Quantitative Imaging Assessment of Bioresorbable Scaffolds: Preprocedural Sizing and Acute Performance

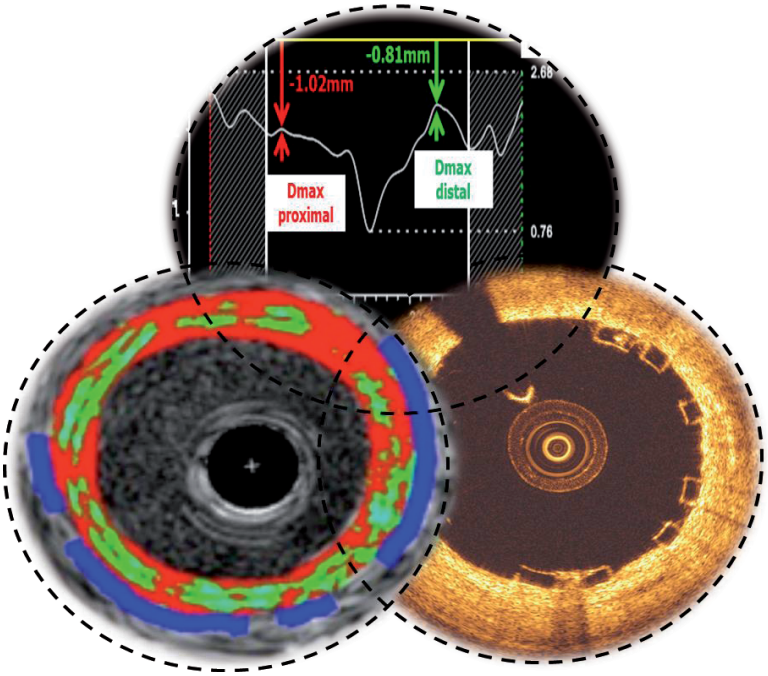

YUKI ISHIBASHI

Erasmus MC
Universitair Medisch Centrum Rotterdam

Quantitative Imaging Assessment of Bioresorbable Scaffolds: Preprocedural Sizing and Acute Performance

Yuki Ishibashi

Financial support by St. Marianna University, Abbott Vascular Japan and Apex International for the publication of this thesis is gratefully acknowledged.

Printed by Optima Grafische Communicatie, Rotterdam, The Netherlands

ISBN: 978-94-6169-882-7

Quantitative Imaging Assessment of Bioresorbable Scaffolds: Preprocedural Sizing and Acute Performance

Quantitative Imaging Evaluatie van Bioresorbeerbare Scaffolds: preprocedurale Sizing en Acute Prestaties

Thesis

to obtain the degree of Doctor from the Erasmus University Rotterdam
by command of the rector magnificus

Prof. dr. H.A.P.Pols

and in accordance with the decision of the Doctorate Board

The public defense shall be held on
Monday the 23rd May 2016 at 11:30 o'clock

by

Yuki Ishibashi
born in Japan

DOCTORAL COMMITTEE

Promotor

Prof.dr. P.W.J.C. Serruys

Prof. dr. R.J.M. van Geuns

The inner doctoral committee

Prof.dr. J.H.C. Reiber

Prof. dr. D.J. Duncker

Dr. Evelyn Regar

The plenary doctoral committee

Dr. Pieter R. Stella

Prof. dr. Y. Ozaki

Prof.dr. Y. J. Akashi

To my parents, Emi and Kyosuke

TABLE of CONTENTS

* Equally contributed to the first author

CHAPTER 1.5 Post-implantation intravascular ultrasound assessment of eccentricity and asymmetry of Xience and Absorb in the ABSORB II trial : impact on adverse cardiovascular events.

Suwannasom P, Sotomi Y, Ishibashi Y, Cavalcante R, Albuquerque FN, Macaya C, Ormiston JA, Hill J, Lang IM, Egred M, Fajadet J, Lesiak M, Tijssen JG, Wykrzykowska JJ, J.de Winter MR, Chevalier B, Onuma Y, Serruys PW

JACC Cardiovasc Interv. 2016 in press. [Original research paper, IF 7.44]

CHAPTER 1.6 A bioresorbable everolimus-eluting scaffold versus a metallic everolimus-eluting stent for ischaemic heart disease caused by de-novo native coronary artery lesions (ABSORB II): an interim 1-year analysis of clinical and procedural secondary outcomes from a randomised controlled trial.

Serruys PW, Chevalier B, Dudek D, Cequier A, Carrié D, Iniguez A, Dominici M, van der Schaaf RJ, Haude M, Wasungu L, Veldhof S, Peng L, Staehr P, Grundeken MJ, Ishibashi Y, Garcia-Garcia HM, Onuma Y.

Lancet. 2015 Jan 3;385(9962):43-54. [Original research paper, IF 39.21]

CHAPTER 1.7 Everolimus-eluting bioresorbable vascular scaffolds for treatment of patients presenting with ST-segment elevation myocardial infarction: BVS STEMI first study.

Diletti R, Karanasos A, Muramatsu T, Nakatani S, Van Mieghem NM, Onuma Y, Nauta ST, Ishibashi Y, Lenzen MJ, Ligthart J, Schultz C, Regar E, de Jaegere PP, Serruys PW, Zijlstra F, van Geuns RJ.

Eur Heart J. 2014 Mar;35(12):777-86 [Original research paper, IF 14.72]

CHAPTER 1.8

Expanded clinical use of everolimus eluting bioresorbable vascular scaffolds for treatment of coronary artery disease:The BVS-Expand Study.

Diletti R, Ishibashi Y, Felix C, Onuma Y, Nakatani S, Van Mieghem NM, Regar E, Valgimigli M, De Jaegere PP, van Ditzhuijzen N, Fam Ming J, Ligthart JMR, Lenzen MJ, Serruys PW, Zijlstra F, Van Geuns R

Submitted [Original research paper, IF xx]

PART 2: Failure Mode of Bioresorbable Scaffolds.

CHAPTER 2.1 Lessons learned from acute and late scaffold failures in the ABSORB EXTEND trial.
Ishibashi Y, Onuma Y, Muramatsu T, Nakatani S, Iqbal J, Garcia-Garcia HM, Bartorelli AL, Whitbourn R, Abizaid A, Serruys PW; ABSORB EXTEND Investigators.
EuroIntervention. 2014 Aug;10(4):449-57. [Original research paper, IF 3.76]

CHAPTER 2.2 Definite and probable bioresorbable scaffold thrombosis in stable and ACS patients.
Ishibashi Y, Nakatani S, Onuma Y.
EuroIntervention. 2014 Sep 22.[Letter to editor, IF 3.76]

CHAPTER 2.3 Early (before 6 months), late (6-12 months) and very late (after 12 months) angiographic scaffold restenosis in the ABSORB Cohort B trial.
Nakatani S, Onuma Y, Ishibashi Y, Muramatsu T, Iqbal J, Zhang YJ, van Geuns RJ, Ormiston JA, Serruys PW.
EuroIntervention. 2014 Feb 27. [Original research paper, IF 3.76]

PART 3: Validation and application of bifurcation algorithm

CHAPTER 3.1 The need for dedicated bifurcation Quantitative Coronary Angiography (QCA) software algorithms to evaluate bifurcation lesions.
Grundeken MJ, Ishibashi Y, Ramcharitar S, Tuinenburg JC, Reiber JH, Tu S, Girasis C, Wentzel JJ, Onuma Y, Serruys PW.
EuroIntervention. 2015 May;11 Suppl V:V44-9. [Review paper, IF 3.76]

CHAPTER 3.2 In vitro validation and comparison of different software packages or algorithms for coronary bifurcation analysis using calibrated phantoms: Implications for clinical practice and research of bifurcation stenting.
Ishibashi Y, Grundeken MJ, Nakatani S, Iqbal J, Morel MA, Généreux P, Girasis C, Wentzel JJ, Garcia-Garcia HM, Onuma Y, Serruys PW.
Catheter Cardiovasc Interv. 2015 Mar;85(4):554-63. [Original research paper, IF 2.40]

CHAPTER 3.3 Inter-Core Lab Variability in Analyzing Quantitative Coronary Angiography for

Bifurcation Lesions: A Post-Hoc Analysis of a Randomized Trial.
Grundeken MJ, Ishibashi Y, Généreux P, LaSalle L, Iqbal J, Wykrzykowska JJ, Morel MA, Tijssen JG, de Winter RJ, Girasis C, Garcia-Garcia HM, Onuma Y, Leon MB, Serruys PW.
JACC Cardiovasc Interv. 2015 Feb;8(2):305-14. [Original research paper, IF 7.44]

CHAPTER 3.4 Comparison Between Two-dimensional and Three-dimensional Quantitative Coronary Angiography For the Assessment of Bifurcation Lesions: A Sub-analysis of the TRYTON Pivotal IDE Coronary Bifurcation Trial.
Muramatsu T, Grundeken MJ, Ishibashi Y, Nakatani S, Girasis C, Campos CM, Morel MA, Jonker H, de Winter RJ, Wykrzykowska JJ, García-García HM, Leon MB, Serruys PW, Onuma Y; TRYTON Pivotal IDE Coronary Bifurcation Trial Investigators.
Catheter Cardiovasc Interv. 2015 Sep;86(3). [Original research paper, IF 2.40]

PART 4: Long Term Assessment of Bioresorbable Scaffolds.

CHAPTER 4.1 Echogenicity as a surrogate for bioresorbable everolimus-eluting scaffold degradation: analysis at 1-, 3-, 6-, 12- 18, 24-, 30-, 36- and 42-month follow-up in a porcine model.
Campos CM, Ishibashi Y, Eggermont J, Nakatani S, Cho YK, Dijkstra J, Reiber JH, Sheehy A, Lane J, Kamberi M, Rapoza R, Perkins L, Garcia-Garcia HM, Onuma Y, Serruys PW.
Int J Cardiovasc Imaging. 2015 Jan 28. [Original research paper, IF 2.32]

CHAPTER 4.2 Temporal evolution of strut light intensity after implantation of bioresorbable polymeric intracoronary scaffolds in the ABSORB cohort B trial-an application of a new quantitative method based on optical coherence tomography.
Nakatani S, Onuma Y, Ishibashi Y, Eggermont J, Zhang YJ, Campos CM, Cho YK, Liu S, Dijkstra J, Reiber JH, Perkins L, Sheehy A, Veldhof S, Rapoza R, van Es GA, Garcia-Garcia HM, van Geuns RJ, Serruys PW; ABSORB Cohort B investigators.
Circ Journal. 2014;78(8):1873-81. [Original research paper, IF 3.69]

CHAPTER 4.3 Bioresorption and Vessel Wall Integration of A Fully Bioresorbable Polymeric Everolimus-Eluting Scaffold: Optical Coherence Tomography (OCT), Intravascular Ultrasound (IVUS) and Histological 3 Study in Porcine Model with Four Years Follow-up.
Nakatani S, Ishibashi Y, Perkins L, Eggermont J, Sotomi Y, Grundeken MJ, Dijkstra J, Rapoza R, Virmani R, Serruys,PW, Onuma Y.

JACC Cardiovasc Interv. 2016 in press. [Original research paper, IF 7.44]

CHAPTER 4.4 Development and receding of a coronary artery aneurysm after implantation of a fully bioresorbable scaffold.
Nakatani S, Ishibashi Y, Suwannasom P, J Grundeken M, Høj Christiansen E, Onuma Y, Serruys PW; ABSORB Cohort B Investigators.
Circulation. 2015 Feb 24;131(8):764-7. [Case report, IF 14.95]

CHAPTER 4.5 A medium term follow-up by Multislice Computed Tomography Coronary Angiography assessing the persistent presence of Bioresorbable Vascular Scaffold metallic radiopaque markers at the site of implantation.
Suwannasom P, Onuma Y, Campos CM, Nakatani S, Ishibashi Y, Grundeken MJ, Stanetic B, Nieman K, Jonker H, Garcia-Garcia HM, Serruys PW.On behalf of the investigators of ABSORB Cohort A, B and EXTENDs.
JACC Cardiovasc Interv. 2015 Jul;8(8):1130-2. [Letter, IF 7.44]

CHAPTER 4.6 Scaffold and edge vascular response following implantation of everolimus-eluting bioresorbable vascular scaffold: a 3-year serial optical coherence tomography study.
Zhang YJ, Iqbal J, Nakatani S, Bourantas CV, Campos CM, Ishibashi Y, Cho YK, Veldhof S, Wang J, Onuma Y, Garcia-Garcia HM, Dudek D, van Geuns RJ, Serruys PW; ABSORB Cohort B Study Investigators..
JACC Cardiovasc Interv. 2014 Dec;7(12):1361-9 [Original research paper, IF 7.44]

PART 5: Summary and Conclusions
(summarize abstracts for each chapter and make a big conclusion)

Summary and Conclusions (Samenvatting en Conclusies)

Acknowledgements

Curriculum Vitae

Appendix

Introduction

INTRODUCTION

In 2006, a fully bioresorbable everolimus-eluting polylactide scaffold, namely the Absorb scaffolds, was introduced. The implantation of a bioresorbable scaffold is a new approach that provides transient vessel support with drug delivery capability, potentially without the limitations of permanent metallic implants. By liberating the coronary artery from the metallic caging, the vessel recovers pulsatility and becomes responsive to shear stress and physiological cyclic strain. The vessel wall, theoretically, can remodel and exhibit plaque reduction in response to pharmacological treatment and physiological stimuli. BRS technology has been so-called "the 4th revolution in coronary interventions" that may have potential clinical advantages over the metallic stent technologies. This novel technology has been extensively investigated in the ABSORB Clinical Program, in that the first-in-man ABSORB Cohort B trial using the current generation Absorb scaffolds showed excellent results in terms of safety and efficacy. Since September 2012, this device has been widely used in the clinical setting.

As the Absorb scaffold has a strict upper limit of expansion, quantitative coronary angiography (QCA)-guided implantation was a mandatory requirement in the most of ABSORB trials. The concerns about appropriate deployment of the Absorb scaffold with angiography guidance arose mainly from optical coherence tomography (OCT) substudies demonstrating an increased frequency of malapposition when the Absorb scaffold was implanted in a too large vessel. Another matter of concern is the risk of scaffold disruption, particularly when the device has already reached its maximal limit of expansion and is overexpanded in an attempt to correct persistent malapposition. Conversely, an OCT substudy showed an excess of proximal and/or distal edge dissections when the Absorb scaffold was implanted in vessels smaller than the device nominal size. However, the impact of quantitative angiographic guidance on clinical outcomes was so far unknown. **Chapter1** describes vessel sizing, acute performance and patient outcome after implantation of bioresorbable scaffolds. The main part of this thesis relates to angiographic and intra coronary imaging assessment of bioresorbable scaffolds.

In the early Absorb studies, several technical failure and adverse events are documented. Acute vessel closure, due to dislodgement of a coronary stent during deployment or an

early stent thrombosis, is a rare but potentially fatal complication of percutaneous coronary intervention. Late or very late thrombosis also remains a long-term concern with metallic drug-eluting stents, due to delayed healing potentially caused by the permanent presence of foreign bodies such as metals and coating materials. After complete bioresorption of the polymeric struts, the risk of very late scaffold thrombosis may theoretically be reduced due to the absence of foreign material. On the other hand, the thick polymeric struts (total strut thickness=156 μm) crimped onto the delivery balloon contribute to the large profile of the device that may cause friction between the device and the diseased vessel wall or any daughter catheter, resulting in dislodgement of the scaffold. We discuss the potential reasons and then share such cases in the early phase of the BRS technology in **Chapter2**.

Considering the use of the Absorb scaffolds in bifurcation lesions, we review the reappraisal angiographic assessment. Angiographic assessment of bifurcation lesion still remains to be a challenging field of research. When revisit single-vessel vs. dedicated bifurcation QCA in clinical bifurcation trials and phantom study, QCA results of the trial are affected following alignment of the methodology. This chapter emphasizes the importance of using the appraisal QCA methodology in **Chapter3**.

Long term assessment of bioresorbable scaffolds beyond angiography is described in **chapter4**. Intravascular ultrasound-derived parameters have shown to be useful to assess the BRS resorption of metallic and polymeric scaffolds in humans. One of the most studied intravascular ultrasound (IVUS) techniques to evaluate the resorption process is called differential echogenicity. This method consists in an automated and quantitative three-dimensional analysis of coronary tissue components scored for echogenicity using as reference the mean level of the adventitia brightness where scaffold struts appear as bright hyperechogenic structures. In clinical studies, a continuous decrease of echogenicity over time has been shown in regions treated with BRS, being putatively correlated to BRS degradation. However, in serial human assessments, changes in the adventitia and plaque-media compartment of the treated regions during the follow-up period could possibly affect these interpretations. This chapter highlights the multimodality imaging assessment for the BRS, mainly focusing on the clinical application of the Absorb scaffolds.

The aims of this thesis are 1) to investigate vessel sizing, acute performance and patient

outcome after implantation of bioresorbable scaffolds; 2) to discuss failure mode of bioresorbable scaffolds;; 3) to validate bifurcation QCA and finally 4) to explore long term assessment of bioresorbable scaffolds beyond angiography.

Chapter 1

Vessel Sizing, Acute Performance and Patient Outcome After Implantation of Bioresorbable Scaffolds

---

1.1 Bioresorbable Scaffold Sizing Using QCA-Dmax

Relation Between Bioresorbable Scaffold Sizing Using QCA-Dmax and Clinical Outcomes at 1 Year in 1,232 Patients From 3 Study Cohorts (ABSORB Cohort B, ABSORB EXTEND, and ABSORB II)

JACC Cardiovasc Interv. 2015 Nov;8(13):1715-26.
[Original research paper, IF 7.44]

Ishibashi Y, Nakatani S, Suwannasom P, Grundeken MJ, Garcia-Garcia HM, Bartorelli A, Whitbourn R, Chevalier B, Abizaid A, Ormiston JA, Rapoza R, Veldhof S, Onuma Y, Serruys PW

Relation Between Bioresorbable Scaffold Sizing Using QCA-Dmax and Clinical Outcomes at 1 Year in 1,232 Patients From 3 Study Cohorts (ABSORB Cohort B, ABSORB EXTEND, and ABSORB II)

Yuki Ishibashi, MD, PhD,* Shimpei Nakatani, MD,* Yohei Sotomi, MD,† Pannipa Suwannasom, MD,*†‡ Maik J. Grundeken, MD,† Hector M. Garcia-Garcia, MD, PhD,* Antonio L. Bartorelli, MD,§ Robert Whitbourn, MD,‖ Bernard Chevalier, MD,¶ Alexandre Abizaid, MD, PhD,# John A. Ormiston, MB, ChB, PhD,** Richard J. Rapoza, PhD,†† Susan Veldhof, RN,‡‡ Yoshinobu Onuma, MD, PhD,* Patrick W. Serruys, MD, PhD§§

ABSTRACT

OBJECTIVES This study sought to investigate the clinical outcomes based on the assessment of quantitative coronary angiography-maximal lumen diameter (Dmax).

BACKGROUND Assessment of pre-procedural Dmax of proximal and distal sites has been used for Absorb scaffold size selection in the ABSORB studies.

METHODS A total of 1,248 patients received Absorb scaffolds in the ABSORB Cohort B (ABSORB Clinical Investigation, Cohort B) study (N = 101), ABSORB EXTEND (ABSORB EXTEND Clinical Investigation) study (N = 812), and ABSORB II (ABSORB II Randomized Controlled Trial) trial (N = 335). The incidence of major adverse cardiac events (MACE) (a composite of cardiac death, any myocardial infarction [MI], and ischemia-driven target lesion revascularization) was analyzed according to the Dmax subclassification of scaffold oversize group versus scaffold nonoversize group.

RESULTS Of 1,248 patients, pre-procedural Dmax was assessed in 1,232 patients (98.7%). In 649 (52.7%) patients, both proximal and distal Dmax values were smaller than the nominal size of the implanted scaffold (scaffold oversize group), whereas in 583 (47.3%) of patients, the proximal and/or distal Dmax were larger than the implanted scaffold (scaffold nonoversize group). The rates of MACE and MI at 1 year were significantly higher in the scaffold oversize group than in the scaffold nonoversize group (MACE 6.6% vs. 3.3%; log-rank $p < 0.01$, all MI: 4.6% vs. 2.4%; log-rank $p = 0.04$), mainly driven by a higher MI rate within 1 month post-procedure (3.5% vs. 1.9%; $p = 0.08$). The independent MACE determinants were both Dmax smaller than the scaffold nominal size (odds ratio [OR]: 2.13, 95% confidence interval [CI]: 1.22 to 3.70; $p < 0.01$) and the implantation of overlapping scaffolds (OR: 2.10, 95% CI: 1.17 to 3.80; $p = 0.01$).

CONCLUSIONS Implantation of an oversized Absorb scaffold in a relatively small vessel appears to be associated with a higher 1-year MACE rate driven by more frequent early MI. (ABSORB Clinical Investigation, Cohort B [ABSORB Cohort B], NCT00856856; ABSORB EXTEND Clinical Investigation [ABSORB EXTEND], NCT01023789; ABSORB II Randomized Controlled Trial [ABSORB II], NCT01425281) (J Am Coll Cardiol Intv 2015;8:1715-26) © 2015 by the American College of Cardiology Foundation.

From the *Thoraxcenter, Erasmus University Medical Center, Rotterdam, the Netherlands; †Academic Medical Center, University of Amsterdam, Amsterdam, the Netherlands; †Northern Region Heart Center, Maharaj Nakorn Chiang Mai Hospital, Faculty of Medicine, Chiang Mai University, Chiang Mai, Thailand; §Centro Cardiologico Monzino, IRCCS, University of Milan, Milan, Italy; ‖St. Vincent's Hospital, Fitzroy, Victoria, Australia; ¶Institut Cardiovasculaire Paris Sud, Massy, France; #Instituto de Cardiologia Dante Pazzanese, São Paulo, Brazil; **Auckland City Hospital, Auckland, New Zealand; ††Abbott Vascular, Santa Clara, California; ‡‡Abbott Vascular, Diegem, Belgium; and the §§International Centre for Cardiovascular Health, Imperial College, London, United Kingdom. Abbott Vascular sponsored and funded the work. Drs. Garcia-Garcia, Onuma, and Serruys are on the advisory board of Abbott Vascular. Dr. Chevalier is a consultant for Abbott Vascular. Dr. Abizaid has received research grants for Abbott Vascular. Dr. Ormiston has received minor honoraria and is on the advisory board of Boston Scientific. Dr. Rapoza and Ms. Veldhof are

ABBREVIATIONS AND ACRONYMS

CI = confidence interval

Dmax = maximal lumen diameter

ID = ischemia-driven

MACE = major adverse cardiac event(s)

MI = myocardial infarction

MLD = minimal lumen diameter

OCT = optical coherence tomography

PMI = periprocedural myocardial infarction

QCA = quantitative coronary angiography

OR = odds ratio

ST = scaffold thrombosis

TLR = target lesion revascularization

TVMI = target vessel myocardial infarction

QCA = quantitative coronary angiography

The performance of the second-generation Absorb bioresorbable everolimus-eluting scaffold was investigated in the ABSORB II (ABSORB II Randomized Controlled Trial) as well as in the Cohort B1, Cohort B2, and ABSORB EXTEND (ABSORB EXTEND Clinical Investigation) studies, and demonstrated excellent clinical results (1-7). As the Absorb scaffold has a strict upper limit of expansion, quantitative coronary angiography (QCA)-guided implantation was a mandatory requirement in ABSORB EXTEND (7) and ABSORB II (1). The aim was to allow the selection of a scaffold size matching that of the reference vessel diameter. For reasons related to the potential labeling by the regulator, the sponsoring corporation did not want to require the use of intravascular imaging for sizing the vessel and for selection of the device size. The concerns about appropriate deployment of the Absorb scaffold with angiography guidance arose mainly from optical coherence tomography (OCT) substudies demonstrating an increased frequency of malapposition when the Absorb scaffold was implanted in a too large vessel (8). Another matter of concern is the risk of scaffold disruption (9), particularly when the device has already reached its maximal limit of expansion and is overexpanded in an attempt to correct persistent malapposition. Conversely, an OCT substudy showed an excess of proximal and/or distal edge dissections when the Absorb scaffold was implanted in vessels smaller than the device nominal size (8). However, the impact of quantitative angiographic guidance on clinical outcomes is so far unknown. Therefore, the aim of this study was to investigate the relationship between clinical outcomes and maximal diameter (Dmax) by QCA, which was used as a guide for appropriate selection and deployment of the Absorb scaffold in 2 cohorts of patients from the ABSORB Cohort B study, ABSORB EXTEND study, and ABSORB II trial.

METHODS

STUDY DESIGN AND POPULATION. We analyzed the results of Absorb scaffold implantation in 1,248 patients enrolled between 2009 and 2013 in the ABSORB Cohort B study (2,4), ABSORB EXTEND study (7), and ABSORB II (1) randomized controlled trial. The design of each study is described elsewhere (4,6,7,10). In the ABSORB Cohort B, a 3.0 × 18-mm Absorb scaffold only was available. In the ABSORB EXTEND and ABSORB II studies, patients were treated as follows (1,7): 1) a 3.5-mm Absorb scaffold was used when both the proximal and distal Dmax were within an upper limit of 3.8 mm and a lower limit of 3.0 mm: 2) a 3.0-mm Absorb scaffold was used when both the proximal and distal maximal lumen diameters were within an upper limit of 3.3 mm and a lower limit of 2.5 mm: 3) a 2.5-mm Absorb scaffold was used when both the proximal and the distal Dmax were within an upper limit of 3.0 mm and a lower limit of 2.25 mm: and 4) scaffold overlap was allowed. Patients demographic data and baseline characteristics were similar among 3 studies as well as pre-procedure minimal lumen diameter (MLD) and % diameter stenosis. All of these trials were sponsored and funded by Abbott Vascular. The research ethics committee of each participating institution approved the protocol, and all enrolled patients provided written informed consent before inclusion.

STUDY DEVICE. The details of the study device (Absorb, Abbott Vascular, Santa Clara, California) have been described in detail previously (5,6). In brief, the balloon-expandable Absorb scaffold comprises a poly-L-lactide backbone (6) coated with an amorphous drug-eluting coating matrix composed of poly-D,L-lactide polymer containing everolimus.

QCA ANALYSIS. QCA guidance of Absorb implantation relies on the angiographic diameter function curve of the pre-treatment vessel segment that contains 3 nonambiguous data points; namely, the MLD and the Dmax with respect to the MLD of the proximal (proximal Dmax) and distal (distal Dmax) vessel segments of interest (8,11) (**Figure 1**). QCA analyses were undertaken by the sites before Absorb implantation, and post-procedurally by an independent core laboratory (Cardialysis BV, Rotterdam, the Netherlands) using a Coronary Angiography Analysis System (Pie Medical Imaging, Maastricht, the Netherlands).

DEFINITIONS AND ENDPOINTS. The patient population in the present study was stratified by the difference between the angiographic maximal diameter

employees of Abbott Vascular. All other authors have reported that they have no relationships relevant to the contents of this paper to disclose.

Manuscript received June 1, 2015; revised manuscript received July 21, 2015, accepted July 30, 2015.

FIGURE 1 The Method to Measure QCA Proximal and Distal Dmax

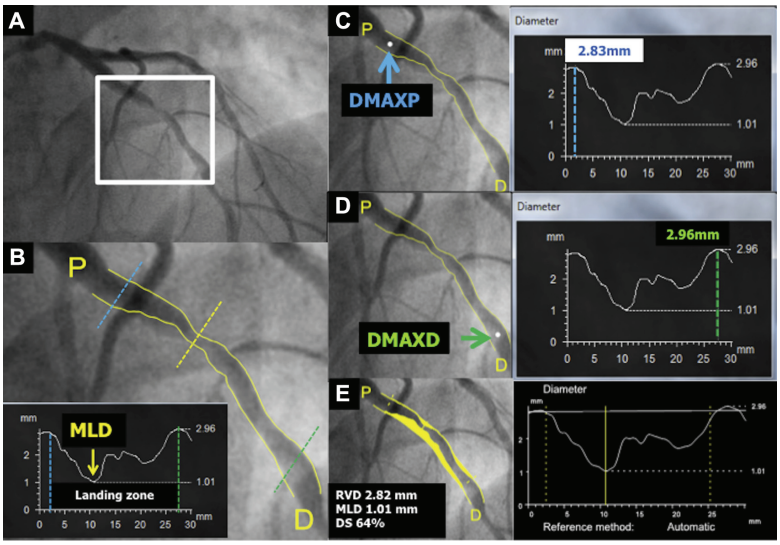

The method used to measure proximal and distal Dmax with QCA is shown. In the pre-procedural angiography **(A)**, the operator has to define the landing zone where the scaffold will be implanted **(B)**. Within the landing zone, the peak of the diameter function curve proximal to the minimal lumen diameter is defined as proximal (P) Dmax **(C)**, whereas the peak diameter function curve distal **(D)** to the minimal lumen diameter is defined as distal Dmax **(D)**. In this case, the proximal and distal Dmax of 2.83 and 2.96 mm led to the correct sizing of the Absorb (3.0 mm) with regard to the vessel diameter **(E)**. DMAXD = maximal lumen diameter distal; DMAXP = maximal lumen diameter proximal; MLD = minimal lumen diameter; QCA = quantitative coronary angiography; RVD = reference vessel diameter.

and the nominal diameter of the implanted scaffold. The selection of device size was considered "oversized" (scaffold oversize group) when the patient received 1 or more devices in vessels in which both the proximal and the distal Dmax were smaller than the nominal size of the device. Patients who received Absorb scaffolds in vessels with either a proximal or a distal Dmax or both Dmax larger than the nominal size of the device constituted the "scaffold nonoversize group". When a patient received 2 or 3 overlapping Absorb scaffolds in a long lesion, the nominal size of the proximally implanted device was compared with the proximal Dmax, whereas the nominal size of the distally implanted device was compared with the distal Dmax. In the cases of device failure (n = 10), the difference between Dmax and the implanted metallic stent was calculated. An additional analysis was performed using a different criterion (nominal scaffold diameter within 0.4 or 0.5 mm of Dmax) and is presented in Online Tables 1 and 2.

In the present analysis, the primary clinical outcome assessed was ischemia-driven major adverse cardiac events (ID-MACE), defined as a composite of cardiac death, any myocardial infarction (MI classified as Q-wave or non-Q-wave MI), and ischemia-driven target lesion revascularization (ID-TLR) by coronary artery bypass graft or percutaneous coronary intervention. Cardiac death was defined as any death due to a proximate cardiac cause (e.g., MI, low-output failure, fatal arrhythmia). Unwitnessed death and death of unknown cause were classified as cardiac death. MI classification and criteria for diagnosis were defined according to the per-protocol definition. Q-wave MI was the development of a new, pathological Q-wave. Non-Q-wave MI was adjudicated if there was an elevation of CK levels to ≥2 times the upper limit of normal with

FIGURE 2 Proximal and Distal Dmax Compared With Nominal Size of the Scaffold

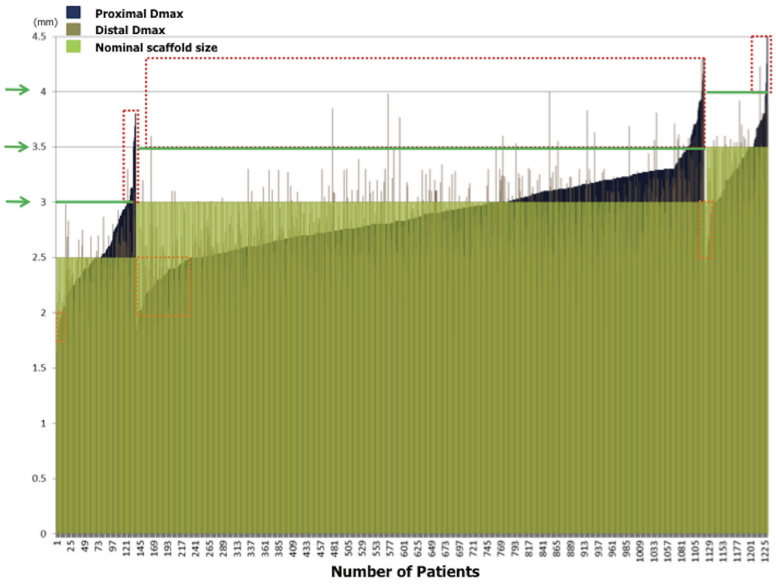

The graph represents the proximal Dmax value, the distal Dmax value and the nominal size of the implanted Absorb scaffold(s) in 1,232 patients. The Dmax measurement is based on core lab assessment. According to the manufacturer, the 2.5-mm, 3.0-mm, and 3.5-mm scaffolds cannot be dilated beyond their nominal size of 3.0 mm, 3.5 mm, and 4.0 mm, respectively. The limit of expansion of the scaffold is depicted by a **green continuous line**. Theoretically, **dotted red areas** indicate implantation of a too "small" Absorb scaffold in a relatively large vessel, and **dotted orange areas** indicate implantation of a too "large" Absorb scaffold in a relatively small vessel. Device size selection with regard to Dmax was considered appropriate in 867 (70.4%) patients and inappropriate in 365 (29.6%) patients. Dmax = maximal lumen diameter.

elevated creatine kinase-myocardial band levels in the absence of new pathological Q waves (12). Notably, this definition of per-protocol MI was consistently applied in all trials included in the present analysis. Target vessel myocardial infarction (TVMI) was defined as MI that occurred in the entire major coronary vessel proximal and distal to the target lesion, which includes upstream and downstream branches and the target lesion itself. ID-TLR was defined as any repeat percutaneous intervention of the target lesion or bypass surgery of the target vessel with either a positive functional ischemia study, ischemic symptoms, or an angiographic MLD stenosis ≥50% by core laboratory QCA, or revascularization of a target lesion with diameter stenosis ≥70% by core laboratory QCA without either ischemic symptoms or a positive functional study. Definite and probable scaffold thrombosis (ST) was adjudicated according to the Academic Research Consortium definitions (13-15). All clinical outcomes were adjudicated by an independent clinical events committee.

SOURCE DOCUMENT VERIFICATION AND CLINICAL FOLLOW-UP. In the ABSORB Cohort B and ABSORB II studies, we verified source documents in 100% of patients through 1-year follow-up. In the ABSORB EXTEND trial, source document verification was routinely performed in 100% of patients through 30-day follow-up, subsequently in a random 20% of patients, and in 100% of all reported events for the remaining follow-up period.

STATISTICAL ANALYSIS. All analyses were conducted using the intention-to-treat population. For the

present analyses, individual data were based on a patient-level basis. Categorical variables were compared by Fisher exact test. Continuous variables are presented as mean ± SD and were compared by nonparametric test. Time-to-event variables are presented as Kaplan-Meier curves. To determine the independent predictors of MACE, firstly univariate logistic regression models were constructed using the following variables: age, male sex, current smoking, hypertension requiring treatment, dyslipidemia requiring treatment, any diabetes, unstable angina, pre-procedural diameter stenosis, pre-procedural MLD, lesion length, angulation >45°, bifurcation lesions, calcified lesions, pre-procedural visible thrombus, Type B2/C lesions, target vessel treatment with 2.5-mm device, treatment with overlapping scaffolds, and scaffold implantation in a vessel with both proximal and distal Dmax smaller than the nominal device size. Secondly, significant variables ($p < 0.10$) in the univariate analysis were forcedly entered into a multivariable logistic regression model to predict for MACE. A 2-sided p value <0.05 was considered significant for all tests. All statistical tests were performed with SPSS, version 22.0 for windows (IBM, Chicago, Illinois).

RESULTS

Of a total population of 1,248 patients, pre-procedural Dmax was assessed by the core laboratory in 1,232 (98.7 %) patients. **Figure 2** displays individual values of proximal and distal Dmax in patients who received Absorb scaffolds of either 2.5-mm, 3.0-mm, or 3.5-mm nominal size. The nominal size of the implanted Absorb scaffold was larger than both proximal and distal Dmax in 649 patients (scaffold oversize group 52.7%).

Clinical and angiographic characteristics between the scaffold oversize group and the scaffold nonoversize group are detailed in **Table 1**. The 2 groups did not significantly differ with regard to main baseline clinical characteristics, whereas pre-procedural MLD, reference vessel diameter, and both proximal and distal Dmax were significantly smaller in the scaffold oversize group than in the scaffold nonoversize group.

The scaffold oversize group was associated with a higher risk of ID-MACE than the scaffold nonoversize group. As illustrated in **Figure 3**, the graphical presentation clearly shows that a higher number of these patients can be seen in the lower left quadrant (scaffold oversize group) than in the other quadrants of the graph (6.6% vs. 3.3%, $p < 0.01$). MACE occurred in 46 of 760 patients when a relatively large device size was selected, whereas it occurred in 16 of 472 patients when a relatively small device size was selected (6.1% vs. 3.4%, $p = 0.04$).

The MACE and MI rates at 1 year and 2 years were significantly higher in the scaffold oversize group

TABLE 1 Clinical and Pre- and Post-Procedural Angiographic Characteristics

	Scaffold Oversize Group (n = 649)	Scaffold Nonoversize Group (n = 583)	p Value
Age, yrs	61.6 ± 10.7	60.8 ± 10.1	0.20
Male	73.8 (479)	75.1 (438)	0.60
Current smoker	1.7 (141)	24 (140)	0.34
Hypertension requiring treatment	67.6 (439)	67.9 (396)	0.95
Dyslipidemia requiring treatment	69.8 (453)	69 (402)	0.76
Any diabetes mellitus	24 (156)	26.2 (153)	0.39
Unstable angina	24.8 (161)	22.9 (133)	0.46
Prior history of myocardial infarction	28.1 (182)	27.8 (162)	0.95
Lesion location			
Right coronary artery	21.9 (142)	33.6 (196)	<0.01
Left anterior descending artery	49.8 (323)	41.9 (244)	0.01
Left circumflex artery or ramus	9.9 (64)	9.6 (56)	0.92
Left main coronary artery	0 (0)	0.2 (1)	0.47
ACC/AHA lesion complexity			
A	1.9 (12)	2.1 (12)	0.84
B1	53.9 (349)	52.8 (307)	0.73
B2	41.2 (267)	43.5 (25)	0.45
C	3.1 (20)	1.7 (10)	0.14
TIMI flow grade 0 or 1	0.6 (4)	0.2 (1)	0.38
Calcification (moderate or severe)	13.4 (87)	14.4 (84)	0.62
Angulation ≥45°	2.6 (17)	2.2 (13)	0.71
Bifurcation	4.0 (26)	4.8 (28)	0.58
Thrombus	1.5 (10)	1.9 (11)	0.67
Pre-procedural			
Reference vessel diameter, mm	2.50 ± 0.33	2.79 ± 0.39	<0.01
Proximal Dmax, mm	2.66 ± 0.30	3.11 ± 0.34	<0.01
Distal Dmax, mm	2.58 ± 0.31	2.94 ± 0.38	<0.01
Minimal lumen diameter, mm	1.05 ± 0.30	1.15 ± 0.33	<0.01
Diameter stenosis, %	57.9 ± 10.9	58.6 ± 10.2	0.22
Obstruction lesion length, mm	12.2 ± 5.9	13.0 ± 5.7	0.03
Device related			
2.5-mm scaffold	8.6 (56)	13.9 (81)	<0.01
3.0-mm scaffold	82.4 (535)	77.4 (451)	0.03
3.5-mm scaffold	8.9 (58)	8.8 (51)	0.92
Average nominal diameter	2.97 ± 0.24	3.00 ± 0.21	0.03
Post-procedural			
Reference vessel diameter, mm	2.58 ± 0.30	2.82 ± 0.34	<0.01
Minimal lumen diameter, mm	2.19 ± 0.28	2.37 ± 0.31	<0.01
Diameter stenosis, %	15.3 ± 6.5	15.9 ± 10.2	0.09
Acute decrease, % diameter stenosis	42.5 ± 12.5	42.5 ± 12.4	0.98
Acute gain, mm	1.13 ± 0.34	1.21 ± 0.38	<0.01
Acute gain/pre-procedural RVD, mm	0.46 ± 0.14	0.44 ± 0.14	0.02
Bailout treatment with metallic stent	1.9 (12)	0.7 (4)	0.08

Values are mean ± SD, or % (n). Clinical and pre- and post-procedural angiographic characteristics are according to the distribution of Dmax measurements minus the nominal scaffold size in the scaffold oversize group versus the scaffold nonoversize group.

ACC/AHA = American College of Cardiology/American Heart Association lesion characteristics; Dmax = maximal lumen diameter; RVD = reference vessel diameter; TIMI = Thrombolysis In Myocardial Infarction.

FIGURE 3 Distribution of the Difference Between Dmax and Nominal Scaffold

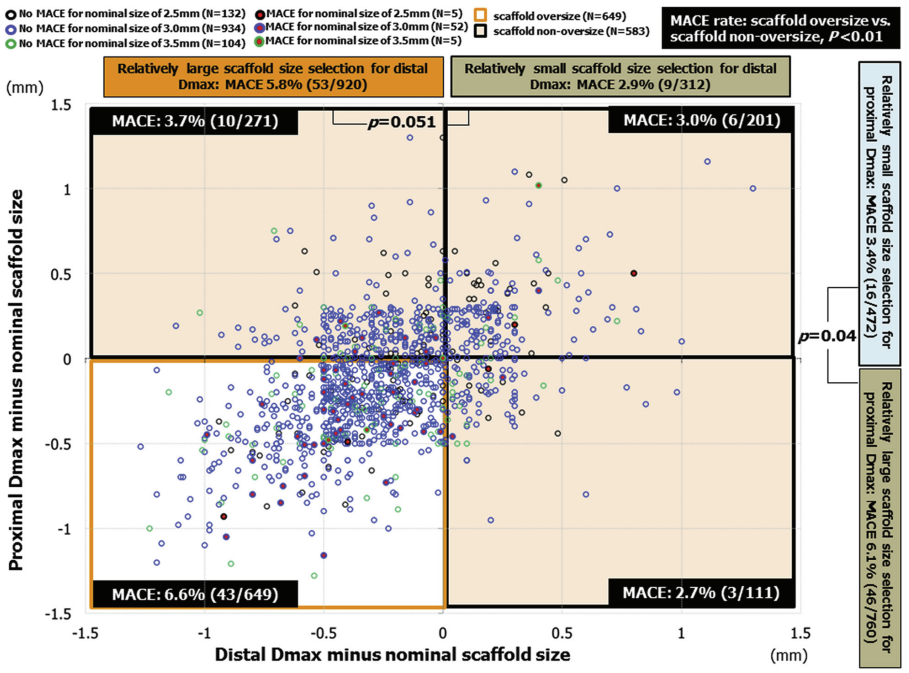

Distribution of proximal and distal Dmax measurements minus nominal scaffold size in patients with or without major adverse cardiac events is shown. When the appropriateness of scaffold size was defined by nominal scaffold diameter within 0.5 mm of Dmax, the differences between the distal Dmax and nominal scaffold size are plotted on the y-axis and x-axis, respectively. The **red filled circles** represent the patients who experienced ID-MACE at 1 year. The graphical presentation demonstrates that major adverse cardiac events (MACE) were more frequently observed in patients in whom both proximal and distal Dmax were smaller than the device nominal size (6.6% vs. 3.3%, p < 0.01) **(lower left quadrant)**. Dmax = maximal lumen diameter; ID-MACE = ischemia-driven major adverse cardiac event(s).

than in scaffold nonoversize group (1-year MACE: 6.6% vs. 3.3%; log-rank p < 0.01, 2-year MACE: 8.7% vs. 5.9%; log-rank p = 0.03, 1-year TVMI: 4.5% vs. 2.1%, 2-year MI: 5.5% vs. 3.0%; log-rank p = 0.04), mainly driven by a higher rate of TVMI within 1 month after the procedure (3.5% vs. 1.9%; p = 0.08) (**Figure 4**, **Tables 2** and **3**). Among the events of MI (44 of 1,232), periprocedural MI (PMI) occurred in 28 cases (63.6%). MI occurred after 48 h in 36% of all MI events. In the scaffold oversize group, PMI occurred in 64% (18 cases), whereas in the scaffold nonoversize group, the PMI rate was 35.7% (10 cases). There were no statistically significant differences in the incidence of overall angiographic complications that could be documented at the end of the procedure for patients who had TVMI within 1 month (3.1% vs. 1.7%; p = 0.14) (**Table 3**). The incidence of ST tended to be higher in the scaffold oversize group than in the scaffold nonoversize group (**Table 2**) (1.54% vs. 0.51%, OR: 3.03 [0.83 to 11.05]; p = 0.10). The acute definite ST rate was 0.15% and 0% in the scaffold oversize group and the scaffold nonoversize group, respectively (p = 1.0). Subacute and late definite ST were not significantly different among the 2 groups (Online Table 3). A case of a definite early ST is shown in **Figure 5**.

When the appropriateness of scaffold size was defined by nominal scaffold diameter within 0.5 mm

FIGURE 4 Time-to-Event Curves of MACE and Its Components

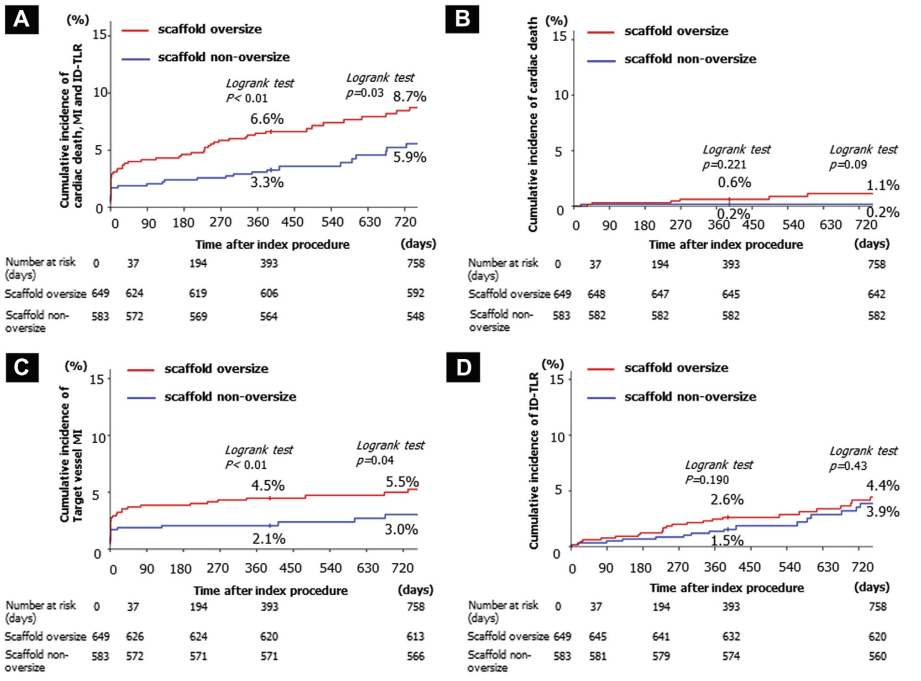

Time-to-event curves of MACE **(A)** and its components (**B**: death, **C**: target vessel MI; **D**: ID-TLR) at 2 years, according to study group. ID-TLR = ischemia-driven target lesion revascularization; MACE = major adverse cardiac event(s); MI = myocardial infarction.

of Dmax, there was no statistically significant difference in MACE between the 2 groups, (appropriate 4.5% vs. inappropriate 6.3%; p = 0.20). When the cutoff of 0.4 mm is used, there was a significant difference in MACE between appropriate and inappropriate scaffold deployment (3.4% vs. 6.8%; p = 0.006) (Online Figures 1 and 2, Online Table 3).

INDEPENDENT PREDICTOR OF MACE AFTER IMPLANTATION OF ABSORB SCAFFOLD(S). With multivariable logistic regression analysis, the independent determinants of 1-year MACE were: implantation of the Absorb scaffold(s) in a vessel with both proximal and distal Dmax smaller than the device nominal size (OR: 2.13, 95% CI: 1.22 to 3.70; p < 0.01) and overlapping scaffolds (OR: 2.10, 95% CI: 1.17 to 3.80; p = 0.01) (**Table 4**).

DISCUSSION

The main findings of this study are: 1) 52.7% (n = 649) of patients had an "oversize" scaffold implantation; 2) The MACE and MI rates at 1 year were significantly higher in the scaffold oversize group than in the scaffold nonoversize group (MACE: 6.6% vs. 3.3%, log-rank p < 0.01, all MI: 4.6% vs. 2.4%; log-rank p = 0.04), mainly driven by a higher rate of MI within 1 month after the procedure (3.5% vs. 1.9%; p = 0.08); the incidence of definite ST tended to be higher in the scaffold oversize group than in the scaffold nonoversize group (1.54% vs. 0.51%,OR: 3.03 [0.83 to 11.05]; p = 0.10); 3) The independent determinants of MACE were both Dmax smaller than the device nominal size (OR: 2.13, 95% CI: 1.22 to 3.70;

TABLE 2 Incidence of Clinical Events at 1 Year

Clinical Outcomes	Scaffold Oversize Group (n = 649)		Scaffold Nonoversize Group (n = 583)			
	% (n)	95% CI	% (n)	95% CI	OR [95% CI]	p Value
Cardiac death	0.62 (4)	0.17–1.57	0.17 (1)	0.00–0.95	3.61 (0.40–32.39)	0.38
Myocardial infarction	4.62 (30)	3.14–5.53	2.40 (14)	1.32–4.00	1.97 (1.03–3.75)	0.049
QMI	1.23 (8)	0.53–2.41	0.34 (2)	0.04–1.23	3.63 (0.77–17.14)	0.11
NQMI	3.39 (22)	2.14–5.09	2.06 (12)	1.07–3.57	1.67 (0.82–3.40)	0.17
TVMI	4.47 (29)	3.01–6.35	2.06 (12)	1.07–3.57	2.23 (1.13–4.40)	0.025
Ischemia-driven TLR	2.62 (17)	1.53–4.16	1.54 (9)	0.71–2.91	1.72 (0.76–3.88)	0.23
Composite of cardiac death, all MI, and clinically indicated target lesion revascularization (MACE)	6.63 (43)	4.84–8.82	3.26 (19)	1.97–5.04	2.11 (1.21–3.66)	<0.01
Composite of cardiac death, target vessel MI, and clinically indicated target lesion revascularization (DoCE)	6.32 (41)	4.57–8.47	2.92 (17)	1.71–4.63	2.25 (1.26–3.99)	<0.01
Composite of all death, all MI, and all revascularization (PoCE)	8.01 (52)	6.04–10.37	4.46 (26)	2.93–6.47	1.87 (1.15–3.03)	0.01
Scaffold thrombosis	1.54 (10)	0.74–2.82	0.51 (3)	0.11–1.50	3.03 (0.83–11.05)	0.10
Definite ST	0.92 (6)	0.34–2.00	0.51 (3)	0.11–1.50	1.80 (0.45–7.25)	0.51
Probable ST	0.31 (2)	0.04–1.11	0 (0)	0.00–1.01	NA	1.0
Possible ST	0.31 (2)	0.04–1.11	0 (0)	0.00–1.01	NA	1.0

Incidence of clinical events at 1 year are according to the distribution of Dmax measurements minus the nominal scaffold size in the scaffold oversize group versus the scaffold nonoversize group.

CI = confidence interval; Dmax = maximal lumen diameter; DoCE = device-oriented composite endpoint; MACE = major adverse cardiac event(s); MI = myocardial infarction; NQMI = non-Q-wave myocardial infarction; OR = odds ratio; PoCE = patient-oriented composite endpoint; QMI = Q-wave myocardial infarction; ST = scaffold thrombosis; TLR = target lesion revascularization; TVMI = target vessel myocardial infarction.

p < 0.01) and overlapping scaffolds (OR: 2.10, 95% CI: 1.17 to 3.80; p = 0.01).

As illustrated in the scaffold oversize group in Figure 3, proximal and distal Dmax were significantly smaller than in the scaffold nonoversize group (proximal Dmax: 2.66 ± 0.30 mm vs. 3.11 ± 0.34 mm; p < 0.01, distal Dmax: 2.58 ± 0.31 mm vs. 2.94 ± 0.38 mm; p < 0.01, respectively) (Table 1). In the population described in the scaffold oversize group, 2.5-mm device size scaffolds were less frequently selected (8.6% vs. 13.9%; p < 0.01) as compared with 3.0-mm scaffolds (82.4% vs. 77.4%; p = 0.03). In the scaffold oversize group, acute gain normalized for preprocedural reference vessel diameter was higher (0.46 ± 0.14 vs. 0.44 ± 0.14; p = 0.02) and bailout treatment with metallic stents was more frequently performed (1.9% vs. 0.7%; p = 0.08) compared with the nonoversize group (Table 1). Implanting Absorb scaffold(s) in a vessel with both proximal and distal Dmax smaller than the device nominal size may cause edge dissections due to the higher balloon/device-artery ratio during scaffold deployment.

TABLE 3 Incidence of TVMI

	Scaffold Oversize Group (n = 649)	Scaffold Nonoversize Group (n = 583)	p Value
TVMI at 12 months after index procedure	4.5 (29)	2.1(12)	0.025
TVMI within 1 month after index procedure	3.5 (23)	1.9 (113)	0.08
TVMI between 1 month and 12 months after index procedure	0.9 (6)	0.2 (1)	0.13
Overall angiographic complications at the end of procedure for TVMI within 1 month	3.1 (20)	1.7 (10)	0.14
Side-branch occlusion	2.3 (15)	1.4 (8)	0.29
Coronary dissection	1.1 (7)	0.3 (2)	0.18
Side branch occlusion + coronary dissection	0.3 (2)	0 (0)	0.50
Not relating to device caused angiographic complications for TVMI within 1 month	0.3 (2)	0.3 (2)	1.0
Coronary dissection due to balloon dilation			

Values are % (n).

Abbreviations as in Table 2.

Retrospective subanalysis (8) of the ABSORB Cohort B study demonstrated that after implantation of a 3.0 × 18-mm device, patients with a Dmax ranging between 2.5 and 3.3 mm had better acute OCT outcomes as compared with patients with a Dmax out of range. The implantation of a "small" Absorb scaffold in a relatively large vessel can cause incomplete strut apposition at the edge and may be associated with scaffold disruption (9) when aggressive postdilation with a larger balloon is attempted to correct such malapposition (Figure 6A). Conversely, implantation of a "large" Absorb scaffold in a relatively small vessel can cause vessel injury or underexpansion of the scaffold (Figure 6B).

CLINICAL OUTCOMES WITH RESPECT TO Dmax. The present study clearly demonstrates that implanting Absorb scaffold(s) in a vessel with both proximal and distal Dmax smaller than the device

FIGURE 5 A Case Example of a Definite Early Thrombosis of Absorb Scaffold Implanted in the Mid-LAD

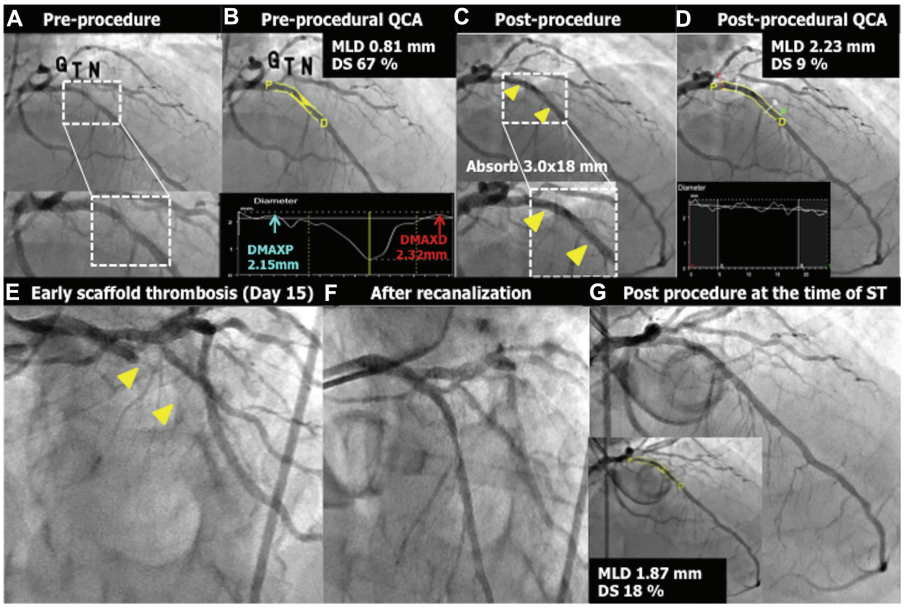

The patient received a 3.0-mm device in a too-small vessel (proximal and distal Dmax 2.15 mm and 2.32 mm, respectively **[A and B]**). After Absorb scaffold implantation **(C and D, arrowheads)**, QCA showed an excellent result with a residual DS of 9%. Fifteen days after the procedure, the patient presented with a STEMI due to early scaffold thrombosis **(E)** that was treated with a manual aspiration only **(F and G)**. DS = diameter stenosis; LAD = left anterior descending coronary artery; ST = scaffold thrombosis; STEMI = ST-segment elevation myocardial infarction; other abbreviations as in **Figure 1**.

nominal size is associated with a higher risk of ID-MACE (6.6% vs. 3.3%; $p < 0.01$). The difference in 1-year MACE was observed in the scaffold oversize group and was mainly driven by a higher MI rate (4.5% vs. 2.1%; $p < 0.01$). Scaffold expansion below nominal diameters can lead to a denser polymer surface pattern and a higher polymer-to-artery ratio (Online Figure 3). Furthermore, the expanding radial force may be suboptimal in these underdeployed configurations; presumably, these unfavorable final expansion diameters might cause micro thrombus formation at the strut level and side-branch occlusion. However, no statistically significant difference in the incidence of overall angiographic complications could be documented at the end of the procedure for the patients who sustained MI within 1 month (scaffold oversize group: 3.1% vs. scaffold nonoversize group: 1.7%; $p = 0.14$) (**Table 3**).

With multivariable logistic regression analysis, the independent determinants of 1-year MACE were: implantation of an Absorb scaffold(s) in a vessel with both proximal and distal Dmax smaller than device nominal size (OR: 2.13, 95% CI: 1.22 to 3.70; $p < 0.01$) and overlapping scaffolds (OR: 2.10, 95% CI: 1.17 to 3.80; $p = 0.01$) (**Table 4**). Of note, in a juvenile porcine model, overlapping Absorb scaffolds showed delayed healing on histology and with OCT assessment and slower tissue coverage than nonoverlapping scaffolds. Indeed, the neoendothelial coverage of the overlapping segments was 80.1% and 99.5% at 28 and 90 days after implantation, respectively; accordingly, coverage in humans may need up to 18 months to be completed (16). Among the 62 patients with MACE,

TABLE 4 Predictors of MACE After Implantation of the Absorb Scaffold(s)

	Univariate Logistic Regression		Multivariate Logistic Regression	
	OR (95% CI)	p Value	OR (95% CI)	p Value
Age, yrs	1.01 (0.98–1.03)	0.64	–	–
Male	0.83 (0.47–1.46)	0.52	–	–
Current smoker	0.80 (0.42–1.53)	0.51	–	–
Hypertension requiring treatment	1.00 (0.90–1.10)	0.96	–	–
Dyslipidemia requiring treatment	1.54 (0.84–2.83)	0.16	–	–
Any diabetes mellitus	0.78 (0.42–1.46)	0.44	–	–
Unstable angina	0.69 (0.35–1.34)	0.27	–	–
Prior myocardial infarction	1.01 (0.99–1.04)	0.20	–	–
Pre-procedural diameter stenosis, %	0.99 (0.97–1.02)	0.55	–	–
Pre-procedural MLD, mm	0.76 (0.33–1.72)	0.51	–	–
Obstruction length, mm	0.99 (0.94–1.04)	0.64	–	–
Smallest Dmax (proximal and distal)	0.51 (0.22–1.14)	0.10	–	–
Angulation ≥45°	0.64 (0.09–4.81)	0.67	–	–
Moderate/severe calcification	0.65 (0.28–1.54)	0.33	–	–
Pre-procedural visible thrombus	0.94 (0.12–7.13)	0.95	–	–
Bifurcation lesion	CS	CS	–	–
Type B2/C lesion	1.02 (0.61–1.71)	0.93	–	–
Left anterior descending artery	0.73 (0.43–1.23)	0.24	–	–
Nominal scaffold size/post-procedural MLD	3.11 (0.73–13.16)	0.12	–	–
Treatment with overlapping devices	2.08 (1.15–3.75)	0.02	2.10 (1.17–3.80)	0.01
2.5-mm device implanted	0.69 (0.27–1.75)	0.44	–	–
Implanting Absorb scaffold(s) in a vessel with both proximal and distal Dmax smaller than nominal size of the device	2.11 (1.21–3.66)	0.01	2.13 (1.22–3.70)	<0.01

CS = complete separation; ITT = intention to treat; MLD = minimal lumen diameter; other abbreviations as in Table 2.

MI occurred in 14 (22.6%) patients who were treated with overlapping scaffolds and were mainly PMI (12 [19.4%]). Thus, overlapping of scaffolds might be a contributing factor of MACE.

PRACTICAL IMPLICATIONS OF THE SELECTION OF APPROPRIATELY SIZED ABSORB SCAFFOLDS. Previously, we have focused mainly on the upper limit of 0.5 mm Dmax due to the well-known issues of device malapposition and disruption in case of over dilation. However, scaffold underexpansion due to the deployment of a scaffold in a vessel with a smaller size, may be associated with a higher post-procedural MI rate due to several different mechanisms. The oversized scaffold could create vessel dissection or microperforation in a small target vessel. Alternatively, the underexpansion of the scaffold may lead to a denser polymer surface pattern and a larger strut footprint to vessel surface area causing side branch occlusion or microthrombus formation.

In the present study, the size selection of Absorb scaffolds with the cutoff value of 0.5-mm Dmax has been shown to be clinically relevant. As presented in the Results and Online Appendix, more events were observed when the mismatch between the device and the vessel size was beyond 0.4 mm. It could therefore be recommended that the device-vessel mismatch regarding Dmax should be within 0.4 mm.

The current analysis showed that the device-vessel mismatch regarding the pre-procedural angiography has a clinical impact. There were no differences in MACE in the population with a post-procedure diameter stenosis ≥10% and <10% (MACE: 5.3% vs. 4.1%; p = 0.46) or in patients with a diameter stenosis ≥20% and <20% (MACE: 5.14% vs. 4.69%; p = 0.77). Therefore, the observed relationship between device-vessel mismatch and clinical outcomes seems to specifically relate to pre-procedural angiographic measurement. It is still unclear how far the pre-procedural device-vessel mismatch could be corrected by post-dilation with high-pressure or low-pressure balloons. Currently, operators with a large experience of BRS implantation are intuitively promoting a strategy of a high-pressure post-dilation with a noncompliant balloon size 0.25 or 0.5 mm larger than the nominal size of the device. A randomized trial on post-dilation strategy (systematic vs. nonsystematic) will be able to clarify what the optimal implantation technique for this polymeric coronary device is.

It has been shown that QCA underestimates coronary lumen diameter, whereas OCT provides correct assessment of lumen dimension (17). Mattesini et al. (18,19) reported that when OCT is used to guide and optimize Absorb scaffold implantation, post-implantation area stenosis, minimal lumen area, and eccentricity index were similar to those observed after deployment of second-generation metallic drug-eluting stents. The different approach for lesion preparation and routine use of OCT guidance during Absorb scaffold implantation might have contributed to these results. In addition, recent studies demonstrated with multivariable analysis that peristent dissections shown by OCT were independent predictors of PMI (OR: 5.3, 95% CI: 1.2 to 24.3), raising concerns about the relationship between these minor vessel injuries and a potential higher risk of early TVMI (20). Taking into account the weakness of QCA for accurately measuring vessel lumen dimension and its inability to assess incomplete scaffold apposition and/or acute scaffold disruption, coregistration (21) of OCT imaging and x-ray angiography may be useful for optimizing the percutaneous treatment of coronary artery disease with bioresorbable vascular scaffolds. In future studies, a clinical scientific question would be whether the pre-procedural usage of intravascular imaging could further improve clinical outcomes.

FIGURE 6 The Potential Consequences of a Device-Vessel Mismatch Implantation

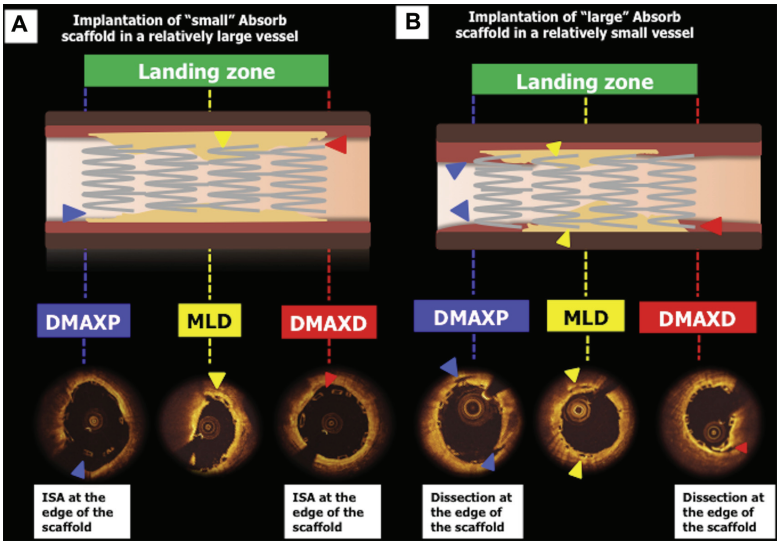

Implantation of a too "small" Absorb scaffold in a relatively large vessel can cause incomplete apposition of the device edges **(A, top panel, blue and red arrowheads)**. Incomplete scaffold apposition **(blue and red arrow heads)** and scaffold under-expansion **(yellow arrowhead)** are visible in the OCT images **(A, bottom panel)**. Implantation of a too "large" Absorb scaffold in a relatively small vessel can cause vessel injury **(B, top panel, blue and red arrowheads)**. Edge dissections **(blue and red arrowheads)** are visible in the OCT images **(B, bottom panel)**. ISA = incomplete scaffold apposition; OCT = optical coherence tomography; other abbreviations as in Figure 1.

STUDY LIMITATIONS. The current study does not provide mechanistic data to support the occurrence of clinical adverse events caused by sizing mismatch due to a lack of routine intravascular imaging (e.g., intravascular ultrasound, OCT, etc.). Further investigation using intravascular imaging is needed to establish the relationship between acute mechanistic complications (such as underexpansion, dissection, and malapposition, and so on) and late adverse events.

CONCLUSIONS

Selection of an appropriate scaffold size according to the vessel Dmax showed a trend toward less frequent ID-TLR, whereas implantation of an oversized Absorb scaffold in a relatively small vessel may be associated with a higher risk of MACE at 1 year. The current results need to be confirmed in the large-scale randomized trials that are on-going, and the mechanistic etiologies should be further elucidated in imaging studies.

REPRINT REQUESTS AND CORRESPONDENCE: Dr. Yoshinobu Onuma, Erasmus Medical Center, 's-Gravendijkwal 230, Rotterdam 3015CE, the Netherlands. E-mail: yoshinobuonuma@gmail.com.

PERSPECTIVES

WHAT IS KNOWN? QCA-Dmax–guided scaffold size selection has been proposed to optimize the scaffold implantation procedure. However, the relationship between clinical outcomes and QCA-Dmax is unknown.

WHAT IS NEW? The device-vessel size mismatch has an impact on clinical event after implantation of Absorb scaffold.

WHAT IS NEXT? The current results should be confirmed in large-scale randomized trials, and the mechanistic etiologies should be further elucidated in studies using intravascular imaging.

REFERENCES

1. Serruys PW, Chevalier B, Dudek D, et al. A bioresorbable everolimus-eluting scaffold versus a metallic everolimus-eluting stent for ischaemic heart disease caused by de-novo native coronary artery lesions (ABSORB II): an interim 1-year analysis of clinical and procedural secondary outcomes from a randomised controlled trial. Lancet 2015;385:43–54.

2. Serruys PW, Onuma Y, Garcia-Garcia HM, et al. Dynamics of vessel wall changes following the implantation of the Absorb everolimus-eluting bioresorbable vascular scaffold: a multi-imaging modality study at 6, 12, 24 and 36 months. EuroIntervention 2014;9:1271–84.

3. Onuma Y, Dudek D, Thuesen L, et al. Five-year clinical and functional multislice computed tomography angiographic results after coronary implantation of the fully resorbable polymeric everolimus-eluting scaffold in patients with de novo coronary artery disease: the ABSORB cohort A trial. J Am Coll Cardiol Intv 2013;6:999–1009.

4. Serruys PW, Onuma Y, Dudek D, et al. Evaluation of the second generation of a bioresorbable everolimus-eluting vascular scaffold for the treatment of de novo coronary artery stenosis: 12-month clinical and imaging outcomes. J Am Coll Cardiol 2011;58:1578–88.

5. Serruys PW, Ormiston JA, Onuma Y, et al. A bioabsorbable everolimus-eluting coronary stent system (ABSORB): 2-year outcomes and results from multiple imaging methods. Lancet 2009;373:897–910.

6. Ormiston JA, Serruys PW, Regar E, et al. A bioabsorbable everolimus-eluting coronary stent system for patients with single de-novo coronary artery lesions (ABSORB): a prospective open-label trial. Lancet 2008;371:899–907.

7. Abizaid A, Costa JR Jr., Bartorelli AL, et al. The ABSORB EXTEND study: preliminary report of the twelve-month clinical outcomes in the first 512 patients enrolled. EuroIntervention 2015;10:1396–401.

8. Gomez-Lara J, Diletti R, Brugaletta S, et al. Angiographic maximal luminal diameter and appropriate deployment of the everolimus-eluting bioresorbable vascular scaffold as assessed by optical coherence tomography: an ABSORB cohort B trial sub-study. EuroIntervention 2012;8:214–24.

9. Onuma Y, Serruys PW, Muramatsu T, et al. Incidence and imaging outcomes of acute scaffold disruption and late structural discontinuity after implantation of the absorb everolimus-eluting fully bioresorbable vascular scaffold: optical coherence tomography assessment in the ABSORB Cohort B trial (A Clinical Evaluation of the Bioabsorbable Everolimus Eluting Coronary Stent System in the Treatment of Patients With De Novo Native Coronary Artery Lesions). J Am Coll Cardiol Intv 2014;7:1400–11.

10. Diletti R, Serruys PW, Farooq V, et al. ABSORB II randomized controlled trial: a clinical evaluation to compare the safety, efficacy, and performance of the Absorb everolimus-eluting bioresorbable vascular scaffold system against the XIENCE everolimus-eluting coronary stent system in the treatment of subjects with ischemic heart disease caused by de novo native coronary artery lesions: rationale and study design. Am Heart J 2012;164:654–63.

11. Farooq V, Gomez-Lara J, Brugaletta S, et al. Proximal and distal maximal luminal diameters as a guide to appropriate deployment of the ABSORB everolimus-eluting bioresorbable vascular scaffold: a sub-study of the ABSORB Cohort B and the on-going ABSORB EXTEND Single Arm Study. Catheter Cardiovasc Interv 2012;79:880–8.

12. Vranckx P, Farooq V, Garg S, et al. Different cardiac biomarkers to detect peri-procedural myocardial infarction in contemporary coronary stent trials: impact on outcome reporting. Heart 2012;98:1424–30.

13. Vranckx P, Kint PP, Morel MA, Van Es GA, Serruys PW, Cutlip DE. Identifying stent thrombosis, a critical appraisal of the academic research consortium (ARC) consensus definitions: a lighthouse and as a toe in the water. EuroIntervention 2008;4 Suppl C:C39–44.

14. Applegate RJ, Sacrinty MT, Little WC, Santos RM, Gandhi SK, Kutcher MA. Incidence of coronary stent thrombosis based on academic research consortium definitions. Am J Cardiol 2008;102:683–8.

15. Mauri L, Hsieh WH, Massaro JM, Ho KK, D'Agostino R, Cutlip DE. Stent thrombosis in randomized clinical trials of drug-eluting stents. N Engl J Med 2007;356:1020–9.

16. Farooq V, Serruys PW, Heo JH, et al. Intracoronary optical coherence tomography and histology of overlapping everolimus-eluting bioresorbable vascular scaffolds in a porcine coronary artery model: the potential implications for clinical practice. J Am Coll Cardiol Intv 2013;6:523–32.

17. Tsuchida K, van der Giessen WJ, Patterson M, et al. In vivo validation of a novel three-dimensional quantitative coronary angiography system (CardiOp-B): comparison with a conventional two-dimensional system (CAAS II) and with special reference to optical coherence tomography. EuroIntervention 2007;3:100–8.

18. Mattesini A, Pighi M, Konstantinidis N, et al. Optical coherence tomography in bioabsorbable stents: mechanism of vascular response and guidance of stent implantation. Minerva Cardioangiol 2014;62:71–82.

19. Mattesini A, Secco GG, Dall'Ara G, et al. ABSORB biodegradable stents versus second-generation metal stents: a comparison study of 100 complex lesions treated under OCT guidance. J Am Coll Cardiol Intv 2014;7:741–50.

20. Porto I, Di Vito L, Burzotta F, et al. Predictors of periprocedural (type IVa) myocardial infarction, as assessed by frequency-domain optical coherence tomography. Circ Cardiovasc Interv 2012;5:89–96, S1–6.

21. Hebsgaard L, Nielsen TM, Tu S, et al. Co-registration of optical coherence tomography and X-ray angiography in percutaneous coronary intervention. The Does Optical Coherence Tomography Optimize Revascularization (DOCTOR) fusion study. Int J Cardiol 2014;182C:272–8.

KEY WORDS bioresorbable scaffold, major adverse cardiac event(s), maximal lumen diameter

APPENDIX For supplemental figures and tables, please see the online version of this article.

1.2 Conformability in Bioresorbable Scaffolds

Conformability in Everolimus-Eluting Bioresorbable Absorb Scaffolds compared with Metal Platform Coronary Stents in Long lesions.

Submitted [Original research paper]

Fam JM, **Ishibashi Y**, Felix C, Diletti1 R, Van Mieghem N, Regar E, van Domburg E, Wentzel J, Gijsen F, Onuma Y, van Geuns RJ

Conformability in Everolimus-Eluting Bioresorbable Absorb Scaffolds compared with Metal Platform Coronary Stents in Long lesions

Jiang Ming Fam[1,2], Yuki Ishibashi[1], Cordula Felix[1], Roberto Diletti[1], Nicolas Van Mieghem[1], Evelyn Regar[1], Ron van Domburg[1], Jolanda Wentzel[1], Frank Gijsen[1], Yoshinobu Onuma[1], Robert- Jan van Geuns[1]

1-Thorax Centre, Erasmus Medical Centre, Rotterdam, Netherlands

2-National Heart Centre Singapore

Address for correspondence:

Robert-Jan M. van Geuns, MD, PhD

Department of Cardiology

Thoraxcentre, room Ba-585

Erasmus University Medical Centre

's-Gravendijkwal 230

3015 GE Rotterdam, The Netherlands

Tel: +31 (0)10 703 33 48

Fax: +31 (0)10 703 52 54

E-mail: r.vangeuns@erasmusmc.nl

Total Word Count: 3276 (Main text, references, legends)

Acknowledgements: The BVS Expand and BVS STEMI First registries are supported by research grants from Abbott Vascular. Prof Robert-Jan van Geuns received speaker's fees from Abbott Vascular.

Structured Abstract

Objectives

The aim of this study was to determine if there are significant differences in curvature of the treated vessel after the deployment of a polymeric BRS or MPS in long lesions.

Background

The impact of long polymeric Bioresorbable Absorb scaffolds (BRS) compared with metallic platform stents (MPS) on vessel curvature is unknown.

Methods

This retrospective study compares 32 patients who received a single everolimus-eluting BRS with 32 patients treated with a single MPS of 28mm. Quantitative coronary angiography (QCA) was used to evaluate curvature of the treatment and peri-treatment region before and after percutaneous coronary intervention (PCI).

Results

Baseline demographic and angiographic characteristics were similar between the BAS and MPS groups. Pretreatment lesion length was 22.19 mm vs 20.38 mm in the BRS and MPS groups respectively (p=0.803). After treatment, there was a decrease in median diastolic curvature in the MPS group (from 0.257cm^{-1} to 0.199cm^{-1}, p= 0.001). A similar trend was observed in the BRS group but did not reach statistical significance (median diastolic curvature from 0.305cm^{-1} to 0.283cm^{-1}, p= 0.056). Median Percentage relative change in diastolic curvature was lower in the BRS group compared with the MPS group (BRS vs MPS: 7.48% vs 29.4%, p= 0.013). By

univariate analysis, use of MPS was an independent predictor of change in diastolic curvature (p = 0.022).

Conclusions

In the deployment of long coronary scaffolds/ stents (28mm in length), BRS provides better conformability compared with MPS.

Word Count Limit: 231 words

Key Words:

Bioresorbable Absorb scaffolds

Curvature

Conformability

Drug Eluting Stents

Long coronary lesions

Metallic Platform stents

Abbreviations:

AMI- Acute Myocardial Infarct

BRS- Bioresorbable Absorb scaffold (BRS)

CABG- Coronary Artery Bypass Graft

CoCr- EES- Cobalt Chromium- Everolimus Eluting Stent

Cv- curvature

CVA- Cerebrovascular Accident

DES- Drug Eluting stent

LAD- Left anterior descending artery

LCX- Left circumflex artery

MLD- Minimal luminal diameter

MPS- Metallic Platform stent

PCI- Percutaneous Coronary Intervention

PLLA- poly-L-lactic acid

QCA- Quantitative coronary angiography

RCA- Right coronary artery

RVD- Reference vessel diameter

STEMI- ST elevation Myocardial Infarct

Introduction

The everolimus-eluting Bioresorbable Absorb scaffold (BRS) (Abbott Vascular, Santa Clara, California) represented a novel change in the treatment of coronary artery lesions. The BRS is composed of a poly-L-lactic acid (PLLA) - based platform which had been shown to provide similar outcomes to best-in-class metallic drug eluting stents (DES)[1]. Besides the ability to have complete strut resorption at 36 months, there are several potential benefits of BRS including no trigger for thrombosis after resorption, reduced requirements for long term dual antiplatelet therapy and restoration of vasoreactivity[2]. As implantation of coronary stents/ scaffolds can alter blood rheology especially at the inflow and outflow edge of the stents, the vessel distortion post device implantation may contribute to early and late stent failure. Geometric changes in the arteries post implantation are largely determined by the conformability of the stent[3]. The conformability of the stent has been described as the flexibility of a stent in its expanded state with adaptation to the natural shape of the vessel. A higher conformability of the stent is associated with less potential for vessel distortion and trauma[4].

Previous studies using BRS in short lesions demonstrate favorable clinical outcomes out to 3-year follow-up[5] and better conformability compared to MPS in the acute setting[6]; however, the acute effects of its implantation on vessel geometry in long coronary lesions are yet to be investigated. The aim of this study was to determine if there are any significant differences in terms of curvature of the treated vessel after the deployment of a polymeric scaffold device in long lesions and compare this to a MPS.

Methods

Study design, population, and treatment device.

This is a nonrandomized, 2-arm, retrospective study performed with patients from the onging BVS Expand and BVS STEMI First registries that received a Everolimus Eluting BRS (BRS-Absorb; Abbott Vascular, Santa Clara, CA, US) compared with a subset of historical controls from the same institutional registries (X-SEARCH) who received a Cobalt Chromium-Everolimus Eluting Stent (CoCr-EES; XIENCE^{R} stent, Abbott Vascular, Santa Clara, CA, US).

In brief, the common inclusion criteria for this study are patients who had received a single BRS or CoCr EES that are 28mm in length in long coronary lesions. The patients in the BRS group are selected from the BVS Expand and BVS STEMI registries which are single centre prospective observational registries conducted at Thorax Centre, Erasmus Medical Centre that evaluates the long term safety and performance of the BRS-Absorb coronary stent in routine clinical practice post market registration. Informed, written consent was obtained from the patients before they undergo any procedure. The lesions are also more complex with more bifurcations and calcified lesions. From the X-SEARCH registry, patients with similar angiographic characteristics were selected for this study.

The BRS-Absorb vascular scaffold is a balloon-expandable device, consisting of a polymer backbone of PLLA coated with a thin layer of a 1:1 mixture of an amorphous matrix of PLLA polymer containing 100ug/cm2 of the antiproliferative drug everolimus. The implant is radiolucent but has 2 platinum markers at each edge that allow visualization on angiography and other imaging modalities. Physically the scaffold has struts with an approximate thickness of 150 um, which are arranged as in-phase zigzag hoops linked together by 3 longitudinal links (Figure 1A).

The metallic platform of the everolimus-eluting XIENCE^{R} family stent (EES) is composed of a cobalt chromium (CoCr) alloy. The platform has a design similar to the Absorb platform and consists of serpentine rings connected by links fabricated from a single piece (Figure 1B). The strut width of the CoCr-EES is 91um. The polymer and drug coating add a combined thickness of 7 um. The metallic platforms of the CoCr EES are constructed by a strut thickness of 81 um each[7].

Treatment procedure.

Patients underwent angiographic and interventional procedures according to guideline recommendations. The BRS was implanted at a pressure not exceeding the rated burst pressure (16 atm). Pre and Post-dilation with a balloon (of length shorter than the implanted device) was performed at the discretion of the operator. Patients were prescribed with standard guideline recommended medical therapy including antiplatelet medications and antianginal therapy when appropriate.

Quantitative coronary angiography (QCA) evaluation.

Angiographic views with minimal foreshortening of the lesion and limited overlap with other vessels were used whenever possible for all phases of the treatment: preprocedural angiography, and after obtaining final result[8]. Comparison between pre and post treatment, were performed in matched angiographic views of 10 degrees or less. The 2-dimensional (2D) angiograms were analyzed with the CASS 5.10 analysis system (Pie Medical BV, Maastricht, the Netherlands). In each patient, the treated region and the peri-treated regions (defined by 5 mm proximal and distal

to the device edge) were analyzed. The computer defined minimal luminal diameter, reference diameter obtained by an interpolated method, and percentage diameter stenosis in the post procedure angiogram.

The definition of "Curvature" is the infinitesimal rate of change in the tangent vector at each point of the centerline. This measurement has a reciprocal relationship to the radius of the perfect circle defined by the curve at each point. The curvature of the vessel is calculated as 1/radius of the circle in cm^{-1}, with a research program installed in the QCA Analysis software (CASS 5.10, Pie Medical Imaging)[9]. The segment of interest was defined as the stented/ scaffolded length. To enable analysis of curvature in the same anatomical region, the scaffold position was superimposed on the preprocedural angiogram (Fig 2). The software automatically detects the lumen contours of the selected segment and configures the centerline. Three points are then defined according to the centerline: 1 at the proximal, 1 at the distal, and 1 at the center of the defined segment. Next, a perfect circle is drawn through these points, calculating the radius of the circle and the curvature value. Prior to and after the procedure, the curvature of the segment of interest was repeatedly measured both during systole and diastole. Percentage relative change in curvature (Cv) was calculated as % (postCv- preCv)/preCv in the respective cardiac phases. Cyclic changes in vessel curvature were estimated as differences between systole and diastole at both pre-treatment and post-treatment.

Statistical analysis.

The Kolmogorov-Smirnov test was used to evaluate the normality assumptions of all continuous variables. Descriptive statistical analysis was performed with continuous variables expressed as median (interquartile range) and with categorical variables presented as counts (percentage). For

comparison between groups, Mann-Whitney *U* test were used for the continuous variables. The chi-square test has been used to assess differences in categorical variables. Pre and post treatment comparisons within groups were assessed with Wilcoxon signed rank tests. Because the curvature, cyclic changes of curvature, and difference of curvature between pre- and post-treatment did not have a normal distribution, a log transformation was performed to achieve a normal distribution. A univariate analysis was performed between curvature and angulation changes with baseline demographic and angiographic variables. Variables that were found to be significant at the univariate level were tested with a multivariate linear regression model. (The thresholds for entry into and removal from the model were 0.1.) All statistical tests were carried out at the 5% level of significance. All analysis were performed by SPSS version 21 (SPSS, Inc., Chicago Illinois).

Results

The baseline clinical and angiographic characteristics are shown in Table 1. A total of 64 patients were involved in this study of which 32 were treated with the BRS and 32 with the MPS. A flow chart summarizing patient selection is shown in Figure 3. There was no difference in median age [BRS vs MPS: 59.6 years vs 64.9 years, p=0.453)] or gender. There was a significant difference in clinical presentation of ACS/STEMI (BRS vs MPS: 68.8% vs 40.6%, p= 0.024). There were no significant differences in the cardiovascular risk factors.

The left anterior descending artery was the most commonly treated vessel in the study population. The pre treatment region length is 21.38mm (17.67- 25.58) in the overall group. There were no significant differences in reference vessel diameter, minimal lumen diameter and percentage diameter stenosis in both groups. Pretreatment curvature was similar between the BRS and MPS

groups in both systole and diastole phases [systole: 0.290 (0.155-0.639) cm^{-1} vs 0.283 (0.125-0.519) respectively, p =0.803 and diastole: 0.305 (0.193- 0.580) cm^{-1} vs 0.257 (0.151-0.518) cm^{-1}respectively, p= 0.803].

Geometric changes within and between groups. Table III shows the changes in curvature in both systole and diastole of the treated vessel in the BRS and MPS groups. After implantation of MPS, there was a significant decrease in median diastolic curvature (from 0.257 cm^{-1} to 0.199 cm^{-1}, p= 0.001) and median systolic curvature (0.283 cm^{-1} to 0.194 cm^{-1}, p <0.001) representing a percentage reduction of 16.0% and 28.6% respectively. Following an Absorb scaffold implantation, there was a trend towards a decrease in the median diastolic curvature (from 0.305 cm^{-1} to 0.283 cm^{-1}, p= 0.056) and median systolic curvature (from 0.290 cm^{-1} to 0.282 cm^{-1}, p= 0.061) which trends towards significance. As a result, the diastolic curvature was significantly higher in the BRS compared with the MPS group post treatment [BRS vs MPS; 0.283 cm^{-1} (0.150-0.541) vs 0.199 cm^{-1} (0.089-0.357), p= 0.035] (Figure 4). Post treatment, Percentage relative reduction in curvature was also smaller in the BRS group compared with MPS group in both the diastole and systole phases [BRS vs MPS; 7.48% vs 29.4%, p= 0.013; 9.04% vs 28.2%, p= 0.010 respectively]. Cyclic changes in curvature (i.e., between systole and diastole) were similar between the BRS than the MPS after the deployment in curvature (p = 0.271).

Predictive factors of modifying curvature. In univariate analysis, the use of MPS predicts a greater reduction in curvature with a coefficient of 23.33 (95% confidence interval: 3.81- 42.85, p = 0.02).

Discussion

In summary, the major finding of this study showed that in the deployment of long coronary devices (28mm in length), BRS showed a non-significant decrease in curvature in the post treated vessel compared with a significant reduction in curvature of the treated vessel with deployment of a MPS. Use of MPS was an independent predictor of vessel curvature change post deployment.

Stent conformability is dependent on both the material and design of the stent and differs between the commercial devices that are available[10-12]. An open cell stent design would have higher conformability compared to a closed cell design. The difference in curvature post treatment between BRS and MPS could be attributed to the difference in underlying material composition of the devices in that a polymeric bioresorbable scaffold has better conformability to vessel geometry compared to metallic stents. In a study evaluating the bending stiffness of the BRS compared to the MPS in-vitro, the maximum compressive load of a BRS from ABSORB COHORT B trial was significantly lower compared to the XIENCE^{R} stent which signifies better conformability of the BRS (Figure 5)[13]. This is despite the fact that the strut thickness of the ABSORB Cohort B stent is thicker than that of the XIENCE^{R} stent (strut thickness 152.4 μm vs 81.3 μm). A previous study had shown that the use of relatively shorter (18mm) BRS and MPS devices modify baseline vessel curvature but the change was more marked in the MPS compared with the BRS[6]. In this study, the median pretreatment lesion length was 16.3 mm and 16.8 mm in the BRS and MPS groups respectively which are comparatively shorter compared to our study population. To our knowledge, this is the first in vivo study that shown that BRS does not affect the curvature of the treated vessel significantly in the deployment of long scaffolds. This might be of useful significance as we treat longer lesions with overlap scaffold required.

Vascular geometry is the most important determinant of local wall shear stress, and improved conformability might have clinical implications. Studies have demonstrated that low wall shear stress promotes atherosclerosis and plaque progression in native arteries[14] and greater intimal hyperplasia after stent deployment[15]. Metallic stents deployed in curved porcine coronary arteries were noted to cause vessel straightening in the stented segment and increased curvature at the stent edges[16]. A study by Gyongyosi et al had further showed that a longitudinal straightening of stents is an additional predictor of major adverse events[17]. There are possible physiological and clinical benefits arising from the improvement in conformability in the bioresorbable scaffolds. An increased conformability of the BRS platform may result in physiological wall shear stress at the stent edges due to less vessel distortion. This may translate to clinical benefits such as reduced risk of scaffold edge restenosis. However, the clinical benefits associated with better conformability still needs further evaluation.

Stent flexibility (and conformability) is also one of the key determinants of stent fracture, a common cause of late stent failure. Hinge motion (i.e. rocking back and forth on a bend) was one of the factors that can increase the risk of stent strut fracture. Our results suggest that there is a subtle but certain cyclic change of curvature after device implantation in both groups. Although there is no difference between groups, one can speculate that this cyclic movement repeating greater than 86400 times a day (based on average heart rate of 60 beats per minute) can cause mechanical failure at the metallic struts. In a study looking at predictors of stent fracture, stent fracture was identified in 2.9% of 1339 lesions treated with the XIENCE^{R} stent in only 6-9 months after placement[18]. In that study, the three major determinants of stent fracture in order of importance were hinge motion, ostial location and tortuosity. Since the BRS is programmed to

get dismantled in the due course of the bioresorption, this might cause less problem with BRS than with MPS.

Limitations

We acknowledge the following limitations. The study is non-randomized and population in each group is relatively small. 2D angiographic analysis may also not be the most optimal imaging modality to assess the geometry of coronary vessels. However the differences between the pre and post treatment angiographic views were less than 10°, indicating that the analysis were mainly performed in the same angiographic view.

Conclusion

In the deployment of long coronary scaffolds/ stents (28mm in length), bioresorbable vascular scaffolds provides better conformability compared with MPS. The findings of this study and its clinical significance merits further evaluation.

Acknowledgements: The BVS Expand and BVS STEMI First registries are supported by research grants from Abbott Vascular. Prof Robert-Jan van Geuns received speaker's fees from Abbott Vascular.

References

1. Serruys PW, Ormiston JA, Dudek D, et al. A bioabsorbable everolimus-eluting coronary stent system (ABSORB): 2-year outcomes and results from multiple imaging methods. Lancet 2009;373:897–910

2. Sarno G, Bruining N, Serruys PW, et al. Morphological and functional evaluation of the bioresorption of the bioresorbable everolimus-eluting vascular scaffold using IVUS, echogenicity and vasomotion testing at two year follow-up: A patient level insight into the ABSORB A clinical trial. Int J Cardiovasc Imaging 2012;28:51–58.

3. Colombo A, Stankovic G, Moses JW. Selection of coronary stents. J Am Coll Cardiol 2002;40:1021–33.

4. Ormiston JA, Dixon SR, Webster MW, et al. Stent longitudinal flexibility: a comparison of 13 stent designs before and after balloon expansion. Catheter Cardiovasc Interv 2000;50:120–4.

5. Onuma Y, Serruys PW, Ormiston JA, et al. Three-year results of clinical follow-up after a bioresorbable everolimus-eluting scaffold in patients with de novo coronary artery disease: the ABSORB trial. EuroIntervention 2010;6:447–53

6. Josep Gomez-Lara, Hector M. Garcia-Garcia, Patrick W. Serruys, et al. A Comparison of the Conformability of Everolimus-Eluting Bioresorbable Vascular Scaffolds to Metal Platform Coronary Stents. J Am Coll Cardiol Intv 2010;3:1190–8

7. Gregg W. Stone. Teirstein PS, Dawkins KD, et al. A Prospective, Randomized Evaluation of a Novel Everolimus-Eluting Coronary Stent The PLATINUM (A Prospective, Randomized, Multicenter Trial to Assess an Everolimus-Eluting Coronary Stent System [PROMUS Element] for the Treatment of up to Two De Novo Coronary Artery Lesions) Trial for the PLATINUM TRIAL Investigators. J Am Coll Cardiol 2011;57:1700–8

8. Tanimoto S, Serruys PW, Thuesen L, et al. Comparison of in vivo acute stent recoil between the bioabsorbable everolimus-eluting coronary stent and the everolimus-eluting cobalt chromium coronary stent: insights from the ABSORB and SPIRIT trials. Catheter Cardiovasc Interv 2007;70:515–23.

9. Choi G, Cheng CP, Wilson NM, Taylor CA. Methods for quantifying three-dimensional deformation of arteries due to pulsatile and nonpulsatile forces: implications for the design of stents and stent grafts. Ann Biomed Eng 2009;37:14 –33.

10. Schmidt W, Lanzer P, Behrens P, Topoleski LD, Schmitz KP. A comparison of the mechanical performance characteristics of seven drug-eluting stent systems. Catheter Cardiovasc Interv 2009;73: 350 – 60.

11. Sangiorgi G, Melzi G, Agostoni P, et al. Engineering aspects of stents design and their translation into clinical practice. Ann Ist Super Sanita 2007;43:89 –100.

12. Rieu R, Barragan P, Sainsous J, et al. Assessment of the trackability, flexibility and conformability of coronary stents: a comparative analysis. Catheter Cardiovascular Intervention. 2003; 59 (4): 496-503.

13. James P. Oberhauser, Syed Hossainy, Richard J. Rapoza. Design principles and performance of bioresorbable polymeric vascular scaffolds. EuroIntervention Supplement (2009) Vol. 5 (Supplement F) F15-F22.

14. Samady H, Eshtehardi P, Giddens DP, et al. Coronary artery wall shear stress is associated with progression and transformation of atherosclerotic plaque and arterial remodeling in patients with coronary artery disease. Circulation. 2011 Aug 16;124(7):779-88.

15. Wentzel JJ, Krams R, Schuurbiers JC, et al. Relationship between neointimal thickness and shear stress after Wallstent implantation in human coronary arteries. Circulation 2001;103:1740 –5.

16. Wentzel JJ, Whelan DM, van der Giessen WJ, et al. Coronary stent implantation changes 3-D vessel geometry and 3-D shear stress distribution. J Biomech 2000;33:1287–95.

17. Gyöngyösi M, Yang P, Glogar D, et al. Austrian Wiktor Stent Study Group and European Paragon Stent Investigators. Longitudinal straightening effect of stents is an additional predictor for major adverse cardiac events. JACC. 2000; 35 (6): 1580-9.

18. Kuramitsu S, Iwabuchi M, Hyodo M, et al. Incidence and clinical impact of stent fracture after everolimus-eluting stent implantation. Circ Cardiovasc Interv. 2012 Oct;5 (5):663-671.

Legends

Figure 1A Bioresorbable Absorb scaffold: The second generation ABSORB BRS (revision 1.1) has a strut thickness of 150um, consisting of in-phase zigzag hoops linked by bridges. The device is radiolucent but has 2 radioopaque platinum markers at each proximal and distal edge that facilitate ease of visualization on angiography.

Figure 1B Cobalt Chromium Everolimus- Eluting Stent (CoCr EES- XIENCE^{R}): The XIENCE^{R} are the metal platform stents and consist of a metallic platform made of cobalt chromium alloy. The struts are serpentine rings connected by links fabricated from a single piece. The XIENCE^{R} is covered by an everolimus coating.

Figure 2 Curvature Analysis of the BRS and MPS: Curvature analysis before and after deployment of a BRS (Figure 2A and 2B) and a MPS (Figure 2C and 2D). After implantation of a BRS, the curvature changed from 0.58 cm^{-1} to 0.49 cm^{-1} wheras after the MPS was implanted, the curvature changed from 0.85cm^{-1} to 0.23 cm^{-1}. BRS- Bioresorbable Absorb scaffold; MPS- Metallic platform stent

Figure 3 Flow Chart of Patient Selection. BRS- Bioresorbable Absorb Scaffold; CTO- Chronic Total Occlusion; MPS- Metallic Platform stents; STEMI- ST elevation Myocardial Infarct

Figure 4 Change in curvature post treatment in BRS and MPS. This boxplot illustrates the difference in median diastolic curvature post treatment in the BAS compared to the MPS group.

Figure 5 Maximum compressive force of ABSORB Cohort B scaffold and XIENCE V stent. This figure shows the maximum compressive force applied to deflect the ABSORB Cohort B and XIENCE V 3.0 x 18mm devices by 1.1 mm using 3 point- bend test (n=5). Statistical analysis yielded p= 0.004 using One- way ANOVA and Tukey- Kramer HSD. Tests were performed by and data are on file at Abbott Vascular. **(Reproduced with permission by James P. Oberhauser et al Eurointervention)**

Tables

Table I Baseline Clinical and Angiographic Characteristics

	BRS (N=32)	MPS (N=32)	p value
Age (years)	59.6 (52.5, 67.8)	64.9 (57.7, 70.7)	0.453
Men	22 (68.8)	22 (68.8)	1.000
Hypertension	18 (56.2)	20 (62.5)	0.611
Hypercholesterolemia	15 (46.9)	17 (53.1)	0.617
Diabetes mellitus	5 (15.6)	8 (25.0)	0.351
Smoker (Active)	12 (37.5)	7 (21.9)	0.391
Family History			
Previous CVA	2 (6.2)	2 (6.2)	1.000
Previous AMI	6 (18.8)	12 (37.5)	0.095
Previous PCI	5 (15.6)	9 (28.1)	0.226
Previous CABG	0	0	
Clinical presentation			0.024
Stable or silent angina	10 (31.2)	19 (59.4)	
Unstable angina/STEMI	22 (68.8)	13 (40.6)	
Target Vessel			0.857
LAD	15 (46.9)	13 (40.6)	
LCX	6 (18.8)	6 (18.8)	
RCA	11 (34.4)	13 (40.6)	
RVD (mm)	2.90 (2.49, 3.18)	2.91 (2.29, 3.26)	0.803
MLD (mm)	0.92 (0.77, 1.57)	1.20 (0.75, 1.55)	0.453
Diameter stenosis (%)	60.00 (47.25, 72.75)	56.00 (46.00, 76.75)	0.452
Pre-treatment region length (mm)	22.19 (17.67, 25.08)	20.38 (17.05, 25.75)	0.803

Values are presented as number (percentages) or median (interquartile range)
AMI- Acute Myocardial Infarct; BRS- Bioresorbable Absorb scaffold; CABG- Coronary Artery Bypass Graft; CVA- Cerebrovascular Accident; LAD= left anterior descending artery; LCX= Left circumflex artery; MLD= Minimal luminal diameter; MPS- Metallic Platform stent; PCI- Percutaneous Coronary Intervention; RCA- Right coronary artery; RVD= Reference vessel diameter, STEMI- ST elevation Myocardial Infarct

Table II Changes in curvature of the Study Population

	BRS (N=32)	MPS (N=32)	p value
Pre-treatment Curvature(cm^{-1})			
Systole	0.290 (0.155, 0.639)	0.283 (0.125, 0.519)	0.648
Diastole	0.305 (0.193, 0.580)	0.257 (0.151, 0.518)	0.460
Post-treatment Curvature(cm^{-1})			
Systole	0.282 (0.147, 0.549)	0.194 (0.097, 0.407)	0.077
Diastole	0.283 (0.150, 0.541)	0.199 (0.089, 0.357)	0.035
Percentage reduction in curvature post-pretreatment			
Systole	2.76	28.6	
Diastole	7.21	16.0	
p value for comparison between Pre and post curvature in systole	0.061	<0.001	
p value for comparison between Pre and post curvature in diastole	0.056	0.001	
Absolute reduction in curvature (cm^{-1})			
Systole	0.024 (0.015, 0.087)	0.064 (0.010, 0.230)	0.034
Diastole	0.021 (0.025, 0.098)	0.090 (0.011, 0.192)	0.066
Percentage Relative change in curvature (cm^{-1})			
Systole	-9.035(-22.128, 7.911)	-28.17 (-46.22, -6.64)	0.010
Diastole	-7.484(-23.193, 8.355)	-29.43 (-50.31, -3.55)	0.013
Pre-treatment Cyclic change in curvature (cm^{-1})	-0.021 (-0.072, 0.061)	0.002 (-0.086, 0.096)	0.398
Post-treatment Cyclic change in curvature (cm^{-1})	-0.026(-0.054, 0.023)	-0.041 (-0.04, 0.125)	0.271

Values are presented as numbers or median (interquartile range).
BRS- Bioresorbable Absorb scaffold; MPS- Metallic Platform stent

Figures

Figure 1A Bioresorbable Absorb scaffold

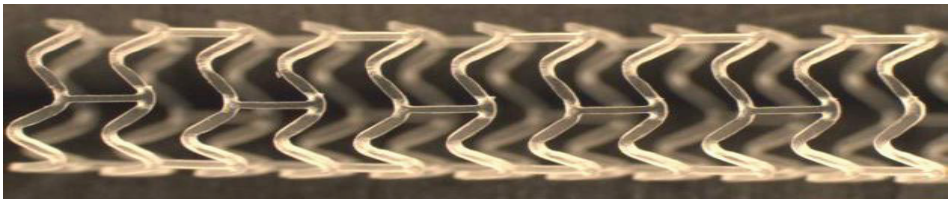

The second generation ABSORB BRS (revision 1.1) has a strut thickness of 150 µm, consisting of in-phase zigzag hoops linked by bridges. The device is radiolucent but has 2 radioopaque platinum markers at each proximal and distal edge that facilitate ease of visualization on angiography.

Figure 1B Cobalt Chromium Everolimus- Eluting Stent (CoCr EES- XIENCE^{R})

The XIENCE^{R} are the metal platform stents and consist of a metallic platform made of cobalt chromium alloy. The struts are serpentine rings connected by links fabricated from a single piece. The XIENCE^{R} is covered by an everolimus coating.

Figure 2 Curvature Analysis of the BRS and MPS

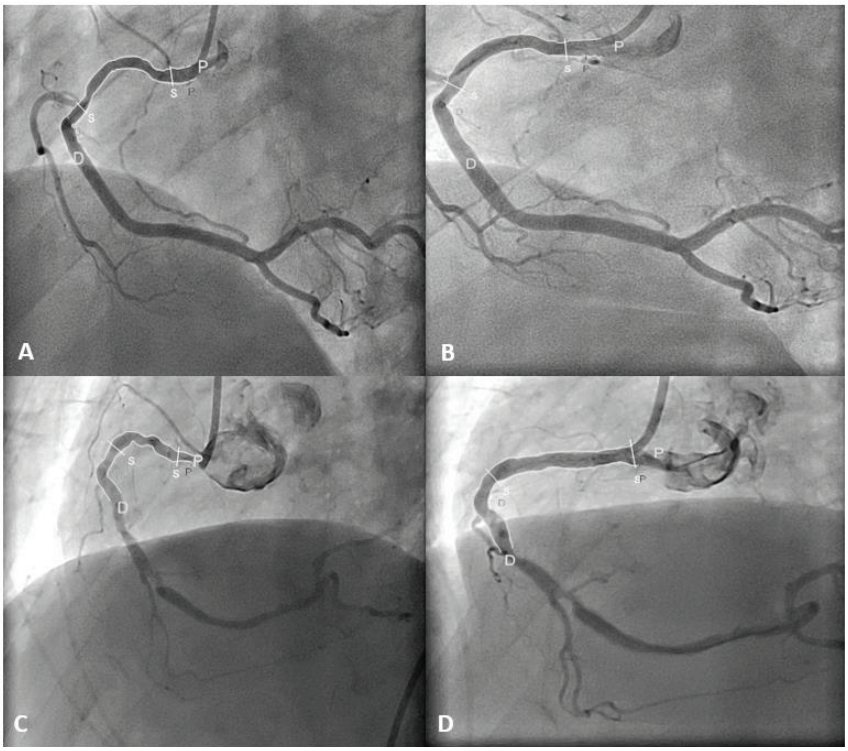

Curvature analysis before and after deployment of a BRS (Figure 2A and 2B) and a MPS (Figure 2C and 2D). After implantation of a BRS, the curvature changed from 0.58 cm^{-1} to 0.49 cm^{-1} wheras after the MPS was implanted, the curvature changed from 0.85cm^{-1} to 0.23 cm^{-1}. BRS- Bioresorbable Absorb scaffold; MPS- Metallic platform stent

Figure 3 Flow Chart of Patient Selection

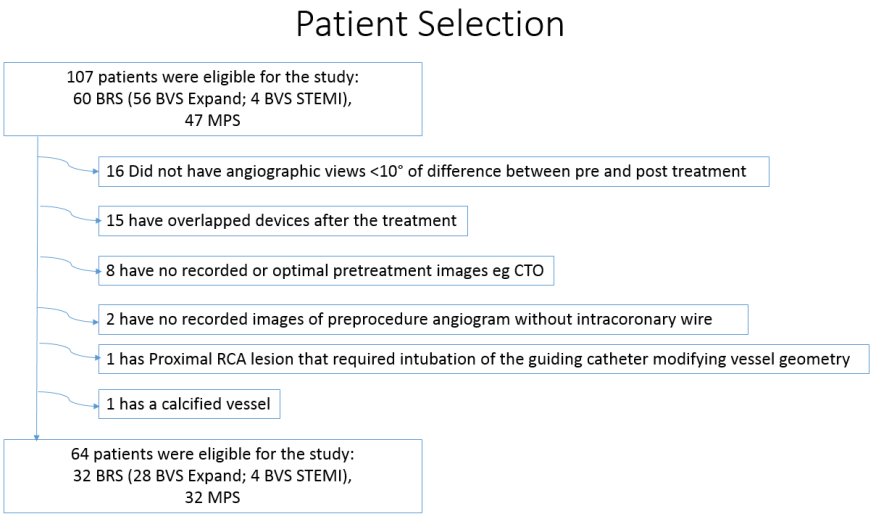

BRS- Bioresorbable Absorb Scaffold
CTO- Chronic Total Occlusion
MPS- Metallic Platform stents
STEMI- ST elevation Myocardial Infarct

Figure 4 Change in curvature post treatment in BRS and MPS

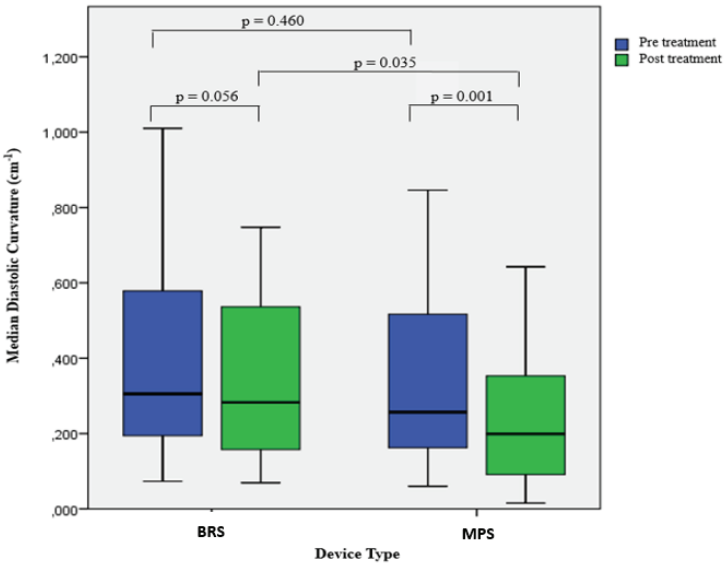

This boxplot illustrates the difference in median diastolic curvature post treatment in the BAS compared to the MPS group.

Figure 5 Maximum compressive force of ABSORB Cohort B scaffold and XIENCE V stent

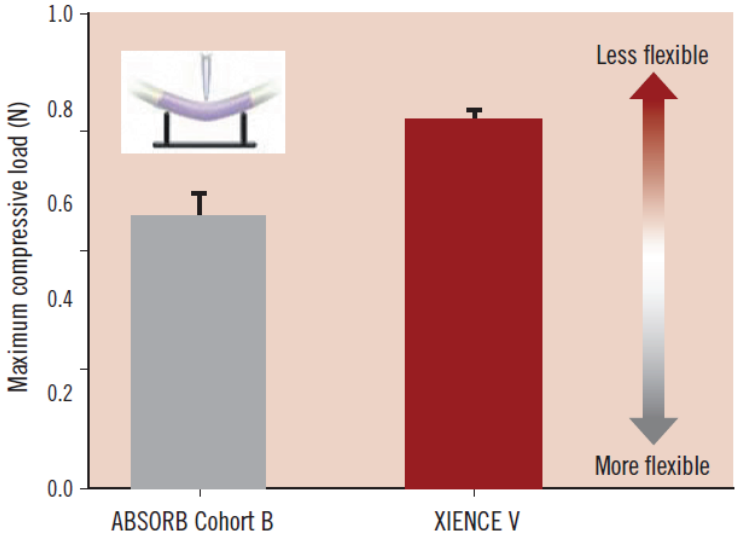

This figure shows the maximum compressive force applied to deflect the ABSORB Cohort B and XIENCE V 3.0 x 18mm devices by 1.1 mm using 3 point- bend test (n=5). Statistical analysis yielded p= 0.004 using One- way ANOVA and Tukey- Kramer HSD. Tests were performed by and data are on file at Abbott Vascular. **(Reproduced with permission by James P. Oberhauser et al Eurointervention)**

1.3 Potential Mechanism(s) of Post-procedural Rise of Cardiac Biomarker

Incidence and Potential Mechanism(s) of Post-procedural Rise of Cardiac Biomarker in Patients with Coronary Artery Narrowing after Implantation of an Everolimus Eluting Bioresorbable Vascular Scaffold or Everolimus Eluting Metallic Stent.

JACC Cardiovasc Interv. 2015 Jul;8(8):1053-63.
[Original research paper, IF 7.44]

Ishibashi Y, Muramatsu T, Grundeken MJ, Nakatani S, Cho YK, Suwannasom P, Garcia-Garcia HM, Boven AJV, Piek JJ, Sabaté M, Helqvist S, Baumbach A, McClean D, Almeida MS, Wasungu L, Miquel K, Chevalier B, Onuma Y, Serruys PW.

Incidence and Potential Mechanism(s) of Post-Procedural Rise of Cardiac Biomarker in Patients With Coronary Artery Narrowing After Implantation of an Everolimus-Eluting Bioresorbable Vascular Scaffold or Everolimus-Eluting Metallic Stent

Yuki Ishibashi, MD, PhD,* Takashi Muramatsu, MD, PhD,*† Shimpei Nakatani, MD,* Yohei Sotomi, MD,‡ Pannipa Suwannasom, MD,* Maik J. Grundeken, MD,‡ Yun-kyeong Cho, MD, PhD,* Hector M. Garcia-Garcia, MD, PhD,* Ad J. van Boven, MD, PhD,§ Jan J. Piek, MD, PhD,‡ Manel Sabaté, MD, PhD,‖ Steffen Helqvist, MD,¶ Andreas Baumbach, MD, PhD,# Dougal McClean, MD,** Manuel de Sousa Almeida, MD, PhD,†† Luc Wasungu, PhD,‡‡ Karine Miquel-Hebert, PhD,‡‡ Dariusz Dudek, MD,§§ Bernard Chevalier, MD,‖‖ Yoshinobu Onuma, MD, PhD,* Patrick W. Serruys, MD, PhD¶¶

ABSTRACT

OBJECTIVES This study sought to evaluate the mechanism of post-procedural cardiac biomarker (CB) rise following device implantation.

BACKGROUND A fully bioresorbable Absorb scaffold, compared with everolimus-eluting metallic stents (EES), might be associated with a higher incidence of periprocedural myocardial injury.

METHODS In 501 patients with stable or unstable angina randomized to either Absorb (335 patients) or EES (n = 166) in the ABSORB II trial, 3 types of CB (creatine kinase, creatine kinase-myocardial band, and troponin) were obtained before and after procedure. Per protocol, periprocedural myocardial infarction (PMI) was defined as creatine kinase rise >2× the upper limit of normal with creatine kinase-myocardial band rise.

RESULTS Incidence of side branch occlusion and any anatomic complications assessed by angiography was similar between the 2 treatment arms (side branch occlusion: Absorb: 5.3% vs. Xience: 7.6%, p = 0.07; any anatomic complication: Absorb: 16.4% vs. EES: 19.9%, p = 0.39). Fourteen patients who presented with recent myocardial infarction at entry with normalized creatine kinase-myocardial band according to the protocol were excluded for post-CB analysis. The overall compliance for CB was 97.8%. The CB rise subcategorized in 7 different ranges was comparable between the 2 treatment arms. PMI rate was numerically higher in the Absorb arm according to the per-protocol definitions, and treatment with overlapping devices was the only independent determinant of per-protocol PMI (odds ratio: 5.07, 95% confidence interval: 1.78 to 14.41, p = 0.002).

CONCLUSIONS There were no differences in the incidence of CB rise and PMI between Absorb and EES. Device overlap might be a precipitating factor of myocardial injury. (ABSORB II Randomized Clinical Trial: A Clinical Evaluation to Compare the Safety, Efficacy, and Performance of Absorb Everolimus Eluting Bioresorbable Vascular Scaffold System Against Xience Everolimus Eluting Coronary Stent System in the Treatment of Subjects With Ischemic Heart Disease Caused by De Novo Native Coronary Artery Lesions [ABSORB II]; NCT01425281). (J Am Coll Cardiol Intv 2015;8:1053–63)

ABBREVIATIONS AND ACRONYMS

CB = cardiac biomarker

CI = confidence interval

CK = creatine kinase

CK-MB = creatine kinase-myocardial band

EES = everolimus-eluting stent(s)

IVUS = intravascular ultrasound

OR = odds ratio

PMI = periprocedural myocardial infarction

RVD = reference vessel diameter

SBO = side branch occlusion

TIMI = Thrombolysis In Myocardial Infarction

ULN = upper limit of the normal

The bioresorbable everolimus-eluting scaffold (Absorb, Abbott Vascular, Santa Clara, California) was developed to provide a novel approach to treat coronary artery stenosis with transient vessel support and drug delivery (1-4). The performance of the second-generation Absorb was investigated in the ABSORB Cohort B trial (ABSORB Clinical Investigation, Cohort B), which reported excellent clinical results (5-7). However, the clinical relevance of this technology in comparison with metallic drug-eluting stents still remains a matter of debate due to the absence of randomized comparative data between the Absorb and conventional metallic drug-eluting stents. The ABSORB II (ABSORB II Randomized Clinical Trial: A Clinical Evaluation to Compare the Safety, Efficacy, and Performance of Absorb Everolimus Eluting Bioresorbable Vascular Scaffold System Against Xience Everolimus Eluting Coronary Stent System in the Treatment of Subjects With Ischemic Heart Disease Caused by De Novo Native Coronary Artery Lesions) (8) is the first randomized clinical trial assessing the clinical outcomes in 501 patients treated with either the Absorb or the metallic everolimus-eluting stent (EES) (Xience, Abbott Vascular).

In a nonrandomized comparison using historical data, the Absorb scaffold was associated with a higher incidence of post-procedural side branch occlusion (SBO) than EES was (9). Given the increased strut thickness of Absorb, a potential concern exists that it might be associated with a higher incidence of periprocedural myocardial injury and periprocedural myocardial infarction (PMI) than newer-generations of DES are (9). Therefore, the aim of this study is to investigate the incidence and mechanism of post-procedural cardiac biomarker (CB) rise following Absorb scaffold versus metallic EES implantation.

METHODS

STUDY DESIGN. The ABSORB II randomized controlled trial design has been described in detail previously (8). In brief, the ABSORB II trial was prospective, multicenter, single-blinded, randomized controlled trial that compared the safety and efficacy of the Absorb versus the EES in patients with stable or unstable angina due to up to 2 de novo coronary artery lesions, each located in different major epicardial vessels, all with an angiographic maximal luminal diameter between 2.25 and 3.8 mm as estimated by online quantitative coronary angiography and a lesion length of ≤48 mm. The detail of both study devices is provided in the Online Appendix (2,10,11). A total of 501 patients were randomized 2:1 into either the Absorb arm or the EES arm in Europe and New Zealand.

QUALITATIVE AND QUANTITATIVE ANGIOGRAPHIC ASSESSMENT. SBO, occurrence of no-reflow, abrupt closure, dissection, and distal embolization in main and side branches were assessed qualitatively at preprocedure, after balloon pre-dilation, after device deployment, and after final balloon inflation. Coronary dissections were assessed using the National Heart, Lung and Blood Institute criteria (12,13). In the present study, according to the underlying "anatomic complications" (assessed by angiography), CB rise and PMI were classified into 3 types: type 1—CB rise and PMI due to SBO; type 2—CB rise and PMI due to other anatomic complications (e.g., slow flow or no-reflow, distal embolization, thrombus during procedure, flow-limiting dissection, coronary dissection of National Heart, Lung and Blood Institute type D or E, or disruption of collateral flow); type 3—CB rise and PMI without angiographically identifiable causes for the CB rise (**Figure 1**).

The quantitative angiographic analysis by the 2-dimensional single-vessel quantitative coronary angiography (CAAS 5.10, Pie Medical BV, Maastricht,

From the *Thoraxcenter, Erasmus University Medical Center, Rotterdam, the Netherlands; †Department of Cardiology, Fujita Health University Hospital, Toyoake, Japan; ‡The Heart Center, Academic Medical Center, Amsterdam, the Netherlands; §Medical Center Leeuwarden, Leeuwarden, the Netherlands; ||Thorax Institute, Hospital Clinic, University of Barcelona, Institut d'Investigacions Biomèdiques August Pi i Sunyer (IDIBAPS), Barcelona, Spain; ¶Rigshospitalet, University of Copenhagen, Copenhagen, Denmark; #Bristol Heart Institute, Bristol, United Kingdom; **Christchurch Hospital, Christchurch, New Zealand; ††Hospital Santa Cruz, Carnaxide, Portugal; ‡‡Abbott Vascular, Diegem, Belgium; §§Jagiellonian University, Krakow, Poland; |||Institut Jacques Cartier, Massy, France; and the ¶¶International Centre for Cardiovascular Health, Imperial College, London, United Kingdom. This study was funded by Abbott Cardiovascular Systems, Inc. Dr. Wasungu is a contractor employed by Abbott Vascular. Dr. Miquel-Hebert is an employee of Abbott Vascular. Drs. Onuma and Serruys are members of the advisory board of Abbott Vascular. Drs. Baumbach and Chevalier are consultants with Abbott Vascular. All other authors have reported that they have no relationships relevant to the contents of this paper to disclose.

Manuscript received April 9, 2015; revised manuscript received May 27, 2015, accepted June 1, 2015.

FIGURE 1 Classification According to Angiographic Mechanism After Revascularization

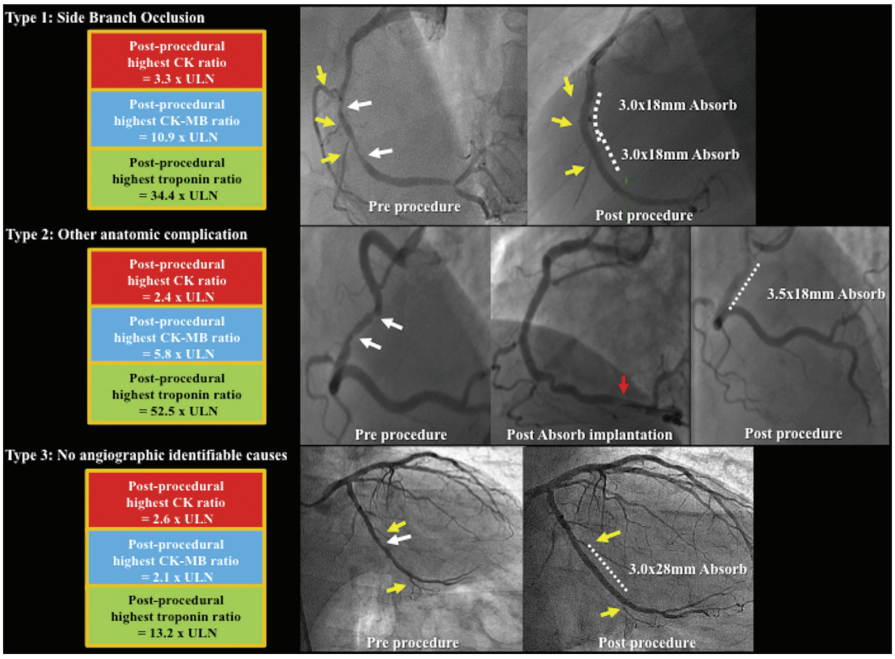

Type 1: cardiac biomarker rise due to side branch occlusion. Type 2: cardiac biomarker rise due to other anatomic complications. Type 3: cardiac biomarker rise without any identifiable anatomic causes in the coronary artery. Pre-procedure angiography showed a focal stenosis **(white arrows)**, side branches in the target lesion **(yellow arrows)**, and distal embolization was observed after device implantation **(red arrow)**.

the Netherlands) included the reference size of the side branch and the percentage of diameter stenosis of any side branch lesion as well as the side branch TIMI (Thrombolysis In Myocardial Infarction) flow grade at the following time points: pre-procedure; after pre-dilation; after post-dilation; and post-procedure (9). The region of interest was defined as the study device implantation site and the 5-mm proximal and distal margins in the main branch (**Figure 2**). A detailed side branch analysis was performed of all side branches identified within the region of interest pre-procedurally, during the course of the intervention to capture any transient complications, and post-procedure. SBO was defined as a reduction in the TIMI flow grade 0 to 1. Accordingly, side branches with pre-procedural TIMI flow grade 0 or 1 were excluded. Transient or final SBO was defined as SBO that occurred during the procedure and either disappeared or persisted at the end of the procedure. Angiographic assessment of the side branch was based on the consensus of 3 experienced cardiologists (Y.I., T.M., and Y.C.) and assessed in at least 2 different projections, with angiographic assessment for each side branch.

IVUS IMAGE ACQUISITION. Intravascular ultrasound (IVUS) was mandatory before and after the procedure. The detail of an image acquisition is described in Online Figure 1.

BLOOD SAMPLING. The protocol mandated that blood sampling for cardiac enzymes was to be collected within 6 h before the index percutaneous

FIGURE 2 Detailed Analysis of SBO

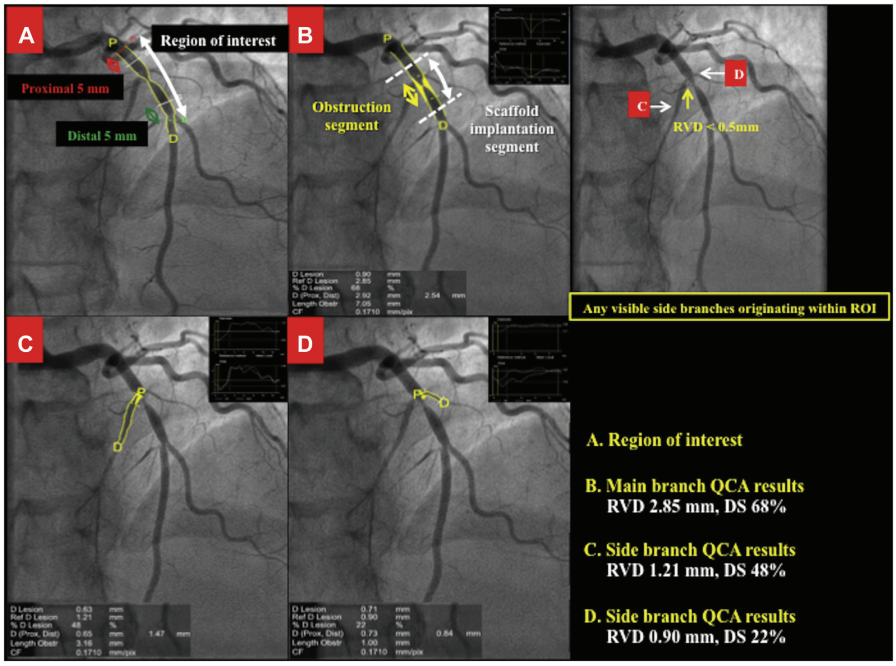

The QCA analysis delineates 5-mm proximal **(A) (red double arrow)** and distal segment **(A) (green double arrow)** to the intended device implantation site **(B) (white double arrow)**. Any visible side branches originating from this region of interest were analyzed. The conventional QCA analysis automatically delineates an obstruction segment in the main branch **(B) (yellow double arrow)**. An example of side branch analysis is shown in **C** and **D**. DS = diameter stenosis; QCA = quantitative coronary angiography; RVD = reference vessel diameter; SBO = side branch occlusion.

coronary intervention procedure and at 6, 12, and 18 h after the procedure or at hospital discharge, whichever came first. These blood samples were sent to the central core laboratory (ICON Laboratories, Dublin, Ireland) and to local hospital laboratories for analysis. Whenever clinically indicated, additional sampling could be taken and analyzed by the local hospital laboratories.

This yielded a mixture of local and central laboratories' biomarker results with different upper limits of normal (ULN). When both local and central laboratories' cardiac enzyme data were available at the same time, the clinical events committee used the central laboratories' results for the adjudication of MI.

DEFINITIONS OF PERIPROCEDURAL MYOCARDIAL INFARCTION. In this study protocol, MI was defined according to the following definitions (14-16): 1) per-protocol (modified World Health Organization) definition; and 2) extended historical definition (14). In the protocol, MI without distinction of being spontaneous or PMI is defined by elevation of total creatine kinase (CK) to >2× ULN along with elevated or "positive" creatine kinase-myocardial band (CK-MB). A hierarchical approach was used for the adjudication of PMI based on CB availability when an analyzable CB was missing (extended historical definition: CK-MB mass when CK was not available, cardiac troponin when CK and CK-MB mass were not available). All protocol defined clinical outcomes were

adjudicated by an independent Clinical Events Committee. Fourteen patients presented with recent MI at entry with normalized CK-MB according to the protocol, but with/without troponin elevation. These patients were excluded for post-CB analysis. Post-hoc adjudication was performed according to Society of Cardiovascular Angiography and Interventions definition and the universal third definition. The details are described in the Online Appendix.

STATISTICAL ANALYSIS. All analyses were performed on the intention-to-treat basis, using all patients randomized in the study, regardless of the treatment actually received. The counts of PMI are summarized and tabulated according to the frequency. Categorical variables were compared by Fisher exact test. Continuous variables are presented as mean ± SD and were compared by nonparametric test. The logistic regression model was performed for Table 5. Detail of statistical analysis is provided in the Online Appendix. In addition to the device type, significant variables ($p < 0.10$) in the univariate analysis were forced into a multivariate logistic regression model to predict PMI. All statistical tests were performed with SPSS (version 22.0 for Windows, SPSS, Chicago, Illinois). A 2-sided p value of <0.05 was considered to indicate statistical significance.

RESULTS

PATIENT AND PROCEDURAL CHARACTERISTICS. Patient demographics were comparable in both arms (Table 1). The lesion characteristics such as type B2/C lesions, bifurcation lesions, eccentricity, moderate/severe tortuosity, thrombus, and moderate/severe calcification were similar between the 2-treatment arms.

AVAILABILITY OF CARDIAC BIOMARKERS OF MYOCARDIAL INJURY. Within 24 h before the index procedure, 920 blood time points for the assessment of CB were available with 458 central and 462 local biomarker data. At least 1 of the 3 CB was available in 486 patients (97.0%) within 6 h and in 495 patients (98.8%) within 24 h before the index procedure. At least 1 of the 3 CB was available in 490 patients (97.8%) within 48 h after the index procedure. In the serial sample analysis, 1,446 blood time points for the assessment of CB were available with 572 central and 874 local biomarker data (Figure 3). A total of 3,813 blood samples with 1,257 CK, 1,253 CK-MB, and 1,303 troponin values were available. For the post-procedural peak-level assessment of each CB, the central biomarker data was used in 58.4% for CK (271 of 464), 70.9% for CK-MB (337 of 475), and 45.0% for troponin (213 of 473). The availability of paired biomarkers (CK and CK-MB) for per-protocol PMI adjudication at post-procedure was available in 93.4% (313 of 335) of the Absorb arm and 96.4% (160 of 166) of the EES arm. Troponin was available in 98.8% (325 of 335) of the Absorb arm and 97.6% (160 of 166) of the EES arm.

TABLE 1 Baseline Demographic Data and Angiographic Characteristics in Patients

	Absorb (335 Patients, 364 Lesions)	EES (166 Patients, 182 Lesions)	p Value
Age, yrs	61.5 ± 10.0	60.9 ± 10.0	0.51
Male	253 (75.5)	132 (79.5)	0.32
Body mass index, kg/m^2	27.9 ± 4.1	28.1 ± 3.7	0.56
Current smoker	79 (23.6)	36 (21.7)	0.64
Hypertension requiring treatment	220 (65.7)	112 (67.5)	0.69
Dyslipidemia requiring treatment	238 (71.0)	123 (74.1)	0.47
Any diabetes mellitus	80 (23.9)	40 (24.1)	0.96
Unstable angina	68 (20.3)	37 (22.3)	0.61
Family history of coronary artery disease	112 (36.6)	64 (41.3)	0.33
Previous history of myocardial infarction	93 (28.0)	48 (28.9)	0.83
Number of lesions/patient	1.1 ± 0.3	1.1 ± 0.3	0.81
Lesion location			
Right coronary artery	95 (26.1)	56 (30.8)	0.25
Left anterior descending artery	163 (44.8)	84 (46.2)	0.76
Left circumflex artery or ramus	106 (29.1)	42 (23.1)	0.13
ACC/AHA lesion complexity			
A	5 (1.4)	1 (0.6)	0.67
B1	193 (53.2)	90 (50.0)	0.49
B2	159 (43.8)	87 (48.3)	0.32
C	6 (1.7)	2 (1.1)	1.00
TIMI flow grade 0 or 1	1 (0.3)	2 (1.1)	0.26
Calcification, moderate or severe	46 (12.7)	28 (15.5)	0.37
Tortuosity, moderate or severe	34 (9.4)	13 (7.2)	0.39
Eccentric	357 (98.3)	178 (99.4)	0.43
Thrombus	5 (1.4)	4 (2.2)	0.49
Bifurcation	13 (3.6)	5 (2.8)	0.62
Reference vessel diameter, mm	2.59 ± 0.38	2.63 ± 0.40	0.36
Percentage of diameter stenosis	58.6 ± 11.1	59.7 ± 11.6	0.30
Obstruction lesion length, mm	13.8 ± 6.5	13.8 ± 6.6	1.00

Values are mean ± SD or n (%).
ACC = American College of Cardiology; AHA = American Heart Association; EES = everolimus-eluting stent(s).

QUALITATIVE AND QUANTITATIVE ANGIOGRAPHIC ASSESSMENT. The frequencies of "angiographic complications" are shown in Table 2. In the present analysis, 335 patients with 988 side branches in the Absorb arm and 166 patients with 503 side branches in the EES arm were assessed. Incidence of any "angiographic complications" and SBO was similar between the 2 treatment arms (any complications: Absorb: 16.4% vs. EES: 19.9%, p = 0.39; SBO: 5.3% vs. 7.6%, p = 0.07). The incidence of post-procedural SBO in the obstruction segment was significantly lower in the Absorb arm than in the EES arm (4.3% vs. 6.8%,

FIGURE 3 Time Points and Availability for the Assessment of CB Pre- and Post-Procedure

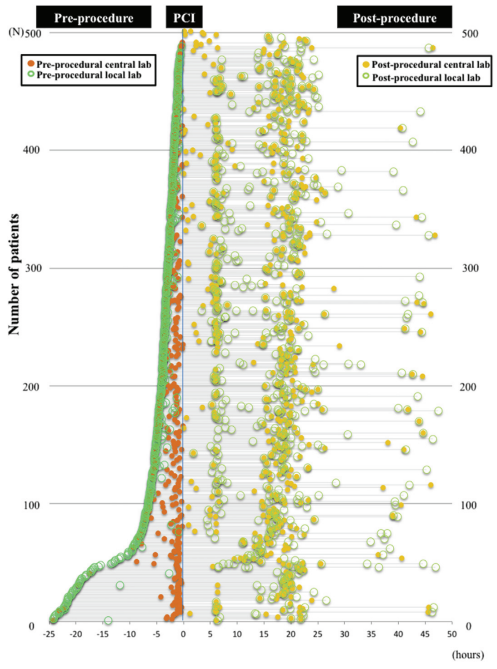

A total of 920 blood time points for the assessment of cardiac biomarkers (CB) were available with 458 central and 462 local biomarker data within 24 h before the index procedure. At least 1 of the 3 CB was available in 486 patients (97.0%) within 6 h and 495 patients (98.8%) within 24 h before the index procedure. At least 1 of the 3 CB was available in 490 patients (97.8%) within 48 h after the index procedure. In the serial sample analysis, 1,446 blood time points for the assessment of CB were available with 572 central and 874 local biomarker data.

p = 0.046), although there were no significant differences in the incidence of SBO according to the reference vessel diameter (RVD) size (RVD ≤ 0.5 mm, 0.5 mm < RVD ≤ 1.0 mm, 1.0 mm < RVD). Each type (type 1, type 2, and type 3) of "anatomic complications" after revascularization was similar between the 2 treatment arms. However, 2 abrupt occlusions were documented after EES implantation (**Table 2**).

INCIDENCE OF CARDIAC BIOMARKER RISE AND PERIPROCEDURAL MI. As recently described (17), we compared the peak value of the 3 CB values post-procedure according to 5 rise categories (CB: >2× ULN, >5× ULN, >10× ULN, > 35× ULN, and >70× ULN) after scaffold or stent implantation. In the present study, the rise of 3 CB subcategorized in 7 different ranges was comparable between the 2 treatment arms (**Table 3**).

Per-protocol PMI (World Health Organization definition) occurred in 13 of 335 patients (3.9%) in the Absorb arm and 2 of 166 patients (1.2%) in the EES arm (p = 0.16). Incidence of PMI per protocol according to "anatomic complications" assessed by angiography was similar between the 2 treatment arms (**Table 4**). In the post-hoc adjudication, the PMI rates according to the third universal definition and the Society of Cardiovascular Angiography and Interventions definition were 14.2% versus 10.6% (p = 0.31) and 0.6% versus 0.6% (p = 1.00), respectively.

CARDIAC BIOMARKER RISE, ANGIOGRAPHY, AND GRAYSCALE/RADIOFREQUENCY IVUS. **Figure 4** shows the magnitude of post-procedural CB rise in patients with "anatomic complications" (type 1 and type 2) assessed by angiography. CB rise subcategorized in 5 different ranges was similar between the 2 treatment arms in the patients with "anatomic complications." Incidence of CB rise assessed by IVUS (data not shown) was similar between the 2 treatment arms as well as "angiographic complications." There was no statistical significance between IVUS finding and post-procedure CB rising (Online Appendix).

PREDICTORS OF PERIPROCEDURAL MYOCARDIAL INFARCTION. In the multivariable analyses, treatment with overlapping devices was the only independent determinant of per-protocol PMI (odds ratio [OR]: 5.07, 95% confidence interval [CI]: 1.78 to 14.41, p = 0.002) (**Table 5**).

DISCUSSION

The present study is the first randomized clinical trial to analyze the difference in frequencies of PMI and CB rise after implantation of Absorb scaffold or EES. The main findings of this study follow: 1) Incidence of any anatomic complications including SBO assessed by angiography was similar between the 2 treatment arms (Absorb: 16.4% vs. EES: 19.9%, p = 0.39). 2) Per-protocol PMI (World Health Organization definition) occurred in 13 of 335 patients (3.9%) in the Absorb arm and 2 of 166 patients (1.2%) in the EES arm (p = 0.16). Of 15 patients with per-protocol PMI, 10 PMI (66.7%) were caused by SBO, whereas 3 (20.0%) were due to other anatomical complications. 3) Treatment with overlapping devices was an independent

determinant of per-protocol PMI (OR: 5.07, 95% CI: 1.78 to 14.41, p = 0.002). 4) The CB rise subcategorized in 7 different ranges was comparable between the 2 treatment arms.

AVAILABILITY OF CARDIAC BIOMARKER AND PERIPROCEDURAL CARDIAC BIOMARKER RISE. This is the first scaffold or metallic stent study in which 3 different CB values were available at a central core laboratory, the compliance of enzyme collection was high (CK: 95.3%, CK-MB: 97.5%, troponin: 97.1%). Of note, in the RESOLUTE-All Comers (A Randomized Comparison of a Zotarolimus-Eluting Stent With an Everolimus-Eluting Stent for Percutaneous Coronary Intervention) trial (14), an analyzable dataset for cardiac troponin was available in 55.3% (1,173 of 2,121) of patients. In addition, 44.1% (935 of 2,121) of patients had an analyzable dataset for both cardiac troponin and CK-MB (14). In 10 patients, 3 CB simultaneously increased, whereas in 127 patients, discordance in CB rise was documented, suggesting that the sensitivity of CB to detect myocardial damage varies according to the criteria and type of CB (Online Figure 2).

The prognostic relevance of CB rise is shown by Park et al. (18), in a large cohort of 23,604 patients, the prognostic implication of a CK-MB rise 3× to 5× ULN. Myint et al. (19) reported that prognostic significance of troponin in acute coronary syndrome attenuates with increased age and that older age is associated with a worse prognosis compared with the prognosis of younger counterparts given the same level of troponin rise, even at very low levels of troponin.

TABLE 2 Anatomic Complications Assessed by Angiography

Per-Patient Analysis	Absorb (n = 335)	EES (n = 166)	p Value
Any anatomic complications assessed by angiography	16.4 (56)	19.9 (33)	0.39
Type 1 anatomic complication assessed by angiography			
SBO	12.5 (43)	15.7 (26)	0.41
SBO after pre-dilation	0 (0)	0 (0)	1.00
SBO after device implantation	12.5 (43)	15.7 (26)	0.41
SBO improvement after NTG	0.9 (3)	0 (0)	0.55
SBO after procedure	11.6 (40)	15.7 (26)	0.26
Type 2 anatomic complication assessed by angiography			
Abrupt closure	0 (0)	1.8 (2)	0.11
Distal embolization	0.3 (1)	0 (0)	1.00
Coronary perforation	0.6 (2)	0 (0)	1.00
Flow-limiting dissection (NHLBI type F)	0.3 (1)	0 (0)	1.00
Coronary dissection after pre-dilation (NHLBI type D or E)	1.8 (6)	1.2 (2)	1.00
Coronary dissection after device implantation	0.3 (1)	0.6 (1)	1.00
Thrombus during procedure	0.3 (1)	0 (0)	1.00
Disruption of collateral flow	0.3 (1)	1.2 (2)	0.26
Per-Side Branch Analysis	**(n = 998)**	**(n = 503)**	
Incidence of SBO after procedure	5.3 (52)	7.6 (39)	0.07
Location of occluded side branch			
Outside scaffold segment	0 (0)	0 (0)	1.00
To-be-scaffold segment outside obstruction	0.9 (9)	1.0 (5)	1.00
Obstruction segment	4.3 (42)	6.8 (34)	0.046
RVD of occluded side branch			
RVD > 1.0 mm	0.9 (9)	1.2 (6)	0.59
0.5 mm < RVD ≤ 1.0 mm	2.9 (29)	4.2 (21)	0.22
RVD ≤ 0.5 mm	1.3 (13)	2.4 (12)	0.14

Values are % (n).

EES = everolimus-eluting stent(s); NHLBI = National Heart, Lung, and Blood Institute; NTG = nitroglycerin; RVD = reference vessel diameter; SBO = side branch occlusion.

ANATOMIC COMPLICATIONS ASSESSED BY ANGIOGRAPHY/IVUS AND PERIPROCEDURAL CARDIAC BIOMARKER RISE WITH ABSORB OR EES. In the previous publication using the data of the Absorb Extend registries with a matched cohort from SPIRIT (Clinical Evaluation of the Xience V Everolimus Eluting Coronary Stent System) trials (9), it was reported that the Absorb scaffold was associated with a higher SBO rate than Xience was. The difference was more pronounced with small side branches with an RVD ≤0.5 mm. However, there was no significant difference in the incidence of post-procedure CK-MB elevation. It was hypothesized that the difference in SBO was due to the difference in the design of the 2 devices. The Absorb scaffold has thicker (156 μm) and wider struts (up to 800 μm) with a higher surface coverage ratio (26% to 32%) than Xience does (thickness: 90 μm, widths: up to 428 μm, surface coverage: 13%). Therefore small side branches could be more frequently occluded by the implantation of Absorb scaffold. At variance with the report by Muramatsu et al. (9), the Absorb, compared with EES, showed a trend toward lower incidence of post-procedural SBO. Of note, most of the SBO occurred in small side branches of RVD <1.0 mm in both of treatment arms (**Table 2**). Although the nominal sizes of devices used (3.01 ± 0.31 mm vs. 3.05 ± 0.28 mm, p = 0.10) and frequency of post-device dilation were comparable (60.7% vs. 58.8%, p = 0.67), the nominal balloon size and the pressure used during either implantation or post-dilation was larger and higher in the EES arm, so that the expected balloon diameter tended to be larger accordingly (3.29 ± 0.35 mm vs. 3.35 ± 0.37 mm, p = 0.15) (17), the acute gain in minimal lumen diameter (quantitative coronary angiography measurement by the core laboratory) was significantly larger in the EES arm (1.15 ± 0.38 mm vs. 1.46 ± 0.38 mm, p < 0.001) (17). Whether the aggressive (post)-dilation may have resulted in a higher incidence

TABLE 3 Comparison of the Peak Value of Cardiac Enzyme Rise Post-Procedure Using Central Lab and/or Local Lab Results

	CK n = 464 of 487 (95.3%)			CK-MB* n = 475 of 487 (97.5%)			cTn n = 473 of 487 (97.1%)		
	Absorb (n = 306)	Xience (n = 158)	p Value	Absorb (n = 315)	Xience (n = 160)	p Value	Absorb (n = 316)	Xience (n = 157)	p Value
Mean ± SD	0.71 ± 0.63	0.65 ± 0.64	0.380	1.33 ± 2.12	1.09 ± 1.65	0.180	12.09 ± 30.24	8.28 ± 20.20	0.138
>2× ULN	5.2 (16)	1.9 (3)	0.135	13.7 (43)	10.0 (16)	0.304	48.1 (152)	45.9 (72)	0.696
>5× ULN	0 (0)	0.6 (1)	0.341	5.1 (16)	2.5 (4)	0.232	29.7 (94)	25.5 (40)	0.386
>10× ULN	0 (0)	0 (0)	1.000	0.6 (2)	0.6 (1)	1.000	19.0 (60)	15.3 (24)	0.372
>35× ULN	0 (0)	0 (0)	1.000	0 (0)	0 (0)	1.000	6.0 (19)	3.8 (6)	0.387
>70× ULN	0 (0)	0 (0)	1.000	0 (0)	0 (0)	1.000	3.5 (11)	1.3 (2)	0.236

Values are % (n) unless otherwise indicated. *Fourteen patients presented with recent myocardial infarction at entry with normalized CKMB according to the protocol were excluded for post CB analysis.

CK = creatine kinase; CK-MB = creatine kinase-myocardial band; cTn = cardiac troponin; EES = everolimus-eluting stent(s); ULN = upper limit of normal.

of post-procedural SBO in the EES arm—due to the presence of the bifurcation carina shift and/or plaque shift into the orifice of side branch (16,20)—remains speculative. Among the patients with post-dilation, the peak ratio of CK-MB post-procedure was significantly higher in the Absorb arm than in the EES arm (1.43 ± 2.41 vs. 1.00 ± 1.89, p = 0.02). The current protocol did not recommend post-dilation of the Absorb device with a balloon larger than 0.25 mm with respect to the nominal size of the device. The post-procedural CB rise with the patients who underwent post-dilation seems to justify retrospectively this conservative recommendation.

TABLE 4 Incidence of Per-Protocol PMI According to Anatomic Complications Assessed by Angiography

	Absorb (n = 335)	EES (n = 166)	p Value
Per-protocol PMI	3.9 (13)	1.2 (2)	0.16
Type 1: SBO	2.7 (9)	0.6 (1)	0.18
SBO after pre-dilation	0 (0)	0 (0)	1.00
SBO after device implantation	2.7 (9)	0.6 (1)	0.18
SBO improvement after NTG	0 (0)	0 (0)	1.00
SBO after procedure	2.7 (9)	0.6 (1)	0.18
Type 2: angiographic other complication	0.6 (2)	0.6 (1)	1.00
Abrupt closure	0 (0)	0.6 (1)	1.00
Distal embolization	0.3 (1)	0 (0)	1.00
Coronary perforation	0 (0)	0 (0)	1.00
Flow-limiting dissection, NHLBI type F	0 (0)	0 (0)	1.00
Coronary dissection after pre-dilation, NHLBI type D or E	0.3 (1)	0 (0)	1.00
Coronary dissection after device implantation	0 (0)	0 (0)	1.00
Thrombus during procedure	0 (0)	0 (0)	1.00
Disruption of collateral flow	0 (0)	0 (0)	1.00
Nonindentifiable mechanism causes	0.6 (2)	0 (0)	1.00

Per-protocol PMI is defined as the elevation of total CK to >2× ULN along with elevated or "positive" CK-MB without clinical symptom and electrocardiogram change.

PMI = periprocedural myocardial infarction; other abbreviations as in Tables 1 to 3.

As previously reported, atherosclerotic plaque burden pre-intervention is correlated with an increased rate of PMI as evidenced by subsequent CB rise (21). Atherosclerotic plaque with larger necrotic core are at higher risk of plaque rupture and microembolization during percutaneous coronary intervention with subsequent CB rise (22,23). The present study also documented that dyslipidemia requiring treatment was protective for troponin rise >5× ULN, whereas the incidence of CB rise assessed by IVUS was similar between the 2 treatment arms. It has been hypothesized that statins may exert anti-inflammatory effects, resulting in reduction of microembolization by stabilizing the underlying plaque (24).

ANATOMIC COMPLICATIONS ASSESSED BY ANGIOGRAPHY AND PERIPROCEDURAL MI WITH ABSORB OR EES. Previous studies revealed that SBO was the most common cause of PMI (20,25). In the present study, 15 patients with per-protocol PMI, 10 (66.7%) were angiographically classified as type 1 (SBO) whereas 3 (20.0%) were type 2 (other anatomic complication). In 2 patients (13.3%), no angiographic complications could be identified. Thus, our results are in concordance with previous studies (16,26,27).

PREDICTORS FOR PERIPROCEDURAL RISE OF CARDIAC BIOMARKER FOR INJURY. The predictors of PMI can be broadly categorized as patient-, lesion-, and procedure-related risk factors (16,20). In the SPIRIT IV trial, which randomized 3,687 patients in a 2:1 fashion to receive either EES or PES, the total stent length was a strong predictor of PMI by criteria using CK or troponin (16). In the present study, by multivariable analysis, treatment with overlapping devices was the independent determinant of per-protocol PMI (OR: 5.07, 95% CI: 1.78 to 14.41, p = 0.002), whereas there was overall no significant difference in PMI between the 2 device types (Absorb vs. EES). In the Absorb

FIGURE 4 Anatomic Complication Assessed by Angiography and Periprocedural CB Rise

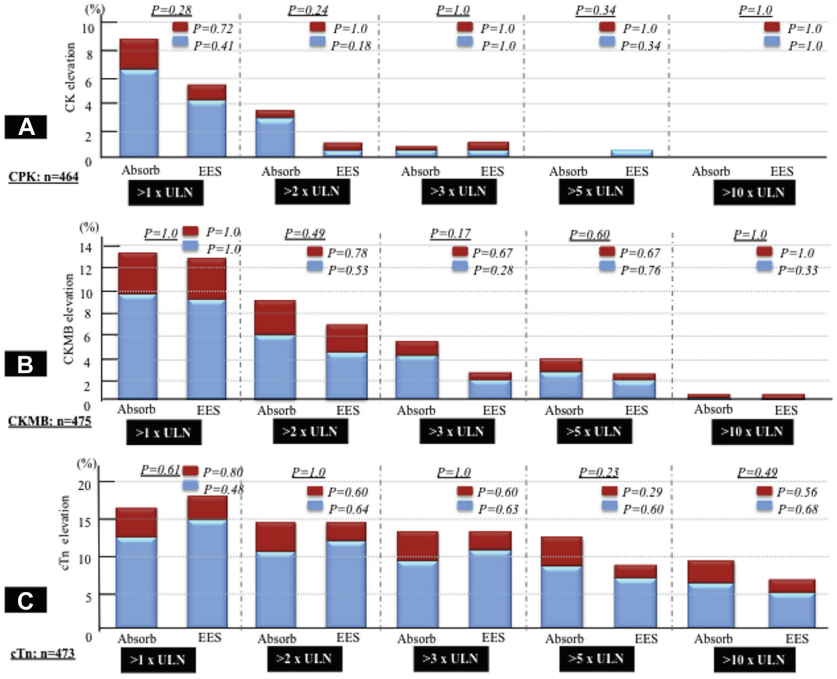

The figure shows magnitude of post-procedural CB rise—**(A)** CK, **(B)** CK-MB, **(C)** cTn—for the patients with side branch occlusion after percutaneous coronary intervention **(blue bars)** and those with the other anatomical complications **(red bars)**. *Fourteen patients presented with recent myocardial infarction at entry with normalized CK-MB according to the protocol were excluded for post-CB analysis. CB = cardiac biomarkers; CK = creatine kinase; CK-MB = creatine kinase-myocardial band; cTn = cardiac troponin.

arm, the treatment with overlapping was associated with risk of PMI with a 3.59 OR (p = 0.03), whereas in the EES arm, OR was 5.07 (p = 0.28) in the EES arm. The p value for interaction was not significantly different (p = 0.65), suggesting that overlapping is associated with higher risk of MI in both the Absorb and Xience arms. One MI (non-Q-wave) was attributed to definite scaffold thrombosis involving overlapping scaffolds. Of note, in a juvenile porcine model (28), overlapping Absorb scaffolds, compared with nonoverlapping scaffolds, showed delayed healing on histology and optical coherence tomography and slower tissue coverage: the coverage of the overlapping segment was 80.1% and 99.5% at 28 and 90 days after implantation respectively, suggesting that complete coverage in humans may take up to 18 months. Similar findings (29,30)—delayed healing and promotion of inflammation at sites of overlap—have been reported in the atherosclerotic rabbit model implanted with EES, suggesting the general detrimental effect and potential biohazard of overlapping devices. Adjacent implantation of scaffolds instead of true overlapping may circumvent this problem.

STUDY LIMITATIONS. The results of the current substudy are a post-hoc analysis. The study was not powered to detect difference in clinical events such as PMI and per-protocol definition of PMI does not include clinical symptoms or electrocardiographic changes. Given the mixture and wide range of troponin assays used across participating hospitals,

TABLE 5 Predictors of Per-Protocol PMI

	Univariate Logistic Regression		Multivariate Model (I, II, III, IV,V and Device Type)	
	OR (95% CI)	p Value	OR (95% CI)	p Value
Patient-related factors				
Age, yrs	1.02 (0.96–1.07)	0.56	–	–
Male	1.21 (0.34–4.37)	0.77	–	–
Body mass index, kg/m^2	0.94 (0.81–1.08)	0.36	–	–
Current smoker	1.71 (0.57–5.11)	0.34	–	–
Hypertension requiring treatment	0.43 (0.15–1.22)	0.11	–	–
Dyslipidemia requiring treatment	0.57 (0.20–1.64)	0.30	–	–
Any diabetes mellitus	0.48 (0.11–2.16)	0.34	–	–
Unstable angina	0.94 (0.26–3.40)	0.93	–	–
Lesion-related factors assessed by angiography				
Pre-procedural diameter stenosis, %	0.98 (0.93–1.02)	0.28	–	–
Pre-procedural minimal lumen diameter, mm	1.38 (0.28–6.72)	0.69	–	–
Pre-procedural reference diameter, mm	0.48 (0.12–1.92)	0.30	–	–
Obstruction length, mm	0.99 (0.92–1.08)	0.85	–	–
Pre-procedural curvature, cm^{-1}	0.20 (0.19–2.16)	0.19	–	–
Lesion-related factors assessed by grayscale IVUS				
Pre-procedural minimal lumen area, mm^2	0.78 (0.35–1.70)	0.53	–	–
Pre-procedural EEM, mm^2	0.99 (0.86–1.16)	0.98	–	–
Pre-procedural mean total plaque area in treated region, mm^2	1.05 (0.88–1.27)	0.58	–	–
Pre-procedural total plaque volume in treated region, mm^3	1.00 (1.00–1.01)	0.22	–	–
Pre-procedural plaque burden in treated region, %	1.03 (0.99–1.07)	0.14	–	–
Lesion-related factors assessed by IVUS-VH				
Pre-procedural dense calcium, mm^2	1.86 (0.15–23.83)	0.63	–	–
Pre-procedural necrotic core, mm^2	1.16 (0.34–3.99)	0.81	–	–
Pre-procedural fibrotic tissue, mm^2	1.33 (0.70–2.51)	0.39	–	–
Pre-procedural fibro-fatty tissue, mm^2	0.92 (0.63–1.34)	0.67	–	–
Treatment-related factors				
Treatment with overlapping devices	5.32 (1.88–15.05)	<0.01	5.07 (1.78–14.41)	0.002
Device type, Absorb vs. EES	0.30 (0.07–1.35)	0.12	3.03 (0.67–13.74)	0.150
Post-dilation	1.18 (0.40–3.50)	0.77	–	–
Bail-out	3.79 (0.45–31.96)	0.22	–	–
Expected balloon diameter of the last balloon, mm	3.06 (0.76–12.33)	0.12	–	–

Dashes indicate that there were no applicable data.

CI = confidence interval; IVUS = intravascular ultrasound; OR = odds ratio; VH = virtual histology; other abbreviations as in Tables 1 and 4.

the proportion of elevated troponin and periprocedural rise could be depended on the proportion of contemporary or sensitive assays compared with conventional troponin assays. The difference in the health care system could influence the long-term clinical outcomes, however, such variances are less relevant to the current analysis focusing on the acute procedural outcomes.

CONCLUSIONS

There were no statistically significant differences in the incidence of CB rise and PMI between Absorb and EES. Overlapping of scaffolds or stents might be a precipitating factor of myocardial injury. Larger randomized trials are currently ongoing to confirm these findings. As demonstrated in the present study, which collected all 3 CB, binary definition of PMI is not only dependent on the selection of CB but also on the thresholds of the CB rise which are arbitrarily chosen.

ACKNOWLEDGMENTS The authors wish to express their sincere appreciation to Dr. Charles Simonton and Ms. Susan Veldhof for the critical review of the manuscript and Dr. Jan G.P. Tijssen and Ms. Lei Peng for statistical assistance.

REPRINT REQUESTS AND CORRESPONDENCE: Prof. Patrick W. Serruys, International Centre for Circulatory Health, National Heart and Lung Institute, Imperial College London, South Kensington Campus, London SW7 2AZ, United Kingdom. E-mail: patrick.w.j.c.serruys@gmail.com.

PERSPECTIVES

WHAT IS KNOWN? A potential concern exists that a bioresorbable vascular scaffold, compared with newer-generations of DES, might be associated with a higher incidence of periprocedural myocardial injury and PMI.

WHAT IS NEW? Our results confirmed that there were no differences in the incidence of CB rise and PMI between Absorb and EES.

WHAT IS NEXT? Device overlap might be a precipitating factor of myocardial injury.

REFERENCES

1. Serruys PW, Ormiston JA, Onuma Y, et al. A bioabsorbable everolimus-eluting coronary stent system (ABSORB): 2-year outcomes and results from multiple imaging methods. Lancet 2009;373:897-910.

2. Ormiston JA, Serruys PW, Regar E, et al. A bioabsorbable everolimus-eluting coronary stent system for patients with single de-novo coronary artery lesions (ABSORB): a prospective open-label trial. Lancet 2008;371:899-907.

3. Ormiston JA, Webster MW, Armstrong G. First-in-human implantation of a fully bioabsorbable drug-eluting stent: the BVS poly-L-lactic acid everolimus-eluting coronary stent. Catheter Cardiovasc Interv 2007;69:128-31.

4. Onuma Y, Serruys PW, Ormiston JA, et al. Three-year results of clinical follow-up after a bioresorbable everolimus-eluting scaffold in patients with de novo coronary artery disease: the ABSORB trial. EuroIntervention 2010;6:447-53.

5. Serruys PW, Onuma Y, Dudek D, et al. Evaluation of the second generation of a bioresorbable everolimus-eluting vascular scaffold for the treatment of de novo coronary artery stenosis: 12-month clinical and imaging outcomes. J Am Coll Cardiol 2011;58:1578–88.

6. Serruys PW, Onuma Y, Ormiston JA, et al. Evaluation of the second generation of a bioresorbable everolimus drug-eluting vascular scaffold for treatment of de novo coronary artery stenosis: six-month clinical and imaging outcomes. Circulation 2010;122:2301–12.

7. Serruys PW, Onuma Y, Garcia-Garcia HM, et al. Dynamics of vessel wall changes following the implantation of the Absorb everolimus-eluting bioresorbable vascular scaffold: a multi-imaging modality study at 6, 12, 24 and 36 months. EuroIntervention 2014;9:1271-84.

8. Diletti R, Serruys PW, Farooq V, et al. ABSORB II randomized controlled trial: a clinical evaluation to compare the safety, efficacy, and performance of the Absorb everolimus-eluting bioresorbable vascular scaffold system against the XIENCE everolimus-eluting coronary stent system in the treatment of subjects with ischemic heart disease caused by de novo native coronary artery lesions: rationale and study design. Am Heart J 2012;164: 654–63.

9. Muramatsu T, Onuma Y, Garcia-Garcia HM, et al., for the ABSORB-EXTEND Investigators. Incidence and short-term clinical outcomes of small side branch occlusion after implantation of an everolimus-eluting bioresorbable vascular scaffold: an interim report of 435 patients in the ABSORB-EXTEND single-arm trial in comparison with an everolimus-eluting metallic stent in the SPIRIT first and II trials. J Am Coll Cardiol Intv 2013;6:247-57.

10. Garg S, Serruys PW. Coronary stents: current status. J Am Coll Cardiol 2010;56 Suppl 10:S1–42.

11. Onuma Y, Ormiston J, Serruys PW. Bioresorbable scaffold technologies. Circ J 2011;75:509–20.

12. Roubin GS, Cannon AD, Agrawal SK, et al. Intracoronary stenting for acute and threatened closure complicating percutaneous transluminal coronary angioplasty. Circulation 1992;85:916–27.

13. Bell MR, Reeder GS, Garratt KN, Berger PB, Bailey KR, Holmes DR Jr. Predictors of major ischemic complications after coronary dissection following angioplasty. Am J Cardiol 1993;71: 1402–7.

14. Vranckx P, Farooq V, Garg S, et al. Different cardiac biomarkers to detect peri-procedural myocardial infarction in contemporary coronary stent trials: impact on outcome reporting. Heart 2012;98:1424-30.

15. Thygesen K, Alpert JS, Jaffe AS, et al., for the Joint ESC/ACCF/AHA/WHF Task Force Members Chairpersons. Third universal definition of myocardial infarction. J Am Coll Cardiol 2012;60: 1581–98.

16. Pervaiz MH, Sood P, Sudhir K, et al. Periprocedural myocardial infarction in a randomized trial of everolimus-eluting and paclitaxel-eluting coronary stents: frequency and impact on mortality according to historic versus universal definitions. Circ Cardiovasc Interv 2012;5:150–6.

17. Serruys PW, Chevalier B, Dudek D, et al. A bioresorbable everolimus-eluting scaffold versus a metallic everolimus-eluting stent for ischaemic heart disease caused by de-novo native coronary artery lesions (ABSORB II): an interim 1-year analysis of clinical and procedural secondary outcomes from a randomised controlled trial. Lancet 2015;385:43-54.

18. Park DW, Kim YH, Yun SC, et al. Frequency, causes, predictors, and clinical significance of peri-procedural myocardial infarction following percutaneous coronary intervention. Eur Heart J 2013;34:1662-9.

19. Myint PK, Kwok CS, Bachmann MO, Stirling S, Shepstone L, Zaman MJ. Prognostic value of troponins in acute coronary syndrome depends upon patient age. Heart 2014;100:1583–90.

20. Lansky AJ, Stone GW. Periprocedural myocardial infarction: prevalence, prognosis, and prevention. Circ Cardiovasc Interv 2010;3:602–10.

21. Mehran R, Dangas G, Mintz GS, et al. Atherosclerotic plaque burden and CK-MB enzyme elevation after coronary interventions: intravascular ultrasound study of 2256 patients. Circulation 2000;101:604–10.

22. Maehara A, Mintz GS, Weissman NJ. Advances in intravascular imaging. Circ Cardiovasc Interv 2009;2:482–90.

23. Kawamoto T, Okura H, Koyama Y, et al. The relationship between coronary plaque characteristics and small embolic particles during coronary stent implantation. J Am Coll Cardiol 2007;50: 1635–40.

24. Merla R, Reddy NK, Wang FW, Uretsky BF, Barbagelata A, Birnbaum Y. Meta-analysis of published reports on the effect of statin treatment before percutaneous coronary intervention on periprocedural myonecrosis. Am J Cardiol 2007; 100:770–6.

25. Farooq V, Serruys PW, Vranckx P, et al. Incidence, correlates, and significance of abnormal cardiac enzyme rises in patients treated with surgical or percutaneous based revascularisation: a substudy from the Synergy between Percutaneous Coronary Interventions with Taxus and Cardiac Surgery (SYNTAX) trial. Int J Cardiol 2013;168: 5287–92.

26. Herrmann J. Peri-procedural myocardial injury: 2005 update. Eur Heart J 2005;26:2493-519.

27. Park DW, Kim YH, Yun SC, et al. Impact of the angiographic mechanisms underlying periprocedural myocardial infarction after drug-eluting stent implantation. Am J Cardiol 2014;113: 1105–10.

28. Farooq V, Serruys PW, Heo JH, et al. Intracoronary optical coherence tomography and histology of overlapping everolimus-eluting bioresorbable vascular scaffolds in a porcine coronary artery model: the potential implications for clinical practice. J Am Coll Cardiol Intv 2013;6: 523–32.

29. Nakazawa G, Nakano M, Otsuka F, et al. Evaluation of polymer-based comparator drug-eluting stents using a rabbit model of iliac artery atherosclerosis. Circ Cardiovasc Interv 2011;4:38–46.

30. Palmerini T, Biondi-Zoccai G, Della Riva D, et al. Stent thrombosis with drug-eluting stents: is the paradigm shifting? J Am Coll Cardiol 2013;62: 1915–21.

KEY WORDS bioresorbable scaffold, cardiac biomarker, device overlap, periprocedural myocardial infarction

APPENDIX For the Protocol and Statistical Analysis Plan as well as supplemental tables and figures, please see the online version of this paper.

1.4 Acute Gain of Everolimus-Eluting Bioresorbable Absorb Scaffolds

Acute Gain in Minimal Lumen Area Following Implantation of Everolimus-Eluting ABSORB Biodegradable Vascular Scaffolds or Xience Metallic Stents: Intravascular Ultrasound Assessment from the ABSORB II Trial.

JACC Cardiovasc Interv. 2016 in press.
[Original research paper, IF 7.44]

Sotomi Y*****, **Ishibashi Y***, Suwannasom P, Nakatani S, Cho YK, MD, Grundeken MJ, Zeng Y MD, Tateishi H, Smits PC, Barragan P, Kornowski R, Gershlick AH, Windecker S, Van Geuns RJ, Bartorelli AL, de Winter RJ, Tijssen J, Serruys PW, Onuma Y.
*** Equally contributed to the first author**

Acute Gain in Minimal Lumen Area Following Implantation of Everolimus-Eluting ABSORB Biodegradable Vascular Scaffolds or Xience Metallic Stents: Intravascular Ultrasound Assessment from the ABSORB II Trial

Yohei Sotomi, MD[1,2*]; Yuki Ishibashi, MD, PhD[1*]; Pannipa Suwannasom, MD[1,2,3]; Shimpei Nakatani, MD[1]; Yun-Kyeong Cho, MD, PhD[1]; Maik J. Grundeken, MD [2]; Yaping Zeng MD, PhD[1]; Hiroki Tateishi, MD, PhD[1]; Pieter C. Smits, MD, PhD[4]; Paul Barragan, MD, PhD[5]; Ran Kornowski, MD[6]; Anthony H Gershlick, MD, PhD[7]; Stephan Windecker, MD, PhD[8]; Robert-Jan van Geuns, MD, PhD[1]; Antonio L. Bartorelli, MD, PhD[9]; Robbert J. de Winter, MD, PhD[2], Jan Tijssen, MD, PhD[2], Patrick W. Serruys, MD, PhD[10]; Yoshinobu Onuma, MD, PhD[1]

*** These authors equally contributed to this work.**

Word Count: 3704 words

Authors' affiliation:

1. ThoraxCenter, Erasmus Medical Center, Rotterdam, The Netherlands
2. The Heart Center, Academic Medical Center, Amsterdam, The Netherlands
3. Northern Region Heart Center, Faculty of Medicine, Chiang Mai University, Chiang Mai, Thailand
4. Maasstad Ziekenhuis, Rotterdam, The Netherlands
5. Polyclinique les Fleurs, Ollioules, France
6. Rabin Medical Center, Petah Tikva, Israel
7. Glenfield Hospital, Leicester, United Kingdom

8. Bern University Hospital, Bern, Switzerland
9. Centro CardiologicoMonzino, University of Milan, Milan, Italy
10. International Centre for Circulatory Health, NHLI, Imperial College London, London, United Kingdom

KEY WORDS: bioresorbable vascular scaffold; drug-eluting stent; intravascular ultrasound

Running title: IVUS acute gain in BVS vs. EES

Corresponding author;

Prof. P.W. Serruys, MD, PhD

International Centre for Circulatory Health, NHLI, Imperial College London, London, United Kingdom

Emeritus Professor of medicine, Erasmus MC, Rotterdam, the Netherlands

Professor in cardiology

E-mail: patrick.w.j.c.serruys@gmail.com

Author Disclosures:

YO and PWS are members of the advisory board of Abbott Vascular. PCS has received research grants and speaker fees from Abbott Vascular. SW has received research grants to the institution by Abbott Vascular. RJvG has received speaker fees and research grants to the institution by Abbott Vascular. ALB has received speaker fees and travel support from Abbott Vascular. MG and RJdW institution receives a research grant from Abbott Vascular.

The other authors have no conflicts of interest to declare regarding the manuscript

Funding: The ABSORB II Study was sponsored by Abbott Vascular , Santa Clara, CA, USA

Abstract (249 words)

Background: The study aimed to compare, by intravascular ultrasound (IVUS), the acute gain (AG) at the site of the pre-procedural minimal lumen area (MLA) achieved by either the Absorb scaffold or the Xience stent and to identify the factors contributing to the acute performance of these devices.

Methods: Out of a total of 501 patients (546 lesions) in the ABSORB II randomized trial, 445 patients with 480 lesions were investigated by IVUS pre- and post-procedure. Comparison of MLA pre- and post-procedure was performed at the MLA site by matching pre- and post-procedural IVUS pullbacks.

Results: Lower AG on IVUS (lowest tertile) occurred more frequently in the Absorb arm than in the Xience arm (3.46 mm^2 vs. 4.27 mm^2, $p<0.001$; risk ratio, 3.04; 95%CI, 1.94-4.76). The plaque morphology at the MLA cross-section was not independently associated with IVUS acute gain. The main difference in acute gain in MLD by angiography was observed at the time of device implantation (EES vs. BVS, Δ+1.50mm vs. Δ+1.23mm), while the gain from post-dilatation was similar between the two arms (Δ+0.16mm vs. Δ+0.16mm) when patients underwent post-dilatation, although expected balloon diameter was smaller in the Absorb-arm than in the Xience-arm ($p=0.003$) during the post-dilatation.

Conclusions: At the site of the pre-procedural MLA, the increase of the lumen post-procedure was smaller in the Absorb-arm than in the Xience-arm. To achieve equivalent AG to Xience, the implantation of Absorb may require more aggressive strategies at implantation and post-dilatation than the technique used in the Absorb II trial.

Introduction

The fully bioresorbable scaffold is a novel device to treat coronary artery stenosis, potentially minimizing the long-term complications seen with metallic drug-eluting stents. The everolimus-eluting Absorb bioresorbable vascular scaffold (Absorb, Abbott Vascular, Santa Clara, CA) made of poly-L lactide (PLLA) provides a temporary coronary scaffolding for at least 6 months and becomes fully resorbed by approximately 3 years.[1] The first-in-man (FIM) trial using the Absorb showed excellent safety results with potential late benefits such as late lumen enlargement and restoration of vasomotion.[2] The ABSORB II study is the first randomized trial between the Absorb scaffold and Xience metallic stents in patients with up to two de novo native coronary lesions.[3, 4]

It is warranted that the acute performance of Absorb matches that of metallic stents; however, concern exists about acute expansion and lumen gain with the use of a polymeric device. In the ABSORB FIM trial, post-procedural intravascular ultrasound (IVUS) imaging demonstrated that implantation of an Absorb scaffold resulted in a more eccentric lumen with non-homogeneous scaffold expansion compared with metallic stents.[5] Furthermore, non-randomized matched population from the ABSORB and SPIRIT trials demonstrated that angiographic acute gain in lumen diameter tends to be smaller in the Absorb than in the Xience.[6] This trend was also observed in the randomized ABSORB Japan trial.[7-9] In the ABSORB II randomized trial (Clinical trials. gov NCT01425281), pre-procedural and post-procedural documentary IVUS imaging were mandatory and provided an unique opportunity to evaluate the scaffold/stent expansion at the precise site of pre-procedural minimal lumen area (MLA) and to relate the degree of expansion to the mechanical performance of both devices, procedural parameters of implantation, and tissue composition derived from IVUS analyses.[4]

Therefore, the purpose of this study is to investigate the IVUS acute gain at the site of minimal lumen area between the Absorb scaffold and the Xience stent and to identify the factors contributing to the acute performance of these devices.

Methods

Study design and population

The ABSORB II study is a randomized controlled trial comparing the safety and efficacy of the Absorb everolimus-eluting bioresorbable vascular scaffold and the Xience everolimus-eluting metallic stent in patients with up to two *de novo* native coronary lesions. The details of the study are available elsewhere.[3] After successful pre-dilatation of the target lesion, 2:1 randomization was performed. Out of a total of 501 patients (546 lesions), 335 patients (364 lesions) were randomly assigned to receive the Absorb and 166 patients (182 lesions) were assigned to receive the Xience. Grayscale IVUS and IVUS-virtual histology (VH) imaging pre-procedure and post- implantation was mandatory but documentary. No treatment recommendation based on IVUS imaging was made in the protocol.

Study device

The Absorb has an amorphous poly-DL-lactide (PDLLA) coating that contains and controls the release of the antiproliferative drug everolimus. The scaffold is made of semi-crystalline PLLA. PLLA is completely biodegraded by hydrolysis into water via the Krebs cycle. Physically, the scaffold has struts with an approximate thickness of 150 μm. The Xience is an everolimus-eluting, cobalt chromium alloy device with a platform consisting of serpentine rings connected by links fabricated from a single piece. The overall strut thickness including

the drug coating is approximately 90 μm.

Procedure and IVUS acquisition

Pre-procedural IVUS was mandatory before dilatation of the target lesion. If it was not technically feasible (for example, the IVUS catheter could not cross the lesion), pre-dilatation with a small balloon was allowed to facilitate the IVUS catheter insertion.

IVUS images were obtained with a rotational 45 MHz IVUS catheter (Revolution™; Volcano Corporation, Rancho Cordova, CA, USA). After intracoronary injection of 200μg nitroglycerin, IVUS pullbacks were performed with the use of an automated motorized device at a pullback speed of 0.5 mm/s. Lesions were treated with routine interventional techniques that included mandatory pre-dilation with a balloon shorter, and 0.5 mm smaller in diameter, than the study device. The size of stent/scaffold was determined by the target vessel diameter which was measured by pre-procedural on-line quantitative coronary angiography (QCA)[3, 10]. All patients enrolled in the ABSORB II trial were treated as follows: 1) a 3.5-mm device was used when both the proximal and distal maximum lumen diameters were within an upper limit of 3.8 mm and a lower limit of 3.0 mm; 2) a 3.0-mm device was used when both the proximal and distal maximum lumen diameters were within an upper limit of 3.3 mm and a lower limit of 2.5 mm; 3) a 2.5-mm device was used when both the proximal and the distal maximum lumen diameters were within an upper limit of 3.0 mm and a lower limit of 2.25 mm; 4) scaffold/stent overlap was allowed. Post-dilatation with a balloon shorter than the implanted scaffold/stent was performed at the discretion of the operators. Post-procedural IVUS images were obtained at the end of the procedure (post-device implantation or post-dilatation). All pullbacks were analyzed off-line by an independent core laboratory (Cardialysis BV, Rotterdam, The Netherlands) using a

commercial software (QIvus 2.2, Medis, Leiden, The Netherlands).

Measurement of acute gain on IVUS

To assess the acute performance of the Absorb and Xience stent at the site of the worst stenosis pre-procedure, the difference of lumen area between pre- and post-procedural IVUS images at the site of the pre-procedural minimal lumen area (MLA) was measured as acute gain in MLA. Pre-procedural MLA was defined as the smallest lumen area within the target lesion. After identifying the frame of the pre-procedural MLA site, matching of pre- and post-procedural IVUS images was performed by identifying common landmarks, such as side branches, bifurcations, large calcifications, or echogenic metallic marker on the device. Matching was performed using a dedicated software (QCU-CMS software, Medis, Leiden, The Netherlands). The pre-procedural image of the MLA was matched and compared with the post-procedural lumen area at the same site. The lower acute gain was defined as the lowest tertile from the whole population.

Analysis of IVUS and procedural parameters

Contour detection was performed by experienced IVUS core lab analysts. IVUS metrics including vessel, stent/scaffold, and lumen area were measured at 0.5-mm intervals. To identify the lesion factors in the evaluation of acute gain, analysis was also performed using the following parameters: plaque burden, lumen eccentricity, presence of calcium, remodeling index[11] from grayscale IVUS and tissue composition parameters (absolute value and percentage) from IVUS-VH. Plaque burden was obtained by the plaque plus media cross-sectional area (CSA) divided by the vessel CSA.[12] Eccentricity index (EI) was

calculated as the ratio of the projected minimal and maximal lumen or scaffold/stent diameter at the MLA cross-section[5, 13]. Pre-treatment reference segments were selected as sites with the least amount of plaque proximal and distal to the MLA sites prior to the take-off of any major side branch. [11] The remodeling index (RI) was calculated as the vessel area at the MLA site divided by the average of the proximal and distal reference vessel areas. Negative remodeling was defined as an RI <0.88, intermediate remodeling as an RI of 0.88 to 1.00, and positive remodeling as an RI >1.00. [11]

Location and circumferential distribution of calcium was quantified in grayscale IVUS. Calcium was defined as bright echoes with acoustic shadowing. The location of the calcium was defined as superficial, deep, or both.[14] If the leading edge of the acoustic shadowing appeared within the shallowest 50% of the plaque thickness, it was defined as superficial calcium. If the leading edge of the acoustic shadowing appeared within the deepest 50% of the plaque thickness, it was defined as deep calcium. The largest continuous arc of calcium and summed arc of calcium at the site of pre-interventional lumen area were measured in degrees with a protractor centered on the lumen. In addition, the arc of calcium was classified as 1 quadrant (≤90°), 2 quadrants (91° to 180°), 3 quadrants (181° to 270°), or 4 quadrants (271° to 360°). By IVUS-VH analysis, tissue at the site of pre-procedural MLA was categorized into the 4 basic plaque tissue components: fibrous tissue (FI) - dark green; fibro-fatty (FF) - light green; necrotic core (NC) - red; and dense calcium (DC) – white.[15]

In the compliance charts (pressure-diameter relationship) for the Absorb and the Xience (Prime, Xpedition, etc.) provided by the manufacturer, the inner diameters of the devices were described. Expected device diameter was obtained from the device compliance chart, using the nominal device diameter and the maximum pressure during implantation. During post-dilatation, the expected balloon diameter was obtained from the balloon compliance

chart data provided by the various manufacturers of balloons, using the nominal diameter of the balloon and the maximum pressure during the procedure. In case the pressure during the procedure exceeded the highest pressure on the chart, the highest diameter on the chart was used for the calculation.

Angiographic assessment

On-line QCA analyses were undertaken by the sites prior to Absorb implantation to define Dmax[10], and pre- and post-procedural off-line QCA were performed by an independent core laboratory (Cardialysis BV, Rotterdam, The Netherlands) using Coronary Angiography Analysis System (Pie Medical Imaging, Maastricht, Netherlands). The minimum lumen diameter (MLD) changes at different phases of the procedure were measured: i) before procedure, ii) after device implantation, and iii) immediately after post-dilatation. Additionally, minimal diameter of balloon was measured: i) during scaffold/stent implantation at maximum inflation pressure and ii) during post-dilatation at maximum inflation pressure.

Acute recoil was defined as follows: When a stent/scaffold delivery balloon was used for stent/scaffold expansion, acute absolute stent/scaffold recoil was defined as the difference between the mean diameter of the stent/scaffold delivery balloon at the highest pressure at implantation of the stent/scaffold (X) and the mean luminal diameter of the stented/scaffolded segment after implantation (Y). Acute absolute stent/scaffold recoil was calculated as X – Y. When a post-dilation balloon was used in the procedure, acute absolute recoil was defined as the difference between the mean diameter of the post-dilation balloon at the highest pressure in the post-dilated segment (X') and the mean luminal diameter after post-dilation (Y'). The angiogram of X and Y was performed in the same angiographic view so that the two images

were perfectly matched.

Statistical analysis

Categorical variables are presented as counts and percentages. Continuous variables are presented as means ± standard deviation. A value of $P < 0.05$ was considered statistically significant. Paired analysis was performed in the patients with analyzable pre- and post-procedural IVUS images. Logistic regression analysis was performed to find the relation of the following factors with IVUS lower acute gain in lumen area: gender, age, obesity (body mass index ≥30 kg/m^2), treated vessel, pre-procedural MLA, pre-procedural lumen eccentricity, plaque area, vessel area (all measurements at the site of MLA); In addition, presence or absence of calcium as well as arc of calcium at the site of MLA, tissue composition at the site of MLA, remodeling index[11], type of stent/scaffold, and maximal expected inner device or balloon diameter throughout procedure (in cases with or without post-dilatation) were also included in the logistic regression analysis. In the multivariate model, MLA was not included due to strong interaction with plaque area and vessel area. Statistical analyses were performed with SPSS (version 23.0.0, IBM, New York).

Results

Baseline characteristics

Out of 501 patients with 546 lesions who were enrolled in the ABSORB II trial, 445 patients with 480 lesions (291 patients with 313 lesions in the Absorb arm and 154 patients with 167 lesions in the Xience arm) had both pre-procedural and post-procedural IVUS analyses for acute lumen area gain assessment (**Figure 1**). There were no significant differences in

baseline patient demographics and pre-procedural angiography data (**Table 1**).

Differences in procedural implantation strategy between Absorb and Xience

Table 1 indicates the differences in procedural strategy between Absorb and Xience. Pre-dilatation strategy was comparable between both arms. At the time of the device implantation, no differences in device size selection and expected inner device diameter were observed, while maximal pressure during device implantation was higher in Xience than in Absorb. At the time of post dilatation, nominal diameter of the balloon, maximal pressure, and expected balloon diameter were smaller in the Absorb arm than in the Xience arm.

IVUS analysis

A representative case of acute gain in MLA is presented in **Figure 2**. Overall, the pre-procedural MLA was comparable between the two arms. However, pre-procedural vessel area (11.61 mm^2 vs.10.71 mm^2, p=0.013) and plaque area (9.47 mm^2 vs.8.63 mm^2, p=0.014) at the site of MLA were significantly larger in the Xience arm than in the Absorb arm. The post-procedural lumen area at the site of pre-procedural MLA was significantly smaller in the Absorb arm (5.55 mm^2 vs. 6.40 mm^2, p<0.001). The amount of change in plaque area and plaque burden was significantly smaller in the Absorb arm than in the Xience arm (-1.12 vs. -1.60 mm^2, p=0.005, -22.6 vs. -25.9 %, p<0.001, respectively) The increase of vessel area tended to be smaller in the Absorb arm (2.34 vs. 2.66 mm^2, p=0.066). As a result, there was a significant difference in acute gain for the minimal lumen area (3.46 mm^2 vs. 4.27 mm^2, p<0.001) (**Table 2, Figure 3**).

Device expansion in minimal lumen area

When device expansion [16, 17] was defined as the ratio of post-procedural lumen area at the site of e pre-procedural MLA to the expected inner device area calculated from the largest balloon used during procedure, the Absorb scaffold achieved on average 62±12% only of the predicted lumen area, while the Xience stent achieved 71±15% ($p< 0.001$) (**Figure 4**). Location of calcium as well as the arc of calcium and the amount of NC did not affect device expansion (**Figure 5**).

QCA MLD changes at different phases during procedure

Figure 6 shows the minimum lumen diameter (MLD) by QCA and MLA by IVUS changes at different phases during the procedure in the patients who had both pre- and post-procedural IVUS analyses.

The main difference in acute gain in MLD by QCA was observed at the time of device implantation (EES vs. BVS, Δ+1.50mm vs. Δ+1.23mm), while the gain from post-dilatation was similar between the two arms (Δ+0.16mm vs. Δ+0.16mm) when patients underwent post-dilatation. Acute recoil in cases with/without post-dilatation was comparable in both groups (EES vs. BES, 0.25±0.23 mm vs. 0.23±0.23 mm, $p = 0.421$).

Predictors of lower acute gain

Lower acute gain (lowest tertile) occurred more frequently in the Absorb arm than in the Xience arm (risk ratio, 3.04; 95%CI, 1.94-4.76) (**Table 3**). Results of logistic regression analysis are summarized in **Online supplement Table 1**. Gender, age, obesity, treated vessel, pre-procedural lumen eccentricity at the site of MLA, presence or absence of calcium as well

as arc of calcium at the site of MLA, tissue composition at the site of MLA were not independent predictors for lower acute gain. The following variables were significantly associated with lower acute gain in the multivariate model: Absorb use, maximal inner device or balloon diameter throughout procedure, vessel area and plaque area at the MLA site and negative remodeling. The differences in IVUS acute gain between Absorb and Xience were consistent across these variables (**Table 3**).

Discussion

Main findings

The main findings of this study are: 1) Lower acute gain occurred more frequently in the Absorb arm than in the Xience arm (3.46 mm^2 vs. 4.27 mm^2, $p<0.001$; risk ratio, 3.04; 95%CI, 1.94-4.76); 2) The plaque morphology at the MLA cross-section was not independently associated with acute gain; 3) On angiography, device acute recoil was comparable but expansion of the device was different. The influence of post-dilatation on MLD was somewhat limited.

Impact of lesion morphology on lumen enlargement

There are conflicting data about the impact of lesion morphology on lumen enlargement. In the previous reports, the expansion of drug-eluting stents was drastically influenced by IVUS (grayscale / virtual histology) plaque morphology (including the arc and length of lesion calcium) or quantitative lesion site geometry (lesion vessel area, plaque area and plaque burden).[16-18] In the present study, the impact of plaque component on acute gain in lumen area was not retained in the multivariate analysis, although in the univariate analysis higher

amounts of fibrotic plaque, necrotic core, and dense calcium showed lower acute gain in lumen area in both arms. In the present study, presence or absence of calcium as well as the arc of calcium by IVUS grayscale did not affect the acute gain and device expansion at MLA (**Figure 5**).

Differences in procedural strategy between Absorb and Xience

Differences in acute performance can be driven not only by differences in the mechanical properties of the Absorb scaffold and the Xience metallic stent but also by different initial implantation strategy[6, 19, 20]. Within precise boundaries of expansion (e.g. 3.0-3.5 mm for a device of 3.0 mm), the stress strain relationship of the metallic and polymeric struts are comparable; and the mechanical strength of the Absorb scaffold is not different from the metallic stent.[21] However, when the scaffold is over-expanded (>3.5 mm for a 3.0 mm device), the strut crowns begin approaching their geometrical limit. The radial support is maximized, while their tensile limit is also reached[22]. Therefore, pre-dilatation, optimal expansion, and avoidance of over-expansion are encouraged during the procedure with Absorb.

Maximal expected diameter of balloon with or without post-dilatation was similar between Absorb and Xience. However, the ratio of post-procedural lumen area at the site of pre-procedural MLA to the expected inner device area calculated from the largest balloon used during procedure was smaller in the Absorb than in the Xience (**Figure 4**). This result might imply the necessity of more aggressive strategy during implantation and post-dilatation of Absorb compared to Xience due to the device mechanical properties.

When QCA was performed to assess MLD changes at different phases during the procedure, the difference between the two arms was already significant at the time of device balloon

expansion (Δ+1.50mm for Xience vs. Δ+1.23mm for Absorb, p< 0.01) (**Figure 6**), despite the fact that the expected inner device diameter at implantation was similar in both arms. The acute device recoil was comparable between the two arms[4]. Despite less aggressive post-dilatation in the Absorb arm than in the Xience arm, the angiographic gain from post-dilatation was similar between the two arms (Δ+0.16 mm vs. Δ+0.16mm, p=0.97) (**Figure 6**). These angiographic analyses implied the difference of the mechanical properties of both devices and the necessity of different procedural strategies for implantation.

Clinical implication

On the basis of previous reports[23] of disrupted polymeric scaffolds due to over-expansion, the protocol did not recommend post-dilatation of the bioresorbable scaffold device. However, on angiography, a significant difference in the initial expansion was noted (Absorb < Xience). To achieve with the Absorb an acute lumen gain equivalent to that of the Xience, device balloon expansion with higher pressures and/or more aggressive post-dilatation should be considered within the limits of the recommended diameters. Since the device balloon of the Absorb is semi-compliant, implantation with a high pressure might result in over-expansion of the device or edge dissection. One of the possible contributing factors to lower acute gain in the Absorb is the lack of systematic post-dilatation with a non-compliant balloon with a diameter of 0.25 or 0.5 mm larger than the nominal diameter of the polymeric device.

The following clinical questions still remain; i) How does an aggressive lesion preparation (pre-dilatation, rotational atherectomy or cutting/scoring balloon) impact acute gain? ii) Can a high implantation pressure with the Absorb device improve acute gain? iii) How does an aggressive post-dilatation impact acute gain? These questions should be answered in future trials

Study limitations

There are several limitations in this analysis. If the IVUS catheter could not cross the lesion, pre-dilatation with a small balloon was performed. The incidence of pre-dilation before IVUS was similar between the Absorb and Xience arms, but initial lesion geometry and morphology could not be evaluated in 12 % of lesions. Aorto-ostial lesions, bifurcations, chronic total occlusions, and lesions with heavy calcification on angiography were excluded from the present study. Thus, our conclusions should not be extrapolated to more complex lesion subsets.

Conclusions

At the site of pre-procedural MLA, the Absorb scaffold showed lower acute gain than Xience stents. To achieve acute gain equivalent to that of Xience, Absorb deployment may require more aggressive strategies at implantation and post-dilatation than the technique used in the Absorb II trial.

References

1. Serruys PW, Onuma Y, Garcia-Garcia HM, Muramatsu T, van Geuns RJ, de Bruyne B, Dudek D, Thuesen L, Smits PC, Chevalier B, McClean D, Koolen J, Windecker S, Whitbourn R, Meredith I, Dorange C, Veldhof S, Hebert KM, Rapoza R and Ormiston JA. Dynamics of vessel wall changes following the implantation of the Absorb everolimus-eluting bioresorbable vascular scaffold: a multi-imaging modality study at 6, 12, 24 and 36 months. *EuroIntervention : journal of EuroPCR in collaboration with the Working Group on Interventional Cardiology of the European Society of Cardiology*. 2013.

2. Onuma Y and Serruys PW. Bioresorbable scaffold: the advent of a new era in percutaneous coronary and peripheral revascularization? *Circulation*. 2011;123:779-97.

3. Diletti R, Serruys PW, Farooq V, Sudhir K, Dorange C, Miquel-Hebert K, Veldhof S, Rapoza R, Onuma Y, Garcia-Garcia HM and Chevalier B. ABSORB II randomized controlled trial: a clinical evaluation to compare the safety, efficacy, and performance of the Absorb everolimus-eluting bioresorbable vascular scaffold system against the XIENCE everolimus-eluting coronary stent system in the treatment of subjects with ischemic heart disease caused by de novo native coronary artery lesions: rationale and study design. *American heart journal*. 2012;164:654-63.

4. Serruys PW, Chevalier B, Dudek D, Cequier A, Carrie D, Iniguez A, Dominici M, van der Schaaf RJ, Haude M, Wasungu L, Veldhof S, Peng L, Staehr P, Grundeken MJ, Ishibashi Y, Garcia-Garcia HM and Onuma Y. A bioresorbable everolimus-eluting scaffold versus a metallic everolimus-eluting stent for ischaemic heart disease caused by de-novo native coronary artery lesions (ABSORB II): an interim 1-year analysis of clinical and procedural secondary outcomes from a randomised controlled trial. *Lancet*. 2014.

5. Brugaletta S, Gomez-Lara J, Diletti R, Farooq V, van Geuns RJ, de Bruyne B, Dudek D,

Garcia-Garcia HM, Ormiston JA and Serruys PW. Comparison of in vivo eccentricity and symmetry indices between metallic stents and bioresorbable vascular scaffolds: insights from the ABSORB and SPIRIT trials. *Catheterization and cardiovascular interventions : official journal of the Society for Cardiac Angiography & Interventions*. 2012;79:219-28.

6. Zhang YJ, Bourantas CV, Muramatsu T, Iqbal J, Farooq V, Diletti R, Campos CA, Onuma Y, Garcia-Garcia HM and Serruys PW. Comparison of acute gain and late lumen loss after PCI with bioresorbable vascular scaffolds versus everolimus-eluting stents: an exploratory observational study prior to a randomised trial. *EuroIntervention : journal of EuroPCR in collaboration with the Working Group on Interventional Cardiology of the European Society of Cardiology*. 2014.

7. Kimura T, Kozuma K, Tanabe K, Nakamura S, Yamane M, Muramatsu T, Saito S, Yajima J, Hagiwara N, Mitsudo K, Popma JJ, Serruys PW, Onuma Y, Ying S, Cao S, Staehr P, Cheong WF, Kusano H, Stone GW and Investigators AJ. A randomized trial evaluating everolimus-eluting Absorb bioresorbable scaffolds vs. everolimus-eluting metallic stents in patients with coronary artery disease: ABSORB Japan. *European heart journal*. 2015.

8. Gao R, Yang Y, Han Y, Huo Y, Chen J, Yu B, Su X, Li L, Kuo HC, Ying SW, Cheong WF, Zhang Y, Su X, Xu B, Popma JJ and Stone GW. Bioresorbable Vascular Scaffolds Versus Metallic Stents in Patients With Coronary Artery Disease: ABSORB China Trial. *Journal of the American College of Cardiology*. 2015;66:2298-309.

9. Ellis SG, Kereiakes DJ, Metzger DC, Caputo RP, Rizik DG, Teirstein PS, Litt MR, Kini A, Kabour A, Marx SO, Popma JJ, McGreevy R, Zhang Z, Simonton C and Stone GW. Everolimus-Eluting Bioresorbable Scaffolds for Coronary Artery Disease. *The New England journal of medicine*. 2015;373:1905-15.

10. Ishibashi. Y, Nakatani S, Sotomi Y, Suwannasom P, Grundeken MJ, Garcia-Garcia HM, Bartorelli AL, Whitbourn R, Chevalier B, Abizaid A, Ormiston JA, Rapoza RJ, Veldhof S,

Onuma Y and Serruys PW. Relation Between Bioresorbable Scaffold Sizing Using QCA-Dmax and Clinical Outcomes at 1 Year in 1,232 Patients From Study Cohorts (ABSORB Cohort B, ABSORB EXTEND, and ABSORB II). *JACC Cardiovascular interventions*. in press.

11. Inaba S, Mintz GS, Farhat NZ, Fajadet J, Dudek D, Marzocchi A, Templin B, Weisz G, Xu K, de Bruyne B, Serruys PW, Stone GW and Maehara A. Impact of positive and negative lesion site remodeling on clinical outcomes: insights from PROSPECT. *JACC Cardiovascular imaging*. 2014;7:70-8.

12. Mintz GS, Nissen SE, Anderson WD, Bailey SR, Erbel R, Fitzgerald PJ, Pinto FJ, Rosenfield K, Siegel RJ, Tuzcu EM and Yock PG. American College of Cardiology Clinical Expert Consensus Document on Standards for Acquisition, Measurement and Reporting of Intravascular Ultrasound Studies (IVUS). A report of the American College of Cardiology Task Force on Clinical Expert Consensus Documents. *Journal of the American College of Cardiology*. 2001;37:1478-92.

13. de Jaegere P, Mudra H, Figulla H, Almagor Y, Doucet S, Penn I, Colombo A, Hamm C, Bartorelli A, Rothman M, Nobuyoshi M, Yamaguchi T, Voudris V, DiMario C, Makovski S, Hausmann D, Rowe S, Rabinovich S, Sunamura M and van Es GA. Intravascular ultrasound-guided optimized stent deployment. Immediate and 6 months clinical and angiographic results from the Multicenter Ultrasound Stenting in Coronaries Study (MUSIC Study). *Eur Heart J*. 1998;19:1214-23.

14. Mintz GS, Popma JJ, Pichard AD, Kent KM, Satler LF, Chuang YC, Ditrano CJ and Leon MB. Patterns of calcification in coronary artery disease. A statistical analysis of intravascular ultrasound and coronary angiography in 1155 lesions. *Circulation*. 1995;91:1959-65.

15. Garcia-Garcia HM, Costa MA and Serruys PW. Imaging of coronary atherosclerosis:

intravascular ultrasound. *European heart journal*. 2010;31:2456-69.

16. de Ribamar Costa J, Jr., Mintz GS, Carlier SG, Fujii K, Sano K, Kimura M, Tanaka K, Costa RA, Lui J, Na Y, Castellanos C, Biro S, Moussa I, Stone GW, Moses JW and Leon MB. Intravascular ultrasound assessment of drug-eluting stent expansion. *American heart journal*. 2007;153:297-303.

17. He Y, Maehara A, Mintz GS, Bharaj H, Castellanos C, Kesanakurthy S, Wu X, Guo N, Choi SY, Leon MB, Stone GW, Mehran R, Rabbani LE and Moses JW. Intravascular ultrasound assessment of cobalt chromium versus stainless steel drug-eluting stent expansion. *The American journal of cardiology*. 2010;105:1272-5.

18. Lee WS, Kim SW, Lee KJ, Kim TH, Kim CJ and Ryu WS. Under-expansions of Drug Eluting Stents in Patients With Acute Coronary Syndrome Are Associated With Plaque Components as Well as Vessel Size or Plaque Burden. *Circulation*. 2009;120:S913.

19. Onuma Y, Serruys PW, Gomez J, de Bruyne B, Dudek D, Thuesen L, Smits P, Chevalier B, McClean D, Koolen J, Windecker S, Whitbourn R, Meredith I, Garcia-Garcia H, Ormiston JA, A AC and investigators B. Comparison of in vivo acute stent recoil between the bioresorbable everolimus-eluting coronary scaffolds (revision 1.0 and 1.1) and the metallic everolimus-eluting stent. *Catheterization and cardiovascular interventions : official journal of the Society for Cardiac Angiography & Interventions*. 2011;78:3-12.

20. Tanimoto S, Bruining N, van Domburg RT, Rotger D, Radeva P, Ligthart JM and Serruys PW. Late stent recoil of the bioabsorbable everolimus-eluting coronary stent and its relationship with plaque morphology. *Journal of the American College of Cardiology*. 2008;52:1616-20.

21. Ormiston JA, Serruys PW, Regar E, Dudek D, Thuesen L, Webster MW, Onuma Y, Garcia-Garcia HM, McGreevy R and Veldhof S. A bioabsorbable everolimus-eluting coronary stent system for patients with single de-novo coronary artery lesions (ABSORB): a

prospective open-label trial. *Lancet*. 2008;371:899-907.

22. Onuma Y, Serruys PW, Perkins LE, Okamura T, Gonzalo N, Garcia-Garcia HM, Regar E, Kamberi M, Powers JC, Rapoza R, van Beusekom H, van der Giessen W and Virmani R. Intracoronary optical coherence tomography and histology at 1 month and 2, 3, and 4 years after implantation of everolimus-eluting bioresorbable vascular scaffolds in a porcine coronary artery model: an attempt to decipher the human optical coherence tomography images in the ABSORB trial. *Circulation*. 2010;122:2288-300.

23. Onuma Y, Serruys PW, Muramatsu T, Nakatani S, van Geuns RJ, de Bruyne B, Dudek D, Christiansen E, Smits PC, Chevalier B, McClean D, Koolen J, Windecker S, Whitbourn R, Meredith I, Garcia-Garcia HM, Veldhof S, Rapoza R and Ormiston JA. Incidence and Imaging Outcomes of Acute Scaffold Disruption and Late Structural Discontinuity After Implantation of the Absorb Everolimus-Eluting Fully Bioresorbable Vascular Scaffold: Optical Coherence Tomography Assessment in the ABSORB Cohort B Trial (A Clinical Evaluation of the Bioabsorbable Everolimus Eluting Coronary Stent System in the Treatment of Patients With De Novo Native Coronary Artery Lesions). *JACC Cardiovascular interventions*. 2014;7:1400-11.

Figure legends

Figure 1

Out of 501 patients with 546 lesions who were enrolled in the ABSORB II trial, 445 patients with 480 lesions (291 patients with 313 lesions in Absorb and 154 patients with 167 lesions in Xience) had both pre-procedural and post-procedural IVUS analyses for acute lumen area gain at the original minimal lumen area site.

Figure 2

Examples of IVUS pullbacks before (panel A-E) and after procedure (panel F-I). Vessel and lumen contours were drawn (panel C) at the site of pre-procedural minimal lumen area (dotted line in longitudinal view; panel E and F). Calcium, defined as bright echoes with acoustic shadowing, was measured in its circumferential extension (largest continuous arc of calcium [solid arc]: 101.3 degrees, summed arc of calcium [solid and dotted arc]: 214.1 degrees in B) and location (superficial calcium). Tissue component (panel D) was assessed by IVUS-VH. After matching pre- (panel E) and post-procedural IVUS pullbacks (panel F), vessel and lumen areas were obtained at the corresponding site (panel H). The lumen area in panel C was 1.77 mm^2 and 4.87 mm^2 in panel H. Therefore, acute lumen gain was 3.10 mm^2. (green line: vessel contour, red line: lumen contour, blue colored asterisk on longitudinal display: side branch, blue colored dagger on longitudinal display: calcification) Abbreviations: MLA, minimum lumen area; LA, lumen area.

Figure 3

Cumulative frequency distribution curve of acute gain (AG) at the minimal lumen area (MLA) site pre-procedure ($AG = MLA_{post} - MLA_{pre}$) for Absorb and Xience. Pre-procedural MLA

was similar between the two arms. The post-procedural lumen area at the site of the pre-procedural MLA was significantly smaller in the Absorb arm (5.55 mm^2 vs. 6.40 mm^2, $p<0.001$). The amount of change in lumen area was significantly smaller in the Absorb arm than in the Xience arm (3.46 mm^2 vs. 4.27 mm^2, $p<0.001$).

Figure 4

When device expansion was defined as the ratio of post-procedural lumen area at the site of the pre-procedural MLA to the expected inner device area calculated from the largest balloon used during procedure, the Absorb scaffold achieved on average 62±12% only of the predicted lumen area, while the Xience stent achieved 71±15% ($p< 0.001$). Abbreviation: MLA, minimum lumen area.

Figure 5

The figure shows the relationship between circumferential distribution of calcium and acute gain (**blue circle: Absorb, red circle: Xience**). Presence or absence of calcium as well as the arc of calcium by IVUS grayscale did not affect acute gain and device expansion at the site of minimum lumen area.

Figure 6

Figure shows the minimum lumen diameter (MLD) changes by quantitative coronary angiography (QCA, line graph) and minimum lumen area (MLA) changes by intravascular ultrasound (IVUS, bar graph) at different phases of the procedure in the patients who had both pre- and post-procedural IVUS analyses. The change of MLD by QCA and MLA by IVUS of the Absorb and the Xience are depicted by blue and red, respectively. The dotted

lines show the MLD changes for those lesions that were not post-dilated, while solid lines show the MLD change of the lesions that underwent post-dilatation.

The difference in acute gain was mainly observed at the time of device implantation (Δ+1.50mm vs. Δ+1.23mm), while the gain from post-dilatation was similar between the two arms (Δ+0.16mm vs. Δ+0.16mm), when patients underwent post-dilatation.

Table 1. Clinical characteristics and procedural variables

all = 445 patients	ABSORB 291 patients	XIENCE 154 patients	*P* value
Demographics			
Male gender	217 (74.6)	123 (79.9)	0.241
Age (years)	61 ± 10	61 ± 10	0.786
Current smoking	77 (26.5)	33 (21.4)	0.251
Lipid disorder requiring medication	201 (69.1)	116 (75.3)	0.258
Hypertension requiring medication	188 (64.6)	104 (67.5)	0.802
Diabetes mellitus	64 (22.0)	38 (24.7)	0.554
Stable angina	187 (64.3)	100 (64.9)	0.917
Body mass index (BMI, kg/m^2)	27.8 ± 4.1	28.1 ± 3.7	0.542
Obesity (BMI ≥30 kg/m^2)	67 (23.1)	44 (28.6)	0.208
all = 480 lesions	**313 lesions**	**167 lesions**	
Pre-procedural angiography			
Lesion location			0.184
Left anterior descending artery	146 (46.7)	81 (48.5)	
Left circumflex artery	88 (28.1)	35 (21.0)	
Right coronary artery	79 (25.2)	51 (30.5)	
Lesion classification†			0.456
A	4 (1.3)	1 (0.6)	
B1	181 (58.0)	85 (51.5)	
B2	125 (40.1)	78 (47.3)	
C	2 (0.6)	1 (0.6)	

Quantitative coronary angiography				
Interpolated percent diameter stenosis (%)	58.3 ± 11.1	59.1 ± 11.4	0.448	
Minimal lumen diameter (mm)	1.08 ± 0.32	1.07 ± 0.31	0.627	
Reference vessel diameter (mm)	2.60 ± 0.37	2.64 ± 0.40	0.327	
Maximal diameter at proximal reference segment (mm)	2.84 ± 0.45	2.87 ± 0.46	0.476	
Maximal diameter at distal reference segment (mm)	2.69 ± 0.45	2.74 ± 0.43	0.258	
Procedural variables				
Pre-dilatation				
Pre-dilatation before IVUS	115 (36.7)	59 (35.3)	0.842	
Pre-dilatation performed	313 (100.0)	165 (98.8)	0.121	
Nominal diameter of pre-dilatation balloon (mm)	2.60 ± 0.36	2.64 ± 0.35	0.236	
Maximal pressure during pre-dilatation (atm)	12.2 ± 3.0	12.5 ± 3.1	0.300	
Device implantation				
Nominal diameter of device			0.139	
2.5 mm	52 (16.6)	17 (10.2)		
2.75 mm	0 (0)	1 (0.6)		
3.0 mm	190 (60.7)	107 (64.1)		
3.5 mm	71 (22.7)	42 (25.1)		
Maximal pressure during device implantation (atm)	13.1 ± 2.7	13.8 ± 2.5	0.008	
Expected inner device diameter (mm)	3.34 ± 0.33	3.28 ± 0.33	0.109	*
Post-dilatation				
Post-dilatation performed	194 (62.0)	102 (61.1)	0.844	
Nominal diameter of post-dilatation balloon (mm)‡	3.16 ± 0.34	3.28 ± 0.37	0.01	*
Maximal pressure during post-dilatation (atm)¶	15.3 ± 3.2	16.7 ± 3.4	0.001	*
Expected diameter of post-dilatation balloon (mm)¶	3.27 ± 0.35	3.40 ± 0.39	0.003	*

Maximal expected diameter of balloon (with or without post-dilatation, mm)	3.37 ± 0.33	3.38 ± 0.36	0.896

Data are expressed as mean ± SD, as n (%)
* $p < 0.05$
† Data was available in 477 lesions.
‡ Data was available in 292 lesions.
¶ Data was available in 290 lesions.

Table 2. IVUS data at the site of pre-procedural minimal lumen area

	Pre-procedure			Post-procedure			Change between pre and post		
	ABSORB	**XIENCE**	**P value**	**ABSORB**	**XIENCE**	**P value**	**ABSORB**	**XIENCE**	**P value**
all=480	n=313	n=167		n=313	n=167		n=313	n=167	
Grayscale IVUS									
Lumen area (mm^2)	2.08 ± 0.76	2.13 ± 0.85	0.489	5.55 ± 1.46	6.40 ± 1.68	<0.001	3.46 ±1.35	4.27 ±1.46	<0.001
Vessel area (mm^2)	10.71 ± 3.67	11.61 ± 3.89	0.013	13.05 ± 3.83	14.28 ± 4.01	0.001	2.34 ±1.80	2.66 ±1.82	0.066
Plaque area (mm^2)	8.63 ± 3.47	9.47 ± 3.71	0.014	7.51 ± 2.82	7.88 ± 2.94	0.177	-1.12 ±1.75	-1.60 ±1.76	0.005
Plaque burden (%)	79.0 ± 8.3	80.2 ± 8.5	0.141	56.4 ± 8.1	54.3 ± 7.8	0.008	-22.6 ± 8.2	-25.9 ±7.3	<0.001
Minimal lumen diameter (mm)	1.47 ± 0.23	1.48 ± 0.25	0.653	2.41 ± 0.37	2.66 ± 0.45	<0.001			
Maximal lumen diameter (mm)	1.75 ± 0.37	1.77 ± 0.38	0.587	2.86 ± 0.40	3.00 ± 0.41	<0.001			
Lumen eccentricity	0.86 ± 0.10	0.85 ± 0.10	0.716	0.84 ± 0.08	0.89 ± 0.11	<0.001			
Presence or absence of calcium (%)			0.987						
No	114 (36.4)	61 (36.5)							
1 quadrant (1~90 degrees)	130 (41.5)	67 (40.1)							
2 quadrants (91~180 degrees)	41 (13.1)	24 (14.4)							
3 quadrants (181~270 degrees)	15 (4.8)	9 (5.4)							
4 quadrants (270~360 degrees)	13 (4.2)	6 (3.6)							
Largest continuous arc of calcium (degrees)	45.5 ± 58.8	51.8 ± 67.0	0.288						
Summed arc of calcium (degrees)	54.3 ± 69.3	60.7 ± 75.0	0.352						
Remodeling pattern (%)[§]			0.802						
Positive remodeling	94 (30)	46 (28)							

Intermediate remodeling	83 (27)	43 (26)							
Negative remodeling	132 (42)	75 (45)							
IVUS-VH									
Fibrous tissue (% of total plaque area)	27.70 ± 16.07	26.70 ± 14.69	0.517	27.30 ± 10.99	21.71 ± 8.86	<0.001	-0.41 ± 15.11	-4.99 ± 15.22	0.002
Fibro-fatty tissue (% of total plaque area)	52.70 ± 22.81	54.00 ± 21.61	0.558	31.49 ± 19.77	30.08 ± 17.65	0.456	-21.25 ± 20.07	-23.92 ± 17.17	0.159
Necrotic core (% of total plaque area)	15.64 ± 10.23	15.48 ± 9.94	0.868	28.58 ± 10.70	30.65 ± 10.12	0.048	13.03 ± 10.96	15.17 ± 10.65	0.047
Dense calcium (% of total plaque area)	3.95 ± 6.02	3.82 ± 5.81	0.824	12.56 ± 11.21*	17.56 ± 12.90*	<0.001	8.56 ± 10.13	13.74 ± 12.47	<0.001

Data are expressed as mean ± SD, as n (%). § 7 missing data.
* The polymeric or metallic struts are detected as (pseudo)calcium on IVUS-VH.

Table 3. Incidence of lower acute gain

Incidence of lower acute gain

	Absorb		Xience		Risk ratio	p value for interaction
All patients	41%	(128/313)	19%	(31/167)	3.04 (1.94-4.76)	
Maximal expected diameter of balloon with or without post-dilatation						
Lower tertile (≤3.28)	70%	(78/112)	35%	(25/72)	4.31 (2.30-8.10)	
Mid-tertile (>3.28, ≤3.40)	32%	(37/117)	9%	(3/34)	4.78 (1.37-16.64)	0.872
Higher tertile (>3.40)	16%	(13/84)	5%	(3/61)	3.54 (0.96-13.02)	
Vessel Area at MLA site						
Lower tertile (≤9.10)	67%	(75/112)	45%	(21/47)	2.51 (1.25-5.04)	
Mid-tertile (>9.10, <12.30)	33%	(35/105)	13%	(7/53)	3.29 (1.35-8.02)	0.305
Higher tertile (≥12.30)	19%	(18/96)	5%	(3/67)	4.92 (1.39-17.46)	
Plaque Area at MLA site						
Lower tertile (≤7.10)	69%	(79/114)	46%	(20/44)	2.71 (1.33-5.53)	
Mid-tertile (>7.10, <9.95)	35%	(35/101)	16%	(9/58)	2.89 (1.27-6.56)	0.475
Higher tertile (≥9.95)	14%	(14/98)	3%	(2/65)	5.25 (1.15-23.94)	
Remodeling†						
Negative (RI<0.88)	41%	(54/132)	17%	(13/75)	3.30 (1.65-6.59)	
Intermediate (0.88≤ RI≤1.00)	39%	(32/83)	26%	(11/43)	1.83 (0.81-4.13)	0.835
Positive (RI>1.0)	43%	(40/94)	15%	(7/46)	4.13 (1.67-10.18)	

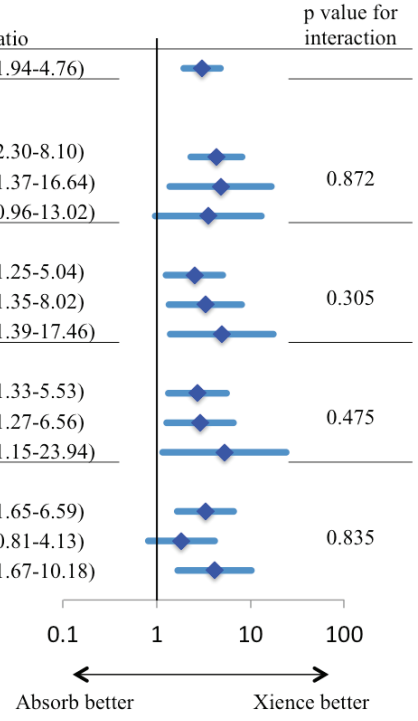

Abbreviations: MLA, minimum lumen area; RI, remodeling index. †Remodeling index: 7 missing data

Figure 1

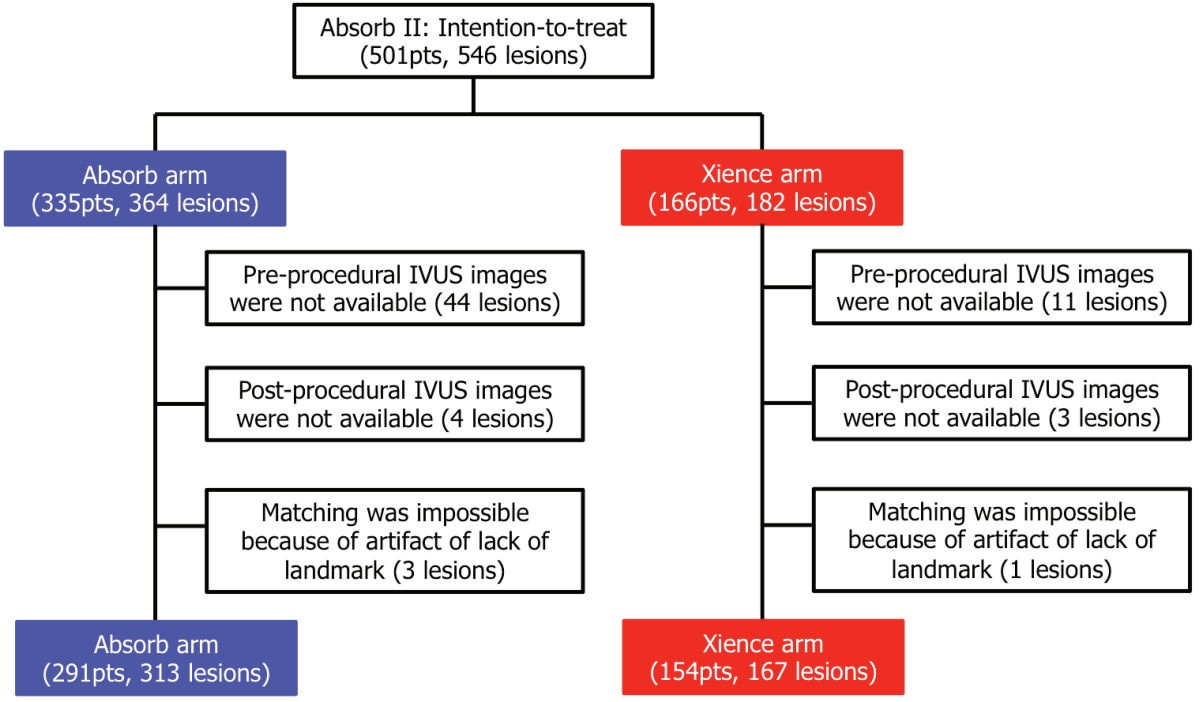
Absorb II: Intention-to-treat
(501pts, 546 lesions)
Absorb arm
(335pts, 364 lesions)
Xience arm
(166pts, 182 lesions)
Pre-procedural IVUS images were not available (44 lesions)
Post-procedural IVUS images were not available (4 lesions)
Matching was impossible because of artifact of lack of landmark (3 lesions)
Pre-procedural IVUS images were not available (11 lesions)
Post-procedural IVUS images were not available (3 lesions)
Matching was impossible because of artifact of lack of landmark (1 lesions)
Absorb arm
(291pts, 313 lesions)
Xience arm
(154pts, 167 lesions)

Figure 2

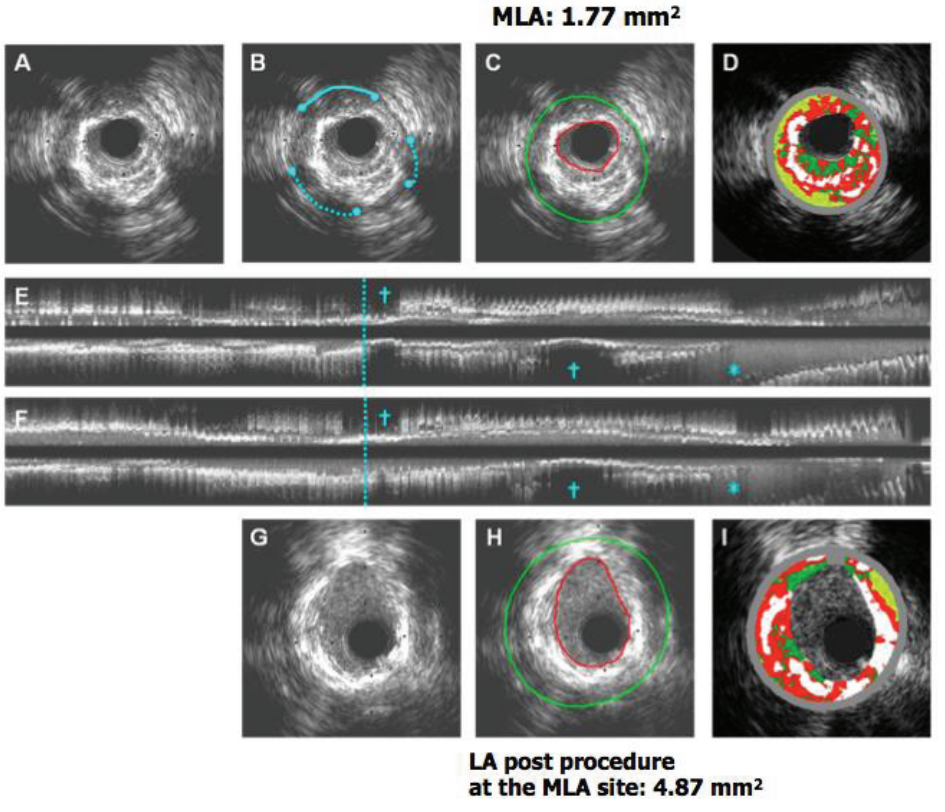
MLA: 1.77 mm²
A
B
C
D
E
F
G
H
I
LA post procedure
at the MLA site: 4.87 mm²

Figure 3

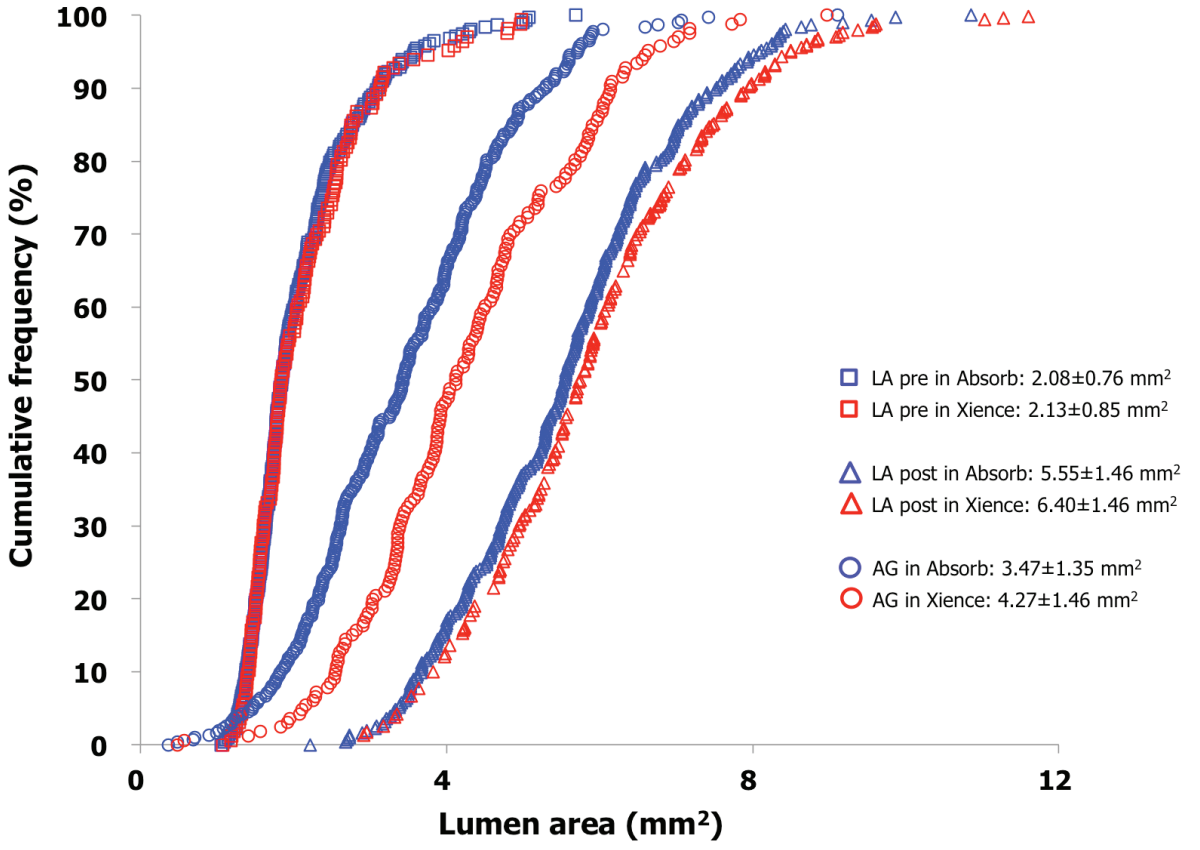
Cumulative frequency (%)
100
90
80
70
60
50
40
30
20
10
0
0
4
8
12
Lumen area (mm²)
LA pre in Absorb: 2.08±0.76 mm²
LA pre in Xience: 2.13±0.85 mm²
LA post in Absorb: 5.55±1.46 mm²
LA post in Xience: 6.40±1.46 mm²
AG in Absorb: 3.47±1.35 mm²
AG in Xience: 4.27±1.46 mm²

Figure 4

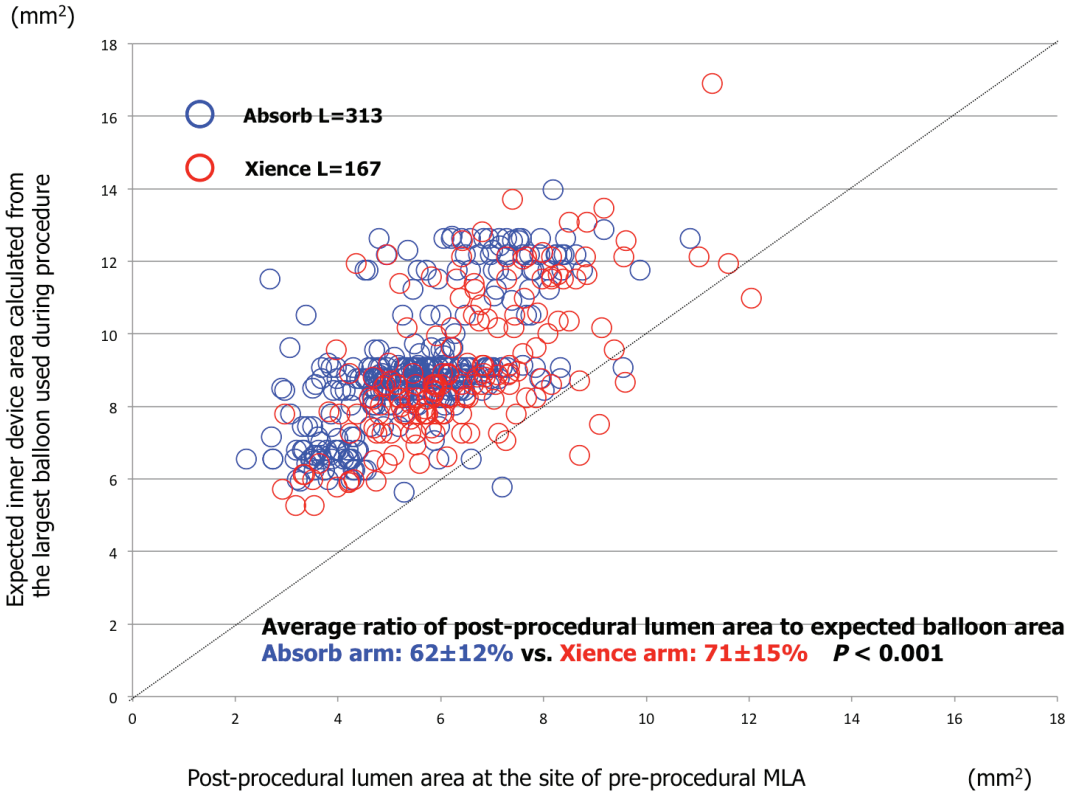
(mm²)
Expected inner device area calculated from the largest balloon used during procedure
Absorb L=313
Xience L=167
Average ratio of post-procedural lumen area to expected balloon area
Absorb arm: 62±12% vs. Xience arm: 71±15% P < 0.001
Post-procedural lumen area at the site of pre-procedural MLA
(mm²)
0
2
4
6
8
10
12
14
16
18

Figure 5

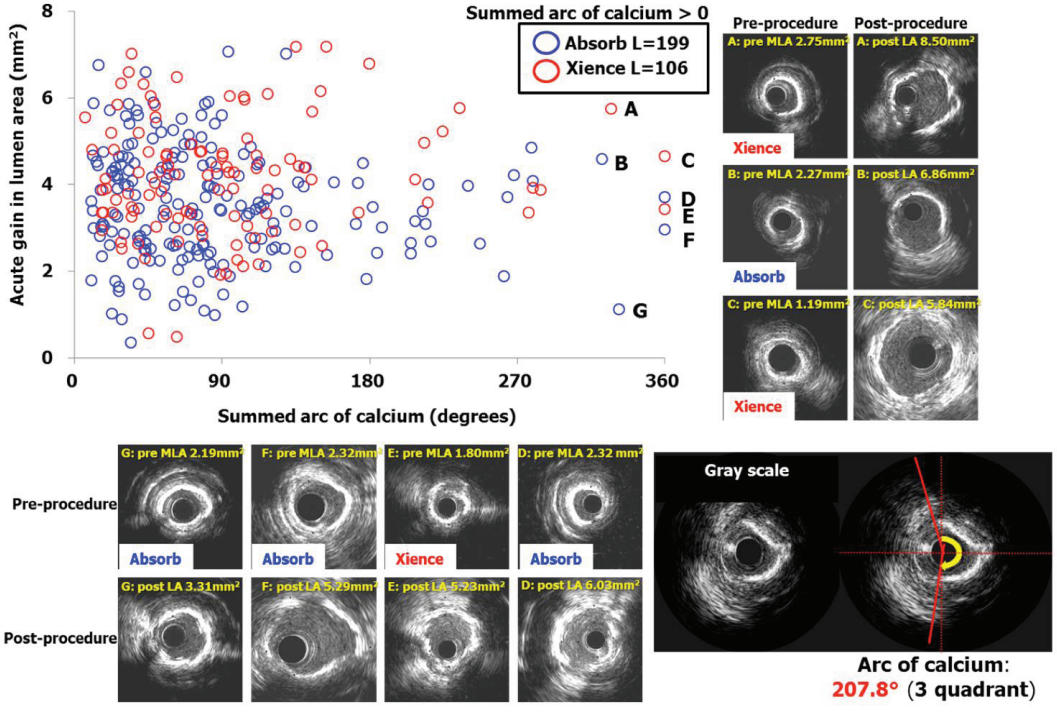
Summed arc of calcium > 0
Absorb L=199
Xience L=106
Acute gain in lumen area (mm²)
Summed arc of calcium (degrees)
0
90
180
270
360
2
4
6
8
A
B
C
D
E
F
G
Pre-procedure
Post-procedure
A: pre MLA 2.75mm²
A: post LA 8.50mm²
Xience
B: pre MLA 2.27mm²
B: post LA 6.86mm²
Absorb
C: pre MLA 1.19mm²
C: post LA 5.84mm²
Xience
Pre-procedure
Post-procedure
G: pre MLA 2.19mm²
F: pre MLA 2.32mm²
E: pre MLA 1.80mm²
D: pre MLA 2.32 mm²
Absorb
Absorb
Xience
Absorb
G: post LA 3.31mm²
F: post LA 5.29mm²
E: post LA 5.23mm²
D: post LA 6.03mm²
Gray scale
Arc of calcium:
207.8° (3 quadrant)

Figure 6

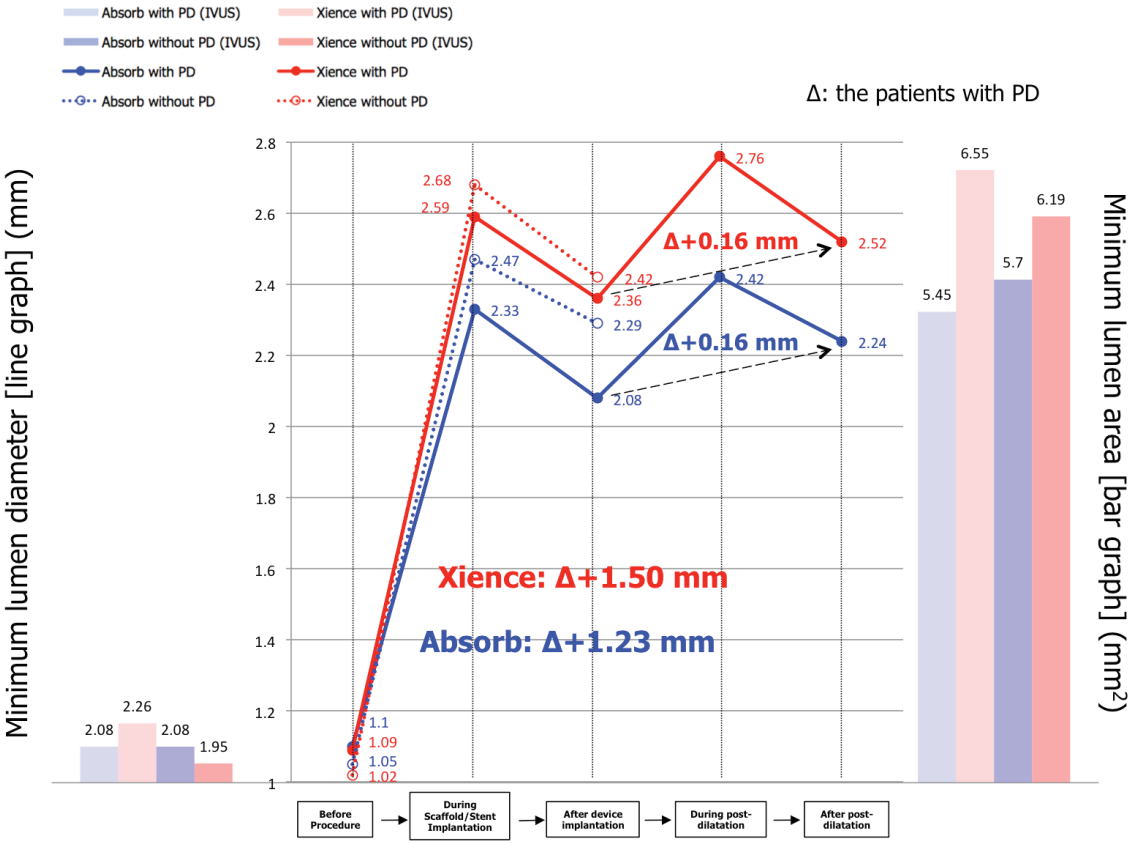
Absorb with PD (IVUS)
Absorb without PD (IVUS)
Absorb with PD
Absorb without PD
Xience with PD (IVUS)
Xience without PD (IVUS)
Xience with PD
Xience without PD
Δ: the patients with PD
Minimum lumen diameter [line graph] (mm)
Minimum lumen area [bar graph] (mm²)
Δ+0.16 mm
Δ+0.16 mm
Xience: Δ+1.50 mm
Absorb: Δ+1.23 mm
Before Procedure
During Scaffold/Stent Implantation
After device implantation
During post-dilatation
After post-dilatation

Online supplement table 1. Independent predictors for lower acute gain

	Univariate analysis			Multivariate analysis			
				Variables in model			Variables not in model
	OR [95%CI]	P value		OR [95%CI]	P value		P value
Male gender	0.543 [0.352-0.837]	0.006	*				0.483
Age (year)	0.998 [0.98-1.018]	0.874					0.906
Obesity (BMI>30 kg/mm2)	0.582 [0.368-0.923]	0.021	*				0.375
Absorb usage	3.035 [1.935-4.763]	<0.001	*	5.028 [2.659-9.507]		*	
Target vessel (Reference: LCX)							
LAD	1.031 [0.705-1.508]	0.876					0.987
RCA	0.433 [0.269-0.697]	0.001	*				0.504
Maximal expected diameter of balloon with or without post-dilatation (mm)	0.016 [0.006-0.040]	<0.001	*	0.010 [0.003-0.035]		*	
At the site of minimum lumen area							
Pre-procedural minimum lumen area**	1.155 [0.914-1.461]	0.228					
Pre-procedural lumen eccentricity	1.779 [0.236-13.395]	0.576					0.205
Pre-procedural plaque area	0.674 [0.618-0.736]	<0.001	*	0.213 [0.134-0.340]		*	

Pre-procedural vessel area	0.726 [0.674-0.783]	<0.001	*	3.078 [2.041-4.640]	*	
Presence of calcium at the site of MLA	0.785 [0.53-1.161]	0.225				0.334
Total arc of calcium at the site of MLA	0.998 [0.996-1.001]	0.258				0.493
Remodeling index (Reference: 0.88 - 1.00)						
< 0.88 (Negative remodeling)	0.942 [0.641-1.383]	0.759		0.461 [0.250-0.850]	*	
1.00 < (Positive remodeling)	1.029 [0.678-1.562]	0.894				0.530
Tissue composition						
Fibrotic	1.021 [1.009-1.034]	0.001	*			0.670
Fibrofatty	0.979 [0.97-0.988]	<0.001	*			0.550
Necrotic core	1.034 [1.014-1.054]	0.001	*			0.324
Dense calcium	1.039 [1.006-1.072]	0.02	*			0.152

* $p < 0.05$
** Minimu lumen area was not included in the multivariate model due to strong interaction with plaque area and vessel area
Abbreviations: MLA, minimum lumen area; LAD, left anterior descending artery; LCX, left circumflex artery; RCA, right coronary artery.

Post-implantation intravascular ultrasound assessment of eccentricity and asymmetry of Xience and Absorb in the ABSORB II trial : impact on adverse cardiovascular events

Pannipa Suwannasom[1,2,3,] MD; Yuki Ishibashi[1] MD, PhD; Yohei Sotomi[2], MD; Rafael Cavalcante, MD, PhD[1]; Felipe N. Albuquerque[4], MD; Carlos Macaya[5], MD; John A. Ormiston[6], MD; Jonathan Hill[7], MD; Irene M. Lang[8], MD; Mohanded Egred[9], MD; Jean Fajadet[10], MD; Maciej Lesiak[11], MD; Jan G. Tijssen[2], MD, PhD; Joanna J. Wykrzykowska[2], MD, PhD; Robbert J.de Winter[2], MD, PhD; Bernard Chevalier[12], MD; Yoshinobu Onuma[1], MD, PhD; Patrick W. Serruys[13], MD, PhD*

***Address for correspondence:**

Professor. Patrick W. Serruys, MD, PhD.

International Centre for Circulatory Health, NHLI, Imperial College London, London,

The United Kingdom

P.O. Box 2125, 3000 CC Rotterdam, The Netherlands

Email: patrick.w.j.c.serruys@gmail.com

Telephone: +31-102062828

Brief title: eccentricity and asymmetry indices and DoCE

Keywords: Bioresorbable vascular scaffolds, Eccentricity, Asymmetry

Total words: 4,483

Number of figures: 4

Number of tables: 5

Online supplement: 1 file

Author's affiliation:

1 ThoraxCenter, Erasmus University Medical Center, Rotterdam, The Netherlands

2 Academic Medical Center, Amsterdam, The Netherlands

3 Northern Region Heart Center, Maharaj Nakorn Chiang Mai Hospital, Faculty of Medicine, Chiang Mai University, Chiang Mai, Thailand.

4 Montefiore Medical Center, Albert Einstein College of Medicine New York - NY.

5 Hospital Universitario Clínico San Carlos, Madrid, Spain

6 Green Lane Cardiovascular Service, Auckland City Hospital, Auckland

7 King's College Hospital, London, United Kingdom

8 Division of Cardiology, Department of Internal Medicine II, Medical University of Vienna, Vienna, Austria

9 Freeman Hospital , Newcastle upon Tyne , UK

10 Department of Cardiology, Pasteur Hospital, Toulouse, France

11 Ist Department of Cardiology, Medical University of Poznan, Poland.

12 Institut Jacques Cartier, Massy, France

13 International Centre for Circulatory Health, NHLI, Imperial College London, London, United Kingdom

Declaration of interests

PW Serruys, B Chevalier and Y Onuma are members of the international advisory board of Abbott Vascular. All other authors declare no conflict of interest.

The Absorb trial was sponsored by Abbott Vascular.

1.5 Post-implantation assessment of eccentricity and asymmetry

Post-implantation intravascular ultrasound assessment of eccentricity and asymmetry of Xience and Absorb in the ABSORB II trial : impact on adverse cardiovascular events.

JACC Cardiovasc Interv. 2016 in press.
[Original research paper, IF 7.44]

Suwannasom P, Sotomi Y, **Ishibashi Y**, Cavalcante R, Albuquerque FN, Macaya C, Ormiston JA, Hill J, Lang IM, Egred M, Fajadet J, Lesiak M, Tijssen JG, Wykrzykowska JJ, J.de Winter MR, Chevalier B, Onuma Y, Serruys PW.

Structured Abstract (total words = 298)

Background: Mechanical properties of a fully bioresorbable polylactide scaffold are inherently different from those of permanent metallic stent.

Objectives: This study investigated the relationship between post-implantation eccentricity and asymmetry of metallic everolimus-eluting stent (Xience) and fully bioresorbable scaffold (Absorb) and their respective impact on clinical events at 1-year follow-up.

Methods: The ABSORB II trial compared the Absorb bioresorbable scaffold and the Xience stent in the treatment of a de novo coronary artery stenosis. Protocol-mandated IVUS imaging was performed pre and post implantation in 470 patients with 506 lesions. The eccentricity index (EI) and asymmetry index (AI) were calculated. The incidence of device-oriented composite endpoint (DoCE: a composite of cardiac death, myocardial infarction not-attributed to non-target vessels, and ischemic driven target lesion revascularization) was stratified in 3 groups characterized by the following geometrical parameters; i) concentric and symmetric (CS group, EI $\geq$ 0.7 and AI $\leq$ 0.3); ii) concentric and asymmetric (CA group, EI $\geq$ 0.7 and AI > 0.3); iii) eccentric and asymmetric (EA group, EI < 0.7 and AI > 0.3).

Results: 224(49.2%) lesions were classified to the CS group followed by the CA group (n= 149 lesions, 31.4%) and the EA group (n= 97 lesions,19.4%). At 1-year, the DoCE rates were 8.2%, 6.0% and 1.8% in the EA group, CA group and CS group, respectively (log-rank p=0.04). The principal independent determinants of eccentric and asymmetric device morphology were: high pre-implantation EI [OR 0.03(0.00-0.31), p=0.003] and, treatment with the Absorb [OR 7.29(3.24-16.37), p<0.001]. The independent determinants of DoCE were: lesions with negative

arterial remodeling [HR 3.26(1.08-9.86), p=0.04] and AI > 0.30 after device implantation [3.58(1.12-11.49), p-value=0.03]

Conclusion: Asymmetric device morphology is independently associated with adverse events following percutaneous coronary intervention. Absorb implantation is more frequently associated with post-implantation eccentric and asymmetric morphology compared to the Xience stent.

[ABSORB-II: NCT01425281]

Condensed abstract (Total words = 86)

The relationship between the IVUS geometrical morphologies and clinical events has never been investigated in the context of a randomized trial. This study investigated the relationship between post-implantation eccentricity and asymmetry of implanted devices and clinical events at 1 year follow-up in the ABSORB II randomized trial. The principal independent determinants of eccentric and asymmetric morphology of scaffold/stent post implantation were high pre-implantation EI [OR 0.03(0.00-0.31), p=0.003] and treatment with Absorb [OR 7.29(3.24-16.37), p<0.001]. Lesions with pre-implantation negative remodeling and high post-implantation AI were independently associated with 1-year DoCE.

Abbreviation

AI = asymmetry index

BVS = bioresorbable vascular scaffold

EES = metallic everolimus-eluting stent

EI = eccentricity index

IVUS = intravascular ultrasound

DoCE = device-oriented composite endpoint

MI= myocardial infarction

MLA = minimal lumen area

MLD = minimal lumen diameter

QCA= quantitative coronary angiography

INTRODUCTION

Bioresorbable vascular scaffolds (Absorb; Abbott Vascular, Santa Clara, CA) have emerged as a novel technology with several potential advantages compared to permanent metallic stents in the treatment of coronary artery disease(1). Bioresorbable vascular scaffolds (BVS) have a lesser radial strength than metallic drug-eluting stents (DES).(2) An over-stretching of BVS may cause loss of its radial strength and even causes mechanical disruption of the device.(3) Therefore, the inherent differences in mechanical property between polymeric and metallic device, precluded aggressive post-dilation in BVS. That last fact could explain the low acute gain of Absorb when compared to the metallic everolimus-eluting stent (EES) in the randomized controlled trial ABSORB-II(4) due to lower pressure used during inflation and smaller post-dilation balloon. Nevertheless, there were similar 1-year clinical outcomes between Absorb and metallic EES.(4)

Eccentricity index (EI) and asymmetry index (AI) assessed by intravascular ultrasound (IVUS) are known as indicators of acute performance of coronary devices. A prior study suggested a possible association between thrombus formation and low eccentricity index lesions after sirolimus-eluting stent implantation at 6-month follow-up.(5) The MUSIC trial showed that EI > 0.7 reflected optimal stent expansion, confirmed by favorable angiographic results seen at 6 months follow-up.(6) However, the understanding of the prognostic value of the eccentricity and asymmetry indices in clinical practice remain limited mainly due to observational studies using old stent platform(6), small sample size(5) and short follow-up duration.(5,6)

A comparison of the acute performance between Absorb and metallic EES in the absence of specific and mandatory intracoronary imaging guidance in the Absorb first-in-man and SPIRIT

FIRST trial has been reported, immediately after implantation, Absorb was more eccentric and asymmetric as compared to a metallic EES, without detectable impact on MACE at 6 months.(7)

It is of interest to investigate the acute performance of a new scaffold/stent platform and, their relationships to device-oriented composite endpoint (DoCE) in a larger sample size and in the context of a randomized trial(4). The aim of this study was to investigate the mechanistic response of lesions after devices implantation and to assess the impact of post-implantation eccentricity and asymmetry indices on early and late clinical events treated either with a metallic or a polymeric device.

METHODS

Study Population

The ABSORB II randomized controlled trial design has been described in detail previously(8). In summary, the ABSORB II trial is a prospective, single blinded, randomized, active –controlled trial. The study included 501 patients with de novo coronary lesions, randomized in 2:1 ratio to receive either treatment with an everolimus eluting bioresorbable scaffold (Absorb, Abbott Vascular, Santa Clara, CA, USA) or with an everolimus-eluting metallic stent (Xience, Abbott Vascular, Santa Clara, CA, USA). The inclusion criteria were patients aged 18–85 years with evidence of myocardial ischemia with one or two de-novo native lesions in different epicardial vessels with a maximum lumen diameter between 2.25 mm and 3.8 mm assessed by online quantitative coronary angiography (QCA) and a maximum lesion length of 48 mm.

Study device

The details of the study device (Absorb) have been described previously(8,9). In brief, the balloon expandable Absorb scaffold is comprised of a Poly-L lactide (PLLA) backbone coated with an amorphous drug-eluting coating matrix composed of Poly-D, L-lactide (PDLLA) polymer containing everolimus 100 μg/cm^2. The control device was the second-generation everolimus-eluting stent Xience (Abbott Vascular, Santa Clara, CA), which is a balloon-expandable metallic stent, manufactured from a flexible cobalt chromium alloy, and coated with a thin nonadhesive, durable, biocompatible acrylic, and fluorinated everolimus-releasing copolymer(8).The Xience stent and Absorb scaffold share the same basic MULTI-LINK design, and both devices are similar in terms of drug, drug dose density, and elution profile.

Imaging acquisition and analysis

Quantitative Angiographic Assessment

Two-dimensional quantitative coronary analysis (QCA) was performed at an independent core lab (Cardialysis BV, Rotterdam, The Netherlands) with the CAAS system (CAAS 5.10; Pie Medical BV, Maastricht, The Netherlands). In each patient, the stent/scaffold segment and the peri-stent/scaffold segments (defined by a length of 5 mm, proximal and distal to the scaffold edge) were analyzed pre- and post-implantation. The details of QCA and measurement of QCA maximal lumen diameters [QCA-Dmax: maximal lumen diameter immediately adjacent to the proximal or distal edges of the scaffold] have been described elsewhere(8,10,11).

IVUS acquisition

For the purpose of the study, IVUS was performed before intervention and after final procedure. IVUS gray-scale was acquired with a 3.2-French, 45-MHz rotational IVUS catheter. (Revolution® 45 MHz; Volcano Corporation, Rancho Cordova, CA), using automated pullbacks at 0.5 mm per second and 30 frames per second. All pullbacks were analyzed off-line at 1 mm longitudinal intervals and analyzed by an independent core laboratory (Cardialysis BV, Rotterdam, The Netherlands) using a commercial software (QIvus 2.2, Medis, Leiden, The Netherlands).

Pre- and post-implantation IVUS analysis

The methods of quantitative IVUS have been previously reported.(4,8) The pre-implantation segments were defined by co-registration with post-implantation IVUS using identical landmarks such as side-branches and calcium locations. Matching was done using dedicated software (IvusOctRegistration, Division of Image Processing [LKEB], Leiden, The Netherlands). Pre-treatment reference segments were selected as sites with the least amount of plaque proximal and distal to the minimal lumen area (MLA) sites prior to the takeoff of any major side branches. The scaffold/stent segments were identified by the first and the last cross-sectional IVUS frame in which scaffold/stent struts could be identified and/or where the proximal or distal metallic markers could be identified. The post-implantation region of interest, was the segment beginning 5 mm distal to, and extending 5 mm proximal to the scaffold/stent segments.(12)

IVUS parameter definitions

Incomplete apposition was defined as one or more scaffold/stent struts separated from the vessel wall. Plaque burden was calculated as plaque area/vessel area. Remodeling was assessed by means of the remodeling index (RI), expressed as the vessel area at the MLA site divided by the

average of the proximal and distal reference segment. Three remodeling categories were defined as follows: positive remodeling, RI >1.00; intermediate remodeling, RI between 0.88 and 1.00; and negative remodeling, RI < 0.88.(13) Calcification on IVUS appears as bright echoes with acoustic shadowing of the deeper arterial structures. Location and circumferential distribution of calcium were quantified on gray-scale IVUS. The largest continuous arc of calcium and summed arc of calcium at the site of pre-interventional lumen area were measured in degrees with a protractor centered on the lumen.

Eccentricity index (EI) was calculated as the ratio of the projected minimal and maximal lumen or scaffold/stent diameter(6,7). The IVUS cross-section with the lowest eccentricity index value per pullback was used for the analysis. Asymmetry index (AI) was calculated per lesion as (1 – projected minimum lumen or scaffold/stent diameter / projected maximal lumen or scaffold/stent diameter throughout an entire pullback)(7) **(Figure 1A)**.

Geometrical morphologies definitions and clinical endpoints

The study population was stratified according to the IVUS criteria of eccentricity and asymmetry(6,7). A lesion was characterized as eccentric when the value of EI was below 0.7.(6) Conversely, a lesion with post-implantation scaffold/stent EI ≥ 0.7 was defined as concentric. A lesion was characterized as asymmetric when the value of AI was over 0.3.(6) Therefore, all post-implantation lesions were classified into three geometrical morphologies as follow; i) "concentric and symmetric", CS group (EI ≥ 0.7 and AI ≤ 0.3); ii) "concentric and asymmetric", CA group (EI ≥ 0.7 and AI > 0.3); iii) "eccentric and asymmetric", EA group (EI < 0.7 and AI > 0.3). **(Figure 1B)**.

In the present analysis, the primary clinical outcome was a device-oriented composite endpoint (DoCE) at 1-year, defined as a composite of cardiac death, myocardial infarction (MI, defined by Q-wave and non-Q-wave MI from non-attributed to non-target vessels) and ischemia-driven target lesion revascularization (ID-TLR) by coronary bypass graft or percutaneous coronary intervention. All clinical endpoints definitions are described in the **online appendix**. Definite and probable scaffold thrombosis (ST) was adjudicated according to the Academic Research Consortium definitions (14-16). An independent clinical events committee adjudicated all clinical outcomes**.**

Statistical Analysis

All statistical analyses were performed using SAS release 9.1 (SAS Institute Inc, Cary, NC) or SPSS (version 17.0, SPSS Inc, Chicago, IL). QCA and IVUS were analyzed per lesion. All continuous variables were presented as mean±standard deviation (SD) or median and interquartile range (IQR; 1st to 3rd quartile) as appropriate. One-way ANOVA with Tukey's post-hoc test or Kruskal-Wallis test were used for comparisons of continuous variables and Chi-square test was used for categorical variables. The endpoint analyses were performed according to the intention-to-treat principle and presented at a patient-level. Whenever a patient received more than one lesion treatment, the lesion with the lowest scaffold/stent EI was selected as representative of that patient. One-year clinical outcomes among the three groups are compared with the log-rank test. Several patient-related, lesion-related, pre and post-procedure-related variables were assessed in univariate analyses.Variables with $p<0.10$ in the univariate analysis were included in the multivariable Cox regression model. A multivariable Cox proportional hazards model was used to determine the independent determinants of DoCE. A multivariate logistic regression analysis was used to determine the independent factors associated with

eccentric and asymmetric morphology after scaffold/stent implantation. Receiver operating characteristic (ROC) curves and c-indices were used to assess the sensitivity and specificity value of eccentricity and asymmetry on clinical outcomes. All reported p-values were 2-sided, and values of $p<0.05$ were considered statistically significant.

RESULTS

Patient demographics and baseline clinical characteristics.

Out of 501 patients who were randomly assigned to either the Absorb arm (335 patients) or the metallic EES arm (166 patients) with 31 patients were excluded from the post-implantation IVUS analysis **(Figure 2).** Consequently, the total sample size consisted of 470 patients with 506 lesions. The CS group comprised the largest proportion of patients (n= 224 lesions, 49.2%) followed by the CA group (n= 149 lesions, 31.4%) and the EA group (n= 97 lesions,19.4%). There were similar baseline clinical characteristics among the three groups **(Table 1).**

Pre-implantation lesion characteristics and details of the procedure

Pre-implantation lesion characteristics, QCA and IVUS measurements are summarized in **Table 2.** When population was stratified according to the post-implantation eccentricity and asymmetry indices, the EA group had lower pre-implantation EI and higher pre-implantation AI than other groups. Lower values of pre-implantation EI were observed more frequently in the metallic EES compared to the Absorb (0.59±0.11 vs. 0.61±0.11, p= 0.048) while asymmetry indices were comparable in both arms. The presence of calcium and the proportion of negative remodeling lesions were comparable among the three groups but the sum arc of calcium was significantly higher in the EA groups. The CS group had a comparable proportion of Absorb and metallic EES (Absorb 50.2% vs. metallic EES 49.8%, p = 0.95) while there was a higher proportion of Absorb

in the CA group (72.3% vs. 27.7%, p<0.01) and an even higher proportion in the EA group (91.8% vs.8.2%, p <0.001). A higher proportion of overlapped implantation was observed in the EA group compared to others (EA, 30.6%; CA, 20.8%; CS, 7.6%, p overall <0.01). The rates of post-dilation were equal among the 3 groups. Details of procedural characteristics are summarized in **online table 1.**

Post-implantation QCA and IVUS measurement

Post-implantation QCA showed that both MLD and acute gain were significantly higher in the CS group compared to both the EA group and CA groups, respectively. The CS group had also a larger mean scaffold/stent area than EA and CA group, respectively **(Table 3).** Nevertheless, the expansion indices were not statistically significant between CS and EA group (CS group 0.75±0.13 vs. EA 0.72±0.16, p=0.10). The change in EI and AI from pre- to post-implantation was lowest in the EA group**.**

Post-implantation, lesions treated with metallic EES were found to be more concentric (metallic EES EI 0.81±0.05 vs. Absorb EI 0.74±0.07, p<0.001) and symmetric (metallic EES AI 0.27±0.06 vs. Absorb AI 0.33±0.08, p<0.001) than lesions treated with Absorb **(online table 2).**

Post-implantation geometrical morphologies and clinical outcomes

One-year clinical follow-up was completed in all patients. The DoCE rates were 8.2%, 6.0% and 1.8% in EA group, CA group and CS groups, respectively (log-rank p=0.04) **(Fig 3).** A higher event rate in the EA group was driven mainly by ID-TLR and partially by non-attributed to non-target vessels MI while the incidences of cardiac death, definite or probable scaffold/stent thrombosis were not significantly different among the groups **(Table 4).** To further investigate the events, a comparison of the symmetric lesions (CS group) vs. asymmetric lesion (CA and EA

group) was performed and the MI rate was noted to be higher in the asymmetric group (symmetric 0.9% vs. asymmetric 5.7%, p-value=0.01). The type of devices implanted was not significantly different in each of the DOCE components **(online table 3)**.

Independent predictors of post-implantation eccentric and asymmetric morphology in a scaffold/stent

Since there was no major imbalance in clinical parameters, the logistic regression analysis were performed exclusively at a lesion level **(online table 4).** The independent determinants of eccentric and asymmetric morphology after scaffold/stent implantation were: i) pre-implantation high lumen EI [OR 0.03(0.00-0.31), p=0.003]; ii) treatment with Absorb [OR 7.29(3.24-16.37), p <0.001]; iii) pre-dilation balloon diameter [OR 2.79(1.38-5.66), p=0.004]; and iv) pre-dilation pressure [OR 1.10(1.01-1.19), p=0.03].

Independent predictors of DoCE after scaffold/stent implantation

The independent predictors for DoCE were i) pre-implantation negative arterial remodeling [HR 3.23(1.04-10.00), p=0.04] and; ii) asymmetry index > 0.3 after implantation [HR 3.58(1.12-11.49), p=0.03]**(Table 5)**. Of note, even when the device type and final minimal lumen area were forced to enter into the multivariate models, the two variables were not significant, moreover, eccentricity was not independently associated with DoCE **(online table 5).** The AI cutoff value of more than 0.3 showed a 81%sensitivity, 51% specificity and an area under the ROC curve (AUC) of 0.65 (p=0.02) while the EI cutoff value of less than 0.7 showed a 62%sensitivity, 20% specificity and AUC of 0.62 (p=0.07)**(Fig 5).**

DISCUSSION

The major findings of this study are the following:

1) The metallic EES had a more symmetric and concentric morphology than the Absorb immediately post-implantation.
2) Pre-implantation lumen EI, treatment with Absorb, pre-dilation balloon diameter and pre-dilation pressure were independent determinants of device eccentricity and asymmetry after implantation.
3) A higher DoCE rate was observed in patients with eccentric and asymmetric lesions compared to patients with concentric and symmetric lesions.
4) The independent predictors of DoCE were pre-implantation negative arterial remodeling and AI > 0.3 after implantation.

Type of device and post-implantation geometrical morphology.

While the pre-implantation EI of the metallic EES arm was lower than in the Absorb arm, lesions treated by the metallic EES became more concentric and symmetric post-implantation. A decreased radial strength of Absorb may be a plausible explanation why the polymeric device could not overcome the lumen eccentricity prior to the implantation.(2) Recently, Foin et al. reported that the 3.0 mm and 3.5 mm scaffold sizes could be expanded up to 1 mm above their nominal diameters without any strut fracture when deployed without an external constraining model. By contrast, when both scaffold sizes were repeated using a constraining silicone lesion model, post-expansion with an NC balloon size 0.5 mm larger than the scaffold nominal sizes could cause strut fractures.[3] Our findings alternatively can be explained by the lower pressure applied during scaffold implantation and by less aggressive post-dilation in the Absorb arm to

avoid scaffold overexpansion. Therefore, it is not surprising to see in the multivariable logistic regression that the use of Absorb when compared to metallic EES has an odd ratio of 7.29 as far as the eccentricity and asymmetry of the lumen post-implantation is concerned.

Asymmetry index is impacting DoCE

Previous trials focused on the optimal device performance and have tried to correlate IVUS parameters and clinical outcomes.(6,18) The expansion index, eccentricity index, minimal stent area have been widely used as indicators of the optimal scaffold/stent expansion while less attention has been paid to the asymmetry index. Although the present study was not powered to determine independent predictors of DoCE, it shows that the AI is an appropriate parameter which relates better to the clinical outcomes than EI. The superiority of AI over EI and expansion index may be explained by the more global assessment of AI which represents the whole treated lesion while EI characterizes only one cross-section of the lesions. The expansion index was calculated using the reference lumen areas that could potentially be influenced by the presence of proximal or distal side branch that makes unavailable the inclusion of either the proximal or distal segments. In previous studies, a correlation between negative arterial remodeling with neointimal hyperplasia(19) could explain the impact of negative arterial remodeling as a determinant of DoCE.

Theoretical relationships between geometrical morphologies and DoCE

Otake et al have reported that eccentricity index assessed by OCT and longer stent length were determinants of thrombus formation following sirolimus-eluting stent implantation at 6 months.(5) The present analyses demonstrated that eccentric and asymmetric lesions irrespective of the type of devices, showed significant increase in DoCE that was mainly driven by a higher

rate of TLR. Pharmacokinetic models have shown that substantial drug concentration inhomogeneities exist for different strut placements and geometry.(17) An inhomogenous strut distribution in eccentric and asymmetric lesions may cause lower local drug concentration, subsequent neointimal hyperplasia and restenosis.

How can we achieve optimal scaffold/stent geometrical morphology?

It remains uncertain whether post-implantation eccentricity and asymmetry of scaffold/stent could be corrected by aggressive post-dilation or this should be avoided by means of aggressive lesions preparation. Previous report from Mattesini and colleagues showed that both Absorb and second-generation DES could achieve similar eccentricity indices, mean stent and mean lumen areas when the procedure was performed under OCT-guidance to achieve optimal expansion by further post-dilation.(20) By contrast, the present study suggested that the initial lesion eccentricity and asymmetry as well as the lesion preparation impact on the post-implantation geometrical morphology. The attempt to correct the eccentricity and asymmetry of the implanted devices during post-dilation may not be effective as the post-dilation procedure was not an independent determinant of eccentricity and asymmetry post-implantation. The discrepancy results of the present study and the previous one may be addressed as follow; i) From Mattesini paper, the operators performed aggressive lesion preparation by using cutting balloon and rotational atherectomy prior to device implantation when appropriate. The aggressive lesions preparation may had corrected the initial eccentricity and asymmetry of the lesions pre-implantation and, therefore, the performance of both devices were comparable; ii) Utilization of larger pre-dilation balloon diameters and high pre-dilation pressure are independent determinants of eccentricity and asymmetry post-implantation in the present study, suggesting that the operators struggled to correct the existing eccentric and asymmetric morphology pre-

implantation. In addition, the presence of calcium and the eccentric and asymmetric appearance of the lesion on IVUS may also have an influence on the operator's decision to select the pre-dilation balloon diameter and to use high pressure; iii) the ABSORB-II trial was designed to compare the efficacy of both Absorb and metallic EES according to the current practice without mandatory imaging guidance and therefore, there were no strict criteria to be achieved during the procedure.(8) Consequently, minimal lumen diameter, acute gain and mean lumen area were significant lower in Absorb than in the metallic DES.(4) Further trials on lesion preparation and imaging guidance to achieve optimal geometrical morphologies and stent/scaffold expansion are of interest to clarify their impact on clinical outcomes.

Limitation

Our study findings may be limited by 1) the low rates of adverse cardiovascular events; 2) the relatively simple lesions characteristics which may limit our ability to generalize our findings, especially to the patients with complex lesions that we commonly see in the daily clinical practice; 3) since the 1-year follow-up of the ABSORB-II trial is purely clinical, we could not evaluate the restenosis process on angiography or IVUS and relate the eccentricity and asymmetry assessment to neointimal hyperplasia.

Conclusion

The scaffold/stent performance is determined by pre-intervention lesion characteristics. The occurrence of DoCE were significantly related to post-implantation eccentricity and asymmetry. Scaffold/stent asymmetry index > 0.3 may be considered as one key IVUS independent determinant of adverse cardiac events.

Reference

1. Onuma Y, Serruys PW. Bioresorbable scaffold: the advent of a new era in percutaneous coronary and peripheral revascularization? Circulation 2011;123:779-97.
2. Ormiston JA, Webber B, Ubod B, Darremont O, Webster MW. An independent bench comparison of two bioresorbable drug-eluting coronary scaffolds (Absorb and DESolve) with a durable metallic drug-eluting stent (ML8/Xpedition). EuroIntervention 2015;11:60-7.
3. Foin N, Lee R, Mattesini A et al. Bioabsorbable vascular scaffold overexpansion: insights from in vitro post-expansion experiments. EuroIntervention 2015;11 [Epub ahead of print].
4. Serruys PW, Chevalier B, Dudek D et al. A bioresorbable everolimus-eluting scaffold versus a metallic everolimus-eluting stent for ischaemic heart disease caused by de-novo native coronary artery lesions (ABSORB II): an interim 1-year analysis of clinical and procedural secondary outcomes from a randomised controlled trial. Lancet 2015;385:43-54.
5. Otake H, Shite J, Ako J et al. Local determinants of thrombus formation following sirolimus-eluting stent implantation assessed by optical coherence tomography. JACC Cardiovascular interventions 2009;2:459-66.
6. de Jaegere P, Mudra H, Figulla H et al. Intravascular ultrasound-guided optimized stent deployment. Immediate and 6 months clinical and angiographic results from the Multicenter Ultrasound Stenting in Coronaries Study (MUSIC Study). European heart journal 1998;19:1214-23.
7. Brugaletta S, Gomez-Lara J, Diletti R et al. Comparison of in vivo eccentricity and symmetry indices between metallic stents and bioresorbable vascular scaffolds: insights from the ABSORB and SPIRIT trials. Catheterization and cardiovascular interventions 2012;79:219-28.
8. Diletti R, Serruys PW, Farooq V et al. ABSORB II randomized controlled trial: a clinical evaluation to compare the safety, efficacy, and performance of the Absorb everolimus-eluting bioresorbable vascular scaffold system against the XIENCE everolimus-eluting coronary stent

system in the treatment of subjects with ischemic heart disease caused by de novo native coronary artery lesions: rationale and study design. American heart journal 2012;164:654-63.

9. Serruys PW, Onuma Y, Ormiston JA et al. Evaluation of the second generation of a bioresorbable everolimus drug-eluting vascular scaffold for treatment of de novo coronary artery stenosis: six-month clinical and imaging outcomes. Circulation 2010;122:2301-12.

10. Gomez-Lara J, Diletti R, Brugaletta S et al. Angiographic maximal luminal diameter and appropriate deployment of the everolimus-eluting bioresorbable vascular scaffold as assessed by optical coherence tomography: an ABSORB cohort B trial sub-study. EuroIntervention : journal of EuroPCR in collaboration with the Working Group on Interventional Cardiology of the European Society of Cardiology 2012;8:214-24.

11. Farooq V, Gomez-Lara J, Brugaletta S et al. Proximal and distal maximal luminal diameters as a guide to appropriate deployment of the ABSORB everolimus-eluting bioresorbable vascular scaffold: a sub-study of the ABSORB Cohort B and the on-going ABSORB EXTEND Single Arm Study. Catheterization and cardiovascular interventions 2012;79:880-8.

12. Mintz GS, Nissen SE, Anderson WD et al. American College of Cardiology Clinical Expert Consensus Document on Standards for Acquisition, Measurement and Reporting of Intravascular Ultrasound Studies (IVUS). A report of the American College of Cardiology Task Force on Clinical Expert Consensus Documents. Journal of the American College of Cardiology 2001;37:1478-92.

13. Inaba S, Mintz GS, Farhat NZ et al. Impact of positive and negative lesion site remodeling on clinical outcomes: insights from PROSPECT. JACC Cardiovascular imaging 2014;7:70-8.

14. Vranckx P, Kint PP, Morel MA, Van Es GA, Serruys PW, Cutlip DE. Identifying stent thrombosis, a critical appraisal of the academic research consortium (ARC) consensus definitions: a lighthouse and as a toe in the water. EuroIntervention 2008;4 Suppl C:C39-44.

15. Applegate RJ, Sacrinty MT, Little WC, Santos RM, Gandhi SK, Kutcher MA. Incidence of coronary stent thrombosis based on academic research consortium definitions. The American journal of cardiology 2008;102:683-8.

16. Mauri L, Hsieh WH, Massaro JM, Ho KK, D'Agostino R, Cutlip DE. Stent thrombosis in randomized clinical trials of drug-eluting stents. The New England journal of medicine 2007;356:1020-9.

17. Hwang CW, Wu D, Edelman ER. Physiological transport forces govern drug distribution for stent-based delivery. Circulation 2001;104:600-5.

18. Chieffo A, Latib A, Caussin C et al. A prospective, randomized trial of intravascular-ultrasound guided compared to angiography guided stent implantation in complex coronary lesions: the AVIO trial. American heart journal 2013;165:65-72.

19. Mintz GS, Tinana A, Hong MK et al. Impact of preinterventional arterial remodeling on neointimal hyperplasia after implantation of (non-polymer-encapsulated) paclitaxel-coated stents: a serial volumetric intravascular ultrasound analysis from the ASian Paclitaxel-Eluting Stent Clinical Trial (ASPECT). Circulation 2003;108:1295-8.

20. Mattesini A, Secco GG, Dall'Ara G et al. ABSORB biodegradable stents versus second-generation metal stents: a comparison study of 100 complex lesions treated under OCT guidance. JACC Cardiovascular interventions 2014;7:741-50.

Table legend

Table 1 Baseline patient characteristics (n=470 patients)

Table 2 Baseline lesion characteristics, pre-implantation angiographic and IVUS measurements (n=506 lesions)

Table 3 Post-implantation angiographic and IVUS measurements (n=506 lesions)

Table 4 Incidence of device oriented clinical endpoints at 1-year follow-up according to the geometrical morphology (n=470 patients)

Table 5 Predictors of device-oriented composite endpoint (DoCE) after scaffold/stent implantation.

Table 1 Baseline patient characteristics (n=470 patients)

	All patients	CS group n = 224	CA group n = 149	EA group n = 97	p-value*
Age, year, mean ± SD	63.5±9.9	63.8±10.0	63.8±9.4	62.4±10.4	0.43
Male sex, n(%)	359(76.4)	176(78.6)	108(72.5)	75(77.3)	0.39
Current smokers, n(%)	113(24.0)	46(20.5)	41(27.5)	26(26.8)	0.24
Diabetes, n(%)	108(23.0)	61(27.2)	29(19.5)	18(18.6)	0.11
Hypertension, n(%)	145(30.9)	158(70.5)	101(67.8)	66(68.0)	0.82
Hyperlipidemia requiring medication, n(%)	338(71.7)	149(66.5)	95(63.8)	64(66.0)	0.88
Previous PCI, n(%)	165(35.1)	75(33.5)	53(35.6)	37(38.1)	0.72
Previous myocardial infarction, n(%)	133(28.3)	58(25.9)	44(29.5)	31(32.0)	0.47
Clinical indication					0.39
Stable angina, n(%)	303(64.5)	148(66.1)	94(63.1)	61(62.9)	
Unstable angina, n(%)	97(20.6)	49(21.9)	32(21.5)	16(16.5)	
Silent ischemia, n(%)	57(12.2)	24(10.7)	18(12.1)	15(15.5)	

Data are shown in mean±SD, or n(%). *comparison among 3 geometrical morphologies

Abbreviation: CS:concentric and symmetric; CA:concentric and asymmetric; EA: eccentric and asymmetric**;** PCI:percutaneous coronary intervention

Table 2 Baseline lesion characteristics, pre-implantation angiographic and IVUS measurements (n=506 lesions)

	CS group n = 249	CA group n = 159	EA group n = 98	p-value Overall	p-value *	p-value †	p-value ‡
Target vessel				0.38			
Left anterior descending	118(47.4)	71(44.7)	45(45.9)				
Left circumflex	56(22.5)	49(30.8)	28(28.6)				
Right coronary artery	75(30.1)	39(24.5)	25(25.5)				
AHA/ACC lesion classification				**0.007**			
A	3(1.2)	1(0.6)	1(1.0)				
B1	157(63.1)	73(45.9)	43(43.9)				
Type B2/C lesion	89(35.7)	85(53.5)	54(55.1)	**<0.001**	**<0.001**	**0.001**	0.79
Moderate/severe calcification	23(9.3)	25(15.7)	19(19.6)	**0.02**	**0.049**	**0.009**	0.43
Pre-implantation Quantitative Coronary Angiography							
Reference vessel diameter, mm	2.66±0.37	2.55±0.40	2.58±0.36	**0.01**	0.01	0.19	0.81
Proximal Dmax, mm	2.86±0.43	2.82±0.49	2.86±0.43	0.71			
Distal Dmax, mm	2.75±0.40	2.64±0.50	2.70±0.42	0.05	0.04	0.63	0.52
Minimal lumen diameter, mm	1.09±0.33	1.04±0.32	1.06±0.27	0.18			
Mean lumen diameter, mm	2.38±0.32	2.26±0.35	2.27±0.33	**<0.001**	**0.001**	**0.02**	0.94
Diameter stenosis,%	58.6±11.7	59.2±11.2	58.8±9.6	0.87			
Lesion length, mm	12.58±5.40	14.61±6.71	15.18±7.49	**<0.001**	**0.004**	**0.002**	0.76
Curvature pre-implantation, cm^{-1}	0.37±0.32	0.33±0.27	0.32±0.25	**0.29**			
Pre-implantation Intravascular Ultrasound							
Lesion length, mm	20.8±6.0	25.5±8.6	25.6±8.4	**<0.001**	**<0.001**	**<0.001**	0.99
Mean lumen area, mm^2	5.10±1.46	4.69±1.36	4.71±1.37	**0.007**	**<0.001**	**0.002**	0.55
Lumen eccentricity index	0.62±0.11	0.60±0.11	0.57±0.11	**<0.001**	0.25	**<0.001**	**0.04**
Lumen asymmetry index	0.59±0.08	0.61±0.07	0.62±0.07	**<0.001**	**0.02**	**0.001**	**0.38**
Mean vessel area, mm^2	12.30±43.45	11.11±3.49	11.47±3.03	**0.002**	**0.002**	0.09	0.69
Minimal vessel area, mm^2	9.68±3.27	7.96±2.99	8.38±2.65	**<0.001**	**<0.001**	**<0.001**	0.55

	CS group n = 249	CA group n = 159	EA group n = 98	p-value Overall	p-value *	p-value †	p-value ‡
Total plaque area, mm^2	7.23±2.73	6.41±2.49	6.75±2.22	**0.009**	**0.007**	0.29	0.57
Remodeling index (mean)	0.93±0.18	0.90±0.22	0.92±0.19	0.57			
Negative remodeling, n(%)	101(41.7)	68(46.3)	40(42.6)	0.68			
Presence of calcium, n(%)	147(60.7)	95(63.8)	64(70.3)	0.31			
Sum arc of calcium	25.2 (0.0-58.3)	32.7 (0.0-70.9)	47.2 (0.0-84.9)	**0.04**	0.33	**0.03**	0.19

Data are shown in n(%) or mean±SD. *CS group vs. CA group; † CS group vs. EA group; ‡ CA group vs. EA group.
Abbreviation: CS:concentric and symmetric; CA:concentric and asymmetric; EA: eccentric and asymmetric

Table 3 Post-implantation angiographic and IVUS measurements (n=506 lesions)

	CS group n = 249	CA group n = 159	EA group n = 98	p-value overall	p-value *	p-value †	p-value ‡
Post-implantation Quantitative Coronary Angiography							
Minimal lumen diameter, mm	2.45±0.33	2.21±0.34	2.25±0.33	**<0.001**	**<0.001**	**<0.001**	.59
Mean lumen diameter, mm	2.80±0.34	2.65±0.36	2.72±0.31	**<0.001**	**<0.001**	.09	.25
Diameter stenosis,%	11.5±5.8	15.5±5.8	16.7±6.9	**<0.001**	**<0.001**	**<0.001**	.23
Acute gain, mm	1.35±0.41	1.17±0.38	1.20±0.33	**<0.001**	**<0.001**	**.003**	.81
Percentage acute gain, %	47.1±12.7	43.6±12.1	42.0±10.6	**<0.001**	**0.02**	**.002**	.57
Post-implantation Intravascular Ultrasound							
Reference lumen area	7.05±2.09	6.19±1.96	6.44±1.78	**<0.001**	**<0.001**	0.11	0.17
Mean vessel area, mm^2	14.22±3.58	12.45±3.54	13.35±3.21	**<0.001**	**<0.001**	.09	0.11
Minimal lumen area, mm^2	5.72±1.43	4.46±1.24	4.87±1.33	**<0.001**	**<0.001**	**<0.001**	**.048**
Mean lumen area, mm^2	6.66±1.54	5.83±1.47	6.20±1.41	**<0.001**	**<0.001**	**.03**	0.13
Minimal scaffold/stent area, mm2	5.73±1.44	4.46±1.24	4.86±1.33	**<0.001**	**<0.001**	**<0.001**	**0.05**
Mean scaffold/stent area, mm^2	6.63±1.53	5.79±1.44	6.18±1.40	**<0.001**	**<0.001**	**.03**	0.10
Scaffold/stent eccentricity index	0.82(0.78;0.84)	0.76(0.73;0.79)	0.66(0.62;0.68)	**<0.001**	**<0.001**	**<0.001**	**<0.001**
Scaffold/stent asymmetry index	0.25(0.22;0.27)	0.34(0.32;0.36)	0.39(0.36;0.44)	**<0.001**	**<0.001**	**<0.001**	**<0.001**
Total plaque area, mm2	7.57±2.50	6.62±2.36	7.15±2.25	**<0.001**	**<0.001**	.32	0.19
Percentage of frame with malapposition,%	2.43±8.48	1.78±5.07	2.60±6.66	0.59			
Mean ISA distance, mm	0.42±0.30	0.37±0.45	0.43±0.27	0.82			
ISA area, mm2	1.03±0.99	1.23±2.46	0.82±0.80	0.67			
Expansion index	0.75±0.13	0.68±0.15	0.72±0.16	**<0.001**	**<0.001**	0.27	0.10
Δ pre- vs. post-implantation EI	-0.18 (-0.26;-0.09)	-0.15 (-0.25;-0.15)	-0.08 (-0.15;0.00)	**<0.001**	**0.03**	**<0.001**	**<0.001**
Δ pre- vs. post-implantation AI	0.35±0.09	0.26±0.08	0.22±0.08	**<0.001**	**<0.001**	**<0.001**	**<0.001**

Data are shown in n(%) or mean±SD or median (interquartile range 1^{st} – 3^{rd}). *CS group vs. CA group; † CS group vs. EA group; ‡ CA group vs. EA group

Abbreviation: CS:concentric and symmetric; CA:concentric and asymmetric; EA: eccentric and asymmetric

Table 4 Incidence of device oriented clinical endpoints at 1-year follow-up according to the geometrical morphology (n=470 patients)

Clinical outcomes	CS group n = 224	CA group n = 149	EA group n = 97	p-value 3 groups	p-value*	p-value†	p-value‡	AI > 0.3 (CA & EA) n=246	p-value¶
Cardiac Death, n(%)	0(0.0)	0(0.0)	0(0.0)	NA	–	–	–	0(0.0)	NA
Myocardial infarction, n(%)				0.13	–	–	–		**0.04**
QMI, n(%)	0(0.0)	1(0.7)	1(1.0)					2(0.8)	
NQMI, n(%)	3(1.3)	8(5.4)	4(4.1)					12(4.9)	
Non-attributed to non-target vessels MI, n(%)	2(0.9)	9(6.0)	5(5.2)	**0.05**	**0.01**	**0.046**	0.77	14(5.7)	**0.01**
Peri-procedural MI, n(%)	4(1.8)	7(4.7)	4(4.1)	0.25	–	–	–	11(4.5)	0.09
Ischemia Driven TLR, n(%)	2(0.9)	0(0.0)	5(5.2)	**<0.001**	0.25	**0.02**	**0.005**	5(2.0)	0.31
Composite of cardiac death, target vessel MI and clinically indicated target lesion revascularization (DoCE), n(%)	4(1.8)	9(6.0)	8(8.2)	**0.02**	**0.03**	**0.005**	0.51	17(6.9)	**0.007**
Composite of cardiac death, all MI and clinically indicated target lesion revascularization (MACE) , n(%)	5(2.2)	9(6.0)	8(8.2)	**0.04**	0.058	**0.01**	0.51	17(6.9)	**0.02**
Composite of all death, all MI and all revascularization (PoCE), n(%)	10(4.5)	13(8.7)	8(8.2)	0.20	–	–	–	21(8.5)	0.08
Definite/probable ST, n(%)	0(0.0)	1(0.7)	2(2.1)	0.10	–	–	–	3(1.2)	0.09
-Definite ST, n(%)	0(0.0)	0(0.0)	2(2.1)$					2(0.8)	
-Probable ST, n(%)	0(0.0)	1(0.7)#	0(0.0)					1(0.4)	

Data are shown in n(%).*CS group vs. CA group; † CS group vs. EA group; ‡ CA group vs. EA group; ¶ CS group vs. lesions with asymmetry index > 0.3 (combination of CA and EA group); $ event occur at 0 and 2 days post-implantation; # event occur 335 days post-implantation.

Abbreviation: CS:concentric and symmetric; CA:concentric and asymmetric; EA: eccentric and asymmetric; QMI: Q-wave myocardial infarction; NQMI: non-Q-wave myocardial infarction; TLR: target lesion revascularization; MI: myocardial infarction; MACE: major adverse cardiac events; DoCE: device oriented composite end point; PoCE: patient oriented composite end point; ST: scaffold thrombosis

Table 5 Predictors of device-oriented composite endpoint (DoCE) after scaffold/stent implantation.

	Univariate logistic regression		Multivariate model	
	HR (95%)	**p Value**	**HR (95%)**	**p Value**
I. Patient-related factors				
Age (yrs)	1.02(0.97-1.06)	0.46	–	–
Male	0.53(0.15-1.82)	0.31	–	–
Current smoker	1.09(0.79-1.50)	0.62	–	–
Hypertension requiring treatment	0.94(0.59-1.49)	0.80	–	–
Dyslipidemia requiring treatment	0.79(0.50-1.25)	0.31	–	–
Any diabetes mellitus	0.99(0.76-1.28)	0.93	–	–
Unstable Angina	0.90(0.29-2.74)	0.85	–	–
II. Lesion-related factors assessed by QCA and IVUS pre-implantation				
QCA:type B2/C lesions	0.72(0.30-1.74)	0.47	–	–
QCA:obstruction length per mm	0.95(0.87-1.04)	0.26	–	–
QCA:percentage diameter stenosis†	0.96(0.93-1.00)	0.07	0.96(0.92-1.00)	0.07
QCA:reference diameter per mm	0.50(0.19-1.36)	0.18	–	–
QCA:curvature per cm^{-1}	0.71(0.25-2.01)	0.52	–	–
IVUS:lesion length to MLA ratio†	1.06(0.99-1.13)	0.06	1.02(0.92-1.12)	0.76
IVUS:sum arc of calcium at MLA frame	1.00(0.99-1.00)	0.34	–	–
IVUS:minimal vessel area per mm^2	1.01(0.87-1.17)	0.89	–	–
IVUS:minimal lumen area per mm^2	0.65(0.26-1.65)	0.36	–	–
IVUS:lumen eccentricity index	0.09(0.00-3.57)	0.19	–	–
IVUS:lumen asymmetry index¶	1.13(0.63-2.03)	0.69	–	–
IVUS:total plaque area per mm^2	1.04(0.88-1.24)	0.62	–	–
IVUS:lesion with negative remodeling†	3.26(1.08-9.86)	0.04	3.23(1.04-10.00)	**0.04**
III. Procedure-related factors				
Treatment with Absorb	1.72(0.62-4.79)	0.29	–	–
Pre-dilation balloon diameter per mm	1.30(0.38-4.45)	0.67	–	–
Pre-dilation balloon pressure per atm	1.07(0.93-1.22)	0.38	–	–
Device diameter per mm	0.83(0.19-3.54)	0.80	–	–
Total stent length per mm†	1.05(1.02-1.08)	0.002	1.03(0.99-1.07)	0.08
Overlapping implantation	3.33(1.33-8.34)	0.01	–	–
Post-dilation performed	1.01(0.41-2.49)	0.98	–	–
Post-dilation balloon diameter per mm	1.33(0.37-4.79)	0.66	–	–
Post-dilation balloon length per atm	0.99(0.89-1.08)	0.76	–	–
IV. Post-implantation result				
QCA:percentage diameter stenosis	0.99(0.93-1.06)	0.80	–	–
QCA:percentage of acute gain	0.98(0.94-1.01)	0.19	–	–
QCA:minimal lumen diameter per mm	0.49(0.13-1.81)	0.28	–	–
IVUS:minimum stent area per mm^2	0.85(0.61-1.16)	0.30	–	–
IVUS:mean stent area per mm^2	0.91(0.67-1.22)	0.52	–	–
IVUS:scaffold/stent eccentricity index	0.01(0.00-3.02)	0.12	–	–
IVUS:scaffold/stent asymmetry index¶	1.74(1.03-2.93)	0.04	–	–

	Univariate logistic regression		Multivariate model	
	HR (95%)	**p Value**	**HR (95%)**	**p Value**
IVUS:scaffold/stent expansion index	0.31(0.01-8.91)	0.49	—	—
IVUS:total plaque area per mm^2	1.02(0.85-1.26)	0.86	—	—
Being classified in EA group	2.49(1.00-6.19)	0.05	—	—
Asymmetry index > 0.3 after implantation†	4.08(1.35-12.33)	0.01	3.58(1.12-11.49)	**0.03**

¶ per 0.1 increase; †variables that were selected into multivariable model.

Abbreviation: HR:Hazard ratio; QCA:quantitative coronary angiography; IVUS:intravascular ultrasound; MLA:minimal lumen area; EA:eccentric and asymmetric

Figure legend

Figure 1. Method used to calculate geometrical IVUS parameters after device implantation (A) and example of 3 geometrical morphologies after treated with Absorb and metallic DES

Abbreviations: SD = scaffold/stent diameter; DES = drug eluting stent

Figure 2. Study flow chart

Abbreviations: EES=everolimus-eluting stent; AI=asymmetry index; EI=eccentricity index; IVUS=intravascular ultrasound

Figure 3. Distribution of geometrical morphology according to type of devices in ABSORB II-trial and the incidence of DoCE over 1 year follow-up

Abbreviations: CS=concentric and symmetric group; CA=concentric and asymmetric group; EA=eccentric and asymmetric group; DoCE=device oriented cardiovascular endpoint

Figure 4 Cumulative curves of sensitivity and specificity of scaffold/stent asymmetry index, minimum scaffold/stent eccentricity index and receiver operating characteristic curves of scaffold/stent asymmetry index and 1 minus minimum scaffold/stent eccentricity index to predict device oriented cardiovascular endpoint

Panel A and B showed cumulative curves of sensitivity (magenta line) and specificity (red line) of scaffold/stent asymmetry index >0.3 and minimum scaffold/stent eccentricity index <0.7, respectively.

Panel C demonstrated ROC curves of scaffold/stent asymmetry index (green line) and 1 minus minimal scaffold/stent eccentricity index (blue line).

Abbreviations: AI=asymmetry index; AUC=area under curve; CI=confident interval; EI=eccentricity index

Figure 1

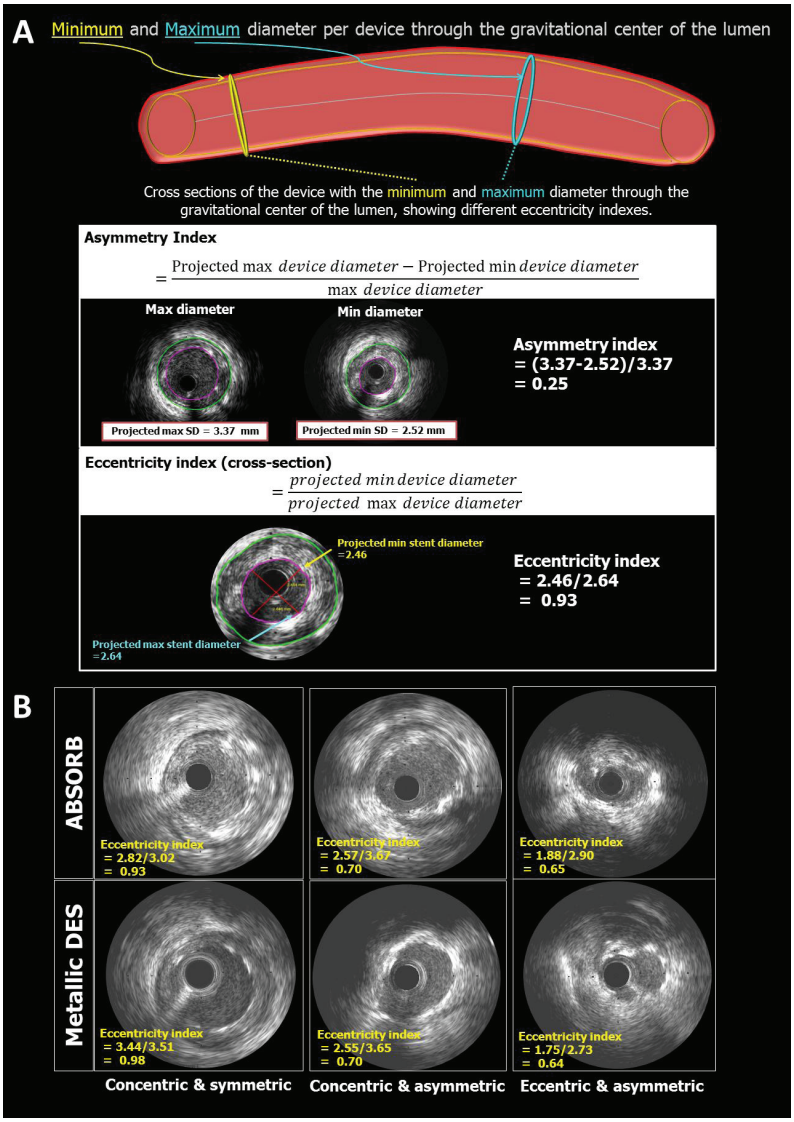
A
Minimum and Maximum diameter per device through the gravitational center of the lumen
Cross sections of the device with the minimum and maximum diameter through the gravitational center of the lumen, showing different eccentricity indexes.
Asymmetry Index
= Projected max device diameter − Projected min device diameter / max device diameter
Max diameter
Min diameter
Projected max SD = 3.37 mm
Projected min SD = 2.52 mm
Asymmetry index
= (3.37-2.52)/3.37
= 0.25
Eccentricity index (cross-section)
= projected min device diameter / projected max device diameter
Projected min stent diameter =2.46
Projected max stent diameter =2.64
Eccentricity index
= 2.46/2.64
= 0.93
B
ABSORB
Metallic DES
Eccentricity index = 2.82/3.02 = 0.93
Eccentricity index = 2.57/3.67 = 0.70
Eccentricity index = 1.88/2.90 = 0.65
Eccentricity index = 3.44/3.51 = 0.98
Eccentricity index = 2.55/3.65 = 0.70
Eccentricity index = 1.75/2.73 = 0.64
Concentric & symmetric
Concentric & asymmetric
Eccentric & asymmetric

Figure 2

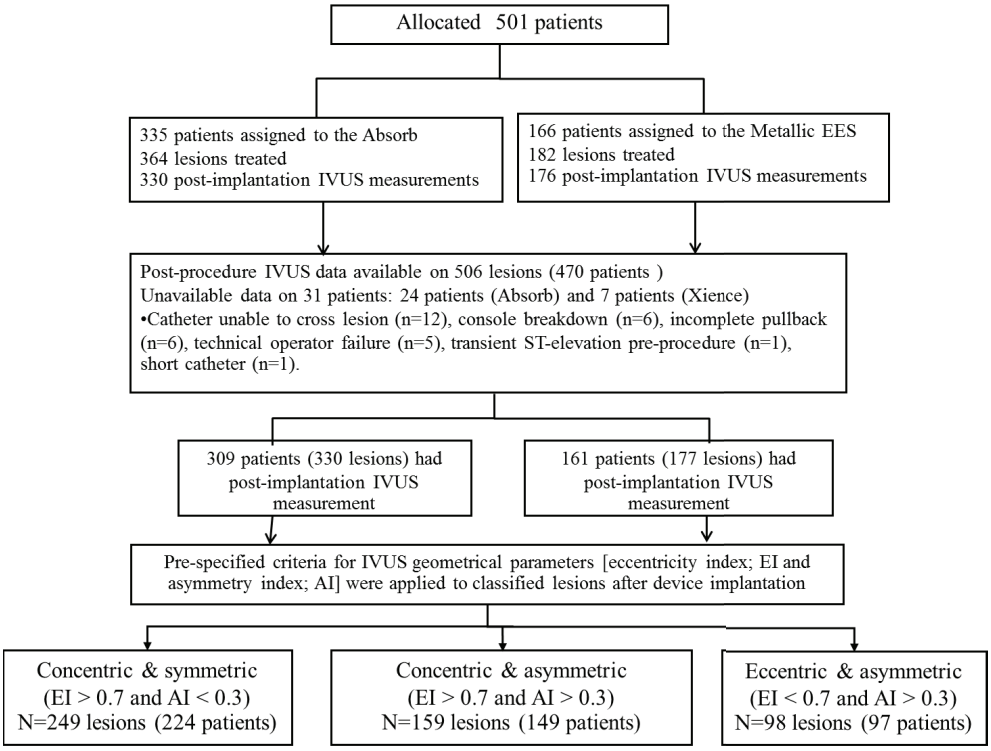
Allocated 501 patients
335 patients assigned to the Absorb
364 lesions treated
330 post-implantation IVUS measurements
166 patients assigned to the Metallic EES
182 lesions treated
176 post-implantation IVUS measurements
Post-procedure IVUS data available on 506 lesions (470 patients)
Unavailable data on 31 patients: 24 patients (Absorb) and 7 patients (Xience)
•Catheter unable to cross lesion (n=12), console breakdown (n=6), incomplete pullback (n=6), technical operator failure (n=5), transient ST-elevation pre-procedure (n=1), short catheter (n=1).
309 patients (330 lesions) had post-implantation IVUS measurement
161 patients (177 lesions) had post-implantation IVUS measurement
Pre-specified criteria for IVUS geometrical parameters [eccentricity index; EI and asymmetry index; AI] were applied to classified lesions after device implantation
Concentric & symmetric
(EI > 0.7 and AI < 0.3)
N=249 lesions (224 patients)
Concentric & asymmetric
(EI > 0.7 and AI > 0.3)
N=159 lesions (149 patients)
Eccentric & asymmetric
(EI < 0.7 and AI > 0.3)
N=98 lesions (97 patients)

Figure 3

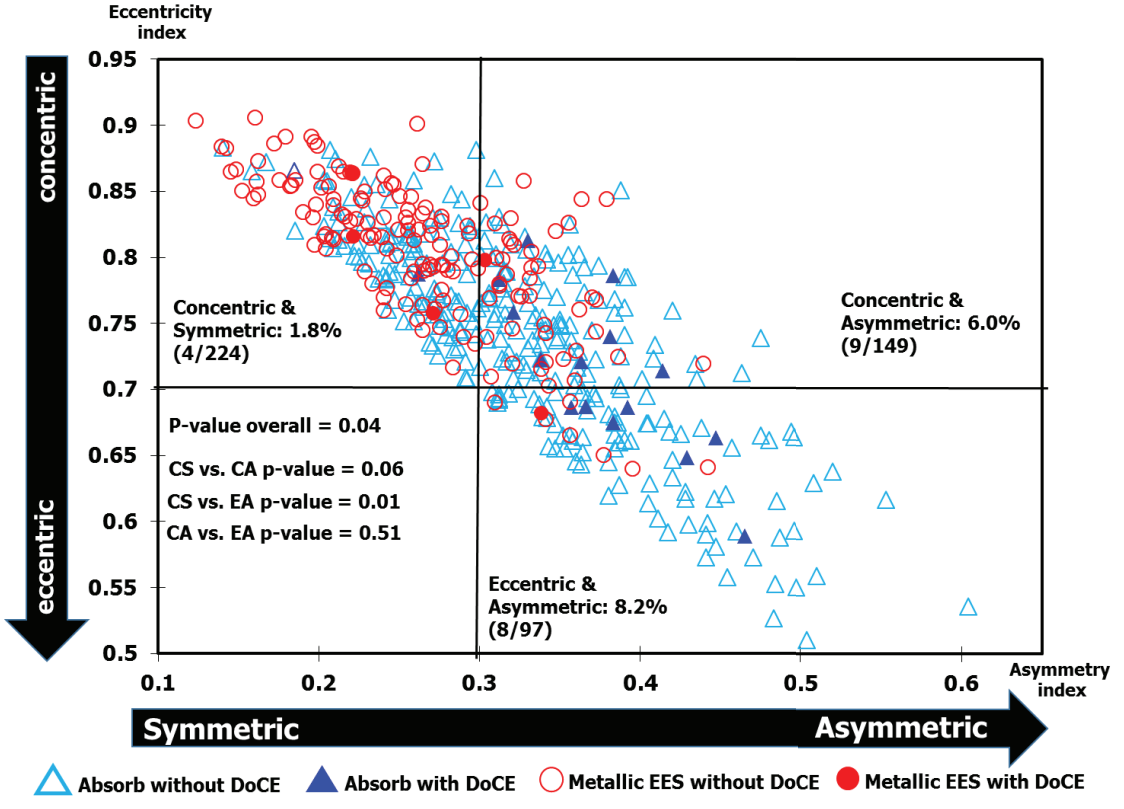
Eccentricity index
concentric
eccentric
0.95
0.9
0.85
0.8
0.75
0.7
0.65
0.6
0.55
0.5
Concentric & Symmetric: 1.8% (4/224)
Concentric & Asymmetric: 6.0% (9/149)
P-value overall = 0.04
CS vs. CA p-value = 0.06
CS vs. EA p-value = 0.01
CA vs. EA p-value = 0.51
Eccentric & Asymmetric: 8.2% (8/97)
0.1
0.2
0.3
0.4
0.5
0.6
Asymmetry index
Symmetric
Asymmetric
Absorb without DoCE
Absorb with DoCE
Metallic EES without DoCE
Metallic EES with DoCE

Figure 4

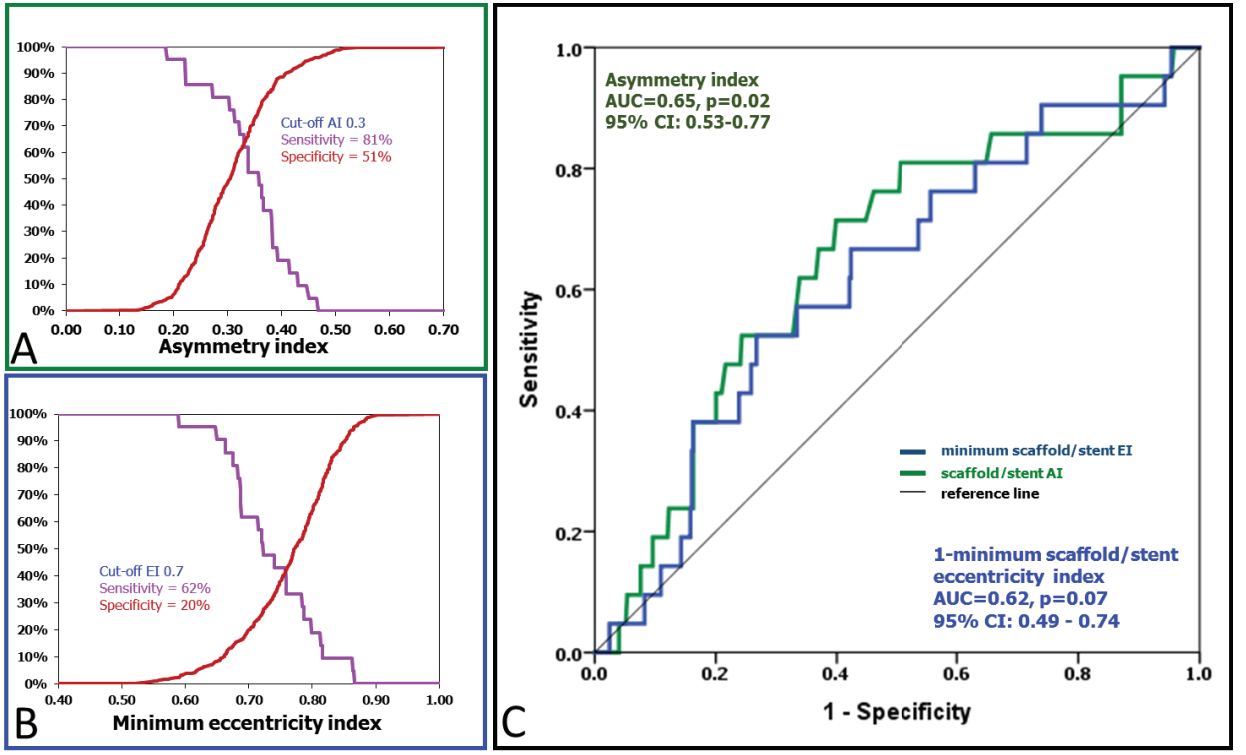
100%
90%
80%
70%
60%
50%
40%
30%
20%
10%
0%
0.00 0.10 0.20 0.30 0.40 0.50 0.60 0.70
Asymmetry index
Cut-off AI 0.3
Sensitivity = 81%
Specificity = 51%
A
100%
90%
80%
70%
60%
50%
40%
30%
20%
10%
0%
0.40 0.50 0.60 0.70 0.80 0.90 1.00
Minimum eccentricity index
Cut-off EI 0.7
Sensitivity = 62%
Specificity = 20%
B
Sensitivity
1 - Specificity
0.0 0.2 0.4 0.6 0.8 1.0
Asymmetry index
AUC=0.65, p=0.02
95% CI: 0.53-0.77
minimum scaffold/stent EI
scaffold/stent AI
reference line
1-minimum scaffold/stent
eccentricity index
AUC=0.62, p=0.07
95% CI: 0.49 - 0.74
C

1.6 Clinical and procedural outcomes from a randomized controlled trial

A bioresorbable everolimus-eluting scaffold versus a metallic everolimus-eluting stent for ischaemic heart disease caused by de-novo native coronary artery lesions (ABSORB II): an interim 1-year analysis of clinical and procedural secondary outcomes from a randomised controlled trial.

Lancet. 2015 Jan 3;385(9962):43-54.
[Original research paper, IF 39.21]

Serruys PW, Chevalier B, Dudek D, Cequier A, Carrié D, Iniguez A, Dominici M, van der Schaaf RJ, Haude M, Wasungu L, Veldhof S, Peng L, Staehr P, Grundeken MJ, **Ishibashi Y**, Garcia-Garcia HM, Onuma Y.

A bioresorbable everolimus-eluting scaffold versus a metallic everolimus-eluting stent for ischaemic heart disease caused by de-novo native coronary artery lesions (ABSORB II): an interim 1-year analysis of clinical and procedural secondary outcomes from a randomised controlled trial

Patrick W Serruys, Bernard Chevalier, Dariusz Dudek, Angel Cequier, Didier Carrié, Andres Iniguez, Marcello Dominici, René J van der Schaaf, Michael Haude, Luc Wasungu, Susan Veldhof, Lei Peng, Peter Staehr, Maik J Grundeken, Yuki Ishibashi, Hector M Garcia-Garcia, Yoshinobu Onuma

Summary

Background Despite rapid dissemination of an everolimus-eluting bioresorbable scaffold for treatment for coronary artery disease, no data from comparisons with its metallic stent counterpart are available. In a randomised controlled trial we aimed to compare an everolimus-eluting bioresorbable scaffold with an everolimus-eluting metallic stent. Here we report secondary clinical and procedural outcomes after 1 year of follow-up.

Methods In a single-blind, multicentre, randomised trial, we enrolled eligible patients aged 18–85 years with evidence of myocardial ischaemia and one or two de-novo native lesions in different epicardial vessels. We randomly assigned patients in a 2:1 ratio to receive treatment with an everolimus-eluting bioresorbable scaffold (Absorb, Abbott Vascular, Santa Clara, CA, USA) or treatment with an everolimus-eluting metallic stent (Xience, Abbott Vascular, Santa Clara, CA, USA). Randomisation was stratified by diabetes status and number of planned target lesions. The co-primary endpoints of this study are vasomotion (change in mean lumen diameter before and after nitrate administration at 3 years) and difference between minimum lumen diameter (after nitrate administration) after the index procedure and at 3 years. Secondary endpoints were procedural performance assessed by quantitative angiography and intravascular ultrasound; composite clinical endpoints based on death, myocardial infarction, and coronary revascularisation; device and procedural success; and angina status assessed by the Seattle Angina Questionnaire and exercise testing at 6 and 12 months. Cumulative angina rate based on adverse event reporting was analysed post hoc. This trial is registered at ClinicalTrials.gov, number NCT01425281.

Findings Between Nov 28, 2011, and June 4, 2013, we enrolled 501 patients and randomly assigned them to the bioresorbable scaffold group (335 patients, 364 lesions) or the metallic stent group (166 patients, 182 lesions). Dilatation pressure and balloon diameter at the highest pressure during implantation or postdilatation were higher and larger in the metallic stent group, whereas the acute recoil post implantation was similar (0·19 mm for both, p=0·85). Acute lumen gain was lower for the bioresorbable scaffold by quantitative coronary angiography (1·15 mm *vs* 1·46 mm, p<0·0001) and quantitative intravascular ultrasound (2·85 mm² *vs* 3·60 mm², p<0·0001), resulting in a smaller lumen diameter or area post procedure. At 1 year, however, cumulative rates of first new or worsening angina from adverse event reporting were lower (72 patients [22%] in the bioresorbable scaffold group *vs* 50 [30%] in the metallic stent group, p=0·04), whereas performance during maximum exercise and angina status by SAQ were similar. The 1-year composite device orientated endpoint was similar between the bioresorbable scaffold and metallic stent groups (16 patients [5%] *vs* five patients [3%], p=0·35). Three patients in the bioresorbable scaffold group had definite or probable scaffold thromboses (one definite acute, one definite sub-acute, and one probable late), compared with no patients in the metallic stent group. There were 17 (5%) major cardiac adverse events in the bioresorbable scaffold group compared with five (3%) events in the metallic stent group, with the most common adverse events being myocardial infarction (15 cases [4%] *vs* two cases [1%], respectively) and clinically indicated target-lesion revascularisation (four cases [1%] *vs* three cases [2%], respectively).

Interpretation The everolimus-eluting bioresorbable scaffold showed similar 1-year composite secondary clinical outcomes to the everolimus-eluting metallic stent.

Funding Abbott Vascular.

Lancet 2015; 385: 43–54

Published **Online** September 14, 2014 http://dx.doi.org/10.1016/S0140-6736(14)61455-0

See **Comment** page 10

International Centre for Cardiovascular Health, Imperial College, London, UK (P W Serruys MD); **Institut Jacques Cartier, Massy, France** (B Chevalier MD); **Jagiellonian University, Department of Cardiology and Cardio Vascular Interventions, University Hospital, Krakow, Poland** (D Dudek MD); **Bellvitge University Hospital, Barcelona, Spain** (A Cequier MD); **Hopital de Rangueil, Toulouse, France** (D Carrié MD); **Hospital de Meixoeiro, Vigo, Spain** (A Iniguez MD); **S Maria University Hospital, Terni, Italy** (M Dominici MD); **OLVG, Amsterdam, Netherlands** (R J van der Schaaf MD); **Städtisches Kliniken Neuss Lukaskrankenhaus GmbH, Neuss, Germany** (M Haude MD); **Abbott Vascular, Diegem, Belgium** (L Wasungu PhD, S Veldhof RN); **Abbott Vascular, Santa Clara, CA, USA** (L Peng MSc, P Staehr MD); **Academic Medical Centre, Amsterdam, Netherlands** (M J Grundeken MD); **Erasmus MC, Rotterdam, Netherlands** (Y Ishibashi MD, H M Garcia-Garcia MD, Y Onuma MD); **and Cardialysis BV, Rotterdam, Netherlands** (H M Garcia-Garcia, Y Onuma)

Correspondence to: Prof P W Serruys, Thoraxcenter, Ba-583, 's Gravendijkwal 230, 3015 CE Rotterdam, Netherlands **patrick.w.j.c.serruys@gmail.com**

Introduction

The implantation of a bioresorbable scaffold is a new approach that provides transient vessel support with drug delivery capability, potentially without the limitations of permanent metallic implants.[1,2] By liberating the coronary artery from the metallic caging, the vessel recovers pulsatility and becomes responsive to shear stress and physiological cyclic strain.[3–5] The vessel wall, theoretically,

can remodel and exhibit plaque reduction in response to pharmacological treatment and physiological stimuli. The potential of this technology has been shown in some studies with up to 3-year follow-up with several imaging modalities.[6–11]

The use of bioresorbable scaffolds has several challenges that justify careful assessment of this technology. First, the mechanical property of the polymeric scaffold should match that of metallic stents; the acute recoil of the scaffold has previously been reported to be similar to that noted with an equivalent device in metal.[12] The mechanical integrity and the absence of recoil has to be maintained for 6 months, during which time the biological process of restenosis (consisting of neointimal formation and constrictive remodelling) fully subsides, therefore not justifying a permanent prosthesis beyond this time.[13] The second challenge to be taken into consideration is that the bioresorption of the polymeric scaffold should not trigger an inflammatory reaction that could result in late renarrowing of the vessel. Over time, the polymer is replaced by a provisional matrix made of proteoglycan that evolves into de-novo connective tissue.[14] Eventual late enlargement of the scaffold and lumen has been documented at 2–3 years, compensating for the intraluminal growth of the neointima.[15]

In a randomised, single-blind, active-controlled trial (the ABSORB II study), we aimed to compare a bioresorbable everolimus-eluting scaffold with a metallic everolimus-eluting stent to treat ischaemic heart disease. Because the bioresorbable scaffold has been commercially available since August, 2012, and has been widely and rapidly disseminated in the absence of comparative data from randomised trials, the steering committee and trial funder decided to report secondary clinical and procedural endpoints at 1 year. Hence, we report secondary endpoints for clinical, procedural, anginal, and disease-related quality-of-life outcomes.

Methods

Study design and participants

The ABSORB II trial is a prospective, randomised, active-controlled, single-blind, parallel two-group, multicentre clinical trial. Eligible participants were aged 18–85 years with evidence of myocardial ischaemia, were suitable for coronary artery bypass graft surgery, and had one or two de-novo native lesions in different epicardial vessels. Patients with acute myocardial infarction before the procedure without normalised cardiac enzymes, evidence of ongoing acute myocardial infarction before the procedure, unstable arrhythmia, or left ventricular ejection fraction less than 30% were excluded. Full inclusion and exclusion criteria are provided in the appendix.

See Online for appendix

A data safety monitoring board reviewed the cumulative safety data from the trial at given intervals for the purpose of safeguarding the interests of the participants. All patients provided informed consent before being included in the trial and all participating sites received medical ethics committee approval for the study.

Randomisation and masking

We randomly assigned patients in a 2:1 ratio to receive either treatment with an everolimus-eluting bioresorbable scaffold (Absorb, Abbott Vascular, Santa Clara, CA, USA) or treatment with an everolimus-eluting metallic stent (Xience, Abbott Vascular, Santa Clara, CA, USA). Randomisation was by a centralised interactive voice–web-based service and was stratified by diabetes status (diabetes *vs* no diabetes) and number of target lesions (single *vs* dual). Patients were masked to treatment allocation (not informed of type of device implanted) for the duration of trial and study staff were instructed not to reveal treatment allocation to patients or referring physicians. Study investigators and physicians doing the procedure were not masked to treatment allocation.

Procedures

The trial protocol allowed the treatment of up to two de-novo native coronary artery lesions, each located in different major epicardial vessels, with a maximum lumen diameter between 2·25 mm and 3·8 mm as assessed by online quantitative coronary angiography and a maximum lesion length of 48 mm. The methods of quantitative coronary angiography, angiographic acute recoil analysis, and quantitative intravascular ultrasound have been previously reported.[12,16] All patients underwent coronary angiography, intravascular ultrasound, and intravascular ultrasound–virtual histology imaging before and after device implantation.

Patients had clinical follow-up at 30 days, 180 days, and 1 year. All patients and treating physicians were asked to adhere to the European Society of Cardiology Guidelines in terms of tobacco usage, exercise, healthy food intake, maintenance of an adequate weight (body-mass index) and waist circumference, achievement of target blood lipid concentrations, and blood pressure control.[17,18] A patient diary was provided to facilitate collection of these data. We collected Seattle Angina Questionnaires at preimplantation, 180 days, and 1-year follow-ups. Exercise testing, including ECG recording, was done at 180 days and 1 year.[19,20] ST-T depression of 0·1 mV at maximum exercise or chest pain during exercise classified as indicative of ischaemia.[17,21] Recurrent or worsening angina as diagnosed by the site was captured on adverse event forms including or excluding the angina episodes that occurred during index admission to hospital or in the 7 days after index procedure (whichever came first).

Three types of biomarkers (creatine kinase, creatine kinase-MB, and troponin I) were simultaneously sampled between 6 h after the procedure and discharge, and were analysed in a central core laboratory (ICON, Dublin, Ireland). When additional local laboratory

values were available, the highest value per reference was taken into consideration for adjudication of myocardial infarction.

Outcomes

The two co-primary endpoints were vasomotion (assessed by change in mean lumen diameter before and after nitrate administration at 3 years by quantitative angiography) and minimum lumen diameter at 3 years after nitrate administration minus minimum lumen diameter postprocedure after nitrate administration (assessed by quantitative angiography). These outcomes will be analysed after 3 years of follow-up.

Intravascular ultrasound secondary endpoints were quantitative analysis of lumen area, plaque area, scaffold area, and neointima area.

Outcomes measured for composite clinical secondary endpoints were death (cardiac *vs* vascular *vs* non-cardiovascular), myocardial infarction (Q-wave *vs* non-Q-wave; attributable *vs* non-attributable to target vessel), target-lesion revascularisation, target-vessel revascularisation, non-target-vessel revascularisation, and all coronary revascularisations (all revascularisations clinically indicated *vs* non-clinically indicated). Composite clinical secondary endpoints were death plus all myocardial infarction; cardiac death plus myocardial infarction attributable to target vessel plus clinically indicated target-lesion revascularisation (ie, target-lesion failure; device-oriented composite endpoint); cardiac death plus all myocardial infarction plus clinically indicated target-lesion revascularisation (ie, major adverse cardiac events); cardiac death plus all myocardial infarction plus clinically indicated target-vessel revascularisation (ie, target-vessel failure); and death plus all myocardial infarction plus all revascularisation (patient-oriented composite endpoint). Myocardial infarction per protocol was defined as the development of new pathological Q-wave or creatine kinase rise of two or more times of upper limit of normal accompanied by creatine kinase-MB rise.[6,8,16]

We also assessed scaffold or stent thrombosis timing (acute *vs* sub-acute *vs* late *vs* very late) and evidence (definite *vs* probable *vs* possible) and acute success (device success and procedural success). We defined device success as successful delivery and deployment of the first study scaffold or stent at the intended target lesion and successful withdrawal of the delivery system with attainment of final in-scaffold or in-stent residual stenosis of less than 50% by quantitative coronary angiography.[16] We defined procedural success as device success without the occurrence of cardiac death, target-vessel myocardial infarction, or repeat target-lesion revascularisation during the hospital stay (maximum of 7 days).

Statistical analyses

The sample size for the trial was calculated on the basis of the first co-primary endpoint (superiority for vasomotion). Assuming a two-tailed superiority *t* test, a 2:1 randomisation ratio, an α of 0·05, and true changes in mean lumen diameter of 0·07 mm for the bioresorbable scaffold and 0 mm for the metallic stent (SD 0·20 for both), we estimated that 260 lesions in the bioresorbable scaffold group and 130 lesions in the metallic stent group would be needed for 90% power. Allowing for a 29% attrition rate and 10% of patients with dual lesions, we estimated that 334 patients in the in the bioresorbable scaffold group and 167 patients in the metallic stent group would be needed.

The endpoint analyses presented in this report were by intention to treat. Binary variables are summarised with counts and percentages. For exact 95% CIs, we used the Clopper-Pearson method. Continuous variables are summarised with means and SDs. For 95% CIs for the mean, we used the Gaussian approximation. χ^2 or Fisher's exact test was used to compare binary variables, and Student's *t*-test or non-parametric test was used to compare continuous variables. All p values in this 1-year report are for descriptive purposes and no formal hypothesis testing was done. The power calculations were done with PASS version 11 and statistical analyses were done with SAS software version 9.2.

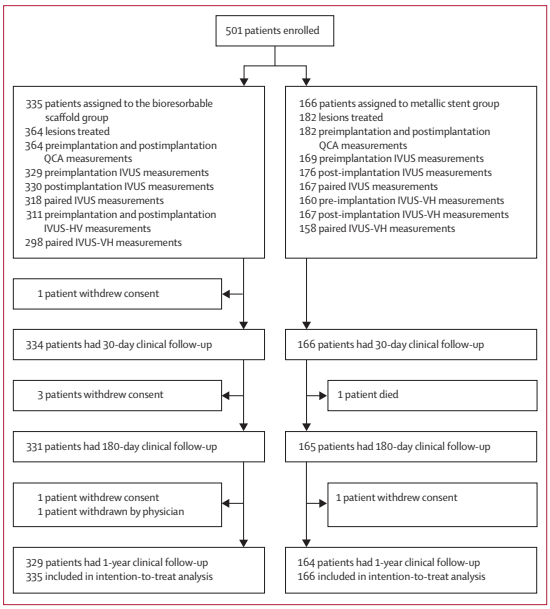

Figure 1: **Trial profile**

This trial is registered at ClinicalTrials.gov, number NCT01425281.

Role of the funding source

The study funder was involved in study design, data collection, data analysis, data interpretation, and writing of this report. The corresponding author had full access to all the data in the study and had final responsibility for the decision to submit for publication.

	Bioresorbable scaffold group	Metallic stent group
Patients		
Number of patients	335	166
Age in years	61·5 (10·0)	60·9 (10·0)
Sex		
Men	253/335 (76%)	132/166 (80%)
Women	82/335 (24%)	34/166 (20%)
Body-mass index (kg/m^2)	27·9 (4·1)	28·1 (3·7)
Current tobacco use	79/335 (24%)	36/166 (22%)
Hypertension (history or needing medication)	231/335 (69%)	119/166 (72%)
Dyslipidaemia (history or needing medication)	252/335 (75%)	133/166 (80%)
LDL cholesterol <2 mmol/L (80 mg/dL)	113/324 (35%)	51/160 (32%)
All diabetes	80/332 (24%)	40/166 (24%)
Diabetes mellitus treated with insulin	22/80 (28%)	14/40 (35%)
Family history of premature coronary artery disease	112/306 (37%)	64/155 (41%)
Previous cardiac intervention in target vessel	14/120 (12%)	5/56 (9%)
Previous myocardial infarction	93/335 (28%)	48/166 (29%)
Recent myocardial infarction with normalised enzyme	11/335 (3%)	3/166 (2%)
Stable angina	214/335 (64%)	107/166(64%)
Stable angina CCS III or IV	47/214 (22%)	24/107 (22%)
Unstable angina	68/335 (20%)	37/166 (22%)
Unstable angina Braunwald Class III	16/68 (24%)	10/37 (27%)
Silent ischaemia	42/335 (13%)	19/166 (11%)
Single-vessel disease	278/335 (83%)	141/166 (85%)
Use of antianginal drugs at baseline		
β blockers	245/335 (73%)	117/166 (70%)
Calcium channel blocker	86/335 (26%)	41/166 (25%)
Nitrate	82/335 (24%)	54/166 (33%)
Dual antiplatelet therapy at 30 days	329/332 (99%)	166/166 (100%)
Target vessel		
Number of lesions	364	182
Left anterior descending artery	163/364 (45%)	84/182 (46%)
Left circumflex artery	106/364 (29%)	42/182 (23%)
Right coronary artery	95/364 (26%)	56/182 (31%)
Two or more lesions treated	29/335 (9%)	16/166 (10%)
Calcification (moderate or severe)	46/363(13%)	28/184 (15%)
ACC/AHA lesion class		
A	5/363 (1%)	1/180 (1%)
B1	193/363 (53%)	90/180 (50%)
B2	159/363 (44%)	87/180 (48%)
C	6/363 (2%)	2/180 (1%)

Data are n/N (%), in which N refers to number of patients with data available, or mean (SD) unless otherwise stated.

Table 1: **Patient and lesion baseline characteristics**

Results

Between Nov 28, 2011, and June 4, 2013, we enrolled 501 patients from 46 sites in Europe and New Zealand, and randomly assigned them to the bioresorbable scaffold group (335 patients) or the metallic stent group (166 patients; figure 1).

Table 1 shows patient demographics, risk factors, and use of antianginal drugs and antiplatelet therapy at baseline. The prevalence of diabetes was 24%, with more than a quarter of these patients being insulin dependent. Roughly 20% of patients presented with unstable angina. More than 80% of patients had single-vessel disease. The complexity of the treated lesions is described according to the AHA/ACC classification.[22]

At 1 year, 329 (98%) patients in the bioresorbable scaffold group and 164 (99%) patients in the metallic stent group were in clinical follow-up. In the bioresorbable scaffold group, six patients withdrew consent by 1 year. In the metallic stent group, one patient died and one patient withdrew consent.

All lesions were predilated with the exception of two lesions in the metallic stent group (table 2). For quantitative coronary angiography, pre-procedural measurements did not differ between the two groups, whereas for quantitative intravascular ultrasound, both pre-procedural vessel area and plaque area were larger in the metallic stent group than in the bioresorbable scaffold group. Rates of clinical device success and clinical procedural success were similar in the two treatment groups (table 2). The nominal size of devices used and the acute recoil after device implantation were also similar between treatment groups. Balloon dilatation after device implantation was done in a similar proportion of patients. However, dilatation pressure was significantly higher and balloon diameter at the highest pressure during implantation or postdilatation of the device was significantly larger in the metallic stent group. Therefore, the acute gain in minimum lumen diameter (by quantitative coronary angiography) and minimum lumen area (by quantitative intravascular ultrasound), and the final minimum lumen diameter and minimum lumen area, were significantly larger in the metallic stent group than in the bioresorbable scaffold group.

The compliance of enzyme collection was high (476 [95%] patients for creatine kinase, 487 [97%] patients for creatine kinase-MB, and 485 [97%] patients for troponin). Overall, we noted no significant differences in the pooled normalised values for each enzyme. When the three enzymes were subcategorised according to the relationship to their upper limit of normal for each respective assay, there were no differences in the rise of creatine kinase-MB and troponin between the bioresorbable scaffold and metallic stent groups. However, for the non-specific creatine kinase enzyme, frequency of the categories of more than one and more than two times higher than upper limit of normal were higher in the bioresorbable scaffold group than in the metallic stent group (table 3).

Figure 2 shows the five domains of Seattle Angina Questionnaire related to angina stability, frequency, physical limitation, disease perception, and treatment satisfaction. We noted substantial improvement in every domain at 6 and 12 months with respect to the pre-procedural assessment, and no significant difference between the two treatment groups. Before the procedure, 94 (29%) patients subsequently assigned to the bioresorbable scaffold group and 48 (29%) patients subsequently assigned to the metallic stent group were free from angina within 1 month before the questionnaire, whereas at 1 year 227 (74%) patients in the bioresorbable group and 113 (74%) patients in the metallic stent group were angina-free within 1 month before to the questionnaire (figure 2).

In a post-hoc analysis, we assessed time and duration of angina through adverse event reporting. Cumulative angina rates at 1 year were lower in the bioresorbable scaffold group than in the metallic stent group (72 [22%] *vs* 50 [30%], p=0·04; figure 3). Likewise, after exclusion of angina episodes that occurred during index admission to hospital or in the 7 days after the index procedure, angina rates were also lower (54 [16%] *vs* 42 [26%], p=0·01). Although the investigators and research staff were instructed to keep blinding intact, 37 patients (32 in the bioresorbable scaffold group and 5 in the metallic stent group) were potentially unblinded mainly through discharge letters to the referring physicians. A sensitivity analysis showed that excluding these 37 patients from the analysis did not affect the outcomes from adverse event reporting (data not shown).

We did a prespecified analysis of exercise testing. 465 (93%) patients received an exercise test at 6 months and 430 (86%) patients received one at 12 months (table 4). At 6 months, we noted ST depression of 0·1 mV or more or chest pain in 56 (18%) patients in the bioresorbable scaffold group and 32 (20%) patients in the metallic stent group (p=0·57), by comparison with 43 patients (15%) and 22 (15%) patients at 1 year (p=0·90), respectively.

	Bioresorbable scaffold group	Metallic stent group	Difference (95% CI)	p value
Procedural details				
Number of lesions	364	182	..	..
Balloon dilatation prior to device implantation	364 (100%)	180 (99%)	1·10% (–0·21, 3·92)	0·11
Planned overlap with the same type of device	56 (15%)	20 (11%)	4·40% (–1·93, 9·94)	0·16
Unforeseen additional implantation with the same device	14 (4%)	11 (6·0)	–2·20% (–6·91, 1·44)	0·25
More than one study device implanted	70 (19%)	27 (15%)	4·40% (–2·57, 10·62)	0·21
Nominal size of study device (mm)	3·01 (0·31)	3·05 (0·28)	–0·04 (–0·10, 0·01)	0·10
Balloon dilatation after device implantation	221 (61%)	107 (59%)	1·92% (–6·66, 10·67)	0·67
Nominal diameter of balloon used (implantation or post-dilatation; mm)	3·08 (0·34)	3·16 (0·36)	–0·08 (–0·14, 0·01)	0·02
Maximum balloon pressure used (implantation or post-dilatation; atm)	14·23 (3·43)	15·03 (3·33)	–0·80 (–1·4, –0·2)	0·01
Expected diameter of balloon used (implantation or post-dilatation; mm)	3·29 (0·35)	3·35 (0·37)	–0·06 (–0·14, 0·02)	0·15
Angiographic acute recoil of device following implantation per device (mm)	0·19 (0·19)	0·19 (0·18)	–0·00 (–0·04, 0·03)	0·85
Device success				
Clinical device success	361 (99%)	182 (100%)	–0·82% (–2·39, 1·31)	0·55
Clinical procedural success	322 (96%)*	164 (99%)*	–2·68% (–5·46, 0·80)	0·16
Angiographic analysis				
Lesion length obstruction (mm)	13·8 (6·5)	13·8 (6·6)	0·00 (–1·18, 1·18)	1·00
Total scaffolded or stented length (mm)	21·1 (8·8)	20·9 (7·4)	0·24 (–1·17, 1·65)	0·74
Reference vessel				
Pre-procedure diameter (mm)	2·59 (0·38)	2·63 (0·40)	–0·03 (–0·10, 0·04)	0·36
Postprocedure diameter (mm)	2·64 (0·36)	2·80 (0·34)	–0·16 (–0·22, –0·09)	<0·001
p between pre-procedure and postprocedure	0·0699	<0·0001	..	..
Minimum lumen diameter				
Pre-procedure diameter (mm)	1·07 (0·32)	1·05 (0·32)	0·02 (–0·03, 0·08)	0·44
Post-procedure in-stent or in-scaffold diameter (mm)	2·22 (0·33)	2·50 (0·33)	–0·28 (–0·34, –0·22)	<0·001
p between pre-procedure and post-procedure	<0·0001	<0·0001		
In-stent/in-scaffold acute gain (mm)	1·15 ± 0·38	1·46 ± 0·38	–0·30 (–0·37, –0·24)	<0·001
Diameter stenosis				
Pre-procedure percent diameter stenosis (%)	59% (11)	60% (12)	–1·07 (–3·11, 0·97)	0·30
Post-procedure in-stent/in-scaffold percent diameter stenosis (%)	16% (7)	10% (5)	5·37 (4·38, 6·36)	<0·001
p between pre-procedure and post-procedure	<0·001	<0·001		
Post-procedural curvature, cm^{-1}	0·29 (0·23)	0·24 (0·19)	0·04 (0·01, 0·08)	0·02

(Table 2 continues on next page)

	Bioresorbable scaffold group	Metallic stent group	Difference (95% CI)	p value
(Continued from previous page)				
Greyscale and radiofrequency intravascular ultrasonographic analysis				
Pre-procedural dense calcium (%)†	4·90% (4·73)	4·68% (4·10)	0·22 (–0·61, 1·05)	0·60
Pre-procedural necrotic core (%)†	16·20% (6·86)	16·15% (6·90)	0·05 (–1·27, 1·37)	0·94
Pre-procedural fibrotic tissue (%)†	31·47% (11·39)	30·62% (11·42)	0·85 (–1·33, 3·04)	0·44
Pre-procedural fibrofatty tissue (%)†	47·43% (16·91)	48·55% (16·86)	–1·12 (–4·35, 2·11)	0·50
Vessel area				
Pre-procedure area, mm²	11·51% (3·40)	12·34% (3·42)	–0·83 (–1·47, –0·19)	0·02
Post-procedure area (mm²)	13·17% (3·55)	14·28% (3·59)	–1·11 (–1·78, –0·44)	0·001
p between pre-procedure and post-procedure	<0·001	<0·001		
Plaque area				
Pre-procedure plaque area / media (mm²)	6·67 (2·52)	7·30 (2·68)	–0·63 (–1·12, –0·13)	0·01
Post-procedure plaque area / media (mm²)	7·11 (2·46)	7·43 (2·44)	–0·32 (–0·78, 0·14)	0·18
p between pre-procedure and post-procedure	<0·001	0·03		
Mean lumen area				
Pre-procedure mean lumen area (mm²)	4·84 (1·39)	5·02 (1·47)	–0·19 (–0·47, 0·08)	0·16
Post-procedure mean lumen area (mm²)	6·06 (1·44)	6·85 (1·60)	–0·80 (–1·09, –0·50)	<0·001
p between pre-procedure and post-procedure	<0·001	<0·001		
Minimal lumen area				
Pre-procedure minimal lumen area (mm²)	2·04 (0·72)	2·13 (0·83)	–0·10 (–0·25, 0·05)	0·20
Post-procedure minimal lumen area (mm²)	4·89 (1·38)	5·73 (1·51)	–0·84 (–1·12, –0·57)	<0·001
p between pre-procedure and post-procedure	<0·001	<0·001		
Acute gain in minimal lumen area (mm²)	2·85 (1·25)	3·60 (1·34)	–0·75 (–0·99, –0·50)	<0·001

Data are n (%) or mean (SD) unless otherwise stated. *Percentage based on number of patients (335 in the bioresorbable scaffold group, 166 in the metallic stent group). †Postprocedural variables not presented.

Table 2: **1-year angiographic and intravascular ultrasound outcomes**

	Creatine kinase			Creatine kinase-MB			Troponin		
	Biosorbable scaffold group (n=315)	Metallic stent group (n=161)	p value	Biosorbable scaffold group (n=324)	Metallic stent group (n=163)	p value	Biosorbable scaffold group (n=325)	Metallic stent group (n=160)	p value
Mean* (SD)	0·69 (0·61)	0·63 (0·63)	0·363	1·27 (1·99)	1·06 (1·64)	0·218	13·38 (30·64)	9·08 (21·01)	0·121
>1×ULN	51 (16%)	14 (9%)	0·024	104 (32%)	42 (26%)	0·150	204 (63%)	99 (62%)	0·848
>2×ULN	16 (5%)	3 (2%)	0·090	43 (13%)	16 (10%)	0·270	158 (49%)	73 (46%)	0·535
>3×ULN	4 (1%)	3 (2%)	0·693	23 (7%)	10 (6%)	0·690	124 (38%)	59 (37%)	0·785
>5×ULN	0	1 (1%)	0·338	16 (5%)	4 (2%)	0·192	97 (30%)	41 (26%)	0·333
>10×ULN	0	0	1·000	2 (1%)	1 (1%)	1·000	62 (19%)	24 (15%)	0·269

Data are n (%) unless otherwise stated. ULN=upper limit of normal. *Mean of the ratio relative to the upper limit of normal for the respective biomarker, as reported by central or local laboratory.

Table 3: **Cardiac biomarkers less than 48 h after the index procedure**

1-year target-lesion failure, a device oriented clinical endpoint (composite of cardiac death, target-vessel myocardial infarction, or clinically indicated target-lesion revascularisation) was 5% (16 patients) in the bioresorbable group and 3% (five patients) in the metallic stent group (p=0·35; table 5). The 1-year patient-oriented clinical endpoint (composite of all death, any myocardial infarction, and all revascularisation) was 7% (24 patients) in the bioresorbable scaffold group compared with 9% (15 patients) in the metallic stent group (p=0·47). We noted only one non-cardiac death, which was due to cancer in the metallic stent group.

Myocardial infarctions (as defined by the protocol) occurred in 15 (4%) patients in the bioresorbable scaffold group and two (1%) patients in the metallic stent group (p=0·06), which were mainly driven by periprocedural non-Q-wave myocardial infarctions occurring in 13 (4%) patients in the bioresorbable scaffold group and two (1%) patients in the metallic stent group (p=0·16). Rates of all revascularisations were 4% (12 patients) and 7% (12 patients) in the bioresorbable scaffold and the metallic stent groups, respectively (p=0·08). We documented two definite scaffold thromboses, one acutely within 24 hours of implantation and the second sub-acutely on

day 2, both in the bioresorbable scaffold group. One probable scaffold thrombosis occurred on day 335. The rate of definite scaffold thrombosis was 0·6% in bioresorbable scaffold and 0% in metallic stent, p=1·0) and the overall rate of definite or probable scaffold thrombosis was 0·9% in bioresorbable scaffold and 0% in metallic stent (p=0·55; table 5).

The incidence of any anatomical complications as assessed by angiography was similar between the two treatment groups (56 patients [16%] in the bioresorbable scaffold group *vs* 33 patients [20%] in the metallic stent group, p=0·39), with sidebranch occlusion occurring more often in the metallic stent group (39/503 [8%] sidebranches) than in the bioresorbable scaffold group (52/998 [5%] sidebranches, p=0·07). Of 15 patients with periprocedural myocardial infarction, 10 (67%) were angiographically classified as type 1 (sidebranch occlusion), whereas three (20%) were type 2 (other angiographic complications).[30,31] In multivariate analysis, treatment with overlapping devices was the only independent determinant of per-protocol periprocedural myocardial infarction (OR 4·36, 95% CI 1·48–12·61, p=0·012).

When we subcategorised cardiac biomarker rise according to contemporary criteria for periprocedural myocardial infarction (the third universal definition[33] and the SCAI definition[32]), periprocedural myocardial infarction rates were 5% in the bioresorbable scaffold group versus 2% in the metallic stent group (creatine kinase-MB >5×upper limit of normal), 30% versus 26% (troponin >5×upper limit of normal), 1% versus 1% (creatine kinase-MB >10× ULN), and 3% versus 1% (troponin >70× upper limit of normal).

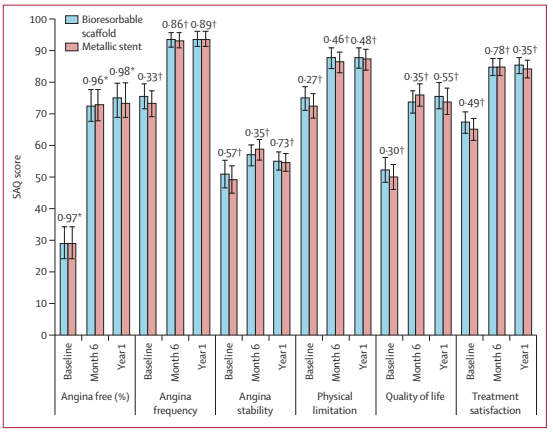

Figure 2: **Seattle Angina Questionnaire responses**
Figure shows five domains of the Seattle Angina Questionnaire related to angina stability, frequency, physical limitation, disease perception, and treatment satisfaction in addition to number of patients with no angina. The bars show 95% CIs. SAQ=Seattle Angina Questionnaire. *p value from post-hoc test. †p value from χ^2 test.

Discussion

The main findings of this interim report of secondary outcomes and post-hoc analysis of 1-year follow-up data are that the device success rate of the bioresorbable scaffold matched that of the metallic stent; acute recoil of both devices were similar; the procedural lumen gain was slightly less with the bioresorbable scaffold than with the metallic stent because of the use of smaller balloons at lower pressure for deployment and dilatation of the bioresorbable scaffold; and that functional assessment, anginal status as assessed by the Seattle Angina Questionnaire, and secondary clinical endpoints did not differ between treatment groups, whereas the cumulative rate of recurrent or worsening angina reported through adverse event forms was lower in the bioresorbable scaffold group than in the metallic stent group (panel).

Despite differences in the crossing profile of the two devices (1·4 mm for Absorb scaffold *vs* 1·1 mm for the Xience stent), the polymeric device achieved success rates in implantation similar to the metallic stent in the context of the simple lesions included in the current trial. However, this finding might not be generalisable to a routine population of patients receiving percutaneous coronary intervention. The current generation of the Absorb scaffold has a strut thickness of 150 µm, compared with 80 µm for the Xience stent. However, intrinsically the polymeric device is more flexible than the metallic device. In this study, we noted the conformability of the coronary anatomy for the bioresorbable scaffold to be better than that of the metallic stent, as previously shown by the increased curvature of scaffolded coronary arteries on quantitative angiography.[23,24]

In this study, the acute recoil of the polymeric device was similar to that described in a previous report.[12,25] However, because of the inherent limitation in elongation-at-break of polylactide, operators tended to restrain themselves from dilating the polymeric device using the aggressive technique typically used for implantation of metallic stents. Accordingly, the differences in acute gain noted on angiography and intravascular ultrasound seem to be related to the significant differences in balloon size and pressure used for deployment and postdilatation. On the basis of previous reports of disrupted polymeric scaffolds due to overexpansion, the protocol did not recommend postdilatation of the bioresorbable scaffold device.[26,27] If this procedure was to be done, balloons had to be at least 0·25 mm larger than the nominal diameter of the bioresorbable scaffold. Mattesini and colleagues[28] reported that the Absorb scaffold showed similar postprocedure area stenosis, minimum lumen area, and eccentricity index to second-generation drug-eluting stent. As concluded by the authors, the different approach for lesion preparation and routine use of optical coherence

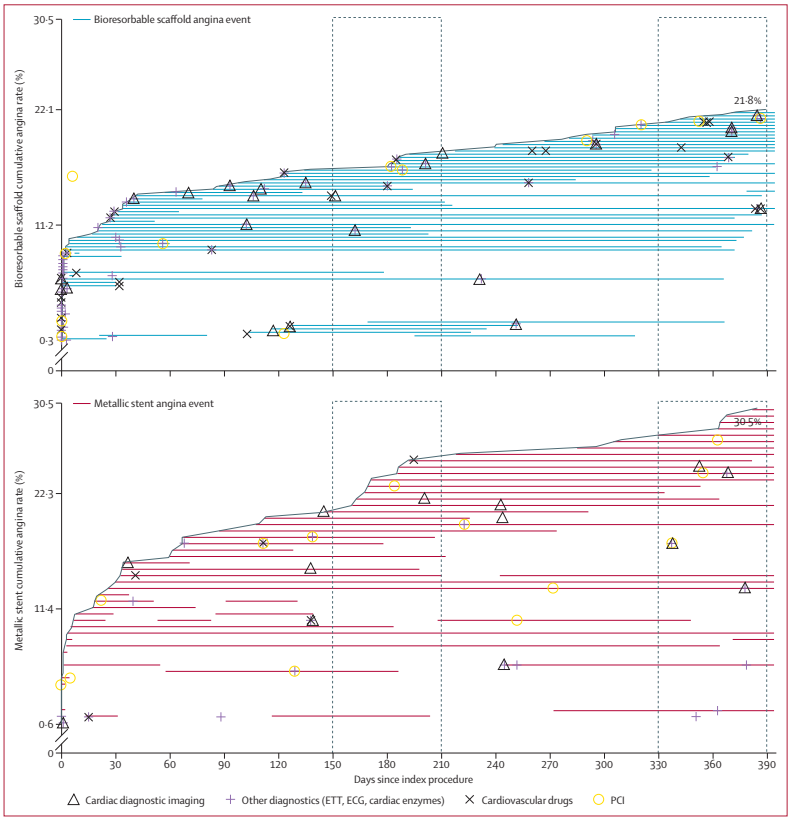

***Figure 3*: Time to first occurrence and duration of angina**

Figure shows time to first occurrence and duration of angina through adverse event reporting (post-hoc analysis). Rectangular frames show the two cross-sectional time windows of 4 weeks during which patients completed Seattle Angina Questionnaires. ETT=exercise tolerance testing. ECG=electrocardiogram. PCI=percutaneous coronary intervention.

tomography guidance during bioresorbable scaffold expansion might have contributed to these results.

Few data about the effect of lesion morphology on acute lumen gain are available. Brown and colleagues[29] showed that in 25 patients with Absorb scaffolds, there was no correlation between the arc of fibrocalcification and scaffold expansion as assessed on optical coherence tomography. In this study, presence of calcium and its circular extension on intravascular ultrasound greyscale did not affect the acute gain in lumen area for both the polymeric and metallic devices. Although we noted differences in postprocedural minimum lumen diameter and minimum lumen area, reassuringly exercise testing showed similar functional results in both groups, suggesting that the subtle differences in postprocedural lumen dimension is clinically negligible.

The rate of per protocol myocardial infarction was 4% in the bioresorbable scaffold group and 1% in the metallic stent group. This difference was mostly due to the non-Q-wave myocardial infarction (4% *vs* 1%) driven by cardiac biomarker rise within 48 h after the index procedure.

	6 months after index procedure				12 months after index procedure			
	Bioresorbable scaffold group (n=335)	Metallic stent group (n=166)	Difference (95% CI)	p value	Bioresorbable scaffold group (n=335)	Metallic stent group (n=166)	Difference (95% CI)	p value
Participated in exercise test	308 (92%)	157 (95%)	−2·64% (−6·89, 2·54)	0·28	288 (86%)	142 (85%)	0·43% (−5·71, 7·42)	0·9
Treadmill	176 (57%)	84 (53%)	3·64% (−5·81, 13·12)	0·45	152 (53%)	74 (52%)	0·67% (−9·24, 10·62)	0·9
Cycling	132 (43%)	73 (46%)	−3·64% (−13·12, 5·81)	0·45	136 (47%)	68 (48%)	−0·67% (−10·62, 9·24)	0·9
Maximum heart rate (beats per min)	131·8 (23·0)	131·5 (23·3)	0·2 (−4·3, 4·7)	0·93	132·6 (21·1)	134·5 (20·7)	−1·9 (−6·1, 2·3)	0·38
Maximum workload (watts)	133·7 (44·1)	138·3 (47·4)	−4·6 (−17·7, 8·4)	0·48	130·8 (42·9)	144·1 (45·8)	−13·3 (−26·4, −0·1)	0·05
Maximum workload (METS)	9·02 (2·81)	9·05 (3·41)	−0·03 (−0·89, 0·83)	0·95	9·32 (2·70)	9·41 (3·05)	−0·09 (−0·92, 0·74)	0·83
Terminated by physician due to >0·2 mV ST depression*	3/70 (4%)	5/29 (17%)	−12·96% (−30·49, −0·69)	0·05	4/82 (5%)	2/34 (6%)	−1·00% (−14·54, 7·19)	1
Test terminated by patient (angina or dyspnea†	43/218 (20%)	20/114 (18%)	2·18% (−7·12, 10·44)	0·63	36/198 (18%)	24/104 (23%)	−4·90% (−15·04, 4·34)	0·31
Exercise duration (min)	8·10 (3·28)	8·53 (3·76)	−0·43 (−1·13, 0·26)	0·22	8·55 (3·73)	8·99 (3·86)	−0·44 (−1·21, 0·33)	0·26
≥0·1 mV ST depression	47 (15%)	28 (18%)	−2·52% (−10·16, 4·32)	0·48	32 (11%)	15 (11%)	0·63% (−6·27, 6·45)	0·85
Chest pain during exercise	15 (5%)	8 (5%)	−0·23% (−5·23, 3·68)	0·92	16 (6%)	12 (8·5%)	−2·90% (−9·01, 1·94)	0·25
≥0·1 mV ST depression or chest pain	56 (18%)	32 (20%)	−2·20% (−10·19, 5·07)	0·57	43 (15%)	22 (15%)	−0·46% (−8·23, 6·36)	0·9
Antianginal medication								
β blocker‡	235/331 (71%)	112/165 (68%)	3·12% (−5·27, 11·90)	0·48	232/329 (71%)	108/164 (66%)	4·66% (−3·88, 13·54)	0·29
Calcium channel blocker	69 (21%)	35 (21%)	−0·37% (−8·32, 6·90)	0·92	78 (24%)	38 (23%)	0·54% (−7·69, 8·12)	0·89
Nitrate	59 (18%)	44 (27%)	−8·84% (−16·98, −1·22)	0·02	64 (19·5%)	43 (26%)	−6·77% (−14·98, 0·91)	0·09
Use of dual antiplatelet therapy	323 (97%)	161 (97%)	0·30% (−2·62, 4·35)	1·00	275 (83%)	138 (83%)	−0·30% (−6·93, 7·11)	0·93

Data are n (%) or mean (SD) unless otherwise stated. *Data are n/N (%), in which N is the number of exercise tests terminated by physician. †Data are n/N (%), in which N is the number of exercise tests terminated by patient. ‡Data are n/N (%), in which N is the number of patients who had available information on medication.

Table 4: **Results of exercise testing**

When we subcategorised periprocedural myocardial infarctions according to biomarker criteria,[32,33] we noted a wide range of values (from <1% to 27–32%) with similar proportions of patients in the two treatment groups, emphasising the arbitrary character of any definition of periprocedural myocardial infarction

The rise of these three cardiac enzymes subcategorised in five different ranges was similar between the two treatment groups (table 3). In particular, only a small proportion of patients with a creatine kinase-MB rise in the range of more than ten times the upper limit of normal was reported and the same (<1%) in both treatment groups. As opposed to lower concentration ranges, this range of more than ten times the upper limit of normal of creatine kinase-MB has been reported as a threshold for worse late outcomes.[34]

Two myocardial infarctions in the bioresorbable scaffold (one Q-wave and one non-Q-wave) were attributed to definite scaffold thrombosis, in one case involving overlapping scaffolds and in the other case involving bifurcation scaffolding (a protocol deviation).

In-vivo assessment of endothelial shear stress with a fusion of frequency domain optical coherence tomography and three-dimensional angiography has demonstrated alternance of high shear stress on top of the protruding struts and low shear stress at the base of the struts.[35,36] Nevertheless, a summary of published and presented data at international meetings suggested that the overall rate of scaffold thrombosis in stable or unstable patients was 0·93% (25 of 2699 patients), a figure comparable with our results. Of note, most thromboses were acute and sub-acute.

	Bioresorbable scaffold group (n=335)	Metallic stent group (n=166)	Difference (95% CI)†	p value
Outcomes				
All deaths	0	1 (1%)	−0·61% (−3·35 to 0·65)	0·33
Cardiac deaths	0	0	0·00% (NA)	1·00
Myocardial infarction per protocol	15 (4%)	2 (1%)	3·32% (−0·25 to 6·26)	0·06
Q-wave	2 (1%)	0	0·60% (−1·71 to 2·18)	1·00
Non-Q-wave	13 (4%)	2 (1%)	2·72% (−0·78 to 5·53)	0·16
All target-lesion revascularisation	4 (1%)	3 (2%)	−0·61% (−4·08 to 1·60)	0·69
Clinically indicated target-lesion revascularisation	4 (1%)	3 (2%)	−0·61% (−4·08 to 1·60)	0·69
All target-vessel revascularisation	8 (2%)	8 (5%)	−2·43% (−7·01 to 0·86)	0·15
Clinically indicated target-vessel revascularisation	6 (2%)	6 (4%)	−1·82% (−6·01 to 1·04)	0·23
Non-clinically indicated target-vessel revascularisation	3 (1%)	3 (2%)	−0·91% (−4·35 to 1·19)	0·40
Non-target-vessel revascularisation	6 (2%)	6 (4%)	−1·82% (−6·01 to 1·04)	0·23
Clinically indicated non-target-vessel revascularisation	5 (1%)	4 (2%)	−0·91% (−4·66 to 1·55)	0·49
Non-clinically indicated non-target-vessel revascularisation	3 (1%)	2 (1%)	−0·31% (−3·46 to 1·63)	1·00
All revascularisation	12 (4%)	12 (7%)	−3·65% (−8·89 to 0·37)	0·08
Clinically indicated revascularisation	9 (3%)	9 (5%)	−2·74% (−7·50 to 0·75)	0·12
Non-clinically indicated revascularisation	6 (2%)	5 (3%)	−1·22% (−5·21 to 1·49)	0·52
Composite secondary endpoints				
Cardiac death, all myocardial infarction, clinically indicated target-vessel revascularisation (target-vessel failure)	18 (5%)	8 (5%)	0·59% (−4·26 to 4·41)	0·78
Cardiac death, target-vessel myocardial infarction, and clinically indicated target-lesion revascularisation (target-lesion failure; device-oriented composite endpoint)	16 (5%)	5 (3%)	1·80% (−2·48 to 5·16)	0·35
Cardiac death, all myocardial infarction, and clinically indicated target-lesion revascularisation (major adverse cardiac events)	17 (5%)	5 (3%)	2·11% (−2·20 to 5·51)	0·28
All death, all myocardial infarction, and all revascularisation (patient-oriented composite endpoint)	24 (7%)	15 (9%)	−1·84% (−7·69 to 2·98)	0·47
Thrombosis endpoints				
Definite scaffold or stent thrombosis	2 (0·6%)	0	0·61% (−1·72 to 2·19)	1·00
Acute (0–1 day)	1 (0·3%)	0	0·30% (−1·98 to 1·67)	1·00
Sub-acute (2–30 days)	1 (0·3%)	0	0·30% (−1·98 to 1·68)	1·00
Late (31–365 days)	0	0	0·00% (NA)	1·00
Definite or probable scaffold or stent thrombosis	3 (0·9%)	0	0·91% (−1·45 to 2·65)	0·55

Data are n (%).

Table 5: **Secondary clinical outcomes at 1-year follow-up**

Panel: **Research in context**

Systematic review

Bioresorbable scaffolds are a novel approach to treat coronary artery stenosis by providing transient scaffolding and local drug delivery, potentially without the long-term limitation of metallic drug-eluting stents such as very late stent thrombosis.[1,2]

The potential of this technology, such as return of vasomotion, cyclic strain and shear stress, has been shown in some observations up to 3-year follow-up using multiple imaging modalities obtained in the ABSORB first-in-man trials.[3-5,6-11] Widespread dissemination of revascularisation with a bioresorbable scaffold has, however, occurred without randomised comparison with its metallic counterpart.

We searched PubMed with the terms "bioresorbable" AND "scaffold" AND "randomized controlled trial" to find papers published between Jan 1, 1999, and Aug 19, 2014, that reported randomised controlled trials which investigated the safety or efficacy of a bioresorbable scaffold compared with a metallic stent. We identified two articles (one related to our own trial design and the second related to a physician-initiated study), both describing the rationale and design of these ongoing trials but found no articles reporting the results of randomised controlled trials.

Interpretation

To our knowledge, this trial is the first randomised controlled comparison of a bioresorbable scaffold with a metallic stent. These data suggest that despite a significant but modest reduction in acute performance, 1-year angina and clinical outcomes of the Absorb bioresorbable scaffold are similar to the Xience metallic stent. The post-hoc observation of reduction in angina through adverse event reporting warrants further investigation.

Although the angina status as assessed by cross-sectional Seattle Angina Questionnaires assessment was similar between the bioresorbable scaffold and metallic stent groups, the cumulative rate of recurrent or worsening angina assessed through adverse event reporting was significantly lower with the bioresorbable scaffold. The Seattle Angina Questionnaires represents assessment of a 4-week window (recall period) and does not take fully into account earlier episodes of angina, whereas the angina assessed through adverse event reporting represents the cumulative rate of angina at 1 year. The decrease in the cumulative rate of angina for bioresorbable scaffold was directionally consistent with the lower reported rates of nitrate use and all revascularisations. This observation is so far unexplained and merits additional research although return of vasomotion, reduction of compliance mismatch, and improved conformability of the bioresorbable scaffold have been reported in previous studies.[3,6,7,9,23,24]

Although the protocol allowed inclusion of long lesions, the population still represents relatively simple lesions compared to the complex lesions frequently encountered in daily practice. The generalisability of the study might therefore be limited.

This report does not present the primary endpoints and endpoints reported were not powered. However, we

thought it important to report these secondary prespecified randomised endpoints in the absence of any current comparative data. Additionally, the angina rate diagnosed by the site was not prespecified and it is thus hypothesis generating. This measure is being investigated in the ABSORB III and IV trials. Both studies have adequately powered prespecified angina endpoints to detect difference between two treatments.

In this randomised comparison, the Absorb everolimus-eluting bioresorbable scaffold showed similar one-year clinical outcomes to the everolimus-eluting Xience metallic stent. Exercise performance and angina status by Seattle Angina Questionnaires were also similar. The reported reduction of angina through adverse event reporting warrants further clinical and physiological investigation.

Contributors

PWS, BC, YO, and SV contributed to the conception and design of the study. BC, DD, AC, DC, AI, MD, RJvdS, and MH contributed to data collection. MJG, YI, HMG-G, YO, LW, SV, LP, PS, BC, and PWS analysed and interpreted the data. PWS, BC, YO, and SV drafted the report, which was critically revised for important intellectual content by DD, MH, MJG, YI, HMG-G, LP, PS, and LW. All authors approved the final version of the report. BC and PWS approved the report and obtained funding. SV and LW provided administrative, technical, or logistical support.

Declaration of interests

PWS is a member of Advisory Board of Abbott Vascular. SV, LP, and PS are employees of Abbott Vascular. BC is a consultant for Abbott Vascular. DD receives lecture fees and is a member of Advisory Board of Abbott Vascular. MD reports grants and non-financial support from Abbott Vascular during the conduct of the study. AC reports grants from Abbott Vascular outside the submitted work. LW is a contractor from Novellas Healthcare working for Abbott Vascular. MH reports minor grants from and consultancy for Abbott Vascular. All other authors declare no competing interests.

References

1 Nakazawa G, Otsuka F, Nakano M, et al. The pathology of neoatherosclerosis in human coronary implants bare-metal and drug-eluting stents. *J Am Coll Cardiol* 2011; **57:** 1314–22.

2 Daemen J, Wenaweser P, Tsuchida K, et al. Early and late coronary stent thrombosis of sirolimus-eluting and paclitaxel-eluting stents in routine clinical practice: data from a large two-institutional cohort study. *Lancet* 2007; **369:** 667–78.

3 Brugaletta S, Gogas BD, Garcia-Garcia HM, et al. Vascular compliance changes of the coronary vessel wall after bioresorbable vascular scaffold implantation in the treated and adjacent segments. *Circ J* 2012; **76:** 1616–23.

4 Lane JP, Perkins LE, Sheehy AJ, et al. Lumen gain and restoration of pulsatility after implantation of a bioresorbable vascular scaffold in porcine coronary arteries. *JACC Cardiovasc Interv* 2014; **7:** 688–95.

5 Serruys PW, Garcia-Garcia HM, Onuma Y. From metallic cages to transient bioresorbable scaffolds: change in paradigm of coronary revascularization in the upcoming decade? *Eur Heart J* 2012; **33:** 16–25b.

6 Ormiston JA, Serruys PW, Regar E, et al. A bioabsorbable everolimus-eluting coronary stent system for patients with single de-novo coronary artery lesions (ABSORB): a prospective open-label trial. *Lancet* 2008; **371:** 899–907.

7 Serruys PW, Ormiston JA, Onuma Y, et al. A bioabsorbable everolimus-eluting coronary stent system (ABSORB): 2-year outcomes and results from multiple imaging methods. *Lancet* 2009; **373:** 897–910.

8 Serruys PW, Onuma Y, Ormiston JA, et al. Evaluation of the second generation of a bioresorbable everolimus drug-eluting vascular scaffold for treatment of de novo coronary artery stenosis: six-month clinical and imaging outcomes. *Circulation* 2010; **122:** 2301–12.

9 Serruys PW, Onuma Y, Dudek D, et al. Evaluation of the second generation of a bioresorbable everolimus-eluting vascular scaffold for the treatment of de novo coronary artery stenosis: 12-month clinical and imaging outcomes. *J Am Coll Cardiol* 2011; **58:** 1578–88.

10 Ormiston JA, Serruys PW, Onuma Y, et al. First serial assessment at 6 months and 2 years of the second generation of absorb everolimus-eluting bioresorbable vascular scaffold: a multi-imaging modality study. *Circ Cardiovasc Interv* 2012; **5:** 620–32.

11 Serruys PW, Onuma Y, Garcia-Garcia HM, et al. Dynamics of vessel wall changes following the implantation of the absorb everolimus-eluting bioresorbable vascular scaffold: a multi-imaging modality study at 6, 12, 24 and 36 months. *EuroIntervention* 2014; **9:** 1271–84.

12 Onuma Y, Serruys PW, Gomez J, et al. Comparison of in vivo acute stent recoil between the bioresorbable everolimus-eluting coronary scaffolds (revision 1.0 and 1.1) and the metallic everolimus-eluting stent. *Catheter Cardiovasc Interv* 2011; **78:** 3–12.

13 Serruys PW, Luijten HE, Beatt KJ, et al. Incidence of restenosis after successful coronary angioplasty: a time-related phenomenon. A quantitative angiographic study in 342 consecutive patients at 1, 2, 3, and 4 months. *Circulation* 1988; **77:** 361–71.

14 Onuma Y, Serruys PW, Perkins LE, et al. Intracoronary optical coherence tomography and histology at 1 month and 2, 3, and 4 years after implantation of everolimus-eluting bioresorbable vascular scaffolds in a porcine coronary artery model: an attempt to decipher the human optical coherence tomography images in the ABSORB trial. *Circulation* 2010; **122:** 2288–300.

15 Bourantas CV, Papafaklis MI, Lakkas L, et al. Fusion of optical coherence tomographic and angiographic data for more accurate evaluation of the endothelial shear stress patterns and neointimal distribution after bioresorbable scaffold implantation: comparison with intravascular ultrasound-derived reconstructions. *Int J Cardiovasc Imag* 2014; **30:** 485–94.

16 Diletti R, Serruys PW, Farooq V, et al. ABSORB II randomized controlled trial: a clinical evaluation to compare the safety, efficacy, and performance of the Absorb everolimus-eluting bioresorbable vascular scaffold system against the XIENCE everolimus-eluting coronary stent system in the treatment of subjects with ischemic heart disease caused by de novo native coronary artery lesions: rationale and study design. *Am Heart J* 2012; **164:** 654–63.

17 Task Force M, Montalescot G, Sechtem U, et al. 2013 ESC guidelines on the management of stable coronary artery disease: the Task Force on the management of stable coronary artery disease of the European Society of Cardiology. *Eur Heart J* 2013; **34:** 2949–3003.

18 Skalidis EI, Vardas PE. Guidelines on the management of stable angina pectoris. *Eur Heart J* 2006; **27:** 2606; author reply -7.

19 Spertus JA, Winder JA, Dewhurst TA, et al. Development and evaluation of the Seattle Angina Questionnaire: a new functional status measure for coronary artery disease. *J Am Coll Cardiol* 1995; **25:** 333–41.

20 Boden WE, O'Rourke RA, Teo KK, et al. Optimal medical therapy with or without PCI for stable coronary disease. *N Engl J Med* 2007; **356:** 1503–16.

21 Gibbons RJ, Balady GJ, Bricker JT, et al. ACC/AHA 2002 guideline update for exercise testing: summary article: a report of the American College of Cardiology/American Heart Association Task Force on Practice Guidelines (Committee to Update the 1997 Exercise Testing Guidelines). *Circulation* 2002; **106:** 1883–92.

22 Ryan TJ, Faxon DP, Gunnar RM, et al. Guidelines for percutaneous transluminal coronary angioplasty. A report of the American College of Cardiology/American Heart Association Task Force on Assessment of Diagnostic and Therapeutic Cardiovascular Procedures (Subcommittee on Percutaneous Transluminal Coronary Angioplasty). *Circulation* 1988; **78:** 486–502.

23 Gomez-Lara J, Brugaletta S, Farooq V, et al. Angiographic geometric changes of the lumen arterial wall after bioresorbable vascular scaffolds and metallic platform stents at 1-year follow-up. *JACC Cardiovasc Interv* 2011; **4:** 789–99.

24 Gomez-Lara J, Garcia-Garcia HM, Onuma Y, et al. A comparison of the conformability of everolimus-eluting bioresorbable vascular scaffolds to metal platform coronary stents. *JACC Cardiovasc Interv* 2010; **3:** 1190–8.

25 Tanimoto S, Serruys PW, Thuesen L, et al. Comparison of in vivo acute stent recoil between the bioabsorbable everolimus-eluting coronary stent and the everolimus-eluting cobalt chromium coronary stent: insights from the ABSORB and SPIRIT trials. *Catheter Cardiovasc Interv* 2007; **70:** 515–23.

26 Onuma Y, Serruys PW, Ormiston JA, et al. Three-year results of clinical follow-up after a bioresorbable everolimus-eluting scaffold in patients with de novo coronary artery disease: the ABSORB trial. *EuroIntervention* 2010; **6:** 447–53.

27 Ormiston JA, De Vroey F, Serruys PW, Webster MW. Bioresorbable polymeric vascular scaffolds: a cautionary tale. *Circ Cardiovasc Interv* 2011; **4:** 535–38.

28 Mattesini A, Pighi M, Konstantidinis N, et al. Optical coherence tomography in bioabsorbable stents: mechanism of vascular response and guidance of stent implantation. *Minerva Cardioangiol* 2014; **62:** 71–82.

29 Brown AJ, McCormick LM, Braganza DM, Bennett MR, Hoole SP, West NE. Expansion and malapposition characteristics after bioresorbable vascular scaffold implantation. *Catheter Cardiovasc Interv* 2014; **84:** 37–45.

30 Herrmann J. Peri-procedural myocardial injury: 2005 update. *Eur Heart J* 2005; **26:** 2493–519.

31 Park DW, Kim YH, Yun SC, et al. Impact of the angiographic mechanisms underlying periprocedural myocardial infarction after drug-eluting stent implantation. *Am J Cardiol* 2014; **113:** 1105–10.

32 Moussa ID, Klein LW, Shah B, et al. Consideration of a new definition of clinically relevant myocardial infarction after coronary revascularization: an expert consensus document from the Society for Cardiovascular Angiography and Interventions (SCAI). *J Am Coll Cardiol* 2013; **62:** 1563–70.

33 Thygesen K, Alpert JS, Jaffe AS, et al. Third universal definition of myocardial infarction. *Eur Heart J* 2012; **33:** 2551–67.

34 Lindsey JB, Marso SP, Pencina M, et al. Prognostic impact of periprocedural bleeding and myocardial infarction after percutaneous coronary intervention in unselected patients: results from the EVENT (evaluation of drug-eluting stents and ischemic events) registry. *JACC Cardiovasc Interv* 2009; **2:** 1074–82.

35 O'Brien CC, Kolachalama VB, Barber TJ, Simmons A, Edelman ER. Impact of flow pulsatility on arterial drug distribution in stent-based therapy. *J Control Release* 2013; **168:** 115–24.

36 Bourantas CV, Papafaklis MI, Kotsia A, et al. Effect of the endothelial shear stress patterns on neointimal proliferation following drug-eluting bioresorbable vascular scaffold implantation: an optical coherence tomography study. *JACC Cardiovasc Interv* 2014; **7:** 315–24.

1.7 Clinical and procedural outcomes of STEMI

Everolimus-eluting bioresorbable vascular scaffolds for treatment of patients presenting with ST-segment elevation myocardial infarction: BVS STEMI first study.

Eur Heart J. 2014 Mar;35(12):777-86
[Original research paper, IF 14.72]

Diletti R, Karanasos A, Muramatsu T, Nakatani S, Van Mieghem NM, Onuma Y, Nauta ST, **Ishibashi Y**, Lenzen MJ, Ligthart J, Schultz C, Regar E, de Jaegere PP, Serruys PW, Zijlstra F, van Geuns RJ.

Everolimus-eluting bioresorbable vascular scaffolds for treatment of patients presenting with ST-segment elevation myocardial infarction: BVS STEMI first study

Roberto Diletti, Antonios Karanasos, Takashi Muramatsu, Shimpei Nakatani, Nicolas M. Van Mieghem, Yoshinobu Onuma, Sjoerd T. Nauta, Yuki Ishibashi, Mattie J. Lenzen, Jurgen Ligthart, Carl Schultz, Evelyn Regar, Peter P. de Jaegere, Patrick W. Serruys, Felix Zijlstra, and Robert Jan van Geuns*

Thoraxcenter, Erasmus MC, 's-Gravendijkwal 230, 3015 CE Rotterdam, the Netherlands

Received 11 September 2013; revised 6 November 2013; accepted 26 November 2013; online publish-ahead-of-print 6 January 2014

See page 753 for the editorial comment on this article (doi:10.1093/eurheartj/ehu005)

Aims We evaluated the feasibility and the acute performance of the everolimus-eluting bioresorbable vascular scaffolds (BVS) for the treatment of patients presenting with ST-segment elevation myocardial infarction (STEMI).

Methods and results The present investigation is a prospective, single-arm, single-centre study, reporting data after the BVS implantation in STEMI patients. Quantitative coronary angiography and optical coherence tomography (OCT) data were evaluated. Clinical outcomes are reported at the 30-day follow-up. The intent-to-treat population comprises a total of 49 patients. The procedural success was 97.9%. Pre-procedure TIMI-flow was 0 in 50.0% of the patients; after the BVS implantation, a TIMI-flow III was achieved in 91.7% of patients and the post-procedure percentage diameter stenosis was 14.7 $\pm$ 8.2%. No patients had angiographically visible residual thrombus at the end of the procedure. Optical coherence tomography analysis performed in 31 patients showed that the post-procedure mean lumen area was 8.02 $\pm$ 1.92 mm^2, minimum lumen area 5.95 $\pm$ 1.61 mm^2, mean incomplete scaffold apposition area 0.118 $\pm$ 0.162 mm^2, mean intraluminal defect area 0.013 $\pm$ 0.017 mm^2, and mean percentage malapposed struts per patient 2.80 $\pm$ 3.90%. Scaffolds with >5% malapposed struts were 7. At the 30-day follow-up, target-lesion failure rate was 0%. Non-target-vessel revascularization and target-vessel myocardial infarction (MI) were reported. A non-target-vessel non-Q-wave MI occurred. No cases of cardiac death or scaffold thrombosis were observed.

Conclusion In the present series, the BVS implantation in patients presenting with acute MI appeared feasible, with high rate of final TIMI-flow III and good scaffold apposition. Larger studies are currently needed to confirm these preliminary data.

Keywords Bioresorbable vascular scaffolds • ST-segment elevation myocardial infarction • Optical coherence tomography

Introduction

Primary percutaneous coronary intervention has been demonstrated to be superior to thrombolytic strategy and is currently the treatment of first choice for patients presenting with ST-segment elevation myocardial infarction (STEMI) in experienced centres with limited time delay.[1] First-generation drug-eluting stents (DES) have been shown to reduce the need for repeat revascularization compared with bare-metal stents (BMS),[2–4] and the newer-generation DES with improved biocompatibility of polymers may lower the rate of clinical events also in acute patients.[5,6] However, the implantation of metal devices is not devoid of important limitations, such as permanent caging of the vessel with permanent impairment of coronary vasomotion, side branch jailing, impossibility of late lumen

*Corresponding author. Tel: +31 10 4635260(33348), Fax: +31 10 4369154, Email: r.vangeuns@erasmusmc.nl

enlargement, non-invasive imaging and future surgical revascularization of stented segments.[7] Moreover, in spite of the beneficial effect of neointimal inhibition, the antiproliferative drug elution has been shown to interfere with the vascular healing processes providing the background for delayed strut coverage and persistent or acquired malapposition.[8,9] The above-mentioned limitations can be proposed for both stable and acute patients; however, primary stenting has additional specific characteristics that should be highlighted. Stent placement in acute thrombotic lesions has been reported to be an independent predictor of late stent malapposition after the BMS[10] or DES[11] implantation. Possible explanations for this phenomenon could be the thrombus sequestration behind the struts—which subsequently resolves—and the vasoconstriction during the acute phase. Both these factors may predispose to stent underdeployment, malapposition and finally to stent thrombosis. The everolimus-eluting bioresorbable vascular scaffold (BVS) has been designed to overcome the general limitations of the metallic stents and recently has been shown to provide excellent results for the treatment of stable patients.[12,13] However, so far very limited data are available on the use of this novel device in patients with acute coronary syndromes (ACS).[14,15] Given this background, a pilot study investigating the feasibility and acute performance of the BVS for the treatment of patients presenting with STEMI was initiated.

Methods

Rationale

As of 1 September 2012, the BVS (ABSORB; Abbott Vascular, Santa Clara, CA, USA) has been commercially available in the Netherlands. Based on previous experience and available evidence, reported in ABSORB Cohort A and B Trial[13,16] our institution initiated the use of BVS for the treatment of patients presenting for PCI in everyday clinical practice, with a preference for patients with a good life expectancy as demonstrated by the presence of limited co-morbidities. As these patients might have more complex lesions compared with the ABSORB study patients[16,17] the BVS-EXPAND registry was initiated. The BVS-EXPAND also included patients with ACS (unstable angina or non-STEMI). After the first experience with ACS patients and an interim analysis, a decision was made to extend BVS utilization to the treatment of STEMI.

As an additional measure for assessing the safety of a treatment approach with BVS in STEMI, optical coherence tomography (OCT) imaging was performed, according to clinical judgement, for a more comprehensive evaluation of the acute procedural outcome.

Study design

The present report is an investigator initiated, prospective, single-arm, single-centre study to assess feasibility and performance of the second-generation everolimus-eluting BVS for the treatment of patients presenting with STEMI.

Subjects enrolled were patients of $\geq$18-year-old admitted with STEMI, defined as at least 1 mm ST-segment elevation in two or more standard leads or at least 2 mm in two or more contiguous precordial leads or new left bundle branch block within 12 h after the onset of symptoms. Culprit lesions were located in vessels within the upper limit of 3.8 mm and the lower limit of 2.0 mm by online quantitative coronary angiography (QCA). The absorb BVS was implanted according to the manufacturer's indication on target-vessel diameter ranges and absorb BVS diameters to be used. The absorb BVS with a nominal diameter of 2.5 mm was implanted in vessels $\geq$2.0 and $\leq$3.0 mm by online QCA; the 3.0 mm BVS was implanted in vessels $\geq$2.5 and $\leq$3.3 mm by online QCA; the 3.5 mm BVS was implanted in vessels $\geq$3.0 and $\leq$3.8 mm. Given the manufacturer's indication on maximum scaffold expansion, for each nominal diameter a further expansion of 0.5 mm was allowed. Enrolled subjects were willing to comply with specified follow-up evaluation and to be contacted by telephone. Exclusion criteria comprise pregnancy, known intolerance to contrast medium, uncertain neurological outcome after cardiopulmonary resuscitation, previous percutaneous coronary intervention with the implantation of a metal stent, left main (LM) disease previous coronary artery bypass grafting (CABG), age superior to 75 years, and participation to another investigational drug or device study before reaching the primary endpoints. The enrolment period started on 1 November 2012 and ended on 30 March 2013. Dual antiplatelet therapy after the BVS implantation was planned to have a duration of 12 months. Baseline and post-BVS implantation QCA analysis, OCT analyses at post-BVS implantation, and clinical outcomes at the 30-day follow-up were evaluated.

Definitions

Success rates were defined as follows: device success was the attainment of $<$30% final residual stenosis of the segment of the culprit lesion covered by the BVS, by angiographic visual estimation. Procedure success was defined as device success and no major periprocedural complications (Emergent CABG, coronary perforation requiring pericardial drainage, residual dissection impairing vessel flow—TIMI-flow II or less). Clinical success was defined as procedural success and no in-hospital major adverse cardiac events (MACE). All deaths were considered cardiac unless an undisputed non-cardiac cause was identified. Myocardial infarction (MI) and scaffold thrombosis were defined according to the Academic Research Consortium definition.[18] Target-lesion revascularization (TLR) was defined as clinically driven if at repeat angiography the diameter stenosis was $>$70%, or if a diameter stenosis $>$50% was present in association with (i) presence of recurrent angina pectoris, related to the target vessel; (ii) objective signs of ischaemia at rest (ECG changes) or during exercise test, related to the target vessel; and (iii) abnormal results of any functional diagnostic test.

The device-oriented endpoint target-lesion failure was defined as the composite of cardiac death, target-vessel MI, or ischaemia-driven TLR. Major adverse cardiac events defined as the composite of cardiac death, any re-infarction (Q- or non-Q-wave), emergent bypass surgery (CABG), or clinically driven TLR. Target-vessel failure (TVF) was defined as cardiac death, target-vessel MI, or clinically driven TVR.

Ethics

This is an observational study, performed according to the privacy policy of the Erasmus MC and to the Erasmus MC regulations for the appropriate use of data in patient-oriented research, which are based on international regulations, including the declaration of Helsinki. The BVS received the CE mark for clinical use, indicated for improving coronary lumen diameter in patients with ischaemic heart disease due to *de novo* native coronary artery lesions with no

restriction in terms of clinical presentation. Therefore, the BVS can be currently used routinely in Europe in different settings comprising the acute MI without a specific written informed consent in addition to the standard informed consent to the procedure. Given this background, a waiver from the hospital Ethical Committee was obtained for written informed consent, as according to Dutch law written consent is not required, if patients are not subject to acts other than as part of their regular treatment.

Study device

The second-generation everolimus-eluting BVS is a balloon expandable device consisting of a polymer backbone of poly-L-lactide acid (PLLA) coated with a thin layer of amorphous matrix of poly-D and -L-lactide acid (PDLLA) polymer (strut thickness 157 μm). The PDLLA controls the release of the antiproliferative drug everolimus (100 $\mu g/cm^2$), 80% of which is eluted within the first 30 days. Both PLLA and PDLLA are fully bioresorbable. The polymers are degraded via hydrolysis of the ester bonds and the resulting lactate and its oligomers are metabolized by the Krebs cycles. Small particles (<2 μm in diameter) may be also phagocytized and degraded by macrophages.[19] According to preclinical studies, the time for complete bioresorption of the polymer backbone is ~2–3 years.[20] The BVS edges contain two platinum markers for accurate visualization during angiography or other imaging modalities.

Quantitative coronary angiography analysis

Quantitative coronary angiography (QCA) analyses were performed using the Coronary Angiography Analysis System (Pie Medical Imaging, Maastricht, Netherlands).

Analyses were performed at pre-procedure, after thombectomy, after balloon dilatation, and after the BVS implantation with a methodology already reported.[21]

In case of thrombotic total occlusion, pre-procedure QCA analysis was performed as proximally as possible from the occlusion (in case of a side branch distally to the most proximal take off of the side branch). Intracoronary thrombus was angiographically identified and scored in five grades as previously described.[22] Thrombus grade was assessed before procedure and after thombectomy.

The QCA measurements included reference vessel diameter (RVD)—calculated with interpolate method—percentage diameter stenosis, minimal lumen diameter (MLD), and maximal lumen diameter (D_{max}). Acute gain was defined as post-procedural MLD minus pre-procedural MLD (MLD value equal to zero was applied when culprit vessel was occluded pre-procedurally). Complications occurring any time during the procedure, such as dissection, spasm, distal embolization, and no-reflow were reported. As additional information, MI SYNTAX I and MI SYNTAX II scores providing long-term risk stratification for mortality and MACE in patients presenting with STEMI were assessed.[23]

Optical coherence tomography image acquisition and analysis

Optical coherence tomography imaging after the BVS implantation was encouraged in all patients but was not mandatory, subordinated to device availability and left at the operator's discretion.

Therefore, OCT imaging of the culprit lesion after treatment was performed in a subset of the population. The image acquisition was performed with C7XR imaging console and the Dragonfly intravascular imaging catheter (both St. Jude Medical, St. Paul, MN, USA). Image acquisition has been previously described.[24] Briefly, after positioning the OCT catheter distally to the most distal scaffold marker, the catheter is pulled back automatically at 20 mm/s with simultaneous contrast infusion by a power injector (flush rate 3–4 mL/s). In cases where the entire scaffold region was not imaged in one pullback, a second more proximal pullback was performed for complete visualization. Images were stored and analysed offline.

Analysis of the OCT images was performed with the St Jude/Lightlab offline analysis software (St. Jude Medical), using previously described methodology for BVS analysis.[17] Analysis was performed in 1-mm longitudinal intervals within the treated culprit segment, after exclusion of frames with <75% lumen contour visibility. Lumen, scaffold, and incomplete scaffold apposition (ISA) area were calculated in accordance with standard methodology for analysis of bioresorbable scaffolds[17] (*Figure 1A* and *B*), while in sites with overlapping scaffolds, analysis was performed using previously suggested modifications[25] (*Figure 1D*). Specifically, the lumen contour is traced at the lumen border and in the abluminal (outer) side of apposed struts, while in the case of malapposed struts the contour is traced behind the malapposed struts. In cases where the scaffold struts are completely covered by tissue or thrombus, the lumen contour is traced above the prolapsing tissue (*Figure 1C*). The scaffold area is traced following interpolation of points located in the mid-point of the abluminal border of the black core in apposed struts and the mid-point of the abluminal strut frame border in malapposed or side branch-related struts, so that the scaffold area is identical to the lumen area in the absence of ISA and tissue prolapse. Incomplete scaffold apposition area is traced in the case of malapposed struts as the area delineated between the lumen and scaffold contours (*Figure 1B*).

A special consideration should be mentioned concerning BVS analysis in MI with the presence of increased tissue prolapse and residual thrombus post-implantation[21,26] (*Figures 1C* and *2*). Tissue prolapse area can be quantified as the difference between the scaffold and the lumen area. For the calculation of prolapse area, in the case that one or more scaffold struts are completely covered by thrombus or tissue, the total black core area of these struts is also measured. Prolapse area is then calculated as [scaffold area + ISA area − lumen area − embedded black core area]. The area of non-attached intraluminal defects (e.g. thrombus) is also measured. Atherothrombotic area is then calculated as the sum of prolapse area and intraluminal defect area and normalized as a percent ratio of the scaffold area (atherothrombotic burden, ATB).[21,26] It should be noted that in the case of bioresorbable scaffolds where measurements of the scaffold area are performed using the abluminal side of the scaffold struts, ATB is overestimated compared with metal platform stents where measurements of the stent area are performed from the adluminal (inner) side of the struts. Additionally, flow area was assessed as [scaffold area + ISA area − atherothrombotic area − total strut area] and the minimal flow area was recorded.

A scaffold strut is defined as incompletely apposed when there is no contact between the abluminal border of the strut and the vessel wall. This does not include struts located in front of side branches or their ostium (polygon of confluence region), which are

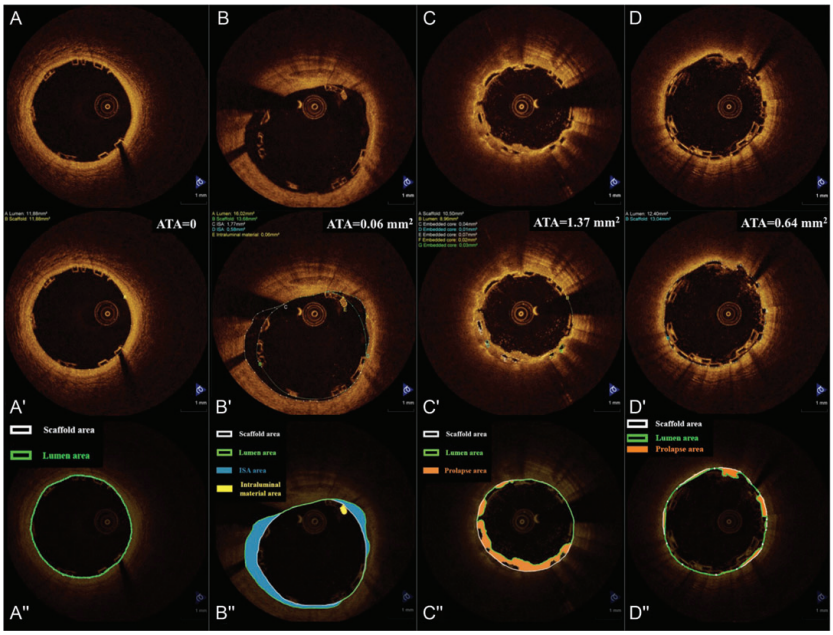

Figure 1 Methodology of optical coherence tomography analysis. (*A*) Good scaffold apposition and absence of incomplete scaffold apposition or tissue prolapse, (*B*) incomplete scaffold apposition, (*C*) sites with high tissue prolapse and struts completely covered by thrombus, and (*D*) overlapping scaffolds. Upper panel shows baseline images, middle panel shows quantitative measurements, and lower panel shows methodology for analysis. ISA, incomplete scaffold apposition; ATA, atherothrombotic area.

defined as side branch-related struts. Intraluminal struts that are part of adjacent clusters of apposed struts in overlapping scaffolds are also not considered malapposed.[25] For illustrative proposes, OCT bi-dimensional images are reported by three-dimensional rendering by dedicated software (Intage Realia, KGT, Kyoto, Japan)[17] (*Figures 2* and *3*).

Statistical analysis

Continuous variables are presented as mean and standard deviation, and categorical variables are reported as count and percentages. Descriptive statistics was provided for all variables. The present study is intended to be a 'first experience investigation' evaluating feasibility and acute performance of the everolimus-eluting BVS for the treatment of patients presenting with STEMI. A patient population of at least 30 patients was planned to be included in the present study. Comparisons among multiple means were performed with analysis of variance (one-way ANOVA). Score (Wilson) confidence intervals were reported for measures of success. Type A intraclass correlation coefficients (ICCs) for absolute agreement were used for assessing intra- and interobserver agreement, while measurement error and 95% limits of agreement were assessed by Bland–Altman analysis. The ICCs were computed with a two-way random effects model (single measures). All statistical tests were performed with SPSS, version 15.0 for windows (IL, USA).

Results

From 1 November 2012 to 30 April 2013, a total of 267 patients presented with acute MI. Twenty-one of those patients were treated percutaneously without any stent implantation (thrombectomy or balloon dilatation alone). Seventy-four had a culprit lesion located in a coronary vessel with a vessel diameter out of the range availability of the BVS (i.e. RVD >4.0 mm). Out of the remaining 172 patients, 125 were meeting the inclusion and none of the exclusion criteria of the present study (47 patients excluded for age, previous PCI or CABG, left main disease). Seventy-six of those patients were treated with metal stents and 49 cases (48 implanted with BVS) were enrolled in the present study (*Figure 4*, *Table 1*). Therefore, the patients implanted with BVS constitute the ~38% of the patients eligible for the present investigation.

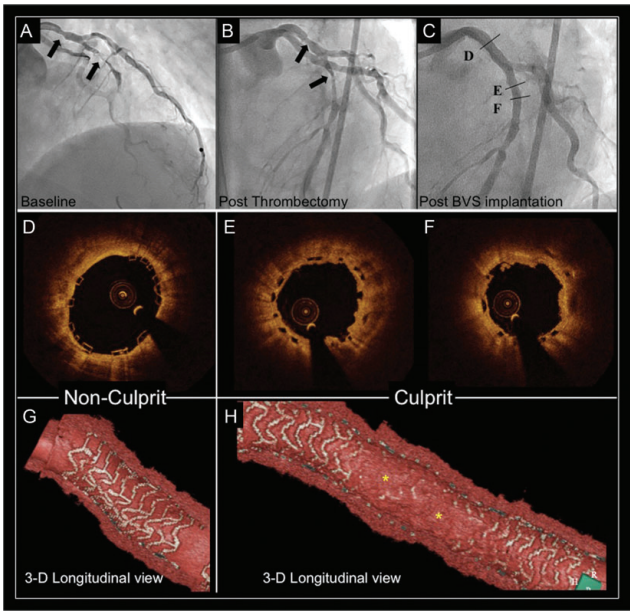

Figure 2 Bioresorbable vascular scaffolds implantation in a culprit and a non-culprit lesion in myocardial infarction. (*A*) Coronary angiography demonstrating a stenotic lesion in proximal LAD (proximal non-culprit lesion) and a total occlusion of the mid-LAD (culprit lesion). (*B*) Angiography following thrombus aspiration. (*C*) Angiography following implantation of a 3.5 × 12 mm bioresorbable vascular scaffolds at the proximal LAD lesion and a 3.0 × 28 mm bioresorbable vascular scaffolds at the mid-LAD lesion. (*D*) Optical coherence tomography image from the proximal non-culprit lesion showing absence of tissue prolapse and thrombus in the 3.5 × 12 mm scaffold. (*E* and *F*) Optical coherence tomography images from the culprit lesion showing complete coverage of the bioresorbable vascular scaffolds by tissue prolapse and presence of small amount of intraluminal defect. (*G*) Three-dimensional optical coherence tomography rendering in the proximal non-culprit lesion with complete scaffold visualization indicating the absence of prolapsing material. (*H*) Conversely, in the three-dimensional rendering of the culprit lesion, the morphology of the bioresorbable vascular scaffolds cannot be fully visualized due to high levels of tissue prolapse (*).

Baseline clinical characteristics of the 172 patients (49 patients included in the intent-to-treat population and 123 patients implanted with metal stents) with vessels size in the range of the BVS availability are reported in *Table 1*. In the intent-to-treat population thirty-eight patients were male (77.6%), mean age was 58.9 ± 10.5 years. Lesions were distributed as follows: left anterior descending 21 (42.9%), right coronary artery 22 (44.9%), and circumflex 6 (12.2%). Baseline clinical data of the enrolled patients were compared with the general population presenting with acute MI and implanted with a metal stent in vessels theoretically suitable for BVS implantation. Minimal differences were observed between the two groups. Namely, age 58.9 ± 10.5 vs. 66.4 ± 12.2, $P < 0.001$ and previous PCI 0% vs. 12.2%, $P = 0.007$. All the other clinical characteristics of the two populations did not show any significant difference.

Mean door-to-balloon time was 31.3 ± 19.5 min. All patients were treated with unfractionated heparin at the dose of 70–100 UI/kg and dual antiplatelet therapy (aspirin plus, prasugrel in 45 patients or clopidogrel in 4 patients). Manual thrombectomy was performed in 38 patients. In 16 cases, direct stenting was performed; a total of 65 scaffolds were implanted (12 patients received overlapping scaffolds—overlap was systematically intended to be minimal). The scaffolds lengths used were 12, 18, and 28 mm, with scaffolds diameters 2.5, 3.0, and 3.5 mm. Mean scaffold length per-lesion was 26.40 ± 13.86 mm, mean scaffold diameter per-lesion was 3.2 ± 34 mm. A highly supportive wire was used in five cases and radial approach was performed in 26 patients (53.0%) (*Table 2*). The procedural success was 97.9% (48/49 patients); in one patient, the delivery of the BVS was unsuccessful (due to the remarkable vessel tortuosity was not

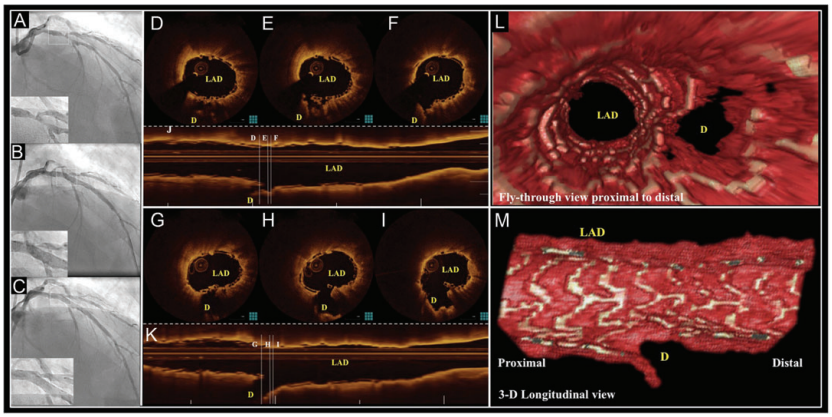

Figure 3 Bioresorbable vascular scaffold implantation in a thrombotic bifurcation lesion treated with provisional approach. (*A*) Coronary angiography pre-intervention. (*B*) Angiography following bioresorbable vascular scaffold implantation in the LAD, showing pinching of the ostium of the diagonal (D). (*C*) Final angiographic result following side branch dilation with 2.0 × 15 mm balloon. (*D–F* and *J*) Optical coherence tomography cross-sectional images and l-mode after bioresorbable vascular scaffolds implantation showing the compromise of the side branch after implantation and presence of thrombus at the side branch ostium. (*G–I* and *K*) Optical coherence tomography cross-sectional images and l-mode after side branch dilation, showing the opening of the carina of the side branch. (*L* and *M*) Three-dimensional reconstructions confirm the opening of the side branch ostium.

possible to advance the BVS at the site of the lesion) and a metallic DES was implanted. Clinical success was 97.9% (48/49 patients).

Quantitative coronary angiography analysis

The QCA is reported only in patients implanted with BVS. In 50.0% of those patients, pre-procedure TIMI-flow was 0 and the RVD was 2.94 ± 0.77 mm. In the non-totally occluded vessels, the RVD was 2.62 ± 0.63 mm, with an MLD of 0.75 ± 0.44 mm and a mean diameter stenosis of 70.8 ± 12.5%. After thrombectomy and balloon dilatation, TIMI-flow grade 0 was present in 2.5 and 0.0% of patients, respectively, and TIMI-flow III in 52.5 and 59.3% of the cases, respectively. After the scaffold implantation, there were no cases of TIMI-flow 0, and a TIMI-flow III was achieved in 91.7% of patients, the mean post-procedure in-scaffold % diameter stenosis was 14.7 ± 8.2%, in-scaffold MLD was 2.44 ± 0.49 mm (*Table 3*). No angiographically visible residual thrombus was observed at post-procedure.

Optical coherence tomography findings

Optical coherence tomography analysis was performed in a subgroup of 31 patients implanted with BVS. Mean lumen area was 8.02 ± 1.92 mm^2, minimum lumen area 5.95 ± 1.61 mm^2, and minimum flow area 5.62 ± 1.66 mm^2. Incomplete scaffold apposition (ISA) was observed in 20 patients with a mean ISA area of 0.118 ± 0.162 mm^2 and a mean percentage of malapposed struts per patients equal to 2.80 ± 3.90%. The mean prolapse area was 0.60 ± 0.26 mm^2, and the mean intraluminal defect area was 0.013 ± 0.017 mm^2. Scaffolds with >5% malapposed struts were 7 (*Table 4*). The OCT analysis stratified by scaffold size (5 BVS 2.5 mm, 13 BVS 3.0 mm, 24 BVS 3.5 mm) showed different lumen, scaffold, and flow areas, but similar amounts of incomplete stent apposition, plaque prolapse, and intraluminal mass areas (*Table 5*). In three cases, the observation of scaffold malapposition by OCT, guided an additional post-dilatation and in one patient the visualization of considerable intraluminal thrombus as assessed by OCT led to a repeated thrombus aspiration.

Intra-observer variability was excellent. Intraclass correlation coefficients were 0.999 for lumen area and 0.999 for scaffold area, and the corresponding measurement errors and limits of agreement were 0.01 mm^2 (−0.12 to 0.15 mm^2) for lumen area and −0.01 mm^2 (−0.20 to 0.17 mm^2) for scaffold area. Similarly, inter-observer intraclass correlation coefficients were 0.997 for lumen area and 0.987 for scaffold area, and the corresponding measurement errors and limits of agreement were −0.01 mm^2 (−0.30 to 0.28 mm^2) for lumen area and −0.22 mm^2 (−0.68 to 0.24 mm^2) for scaffold area.

Clinical outcomes

At the 30-day follow-up, the rate of the device-oriented endpoint, target-lesion failure, was 0%. None of the patients experienced target-vessel re-infarction, emergent bypass surgery, or clinically driven TLR. No cases of cardiac death or scaffold thrombosis were reported. The MACE rate was 2.6% as one patient, after discharge developed a non-Q-wave MI related to a non-target-vessel lesion and underwent a non-target-vessel revascularization within the

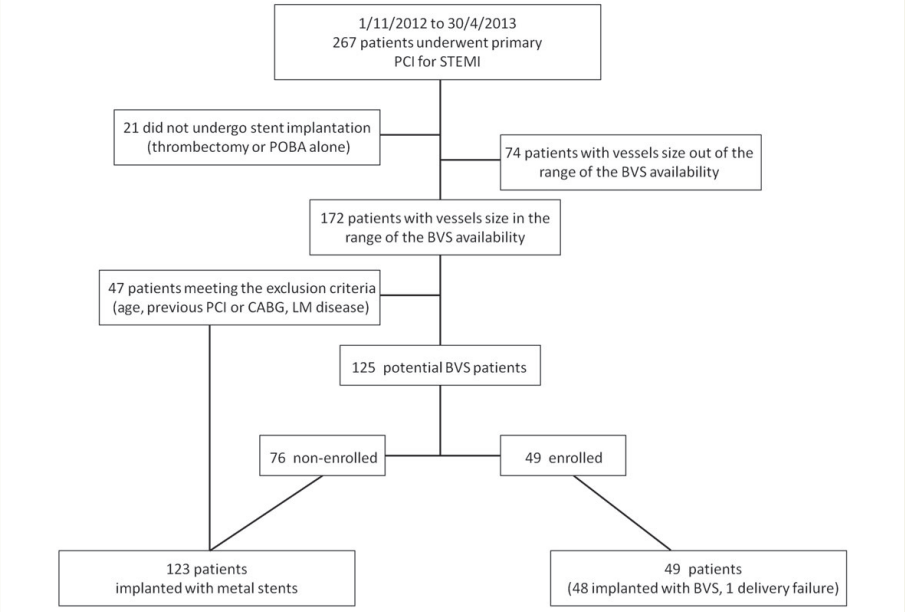

Figure 4 Flow-chart of the study. From 1 November 2012 to 30 April 2013, a total of 267 patients presented with acute myocardial infarction. Twenty-one of those patients were treated percutaneously but without any stent implantation (thrombectomy or balloon dilatation alone). Seventy-four had a culprit lesion located in a coronary vessel with a vessel diameter out of the range availability of the bioresorbable vascular scaffolds (i.e. reference vessel diameter >4.0 mm). Out of the remaining 172 patients, 125 were meeting the inclusion and none of the exclusion criteria of the present study (47 patients excluded for age, previous PCI or CABG, left main disease). Seventy-six of those patients were treated with metal stents and 49 cases (48 implanted with BVS) were included in the present study.

30 days post-procedure. This was the only event reported in the studied population (*Table 6*).

Discussion

The everolimus-eluting BVS has been tested so far only in elective patients with stable, unstable angina, or silent ischaemia;[16,17,27–29] showing promising results up to 4-year follow-up[30] for the first-generation and up to 2 years for the second-generation BVS.[12,13,31] The present study represents an early investigation reporting clinical and angiographic data on the use of the second-generation BVS for the treatment of patients presenting with STEMI and evaluating acute results with high-resolution intracoronary imaging (OCT).

A high device, procedural, and clinical success rates were observed with all the scaffolds achieving a residual stenosis <30% and no in-hospital MACE. Such data are supportive of feasibility and good acute performance of the BVS for the treatment of patients with acute MI.

Angiographic data

The everolimus-eluting BVS was implanted in patients presenting with ST-segment elevation and a thrombus burden 4 or 5 in 63.0% of the cases. A theoretical concern related to the implantation of the BVS in such thrombotic lesions is the fact that scaffold positioning and placement may need a more aggressive lesion preparation (pre-dilatation) compared with standard metal devices, due to its slightly higher profile. We hypothesized that this strategy might be prone to an increase in distal embolization following balloon inflations, favouring no-reflow and reducing the rate of final TIMI-flow III.

However, the analysis of the post-procedural angiographies revealed a TIMI-flow III in 91.7% of the cases; such results are in line with recently reported large trials evaluating the performance of metallic stents in patients presenting with acute MI.[5,6] Less thrombus embolization may result from a different pattern of thrombus dislodgment and compression to the arterial wall after deployment of a device with a larger strut width (157 μm) compared with currently available metallic stents. The percentage of vessel wall area

Table 1 **Baseline clinical characteristics intent-to-treat population and patients treated with metallic stent in the enrolment period**

Clinical characteristics	BVS (*N* = 49)	Metal stents (*N* = 123)	*P*-value
Age (year)	58.9 ± 10.5	66.4 ± 12.2	<0.001
Male, *n* (%)	38 (77.6)	93 (75.6)	0.845
Hypertension, *n* (%)	19 (38.8)	53/105 (50.5)	0.225
Hypercholesterolemia, *n* (%)	11 (22.4)	30/100 (30.0)	0.435
Diabetes, *n* (%)	4 (8.2)	14/116 (12.1)	0.590
Smoke, *n* (%)	27 (69.2)	46/116 (39.7)	0.120
Family history of CAD, *n* (%)	12 (24.5)	31/95 (32.6)	0.343
Peripheral vascular disease, *n* (%)	1 (2.0)	8 (6.5)	0.449
Kidney disease, *n* (%)	1 (2.0)	7 (5.7)	0.442
Prior MI, *n* (%)	1 (2.0)	14 (11.4)	0.070
Prior PCI, *n* (%)	0 (0.0)	15 (12.2)	0.007
Prior CABG, *n* (%)	0 (0.0)	3 (2.4)	0.559
COPD, *n* (%)	2 (4.1)	5 (4.1)	1.000
Culprit vessel			0.624
LM, *n* (%)	0 (0)	2 (1.6)	
LAD, *n* (%)	21 (42.9)	52 (42.3)	
RCA, *n* (%)	22 (44.9)	46 (37.4)	
LCX, *n* (%)	6 (12.2)	21 (17.1)	
SVG, *n* (%)	0 (0)	2 (1.6)	

Patients with vessels diameters not feasible for BVS implantation (i.e. reference vessel diameter ≥4.0 mm) were excluded.
Data are expressed as mean ± SD or number and proportion, *n* (%).
CAD, coronary artery disease; MI, myocardial infarction; PCI, percutaneous coronary intervention; CABG, coronary artery bypass graft; COPD, chronic obstructive pulmonary disease; LM, left main; LAD, left anterior descending; RCA, right coronary artery; LCX, circumflex; SVG, saphenous vein graft.

Table 2 **Procedural data intent-to-treat population**

Procedural data	*N* = 49
Medications	
Aspirin, *n* (%)	49 (100)
Prasugrel, *n* (%)	45 (91.8)
Clopidogrel, *n* (%)	4 (8.2)
Glycoprotein IIb/IIIa antagonists, *n* (%)	17 (34.7)
Unfractionated heparin, *n* (%)	49 (100)
Mean door-to-balloon time (min)	31.3 ± 19.5
Manual thrombectomy, *n* (%)	38 (77.5)
Direct stenting, *n* (%)	16 (32.7)
Pre-dilatation, *n* (%)	33 (67.3)
Mean pre-dilatation balloon diameter per-lesion (mm)	2.6 ± 0.67
Post-dilatation, *n* (%)	10 (20.4)
Mean post-dilatation balloon diameter per-lesion (mm)	3.5 ± 0.47
Overlapping, *n* (%)	12 (24.5)
Overlap scaffolds diameters 3.5 mm–3.5 mm, *n* (%)	5 (10.2)
Overlap scaffolds diameters 3.5 mm – 3 mm *n* (%)	5 (10.2)
Overlap scaffolds diameters 3.5 mm–2.5 mm, *n* (%)	1 (2.0)
Overlap scaffolds diameters, 3 mm–2.5 mm, *n* (%)	1 (2.0)
Total number of scaffolds, *n*.	65
Mean scaffolds per-lesion, *n*.	1.35 ± 0.60
Mean scaffold length per-lesion (mm)	26.40 ± 13.86
Mean scaffold diameter per-lesion (mm)	3.2 ± 34
Supportive wire, *n*. (%)	5 (10.2)
Radial approach, *n*. (%)	26 (53.0)

Data are expressed as mean ± SD or number and proportion, *n* (%).

covered by the BVS polymer (scaffold/vessel ratio) has been previously evaluated to be 26%,[32] a value considerably higher compared with what observed for conventional metallic DES (i.e. EES provides a percentage stent/vessel ratio equal to 12%).[32] This characteristic of the BVS might be associated to an increased capacity of capturing debris and thrombotic material behind the struts before embolization to distal microcirculation. This so-called snow racket concept (entrapment of thrombotic material between the stent and the vessel) is currently the basis for the design of novel devices and clinical studies.[33]

Optical coherence tomography findings

Given its high resolution, OCT allows the assessment of *in vivo* strut apposition and presence of thrombus.[24,34–36]

The present analysis was performed at 1 mm intervals in the OCT pullback. Although, the possibility for a more strict assessment of OCT analysis in thrombotic lesion may be considered,[21] this methodology is the current standard applied in our institution for clinical studies, and the most commonly used in the literature.

Previous reports defined a stent malapposed if at least 5% of struts were observed to be malapposed;[37,38] in the present investigation, only seven scaffolds (22.6%) investigated with OCT showed a strut malapposition of >5%, with an overall mean struts malapposition equal to 2.8 ± 3.90%. A recently reported study using a similar methodology to investigate malapposition after metallic balloon expandable stent implantation in STEMI patients showed a total of 37.1% malapposed stents (stents with >5% malapposition) with a mean percentage of strut malapposition equal to 5.99 ± 7.28%.[38] In addition, the mean ISA area was 0.118 ± 0.162 mm^2, a value in line with data reported for metallic stent implantation in patients presenting with STEMI.[21,38] Similarly, the amount of intraluminal defect after scaffold implantation was minimal and comparable with what is observed in metallic stents.[21] Notably, these results were consistent among different scaffold sizes.

Clinical outcomes

In the present series, none of patients treated with BVS experienced a clinical event related to the treated vessel at the 30-day follow-up. These observations support the feasibility of BVS implantation in patients presenting with acute STEMI.

Table 3 **Angiographic analysis in patients implanted with bioresorbable vascular scaffolds**

Angiographic data	*N* = 48
Pre-procedure	
TIMI-flow, % (*n*)	
0	50.0% (23/46)
1	15.2% (7/46)
2	21.7% (10/46)
3	13.0% (6/46)
Thrombus burden, % (*n*)	
0	0.0% (0/46)
1	6.5% (3/46)
2	17.4% (8/46)
3	13.0% (6/46)
4	13.0% (6/46)
5	50.0% (23/46)
Total occlusion (*N* = 23)	
RVD (mm)	2.94 ± 0.77
Non-total occlusion (*N* = 23)	
RVD (mm)	2.62 ± 0.63
MLD (mm)	0.75 ± 0.44
Diameter stenosis (%)	70.8 ± 12.5
After thrombectomy	
TIMI-flow, % (*n*)	
0	2.5% (1/40)
1	7.5% (3/40)
2	37.5% (15/40)
3	52.5% (21/40)
Thrombus burden, % (*n*)	
0	0.0% (0/40)
1	30.0% (12/40)
2	35.0% (14/40)
3	22.5% (9/40)
4	10.0% (4/40)
5	2.5% (1/40)
After pre-dilatation	
TIMI-flow, % (*n*)	
0	0.0% (0/27)
1	7.4% (2/27)
2	33.3% (9/27)
3	59.3% (16/27)
Before BVS implantation	
RVD (mm)	2.63 ± 0.53
MLD (mm)	1.21 ± 0.46
Diameter stenosis (%)	53.2 ± 16.1
D_{max} (mm)	3.01 ± 0.52
Post-procedure	
TIMI-flow, % (*n*)	
0	0.0% (0/48)
1	0.0% (0/48)
2	8.3% (4/48)
3	91.7% (44/48)
In-scaffold	
RVD (mm)	2.86 ± 0.52
MLD (mm)	2.44 ± 0.49
Diameter stenosis (%)	14.7 ± 8.2
In-segment	
RVD (mm)	2.74 ± 0.59
MLD (mm)	2.20 ± 0.53
Diameter stenosis (%)	21.8 ± 12.0
MI syntax score I[a]	10.0 (7.0–15.0)
MI syntax score II[a]	7.0 (4.25–10.0)
Dominant right coronary artery, % (*n*)	93.8% (45/48)
Scaffold-to-artery ratio	1.19 ± 0.24
Complications occurring any time during the procedure, % (*n*)	
Dissection	6.3% (3/48)
Spasm	4.2% (2/48)
Distal embolism	14.6% (7/48)
No-reflow	2.1% (1/48)

Data are expressed as mean ± SD or proportion (%).
[a]MI syntax scores I and II are expressed as median (interquartile range).

Table 4 **Optical coherence tomography findings post-implantation in patients implanted with bioresorbable vascular scaffolds**

OCT variables	*N* = 31
Analysed length (mm)	28.16 ± 13.29
Analysed struts, *n*	245 ± 135
Minimum lumen area (mm^2)	5.95 ± 1.61
Mean lumen area (mm^2)	8.02 ± 1.92
Lumen volume (mm^3)	225.78 ± 113.63
Minimum scaffold area (mm^2)	6.69 ± 1.94
Mean scaffold area (mm^2)	8.54 ± 1.97
Scaffold volume (mm^3)	240.07 ± 118.48
Minimum flow area (mm^2)	5.62 ± 1.66
ISA area (mm^2) (*N* = 20)	0.118 ± 0.162
Mean prolapse area (mm^2)	0.60 ± 0.26
Mean intraluminal defect area (mm^2)	0.013 ± 0.017
Maximum intraluminal defect area (mm^2)	0.094 ± 0.077
Mean atherothrombotic area (mm^2)	0.61 ± 0.27
Mean atherothrombotic burden (%)	7.29 ± 3.12
Malapposed struts per patient (%)	2.80 ± 3.90
Scaffolds with at least 1 malapposed strut, *n* (%)	20 (64.5)
Scaffolds with >5% malapposed struts, *n* (%)	7 (22.6)

ISA, incomplete scaffold apposition.
Data are expressed as mean ± SD or number and proportion, *n* (%).

Table 5 Optical coherence tomography findings post-implantation stratified by scaffold size in patients implanted with bioresorbable vascular scaffolds

OCT variables				
Scaffold size	**2.5 mm (*N* = 5)**	**3.0 mm (*N* = 13)**	**3.5 mm (*N* = 24)**	***P***
Analysed length (mm)	18.80 ± 1.30	22.23 ± 6.46	21.33 ± 7.38	0.628
Minimum lumen area (mm^2)	4.08 ± 0.24	5.60 ± 0.93	7.18 ± 1.58	0.001
Mean lumen area (mm^2)	5.42 ± 0.75	7.18 ± 1.03	9.25 ± 1.72	0.001
Minimum scaffold area (mm^2)	4.53 ± 0.51	6.13 ± 1.02	8.06 ± 1.82	0.001
Mean scaffold area (mm^2)	5.62 ± 0.28	7.66 ± 0.88	9.82 ± 1.70	0.001
Minimum flow area (mm^2)	3.84 ± 0.28	5.17 ± 0.86	6.77 ± 1.60	0.001
ISA area (mm^2) (*N* = 25)	0.190 ± 0.318 (*N* = 3)	0.063 ± 0.072 (*N* = 10)	0.133 ± 0.177 (*N* = 12)	0.429
Mean prolapse area (mm^2)	0.40 ± 0.19	0.54 ± 0.27	0.62 ± 0.29	0.246
Mean intraluminal defect area (mm^2)	0.007 ± 0.008	0.016 ± 0.021	0.012 ± 0.018	0.628
Maximum intraluminal defect area (mm^2)	0.072 ± 0.081	0.102 ± 0.086	0.068 ± 0.065	0.096
Mean atherothrombotic area (mm^2)	0.40 ± 0.19	0.56 ± 0.27	0.64 ± 0.30	0.237
Mean atherothrombotic burden (%)	6.00 ± 4.66	7.42 ± 3.79	6.20 ± 3.39	0.594

ISA, incomplete scaffold apposition.
Data are expressed as mean ± SD or number and proportion, *n* (%).

Table 6 Clinical outcomes at the 30-day follow-up intent-to-treat population

Clinical events	*N* = 49	95% CI
Target-lesion failure	(0/49) 0%	(0–7.41)
TVF	(0/49) 0%	(0–7.41)
Cardiac death	(0/49) 0%	(0–7.41)
Target-vessel MI	(0/49) 0%	(0–7.41)
Q-wave MI	(0/49) 0%	(0–7.41)
Non Q-wave MI	(0/49) 0%	(0–7.41)
Clinically driven target-vessel revascularization	(0/49) 0%	(0–7.41)
Any MI	(1/49) 2.6%	(0–10.69)
Q-wave MI	(0/49) 0%	(0–7.41)
Non Q-wave MI	(1/49) 2.6%	(0–10.69)
Major adverse cardiac events	(1/49) 2.6%	(0–10.69)
Non-target-vessel revascularization	(1/49) 2.6%	(0–10.69)
Definite or probable scaffold thrombosis	(0/49) 0%	(0–7.41)

Data are expressed number and proportion, *n* (%). 95% CI, 95% confidence interval.

Data showed in the present report with optimal acute performance in terms of final TIMI-flow and scaffold apposition may suggest that everolimus-eluting BVS could be considered for the treatment of patients presenting with STEMI, however, due to the limited number of patients and events, caution should be made in reaching firm conclusions. Further larger studies are needed to fully evaluate the performance of the present device in STEMI patients.

Limitations

The present study represents a feasibility study with a limited number of patients. The small sample size does not allow reaching conclusions in terms of clinical outcomes. The lack of a head-to-head comparison with the current standard of care is a major limitation of the present study. A longer follow-up is needed to fully evaluate the performance of this novel device in patients presenting with acute MI. During the enrolment period, the implantation of either metallic stent or BVS in STEMI patients was left to the operator's discretion; this methodology may be prone to selection bias. Therefore, these data should not stimulate at the current state of knowledge the use of BVS in patients presenting with acute MI. Larger randomized studies are needed to confirm these preliminary observations.

Conclusion

In the present investigation, the implantation of the everolimus-eluting BVS was observed to be feasible in patients presenting with STEMI with optimal acute performance. These data are preliminary and need further confirmation in randomized controlled trials to define the true role of BVS for the treatment of patients presenting with acute myocardial infarction.

Funding

Conflict of interest: Dr R.J. van Geuns received speakers fee from Abbott Vascular. Abbott Vascular is providing institution research grant for the Erasmus MC. Antonios Karanasos received funding support from the Hellenic Heart Foundation and St Jude Medical.

References

1. Task Force on Myocardial Revascularization of the European Society of C, the European Association for Cardio-Thoracic S, European Association for Percutaneous

Cardiovascular I, Wijns W, Kolh P, Danchin N, Di Mario C, Falk V, Folliguet T, Garg S, Huber K, James S, Knuuti J, Lopez-Sendon J, Marco J, Menicanti L, Ostojic M, Piepoli MF, Pirlet C, Pomar JL, Reifart N, Ribichini FL, Schalij MJ, Sergeant P, Serruys PW, Silber S, Sousa Uva M, Taggart D. Guidelines on myocardial revascularization. *Eur Heart J* 2010;**31**:2501–2555.

2. Spaulding C, Henry P, Teiger E, Beatt K, Bramucci E, Carrie D, Slama MS, Merkely B, Erglis A, Margheri M, Varenne O, Cebrian A, Stoll HP, Snead DB, Bode C, Investigators T. Sirolimus-eluting versus uncoated stents in acute myocardial infarction. *N Engl J Med* 2006;**355**:1093–1104.
3. Stone GW, Lansky AJ, Pocock SJ, Gersh BJ, Dangas G, Wong SC, Witzenbichler B, Guagliumi G, Peruga JZ, Brodie BR, Dudek D, Mockel M, Ochala A, Kellock A, Parise H, Mehran R, Investigators H-AT. Paclitaxel-eluting stents versus bare-metal stents in acute myocardial infarction. *N Engl J Med* 2009;**360**:1946–1959.
4. Brar SS, Leon MB, Stone GW, Mehran R, Moses JW, Brar SK, Dangas G. Use of drug-eluting stents in acute myocardial infarction: a systematic review and meta-analysis. *J Am Coll Cardiol* 2009;**53**:1677–1689.
5. Raber L, Kelbaek H, Ostojic M, Baumbach A, Heg D, Tuller D, von Birgelen C, Roffi M, Moschovitis A, Khattab AA, Wenaweser P, Bonvini R, Pedrazzini G, Kornowski R, Weber K, Trelle S, Luscher TF, Taniwaki M, Matter CM, Meier B, Juni P, Windecker S, Investigators CAT. Effect of biolimus-eluting stents with biodegradable polymer vs bare-metal stents on cardiovascular events among patients with acute myocardial infarction: the COMFORTABLE AMI randomized trial. *JAMA* 2012;**308**:777–787.
6. Sabate M, Cequier A, Iniguez A, Serra A, Hernandez-Antolin R, Mainar V, Valgimigli M, Tespili M, den Heijer P, Bethencourt A, Vazquez N, Gomez-Hospital JA, Baz JA, Martin-Yuste V, van Geuns RJ, Alfonso F, Bordes P, Tebaldi M, Masotti M, Silvestro A, Backx B, Brugaletta S, van Es GA, Serruys PW. Everolimus-eluting stent versus bare-metal stent in ST-segment elevation myocardial infarction (EXAMINATION): 1 year results of a randomised controlled trial. *Lancet* 2012;**380**:1482–1490.
7. Serruys PW, Garcia-Garcia HM, Onuma Y. From metallic cages to transient bioresorbable scaffolds: change in paradigm of coronary revascularization in the upcoming decade? *Eur Heart J* 2012;**33**:16–25b.
8. Finn AV, Joner M, Nakazawa G, Kolodgie F, Newell J, John MC, Gold HK, Virmani R. Pathological correlates of late drug-eluting stent thrombosis: strut coverage as a marker of endothelialization. *Circulation* 2007;**115**:2435–2441.
9. Joner M, Finn AV, Farb A, Mont EK, Kolodgie FD, Ladich E, Kutys R, Skorija K, Gold HK, Virmani R. Pathology of drug-eluting stents in humans: delayed healing and late thrombotic risk. *J Am Coll Cardiol* 2006;**48**:193–202.
10. Hong MK, Mintz GS, Lee CW, Kim YH, Lee SW, Song JM, Han KH, Kang DH, Song JK, Kim JJ, Park SW, Park SJ. Incidence, mechanism, predictors, and long-term prognosis of late stent malapposition after bare-metal stent implantation. *Circulation* 2004;**109**:881–886.
11. Hong MK, Mintz GS, Lee CW, Park DW, Park KM, Lee BK, Kim YH, Song JM, Han KH, Kang DH, Cheong SS, Song JK, Kim JJ, Park SW, Park SJ. Late stent malapposition after drug-eluting stent implantation: an intravascular ultrasound analysis with long-term follow-up. *Circulation* 2006;**113**:414–419.
12. Ormiston JA, Serruys PW, Onuma Y, van Geuns RJ, de Bruyne B, Dudek D, Thuesen L, Smits PC, Chevalier B, McClean D, Koolen J, Windecker S, Whitbourn R, Meredith I, Dorange C, Veldhof S, Hebert KM, Rapoza R, Garcia-Garcia HM. First serial assessment at 6 months and 2 years of the second generation of absorb everolimus-eluting bioresorbable vascular scaffold: a multi-imaging modality study. *Circ Cardiovasc Interv* 2012;**5**:620–632.
13. Serruys PW, Onuma Y, Dudek D, Smits PC, Koolen J, Chevalier B, de Bruyne B, Thuesen L, McClean D, van Geuns RJ, Windecker S, Whitbourn R, Meredith I, Dorange C, Veldhof S, Hebert KM, Sudhir K, Garcia-Garcia HM, Ormiston JA. Evaluation of the second generation of a bioresorbable everolimus-eluting vascular scaffold for the treatment of de novo coronary artery stenosis: 12-month clinical and imaging outcomes. *J Am Coll Cardiol* 2011;**58**:1578–1588.
14. Kajiya T, Liang M, Sharma RK, Lee CH, Chan MY, Tay E, Chan KH, Tan HC, Low AF. Everolimus-eluting bioresorbable vascular scaffold (BVS) implantation in patients with ST-segment elevation myocardial infarction (STEMI). *EuroIntervention* 2013;**9**:501–504.
15. Kocka V, Lisa L, Tousek P, Budesinsky T, Widimsky P. ST elevation myocardial infarction treated with bioresorbable vascular scaffold: rationale and first cases. *Eur Heart J* 2013;**34**:2073.
16. Ormiston JA, Serruys PW, Regar E, Dudek D, Thuesen L, Webster MW, Onuma Y, Garcia-Garcia HM, McGreevy R, Veldhof S. A bioabsorbable everolimus-eluting coronary stent system for patients with single de-novo coronary artery lesions (ABSORB): a prospective open-label trial. *Lancet* 2008;**371**:899–907.
17. Serruys PW, Onuma Y, Ormiston JA, de Bruyne B, Regar E, Dudek D, Thuesen L, Smits PC, Chevalier B, McClean D, Koolen J, Windecker S, Whitbourn R, Meredith I, Dorange C, Veldhof S, Miquel-Hebert K, Rapoza R, Garcia-Garcia HM. Evaluation of the second generation of a bioresorbable everolimus drug-eluting vascular scaffold for treatment of de novo coronary artery stenosis: six-month clinical and imaging outcomes. *Circulation* 2010;**122**:2301–2312.
18. Cutlip DE, Windecker S, Mehran R, Boam A, Cohen DJ, van Es GA, Steg PG, Morel MA, Mauri L, Vranckx P, McFadden E, Lansky A, Hamon M, Krucoff MW, Serruys PW, Academic Research C. Clinical end points in coronary stent trials: a case for standardized definitions. *Circulation* 2007;**115**:2344–2351.
19. Onuma Y, Serruys PW. Bioresorbable scaffold: the advent of a new era in percutaneous coronary and peripheral revascularization? *Circulation* 2011;**123**:779–797.
20. Onuma Y, Serruys PW, Perkins LE, Okamura T, Gonzalo N, Garcia-Garcia HM, Regar E, Kamberi M, Powers JC, Rapoza R, van Beusekom H, van der Giessen W, Virmani R. Intracoronary optical coherence tomography and histology at 1 month and 2, 3, and 4 years after implantation of everolimus-eluting bioresorbable vascular scaffolds in a porcine coronary artery model: an attempt to decipher the human optical coherence tomography images in the ABSORB trial. *Circulation* 2010;**122**:2288–2300.
21. Onuma Y, Thuesen L, van Geuns RJ, van der Ent M, Desch S, Fajadet J, Christiansen E, Smits P, Ramsing Holm N, Regar E, van Mieghem N, Borovicanin V, Paunovic D, Senshu K, van Es GA, Muramatsu T, Lee IS, Schuler G, Zijlstra F, Garcia-Garcia HM, Serruys PW, Investigators T. Randomized study to assess the effect of thrombus aspiration on flow area in patients with ST-elevation myocardial infarction: an optical frequency domain imaging study – TROFI trial. *Eur Heart J* 2013;**34**:1050–1060.
22. Sianos G, Papafaklis MI, Daemen J, Vaina S, van Mieghem CA, van Domburg RT, Michalis LK, Serruys PW. Angiographic stent thrombosis after routine use of drug-eluting stents in ST-segment elevation myocardial infarction: the importance of thrombus burden. *J Am Coll Cardiol* 2007;**50**:573–583.
23. Magro M, Nauta S, Simsek C, Onuma Y, Garg S, van der Heide E, van der Giessen WJ, Boersma E, van Domburg RT, van Geuns RJ, Serruys PW. Value of the SYNTAX score in patients treated by primary percutaneous coronary intervention for acute ST-elevation myocardial infarction: The MI SYNTAXscore study. *Am Heart J* 2011;**161**:771–781.
24. Tearney GJ, Regar E, Akasaka T, Adriaenssens T, Barlis P, Bezerra HG, Bouma B, Bruining N, Cho JM, Chowdhary S, Costa MA, de Silva R, Dijkstra J, Di Mario C, Dudek D, Falk E, Feldman MD, Fitzgerald P, Garcia-Garcia HM, Gonzalo N, Granada JF, Guagliumi G, Holm NR, Honda Y, Ikeno F, Kawasaki M, Kochman J, Koltowski L, Kubo T, Kume T, Kyono H, Lam CC, Lamouche G, Lee DP, Leon MB, Maehara A, Manfrini O, Mintz GS, Mizuno K, Morel MA, Nadkarni S, Okura H, Otake H, Pietrasik A, Prati F, Raber L, Radu MD, Rieber J, Riga M, Rollins A, Rosenberg M, Sirbu V, Serruys PW, Shimada K, Shinke T, Shite J, Siegel E, Sonoda S, Suter M, Takarada S, Tanaka A, Terashima M, Thim T, Uemura S, Ughi GJ, van Beusekom HM, van der Steen AF, van Es GA, van Soest G, Virmani R, Waxman S, Weissman NJ, Weisz G, International Working Group for Intravascular Optical Coherence T. Consensus standards for acquisition, measurement, and reporting of intravascular optical coherence tomography studies: a report from the International Working Group for Intravascular Optical Coherence Tomography Standardization and Validation. *J Am Coll Cardiol* 2012;**59**:1058–1072.
25. Farooq V, Onuma Y, Radu M, Okamura T, Gomez-Lara J, Brugaletta S, Gogas BD, van Geuns RJ, Regar E, Schultz C, Windecker S, Lefevre T, Brueren BR, Powers J, Perkins LL, Rapoza RJ, Virmani R, Garcia-Garcia HM, Serruys PW. Optical coherence tomography (OCT) of overlapping bioresorbable scaffolds: from benchwork to clinical application. *EuroIntervention* 2011;**7**:386–399.
26. Magro M, Regar E, Gutierrez-Chico JL, Garcia-Garcia H, Simsek C, Schultz C, Zijlstra F, Serruys PW, van Geuns RJ. Residual atherothrombotic material after stenting in acute myocardial infarction – an optical coherence tomographic evaluation. *Int J Cardiol* 2013;**167**:656–663.
27. Serruys PW, Ormiston JA, Onuma Y, Regar E, Gonzalo N, Garcia-Garcia HM, Nieman K, Bruining N, Dorange C, Miquel-Hebert K, Veldhof S, Webster M, Thuesen L, Dudek D. A bioabsorbable everolimus-eluting coronary stent system (ABSORB): 2-year outcomes and results from multiple imaging methods. *Lancet* 2009;**373**:897–910.
28. Diletti R, Onuma Y, Farooq V, Gomez-Lara J, Brugaletta S, van Geuns RJ, Regar E, de Bruyne B, Dudek D, Thuesen L, Chevalier B, McClean D, Windecker S, Whitbourn R, Smits P, Koolen J, Meredith I, Li D, Veldhof S, Rapoza R, Garcia-Garcia HM, Ormiston JA, Serruys PW. 6-month clinical outcomes following implantation of the bioresorbable everolimus-eluting vascular scaffold in vessels smaller or larger than 2.5 mm. *J Am Coll Cardiol* 2011;**58**:258–264.
29. Diletti R, Serruys PW, Farooq V, Sudhir K, Dorange C, Miquel-Hebert K, Veldhof S, Rapoza R, Onuma Y, Garcia-Garcia HM, Chevalier B. ABSORB II randomized controlled trial: a clinical evaluation to compare the safety, efficacy, and performance of the absorb everolimus-eluting bioresorbable vascular scaffold system against the XIENCE everolimus-eluting coronary stent system in the treatment of subjects with ischemic heart disease caused by de novo native coronary artery lesions: rationale and study design. *Am Heart J* 2012;**164**:654–663.
30. Dudek D, Onuma Y, Ormiston JA, Thuesen L, Miquel-Hebert K, Serruys PW. Four-year clinical follow-up of the ABSORB everolimus-eluting bioresorbable vascular scaffold in patients with de novo coronary artery disease: the ABSORB trial. *EuroIntervention* 2012;**7**:1060–1061.

31. Diletti R, Farooq V, Girasis C, Bourantas C, Onuma Y, Heo JH, Gogas BD, van Geuns RJ, Regar E, de Bruyne B, Dudek D, Thuesen L, Chevalier B, McClean D, Windecker S, Whitbourn RJ, Smits P, Koolen J, Meredith I, Li X, Miquel-Hebert K, Veldhof S, Garcia-Garcia HM, Ormiston JA, Serruys PW. Clinical and intravascular imaging outcomes at 1 and 2 years after implantation of absorb everolimus eluting bioresorbable vascular scaffolds in small vessels. Late lumen enlargement: does bioresorption matter with small vessel size? Insight from the ABSORB cohort B trial. *Heart* 2013;**99**:98–105.
32. Muramatsu T, Onuma Y, Garcia-Garcia HM, Farooq V, Bourantas CV, Morel MA, Li X, Veldhof S, Bartorelli A, Whitbourn R, Abizaid A, Serruys PW, Investigators A-E. Incidence and short-term clinical outcomes of small side branch occlusion after implantation of an everolimus-eluting bioresorbable vascular scaffold: an interim report of 435 patients in the ABSORB-EXTEND single-arm trial in comparison with an everolimus-eluting metallic stent in the SPIRIT first and II trials. *JACC Cardiovasc Interv* 2013;**6**:247–257.
33. Stone GW, Abizaid A, Silber S, Dizon JM, Merkely B, Costa RA, Kornowski R, Abizaid A, Wojdyla R, Maehara A, Dressler O, Brener SJ, Bar E, Dudek D. Prospective, randomized, multicenter evaluation of a polyethylene terephthalate micronet mesh-covered stent (MGuard) in ST-segment elevation myocardial infarction: the MASTER trial. *J Am Coll Cardiol*. 2012;**60**:1975–1984.
34. Otake H, Shite J, Ako J, Shinke T, Tanino Y, Ogasawara D, Sawada T, Miyoshi N, Kato H, Koo BK, Honda Y, Fitzgerald PJ, Hirata K. Local determinants of thrombus formation following sirolimus-eluting stent implantation assessed by optical coherence tomography. *JACC Cardiovasc Interv* 2009;**2**:459–466.
35. Prati F, Guagliumi G, Mintz GS, Costa M, Regar E, Akasaka T, Barlis P, Tearney GJ, Jang IK, Arbustini E, Bezerra HG, Ozaki Y, Bruining N, Dudek D, Radu M, Erglis A, Motreff P, Alfonso F, Toutouzas K, Gonzalo N, Tamburino C, Adriaenssens T, Pinto F, Serruys PW, Di Mario C, Expert's OCTRD. Expert review document part 2: methodology, terminology and clinical applications of optical coherence tomography for the assessment of interventional procedures. *Eur Heart J* 2012;**33**:2513–2520.
36. Prati F, Regar E, Mintz GS, Arbustini E, Di Mario C, Jang IK, Akasaka T, Costa M, Guagliumi G, Grube E, Ozaki Y, Pinto F, Serruys PW, Expert's OCTRD. Expert review document on methodology, terminology, and clinical applications of optical coherence tomography: physical principles, methodology of image acquisition, and clinical application for assessment of coronary arteries and atherosclerosis. *Eur Heart J* 2010;**31**:401–415.
37. Barlis P, Regar E, Serruys PW, Dimopoulos K, van der Giessen WJ, van Geuns RJ, Ferrante G, Wandel S, Windecker S, van Es GA, Eerdmans P, Juni P, di Mario C. An optical coherence tomography study of a biodegradable vs. durable polymer-coated limus-eluting stent: a LEADERS trial sub-study. *Eur Heart J* 2010; **31**:165–176.
38. van Geuns RJ, Tamburino C, Fajadet J, Vrolix M, Witzenbichler B, Eeckhout E, Spaulding C, Reczuch K, La Manna A, Spaargaren R, Garcia-Garcia HM, Regar E, Capodanno D, Van Langenhove G, Verheye S. Self-expanding versus balloon-expandable stents in acute myocardial infarction: results from the APPOSITION II study: self-expanding stents in ST-segment elevation myocardial infarction. *JACC Cardiovasc Interv* 2012;**5**:1209–1219.

1.8 Expanded clinical use of Bioresorbable Scaffolds

Expanded clinical use of everolimus eluting bioresorbable vascular scaffolds for treatment of coronary artery disease:The BVS-Expand Study.

Submitted [Original research paper]

Diletti R, **Ishibashi Y**, Felix C, Onuma Y, Nakatani S, Van Mieghem NM, Regar E, Valgimigli M, De Jaegere PP, van Ditzhuijzen N, Fam Ming J, Ligthart JMR, Lenzen MJ, Serruys PW, Zijlstra F, Van Geuns R.

Expanded clinical use of everolimus eluting bioresorbable vascular scaffolds for treatment of coronary artery disease.

The BVS-Expand Study

Roberto Diletti, MD[1]; Yuki Ishibashi, MD, PhD[1]; Cordula Felix MD[1]; Yoshinobu Onuma, MD[1,2]; Shimpei Nakatani, MD[1]; Nicolas M Van Mieghem, MD[1]; Evelin Regar, MD, PhD[1]; Marco Valgimigli, MD, PhD[1]; Pieter P. de Jaegere MD, PhD[1]; Nienke van Ditzhuijzen MD[1]; Jiang Ming, Fam, MBBS[1]; Jurgen M.R. Ligthart, RT[1]; Mattie J. Lenzen, PhD[1]; Patrick W. Serruys MD, PhD[1]; Felix Zijlstra, MD, PhD[1]; Robert Jan van Geuns MD, PhD[1]

Short title: BVS EXPAND study

[1] Thoraxcenter Erasmus MC, Rotterdam, The Netherlands

[2] Cardialysis BV, Rotterdam, The Netherlands

Corresponding author:

Robert Jan van Geuns MD, PhD

Erasmus MC, 's-Gravendijkwal 230

3015 CE Rotterdam, the Netherlands

Tel.: +31 10 4635260(33348);

Fax: +31 10 4369154.

E-mail address: r.vangeuns@erasmusmc.nl

Abstract

Objectives To report angiographic and clinical outcomes after an expanded clinical use of the everolimus eluting bioresorbable vascular scaffold (BVS)

Background Limited data are currently available on the performance of BVS for treatment of coronary lesions representative of daily practise.

Methods This is a prospective, mono-center, single-arm study. Patients were presenting with stable, unstable angina, or non-ST segment elevation myocardial infarction caused by de novo stenotic lesions in native coronary arteries. No restrictions were applied to lesion complexity. Procedural results and 6-manth clinical outcomes were reported.

Results A total of 180 patients have been evaluated in the present study, with 249 treated coronary lesions. Device Success per lesion was 99.2%. A total of 119 calcified lesions were treated with results comparable among severe, moderate and non-calcified lesions in term of percentage diameter stenosis (%DS) (20.3±10.5%, 17.8±7.7%, 16.8±8.6%; p=0.112) and acute gain (1.36±0.41mm, 1.48±0.44mm, 1.56±0.54 mm; p=0.109). A total of 54 bifurcations were treated, side-branch ballooning after main vessel treatment was often performed (33.3%). The rate of side-branch impairment was low and comparable to metallic stents (9.3%). Total occlusions were 29, after BVS implantation %DS was not different from other lesion types (17.2±9.4%, vs 17.7±8.6%; p=0.780). All cause mortality was reported in 3 cases and 2 patients experienced non-target lesion revascularization. Four cases of definite or possible scaffold thrombosis were reported. None of them was acute or subacute.

Conclusions The implantation of the everolimus eluting bioresorbable vascular scaffold in an expanded range of coronary lesion types and clinical presentations was observed to be safe and feasible with promising angiographic results and mid-term clinical outcomes.

Introduction

The everolimus eluting bioresorbable vascular scaffolds (BVS) represent a novel approach for treatment of coronary artery disease. Similarly to conventional metal stents the absorb BVS provide acute lumen gain, vessel scaffolding and drug elution to the vessel wall immediately after implantation.(1) However, at variance of standard stents, the polymeric structure of this device allows a gradual bioresorption of the implant over time.(2) Complete scaffold bioresorption is hypothesized to offer several advantages over permanent metal devices comprising re-acquirement of physiological vasomotion, late lumen enlargement, non-invasive imaging and future treatment with bypass grafting.(3-5) In addition the absence of a foreign body could avoid phenomena such as permanent side-branch jailing, late acquired malapposition and the occurrence of late and very late stent thrombosis.(5)

The absorb BVS has been initially tested in humans in two cohort studies, both showing promising results in terms of surrogate and clinical endpoints.(6-9) However, being those studies an early evaluation of this technology, they were characterized by a patient population showing stable coronary artery disease and relatively simple lesions.

At the current state of the art, very limited data are available on BVS performance in real-world patients, including those presenting with acute coronary syndromes and complex coronary lesions. A lack of information is especially evident when considering important lesion subsets such as calcified plaques, long lesions, bifurcations, and total occlusions.

Given this background, the present study aims to reports angiographic and clinical data after an expanded clinical use of the second generation BVS, implanted in patients admitted with different clinical presentations including acute coronary syndromes and having a broad range of coronary lesion types.

Methods

This is an investigator initiated, prospective, single-centre, single-arm post market study, aiming to evaluate the feasibility safety and performance of the absorb BVS for treatment of patients with coronary artery disease in routine clinical practice. Enrolled patients were subjects presenting with stable, unstable angina, or non-ST segment elevation myocardial infarction caused by *de novo* stenotic lesions in native coronary arteries. No restrictions were applied to lesion complexity. Due to the absorb BVS size availability, a Dmax (proximal and distal mean lumen diameter) within the upper limit of 3.8 mm and the lower limit of 2.0 mm by online QCA was required. Exclusion criteria were minimal and comprised allergies or contraindications to antiplatelet medication, female patient with childbearing potential or currently breastfeeding, acute ST segment elevation myocardial infarction and post CABG patients

Ethics

This is an observational study, performed according to the privacy policy of the Erasmus MC, and to the Erasmus MC regulations for the appropriate use of data in patient-oriented research, which are based on international regulations, including the declaration of Helsinki. The BVS received the CE mark for clinical use, indicated for improving coronary lumen diameter in patients with ischemic heart disease due to de novo native coronary artery lesions with no restriction in terms of clinical presentation. Therefore the BVS can be currently used routinely in Europe in different settings without a specific written informed consent in addition to the standard informed consent to the procedure. Therefore, a waiver from the hospital Ethical Committee was obtained for written informed consent, as according to Dutch law written consent is not required, if patients are not subject to acts other than as part of their regular treatment.

Study device

The device used in the present study is the second generation Absorb BVS (Abbott Vascular, Santa Clara, CA, USA); a balloon expandable scaffold with a polymer backbone of Poly-L lactide Acid (PLLA) coated with a thin layer of a 1:1 mixture of an amorphous matrix of Poly-D and L lactide acid (PDLLA) polymer, controlling the realise of 100 micrograms/cm^2 of the anti-proliferative drug everolimus. Two platinum markers located at each Absorb BVS edge allowing for accurate visualization of the radiolucent Absorb BVS during angiography or other imaging modalities. Approximately 80% of the drug is eluted within the first 30-days. Both PLLA and PDLLA are fully bioresorbable. The polymers are degraded mainly via hydrolysis resulting oligomers of lactate metabolized by Krebs cycle. Small particles, less than 2 μm in diameter, have also been shown to be phagocytised and degraded by macrophages.

Reinsertion of the device after initial failure to cross the lesion is not currently advised by the manufacturer. However, based on internal Abbott Vascular early bench testing reinsertion was accepted as feasible by our staff up to 30 min after first contact with blood.

Definitions

Device Success was defined as the attainment of <30% final in segment residual stenosis after absorb BVS implantation, by angiographic visual estimation. Procedure Success was defined as device success and no major peri-procedural complications (Emergent CABG, coronary perforation requiring pericardial drainage, residual dissection impairing vessel flow – TIMI-flow II or less -). Clinical success was defined as procedural success and no in-hospital major adverse cardiac events (MACE). All deaths were considered cardiac unless an undisputed non-cardiac cause was identified. Myocardial infarction (MI) and scaffold thrombosis were defined according to the Academic Research Consortium (ARC) definition. Any Target lesion revascularization (TLR) was defined as clinically driven if at repeat angiography a diameter stenosis >70% was observed, or if a diameter

stenosis >50% was present in association with recurrent angina pectoris; objective signs of ischaemia (ECG changes) at rest or during exercise test, likely to be related to the target vessel; abnormal results of any invasive functional diagnostic test.

The device oriented endpoint target lesion failure was defined as the composite of cardiac death, target vessel myocardial infarction, or ischemia driven target lesion revascularization. Major adverse cardiac events (MACE), defined as the composite of cardiac death, any re-infarction (Q or Non Q-Wave), emergent bypass surgery (CABG), or clinically driven target lesion revascularization (TLR). Target vessel failure (TVF) was defined as cardiac death, target vessel myocardial infarction (MI), or clinically driven target vessel revascularization (TVR). Delivery failure was defined as opening of scaffold from its cover and insertion into the guiding-catheter without final implantation. In an attempt to study re-insertion time between registration of product in material list of our database and angiographic recording of implantation was registered. If this was above 5 min, initial lesion passage was presumed failed and reinsertion assumed.

All potential events were adjudicated by a local independent Clinical Events Committee (CEC).

Quantitative coronary angiography

Quantitative coronary angiography (QCA) analyses were performed using the Coronary Angiography Analysis System (Pie Medical Imaging, Maastricht, Netherlands).
The QCA measurements we performed pre and post BVS implantation. The 37 μm platinum radio-markers located at each end of the Absorb BVS aided in the localisation of the non-radio-opaque scaffold for QCA. Analysed parameters included reference vessel diameter (RVD) - calculated with interpolate method - percentage diameter stenosis (%DS) and minimal lumen diameter (MLD). Acute gain was defined as post-procedural MLD minus pre-procedural MLD. The angiographic analysis were performed by three investigators (YI, YO and RD) who where extensively trained in an experienced core-lab (Cardialysis BV, Rotterdam, The Netherlands)

A calcified coronary culprit lesion was defined as already reported(10) 'readily apparent densities noted within the apparent vascular wall at the site of the stenosis.' By qualitative assessment of the angiograms, target lesions were classified as severe ('radioopacities noted without cardiac motion prior to contrast injection generally involving both sides of the arterial wall'), moderate ('densities noted only during the cardiac cycle prior to contrast injection'), or none/mild (lesions other than severe and moderate calcified lesions). The Inter- and intra-observer variability in the qualitative analysis of coronary calcium on coronary angiograms have been already reported. (11)

To provide insights on the coronary bifurcation treatment with BVS we performed a full analysis of techniques and material used and we reported the occurrence of side-branch impairment, an end-point already reported in the literature as "side-branch trouble"(12) and defined as follow: at least 1 of the following procedural parameters: 1) Side-branch TIMI flow grade <3 after main vessel stenting; 2) need of guide-wire(s) different from the workhorse wire to rewire side-branch after main vessel scaffolding; 3) failure to rewire the side-branch after main vessel scaffolding; or 4) failure to dilate the side-branch after main vessel scaffolding and side-branch rewiring.

Statistical analysis

Categorical variables are reported as counts and percentages, continuous variables as mean ± standard deviation; p values were calculated with Fisher's Exact test for binary variables, Wilcoxon's Rank Sum test for continuous variables. Comparisons among multiple means were performed with analysis of variance (1-way ANOVA). A p value<0.05 was considered statistically significant. Statistical analyses were performed using SPSS, version 15.0 for windows (IL,US).

Results

From September 2012 to July 2013 a total of 1529 percutaneous coronary interventions were performed in our center. A total of 180 patients have been enrolled in the present study, with 249 treated coronary lesions. Baseline clinical characteristics are reported in table 1. Seventy-three patients (40.6%) showed multivessel disease. A total of 109 lesions (43.8%) were classified as type B2 or C, mean lesion length was 25.86 mm, bifurcation lesions with side-branch ≥ 2 mm were 54, a total of 119 lesion were defined with severe or moderate calcification and in 29 case was present a total occlusion. (Table 2)

Lesion preparation was performed in a large part of the cases mainly through balloon predilatation (89.2%); rotational atherectomy was necessary in 4.8% of cases. Multiple scaffold implantation per lesion was allowed and often performed, (31.7%) up to the implantation of 5 scaffolds.

Reinsertion of the scaffold, (assumed if time between registration of product in material list and angiographic recording of implantation was > 5 minutes) was reported in 15 cases. No scaffold dislodgment was reported.

Bailout with metal stents was performed in only 2 cases. Balloon post-dilatation was performed in a remarkable percentage of cases (45.0%) with often a balloon/scaffold ratio > 1.0 (41.8%). (Table 3)

The overall device, procedure and clinical success rates per lesion, were respectively 99.2%, 98.8% and 98.8%

QCA analysis The mean pre-procedure reference vessel diameter (RVD) was 2.63 ± 0.43 mm, with a mean percentage diameter stenosis (%DS) of 64.8 ± 14.5% and a mean minimal lumen diameter (MLD) equal to 0.90 ± 0.35 mm. Post-procedure was observed a %DS of 17.60 ± 8.65 % and a mean MLD equal to 2.41 ± 0.41 mm with a mean acute gain of 1.51 ± 0.49 mm. TIMI 3 flow was observed in 99.2% of the final angiograms. (Table 4)

Bifurcation Lesions A total of 54 lesions were located at the site of a bifurcation with a side-branch ≥ 2.0 mm. In 51 cases a provisional T-stenting technique was used, in addition 1 T stenting 1 culotte, 1 T-stenting and small protrusion techniques were performed. In 18 cases branch wire protection was used, pre-dilatation and post-dilatation of the main vessel was often performed. Side branch dilatation post MV stenting was necessary in 18 lesions. A final TIMI flow <3 in the main vessels (MV) was observed in only one case, at the side-branch this was reported in 3 lesions. Failure to re-wire the side-branch was never reported but in one case the operator was unable to re-cross the scaffold with a small balloon of 1.5 mm in diameter. (Table 5) The overall of rate of side-branch impairment was 9.3% (5/54)

Calcified lesions A total of 119 calcified lesions were treated with BVS (33 with severe calcification, 86 with moderate calcification) and compared with non-calcified lesions. Given a non significant difference in pre-procedure RVD, MLD and %DS no differences were observed after treatment between calcified and non calcified lesions in terms of MLD (Severe calcified 2.38 ± 0.38 mm, moderate calcified 2.41 ± 0.39 mm, non-calcified 2.42 ± 0.43 mm; p=0.889), %DS (Severe calcified 20.3 ± 10.5 %, moderate calcified 17.8 ± 7.7%, non-calcified 16.8 ± 8.6%; p=0.112) and acute gain (Severe calcified 1.36 ± 0.41mm, moderate calcified 1.48 ± 0.44 mm, non-calcified 1.56 ± 0.54 mm; p=0.109). These results were achieved with an overall higher use of buddy wires in calcified lesions (severe calcified 18.2%, moderate calcified 9.3%, non-calcified 3.0%; p=0.016)

Lesion preparation was more aggressive in calcified lesions with a higher use of rotational atherectomy (Severe calcified 18.2%, moderate calcified 4.7%, non-calcified 1.5%; p<0.001) and scoring balloons (Severe calcified 15 .2%, moderate calcified 3.5%, non-calcified 0.8%; p=0.001). Success rates were high in calcified vessels showing no significant differences when compare do non-calcified ones. Device success in severe calcified lesions was 97.0%, in moderate calcified 100% and in non-calcified 99.2%; p=0.251. (Table 6)

Total Occlusions Vessels showing a total occlusion were 29. After vessel disobstruction total occluded vessel were treated with BVS achieving a final MLD and %DS not different from other lesion types (MLD: 2.51 ± 0.53 mm vs 2.40 ± 0.39; p=0.163; %DS: 17.2 ± 9.4% vs 17.7 ± 8.6%; p=0.780), with a high rate of final device success (96.6% vs 98.2%; p=0.465) and procedure success (96.6% vs 98.6%; p=0.393). To reach those results supportive wires were used much more frequently in occluded vessels (54.2% vs 2.1%; p<0.001). (Table 7)

Long Lesions In a total of 79 lesions (31.7%) more than one device was implanted. The mean lesion length treated with BVS was 25.86 ± 13.64 mm. The maximum lesion length covered by BVS was 80.01 mm. Overlapping of BVS with BVS was often performed with a total of 76 overlapping. The great majority (96%, 73/76) were performed using scaffold of the same diameter or with a maximum of 0.5 mm difference in nominal diameter. In 3 cases a 3.5 mm scaffold was placed in overlap with a 2.5 mm device.

Clinical outcomes Survival data at 6 months after the procedure were available for 98.9 % of patients. A questionnaire was sent to all living patients with specific queries on re-hospitalization and cardiovascular events. For patients who suffered an adverse event at another center, medical records or discharge letters from the other institutions were systematically reviewed. General practitioners and referring physicians were contacted for additional information if necessary.
At 6-month follow-up all cause-death was reported in 3 cases. In 2 cases non-target vessel revascularisations were performed. A total of 4 definite or probable scaffold thrombosis (ST) occurred within six-month after index procedure; none of them was acute or sub-acute. Of note one of those 4 cases was meeting the ARC criteria for ST but no clear thrombus was observed by optical coherence tomography (OCT). In the remaining 3 cases, severe calcification, bifurcation lesion and long overlap were observed but BVS underexpansion was the factor that was present in all of them.

Description of the Scaffold thrombosis cases

Case 1 A 59-year old male patient, smoker, with history of cerebrovascular accident and stable angina pectoris, was treated after predilatation on long lesion involving the ostial left anterior descending (LAD) and the bifurcation with the first diagonal (D1), using a BVS 3.5 x 28mm. Despite a postdilatation was performed with a 3.5 non-complaint (NC) balloon at high pressure, the BVS remained under-expanded with an impaired flow in the first diagonal. At the day 111 post PCI the patient was re-admitted with NSTEMI and angiographically was observed a total re-occlusion of the LAD beginning from the ostium. After predilatation a DES 3.5 x32mm was implanted. Of note, at day 81 after the second PCI the patients was again re-admitted for instable angina pectoris caused by a re-occlusion also of the metal stent in the proximal LAD. The patients was treated with CABG.

Lesion key characteristics: ***Ostial lesion, long lesion, bifurcation, impaired side-branch TIMI flow and BVS underexpansion***

Case 2 A 69-year old male with history of dyslipidaemia and hypertension was admitted with NSTEMI. Angiographically was observed a long, severely calcified, chronic total occlusion (CTO) of the proximal and mid LAD with severe calcification and involvement of D1. After Predilatation, 2x 3.5 x 18mm BVS were implanted. The procedure was complicated by pinching of D1 and thrombus formation. Additional ballooning of the ostium of the side-branch was performed, but at the end of the procedure remained BVS underexpansion and haziness in the mid LAD. At day 47 the patient developed a non-Q wave MI due to definite scaffold thrombosis in the proximal LAD, which was treated with thrombectomy and DES implantation.

Lesion key characteristics: ***CTO, long lesion, bifurcation, severe calcification, thrombus formation and BVS underexpansion***

Case 3 A 65-year old male patient, smoker, with history of hypertension was admitted with NSTEMI, due to a sub-occlusive lesion in the LAD located at the site of a tortuous trifurcation with the first and second diagonal. The initial TIMI flow was 1. After predilatation, a 3.0 x 18mm BVS was implanted and after postdilatation a TIMI III flow was achieved. At day 142 the patient was re-admitted with NSTEMI. Angiographically a proximal BVS edge sub-total restenosis was observed with a distal TIMI flow 1. A DES stent 3.5 x38mm was deployed covering the BVS and a large proximal segment. Of note, this case was meeting the ARC criteria for stent thrombosis and was adjudicated as such by the CEC, but should be mentioned that an OCT performed before predilatation did not showed any clear intraluminal thrombus.

Lesion key characteristics: ***tortuous trifurcation (no thrombus by OCT)***

Case 4 A 70-year old male, with severe peripheral vascular disease, diabetes mellitus, dyslipidaemia, hypertension, and reduced left ventricular function was admitted with stable angina pectoris. Angiography revealed, a long and severely calcified lesion mid LAD involving two bifurcations (D1 and D2). Aggressive preparation was performed with rotational atherectomy and high-pressure dilatations with NC and cutting balloons. Two overlapping BVS were placed with a quite long segment of overlap (5 mm). Despite extensive postdilatation under-expansion remained at the end of the procedure. Five months after index PCI, the patient underwent non-cardiac surgery. The antiplatelet therapy was interrupted (both aspirin and clopidogrel) and the patient developed a NSTEMI due to a scaffold thrombosis that was treated with balloon dilatation and eptifibatide. Unfortunately, the patient died few days later because of heart failure.

Lesion key characteristics: ***Severe calcification, bifurcation, long overlap, no antiplatelet therapy and BVS underexpansion***

Discussion

The present investigation represents en evaluation of the feasibility of BVS implantation in everyday clinical practise reflected by in a wide range of coronary lesions subsets including bifurcations, calcified vessels, chronic total occlusions and long lesion in patients with stable coronary artery disease and acute coronary syndromes. At variance of previous reports we also aimed to provide a detailed description of procedural data en techniques that were used to allow the use of this novel device in challenging subsets.

Bifurcation lesions A common concern regarding this technology is the fact that implantation of the BVS in bifurcation lesions might result into side-branch compromise due to the thick strut nature of this device. In keeping with this concept, a recent study performed by our group showed that BVS deployment could be associated with an increased small (≤0.5 mm) side-branch occlusion and a consequent increase of enzymes release after procedure.(13)

However, in the present report the effect of BVS implantation in what is commonly considered a bifurcation lesion (with a side branch ≥ 2 mm) was specifically investigated.

Rewiring of the side-branch in those cases and consequent ballooning (mainly with small balloon 1.5-2 mm in diameter) of the SB ostium is feasible as we already reported(13) and safe also in terms of scaffold geometry and fracture.(14,15) In the present study side-branch ballooning was performed in one third of the patients (33%, 18/54) with promising results. In majority of the cases this was done with sequential ballooning and proximal optimization technique (POT), kissing balloon only in 3 cases.

Taking into consideration the rates of TIMI flow < 3 in the main vessel or in the side-branch, the rate of failure to rewire the side-branch and failure to dilate the side-branch, the BVS performed at least as good as metallic stents according to historical data. (12)

In addition the rate of the composite endpoint of side-branch impairment (9.3%) was observed to be encouraging especially when compared with data recently reported by Burzotta et al. with rates of side-branch impairment in sirolimus and everolimus eluting stents respectively 16% and 11%. (12) These data are supportive of the concept that BVS could be used safely in bifurcation lesions with side-branch ≥ 2.0 mm with a single scaffold approach and could provide results similar to metallic stents.

Calcified lesions A total of 119 calcified lesions with a considerable percentage of heavily calcified plaques, were treated with BVS. A large number of those lesions were located in diffusely diseased vessels with an overall mean treated lesion length of more than 36 mm (severe calcified group). QCA analysis showed final MLD, %DS, acute gain and device, procedural and clinical success not different from non-calcified lesions. These results were obtained at the cost of a more aggressive lesion preparation with a considerable use of rotational atherectomy and scoring balloons.

Such approach is needed to facilitate the delivery of the scaffold given its slightly higher profile compared with second generation DES. In addition appropriate lesion preparation could avoid scaffold under-expansion or need for aggressive post-dilatation. This strategy could be relevant also when using metallic stents. (16) Our data might suggest feasibility of BVS implantation in calcified vessels with optimal results given an adequate lesion preparation.

On the other hand, should be mentioned that many of the advantages proposed for BVS namely the restoration of the vasomotion and vessel physiology could be minimized in artery at a very advanced stage of the atherosclerosis process even considering the fact that patients with diffused calcified vessels have also a multivessel disease,(17) that might benefit from a temporary implant allowing future surgical treatments.

T**otal occlusions** Successful re-canalization of total occlusions has been previously associated with a significant improvement in angina symptoms (18,19) and complete coronary revascularization was demonstrated to have an important impact on long-term clinical outcomes.(20)

Vessels with total occlusions have peculiar characteristics in terms of vascular remodeling; this is a dynamic process involving regulation of vascular cell migration and mitosis and apoptosis rates in response to several factors comprising blood flow and pressure, shear stress, circumferential stretch and wall tension.(21) Reduction or even more absence of blood flow in totally occluded vessels might promote negative remodeling and plaque growth; on the other hand restoration of flow could have an opposite effect.

Recently, Park J.J. and colleagues reported, at 6-month follow-up after successful total occlusion revascularization, a flow-dependent vascular remodeling process in human coronary arteries, associated with increases in lumen diameter, lumen area and external elastic membrane area.(22) This process was observed in a large part of treated vessels (69%) with a mean lumen diameter increase of 0.40 ± 0.34 mm. IVUS analysis of those vessels revealed that the amount of incomplete stent apposition increased significantly during 6 months in patients with positive remodeling and lumen area increase but not in those without lumen area increase.

In this scenario choosing a metal stent based on the vessel diameter at the index procedure might lead to stent under-sizing.

Given this background a theoretical advantage of BVS implantation in patients with total occlusion is the fact that it might allow at mid-term follow-up, after the loss of scaffold mechanical integrity, late lumen enlargement without late acquired malapposition, as at that time the remnants of the bioresorbable implant can follow the vessel remodeling.

Long lesions and overlap In the present series, several lesions were treated with more than one scaffold up to a maximum of 5 scaffolds for a maximum lesion length of 80 mm. Operators were advised to minimize the extension of overlapping segment using a marker-to-marker technique.

In the metal stent era, long segments treatment has been associated to an increased risk of stent thrombosis,(23-25) and could results in prevention of future surgical revascularisations. In a juvenile porcine model (paper from Farooq), overlapping Absorb scaffolds showed delayed healing on histology and OCT and slower tissue coverage than in non-overlapping scaffolds: the coverage

of the overlapping segment was 80.1% and 99.5% at 28 and 90 days after implantation respectively, suggesting that complete coverage in humans may take up to 18 months.

Both these issues could be overcome with the use of bioresorbable technologies and the introduction in the near future of bioresorbable scaffold with thinner struts could mitigate the effect of overlap on delayed vascular healing.

Clinical outcomes Mid-term clinical outcomes revealed a relatively reassuring safety profile of the BVS when used in a large range of lesion type and in patients with either stable symptoms or acute coronary syndromes. Regarding the occurrence of scaffold thrombosis (ST), at variance of previous reports no acute or sub-acute STs were observed in the present investigation. This datum could be related to procedural characteristics including a meticulous lesion preparation pre BVS implantation and an advanced stage in learning curve of the operators in terms of BVS implantation.

The revision of the cases with ST revealed that several factors might be associated with such event comprising severe lesion calcification, the presence of bifurcations, long overlap and antiplatelet therapy discontinuation. However, the factor that was particularly consistent was scaffold under-expansion. Previous investigations described stent underexpansion as an important predictor of ST with both bare metal stents and DES,(26-30) with an impact on the occurrence of ST that was hypostasized to be superior to stent malapposition.(31) The mechanisms behind these findings could be the fact that stent underexpansion translates into an abnormal shear stress. In particular increased radial transport of blood components and low wall shear stress, were described to promote platelet-dependent thrombosis.(32) In addition the impact of underexpansion on shear stress could be potentiated by the presence of the BVS thick struts.(33)

Although, given the small number of patients and event reported in the present study it is not possible to reach firm conclusions, our findings suggest that optimal BVS expansion, with lesion preparation and appropriate scaffold postdilatation, should be pursued given the possible relevant clinical implications.

Limitations

The present report is an investigator initiated, single center, single arm study. The choice for BVS implantation was left to operator discretion, this could be source of selection bias. The absence of a comparator arm is limiting the interpretation of our data. The limited number of patients does not allow reaching firm conclusions on clinical outcomes. The short follow-up is preventing the availability of information on long-term safety and efficacy.

Conclusion

The implantation of the everolimus eluting bioresorbable vascular scaffold in an expanded range of coronary lesion types and clinical presentations was observed to be safe and feasible. Larger studies with longer follow-up and a direct comparison with currently available metallic drug eluting stents are needed to fully evaluate the possible additional value of the bioresorbable technologies an all comers setting.

Acknowledgments

This study was supported by an unrestricted grant from Abbott Vascular.
The authors want to thank Isabella Kardijs, Johannes Schaar and Martijn Akkerhuis, for their contribution in the event adjudication.

References

1. Serruys PW, Onuma Y, Ormiston JA et al. Evaluation of the second generation of a bioresorbable everolimus drug-eluting vascular scaffold for treatment of de novo coronary artery stenosis: six-month clinical and imaging outcomes. Circulation 2010;122:2301-12.
2. Onuma Y, Serruys PW, Perkins LE et al. Intracoronary optical coherence tomography and histology at 1 month and 2, 3, and 4 years after implantation of everolimus-eluting bioresorbable vascular scaffolds in a porcine coronary artery model: an attempt to decipher the human optical coherence tomography images in the ABSORB trial. Circulation 2010;122:2288-300.
3. Onuma Y, Serruys PW. Bioresorbable scaffold: the advent of a new era in percutaneous coronary and peripheral revascularization? Circulation 2011;123:779-97.
4. Diletti R, Farooq V, Girasis C et al. Clinical and intravascular imaging outcomes at 1 and 2 years after implantation of absorb everolimus eluting bioresorbable vascular scaffolds in small vessels. Late lumen enlargement: does bioresorption matter with small vessel size? Insight from the ABSORB cohort B trial. Heart 2013;99:98-105.
5. Serruys PW, Garcia-Garcia HM, Onuma Y. From metallic cages to transient bioresorbable scaffolds: change in paradigm of coronary revascularization in the upcoming decade? European heart journal 2012;33:16-25b.
6. Serruys PW, Ormiston JA, Onuma Y et al. A bioabsorbable everolimus-eluting coronary stent system (ABSORB): 2-year outcomes and results from multiple imaging methods. Lancet 2009;373:897-910.
7. Onuma Y, Dudek D, Thuesen L et al. Five-year clinical and functional multislice computed tomography angiographic results after coronary implantation of the fully resorbable polymeric everolimus-eluting scaffold in patients with de novo coronary artery disease: the ABSORB cohort A trial. JACC Cardiovascular interventions 2013;6:999-1009.
8. Serruys PW, Onuma Y, Garcia-Garcia HM et al. Dynamics of vessel wall changes following the implantation of the absorb everolimus-eluting bioresorbable vascular scaffold: a multi-imaging modality study at 6, 12, 24 and 36 months. EuroIntervention : journal of EuroPCR in collaboration with the Working Group on Interventional Cardiology of the European Society of Cardiology 2014;9:1271-84.
9. Diletti R, Onuma Y, Farooq V et al. 6-month clinical outcomes following implantation of the bioresorbable everolimus-eluting vascular scaffold in vessels smaller or larger than 2.5 mm. Journal of the American College of Cardiology 2011;58:258-64.
10. Onuma Y, Tanimoto S, Ruygrok P et al. Efficacy of everolimus eluting stent implantation in patients with calcified coronary culprit lesions: two-year angiographic and three-year clinical results from the SPIRIT II study. Catheterization and cardiovascular interventions : official journal of the Society for Cardiac Angiography & Interventions 2010;76:634-42.
11. Herrman JP, Azar A, Umans VA, Boersma E, von Es GA, Serruys PW. Inter- and intra-observer variability in the qualitative categorization of coronary angiograms. International journal of cardiac imaging 1996;12:21-30.
12. Burzotta F, Trani C, Todaro D et al. Prospective randomized comparison of sirolimus- or everolimus-eluting stent to treat bifurcated lesions by provisional approach. JACC Cardiovascular interventions 2011;4:327-35.

13. Muramatsu T, Onuma Y, Garcia-Garcia HM et al. Incidence and short-term clinical outcomes of small side branch occlusion after implantation of an everolimus-eluting bioresorbable vascular scaffold: an interim report of 435 patients in the ABSORB-EXTEND single-arm trial in comparison with an everolimus-eluting metallic stent in the SPIRIT first and II trials. JACC Cardiovascular interventions 2013;6:247-57.
14. Dzavik V, Colombo A. The absorb bioresorbable vascular scaffold in coronary bifurcations: insights from bench testing. JACC Cardiovascular interventions 2014;7:81-8.
15. Ormiston JA, Webber B, Ubod B, Webster MW, White J. Absorb everolimus-eluting bioresorbable scaffolds in coronary bifurcations: a bench study of deployment, side branch dilatation and post-dilatation strategies. EuroIntervention : journal of EuroPCR in collaboration with the Working Group on Interventional Cardiology of the European Society of Cardiology 2014.
16. Abdel-Wahab M, Baev R, Dieker P et al. Long-term clinical outcome of rotational atherectomy followed by drug-eluting stent implantation in complex calcified coronary lesions. Catheterization and cardiovascular interventions : official journal of the Society for Cardiac Angiography & Interventions 2013;81:285-91.
17. Genereux P, Madhavan MV, Mintz GS et al. Ischemic outcomes after coronary intervention of calcified vessels in acute coronary syndromes. Pooled analysis from the HORIZONS-AMI (Harmonizing Outcomes With Revascularization and Stents in Acute Myocardial Infarction) and ACUITY (Acute Catheterization and Urgent Intervention Triage Strategy) TRIALS. Journal of the American College of Cardiology 2014;63:1845-54.
18. Stone GW, Kandzari DE, Mehran R et al. Percutaneous recanalization of chronically occluded coronary arteries: a consensus document: part I. Circulation 2005;112:2364-72.
19. Stone GW, Reifart NJ, Moussa I et al. Percutaneous recanalization of chronically occluded coronary arteries: a consensus document: part II. Circulation 2005;112:2530-7.
20. Farooq V, Serruys PW, Garcia-Garcia HM et al. The negative impact of incomplete angiographic revascularization on clinical outcomes and its association with total occlusions: the SYNTAX (Synergy Between Percutaneous Coronary Intervention with Taxus and Cardiac Surgery) trial. Journal of the American College of Cardiology 2013;61:282-94.
21. Langille BL. Arterial remodeling: relation to hemodynamics. Canadian journal of physiology and pharmacology 1996;74:834-41.
22. Park JJ, Chae IH, Cho YS et al. The recanalization of chronic total occlusion leads to lumen area increase in distal reference segments in selected patients: an intravascular ultrasound study. JACC Cardiovascular interventions 2012;5:827-36.
23. Park DW, Park SW, Park KH et al. Frequency of and risk factors for stent thrombosis after drug-eluting stent implantation during long-term follow-up. The American journal of cardiology 2006;98:352-6.
24. Moreno R, Fernandez C, Hernandez R et al. Drug-eluting stent thrombosis: results from a pooled analysis including 10 randomized studies. Journal of the American College of Cardiology 2005;45:954-9.
25. Suh J, Park DW, Lee JY et al. The relationship and threshold of stent length with regard to risk of stent thrombosis after drug-eluting stent implantation. JACC Cardiovascular interventions 2010;3:383-9.
26. Fujii K, Carlier SG, Mintz GS et al. Stent underexpansion and residual reference segment stenosis are related to stent thrombosis after sirolimus-eluting stent implantation: an

intravascular ultrasound study. Journal of the American College of Cardiology 2005;45:995-8.
27. Cheneau E, Leborgne L, Mintz GS et al. Predictors of subacute stent thrombosis: results of a systematic intravascular ultrasound study. Circulation 2003;108:43-7.
28. Kasaoka S, Tobis JM, Akiyama T et al. Angiographic and intravascular ultrasound predictors of in-stent restenosis. Journal of the American College of Cardiology 1998;32:1630-5.
29. Sonoda S, Morino Y, Ako J et al. Impact of final stent dimensions on long-term results following sirolimus-eluting stent implantation: serial intravascular ultrasound analysis from the sirius trial. Journal of the American College of Cardiology 2004;43:1959-63.
30. Uren NG, Schwarzacher SP, Metz JA et al. Predictors and outcomes of stent thrombosis: an intravascular ultrasound registry. European heart journal 2002;23:124-32.
31. Liu X, Doi H, Maehara A et al. A volumetric intravascular ultrasound comparison of early drug-eluting stent thrombosis versus restenosis. JACC Cardiovascular interventions 2009;2:428-34.
32. Sukavaneshvar S, Rosa GM, Solen KA. Enhancement of stent-induced thromboembolism by residual stenoses: contribution of hemodynamics. Annals of biomedical engineering 2000;28:182-93.
33. Bourantas CV, Papafaklis MI, Kotsia A et al. Effect of the endothelial shear stress patterns on neointimal proliferation following drug-eluting bioresorbable vascular scaffold implantation: an optical coherence tomography study. JACC Cardiovascular interventions 2014;7:315-24.

Table 1

Baseline clinical characteristics

Clinical characteristics	N = 180
Age	60.8 ± 10.5
Male n. (%)	124 (68.9%)
Hypertension n. (%)	94 (52.2%)
Hypercholesterolemia n. (%)	84 (46.7%)
Diabetes n. (%)	32 (17.8%)
Insulin-dependent n. (%)	8 (4.4%)
Smoke n. (%)	99 (55.0%)
Peripheral vascular disease n. %	19 (10.6%)
CVA n. (%)	14 (7.8%)
Kidney disease n. (%)	11 (6.1%)
Prior MI n. (%)	30 (16.7%)
Prior PCI n. (%)	17 (9.4%)
Prior GABG n. (%)	0 (0.0%)
COPD n. (%)	11 (6.1%)
History of heart failure n. (%)	10 (5.6%)

CVA= cerebrovascular accident; PCI = percutaneous coronary intervention; CABG = coronary artery bypass graft; COPD = chronic obstructive pulmonary disease. Data are expressed as mean ± standard deviation or number and proportion

Table 2

Lesion characteristics

Lesion characteristics	N = 180, L= 249
Number of Diseased Vessel	
One vessel disease	107 / 180 (59.4%)
Two vessel disease	61 / 180 (33.9%)
Three vessel disease	12 / 180 (6.7%)
Number of Treated Lesions per vessel (%)	
0 lesion	1/ 249 (0.4%)
1 lesion	189 / 249 (75.9%)
2 lesions	54 / 249 (21.7%)
3 lesions	4 / 249 (1.6%)
4 lesions	1 / 249 (0.4%)
Lesion Location (%)	
LAD	120 / 249 (48.2%)
LCX	55 / 249 (22.1%)
RCA	66 / 249 (26.5%)
DIAGONAL	7 / 249 (2.8%)
LMCA/Ramus	1 / 249 (0.4%)
AHA/ACC Lesion Classification (%)	
A	38 / 249 (15.3%)
B1	103 / 249 (41.4%)
B2	63 / 249 (25.3%)
C	46 / 249 (18.5%)
Lesion Length (mm)	25.86 ± 13.64
Range min, max (mm)	5.32 - 80.01
Bifurcation Lesion n. (%)	54 / 249 (21.7%)
Total Occlusion (%)	29 / 249 (11.6%)
Calcification Lesion (%)	119/ 249 (47.8%)

Data are expressed as mean ± standard deviation or number and proportion

Table 3

Procedural data per-lesion analysis

Lesion characteristics	L= 249
Number of Scaffold or stent – per lesion (%)	
Average	1.41± 0.75
0 scaffold or stent	1 / 249 (0.4%)
1 scaffold or stent	169 / 249 (67.9%)
2 scaffolds or stents	61 / 249 (24.5%)
3 scaffolds or stents	10 / 249 (4.0%)
4 scaffolds or stents	7 / 249 (2.8%)
5 scaffolds or stents	1 / 249 (0.4%)
Overlapping	78
Overlapping BVS-BVS	76
Overlap scaffolds diameters 3.5mm-3.5mm,n (%)	20 (26.3%)
Overlap scaffolds diameters 3.5mm-3.0mm,n (%)	15 (19.7%)
Overlap scaffolds diameters 3.5mm-2.5mm,n (%)	3 (3.9%)
Overlap scaffolds diameters 3.0mm-3.0mm,n (%)	15(19.7%)
Overlap scaffolds diameters 3.0mm-2.5mm,n (%)	15 (19.7%)
Overlap scaffolds diameters 2.5mm-2.5mm,n (%)	8 (10.5%)
Overlapping BVS-Metal	2 (2.6%)
Bailout scaffold/stent (%) – per lesion	
with BVS	8 / 249 (3.2%)
with Metallic stent	2 / 249 (0.8%)
Pre dilatation (%)	222 / 249 (89.2%)
Type of predilatation balloon*	
Non-compliant	16 / 203 (7.9%)
Semi-compliant	187 / 203 (92.1%)
The usage of scoring (scoreflex or cutting)	9 / 219 (4.1%)
Average size of balloon	2.52 ± 0.36
Balloon / artery (pre RVD) Ratio < 1 (excluding total occlusion before procedure)	100 / 184 (54.3%)
Balloon / scaffold ratio ≤1	198 / 202 (98.0%)
Balloon 0.5mm smaller ≤ scaffold size	172/202 (85.1%)
Max pressure	13.95 ± 2.86
Use of other devices for lesion preparation	

Rotational Atherectomy	12 / 249 (4.8%)
Manual Thrombectomy	11 / 249 (4.4%)
Daughter Catheter	5 / 249 (2.0%)
Buddy wire	18 / 249 (7.2%)
Post dilatation (%)	112 / 249 (45.0%)
Type of postdilatation balloon**	
Compliant	32 / 110 (29.1%)
Noncompliant	78 / 110 (70.9%)
Average size of balloon	3.27 ± 0.46 mm
Max pressure	15.58± 3.46
Balloon / Artery < 1	25 / 110 (22.7%)
Balloon > Scaffold size	46 / 110 (41.8%)
Balloon > Scaffold size+0.25mm	15 / 110 (13.6%)
Device Success per lesion (%)	247 / 249 (99.2%)
Procedure Success per lesion (%)	246 / 249 (98.8%)
Clinical Success per lesion	246 / 249 (98.8%)

*Type of predilatation balloon is reported in a subgroup of 203 patients. ** Type of posdilatation balloon is reported in a subgroup of 110 patients. Data are expressed as mean ± standard deviation or number and proportion

Table 4

Quantitative coronary angiography analysis (QCA)

QCA data	N = 180, L = 249
QCA pre-procedure	
RVD (mm)	2.63 ± 0.43
MLD (mm)	0.90 ± 0.35
% DS (%)	64.8 ± 14.5
Proximal Dmax (mm)	3.92 ± 8.28
Distal Dmax (mm)	2.89 ± 2.31
QCA Post-procedure In-scaffold	
RVD (mm)	2.89 ± 0.42
DS (%)	17.6 ± 8.65
MLD (mm)	2.41 ± 0.41
Scaffold length	29.44± 15.71
Acute gain (mm)	1.51 ± 0.49
TIMI grade 2	2 / 249 (0.8%)
TIMI grade 3	247 / 249 (99.2%)

Data are expressed as mean ± standard deviation or number and proportion

Table 5

BVS implantation in Bifurcation lesions

Procedural characteristics	L=54
LAD	38
CX	12
RCA	4
Involvement of both SB and MV (Medina 111, 101, 011)	15 (27.8%)
1 Scaffold Technique	51 (94.4%)
Provisional T	51 (94.4%)
T-stenting	1 (1.8%)
Culotte	1 (1.8%)
TAP	1 (1.8%)
MV pre-dilatation	44 (81.4%)
MV post-dilatation	26 (44.4%)
SB pre-dilatation	6 (11.1%)
SB dilatation post MV Scaffolding	18 (33.3%)
Kissing balloon	3 (5.6%)
Proximal optimization technique	26 (44.4%)
Final MV TIMI flow <3	1 (1.8%)
Side-branch Timi flow <3	3 (5.6%)
Failure to rewire the SB	0 (0%)
Different wire from the workhorse to rewire SB after MV scaffolding	2 (3.7%)
Failure to dilate SB	1 (1.8%)
Composite of side-branch impairment	5 (9.3%)

Data are expressed as mean ± standard deviation or number and proportion

Table 6

BVS implantation in calcified lesions

Procedural characteristics	Severe calcification (L = 33)	Moderate calcification (L =86)	No calcification (L =130)	P value
Lesion preparation				
Rotational Atherectomy ,% (n)	18.2% (6/33)	4.7% (4/86)	1.5% (2/130)	<0.001
Scoring balloon ,% (n)	15.2% (5/33)	3.5% (3/86)	0.8% (1/130)	0.001
Daughter catheter ,% (n)	3.0% (1/33)	2.3% (2/86)	1.5% (2/130)	0.886
Buddy wire,% (n)	18.2% (6/33)	9.3% (8/86)	3.0% (4/130)	0.016
Average size of balloon	2.48 ± 0.38	2.55 ± 0.35	2.52 ± 0.36	0.702
Non-compliant balloon ,% (n)	13.3% (4/30)	9.5% (7/74)	5.1% (5/99)	0.276
QCA pre-procedure				
RVD (mm)	2.51 ± 0.35	2.66 ± 0.43	2.64 ± 0.46	0.256
MLD (mm)	0.97 ± 0.40	0.92 ± 0.36	0.87 ± 0.34	0.358
% DS (%)	62.3 ± 13.5	65.0 ± 12.6	65.3 ± 15.7	0.592
Lesion length	36.11 ± 2.34	27.99 ± 1.54	22.11 ± 1.16	<0.001
QCA post-procedure				
RVD (mm)	2.97 ± 0.38	2.93 ± 0.39	2.85 ± 0.46	0.244
MLD (mm)	2.38 ± 0.38	2.41 ± 0.39	2.42 ± 0.43	0.889
% DS	20.3 ± 10.5	17.8 ± 7.7	16.8 ± 8.6	0.112
Acute gain (mm)	1.36 ± 0.41	1.48 ± 0.44	1.56 ± 0.54	0.109
Device Success per lesion, % (n)	97.0% (32/33)	100% (86/86)	99.2% (129/130)	0.251
Procedure Success per lesion, % (n)	97.0% (32/33)	98.8% (85/86)	99.2% (129/130)	0.571
Clinical Success (per lesion), % (n)	97.0% (32/33)	98.8% (85/86)	99.2% (129/130)	0.571

Data are expressed as mean ± standard deviation or number and proportion

Table 7

BVS implantation in Total occlusions

	Occluded (L =29)	Non-occluded (L = 220)	P value
QCA post-procedure			
RVD (mm)	3.01 ± 0.47	2.88 ± 0.41	0.103
MLD (mm)	2.51 ± 0.53	2.40 ± 0.39	0.163
% DS (%)	17.2 ± 9.4	17.7 ± 8.6	0.780
Acute gain (mm)	-	1.51 ± 0.49	-
Procedural characteristics			
Daughter catheter, % (n)	3.4% (1/29)	1.8% (4/220)	0.465
Buddy wire, % (n)	10.3% (3/29)	6.8% (15/220)	0.449
Type of first wire (after recanalization)			
Supportive	54.2% (13/ 24)	2.1% (4/195)	<0.001
Non-supportive	45.8% (11/24)	97.9% (191/195)	<0.001
Device Success after disobstruction per lesion, % (n)	100% (29/29)	99.1% (218/220)	1.0
Procedure Success after disobstruction per lesion, % (n)	100% (29/29)	98.6% (217/220)	1.0
Clinical Success after disobstruction per lesion, % (n)	100% (29/29)	98.6% (217/220)	1.0

Data are expressed as mean ± standard deviation or number and proportion

Figure legend

Figure 1

Title: Calcified lesion

Caption: Angiogram showing a long lesion in the RCA (panel A). IVUS pre-procedure (Panel a) shows at the MLA more than 180 degrees superficial calcium (*). Panel B shows the angiogram after pre-dilatation (semi-compliant balloon 3.0 x 20mm). IVUS (panel b) shows clear "cracks" in the calcium (arrowheads), reducing the plaque resistance, thus sufficiently prepared for BVS implantation. Panels C and c show respectively the result on angiogram and on IVUS after implanting a BVS 3.5 x 28mm.

Figure 2

Title: Chronic total occlusion and bifurcation

Caption: Top panels show from left to right the angiograms pre-procedure, after recanalization and scaffold implantation (BVS 3.0 x 28mm with the sequential post dilatation of the diagonal and the scaffold in the main branch) and 2-month follw-up with partial distal vessel positive remodeling. Characters a-c indicate the positions of the OCT cross-sections. OCT (St.Jude Lightlab Dragonfly™) post procedure show distal a well deployed scaffold (Panel A), an well opened carina with the diagonal branch (Panel B *) and the overlap of the proximal marker with the septal branch (Panel C *). The 3D reconstruction (Intage realia™, Cybersystems, Tokyo, Japan) shows the opening of the struts at the carina with the diagonal branch. (Arrowhead bottom panel).

Figure 3

Title: Chronic total occlusion and bifurcation

Caption: The angiogram top left shows the long lesion in the LAD. The mid-panel shows the markers of the two overlapping scaffolds (a & c distal BVS 3.0 x 28mm and b & d proximal BVS 3.5 x 18mm). The top right shows the final result with the OCT cross-section positions indicated by a to d). OCT (St.Jude Lightlab Dragonfly™) shows a well deployed scaffold. Panels B & C show the markers of respectively the proximal and distal scaffolds (*), indicating an overlap of approximately 1 mm.

Chapter 2

Failure Mode of Bioresorbable Scaffolds

2.1 Acute and late scaffold failures: dislodgement and thrombosis

Lessons learned from acute and late scaffold failures in the ABSORB EXTEND trial.

EuroIntervention. 2014 Aug;10(4):449-57.
[Original research paper, IF 3.76]

Ishibashi Y, Onuma Y, Muramatsu T, Nakatani S, Iqbal J, Garcia-Garcia HM, Bartorelli AL, Whitbourn R, Abizaid A, Serruys PW; ABSORB EXTEND Investigators.

Lessons learned from acute and late scaffold failures in the ABSORB EXTEND trial

Yuki Ishibashi[1], MD, PhD; Yoshinobu Onuma[1], MD; Takashi Muramatsu[1], MD, PhD; Shimpei Nakatani[1], MD; Javaid Iqbal[1], MRCP, PhD; Hector M. Garcia-Garcia[1], MD, PhD; Antonio L. Bartorelli[2], MD; Robert Whitbourn[3], MD; Alexander Abizaid[4], MD, PhD; Patrick W. Serruys[1], MD, PhD; on behalf of the ABSORB EXTEND Investigators

1. Thoraxcenter, Erasmus University Medical Center, Rotterdam, The Netherlands; 2. Centro Cardiologico Monzino, IRCCS, University of Milan, Milan, Italy; 3. St Vincent's Hospital, Fitzroy, Victoria, Australia; 4. Instituto de Cardiologia Dante Pazzanese, Sao Paulo, Brazil

GUEST EDITOR: Antonio Colombo, MD; *S. Raffaele Scientific Institute, Milan, Italy*

KEYWORDS

- bioresorbable scaffold
- scaffold dislodgement
- scaffold thrombosis

Abstract

Aims: Bioresorbable scaffolds are increasingly used in patients with coronary artery disease undergoing percutaneous coronary interventions. ABSORB EXTEND is an ongoing study that will recruit 800 patients. This report evaluates acute and late scaffold failure in the first 450 patients enrolled in ABSORB EXTEND who have completed 12 months follow-up.

Methods and results: Clinical event data from the first 450 patients enrolled in ABSORB EXTEND have demonstrated low rates of ischaemia-driven MACE (4.2%) and target vessel failure (4.7%) at 12 months. There have been seven cases of device failure in this study: three cases of scaffold dislodgement (0.67%) and four cases of subacute or late scaffold thrombosis (0.89%). All scaffold dislodgements occurred in the left circumflex (LCX), and in two cases dislodgement was observed after reinsertion of the same device. Two cases of subacute scaffold thrombosis and two late scaffold thromboses were observed. Two out of four cases of scaffold thrombosis seemed to be related to either premature discontinuation of dual antiplatelet therapy (DAPT) or resistance to clopidogrel.

Conclusions: This is the first report specifically describing the incidence and the potential mechanisms of scaffold dislodgement and scaffold thrombosis as seen in the ABSORB EXTEND trial.

**Corresponding author: Thoraxcenter, Ba-583, 's Gravendijkwal 230, 3015 CE Rotterdam, The Netherlands. E-mail: p.w.j.c.serruys@erasmusmc.nl*

SUBMITTED ON 22/07/2013 - REVISION RECEIVED ON 24/09/2013 - ACCEPTED ON 19/11/2013

Introduction

Acute vessel closure, due to dislodgement of a coronary stent during deployment or an early stent thrombosis, is a rare but potentially fatal complication of percutaneous coronary intervention (PCI)[1]. Late or very late thrombosis also remains a long-term concern with metallic drug-eluting stents, due to delayed healing potentially caused by the permanent presence of foreign bodies such as metals and coating materials[1-4].

The Absorb everolimus-eluting poly-L-lactic acid (PLLA) bioresorbable vascular scaffold system (BVS; Abbott Vascular, Santa Clara, CA, USA) is a novel approach to treat coronary lesions[5-8]. After complete bioresorption of the polymeric struts[8], the risk of very late scaffold thrombosis may theoretically be reduced due to the absence of foreign material[9,10]. On the other hand, the thick polymeric struts (total strut thickness=156 μm) crimped onto the delivery balloon contribute to the large profile of the device that may cause friction between the device and the diseased vessel wall or any daughter catheter, resulting in dislodgement of the scaffold[10]. Until now, however, there have been no specific reports of these acute and late complications with the Absorb BVS beyond anecdotal presentations of isolated cases.

ABSORB EXTEND (unique identifier NCT01023789) is an international prospective, single-arm study that will recruit 800 patients with long lesions (length up to 28 mm) or lesions in small vessels (2.0-3.8 mm diameter). Treatment of two *de novo* native coronary artery lesions is also permitted when each lesion is located in a different epicardial vessel. The details of the trial are described in the previous report[11].

The first 450 patients enrolled in ABSORB EXTEND have completed 12 months follow-up and this interim report presents seven cases of device failure detected in this population. Three cases of scaffold dislodgement (0.67%) and four cases of subacute or late scaffold thrombosis (0.89%) are described in detail to evaluate the underlying mechanisms and to make some practical recommendations to avoid these serious complications.

Case descriptions

CASE 1. SCAFFOLD DISLODGEMENT SUBSEQUENTLY CRUSHED BY METALLIC STENTS

In a 74-year-old man coronary angiography showed a severe lesion with a percentage diameter stenosis (DS) of 83% **(Table 1)** in the mid segment of a calcified left circumflex (LCX) coronary artery **(Figure 1A)**. After the first predilatation with a 2.5×15 mm balloon, a 3.0×18 mm Absorb BVS failed to cross the tortuous proximal LCX. After the second dilatation, the same Absorb scaffold was reinserted (time between the first and second insertion of the scaffold is unknown). However, the same Absorb scaffold still failed to cross and unexpectedly dislodged from the balloon at a site of fluoroscopic calcification proximal to the lesion when the device was pushed forward **(Figure 1B, Figure 1C)**. Two 3.0×18 mm metallic everolimus-eluting metallic stents (EES) were deployed in an overlapping fashion to crush the dislodged scaffold against the vessel wall, and an additional 3.0×18 mm EES was deployed at the target lesion **(Figure 1D)**. The follow-up was uneventful during 12 months.

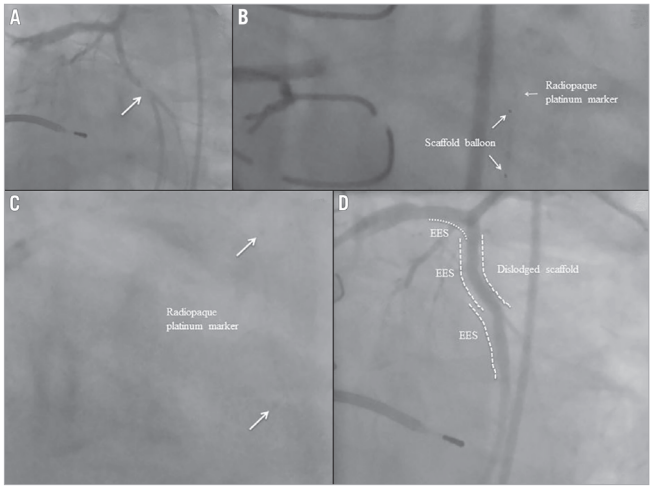

Figure 1. *Case 1. A) Coronary angiography showing a severe lesion in the mid segment of a calcified left circumflex (LCX) coronary artery. B) & C) The same Absorb scaffold still failed to cross and unexpectedly dislodged. D) Two metallic everolimus-eluting metallic stents (EES) were deployed in an overlapping fashion to crush the dislodged scaffold against the vessel wall, and an additional EES was deployed at the target lesion.*

CASE 2. A DISLODGED SCAFFOLD LEFT INSIDE A PREVIOUSLY IMPLANTED METALLIC STENT

In a 60-year-old man diagnostic coronary angiography showed a moderate stenosis **(Table 1)** in the mid segment of a highly tortuous LCX. Two metallic stents had previously been implanted in the left anterior descending coronary artery (LAD) and it seemed that the proximal stent had partially jailed the ostium of the LCX **(Figure 2A)**. After predilation using a 2.5×15 mm balloon, a 3.0×18 mm Absorb BVS was advanced beyond the ostium of the LCX, but it failed to progress into the proximal LCX despite the use of an extra support guidewire **(Figure 2B)**. While the Absorb BVS delivery system and extra support guidewire were being withdrawn, the Absorb scaffold unexpectedly dislodged from the balloon and became positioned with its distal edge in the proximal LCX and its proximal edge in the LMS **(Figure 2C)**. An attempt to retrieve the dislodged scaffold was made with a GooseNeck® snare (ev3 Inc., Plymouth, MN, USA). However, it failed as the dislodged scaffold was inadvertently pushed into the metallic stent located in the proximal LAD. Following this, another guidewire was inserted into the LAD and a second attempt was made to retrieve the dislodged scaffold using the GooseNeck snare, but it failed again. A balloon was

Table 1. QCA analysis before and after the procedure in all cases.

Case No.	MLD, mm	RVD, mm	DS, %	Obstruction length, mm	Curvature, cm^{-1}	Angulation, degree
before procedure						
1	0.37	2.24	83	13.97	0.439	32.6
2	0.98	2.57	62	7.78	0.436	47.4
3	0.91	2.41	62	9.30	0.421	54.9
4	0.91	2.59	65	9.10	0.116	20.5
5	0.74	2.88	74	12.37	0.353	23.8
6	1.00	2.54	61	18.13	0.233	21.4
7	0.88	2.28	61	8.65	0.147	19.7
after procedure						
1	2.16	2.39	11	–	0.413	25.6
2	2.60	2.74	5	–	0.305	40.5
3	2.30	2.46	7	–	0.418	44.8
4	2.03	2.79	27	–	0.118	19.2
5	3.07	3.13	2	–	0.293	21.5
6	2.12	2.44	13	–	0.225	18.7
7	2.02	2.38	15	–	0.144	19.5

DS: diameter stenosis; MLD: minimal lumen diameter; QCA: quantitative coronary angiography; RVD: reference vessel diameter

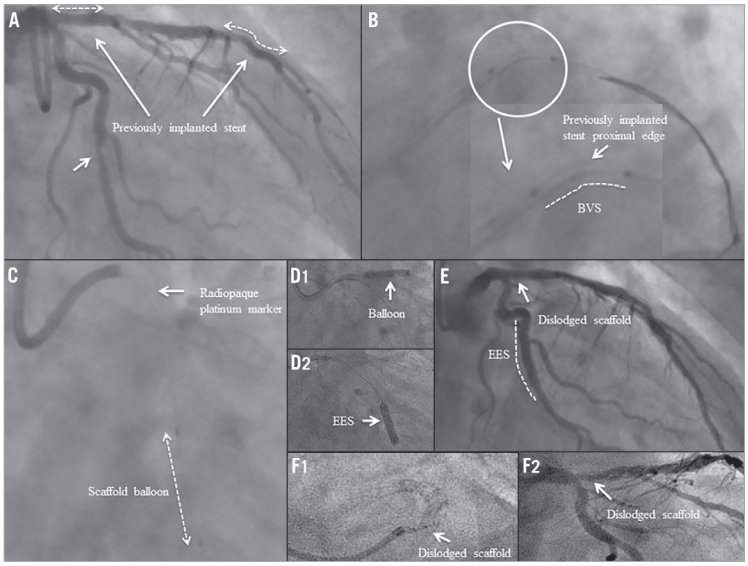

Figure 2. *Case 2. A) Coronary angiography showing a moderate stenosis in the mid segment of a highly tortuous LCX. Two metallic stents had previously been implanted in the left anterior descending coronary artery (LAD) and it seemed that the proximal stent had partially jailed the ostium of the LCX. B) An Absorb BVS was advanced beyond the ostium of the LCX, but it failed to progress. C) The Absorb scaffold unexpectedly dislodged and became positioned with its distal edge in the proximal LCX and its proximal edge in the left main stem (LMS). D1) A balloon was then inflated to crush the dislodged scaffold in the proximal LAD. D2) An EES was successfully deployed at the target lesion. E) Final result. F1) & F2) Five months later, coronary angiography revealed a severe stenosis in the proximal LAD and LCX.*

then inflated to crush the dislodged scaffold in the proximal LAD and finally an EES was successfully deployed at the target lesion **(Figure 2D, Figure 2E)**. Five months later, coronary angiography revealed a severe stenosis in the proximal LAD and proximal LCX **(Figure 2F)**, and the patient was referred for surgical treatment.

CASE 3. SCAFFOLD DISLODGEMENT DUE TO A TORTUOUS VESSEL

A 61-year-old male underwent coronary angiography which showed a moderate stenosis **(Table 1)** in the mid segment of a calcified LCX **(Figure 3A)**. After the first predilatation with a 2.5×15 mm balloon, a 3.0×18 mm Absorb BVS failed to cross the lesion. After two additional predilatations with a 3.0×15 mm balloon, the same Absorb BVS system was reinserted, but it was unable to pass a moderate bend in the LCX proximal to the predilated lesion. Another attempt was made to deliver the scaffold using a GuideLiner™ catheter (Vascular Solutions Inc., Minneapolis, MN, USA) and the scaffold delivery system was apparently positioned at the target lesion **(Figure 3B1)**. However, after balloon inflation, the radiopaque markers at the edges of the scaffold were not visible on fluoroscopy **(Figure 3B1, Figure 3B2)**. When the GuideLiner™, guidewire and the Absorb BVS delivery system were removed together as a single unit, the dislodged scaffold was found to be inside the GuideLiner™. Following this, a 2.75×18 mm EES was successfully deployed at the target lesion without any further procedural complications **(Figure 3C)**. The patient had an uneventful clinical course and was discharged two days after the procedure. Approximately three months after the procedure, the patient passed away at home (unwitnessed sudden death). This event was adjudicated as a possible stent thrombosis by the clinical events committee of the ABSORB EXTEND trial.

CASE 4. SUBACUTE SCAFFOLD THROMBOSIS AT THE SITE OF OVERLAPPING SCAFFOLDS

In a 56-year-old man coronary angiography showed a moderate stenosis **(Table 1)** in the proximal segment of the LCX **(Figure 4A1, Figure 4A2)**. After predilatation, a 3.0×28 mm Absorb scaffold failed to be delivered. Two additional predilatations were performed and the same Absorb BVS system was reinserted over an extra support guidewire (ASAHI GRAND SLAM™; Abbott Vascular, Santa Clara, CA, USA), but was unable to cross. A proximal scaffold deformation was observed (post-withdrawal observation) after having retracted the Absorb BVS system and the guidewire. Following this, two 3.0×18 mm Absorb BVS were successfully deployed **(Figure 4B, Figure 4C)**. The distance between the scaffold radiopaque markers in the overlapping segment was 2.56 mm as measured by QCA.

Six days after the procedure the patient presented with a non-STEMI and was treated with thrombolytic therapy. Angiography on day seven revealed a thrombotic lesion at the site of the overlapping scaffolds in the mid segment of the LCX **(Figure 4D1, Figure 4D2)**. The patient claimed to be fully compliant with dual antiplatelet therapy (DAPT). An EES was successfully implanted to cover the lesion and the overlapping segment of the scaffolds **(Figure 4E, Figure 4F)**.

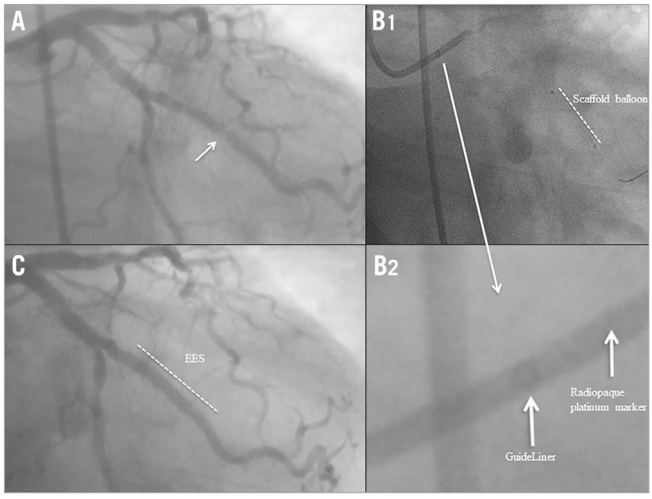

Figure 3. *Case 3. A) Coronary angiography showing a moderate stenosis in the mid segment of a calcified LCX. B1) The scaffold delivery system was apparently positioned at the target lesion. B2) When the GuideLiner™ system was removed together as a single unit, the dislodged scaffold was found to be inside the GuideLiner™. C) An EES was successfully deployed at the target lesion.*

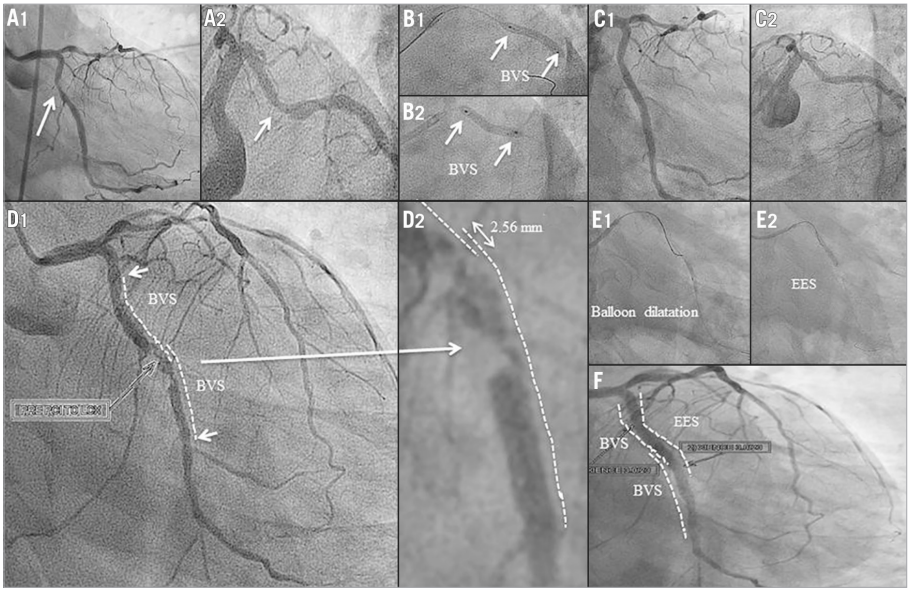

Figure 4. *Case 4. A1) & A2) Coronary angiography showing a moderate stenosis in the proximal segment of the LCX. B1) & B2) Two Absorb BVS were successfully deployed. C1) & C2) Final results. D1) & D2) Angiography on day seven revealed a thrombotic lesion at the site of the overlapping scaffolds in the mid segment of the LCX. E1), E2) & F) An EES was successfully implanted to cover the lesion and the overlapping segment.*

CASE 5. SUBACUTE SCAFFOLD THROMBOSIS OCCURRING TWO DAYS AFTER DISCONTINUATION OF DAPT

A 58-year-old woman underwent PCI with a 3.0×18 mm Absorb BVS in the mid segment of the LAD **(Figure 5A, Figure 5B)**. On day 27, the patient stopped taking both aspirin and clopidogrel. Two days after DAPT discontinuation, she presented with a non-STEMI and was treated by thrombolysis. On day 32, coronary angiography showed a patent LAD with haziness **(Figure 5C, Figure 5D)**. DAPT was restarted and follow-up was uneventful.

CASE 6. LATE SCAFFOLD THROMBOSIS IN A PATIENT WITH RESISTANCE TO CLOPIDOGREL

An 80-year-old woman underwent PCI with a 3.0×18 mm Absorb BVS for a moderate stenosis **(Table 1)** in the mid segment of the LAD **(Figure 6A-Figure 6C)**.

Seventy-five days after the index procedure, she presented with an acute anterior STEMI. Coronary angiography showed complete thrombotic occlusion of the LAD proximal to the scaffold up to the take-off of a diagonal branch **(Figure 6D)**. Primary PCI with a manual thrombectomy and a balloon dilatation was successfully performed **(Figure 6E-Figure 6G)**. At the time of the emergency procedure, the patient reported that she was scrupulously taking her

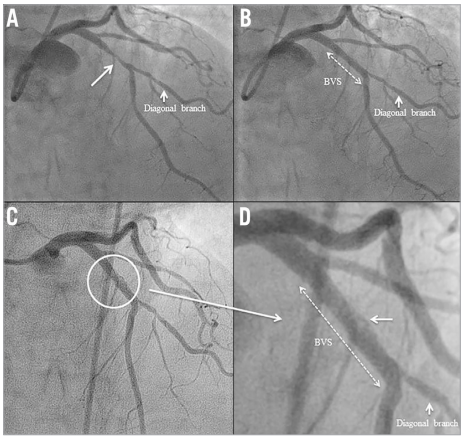

Figure 5. *Case 5. A) Coronary angiography showing a moderate stenosis in the proximal segment of the LAD. B) An Absorb BVS was successfully deployed at the target lesion. C) & D) On day 32, coronary angiography showed a patent LAD with haziness.*

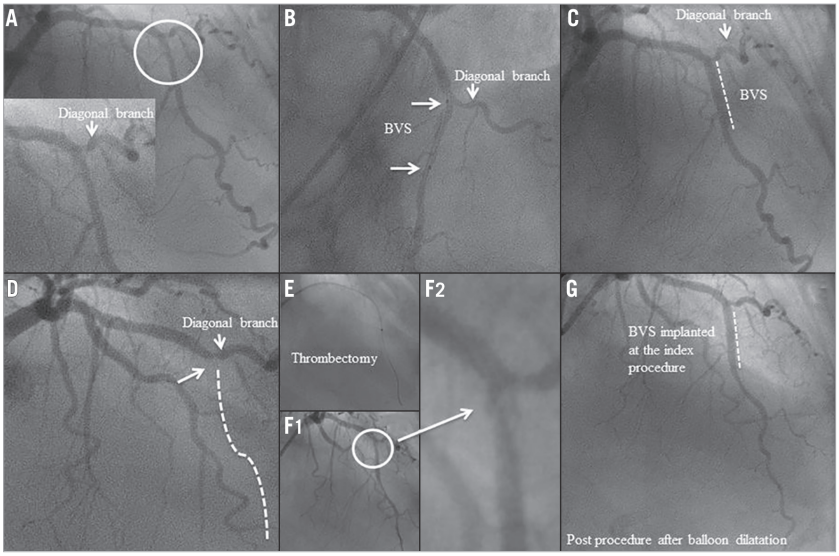

Figure 6 *Case 6. A) Coronary angiography showing a moderate stenosis in the mid segment of the LAD. B) & C) An Absorb BVS was successfully deployed at the target lesion. D) Coronary angiography showed complete thrombotic occlusion of the LAD. E) Primary PCI with a manual thrombectomy was performed. F1) & F2) Coronary angiography showed a patent LAD with haziness after thrombectomy. G) Coronary angiography showed a patent LAD without haziness after balloon dilatation.*

DAPT. However, the platelet aggregation test indicated that she was either not on DAPT or resistant to clopidogrel, since her ADP-induced aggregation of platelets was normal. The patient claimed to be fully compliant with DAPT and hence a higher dose of clopidogrel (150 mg daily) was prescribed to prevent further scaffold thrombosis. The follow-up was uneventful.

CASE 7. LATE SCAFFOLD THROMBOSIS OF UNKNOWN CAUSE

A 56-year-old man with dyslipidaemia, a family history of coronary artery disease (CAD) and angina class II underwent PCI with a 3.0×18 mm Absorb BVS in the mid segment of the LAD **(Figure 7A, Figure 7B)**. After Absorb BVS implantation, post-dilation was performed with a 3.0×9.0 mm balloon (non-compliant balloon) at maximal pressure of 16 atm (rated balloon pressure: 18 atm).

At day 239, following a bee sting, he presented with an acute anterior STEMI. The patient was still on DAPT at that time. Urgent coronary angiography revealed total occlusion of the LAD, proximal to the previously implanted Absorb scaffold **(Figure 7C)**. Following manual thrombectomy, an EES was successfully deployed **(Figure 7D)**.

Discussion

The main findings of the current report are the following: 1) in the first 450 patients enrolled in the ABSORB EXTEND trial, scaffold dislodgement occurred in three cases; 2) all dislodgements occurred

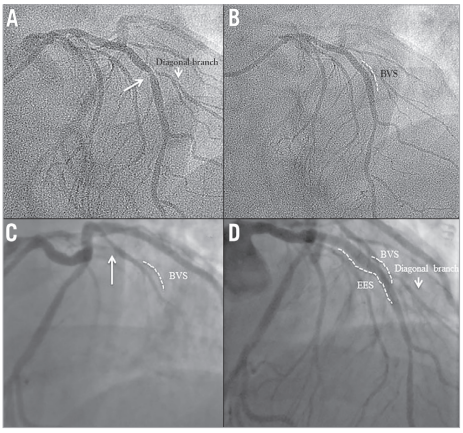

Figure 7. *Case 7. A) Coronary angiography showing a moderate stenosis in the mid segment of the LAD. B) An Absorb BVS was successfully deployed at the target lesion. C) At day 239, coronary angiography revealed a total occlusion of the LAD, proximal to the preciously implanted Absorb scaffold. D) Following manual thrombectomy, an EES was successfully deployed.*

in the LCX, and in two cases dislodgement was observed after reinsertion of the same device; 3) two subacute scaffold thromboses and two late scaffold thromboses were observed; 4) two scaffold thromboses seemed to be related to either premature discontinuation of DAPT or resistance to clopidogrel.

SCAFFOLD DISLODGEMENT

Dislodgement of a metallic stent from the delivery balloon during deployment is a rare complication, reported in 0.32-1.2% of procedures in the early 2000s[12]. Metallic stent dislodgement from the delivery system occurs most often when the stent balloon device is pulled back into the guiding catheter, because the target lesion cannot be either reached or crossed despite a forceful pushing manoeuvre[13-15]. Risk factors for stent dislodgement include severe coronary angulations, coronary tortuosity, diffuse long lesions and calcified lesions. In addition, stent dislodgement has been reported to be the highest in the LMS or LAD[16].

In the current series which included relatively simple lesions (mean lesion length: 11.6 mm, type B2/C lesions according to the American College of Cardiology/American Heart Association: 38.6%, calcification: 13.2%), scaffold dislodgement was observed in 0.67% (3/450). All cases of dislodgement occurred in the LCX (mean baseline vessel angulation: 45.0 degrees; mean baseline vessel curvature: 0.432 cm^{-1}). One scaffold was dislodged when the crimped scaffold was retracted after the delivery failure of the device, one was dislodged from the balloon when the device was advanced through a 6 Fr daughter catheter, and one was observed after crossing the ostium of the LCX jailed by a metallic stent previously implanted in the LAD. Of these three cases, two scaffold dislodgements occurred when the same scaffolds were reinserted after failed delivery attempts.

The Absorb BVS has a crossing profile of 1.4 mm with a strut thickness of 156 μm, and consists of in-phase zigzag hoops linked by straight bridges[17]. Alternative processing techniques have been developed to enhance polymeric scaffold retention, and bench-top testing indicates retention forces equivalent to those observed with metallic stents. However, these thick polymeric struts with a large crossing profile may contribute to friction between the device and a tortuous/calcified vessel or a daughter catheter, resulting in device dislodgement when forcefully pushing the scaffold[10]. In case 3, a 6 Fr GuideLiner™ with a 6 Fr guiding catheter was used, which was not compatible with the current version of the Absorb scaffold. Usage of the 6 Fr GuideLiner™ system should be avoided.

The risk of scaffold dislodgement may increase with the combination of several factors, including tortuous and calcified vessels proximal to the target lesion, prolonged exposure to moisture during repeated removal and reinsertion of a scaffold, and friction against a tightly fitting delivery catheter (such as the GuideLiner™) where enough dimensional clearance for the scaffold is not assured. To prevent scaffold dislodgement, it is recommended to avoid prolonged contact with moisture in the setting of repeated removal and reinsertion of the same device after a failed delivery. It would be advisable to use a new scaffold in such a situation. In the case of heavily calcified lesions, optimal lesion preparation using cutting/scoring balloons or rotational atherectomy should be considered before implantation of the Absorb BVS.

If dislodgement of a device occurs, prompt recognition and an attempt at percutaneous retrieval using a snare system or a multiwire technique is advisable. If the retrieval manoeuvres are not technically feasible or fail, the dislodged scaffold could be crushed against the arterial wall by implantation of a metallic stent. In this case, however, the operator should be aware that the crushed polymeric scaffold will result in a circular and non-laminated structure as seen with crushed metallic stents.

SCAFFOLD THROMBOSIS

Metallic stent thrombosis is multifactorial, including procedure-related factors such as underexpansion, multiple stent use, dissections, and late acquired stent malapposition due to resolution of thrombus on the vessel wall or abnormal vessel healing[1-4,18].

In the current series, two subacute and two late scaffold thromboses were observed (0.89%). Acutely after implantation, PLLA polymer is, at least *in vitro*, somewhat less thrombogenic than a metal without a coating[19]. In the blood flow, however, the presence of thick struts creates alteration of shear stress, resulting in high shear stress on top of the strut and low shear stress behind the strut which may trigger platelet aggregation[20]. Preclinical reports have demonstrated that metallic stents with the thinner struts are less thrombogenic[21,22]. During the acute/subacute phase after implantation of an Absorb scaffold, efficient platelet inhibition is mandatory[22]. The optimal duration of DAPT after implantation of Absorb scaffolds has not been investigated. In a porcine coronary angioplasty model, the polymeric struts were associated with lesser granuloma formation than the first-generation sirolimus-eluting stents, suggesting that the bioresorption process does not provoke any significant inflammation. In the ABSORB Cohort B trial, tissue coverage as assessed by optical coherence tomography (OCT) was almost complete (97%) at six months[5]. The optimal duration of DAPT after implantation of Absorb scaffolds has not been investigated. The protocols of previous ABSORB trials mandated at least six months of DAPT. It is noteworthy that the mean duration of DAPT was 403 days in the ABSORB Cohort B trial[5]. Given the paucity of data, the optimal duration of DAPT should be prospectively assessed in future studies.

In the present series, late scaffold thrombosis occurred in one case with overlapping Absorb scaffolds. In a juvenile porcine model, the overlapping Absorb scaffolds showed delayed healing and slower tissue coverage than in non-overlapping scaffolds[23]: the coverage of the overlapping segment was 80.1% and 99.5% at 28 and 90 days after implantation, respectively, suggesting that complete coverage in humans may take up to 18 months[4]. In case of overlapping scaffolds, a relatively longer duration of DAPT with more potent agents (e.g., ticagrelor or prasugrel) could be considered.

One late scaffold thrombosis occurred following a bee sting. The mechanism responsible for STEMI in this patient could have been

coronary artery spasm (partly mediated by psychological stress related to the intensity of the anaphylactic reaction) with thrombosis secondary to cardiovascular collapse[24]. However, the precise mechanism of scaffold thrombosis in this case remains uncertain.

Conclusion

This is the first report specifically describing the incidence and the potential mechanisms of scaffold dislodgement and scaffold thrombosis seen in the ABSORB EXTEND trial. To avoid scaffold dislodgement, appropriate lesion preparation is mandatory. In case of unsuccessful initial delivery, a second insertion of the same scaffold should be avoided. Adherence to antiplatelet therapy is of paramount importance to avoid acute or subacute scaffold thrombosis.

Impact on daily practice

Bioresorbable scaffolds are increasingly used in patients with coronary artery disease undergoing percutaneous coronary interventions; however, the early clinical experiences in the ABSORB EXTEND trial (n=450) demonstrated scaffold dislodgement in 0.67% and scaffold thrombosis in 0.89% of cases. To avoid scaffold dislodgement, appropriate lesion preparation is mandatory and a second insertion of the same scaffold should be avoided. Adherence to the antiplatelet therapy is of paramount importance to avoid acute or subacute scaffold thrombosis.

Guest Editor

This paper was guest edited by Antonio Colombo, MD, S. Raffaele Scientific Institute, Milan, Italy.

Conflict of interest statement

The authors have no conflicts of interest to declare. The Guest Editor has no conflicts of interest to declare.

References

1. Lüscher TF, Steffel J, Eberli FR, Joner M, Nakazawa G, Tanner FC, Virmani R. Drug-eluting stent and coronary thrombosis. Biological mechanisms and clinical implications. *Circulation*. 2007;115:1051-8.

2. Cook S, Wenaweser P, Togni M, Billinger M, Morger C, Seiler C, Vogel R, Hess O, Meier B, Windecker S. Incomplete stent apposition and very late stent thrombosis after drug-eluting stent implantation. *Circulation*. 2007;115:2426-34.

3. Farb A, Burke AP, Kolodgie FD, Virmani R. Pathological mechanisms of fatal late coronary stent thrombosis in humans. *Circulation*. 2003;108:1701-6.

4. Iakovou I, Schmidt T, Bonizzoni E, Ge L, Sangiorgi GM, Stankovic G, Airoldi F, Chieffo A, Montorfano M, Carlino M, Michev I, Corvaja N, Briguori C, Gerckens U, Grube E, Colombo A. Incidence, predictors and outcome of thrombosis after successful implantation of drug-eluting stents. *JAMA*. 2005;293:2126-30.

5. Onuma Y, Serruys PW, Ormiston JA, Regar E, Webster M, Thuesen L, Dudek D, Veldhof S, Rapoza R. Three-year results of clinical follow-up after a bioresorbable everolimus-eluting scaffold in patients with de novo coronary artery disease: the ABSORB trial. *EuroIntervention*. 2010;6:447-53.

6. Serruys PW, Onuma Y, Dudek D, Smits PC, Koolen J, Chevalier B, de Bruyne B, Thuesen L, McClean D, van Geuns RJ, Windecker S, Whitbourn R, Meredith I, Dorange C, Veldhof S, Hebert KM, Sudhir K, Garcia-Garcia HM, Ormiston JA. Evaluation of the second generation of a bioresorbable everolimus-eluting vascular scaffold for the treatment of de novo coronary artery stenosis: 12-month clinical and imaging outcomes. *J Am Coll Cardiol.* 2011;58:1578-88.

7. Dudek D, Onuma Y, Ormiston JA, Thuesen L, Miquel-Hebert K, Serruys PW. Four-year clinical follow-up of the ABSORB everolimus-eluting bioresorbable vascular scaffold in patients with de novo coronary artery disease: the ABSORB trial. *EuroIntervention*. 2012;7:1060-1.

8. Onuma Y, Serruys PW, Perkins LE, Okamura T, Gonzalo N, García-García HM, Regar E, Kamberi M, Powers JC, Rapoza R, van Beusekom H, van der Giessen W, Virmani R. Intracoronary optical coherence tomography and histology at 1 month and 2, 3, and 4 years after implantation of everolimus-eluting bioresorbable vascular scaffolds in a porcine coronary artery model: an attempt to decipher the human optical coherence tomography images in the ABSORB trial. *Circulation*. 2010;122:2288-300.

9. Serruys PW, Onuma Y, Ormiston JA, de Bruyne B, Regar E, Dudek D, Thuesen L, Smits PC, Chevalier B, McClean D, Koolen J, Windecker S, Whitbourn R, Meredith I, Dorange C, Veldhof S, Miquel-Hebert K, Rapoza R, García-García HM. Evaluation of the second generation of a bioresorbable everolimus drug-eluting vascular scaffold for treatment of de novo coronary artery stenosis: six-month clinical and imaging outcomes. *Circulation*. 2010;122:2301-12.

10. Oberhauser JP, Hossainy S, Rapoza R. Design principles and performance of bioresorbable polymeric vascular scaffolds. *EuroIntervention*. 2009;5:F15-22.

11. Muramatsu T, Onuma Y, García-García HM, Farooq V, Bourantas CV, Morel MA, Li X, Veldhof S, Bartorelli A, Whitbourn R, Abizaid A, Serruys PW; ABSORB-EXTEND Investigators. Incidence and short-term clinical outcomes of small side branch occlusion after implantation of an everolimus-eluting bioresorbable vascular scaffold: an interim report of 435 patients in the ABSORB-EXTEND single-arm trial in comparison with an everolimus-eluting metallic stent in the SPIRIT first and II trials. *JACC Cardiovasc Interv.* 2013;6:247-57.

12. Kwan TW, Chaudhry M, Huang Y, Liou M, Wong S, Zhou X, Pancholy S, Patel T. Approaches for dislodged stent retrieval during transradial percutaneous coronary interventions. *Catheter Cardiovasc Interv.* 2013;81:E245-9.

13. Curran PJ, Currier J, Tobis J. Percutaneous snare retrieval of a partially embedded Wallstent. *Catheter Cardiovasc Interv.* 2004; 61:400-2.

14. Eggebrecht H, Haude M, von Birgelen C, Oldenburg O, Baumgart D, Herrmann J, Welge D, Bartel T, Dagres N, Erbel R. Nonsurgical retrieval of embolized coronary stents. *Catheter Cardiovasc Interv.* 2000;51:432-40.

15. Webb JG, Solankhi N, Carere RG. Facilitation of stent retention and retrieval with an emboli containment device. *Catheter Cardiovasc Interv.* 2000;50:215-7.

16. Laarman G, Muthusamy TS, Swart H, Westendorp I, Kiemeneij F, Slagboom T, van der Wieken R. Direct coronary stent implantation: safety, feasibility and predictors of success of the strategy of direct coronary stent implantation. *Catheter Cardiovasc Interv.* 2001;52:443-8.

17. Okamura T, Garg S, Gutiérrez-Chico JL, Shin ES, Onuma Y, García-García HM, Rapoza RJ, Sudhir K, Regar E, Serruys PW. In vivo evaluation of stent strut distribution patterns in the bioabsorbable everolimus-eluting device: an OCT ad hoc analysis of the revision 1.0 and revision 1.1 stent design in the ABSORB clinical trial. *EuroIntervention*. 2010;5:932-8.

18. Byrne RA, Kastrati A, Massberg S, Wieczorek A, Laugwitz KL, Hadamitzky M, Schulz S, Pache J, Fusaro M, Hausleiter J, Schömig A, Mehilli J; ISAR-TEST 4 Investigators. Biodegradable polymer versus permanent polymer drug-eluting stents and everolimus- versus sirolimus-eluting stents in patients with coronary artery disease: 3-year outcomes from a randomized clinical trial. *J Am Coll Cardiol.* 2011;58:1325-31.

19. Seifert B, Romaniuk P, Groth TH. Bioresorbable, heparinized polymers for stent coating: in vitro studies on heparinization efficiency, maintenance of anticoagulant properties and improvement of stent haemocompatibility. *J Mater Sci Mater Med.* 1996;7:465-9.

20. Onuma Y, Serruys PW. The advent of a new era in percutaneous coronary and peripheral revascularization? *Circulation*. 2011;123:779-97.

21. Daemen J, Wenaweser P, Tsuchida K, Abrecht L, Vaina S, Morger C, Kukreja N, Jüni P, Sianos G, Hellige G, van Domburg RT, Hess OM, Boersma E, Meier B, Windecker S, Serruys PW. Early and late coronary stent thrombosis of sirolimus-eluting and paclitaxel-eluting stents in routine clinical practice: data from a large two-institutional cohort study. *Lancet.* 2007;369:667-78.

22. Lüscher TF, Steffel J, Eberli FR, Joner M, Nakazawa G, Tanner FC, Virmani R. Drug-eluting stent and coronary thrombosis: biological mechanisms and clinical implications. *Circulation*. 2007;115:1051-8.

23. Farooq V, Serruys PW, Heo JH, Gogas BD, Onuma Y, Perkins LE, Diletti R, Radu MD, Räber L, Bourantas CV, Zhang Y, van Remortel E, Pawar R, Rapoza RJ, Powers JC, van Beusekom HM, Garcia-Garcia HM, Virmani R. Intracoronary optical coherence tomography and histology of overlapping everolimus-eluting bioresorbable vascular scaffolds in a porcine coronary artery model: the potential implications for clinical practice. *JACC Cardiovasc Interv.* 2013;6:523-32.

24. Kounis NG, Giannopoulos S, Tsigkas GG, Goudevenos J. Eosinophilic responses to stent implantation and the risk of Kounis hypersensitivity associated coronary syndrome. *Int J Cardiol.* 2012;156:125-32.

2.2 Scaffold thrombosis in stable and ACS patients

Definite and probable bioresorbable scaffold thrombosis in stable and ACS patients.

EuroIntervention. 2014 Sep 22.
[Letter to editor, IF 3.76]

Ishibashi Y, Nakatani S, Onuma Y.

Definite and probable bioresorbable scaffold thrombosis in stable and ACS patients

Yuki Ishibashi, MD, PhD; Shimpei Nakatani, MD; Yoshinobu Onuma*, MD, PhD

Thoraxcenter, Erasmus University Medical Center, Rotterdam, The Netherlands

We read with great interest the recent report by Capodanno et al[1]. In the European multicentre GHOST-EU registry, the authors reported that the rate of definite/probable scaffold thrombosis was 2.1% (definite scaffold thrombosis: 1.8%, probable scaffold thrombosis: 0.3%) in an all-comers population at six months. More specifically, the rate of definite/probable scaffold thrombosis was 1.4% (9/626) in stable/silent angina pectoris (SAP), 2.5% (14/563) in acute coronary syndrome (ACS) and 2.1% (4/192) in ST-segment elevation myocardial infarction (STEMI). This publication prompted us to review the rates of scaffold thrombosis in all-comers, SAP, ACS and STEMI either reported so far in peer review journals or presented at international meetings.

Table 1 summarises the rate of scaffold thrombosis in each individual report. Excluding the GHOST-EU registry, the rate of definite/probable scaffold thrombosis was 0.89% in all-comers, 0.68% in SAP, 1.71% in ACS and 0.67% in STEMI. There were 25 definite and two probable scaffold thromboses. Out of 27 patients with scaffold thrombosis, two had acute (≤24 hours

Table 1. The rate of ST in individual populations*.

Study (journal/ international congress)	Population	Follow-up	Total, N	Acute ST in total, N (%)	Subacute ST in total, N (%)	Early ST in total, N (%)	ST in total, N (%)	SAP, N	ST in SAP, N (%)	ACS, N	ST in ACS, N (%)	STEMI, N	ST in STEMI, N (%)
Kraak et al, AMC single-centre (EIJ 2014)	All-comers	6 mo	135	0 (0%)	3 (2.2%)	3 (2.2%)	4 (3.0%)	82	1 (1.2%)	53	3 (5.7%)	17	0 (0%)
ABSORB FIRST, (EuroPCR 2014)	All-comers	1 mo	800	0 (0%)	2 (0.3%)	2 (0.3%)	2 (0.3%)	295	N/A	505	N/A	N/A	N/A
Azzalini et al, (EuroPCR 2014)	All-comers	N/A	339	0 (0%)	4 (1.2%)	4 (1.2%)	4 (1.2%)	N/A	3 (N/A)	N/A	0 (N/A)	N/A	1 (N/A)
Abizaid et al, ABSORB EXTEND (EIJ 2014)	SAP	12 mo	512	0 (0%)	2 (0.4%)	2 (0.4%)	4 (0.8%)	512	4 (0.8%)	–	–	–	–
Serruys et al, ABSORB B (EIJ 2014)	SAP	36 mo	101	0 (0%)	0 (0%)	0 (0%)	0 (0%)	101	0 (0%)	–	–	–	–
Onuma et al, ABSORB A (JACC CI 2013)	SAP	60 mo	30	0 (0%)	0 (0%)	0 (0%)	0 (0%)	30	0 (0%)	–	–	–	–
CORONARY CTO (EuroPCR 2014)	SAP	6 mo	35	0 (0%)	0 (0%)	0 (0%)	0 (0%)	35	0 (0%)	–	–	–	–
Serruys et al, ABSORB II (Lancet 2014)	SAP/UAP	12 mo	335	1 (0.3%)	1 (0.3%)	2 (0.6%)	3 (0.9%)	267	3 (1.1%)	68	0 (0%)	–	–
ASSURE registry (EuroPCR 2014)	SAP/UAP	12 mo	183	0 (0%)	0 (0%)	0 (0%)	0 (0%)	144	0 (0%)	39	0 (0%)	–	–
BVS EXPAND (EuroPCR 2014)	SAP/UAP	6 mo	200	0 (0%)	0 (0%)	0 (0%)	4 (2.2%)	N/A	N/A	N/A	N/A	–	–
Gori et al (EIJ 2014)	ACS	1 mo	150	1 (0.7%)	1 (0.7%)	2 (1.4%)	4 (2.7%)	–	–	150	4 (2.7%)	66	N/A
POLAR ACS (EuroPCR 2014)	ACS	12 mo	100	0 (0%)	0 (0%)	0 (0%)	0 (0%)	–	–	100	0 (0%)	16	0 (0%)
Kajiya et al (EIJ 2013)	STEMI	3 mo	11	0 (0%)	0 (0%)	0 (0%)	0 (0%)	–	–	–	–	11	0 (0%)
Diletti et al, BVS STEMI (EHJ 2014)	STEMI	1 mo	49	0 (0%)	0 (0%)	0 (0%)	0 (0%)	–	–	–	–	49	0 (0%)
Kocka et al, PRAGUE-19 (EHJ 2014)	STEMI	4 mo	41	0 (0%)	1 (2.4%)	1 (2.4%)	1 (2.4%)	–	–	–	–	41	1 (2.4%)
Wiebe et al (CRC 2014)	STEMI	6 mo	25	0 (0%)	0 (0%)	0 (0%)	0 (0%)	–	–	–	–	25	0 (0%)
Ielasi et al, RAI registry (EIJ in press)	STEMI	6 mo	74	0 (0%)	1 (1.4%)	1 (1.4%)	1 (1.4%)	–	–	–	–	74	1 (1.4%)
Weighted average excluding the GHOST-EU registry	Average F/U: 10.6 months		3,120	0.06%	0.48%	0.54%	0.89%	1,171	0.68%	410	1.71%	299	0.67%
Capodanno et al, GHOST (EIJ 2014)	All-comers	6 mo	1,189	5 (0.4%)	11 (0.9%)	16 (1.3%)	23 (2.1%)	626	9 (1.4%)	563	14 (2.5%)	192	4 (2.1%)
Weighted average including the GHOST-EU registry	Average F/U: 10.3 months		4,309	0.16%	0.60%	0.76%	1.22%	1,797	0.94%	973	2.16%	491	1.22%

*ACS: acute coronary syndrome; SAP: stable/silent angina pectoris; ST: scaffold thrombosis; STEMI: ST-segment elevation myocardial infarction. CRC: Clinical Research in Cardiology; EHJ: European Heart Journal; EIJ: EuroIntervention; JACC CI: JACC Cardiovascular Interventions

*Corresponding author: Thoraxcenter, Room Ee 218, 's-Gravendijkwal 230, 3015 CE Rotterdam, The Netherlands. E-mail: y.onuma@erasmusmc.nl

after procedure) thrombosis (0.06%) and 15 had subacute after one day (≤1 month after procedure) thrombosis (0.48%). Premature discontinuation of dual antiplatelet therapy (DAPT) or resistance to clopidogrel at the time of scaffold thrombosis was documented in 29.4% patients (5/17). The rate of scaffold thrombosis when the GHOST-EU registry is added to the series is tabulated at the bottom of **Table 1**. Potential aetiological causes of scaffold thrombosis could be: 1) suboptimal implantation resulting in underexpansion/acute incomplete strut apposition[2-4] or acute disruption of struts[5]; 2) platelet activation due to low shear stress created by the relatively thick strut[6]; 3) delayed tissue coverage in an overlapped segment[7-9]; 4) discontinuation of DAPT or resistance to DAPT[9].

In the first randomised comparison of ABSORB II[10], the rate of definite scaffold/stent thrombosis was 0.6% in Absorb (one acute and one subacute case) and 0% in XIENCE (p=1.0), and the rate of definite/probable scaffold/stent thrombosis was 0.9% in Absorb and 0% in XIENCE (p=0.55)[10].

Further randomised studies may or may not confirm these scaffold thrombosis rates in the future[11,12].

Conflict of interest statement

The authors have no conflicts of interest to declare.

References

1. Capodanno D, Gori T, Nef H, Latib A, Mehilli J, Lesiak M, Caramanno G, Naber C, Di Mario C, Colombo A, Capranzano P, Wiebe J, Araszkiewicz A, Geraci S, Pyxaras S, Mattesini A, Naganuma T, Munzel T, Tamburino C. Percutaneous coronary intervention with everolimus-eluting bioresorbable vascular scaffolds in routine clinical practice: early and midterm outcomes from the European multicentre GHOST-EU registry. *EuroIntervention.* 2014 Jul 18. [Epub ahead of print].

2. Kolandaivelu K, Swaminathan R, Gibson WJ, Kolachalama VB, Nguyen-Ehrenreich KL, Giddings VL, Coleman L, Wong GK, Edelman ER. Stent thrombogenicity early in high-risk interventional settings is driven by stent design and deployment and protected by polymer-drug coatings. *Circulation*. 2011;123:1400-9.

3. Guagliumi G, Sirbu V, Musumeci G, Gerber R, Biondi-Zoccai G, Ikejima H, Ladich E, Lortkipanidze N, Matiashvili A, Valsecchi O, Virmani R, Stone GW. Examination of the in vivo mechanisms of late drug-eluting stent thrombosis: findings from optical coherence tomography and intravascular ultrasound imaging. *JACC Cardiovasc Interv.* 2012;5:12-20.

4. Siqueira DA, Abizaid AA, Costa Jde R, Feres F, Mattos LA, Staico R, Abizaid AA, Tanajura LF, Chaves A, Centemero M, Sousa AG, Sousa JE. Late incomplete apposition after drug-eluting stent implantation: incidence and potential for adverse clinical outcomes. *Eur Heart J.* 2007;28:1304-9.

5. Ormiston JA, De Vroey F, Serruys PW, Webster MW. Bioresorbable polymeric vascular scaffolds: a cautionary tale. *Circ Cardiovasc Interv.* 2011;4: 535-8.

6. Bourantas CV, Papafaklis MI, Lakkas L, Sakellarios A, Onuma Y, Zhang YJ, Muramatsu T, Diletti R, Bizopoulos P, Kalatzis F, Naka KK, Fotiadis DI, Wang J, Garcia Garcia HM, Kimura T, Michalis LK, Serruys PW. Fusion of optical coherence tomographic and angiographic data for more accurate evaluation of the endothelial shear stress patterns and neointimal distribution after bioresorbable scaffold implantation: comparison with intravascular ultrasound-derived reconstructions. *Int J Cardiovasc Imaging.* 2014;30:485-94.

7. Farooq V, Onuma Y, Radu M, Okamura T, Gomez-Lara J, Brugaletta S, Gogas BD, van Geuns RJ, Regar E, Schultz C, Windecker S, Lefevre T, Brueren BR, Powers J, Perkins LL, Rapoza RJ, Virmani R, Garcia-Garcia HM, Serruys PW. Optical coherence tomography (OCT) of overlapping bioresorbable scaffolds: from benchwork to clinical application. *EuroIntervention.* 2011;7:386-99.

8. Farooq V, Serruys PW, Heo JH, Gogas BD, Onuma Y, Perkins LE, Diletti R, Radu MD, Raber L, Bourantas CV, Zhang Y, van Remortel E, Pawar R, Rapoza RJ, Powers JC, van Beusekom HM, Garcia-Garcia HM, Virmani R. Intracoronary optical coherence tomography and histology of overlapping everolimus-eluting bioresorbable vascular scaffolds in a porcine coronary artery model: the potential implications for clinical practice. *JACC Cardiovasc Interv.* 2013;6:523-32.

9. Ishibashi Y, Onuma Y, Muramatsu T, Nakatani S, Iqbal J, Garcia-Garcia HM, Bartorelli AL, Whitbourn R, Abizaid A, Serruys PW. Lessons learned from acute and late scaffold failures in the ABSORB EXTEND trial. *EuroIntervention.* 2014;10:449-57.

10. Serruys PW, Chevalier B, Dudek D, Cequier A, Carrié D, Iniguez A, Dominici M, Van der Schaaf R, Haude M, Wasungu L, Veldhof S, Peng L, Staehr P, Grundeken M, Ishibashi Y, Garcia-Garcia HM, Onuma Y. A bioresorbable everolimus-eluting scaffold versus a metallic everolimus-eluting stent for ischaemic heart disease caused by de-novo native coronary artery lesions (ABSORB II): an interim 1-year analysis of clinical and procedural secondary outcomes. *Lancet.* 2015;385:43-54.

11. Woudstra P, Grundeken MJ, Kraak RP, Hassell ME, Arkenbout EK, Baan J Jr, Vis MM, Koch KT, Tijssen JG, Piek JJ, de Winter RJ, Henriques JP, Wykrzykowska JJ. Amsterdam Investigator-initiateD Absorb strategy all-comers trial (AIDA trial): a clinical evaluation comparing the efficacy and performance of ABSORB everolimus-eluting bioresorbable vascular scaffold strategy vs the XIENCE family (XIENCE PRIME or XIENCE Xpedition) everolimus-eluting coronary stent strategy in the treatment of coronary lesions in consecutive all-comers: rationale and study design. *Am Heart J.* 2014;167:133-40.

12. Stone GW. The ABSORB III + IV Clinical Trial Program. EuroPCR 2014 Paris, May 2014.

2.3 Early and late scaffold restenosis

Early (before 6 months), late (6-12 months) and very late (after 12 months) angiographic scaffold restenosis in the ABSORB Cohort B trial.

EuroIntervention. 2014 Feb 27.
[Original research paper, IF 3.76]

Nakatani S, Onuma Y, **Ishibashi Y**, Muramatsu T, Iqbal J, Zhang YJ, van Geuns RJ, Ormiston JA, Serruys PW.

Early (before 6 months), late (6-12 months) and very late (after 12 months) angiographic scaffold restenosis in the ABSORB Cohort B trial

Shimpei Nakatani[1], MD; Yoshinobu Onuma[1]*, MD; Yuki Ishibashi[1], MD, PhD; Takashi Muramatsu[1], MD, PhD; Javaid Iqbal[1], MRCP, PhD; Yao-Jun Zhang[1], MD, PhD; Robert-Jan van Geuns[1], MD, PhD; John A. Ormiston[2], MBChB, PhD; Patrick W. Serruys[1], MD, PhD; on behalf of the ABSORB Cohort B investigators

1. Thoraxcenter, Erasmus Medical Center, Rotterdam, The Netherlands; 2. Auckland City Hospital, Auckland, New Zealand

GUEST EDITOR: Rafael Beyar, MD, DSc, MPH, Director; *Rambam Health Care Campus, Women's Division/Dr Phillip and Sara Gotlieb Chair, Department of Medicine and Biomedical Engineering, Technion, Israel*

KEYWORDS

- bioresorbable scaffold
- everolimus
- intravascular imaging
- long-term follow-up
- restenosis

Abstract

Aims: The long-term follow-up of the first-in-man ABSORB Cohort B trial showed that angiographic binary restenosis can occur early, late or very late after implantation of the Absorb everolimus-eluting bioresorbable vascular scaffold (Absorb BVS). Since the mechanical support of the scaffold decreases during bioresorption, the mechanism of in-segment restenosis (ISR) of the Absorb BVS might be different from that of metallic stents. The objective of the current analysis was to review the multimodality imaging of cases with binary restenosis to elucidate the mechanism of ISR after Absorb BVS implantation.

Methods and results: The ABSORB Cohort B trial enrolled 101 patients with a maximum of two *de novo* coronary lesions. At the three-year imaging and clinical follow-up, there were six cases of in-segment binary restenosis: two early ISR (<6 months), one late ISR (6-12 months) and three very late ISR (>12 months). Three of these ISR cases seemed to be induced by anatomical or procedural factors. In the other three cases, intravascular imaging (IVUS/OCT) demonstrated that the main mechanism of restenosis was significant intra-scaffold tissue growth, while the structural circularity and diameter of the scaffold were not affected.

Conclusions: Early and late restenosis after implantation of the Absorb bioresorbable scaffold could be related to anatomical or procedural factors. In this small cohort of patients late or very late restenosis seems to be attributed to pure intra-scaffold tissue growth without extrinsic encroachment of the scaffold.

**Corresponding author: Thoraxcenter, Ba-583, 's Gravendijkwal 230, 3015 CE Rotterdam, The Netherlands. E-mail: yoshinobuonuma@gmail.com*

SUBMITTED ON 29/08/2013 - REVISION RECEIVED ON 09/12/2013 - ACCEPTED ON 08/01/2014

Introduction

The Absorb everolimus-eluting bioresorbable vascular scaffold (Absorb BVS; Abbott Vascular, Santa Clara, CA, USA) shows unique potential in vascular repair, such as late lumen enlargement, restoration of vasomotion and plaque media reduction[1-4]. However, in-scaffold restenosis may occur as frequently as with metallic drug-eluting stents (DES). Since the Absorb BVS loses its mechanical strength during bioresorption, unlike metallic stents, the mechanism of in-scaffold restenosis might be unique and different from DES and bare metal stents (BMS).

The process of lumen loss (LL) is a "time limited phenomenon" due to negative remodelling of the vessel and neointimal hyperplasia inside the stent, which occurs three to six months after implantation[5,6]. Beyond this critical period, the mechanical support of the scaffold and the active pharmacological inhibition of the neointima are no longer necessary. According to this concept, mechanical support of the scaffold could decrease approximately six months after implantation. Actually, it has been established in humans that the mechanical integrity is maintained over a period of six months but subsides afterwards[7]. However, one could speculate that the plaque behind the struts of the scaffold might progress and narrow the lumen once the scaffold has lost its mechanical strength.

Timing of restenosis and its potential mechanism after implantation of the Absorb BVS have not been investigated. We report six cases of ISR (quantitative coronary angiography [QCA] diameter stenosis ≥50% within the scaffolded segment and 5 mm proximal and distal to the scaffolded segment) observed in the ABSORB Cohort B trial (101 patients, 102 lesions) according to the timing, and describe in detail the intravascular findings in an attempt to elucidate the mechanism of this complication. Two cases were early ISR (<6 months), one case was late ISR (6-12 months), and three cases were very late ISR (>12 months) **(Table 1, Figure 1)**.

Case histories

CASE 1. EARLY ISR DUE TO MYOCARDIAL BRIDGE

A 57-year-old man with a history of hypertension, dyslipidaemia, smoking and COPD presented with stable angina. The coronary angiography showed a type B2 lesion in the mid left anterior descending (LAD) artery with severe stenosis in systole (percentage diameter stenosis [%DS]: 84%), but without significant stenosis in diastole (%DS: 26%), thus with typical evidence of a myocardial bridge **(Figure 2A-Figure 2C)**[8]. After predilatation with a 2.75 mm semi-compliant balloon, a 3.0×18 mm Absorb BVS was deployed and post-dilated with a 3.5 mm non-compliant balloon at 16 atm **(Figure 2D)**. On day 89, the patient experienced recurrent angina and underwent re-catheterisation. The angiography revealed a focal ISR at the site of the myocardial bridge (QCA minimum lumen diameter [MLD]: 1.20 mm, %DS: 59.0%, LL: 0.90 mm) **(Figure 2E)**. This ISR was treated by implantation of a 3.5×15 mm XIENCE V stent (Abbott Vascular) inside the Absorb BVS **(Figure 2F)**. At three years, angiography revealed a significant re-ISR of this XIENCE V stent (QCA MLD: 1.20 mm, %DS: 59.0%, LL: 0.90 mm) **(Figure 2G)**.

Table 1. Case summary.

	Case 1	Case 2	Case 3	Case 4	Case 5	Case 6
Timing	Early	Early	Late	Very late	Very late	Very late
Day	89	168	354	383	567	833
Age	57	69	57	76	62	42
Sex	Male	Male	Male	Male	Male	Female
History of DM	no	no	no	no	no	no
Pre procedure						
RVD (mm)	2.51	2.05	2.64	2.82	2.97	2.24
Lesion length	10.3	5.9	12.0	8.1	15.4	10.2
%DS (%)	71.5	72.5	70.0	71.0	64.5	52.5
MLD (mm)	0.72	0.58	0.79	0.82	1.05	1.06
Post procedure						
%DS (%)	16.7	27.0	16.0	24.5	23.5	9.0
MLD (mm)	1.91	1.94	2.08	2.10	1.95	1.93
At TLR						
Clinical presentation	Stable angina	No angina	Stable angina	Unstable angina	Unstable angina	Stable angina
Examination for ischaemia	–	FFR: 0.72	Asynergy on echo.	–	–	Myocardial scintigram positive
%DS (%)	59.0	63.5	64.0	67.0	71.0	63.7
MLD (mm)	1.20	0.89	0.79	0.90	0.81	0.72
LL (mm)	0.90	0.50	1.58	1.20	1.47	1.38

DM: diabetes mellitus; RVD: reference vessel diameter; %DS: % diameter stenosis; MLD: minimum lumen diameter; LL: lumen loss; FFR: fractional flow reserve; TLR: target lesion revascularisation

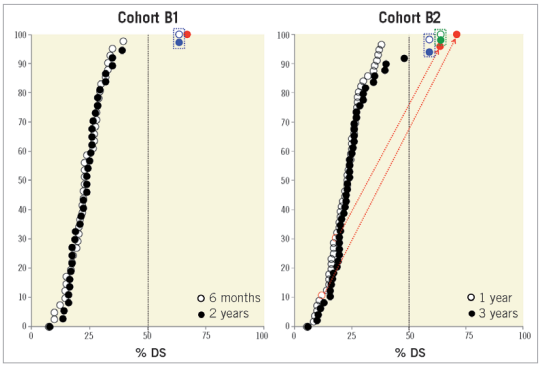

Figure 1. *Cumulative frequency distribution curves of angiographic % diameter stenosis (%DS). A) %DS at 6 (circle) and 24 months (dot) of Cohort B1. B) %DS at 12 (circle) and 36 months (dot) of Cohort B2. If the patient had TLR before the planned angiography, %DS at the time of TLR (before repeat revascularisation) was used for the %DS at the later time point. Blue dots (●) and blue circles (○) represent %DS in TLR patients who experienced early ISR (<6 months). Green dots (●) and green circles (○) represent %DS in TLR patients who experienced late ISR (6-12 months). Red dots (●) and red circles (○) represent %DS in TLR patients who experienced very late ISR.*

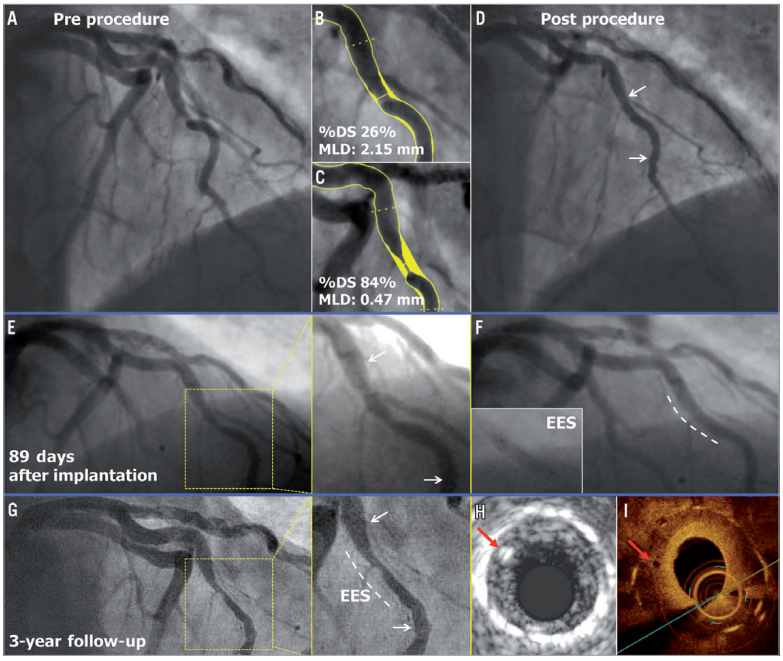

Figure 2. *Early ISR due to myocardial bridge. The white arrows indicate the metallic markers of the implanted scaffold, while the white dotted line illustrates the implanted EES. The red arrows show the scaffold struts of the previously implanted Absorb BVS located inside the metal stent on IVUS (H) and OCT (I).*

Optical coherence tomography (OCT) revealed intra-scaffold tissue growth with homogeneous light reflectivity. Of interest, OCT and intravascular ultrasound (IVUS) showed that some struts of the previously implanted Absorb BVS were located inside the metal stent (**Figure 2H**, **Figure 2I**). Finally, this re-ISR lesion was treated by a coronary artery bypass graft (CABG).

CASE 2. EARLY ISR AT PROXIMAL EDGE

A 69-year-old male with a history of dyslipidaemia and previous coronary intervention of the left circumflex (LCX) artery presented with stable angina. Coronary angiography showed a type B1 severe stenosis in the mid right coronary artery (RCA) **(Figure 3A)**. After predilatation with a 2.5 mm semi-compliant balloon, a 3.0×18 mm Absorb BVS was deployed and post-dilated with a 3.0 mm balloon at 15 atm (expected diameter according to the manufacturer was 3.3 mm) **(Figure 3B)**. As the IVUS catheter failed to pass through the implanted scaffold, the guiding catheter was changed from JR4 to AL1. After repeated attempts to cross the IVUS catheter through the scaffold by seating the guiding catheter deeply up to the proximal edge of the scaffold in order to perform the protocol-related imaging, the operator was unable to cross the scaffold and the procedure was ended **(Figure 3C)**. On day 168, the patient underwent a planned repeat angiography, which showed a type 1B ISR at the proximal edge of the scaffold (QCA MLD: 0.89 mm, %DS: 63.5%, LL: 0.50 mm) without significant restenosis in the scaffold itself **(Figure 3D)**[9]. Greyscale IVUS (IVUS-GS) showed a high-echoic intra-scaffold tissue growth in the segment proximal to the scaffold, with maintained circularity of the scaffold (**Figure 3E**, **Figure 3F**). This ISR was treated by implantation of a 3×28 mm XIENCE V stent with full coverage of the previously implanted Absorb BVS.

CASE 3. LATE ISR WITH HOMOGENEOUS INTRA-SCAFFOLD TISSUE ON OCT

In a 57-year-old man with a history of dyslipidaemia and smoking, and presenting with unstable angina, coronary angiography showed a severe type B1 stenosis in the proximal LAD with TIMI grade 2 flow **(Figure 4A)**. After predilatation with a 2.5 mm

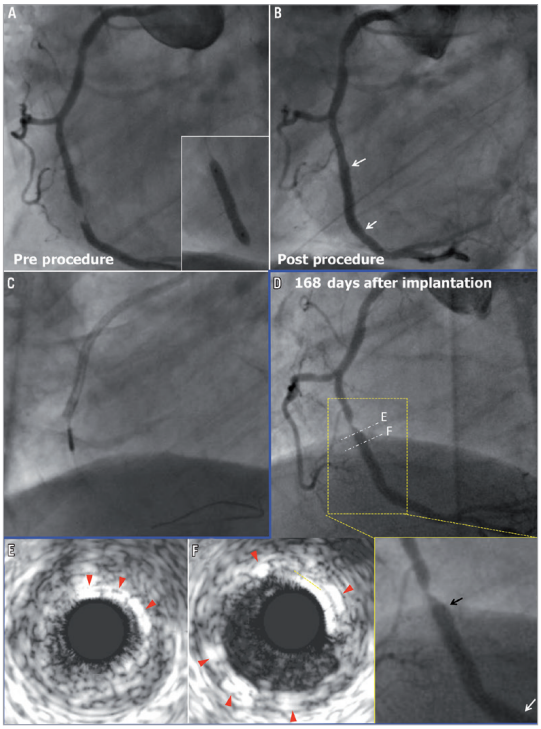

Figure 3. *Early ISR at proximal edge. The white and black arrows indicate the metallic markers of the implanted scaffold. In panels E and F, the red arrows show the polymeric strut on IVUS.*

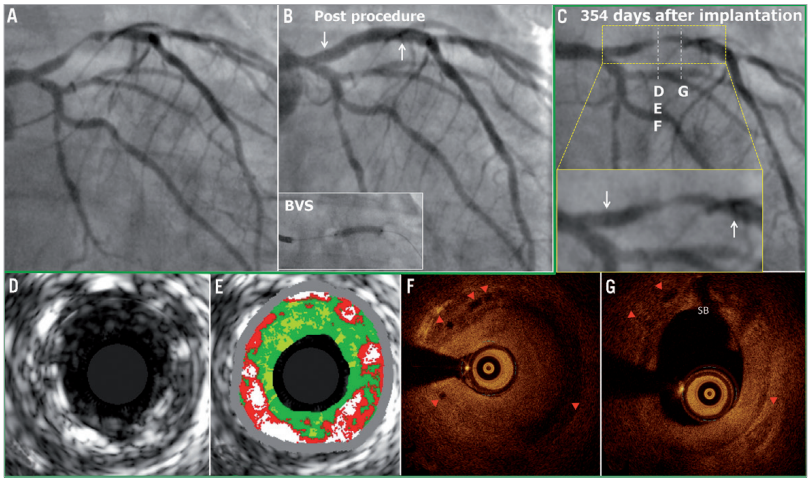

Figure 4. *Late ISR with homogeneous intra-scaffold tissue on OCT. The white arrows show the metallic marker of the implanted scaffold. In panels F and G, the red triangles show the scaffold struts on OCT (case 3).*

semi-compliant balloon, a 3.0×18 mm Absorb BVS was deployed and post-dilated with a 3.0 mm non-compliant balloon at 20 atm **(Figure 4B)**. On day 348, the patient had recurrence of angina pectoris. On day 354, the patient underwent a planned repeat angiography, which showed a significant type 1C ISR (QCA MLD: 0.79 mm, %DS: 64.0%, LL: 1.58 mm) in the body of the scaffold **(Figure 4C)**[9]. OCT showed that the circularity of the scaffold was maintained throughout the pullback (the mean scaffold area was 5.67 mm^2 and the minimum scaffold area was 4.73 mm^2) and all the struts were completely apposed and covered. At the site of the minimal lumen area (MLA), OCT revealed homogeneous signal-rich intra-scaffold tissue (**Figure 4D**-**Figure 4G**). On virtual histology IVUS (IVUS-VH), intra-scaffold tissue was documented as fibrous **(Figure 4E)**. A XIENCE V stent was implanted to cover the previously implanted Absorb BVS.

CASE 4. VERY LATE ISR AT THE PROXIMAL EDGE

A 76-year-old gentleman with a history of dyslipidaemia, chronic kidney failure and coronary intervention to the mid LAD (non-target lesion) presented with stable angina. The coronary angiography showed a type B1 moderate stenosis in the mid LAD **(Figure 5A)**. After predilatation with a 2.5 mm semi-compliant balloon, a 3.0×18 mm Absorb BVS was deployed. However, the Absorb BVS did not cover the proximal part of the predilated segment, resulting in geographical miss **(Figure 5B)**. After implantation of the scaffold, the jailed diagonal branch became occluded. Since this closure resulted in chest pain, bradycardia and hypotension, the side branch was dilated with a 1.5 mm balloon **(Figure 5C)**. OCT post procedure revealed a small dissection in the proximal edge of the scaffold, presumably due to the geographical miss during the procedure **(Figure 5D, Figure 5E)**. The patient refused the scheduled follow-up angiography at six months. One year later, the patient presented with recurrence of angina pectoris, and repeat angiography showed a type 1B ISR in the segment proximal to the scaffold (QCA MLD: 0.90 mm, %DS: 67.0%, LL: 1.20 mm) **(Figure 5F)**, while the scaffolded segment was free from significant restenosis[9]. A 3.0×15 mm XIENCE V stent was implanted to overlap the proximal part of the previously implanted Absorb BVS.

CASE 5. VERY LATE ISR WITH HOMOGENEOUS INTRA-SCAFFOLD TISSUE ON OCT

A 62-year-old man with a history of hypertension, smoking and COPD presented with stable angina. Coronary angiography showed a type B1 severe stenosis in the proximal LAD **(Figure 6A)**. Although the proximal maximum luminal diameter (Dmax) on QCA was 3.90 mm, a 3.0 mm Absorb BVS was planned **(Figure 6B, Figure 6C)**. After predilatation with a 2.5 mm semi-compliant balloon, this 3.0×18 mm Absorb BVS was implanted and post-dilated with a 3.5 mm non-compliant balloon at 12 atm **(Figure 6F)**. Post-procedural OCT showed large incomplete stent apposition (ISA) (max ISA area: 11.89 mm^2, max ISA distance 1.63 mm, the number of cross-sections with ISA: 25 frames) at the proximal edge of the scaffold, but additional dilatation was not performed **(Figure 6D, Figure 6E)**. At one year, the planned follow-up coronary angiography showed patency of the scaffold (QCA MLD: 1.99 mm, %DS: 10.0%, LL: -0.04 mm) **(Figure 6G)**. OCT showed persistent numerous malapposed struts with intraluminal mass attached to or free from the vessel wall at the proximal edge of the previously

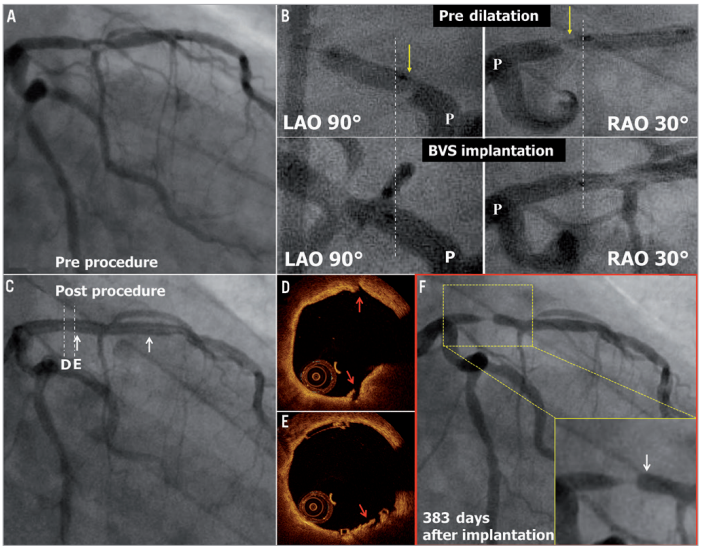

Figure 5. *Very late ISR at the proximal edge. The white arrows show the metallic marker of the implanted scaffold. In panel B, the yellow arrows show the proximal edge of the predilatation balloon. The angiograms are matched anatomically between predilatation and scaffold implantation, and the white dotted lines show the proximal edge of the implanted scaffold. The red arrows show the small dissection observed post procedure on OCT in panels D and E.*

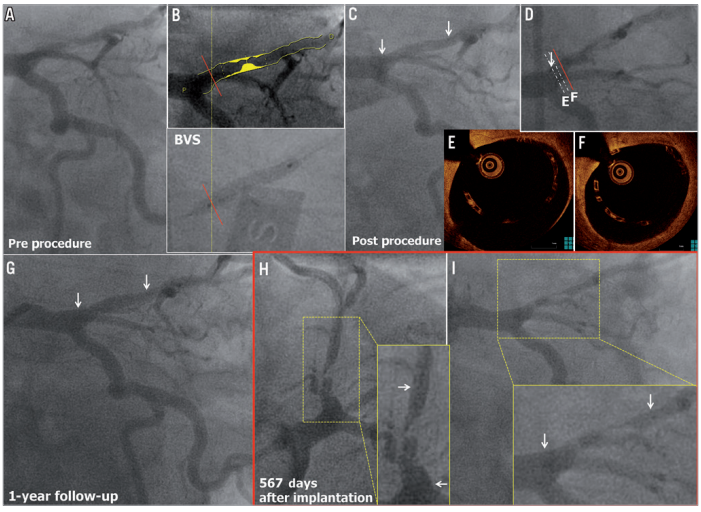

Figure 6. *Very late ISR with homogeneous intra-scaffold tissue on OCT. The white arrows show the metallic marker of the implanted scaffold. The red line shows the point of Dmax on QCA, which is superimposed on the angiogram at scaffold implantation in panel B. The red line is superimposed on the angiogram at OCT study in panel D (case 5).*

implanted scaffold **(Figure 7a)**. On the three-dimensional OCT image, the intraluminal masses were interlinked to the malapposed struts and connected proximally to the vessel wall **(Figure 7a')**. On day 564 the patient was hospitalised with unstable angina and underwent a repeat angiography on day 567, which showed a type 1C ISR in the body of the scaffold (QCA MLD: 0.81 mm, %DS: 71.0% and LL: 1.47 mm)[9]. OCT showed homogeneous signal-rich intra-scaffold tissue in the middle of the scaffold segment with persistent malapposed struts at the proximal edge **(Figure 7B-E)**[10]. After predilatation, repeat OCT revealed an extensive tissue protrusion with maintained circularity of the scaffold **(Figure 7B'-E')**. On OCT analysis, the mean scaffold area was 8.32 mm^2, and the minimum scaffold area was 6.23 mm^2 **(Figure 7A)**. This ISR was treated by implantation of a 3.0×18 mm XIENCE V stent which overlapped the proximal part of the previously implanted Absorb BVS.

CASE 6. VERY LATE ISR WITH ISO-ECHOIC INTRA-SCAFFOLD TISSUE ON IVUS-GS

In a 42-year-old female with a history of smoking presenting with stable angina, coronary angiography demonstrated a type B1 moderate stenosis in the mid LAD **(Figure 8A)**. After predilatation with a 2.5 mm semi-compliant balloon, a 3.0×18 mm Absorb BVS was implanted. After post-dilatation with a 3.0 mm non-compliant balloon at 20 atm, post-procedural angiography showed a residual stenosis of 9.0% **(Figure 8B)**. At one year, a planned repeat angiography showed patency of the previously implanted scaffold (QCA MLD was 1.73 mm, %DS was 18.0% and LL was 0.35 mm) **(Figure 8C)**. On day 833, the patient underwent a repeat angiography because of stable angina with ischaemia on a myocardial scintigraphy: the angiogram showed a type 1B ISR at the distal margin of the scaffold segment (QCA MLD: 0.72 mm, %DS: 63.7% and LL:

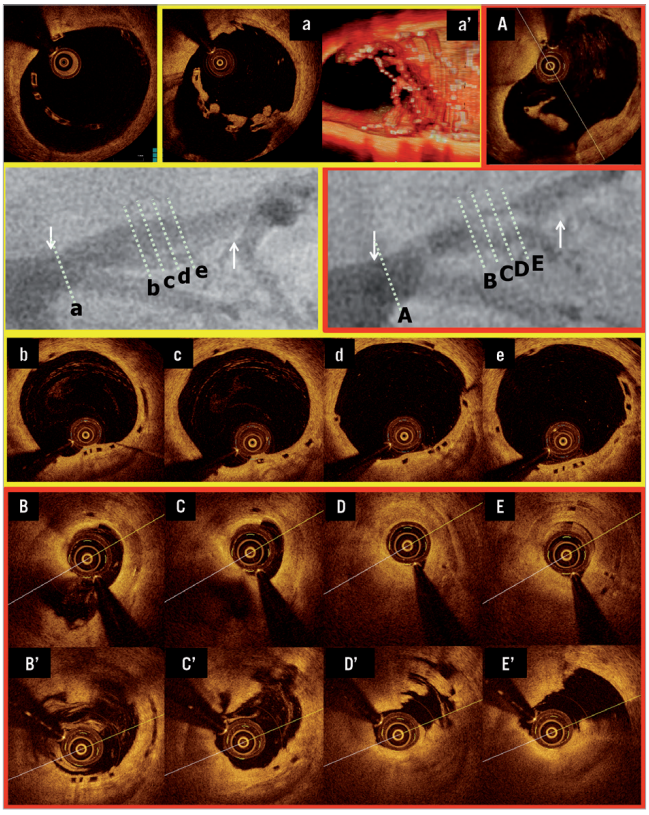

Figure 7. *Very late ISR with homogeneous intra-scaffold tissue on OCT. The white arrows show the metallic marker of the implanted scaffold. OCT images pre TLR before ballooning are shown in panels B to E, and those after ballooning are shown in panels B' to E'. In panels b to e, the corresponding cross-sections to ISR site are shown at 12-month follow-up.*

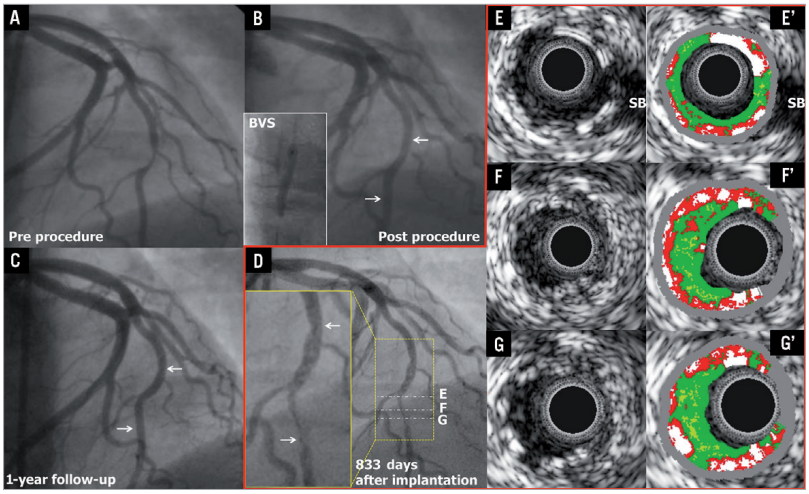

Figure 8. *Very late ISR with iso-echoic intra-scaffold tissue on IVUS-GS. The white arrows show the metallic marker of the implanted scaffold.*

1.38 mm) **(Figure 8D)**[9]. IVUS-GS showed that the scaffold circularity was maintained and that the eccentric intra-scaffold tissue was iso-echoic **(Figure 8E-G)**. On IVUS-VH, small necrotic core and dense calcium were detected in the intra-scaffold tissue **(Figure 8E'-G')**. In this case, the ISR lesion was treated by the implantation of a 3.0×23 mm XIENCE V which overlapped the distal part of the previously implanted Absorb BVS.

Discussion

The main findings of the current report are the following: 1) out of 101 patients enrolled in the ABSORB trial, at three years early restenosis occurred in two cases (2.0%), late ISR in one case (1.0%), and very late ISR in three cases (3.0%); 2) the early ISR was associated with a myocardial bridge (case 1); 3) two of the three late ISR cases may have been caused by procedural edge injury at the index procedure (one case was due to the injury caused by deep insertion of the guiding catheter [case 2], while the other case could be attributed to proximal geographical miss [case 4]); 4) in three cases (one late ISR and two very late ISR), the mechanism of ISR could not be identified (case 3, case 5, and case 6) , but in all cases the circularity of the scaffold was maintained.

It is noteworthy that ISR occurred in patients without diabetes, with relatively large vessels (reference vessel diameter 3 or more mm) and short lesion length (less than 10 mm).

ISR ASSOCIATED WITH MYOCARDIAL BRIDGE

Myocardial bridging (MB) is a potential cause of myocardial ischaemia and in such cases medical therapy, with beta-blockers or calcium channel blockers, is recommended as a first-line strategy[8,11]. Although intracoronary stent implantation is another therapeutic approach to prevent external systolic compression and ischaemia caused by the MB, this therapy is still controversial because of concerns regarding high restenosis rates, plaque prolapse and stent fracture[12,13]. In the current series, one early TLR occurred in a myocardial bridge at three months after implantation of an Absorb BVS, followed by a second failure occurring after implantation of a metallic drug-eluting stent. This case suggests that scaffold implantation for a myocardial bridge treatment should be discouraged. Myocardial bridges generate compressive pressure (up to 300 mmHg) capable of fully closing the vessel in systole. Although the initial radial strength of an Absorb BVS is approximately 900 mmHg and superior to this compressive pressure, this systolic external compression occurs at least 100,000 times/day, and in the course of bioresorption a bioresorbable transient scaffold might yield to such a mechanical stress[3,14].

In this case, at three years, OCT and IVUS detected one scaffold strut inside the area of the metal stent, while post procedure no disrupted strut had been detected on IVUS. The location of a polymeric strut inside the metallic stent may suggest that the discontinued strut could protrude between the metallic mesh of the stent after TLR at three months.

ISR PRESUMABLY TRIGGERED BY PROCEDURAL INJURY

It has been shown that procedural vessel injury might lead to late intra-scaffold tissue growth[15]. In one case in the current series, the deeply inserted AL1 guide catheter might have injured the edge of the scaffold at baseline and led to proximal edge ISR at six months.

Geographical miss is also a known cause of restenosis[16,17]. In one case, the predilatation might have caused "barotrauma" to the proximal plaque and the Absorb BVS did not cover the injured edge segment. Actually, a proximal edge dissection not scaffolded by the Absorb BVS was observed on OCT. The edge ISR could therefore be related to the proximal plaque injury associated with geographical miss[18].

MAINTAINED CIRCULARITY OF SCAFFOLD AREA IN LATE/VERY LATE ISR

As previously described, the radial strength of the fully bioresorbable scaffold declines following polymer hydrolysis at six months, and this device becomes malleable without any supportive properties at 12 months. One could therefore speculate that the scaffold might become encroached by plaque growth behind the struts. In the balloon angioplasty era, Serruys et al demonstrated that the incidence of restenosis reaches a plateau at four months[6]. Ormiston et al demonstrated that the late loss in response to balloon injury reached a maximum before six months and then regressed, while some cases with an intermediate stenosis at six months showed very late lumen narrowing at five years[19].

In this study, we observed three ISR cases without any possible causal relationship with procedural or anatomical factors: one case presented a late ISR and two cases a very late ISR. As shown in **Figure 9**, the circularity of the Absorb BVS, especially at MLA cross-section, was preserved post procedure in all cases. In addition, there were no changes in mean/minimum scaffold area.

This report suggests that the perceived relative weakness of the scaffold related to its polymeric nature does not seem to have any direct impact on the restenosis phenomenon, and late lumen loss seems to be the result of intra-scaffold tissue growth rather than late scaffold recoil.

Late and very late restenosis have also been reported with metallic drug-eluting stents. In the SPIRIT II trial, the rate of ischaemia-driven TLR steadily increased from 1.8% at one year to 3.8% at two years and 4.6% at three years[20-22]. In the ABSORB Cohort B trial, the rate of ischaemia-driven TLR beyond one year increased similarly (4.0% at one year, 5.0% at two years, and 5.9% at three years). These data suggest that ISR with the Absorb BVS occurs as frequently as with metallic DES, and a reduced mechanical strength of the scaffold cannot be implicated in the occurrence of ISR.

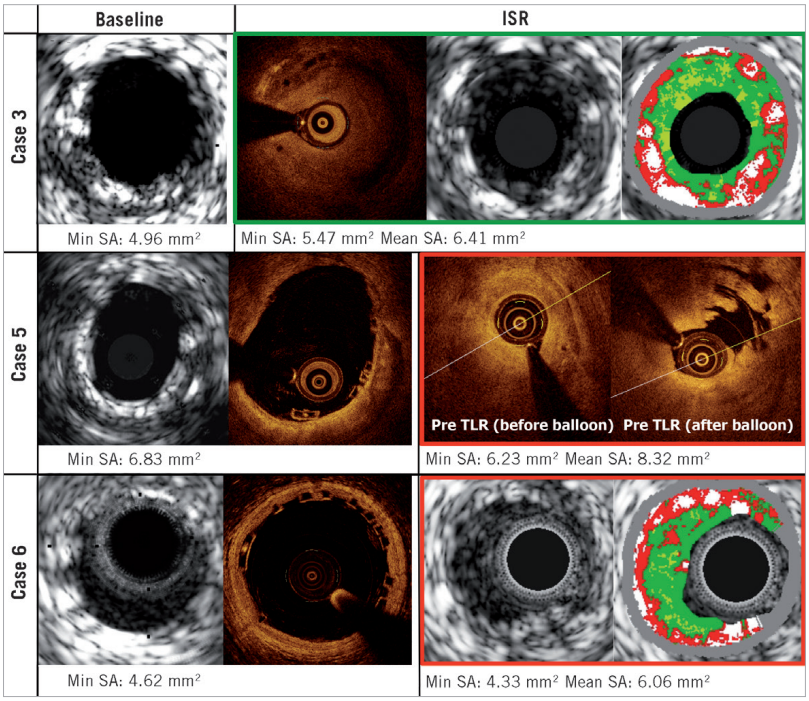

Figure 9. *Intravascular imaging of the late and very late restenosis.*

MORPHOLOGICAL CHARACTERISTICS OF INTRA-SCAFFOLD TISSUE IN LATE/VERY LATE ISR

On IVUS-VH, a typical neointimal restenosis within one year after BMS implantation appears as fibrous or fibro-fatty tissue (green or green-yellow)[23]. Neointima after DES implantation or beyond one year after BMS implantation is sometimes detected as necrotic core tissue (red and red-white) on IVUS-VH[23]. It should be noted that intramural thrombus also has the appearance of fibrous or fibro-fatty tissue[24]. In the current series, two IVUS-VH images were available: one was a late ISR and the other was a very late ISR. In the late ISR case, the intra-scaffold tissue appeared as fibrous tissue, while, in the very late ISR case, the small necrotic core and dense calcium were interspersed in fibrous tissue **(Figure 9)**.

OCT has been used to evaluate the efficacy of stenting by analysing tissue characteristics of in-stent intima[25]. Goto et al demonstrated that homogeneous high-signal band is a typical in-stent intima within one year after BMS implantation, while heterogeneous mixed-signal band is observed at all timing points after DES implantation[24]. In the current series, two OCT images were available: both of them were late ISR. In these cases, the intra-scaffold tissue appeared as a homogeneous tissue **(Figure 9)**.

Limitations

The sample size was small and the first-in-man trial had no control arm. The current findings therefore need to be confirmed in a large randomised trial.

Conclusion

The current analysis suggests that early and late restenosis after implantation of the Absorb bioresorbable scaffold could be related to anatomical or procedural factors. Late or very late restenosis could be attributed to intra-scaffold tissue growth but not to the encroachment of the scaffold.

Impact on daily practice

Since the Absorb everolimus-eluting bioresorbable vascular scaffold (BVS) loses its mechanical strength during bioresorption, the mechanism of in-scaffold restenosis (ISR) could be different from metallic stents. In the ABSORB Cohort B trial, at three years, ISR with the BVS occurs as frequently as with drug-eluting metallic stents. By investigating the ISR according to the time line of the mechanical change of the BVS, the perceived relative weakness of the scaffold does not seem to have any direct impact on the restenosis phenomenon, and seems to be the result of intra-scaffold tissue growth rather than late scaffold recoil and extrinsic encroachment of the scaffold. The disappearance of the device was not found to be a disadvantage in relation to ISR in the current study.

Guest Editor

This paper was guest edited by Rafael Beyar, MD, DSc, MPH, Director, Rambam Health Care Campus, Women's Division/Dr Phillip and Sara Gotlieb Chair, Department of Medicine and Biomedical Engineering, Technion, Israel.

Funding

The ABSORB trial was sponsored by Abbott Vascular.

Conflict of interest statement

The authors have no conflicts of interest to declare. The Guest Editor has no conflicts of interest to declare.

References

1. Ormiston JA, Serruys PW, Onuma Y, van Geuns RJ, de Bruyne B, Dudek D, Thuesen L, Smits PC, Chevalier B, McClean D, Koolen J, Windecker S, Whitbourn R, Meredith I, Dorange C, Veldhof S, Hebert KM, Rapoza R, Garcia-Garcia HM. First serial assessment at 6 months and 2 years of the second generation of absorb everolimus-eluting bioresorbable vascular scaffold: a multi-imaging modality study. *Circ Cardiovasc Interv.* 2012;5:620-32.

2. Serruys PW, Ormiston JA, Onuma Y, Regar E, Gonzalo N, Garcia-Garcia HM, Nieman K, Bruining N, Dorange C, Miquel-Hebert K, Veldhof S, Webster M, Thuesen L, Dudek D. A bioabsorbable everolimus-eluting coronary stent system (ABSORB): 2-year outcomes and results from multiple imaging methods. *Lancet.* 2009;373:897-910.

3. Serruys PW, Onuma Y, Dudek D, Smits PC, Koolen J, Chevalier B, de Bruyne B, Thuesen L, McClean D, van Geuns RJ, Windecker S, Whitbourn R, Meredith I, Dorange C, Veldhof S, Hebert KM, Sudhir K, Garcia-Garcia HM, Ormiston JA. Evaluation of the second generation of a bioresorbable everolimus-eluting vascular scaffold for the treatment of de novo coronary artery stenosis: 12-month clinical and imaging outcomes. *J Am Coll Cardiol.* 2011;58:1578-88.

4. Onuma Y, Serruys PW, Ormiston JA, Regar E, Webster M, Thuesen L, Dudek D, Veldhof S, Rapoza R. Three-year results of clinical follow-up after a bioresorbable everolimus-eluting scaffold in patients with de novo coronary artery disease: the ABSORB trial. *EuroIntervention.* 2010;6:447-53.

5. Nobuyoshi M, Kimura T, Nosaka H, Mioka S, Ueno K, Yokoi H, Hamasaki N, Horiuchi H, Ohishi H. Restenosis after successful percutaneous transluminal coronary angioplasty: serial angiographic follow-up of 229 patients. *J Am Coll Cardiol.* 1988;12:616-23.

6. Serruys PW, Luijten HE, Beatt KJ, Geuskens R, de Feyter PJ, van den Brand M, Reiber JH, ten Katen HJ, van Es GA, Hugenholtz PG. Incidence of restenosis after successful coronary angioplasty: a time-related phenomenon. A quantitative angiographic study in 342 consecutive patients at 1, 2, 3, and 4 months. *Circulation.* 1988;77:361-71.

7. Onuma Y, Serruys PW, Gomez J, de Bruyne B, Dudek D, Thuesen L, Smits P, Chevalier B, McClean D, Koolen J, Windecker S, Whitbourn R, Meredith I, Garcia-Garcia H, Ormiston JA; ABSORB Cohort A and B investigators. Comparison of in vivo acute stent

recoil between the bioresorbable everolimus-eluting coronary scaffolds (revision 1.0 and 1.1) and the metallic everolimus-eluting stent. *Catheter Cardiovasc Interv.* 2011;78:3-12.

8. Ge J, Erbel R, Rupprecht HJ, Koch L, Kearney P, Gorge G, Haude M, Meyer J. Comparison of intravascular ultrasound and angiography in the assessment of myocardial bridging. *Circulation.* 1994;89:1725-32.

9. Mehran R, Dangas G, Abizaid AS, Mintz GS, Lansky AJ, Satler LF, Pichard AD, Kent KM, Stone GW, Leon MB. Angiographic patterns of in-stent restenosis: classification and implications for long-term outcome. *Circulation.* 1999;100:1872-8.

10. Tearney GJ, Regar E, Akasaka T, Adriaenssens T, Barlis P, Bezerra HG, Bouma B, Bruining N, Cho JM, Chowdhary S, Costa MA, de Silva R, Dijkstra J, Di Mario C, Dudek D, Falk E, Feldman MD, Fitzgerald P, Garcia-Garcia HM, Gonzalo N, Granada JF, Guagliumi G, Holm NR, Honda Y, Ikeno F, Kawasaki M, Kochman J, Koltowski L, Kubo T, Kume T, Kyono H, Lam CC, Lamouche G, Lee DP, Leon MB, Maehara A, Manfrini O, Mintz GS, Mizuno K, Morel MA, Nadkarni S, Okura H, Otake H, Pietrasik A, Prati F, Raber L, Radu MD, Rieber J, Riga M, Rollins A, Rosenberg M, Sirbu V, Serruys PW, Shimada K, Shinke T, Shite J, Siegel E, Sonoda S, Suter M, Takarada S, Tanaka A, Terashima M, Thim T, Uemura S, Ughi GJ, van Beusekom HM, van der Steen AF, van Es GA, van Soest G, Virmani R, Waxman S, Weissman NJ, Weisz G; International Working Group for Intravascular Optical Coherence Tomography (IWG-IVOCT). Consensus standards for acquisition, measurement, and reporting of intravascular optical coherence tomography studies: a report from the International Working Group for Intravascular Optical Coherence Tomography Standardization and Validation. *J Am Coll Cardiol.* 2012;59:1058-72.

11. Schwarz ER, Klues HG, vom Dahl J, Klein I, Krebs W, Hanrath P. Functional, angiographic and intracoronary Doppler flow characteristics in symptomatic patients with myocardial bridging: effect of short-term intravenous beta-blocker medication. *J Am Coll Cardiol.* 1996;27:1637-45.

12. Tandar A, Whisenant BK, Michaels AD. Stent fracture following stenting of a myocardial bridge: report of two cases. *Catheter Cardiovasc Interv.* 2008;71:191-6.

13. Arora P, Bhatia V, Parida AK, Kaul U. Myocardial bridge in association with fixed atherosclerotic lesions treated with drug-eluting stents: a follow-up report with quantitative coronary analysis. *Indian Heart J.* 2008;60:594-6.

14. Oberhauser JP, Hossainy S, Rapoza RJ. Design principles and performance of bioresorbable polymeric vascular scaffolds. *EuroIntervention.* 2009;5:F15-22.

15. Lee JH, Kim EM, Ahn KT, Kim MS, Kim KS, Jung IS, Park JH, Choi SW, Seong IW, Jeong JO. Significant left main coronary artery disease from iatrogenic dissection during coronary angiography. *Int J Cardiol.* 2010;138:e35-7.

16. Costa MA, Angiolillo DJ, Tannenbaum M, Driesman M, Chu A, Patterson J, Kuehl W, Battaglia J, Dabbons S, Shamoon F, Flieshman B, Niederman A, Bass TA; STLLR Investigators. Impact of stent deployment procedural factors on long-term effectiveness and safety of sirolimus-eluting stents (final results of the multicenter prospective STLLR trial). *Am J Cardiol.* 2008;101:1704-11.

17. Sabate M, Costa MA, Kozuma K, Kay IP, van der Giessen WJ, Coen VL, Ligthart JM, Serrano P, Levendag PC, Serruys PW. Geographic miss: a cause of treatment failure in radio-oncology applied to intracoronary radiation therapy. *Circulation.* 2000;101: 2467-71.

18. Gogas BD, Onuma Y, van Geuns RJ, Serruys PW. The edge vascular response following implantation of a fully bioresorbable device: 'a miss always counts'. *Int J Cardiol.* 2012;158:455-7.

19. Ormiston JA, Stewart FM, Roche AH, Webber BJ, Whitlock RM, Webster MW. Late regression of the dilated site after coronary angioplasty: a 5-year quantitative angiographic study. *Circulation.* 1997;96:468-74.

20. Claessen BE, Beijk MA, Legrand V, Ruzyllo W, Manari A, Varenne O, Suttorp MJ, Tijssen JG, Miquel-Hebert K, Veldhof S, Henriques JP, Serruys PW, Piek JJ. Two-year clinical, angiographic, and intravascular ultrasound follow-up of the XIENCE V everolimus-eluting stent in the treatment of patients with de novo native coronary artery lesions: the SPIRIT II trial. *Circ Cardiovasc Interv.* 2009;2:339-47.

21. Garg S, Serruys P, Onuma Y, Dorange C, Veldhof S, Miquel-Hebert K, Sudhir K, Boland J, Huber K, Garcia E, te Riele JA; SPIRIT II Investigators. 3-year clinical follow-up of the XIENCE V everolimus-eluting coronary stent system in the treatment of patients with de novo coronary artery lesions: the SPIRIT II trial (Clinical Evaluation of the Xience V Everolimus Eluting Coronary Stent System in the Treatment of Patients with de novo Native Coronary Artery Lesions). *JACC Cardiovasc Interv.* 2009;2:1190-8.

22. Ruygrok PN, Desaga M, Van Den Branden F, Rasmussen K, Suryapranata H, Dorange C, Veldhof S, Serruys PW. One year clinical follow-up of the XIENCE V Everolimus-eluting stent system in the treatment of patients with de novo native coronary artery lesions: the SPIRIT II study. *EuroIntervention.* 2007;3:315-20.

23. Wakabayashi K, Mintz G, Delhaye C, Choi YJ, Doh JH, Ben-Dor I, Gaglia M Jr, Pakala R, Suddath W, Satler L, Kent K, Pichard A, Weissman N, Waksman R. In vivo virtual histology intravascular ultrasound comparison of neointimal hyperplasia within drug-eluting versus bare metal stents. *J Invasive Cardiol.* 2011;23:262-8.

24. Nasu K, Tsuchikane E, Katoh O, Vince DG, Margolis PM, Virmani R, Surmely JF, Ehara M, Kinoshita Y, Fujita H, Kimura M, Asakura K, Asakura Y, Matsubara T, Terashima M, Suzuki T. Impact of intramural thrombus in coronary arteries on the accuracy of tissue characterization by in vivo intravascular ultrasound radiofrequency data analysis. *Am J Cardiol.* 2008;101:1079-83.

25. Gonzalo N, Serruys PW, Okamura T, van Beusekom HM, Garcia-Garcia HM, van Soest G, van der Giessen W, Regar E. Optical coherence tomography patterns of stent restenosis. *Am Heart J.* 2009;158:284-93.

Chapter 3

Validation and application of bifurcation algorithm

3.1 Dedicated bifurcation Quantitative Coronary Angiography (QCA) software

The need for dedicated bifurcation Quantitative Coronary Angiography (QCA) software algorithms to evaluate bifurcation lesions.

EuroIntervention. 2015 May;11 Suppl V:V44-9.
[Review paper, IF 3.76]

Grundeken MJ, **Ishibashi Y**, Ramcharitar S, Tuinenburg JC, Reiber JH, Tu S, Girasis C, Wentzel JJ, Onuma Y, Serruys PW.

The need for dedicated bifurcation quantitative coronary angiography (QCA) software algorithms to evaluate bifurcation lesions

Maik J. Grundeken[1], MD; Yuki Ishibashi[2], MD, PhD; Steve Ramcharitar[3], MD, PhD; Joan C. Tuinenburg[4,5], MSc; Johan H.C. Reiber[4,5], PhD; Shengxian Tu[5,6], PhD; Jean-Paul Aben[7], BSc; Chrysafios Girasis[8], MD, PhD; Joanna J. Wykrzykowska[1], MD, PhD; Yoshinobu Onuma[2], MD, PhD; Patrick W. Serruys[9]*, MD, PhD

1. Academic Medical Center, Amsterdam, The Netherlands; 2. Thoraxcenter, Erasmus Medical Center, Rotterdam, The Netherlands; 3. Wiltshire Cardiac Centre, Swindon, United Kingdom; 4. Medis medical imaging systems bv, Leiden, The Netherlands; 5. Division of Image Processing, Department of Radiology, Leiden University Medical Center, Leiden, The Netherlands; 6. Biomedical Instrument Institute, School of Biomedical Engineering, Shanghai Jiao Tong University, Shanghai, China; 7. Pie Medical Imaging BV, Maastricht, The Netherlands; 8. Onassis Cardiac Surgery Center, Athens, Greece; 9. International Centre for Circulatory Health, NHLI, Imperial College London, London, United Kingdom

The complete references and the accompanying supplementary data are published online at: http://www.pcronline.com/eurointervention/V_issue/10

KEYWORDS

- bifurcation lesions
- bifurcation QCA software
- bifurcation stenting
- quantitative coronary angiography (QCA)
- single-vessel QCA software

Abstract

Single-vessel quantitative coronary angiography (QCA) software is inaccurate when used in bifurcation lesions due to the specific anatomical characteristics of bifurcations, including the natural step-down in diameters after every bifurcation. Dedicated bifurcation QCA software has been developed to overcome the limitations of single-vessel QCA in bifurcations. A phantom validation study has shown the superior accuracy of these bifurcation QCA algorithms compared to the single-vessel QCA software. These QCA software algorithms are currently highly recommended to assess bifurcation lesions.

**Corresponding author: International Centre for Circulatory Health, NHLI, Imperial College London, South Kensington Campus, London, SW7 2AZ, United Kingdom. E-mail: patrick.w.j.c.serruys@gmail.com*

Introduction

Visual estimation of stenosis on coronary angiography has been regarded as unreliable due to a marked intraobserver and interobserver variability[1,2]. Therefore, quantitative coronary angiography (QCA) software was developed to provide an objective, accurate and reproducible quantification of coronary lesions[3,4]. Parameters derived from QCA have subsequently been used as surrogate endpoints in randomised clinical trials evaluating the efficacy of new stent technologies and the effect of new pharmaceutical agents on coronary artery disease progression/regression[5-7]. As described in detail elsewhere in this Bifurcation Supplement[8], the human coronary vasculature tree is subject to fractal geometry. As a result, there is a natural step-down in vessel diameter after every bifurcation. In this review we will outline why this natural step-down phenomenon results in inaccurate QCA measurements when conventional single-vessel QCA software is used and why dedicated bifurcation QCA software algorithms are essential to provide accurate measurements.

Challenges in QCA of bifurcation lesions: why conventional single-vessel algorithms are inaccurate in bifurcations

When conventional single-vessel software is used in bifurcation lesions, two analyses should be performed: one from the proximal main branch to the distal main branch **(Figure 1A)**, and the other from the proximal main branch to the side branch **(Figure 1B)** (or alternatively by starting from the side branch ostium, **Figure 1C**). In 2009, it was already acknowledged that the use of conventional single-vessel software was inaccurate to assess bifurcation lesions for several reasons which we will address here[9].

Why is the use of single-vessel software so problematic? First and foremost, because it completely ignores the natural anatomy of the bifurcation. In the bifurcation core or the so-called polygon of confluence (POC), single-vessel algorithms detect non-existing vessel contours crossing the bifurcation, something which frequently requires manual corrections, which by definition are arbitrary and introduce bias **(Online Figure 1)**. Even more problematic is that it sometimes even creates what we call "pseudo-stenoses", in which the minimal lumen diameter (MLD) is incorrectly located at the site of the side branch ostium in the middle of the POC, instead of locating the MLD at the true MLD site **(Figure 2)**.

Another challenge in QCA of bifurcations is to assess an accurate reference diameter (RefD) to calculate the percent diameter stenosis (%DS). If the single-vessel algorithm is applied to a bifurcation lesion, this will lead to an inaccurate RefD due to the natural differences in diameters proximal and distal to the bifurcation, which is most pronounced at the side branch ostium[10]. The so-called interpolated RefD will be estimated as too large in the ostia of the distal branches because of the larger proximal diameters (compare interpolated RefD lines in **Figure 2B** and **Figure 2C**). Vice versa, the reference diameter of the distal part of the proximal main branch will be underestimated, due to the influence of the smaller distal branch on the interpolated RefD (again, compare interpolated RefD lines in **Figures 2B** and **Figure 2C**). Alternatively, a single reference point could be chosen for each segment (i.e., one proximal for the proximal main branch segment, one distal in the side branch for the side branch segment, and one distal in the main branch for the distal main branch segment). However, choosing such reference points is arbitrary and therefore not reproducible. Furthermore, it is conceivable that a RefD based on a single point is less accurate than when the RefD is based on the complete segment.

Another problem with the use of a single-vessel algorithm in bifurcation lesions is the need for manual segment selection. Because the conventional software does not recognise where the proximal branch stops and the distal main branch or side branch begins, this needs to be indicated by the analyst, which introduces another bias and it will therefore be very challenging to indicate exactly the same segments pre-procedure, post-procedure and at follow-up. This is particularly true because the stenoses are located in close proximity to the ostium of the distal branch in most cases.

Dedicated bifurcation QCA software packages

To overcome the above-mentioned shortcomings of single-vessel software, dedicated bifurcation QCA algorithms were developed. Two different QCA software packages are currently available and will be described in detail below.

CAAS (PIE MEDICAL IMAGING)

The Cardiovascular Angiography Analysis System (CAAS; Pie Medical Imaging BV, Maastricht, The Netherlands) bifurcation QCA software has been validated against a precision-manufactured bifurcation phantom model[10-13]. In the CAAS bifurcation QCA

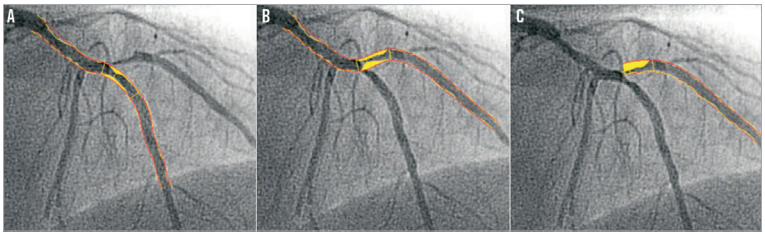

Figure 1. *The use of single-vessel quantitative coronary angiography (QCA) software in a bifurcation. When using single-vessel QCA software, one analysis is performed of the main branch (A), and one of the side branch, starting in the proximal main branch (B) or side branch ostium (C).*

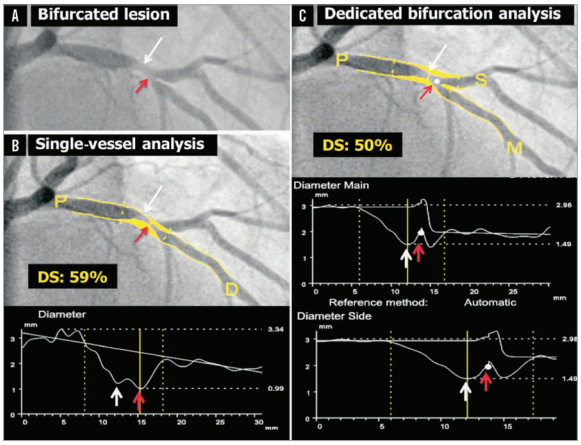

Figure 2. *Quantitative coronary angiography of a bifurcation lesion using single-vessel or bifurcation software. Panel A shows a bifurcation lesion. Panel B shows quantitative coronary angiography (QCA) analysis of this bifurcation lesion using single-vessel software creating a "pseudo-stenosis" (red arrow). Panel C shows QCA analysis of the same bifurcation lesion using the bifurcation software. In all panels, the white arrow indicates the true location of the MLD of the proximal main branch, the red arrow the pseudo-stenosis found with single-vessel QCA at the actual location of the point of bifurcation (white dot in C).*

software, the analysis is initialised by three user-defined points: one indicating the proximal boundary of the main branch and two indicating the distal boundaries of the two daughter branches **(Figure 3A)**. Next, the algorithm automatically detects the contours using the "minimal cost algorithm", a mathematical modelling process based on the differences in the local greyscale and video densitometry **(Figure 3B)**[12,14]. If this modelling system erroneously detects a contour outside the vessel, the contour can be corrected either by drawing the contour manually or by using the "restriction function", excluding an area from the automatic contour detection. The two-dimensional dedicated bifurcation algorithm assumes the bifurcation as a single object with a left, middle and right contour, without making any further assumptions. The "point of bifurcation" (POB) is then defined as the mid-point of the largest possible circle touching all three (i.e., left, middle and right) contours, and is the point where all three centrelines (i.e., the lines through the middle of the vessel) from the proximal main branch, distal main branch and side branch meet **(Figure 3C)**. The intersections of the circle with the centrelines indicate the boundaries of the POC **(Figure 3D, Figure 3E)**. The diameter values are obtained differently inside the POC from those in straight segments outside the POC. Outside the POC, diameters are determined by the shortest distance between the vessel's outer borders, as in the conventional straight-vessel QCA algorithm. Within the POC, however, another mathematical algorithm, the so-called "minimum freedom" approach, is used. This approach uses the shortest distances from a centreline point to the vessel contours. The distance between these two points on the vessel contours is defined as the diameter of the centreline point and hence the true diameter at the bifurcation **(Figure 3F, Moving image 1)**. The RefD outside the POC is determined from the "healthy" (non-stenotic) part of the branch. Within the POC, the RefD is based on a curvature-based interpolation technique, assuming smooth blood flow from the proximal main branch to the distal branches, the curvature being constant at the POC **(Online Figure 2)**.

QANGIO XA (MEDIS MEDICAL IMAGING SYSTEMS)

Some of the first basic steps are essentially the same for the QAngio® XA bifurcation software (Medis medical imaging systems bv, Leiden, The Netherlands) as for the CAAS bifurcation software described above[15,16]. First, the analyst defines the segment of analysis by indicating one proximal start point and an endpoint in each of the distal branches. Then, two wavepath centrelines from proximal to distal are detected. These can be semi-automatically (by providing an additional support point) or manually corrected if necessary **(Online Figure 3B)**. Subsequently, the vessel contour is automatically detected using the minimal cost algorithm **(Online Figure 3C)**. If the vessel contour erroneously detects a contour outside the vessel, the contour can be either semi-automatically corrected (by indicating a support point manually on the vessel edge) or manually corrected by re-drawing the contour by hand. Although the steps above are more or less similar between CAAS and QAngio XA, there is a difference between the two software packages with regard to the anatomic points which are used to define the bifurcation and its measurements. Unlike CAAS using the POB as the cornerstone for its subsequent analyses, QAngio XA uses the carina point on the middle contour as well. This carina point can be manually edited

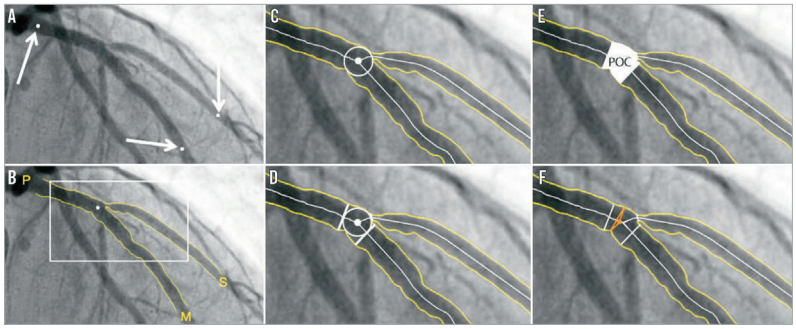

Figure 3. *CAAS bifurcation software (Pie Medical). In the CAAS bifurcation QCA software, the segment of analysis is indicated by one proximal and two distal delimiter points (white arrows, A). After automatic detection of the contours (B), the "point of bifurcation" (POB) is defined as the mid-point of the largest possible circle touching all three contours (C). The intersections of the circle with the centrelines (D) indicate the boundaries of the POC (E). The diameter values within the POC are determined by the "minimum freedom" approach (F).*

by dragging this point to the correct position, if found to be more appropriate by the analyst. Hereafter, the middle contour detection procedure is executed again, based on the available image information and new carina point, which serves as a support point. Besides that, the position of the "proximal delimiter" of the bifurcation core is automatically determined. This proximal delimiter and the carinal point are important landmarks for the software algorithm to define the four "building blocks" of the bifurcation analysis model (proximal main branch, bifurcation core, distal main branch and side branch). QAngio XA has two different bifurcation models. As recommended by the company, the T-shape model should be used in the vast majority (probably ~>90%) of bifurcation lesions and is selected as default setting in the current version of the QAngio XA software. Alternatively, the Y-shape model can be used. Use of the Y-shape model is recommended by the company only in specific anatomical subsets (e.g., in cases with equally sized distal branches and/or a narrow distal bifurcation angle), or when evaluating specific treatment approaches (skirt stenting for example).

In the T-shape model, the bifurcation core is defined as the area in-between the proximal delimiter, the first diameter of the distal main branch and by a virtual contour between the proximal and distal main branch segments **(Figure 4A)**. The virtual contour separates the main branch from the side branch, creating two sections: 1) the main branch section consisting of the proximal main branch, bifurcation core and distal main branch **(Figure 4B, Figure 4C)**; and 2) the side branch section starting at the virtual contour, continuing into the side branch **(Figure 4B, Figure 4D)**. The diameter function is calculated using Medis straight vessel algorithms for the entire main branch section, whereas an adjusted Medis ostial algorithm is used for the side branch section, reconstructing a proximal flare to correspond to the "mouth" of the ostium[17,18]. The bifurcation core is excluded when calculating the RefD function, which is calculated for the proximal main branch segment, distal main branch segment, and side branch section separately. Within the bifurcation core, the interpolated reference diameters are determined linearly by means of a straight RefD function (corresponding to the virtual contour of the bifurcation core) **(Figure 4A, Figure 4C)**.

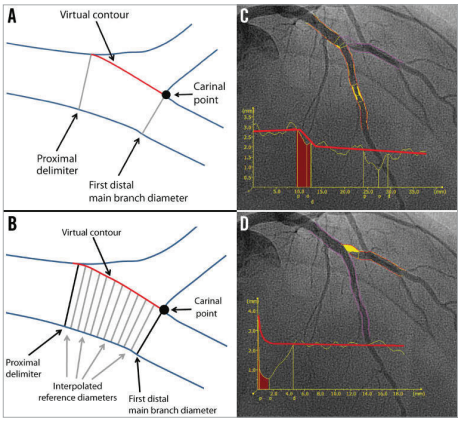

Figure 4. *T-shape model of the QAngio XA bifurcation QCA software. A) The anatomic landmarks used to define the four "building blocks" of the bifurcation analysis model: the proximal delimiter, the first diameter of the distal main branch, the virtual contour between the proximal and distal main branch segments, and the carinal point. B) The interpolated reference diameter (virtual contour) of the bifurcation core, which is determined linearly by means of a straight reference diameter function. C) The QCA (including the diameter function) of the combined main branch, with a separate diameter function for each building block. D) QCA of the side branch, including the diameter function using the adjusted Medis ostial algorithm.*

In the Y-shape model, the bifurcation core is defined as the area between the proximal delimiter and the carinal point **(Figure 5A)**. Three different segments are analysed in the Y-shape model: 1) the proximal section from the proximal boundary to the carina point; 2) the "distal 1" section from the first distal 1 diameter to the distal 1 boundary; and 3) the "distal 2" section from the first distal 2 diameter to the distal 2 boundary. The interpolated RefD functions of the three segments (proximal, distal 1 and distal 2) outside the bifurcation core are derived by an iterative regression technique[17]. The RefD function of the bifurcation core itself is based on two interpolated reference contours (spline-based)[18]. The graph of the RefD function of the proximal main branch displays the combined function of the proximal main branch and the bifurcation core, up to the carinal point. This combined function is straight for the proximal segment and curved in the bifurcation core **(Figure 5B)**. The RefD functions of the distal sections are straight and displayed as one function **(Figure 5C, Figure 5D)**.

Comparison of single-vessel software with dedicated bifurcation QCA software algorithms in a bifurcation phantom

To assess the inaccuracy of the single-vessel software in bifurcation lesions objectively, and to validate both QAngio XA and CAAS bifurcation software algorithms, a phantom validation study was performed by our group. For this analysis, six precision phantoms with a total of 18 bifurcations made from Plexiglas with a tolerance <10 µm were used[13]. The 18 bifurcations were analysed three times: 1) with the conventional single-vessel algorithm of CAAS (version 5.10); 2) with the bifurcation algorithm of CAAS (version 5.10); and 3) with the bifurcation algorithm of QAngio XA (version 7.3) **(Online Figure 4)**[10]. The single-vessel analysis was performed from the proximal main branch to the distal main branch and from the proximal main branch to the side branch[10].

We found that conventional single-vessel analysis underestimated the RefD and %DS in the proximal main branch, whilst these parameters were overestimated in the distal main branch and side branch (case example in **Online Figure 4**). Overall, combining all three segments of the 18 bifurcations (54 segments), the accuracy and precision with single-vessel software was very poor with regard to the RefD (-0.108±0.352 mm) and %DS (5.69±11.28%)[10]. The bifurcation algorithms on the other hand proved to be highly accurate and precise, with comparable accuracy and precision between the CAAS and QAngio XA (with systematic use of the T-shape model) bifurcation software models with regard to MLD (0.012±0.103 vs. 0.012±0.093 mm, p=0.104), RefD (0.050±0.043 vs. –0.045±0.064 mm, p=0.106), and %DS (0.94±4.07 vs. 0.74±3.81%, p=0.121) **(Figure 6)**.

Why is this important?

The most important conclusion from the study above is that the conventional single-vessel QCA method is inaccurate in bifurcation lesions and that both CAAS and QAngio XA (when systematically using the T-shape model) bifurcation algorithms are highly accurate and precise in bifurcation lesions. But why is this so important? Overestimation of the %DS of the distal main and side branch by single-vessel analysis may potentially have clinical implications. We are already aware that ostial side branch stenosis severity is overestimated with visual estimation[19]. However, the side branch stenosis will also be overestimated when single-vessel QCA analysis is used pre-procedure, which may lead to the overtreatment of insignificant stenosis (e.g., treatment of side branch without significant stenosis).

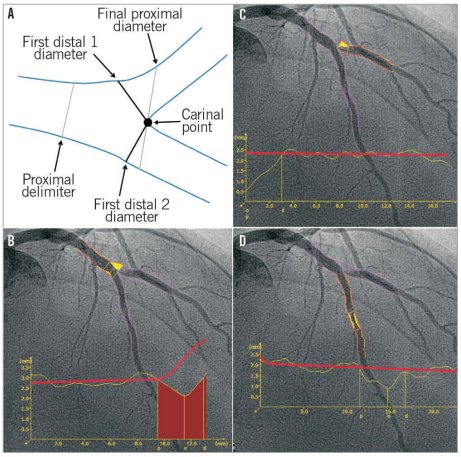

Figure 5. *Y-shape model of the QAngio XA software. A) The anatomic landmarks used to define the four building blocks of the bifurcation analysis. B) The QCA of the proximal section, consisting of the proximal segment (up to the proximal delimiter) and the bifurcation core. C) & D) The QCA and reference vessel diameter functions of the distal 1 and distal 2 branches. Note that the reference diameter functions of the distal sections are straight and displayed as one function.*

Besides clinical implications, use of single-vessel QCA may also have implications in clinical trials. The major randomised trials comparing single stenting with systematic double stenting have used the single-vessel analysis **(Online Table 1)**[20-22]. Inclusion of lesions based on the single-vessel analysis may result in biased selection of target lesions, with an overestimation of "true" bifurcation rates (i.e., Medina 0,1,1; 1,0,1; or 1,1,1)[9]. Furthermore, single-vessel software use in bifurcation trials **(Online Table 1)** or first-in-man/registry studies on dedicated bifurcation stents **(Online Table 2)** with planned repeat angiography will lead to less accurate results of the side branch. A recent example was the Tryton IDE trial showing different QCA outcomes with dedicated bifurcation QCA from those with single-vessel QCA[23,24]. Furthermore, as defined by the Academic Research Consortium[25], justification of target lesion revascularisation (TLR) (i.e., "ischaemia-driven" vs. "non-ischaemia-driven" TLR) is based on %DS assessed by

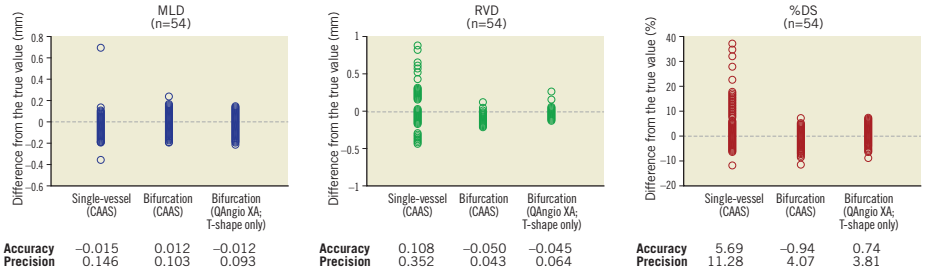

Figure 6. *Accuracy and precision of single-vessel QCA software and bifurcation QCA software in all phantom bifurcation segments (n=54). Differences between the measured values (MLD, RVD and %DS) and the true phantom values for all 54 segments (18 bifurcations) for the single-vessel analysis (CAAS), bifurcation analysis using CAAS, and bifurcation analysis using QAngio XA (T-shape only). The accuracy was defined as the mean difference from the true value, and precision was defined as the standard deviation of the mean difference.*

QCA. The use of single-vessel software in such trials may therefore lead to an increased rate of ischaemia-driven target TLR of the side branch.

European Bifurcation Club recommendations in reporting QCA

The European Bifurcation Club (EBC) recommends reporting the QCA results according to the three segments of the bifurcation (i.e., proximal main, distal main, and side branch)[9,26]. Binary restenosis is best reported as QCA-based Medina scores at every time point (i.e., pre-procedure, post-procedure and follow-up). One of the advantages of such per-segment reporting is that the healing pattern of the bifurcation treatment can be better understood (i.e., more complex restenosis patterns including main and side branch vs. relatively simple restenosis patterns including main branch only). Another important issue is that the MLD can be relocated from one segment to another. When using single-vessel software, the post-procedural MLD might, for example, be located in the (non-stenotic) distal main branch, whilst at follow-up the MLD might be (re-)located in the (stenotic) proximal main branches. Especially when there is a large difference in reference diameters between the proximal and distal main branch, the late lumen loss (LLL) value calculated from these two MLD values might be artificially low. When the LLL is calculated for the three segments separately, the LLL value is probably more accurate in representing the restenotic effect in a particular segment.

Conclusions

Conventional single-vessel QCA software is inaccurate in bifurcation lesions because it completely ignores the natural anatomy of the bifurcation, including the natural "step-down" in diameters after each bifurcation. Dedicated bifurcation software algorithms have been developed: currently, two different software packages are commercially available (CAAS and QAngio XA). The two software packages use slightly different approaches, but both have proven to be highly accurate when validated against precision-manufactured bifurcation phantoms.

Conflict of interest statement

J. Tuinenburg is employed by Medis medical imaging systems bv. J. Reiber is the CEO of Medis medical imaging systems bv. J-P. Aben is employed by Pie Medical Imaging BV. P. Serruys is chairman of the Tryton IDE trial. S. Tu had an employment contract with Medis until June 2014. The other authors have no conflicts of interest to declare.

References

The references can be found in the online version of the paper.

Online data supplement

Online Table 1. Angiographic endpoints and QCA algorithms used in randomised studies, multicentre studies or ongoing studies.

Online Table 2. Angiographic endpoints and QCA algorithms used in first-in-man studies or registries assessing dedicated bifurcation stents.

Online Figure 1. Single-vessel QCA creating a virtual contour crossing the side branch ostium.

Online Figure 2. Curvature-based interpolation technique of CAAS bifurcation software.

Online Figure 3. Introduction steps of QAngio XA bifurcation software.

Online Figure 4. Example of a representative QCA analysis on the bifurcation phantom model.

Moving image 1. "Minimum freedom" approach to determine the diameter function in the polygon of confluence.

Online data supplement

References

1. Zir LM, Miller SW, Dinsmore RE, Gilbert JP, Harthorne JW. Interobserver variability in coronary angiography. *Circulation.* 1976;53:627-32.

2. Galbraith JE, Murphy ML, de Soyza N. Coronary angiogram interpretation. Interobserver variability. *JAMA.* 1978;240:2053-6.

3. Serruys PW, Reiber JH, Wijns W, van den Brand M, Kooijman CJ, ten Katen HJ, Hugenholtz PG. Assessment of percutaneous transluminal coronary angioplasty by quantitative coronary angiography: diameter versus densitometric area measurements. *Am J Cardiol.* 1984;54:482-8.

4. Reiber JH, Serruys PW, Kooijman CJ, Wijns W, Slager CJ, Gerbrands JJ, Schuurbiers JC, den Boer A, Hugenholtz PG. Assessment of short-, medium-, and long-term variations in arterial dimensions from computer-assisted quantitation of coronary cineangiograms. *Circulation.* 1985;71:280-8.

5. Garg S, Serruys PW. Coronary stents: current status. *J Am Coll Cardiol.* 2010;56 (10 Suppl):S43-78.

6. Lichtlen PR, Hugenholtz PG, Rafflenbeul W, Hecker H, Jost S, Deckers JW. Retardation of angiographic progression of coronary artery disease by nifedipine. Results of the International Nifedipine Trial on Antiatherosclerotic Therapy (INTACT). INTACT Group Investigators. *Lancet.* 1990;335:1109-13.

7. de Feyter PJ, Vos J, Deckers JW. Progression and regression of the atherosclerotic plaque. *Eur Heart J.* 1995;16 Suppl I:26-30.

8. Kassab GS, Finet G. Anatomy and function relation in the coronary tree: from bifurcations to myocardial flow and mass. *EuroIntervention.* 2015;11 Suppl V:V13-7.

9. Lansky A, Tuinenburg J, Costa M, Maeng M, Koning G, Popma J, Cristea E, Gavit L, Costa R, Rares A, Van Es GA, Lefevre T, Reiber H, Louvard Y, Morice MC; European Bifurcation Angiographic Sub-Committee. Quantitative angiographic methods for bifurcation lesions: a consensus statement from the European Bifurcation Group. *Catheter Cardiovasc Interv.* 2009; 73:258-66.

10. Ishibashi Y, Grundeken MJ, Nakatani S, Iqbal J, Morel MA, Genereux P, Girasis C, Wentzel JJ, Garcia-Garcia HM, Onuma Y, Serruys PW. In vitro validation and comparison of different software packages or algorithms for coronary bifurcation analysis using calibrated phantoms: implications for clinical practice and research of bifurcation stenting. *Catheter Cardiovasc Interv.* 2015;85:554-63.

11. Girasis C, Schuurbiers JC, Onuma Y, Aben JP, Weijers B, Boersma E, Wentzel JJ, Serruys PW. Two-dimensional quantitative coronary angiographic models for bifurcation segmental analysis: in vitro validation of CAAS against precision manufactured plexiglas phantoms. *Catheter Cardiovasc Interv.* 2011;77:830-9.

12. Girasis C, Schuurbiers JC, Onuma Y, Aben JP, Weijers B, Morel MA, Wentzel JJ, Serruys PW. Advances in two-dimensional quantitative coronary angiographic assessment of bifurcation lesions: improved small lumen diameter detection and automatic reference vessel diameter derivation. *EuroIntervention.* 2012;7: 1326-35.

13. Girasis C, Schuurbiers JC, Onuma Y, Serruys PW, Wentzel JJ. Novel bifurcation phantoms for validation of quantitative coronary angiography algorithms. *Catheter Cardiovasc Interv.* 2011;77: 790-7.

14. Ramcharitar S, Onuma Y, Aben JP, Consten C, Weijers B, Morel MA, Serruys PW. A novel dedicated quantitative coronary analysis methodology for bifurcation lesions. *EuroIntervention.* 2008;3:553-7.

15. Tuinenburg JC, Janssen JP, Kooistra R, Koning G, Corral MD, Lansky AJ, Reiber JH. Clinical validation of the new T- and Y-shape models for the quantitative analysis of coronary bifurcations: an interobserver variability study. *Catheter Cardiovasc Interv.* 2013; 81:E225-36.

16. Tuinenburg JC, Koning G, Rares A, Janssen JP, Lansky AJ, Reiber JH. Dedicated bifurcation analysis: basic principles. *Int J Cardiovasc Imaging.* 2011;27:167-74.

17. Reiber JHC, Tuinenburg JC, Koning G, Janssen JP, Rares A, Lansky AJ, Goedhart B. Chapter 2.2: Quantitative coronary arteriography. In: Oudkerk M, Reiser MF, editors. Coronary Radiology, 2nd Revised ed., Series: Medical Radiology, Subseries: Diagnostic Imaging. Berlin-Heidelberg; Springer-Verlag; 2009.

18. Janssen JP, Rares A, Tuinenburg JC, Koning G, Lansky AJ, Reiber JH. New approaches for the assessment of vessel sizes in quantitative (cardio-)vascular X-ray analysis. *Int J Cardiovasc Imaging.* 2010;26:259-71.

19. Girasis C, Onuma Y, Schuurbiers JC, Morel MA, van Es GA, van Geuns RJ, Wentzel JJ, Serruys PW; 5th meeting of the European Bifurcation Club. Validity and variability in visual assessment of stenosis severity in phantom bifurcation lesions: a survey in experts during the fifth meeting of the European Bifurcation Club. *Catheter Cardiovasc Interv.* 2012;79:361-8.

20. Colombo A, Bramucci E, Sacca S, Violini R, Lettieri C, Zanini R, Sheiban I, Paloscia L, Grube E, Schofer J, Bolognese L, Orlandi M, Niccoli G, Latib A, Airoldi F. Randomized study of the crush technique versus provisional side-branch stenting in true coronary bifurcations: the CACTUS (Coronary Bifurcations: Application of the Crushing Technique Using Sirolimus-Eluting Stents) Study. *Circulation.* 2009;119:71-8.

21. Hildick-Smith D, de Belder AJ, Cooter N, Curzen NP, Clayton TC, Oldroyd KG, Bennett L, Holmberg S, Cotton JM, Glennon PE, Thomas MR, Maccarthy PA, Baumbach A, Mulvihill NT, Henderson RA, Redwood SR, Starkey IR, Stables RH. Randomized trial of simple versus complex drug-eluting stenting for bifurcation lesions: the British Bifurcation Coronary Study: old, new, and evolving strategies. *Circulation.* 2010;121:1235-43.

22. Korn HV, Yu J, Ohlow MA, Huegl B, Schulte W, Wagner A, Wassmer G, Gruene S, Petek O, Lauer B. Interventional therapy of bifurcation lesions: a TIMI flow-guided concept to treat side branches in bifurcation lesions--a prospective randomized clinical study (Thueringer bifurcation study, THUEBIS study as pilot trial). *Circ Cardiovasc Interv.* 2009;2:535-42.

23. Grundeken M, Ishibashi Y, Généreux P, LaSalle L, Iqbal J, Wykrzykowska JJ, Morel MA, Tijssen JG, de Winter RJ, Girasis C, Garcia-Garcia HM, Onuma Y, Leon MB, Serruys PW. Inter-core lab variability in analyzing quantitative coronary angiography for bifurcation lesions: a post-hoc analysis of a randomized trial. *JACC Cardiovasc Interv.* 2015;8:305-14.

24. Généreux P, Kumsars I, Lesiak M, Kini A, Fontos G, Slagboom T, Ungi I, Metzger C, Wykrzykowska JJ, Stella PR, Bartorelli AL, Fearon WF, Lefèvre T, Feldman RL, LaSalle L, Francese DP, Onuma Y, Grundeken MJ, Garcia-Garcia HM, Laak LL, Cutlip DE, Kaplan AV, Serruys PW, Leon MB. A randomized trial of a dedicated bifurcation stent versus provisional stenting in the treatment of coronary bifurcation lesions. *J Am Coll Cardiol.* 2015;65:533-43.

25. Cutlip DE, Chauhan MS, Baim DS, Ho KK, Popma JJ, Carrozza JP, Cohen DJ, Kuntz RE. Clinical restenosis after coronary stenting: perspectives from multicenter clinical trials. *J Am Coll Cardiol.* 2002;40:2082-9.

26. Lassen JF, Holm NR, Stankovic G, Lefevre T, Chieffo A, Hildick-Smith D, Pan M, Darremont O, Albiero R, Ferenc M, Louvard Y. Percutaneous coronary intervention for coronary bifurcation disease: consensus from the first 10 years of the European Bifurcation Club meetings. *EuroIntervention.* 2014;10:545-60.

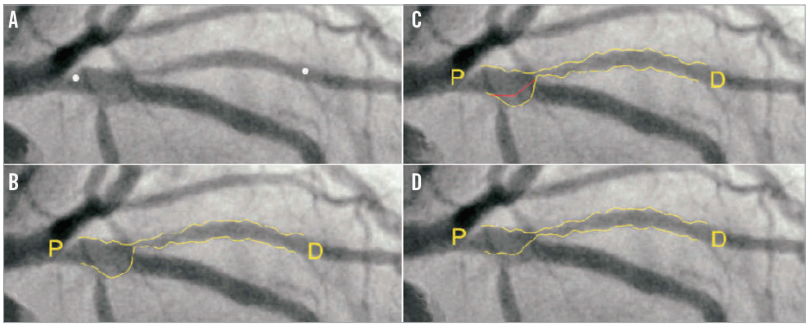

Online Figure 1. *Single-vessel QCA creating a virtual contour crossing the side branch ostium. After indicating the proximal and distal boundaries of the region of interest (white dots) in a left anterior descending-first diagonal bifurcation lesion (A), the vessel contour was detected automatically by the bifurcation software (B). Note that, in the so-called polygon of confluence (POC), the software detected the ostium of a septal side branch as vessel contour. In this case, this was corrected by re-drawing the contour manually, which seems to be arbitrary (C). D) The final vessel contour of the QCA.*

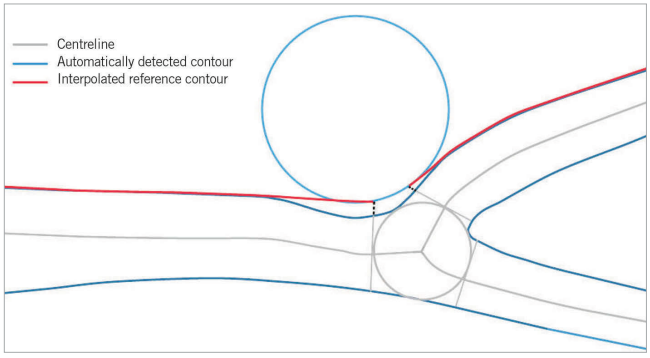

Online Figure 2. *Curvature-based interpolation technique of CAAS bifurcation software.*

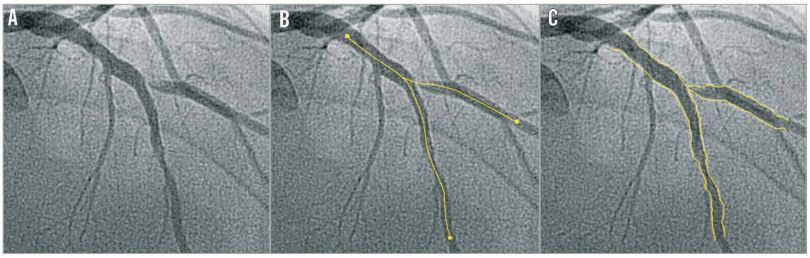

Online Figure 3. *Introduction steps of QAngio XA bifurcation software. A) A left anterior descending artery-diagonal branch bifurcation lesion. First, the analyst defines the segment of analysis by indicating one proximal start point and an endpoint in each of the distal branches, after which two wavepath centrelines from proximal to distal are detected (note that the proximal parts overlap) (B). Subsequently, the vessel contour is automatically detected using the minimal cost algorithm (C).*

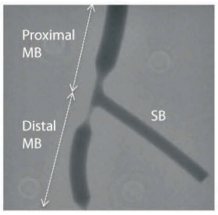

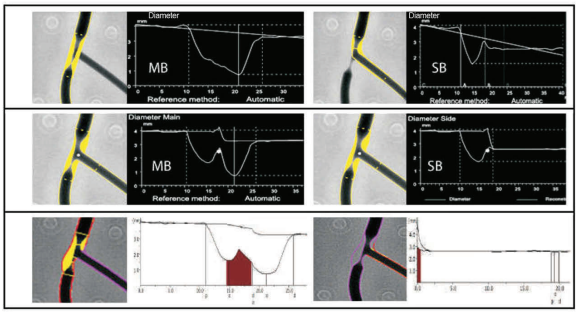

A: Single-vessel analysis by CAAS
B: Bifurcation analysis by CAAS
C: Bifurcation analysis by QAngio XA (T-shape)

Segment - analysis	Phantom values	A: Single-vessel software	B: Bifurcation analysis by CAAS	C: Bifurcation analysis by QAngio XA (T-shape)
Proximal MB-MLD (mm)	**1.59**	**1.41**	1.66	1.59
Proximal MB-DS (%)	**60.30**	55.00	57.54	59.10
Proximal MB-RVD (mm)	**4.00**	**3.62**	4.02	3.88
Distal MB-MLD (mm)	**0.66**	0.74	0.71	0.75
Distal MB-DS (%)	**80.00**	80.00	78.33	77.00
Distal MB-RVD (mm)	**3.30**	**3.51**	3.25	3.24
SB-MLD (mm)	**2.60**	2.53	2.55	2.54
SB-DS (%)	**0.00**	**23.00**	1.16	2.11
SB-RVD (mm)	**2.60**	**3.29**	2.58	2.59

Online Figure 4. *Example of a representative QCA analysis on the bifurcation phantom model. Example of a representative QCA analysis on one of the phantom bifurcations using single-vessel software (A) and dedicated bifurcation software (B & C). Note that, in this particular case, the single-vessel software underestimates the reference vessel diameter in the proximal main branch, while it overestimates the reference vessel diameter in the distal main branch and side branch. Furthermore, the MLD in the proximal main branch is inaccurate.*

Online Table 1. Angiographic endpoints and QCA algorithms used in randomised studies, multicentre studies or ongoing studies.

	Year	No. patients	Primary endpoint	Planned repeat angiography, Yes or No	Angiographic endpoint	QCA software	Algorithm	Randomisation
Prior to introduction of bifurcation software								
Colombo et al	2004	85	Angiographic restenosis (either branch) 6 months	Yes	Binary in-segment restenosis of both the MB and SB at 6 months	QCA-CMS 5.1	Single	Provisional vs. systematic (crush, T, culotte)
Pan et al	2004	91	Composite of cardiac death, MI, and the need for TVR at 6 months	Yes	Angiographic restenosis (either branch) 6 months	CAAS II 4.1.1	Single	Provisional vs. systematic (T)
Introduction of bifurcation software								
NORDIC	2006	413	Death, MI (non-procedural), TVR, or stent thrombosis at 6 months	Yes	Significant restenosis (50% diameter stenosis) of the MV and/or occlusion of the SB	QAngio XA 7.0	Bifurcation	Provisional vs. systematic (crush, culotte, T)
Ferenc et al	2008	202	Angiographic restenosis of the SB at 9 months	Yes	In-segment percent diameter stenosis of the SB at 9 months	QAngio XA 7.0	Bifurcation	Provisional vs. systematic (T)
NORDIC 2	2009	424	Death, MI (non-procedural), TVR, or stent thrombosis at 6 months	Yes	In-segment and in-stent restenosis of MV and/or SB after 8 months	QAngio XA 7.0	Bifurcation	Systematic (crush vs. culotte)
The DIVERGE	2009	302	Composite of death, MI, and TLR at 9 months	Yes	Binary angiographic restenosis at 9 months	QAngioXA 7.1	Bifurcation	No, a prospective multicentre registry (Axxess stent)
DKCRUSH-II	2009	370	Cardiac death, MI, or TVR at 12 months	Yes	Restenosis in the MV and SB at 8 months	CAAS 5.7	Bifurcation	Double kissing crush versus provisional stenting technique for treatment of coronary bifurcation lesions
CACTUS	2009	350	Death, MI, TVR at 6 months	Yes	In-segment restenosis rate at 6 months	QCA-CMS	Single	Provisional vs. systematic crush
Thueringer Bifurcation Study	2009	110	Death, MI, stent thrombosis, CABG, or TLR at 6 months	Yes	Restenosis in the MV and SB at 6 months	Quantcor QCA V2.0	Single	Stenting of the MB (TAXUS stent) and mandatory SB PCI kissing balloons with provisional SB stenting, or stenting of the MB (paclitaxel-eluting stents) with provisional SB-PCI only when the SB had a TIMI flow 2
BBC ONE	2010	500	All-cause death, MI, TVF at 9 months	No	No	Not described	Single	Provisional vs. systematic (crush, culotte)
NORDIC 3	2011	477	Cardiac death, non-procedure-related index lesion MI, stent thrombosis, or TLR by PCI or CABG within 6 months	Yes	In-segment and in-stent restenosis (50% diameter stenosis) of the MV and/or SB at 8 months	QAngio XA 7.2	Bifurcation	Final kissing balloon dilatation versus no final kissing balloon dilatation
TRYTON trial	2013	704	Cardiac death, MI, or TVR at 9 months	Yes	In-segment % DS of the Tryton SB compared to SB balloon angioplasty at 9 months	QAngio XA 7.2 CAAS 5.9 or 5.11*	Single Bifurcation*	The Tryton SB vs. SB balloon angioplasty

CABG: coronary artery bypass graft; MB main branch; MI, myocardial infarction; MV: main vessel; PCI: percutaneous coronary intervention; SB: side branch; TLR: target vessel revascularisation; TVF: target vessel failure; TVR: target vessel revascularisation. * The nine-month follow-up angiograms were re-analysed in both core labs (Cardiovascular Research Foundation, New York, NY, USA; Cardialysis B.V., Rotterdam, The Netherlands) using the bifurcation software.

Online Table 2. Angiographic endpoints and QCA algorithms used in first-in-man studies or registries assessing dedicated bifurcation stents.

	Year	No. patients	Primary endpoint	Planned repeat angiography, Yes or No	Angiographic endpoint	QCA software	Algorithm
Prior to introduction of bifurcation software							
Frontier™ stent	2005	105	Death, MI, and TLR at 6 months	Yes	Angiographic restenosis (either branch) 6 months	CAAS II	Single
Introduction of bifurcation software							
Axxess Plus™ stent	2007	139	Death, MI, CABG and ischaemia-driven TLR at 6 months	Yes	Angiographic late loss at 6 months	Not described	Single
Tryton™ stent	2008	30	In-hospital cardiac death, MI, CABG, TLR and TVR	Yes	TLR and TVR at 6 months	CAAS 5.4	Bifurcation
Petal™ stent	2010	28	Death, MI and TVR at 1 month	Yes	Angiographic restenosis (either branch) 6 months	Medis (not described in detail)	Bifurcation
Stentys™ stent	2011	63	Cardiac death, stroke, MI, CABG, TLR and TVR at 6 months	Yes	Vessel patency , late lumen loss and binary restenosis rate at 6 months	CAAS 5	Bifurcation
BiOSS™ stent	2011	63	Cardiac death, stroke, MI, CABG, TLR and TVR at 12 months	Yes	Late lumen loss, percent diameter stenosis and binary restenosis rate at 12 months	QCA-CMS 5.0	Single
Nile Croco™ stent	2011	151	Acute device success and angiographic success	No	No	Not described	Not described
Sideguard™ stent	2012	20	Stroke, MI, stent thrombosis and TLR/TVR at 6 months	Yes	TVR at 6 months	QAngio XA	Bifurcation

CABG: coronary artery bypass graft; MI: myocardial infarction; TLR: target lesion revascularisation; TVR: target vessel revascularisation

3.2 In vitro validation of phantoms: Implications for clinical practice

In vitro validation and comparison of different software packages or algorithms for coronary bifurcation analysis using calibrated phantoms: Implications for clinical practice and research of bifurcation stenting.

Catheter Cardiovasc Interv. 2015 Mar;85(4):554-63.
[Original research paper, IF 2.40]

Ishibashi Y, Grundeken MJ, Nakatani S, Iqbal J, Morel MA, Généreux P, Girasis C, Wentzel JJ, Garcia-Garcia HM, Onuma Y, Serruys PW.

In Vitro Validation and Comparison of Different Software Packages or Algorithms for Coronary Bifurcation Analysis Using Calibrated Phantoms: Implications for Clinical Practice and Research of Bifurcation Stenting

Yuki Ishibashi,[1] MD, PhD, Maik J. Grundeken,[2] MD, Shimpei Nakatani,[1] MD, Javaid Iqbal,[1] MRCP, PhD, Marie-Angele Morel,[3] BSc, Philippe Généreux,[4] MD, PhD, Chrysafios Girasis,[1,5] MD, Jolanda J. Wentzel,[6] PhD, Hector M. Garcia-Garcia,[1] MD, PhD, Yoshinobu Onuma,[1,3*] MD, PhD, and Patrick W. Serruys,[7] MD, PhD

Background: The accuracy and precision of quantitative coronary angiography (QCA) software dedicated for bifurcation lesions compared with conventional single-vessel analysis remains unknown. Furthermore, comparison of different bifurcation analysis algorithms has not been performed. Methods: Six plexiglas phantoms with 18 bifurcations were manufactured with a tolerance < 10 μm. The bifurcation angiograms were analyzed using Cardiovascular Angiography Analysis System (CAAS; Version 5.10, Pie Medical Imaging, Maastricht, The Netherlands) and QAngio XA (Version 7.3, Medis Medical Imaging System BV, Leiden, The Netherlands) software packages. Results: Conventional single-vessel analysis underestimated the reference vessel diameter and percent diameter stenosis in the proximal main vessel while it overestimated these parameters in the distal main vessel and side branch. CAAS software showed better overall accuracy and precision than QAngio XA (with automatic Y- or T-shape bifurcation algorithm selection) for various phantom diameters including minimum lumen diameter (0.012 ± 0.103 mm vs. 0.041 ± 0.322 mm, $P = 0.003$), reference vessel diameter (−0.050 ± 0.043 mm vs. 0.116 ± 0.610 mm, $P = 0.026$), and % diameter stenosis (−0.94 ± 4.07 % vs. 1.74 ± 7.49 %, $P = 0.041$). QAngio XA demonstrated higher minimal lumen diameter, reference vessel diameter, and % diameter stenosis when compared to the actual phantom diameters; however, the accuracy of these parameters improved to a similar level as CAAS when the sole T-shape algorithm in the QAnxio XA was used. Conclusion: The use of the single-vessel QCA method is inaccurate in bifurcation lesions. Both CAAS and QAngio XA (when the T shape is systematically used) bifurcation software packages are suitable for quantitative assessment of bifurcations.

Key words: bifurcation; quantitative coronary angiography; calibrated phantom

[1]Thoraxcenter, Erasmus Medical Center, Rotterdam, The Netherlands
[2]The Heart Center, Academic Medical Center, Amsterdam, The Netherlands
[3]Cardialysis B.V, Rotterdam, The Netherlands
[4]New York - Presbyterian Hospital and Columbia University Medical Center, New York, New York - Cardiovascular Research Foundation, New York
[5]The Onassis Cardiac Surgery Center, Kallithea, Greek
[6]Biomedical Engineering, Erasmus MC, Rotterdam, The Netherlands
[7]International Centre for Circulatory Health, NHL 1, Imperial College London, London, United Kingdom.

Conflict of interest: Nothing to report.

*Correspondence to: Yoshinobu Onuma, MD, PhD, Thoraxcenter, Ba-583, 's Gravendijkwal 230, 3015 CE Rotterdam, Netherlands. E-mail: y.onuma@erasmusmc.nl

Received 18 March 2014; Revision accepted 21 July 2014

DOI: 10.1002/ccd.25618
Published online 24 July 2014 in Wiley Online Library (wileyonlinelibrary.com)

INTRODUCTION

Two-dimensional quantitative coronary angiography (QCA) analysis in bifurcation remains technically challenging. When a conventional single-vessel analysis is used in a bifurcated lesion, two analyses should be performed: one from the proximal main to the distal main branch and the other from the proximal main to the side branch (SB) [1,2]. In the so-called polygon of confluence [3], the edge detection of single-vessel algorithms are not able to define the vessel contours crossing the bifurcation, which frequently requires manual corrections of contour and may introduce subjectivity or bias. Due to natural tapering after the bifurcation, the interpolated reference diameter calculated for the proximal main vessel (PMV) and tapered distal branches underestimates the % diameter stenosis (DS) of the PMV and overestimate % DS in the distal main vessel (DMV) or SB [4,5].

To overcome these limitations, the dedicated bifurcation algorithms have been developed. Currently, two software packages are commercially available: the Cardiovascular Angiography Analysis System (CAAS; Pie Medical Imaging, Maastricht, The Netherlands) and QAngio XA software (Medis Medical Imaging Systems BV, Leiden, The Netherlands). CAAS has been validated in a phantom model with quantification of minimum lumen diameter (MLD) measurements showing a highly accurate and precise performance across a wide range of diameter values [6,7], whereas bifurcation algorithm of QAngio XA with segments was shown in vivo to be robust and reproducible in two clinical studies [8,9].

However, it remains to be investigated whether the bifurcation algorithms, compared to a single-vessel analysis, significantly improve the accuracy of the analysis. Furthermore, the difference in accuracy between bifurcation analysis algorithms remains unknown. We, therefore, aimed to compare single-vessel analysis and bifurcation QCA analysis using CAAS and QAngio XA in calibrated phantoms.

MATERIALS AND METHODS

Phantom Models

Six plexiglas phantoms, each of them mimicking a vessel with three successive bifurcations, were designed in 3D and manufactured with a tolerance < 10 μm [10]. Every individual bifurcation had a lesion, wherein at least one vessel segment had a DS of >60% with the MLD being located within 3–6 mm from the point of bifurcation. The range of diameters, lesion length, angulation, and Medina class [5] used in the design of these 18 bifurcations reflected the anatomic variation and the fractal nature of bifurcations in the human coronary tree as derived from relevant literature [6,7,11,12].

Acquisition and Calibration of Phantom Models

The digital angiograms were acquired on a biplane angiographic system (Axiom Artis^{TM}; Siemens, Forchheim, Germany) [9]. All phantoms were filled with 100% Iodixanol 320 (Visipaque^{TM}; GE Healthcare, Cork, Ireland) and imaged at 30 frames per second, in a 20 cm field of view, with the center of the phantom placed precisely at the isocenter. For validation purposes, images acquired in anteroposterior (AP) direction by either C-arm were analyzed. Images acquired at 30° rotation, once in right and once in left anterior oblique projection, were also analyzed, to investigate the impact of gantry angulation on the accuracy and precision of the measurements.

Quantitative Angiographic Analysis

QCA was performed off-line by an experienced observer using a single-vessel analysis and a bifurcation segmental analysis. As the bifurcation phantom was made in a flat plane, our analysis was performed in AP view, to minimize errors resulting from foreshortening and/or overlap.

Calibration was performed on a 10-mm grid board and the recording geometry of the x-ray system obtained from the Digital Imaging and Communications in Medicine (DICOM) (National Electrical Manufacturers' Association, DICOM, Rosslyn, VA) header and the phantom thickness were taken into account to determine the true pixel size in the phantom plane, separately for each C-arm [9]. Radiographic system settings, phantom position, table height, and distance from source to the image intensifier distance were kept constant throughout each phantom and centimeter grid acquisition and were identical for all phantoms. Then, the same pixel size was manually entered in each analysis.

MLD, reference vessel diameter (RVD), %DS of PMV, DMV, and SB segments were compared with the phantom diameters (PDs) for vessel segments.

Single-vessel analysis. Angiographic images of the 18 bifurcations were analyzed using single-vessel analysis of the CAAS. The middle frame out of the total frame count of a given acquisition was consistently analyzed to avoid frame selection bias. To obtain the angiographic parameters separately in PMV, DMV, and SB, two analyses were performed per bifurcation: (1) MV analysis; PMV to DMV and (2) SB analysis; PMV to SB. Subsequently the QCA was manually segmented. To allow a comparison with to the bifurcation

TABLE I. The Respective Comparison Between Accuracy Measures Relative to the Calibrated Phantom Values Using the Conventional Single Vessel Analysis and Two Bifurcation Methods

		Single vessel analysis by CAAS			Bifurcation segment analysis by CAAS			Bifurcation segment analysis by QAngio XA (auto)			Bifurcation segment analysis by QAngio XA (T shape)			*P*-value				
		Accuracy			Accuracy			Accuracy			Accuracy							
Lesions	Parameters	1	Precision	Limits of agreement	2	Precision	Limits of agreement	3	Precision	Limits of agreement	4	Precision	Limits of agreement	1 versus 2	1 versus 3	2 versus 3	2 versus 4
All ($n = 54$)	RVD	0.108	0.352	±0.690	−0.050	0.043	±0.085	0.116	0.610	±1.196	−0.045	±0.064	±0.125	0.002	0.032	0.026	0.106
All ($n = 54$)	MLD	−0.015	0.146	±0.286	0.012	0.103	±0.202	0.041	0.322	±0.631	−0.012	0.093	±0.182	0.006	0.183	0.003	0.104
All ($n = 54$)	%DS	5.69	11.28	±22.11	−0.94	4.07	±7.98	1.74	7.49	±14.68	0.74	3.81	±7.47	<0.001	<0.001	0.041	0.121
PMV ($n = 18$)	RVD	−0.263	0.102	±0.200	−0.051	0.035	±0.069	0.374	1.021	±2.001	0.051	0.030	±0.059	<0.0001	<0.0001	0.139	0.028	0.921
	MLD	−0.039	0.130	±0.255	0.031	0.086	±0.169	0.189	0.524	±1.027	0.066	0.048	±0.094	0.042	0.311	0.207	0.353
	%DS	−3.29	3.61	±7.08	−1.71	2.38	±4.66	2.56	11.38	±22.30	2.20	1.44	±2.82	0.040	0.251	0.272	0.588
DMV ($n = 18$)	RVD	0.183	0.138	±0.270	−0.066	0.036	±0.071	−0.028	0.086	±0.169	0.067	0.062	±0.131	0.002	<0.001	0.512	0.957
	MLD	−0.008	0.112	±0.220	0.024	0.097	±0.190	0.013	0.093	±0.182	0.088	0.049	±0.096	0.262	0.348	0.530	0.678
	%DS	3.16	4.88	±9.56	−1.95	3.48	±6.82	−0.89	3.33	±6.53	−0.89	3.37	±4.45	0.196	0.204	0.390	0.488
SB ($n = 18$)	RVD	0.405	0.334	±0.655	−0.032	0.075	±0.147	0.035	0.051	±0.100	0.032	0.039	±0.076	<0.001	<0.001	0.083	0.352
	MLD	0.008	0.045	±0.088	−0.017	0.123	±0.241	−0.050	0.083	±0.163	0.084	0.044	±0.086	0.331	0.226	0.133	0.216
	%DS	17.23	11.26	±22.07	0.88	5.35	±10.49	3.55	4.78	±9.37	3.98	2.08	±4.08	<0.001	<0.001	0.702	0.389

RVD, reference vessel diameter; MLD, minimal lumen diameter; DS, diameter stenosis
P significant < 0.05

analyses, the MV was divided into two segments (PMV and DMV) at the site of the carinal point. For the SB analysis, the start point of the SB was set at the carina.

Bifurcation segmental analysis. The angiography of the bifurcations was analyzed using the CAAS version 5.10 and QAngio XA version 7.3 for 2D bifurcation segmental analyses including the edge segments analysis. Standard procedure for bifurcation analysis has been previously described [9]. Briefly, it consisted of the following steps: (1) the middle frame out of the total frame count of a given acquisition was consistently analyzed to avoid frame selection bias; (2) the same pixel size with single-vessel analysis was manually entered; (3) the bifurcation segmentation was initialized by placing one proximal and two distal delimiter points at the largest possible distance from the bifurcation to be analyzed, however, not touching the adjacent bifurcation lesions or the phantom borders; (4) contours were detected using the lumen detection algorithm and MLD was determined using previously described methodology [6,7].

In QAngio XA software, the two bifurcation models (T shape; a main vessel being a proximal vessel that continues in the same direction into a distal vessel, and a SB at an acute angle and Y shape; a proximal vessel with two distal branches that are approximately equal in size and split off at similar angles) are available [9]. Initially, software was allowed to automatically select the analysis algorithm. Subsequently, all bifurcation analyses with QAngio XA were repeated using both the Y- and the T-shape algorithms.

Statistics

Statistical analysis was performed using JMP®10 for Windows (SAS Institute, Cary, NC). Continuous variables are presented as mean ± standard deviation and paired values were compared by Wilcoxon signed rank test. The individual signed differences were averaged; the mean of these signed differences (bias) is a measure of accuracy; the standard deviation is a measure of precision. The agreement for MLD between the CAAS bifurcation analysis and the PDs, QAngio XA using default Y- or T-shape bifurcation analysis and the PDs or QAngio XA using solely the T shape and the PDs were also performed using the Bland–Altman analysis. The accuracy between the measurements and the PDs and its precision were calculated; the repeatability coefficient (equal to 1.96 * standard deviation of the bias) was determined as the measure of variability. All statistical tests were two sided and a P-value < 0.05 was considered statistically significant.

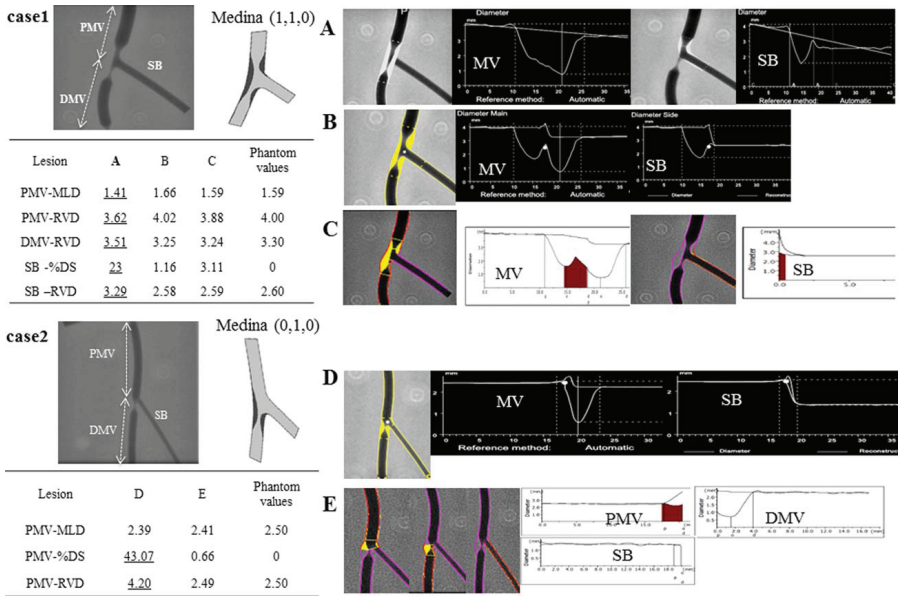

Lesion	A	B	C	Phantom values
PMV-MLD	1.41	1.66	1.59	1.59
PMV-RVD	3.62	4.02	3.88	4.00
DMV-RVD	3.51	3.25	3.24	3.30
SB -%DS	23	1.16	3.11	0
SB –RVD	3.29	2.58	2.59	2.60

Lesion	D	E	Phantom values
PMV-MLD	2.39	2.41	2.50
PMV-%DS	43.07	0.66	0
PMV-RVD	4.20	2.49	2.50

Fig. 1. This is an example of a case of the phantom model results. Quantitative coronary angiography measurement by CAAS and QAngio XA with automatic selection of Y- or T-shape algorithm was shown for a bifurcated lesion in the calibrated phantom. Angiographic parameters including reference diameter, minimal lumen diameter, % diameter stenosis are given in the PMV, DMV, and side branch (SB). Case1; A cine-angiogram demonstrated moderate to severe stenosis both in the proximal main vessel (PMV) and the distal main vessel (DMV) in Medina class (1,1,0) bifurcation. The conventional single-vessel method measured a significantly smaller RVD in the PMV and a larger RVD in the DMV and SB. (A) QCA was shown using the conventional single-vessel algorithm by CAAS. (B) QCA was shown using the bifurcation algorithm by CAAS. (C) QCA was shown using the bifurcation algorithm by QAngio XA with automatic selection of Y or T shape. Case2; A cine-angiogram demonstrated severe stenosis in the distal main vessel (DMV) in Medina class (0,1,0) bifurcation. QAngio XA software using the default Y- or T-shape program, accuracy values for RVD and %DS were quite large (43.07% vs. 0.66%) when Y-shape algorithm was applied as default for Medina class (0,1,0) bifurcation. (D) QCA was shown using the bifurcation algorithm by CAAS. (E) QCA was shown using the bifurcation algorithm by QAngio XA with automatic selection of Y or T shape.

RESULTS

Accuracy and precision of tested software packages for MLD, RVD, and %DS value are presented in Tables I and II including measurements obtained exclusively with the T-shape program.

Comparison Between Angiographic Measurements by Single-Vessel Analyses and PDs

The conventional single-vessel method measured a significantly smaller RVD in the PMV and a larger RVD in the DMV and SB (Fig. 1). Consequently, all the %DS and RVD were overestimated significantly compared to the PDs when using the conventional single-vessel method ($P = 0.003$, $P = 0.014$, respectively). Using single-vessel analyses, MLD values for each segment had an accuracy and precision of -0.039 ± 0.130 mm, -0.008 ± 0.112 mm, and 0.008 ± 0.045 mm for PMV, DMV, and SB, respectively. The values of MLD for all segments did not significantly differ between the conventional single-vessel analysis and the PDs.

CAAS and QAngio XA Bifurcation Algorithms in Reference to PDs

Agreement between the two bifurcation software packages in MLD assessment is presented in Fig. 2. Bland–Altman plots comparing MLD for 54 vessel segments analyzed by CAAS or QAngio XA compared

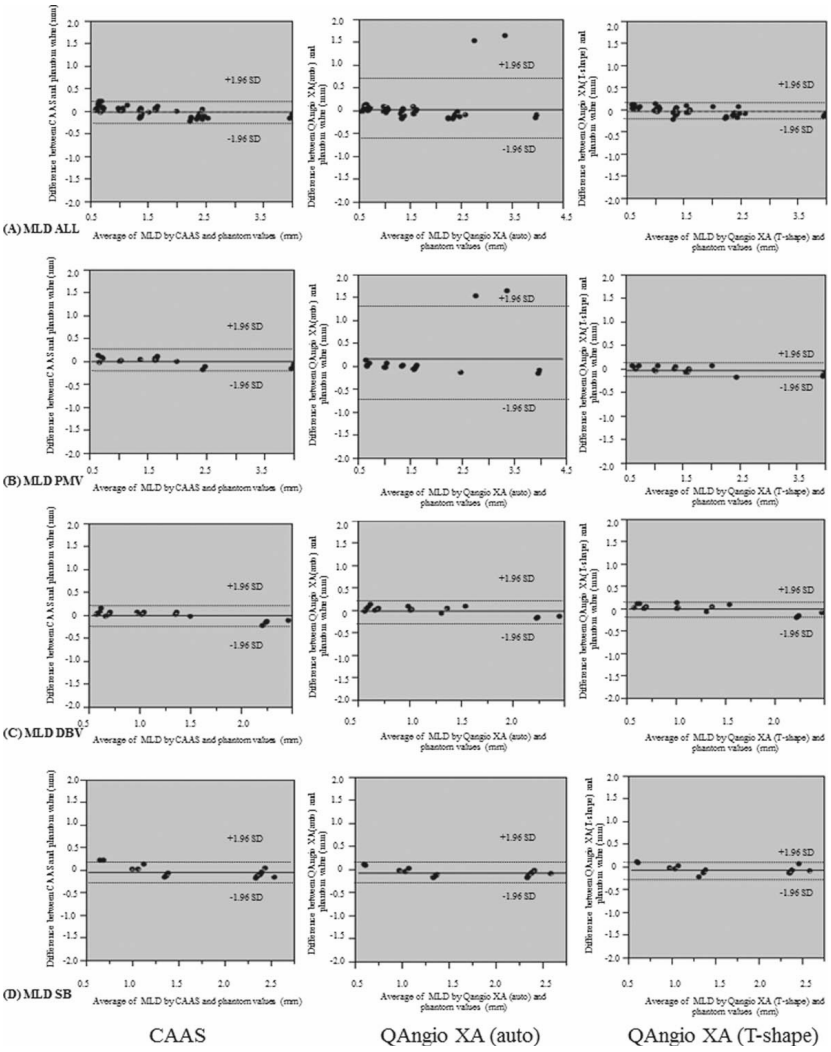

Fig. 2. The agreement for minimum lumen diameter (MLD) between the CAAS and the phantom diameters (PDs), QAngio XA using default Y- or T-shape bifurcation, and the PDs or QAngio XA using solely the T shape were also performed using the Bland–Altman analysis; (A) MLD all, (B) MLD proximal main vessel (PMV), (C) MLD distal main vessel (DMV), (D) MLD side branch (SB). Solid lines represent the mean difference (bias), dotted lines represent the 95% limits of agreement (bias ± 1.96 SD).

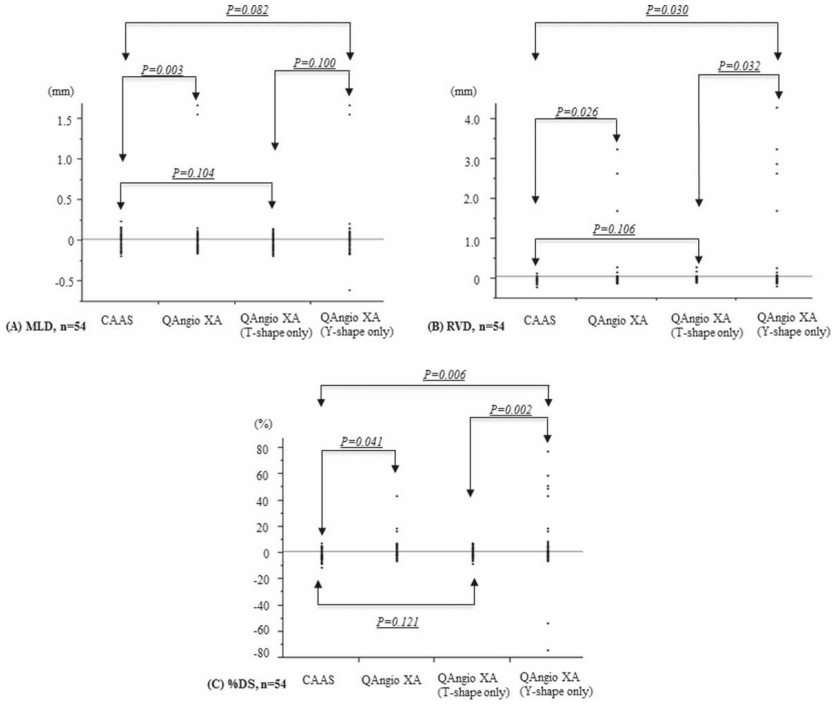

Fig. 3. The respective comparison between accuracy measures relative to the calibrated phantom values using the two bifurcation methods and two bifurcation algorithms were shown for minimum lumen diameter (MLD; panel A), reference vessel diameter (RVD; panel B), and percent diameter stenosis (%DS; panel C).

to the PDs showed that the limit of agreement between CAAS and the PDs, QAngio XA using default Y- or T-shape algorithm and the PDs, or QAngio XA using solely the T shape and the PDs were −0.179 to 0.214, −0.618 to 0.648 mm, and −0.194 to 0.170, respectively (Fig. 2).

The values of MLD did not significantly differ between the QAngio XA using the default Y- or T-shape program and the PDs. Moreover, RVD and %DS in the QAngio XA using the default Y- or T-shape program were overestimated significantly compared to the PDs ($P = 0.002$, $P = 0.047$, respectively). With the CAAS software, MLD and %DS were not significantly different from the PDs.

Accuracy of CAAS and QAngio XA using the default Y- or T-shape program for MLD, RVD, and %DS were 0.012 ± 0.103 mm versus 0.041 ± 0.322 mm ($P = 0.003$), -0.050 ± 0.043 mm versus 0.116 ± 0.610 mm ($P = 0.026$), and -0.94 ± 4.07 % versus 1.74 ± 7.49 % ($P = 0.041$), respectively (Table I). CAAS software provided more precise values than QAngio XA software using the default Y- or T-shape program for MLD, RVD, and %DS measurements.

QAngio XA software using the default Y- or T-shape program, accuracy values for RVD and %DS were quite large in three cases (1.70 mm vs. 0.08 mm and 43.07% vs. 0.66%, 3.23 mm vs. −0.03 mm and 5.32% vs. −0.32%, 2.62 mm vs. −0.09 mm and 18.51% vs. 2.86%) when Y-shape algorithms were applied as default for Medina class (0,1,0) bifurcation (Figs. 1 and 3). As a result, the Y-shape algorithm over-diagnosed binary restenosis in two cases, yielding a positive predictive value of 93%.

When the T-shape algorithm was used in all cases, the accuracy of %DS and RVD improved considerably up to $0.24 \pm 3.80\%$ and -0.025 ± 0.064 mm,

TABLE II. Angiographic Endpoints and Used QCA Algorithms in Randomized Studies, Multicenter Study, or Ongoing Study

	Year	No. patients	Primary endpoint	Planned repeat angiography, Yes or No	Angiographic endpoint	QCA software	Algorithm	Randomization
Colombo et al.	2004	85	Angiographic restenosis (either branch) 6 months	Yes	Binary in-segment restenosis of both the MB and SB at 6months	QCA-CMS 5.1	Single	Provisional vs systematic (crush,T, culotte)
Pan et al.	2004	91	Composite of cardiac death, MI, and the need for TVR at 6 months	Yes	Angiographic restenosis (either branch) 6 months	CAAS II 4.1.1	Single	Provisional vs systematic (T)
NORDIC	2006	413	Death, MI (nonprocedural), TVR, or stent thrombosis at 6 months	Yes	Significant restenosis (50% diameter stenosis) of the MV and/or occlusion of the SB	QAngio XA 7.0	Bifurcation	Provisional vs systematic (crush, culotte, T)
Ferenc et al.	2008	202	Angiographic restenosis of the SB at 9 months	Yes	In-segment per cent diameter stenosis of the SB at 9 months	QAngio XA 7.0	Bifurcation	Provisional vs systematic (T)
NORDIC 2	2009	424	Death, MI (nonprocedural), TVR, or stent thrombosis at 6 months	Yes	in-segment and in-stent restenosis of MV and/or SB after 8 months	QAngio XA 7.0	Bifurcation	Systematic (crush vs culotte)
The DIVERGE	2009	302	Composite of death, MI, and TLR at 9months	Yes	Binary angiographic restenosis at 9months	QAngioXA 7.1	Bifurcation	No, a prospective multicenter registry. (Axxess stent)
DKCRUSH-II	2009	370	Cardiac death, MI, or TVR at 12months	Yes	Restenosis in the MV and SB at 8 months	CAAS 5.7	Bifurcation	Double Kissing Crush versus Provisional Stenting Technique for Treatment of Coronary Bifurcation Lesions
CACTUS[13]	2009	350	Death, MI, TVR at 6 months	Yes	In-segment restenosis rate at 6 months	QCA-CMS	Single	Provisional vs systematic (crush)
Thueringer Bifurcation Study[14]	2009	110	Death, MI, stent thrombosis, CABG, or TLR at 6months	Yes	Restenosis in the MV and SB at 6 months	Quantcor QCA V2.0	Single	Stenting of the MB (Taxus-stent)and mandatory SB PCI kissing balloons with provisional SBstenting, or stenting of the MB (Paclitaxel-eluting stents) with provisional SB-PCI only when the SB had a TIMI flow 2
BBC ONE[15]	2010	500	All cause of death, MI, TVF at 9 months	No	No	Not described	Single	Provisional vs systematic (crush,culotte)
NORDIC 3[16,17]	2011	477	cardiac death, non–procedure-related index lesion MI, stent thrombosis, or TLR by PCI or CABG within 6 months.	Yes	In-segment and in-stent restenosis (50% diameter stenosis) of the MV and/or SB at 8 months	QAngio XA 7.2	Bifurcation	Final Kissing Balloon Dilatation Versus No Final Kissing Balloon Dilatation
The TRYTON trial*a*	2013[a]	704	Cardiac death, MI, or TVR at 9months	Yes	In-segment % DS of the Tryton SB compared to SB balloon angioplasty at 9 months	QAngio XA 7.2 CAAS 5.9 or 5.11[a]	Single bifurcation[a]	The TRYTON SB vs SB balloon angioplasty

TLR, target vessel revascularization; TVR, target vessel revascularization; TVF, target vessel failure; MV, main vessel; MB main branch; SB, side branch; PCI, percutaneous coronary intervention; CABG, coronary artery bypass graft; MI, myocardial infarction

First Results From Pivotal Study of the Tryton Side Branch Stent™ Presented at Transcatheter Cardiovascular Therapeutics (TCT) 2013 Annual Meeting in Late Breaking Clinical Trial Session.

[a]The angiographies of 9 months follow up were reanalyzed in both corelabs (CRF: Cardiovascular Research Foundation, New York, Cardialysis: Cardialysis B.V., Rotterdam).

respectively (Fig. 3). The MLD, RVD, and %DS of the T shape was no longer statistically different from the CAAS bifurcation method. Conversely, when the Y-shape algorithm was consistently applied for all bifurcations, the accuracy of precision for RVD in reference to the PDs became worse (Fig. 3).

DISCUSSION

The main findings of this study are: (1) with conventional single-vessel QCA, the RVD, and %DS were significantly larger than the PDs. (2) CAAS and T shape in the QAngio XA are highly accurate and precise for MLD, RVD, and %DS when compared in vitro with a series of custom-made, precision manufactured Plexiglas phantoms. (3) When algorithms either T shape or Y shape were selected by default mode, QAngio XA demonstrated a higher RVD and %DS than CAAS and the PDs; however, accuracy improved and became comparable to the CAAS algorithm when the T shape was systematically used.

Percutaneous treatment of coronary artery bifurcation lesions is a recognized challenge in interventional cardiology [18–20]. Dedicated software packages for bifurcation assessment can provide angiographic parameters; however, it is important to validated precision and accuracy of available software packages.

The value of MLD in the conventional single-vessel analysis was similar to the PDs; however, our results demonstrated that %DS of DMV and SB is overestimated by the conventional single-vessel analysis. Overestimation of %DS in the DMV and SB has potentially clinical implications. First, when the single-vessel analysis is applied in preprocedural assessment of a bifurcation lesion, the lesion severity would be over exaggerated and may result in the overtreatment of insignificant stenosis. The major bifurcation trials such as BBC ONE, CACTUS, and Thueringer bifurcation study [13–15] have used the single-vessel analysis (Table II). The inclusion of lesion based on the single-vessel analysis may result in biased selection of target lesion [5]. The use of dedicated bifurcation software has been recommended by the European Bifurcation Club Angiographic Sub-Committee to overcome the numerous limitations of standard QCA when applied on bifurcation lesions [5]. Second, in the first-in-man/registry studies testing a dedicated bifurcation stent with a planned repeat angiography (Table III), overestimation of SB at follow up would result in increased rates of ischemia driven target lesion revascularization [13,22,23]. According to the Academic Research Consortium definition [24], at repeat angiography, revascularization for a lesions with >70% stenosis (by corelab QCA) or >50% stenosis with evidence of ischemia are

TABLE III. Angiographic Endpoints and Used QCA Algorithms in First-In-Man Studies or Registries Assessing Dedicated Bifurcation Stent

	Year	No. patients	Primary endpoint	Planned repeat angiography, Yes or No	Angiographic endpoint	QCA software	algorithm
Frontier ™ stent	2005	105	Death, MI, and TLR at 6months	Yes	Angiographic restenosis (either branch) 6 months	CAAS II	Single
Axxess Plus ™ stent21	2007	139	Death, MI, CABG, and ischemia driven TLR at 6 months	Yes	Angiographic late loss at 6 months	Not described	Single
Tryton™ stent22	2008	30	In-hospital Cardiac death, MI, CABG, TLR, and TVR	Yes	TLR and TVR at 6 months	CAAS 5.4	Bifurcation
Petal stent ™	2010	28	Death, MI, and TVR at 1 month	Yes	Angiographic restenosis (either branch) 6 months	Medis (not described in detail)	Bifurcation
Stentys ™ stent	2011	63	Cardiac death, stroke, MI, CABG, TLR, and TVR at 6 months	Yes	Vessel patency, late lumen loss, and binary restenosis rate at 6 months	CAAS 5	Bifurcation
BiOSS™ stent	2011	63	Cardiac death, stroke, MI, CABG, TLR, and TVR at 12 months	Yes	Late lumen loss, percent diameter stenosis, and binary restenosis rate at 12 months	QCA-CMS 5.0	Single
Nile Croco™ stent	2011	151	The acute device success and angiographic success	No	No	Not described	Not described
Sideguard™ stent	2012	20	Stroke, MI, stent thrombosis, and TLR/TVR at 6months	Yes	TVR at 6 months	QAngio XA	Bifurcation

TLR, target vessel revascularization; TVR, target vessel revascularization; MI, myocardial infarction; CABG; coronary artery bypass graft

considered as ischemic driven. In the trial with planned repeat angiography, the usage of single-vessel analysis might influence the event adjudication.

Percentage DS has been less reliable than the MLD in the evaluation of the functional significance of ostial SB stenosis and RVD of a given vessel segment gets interpolated from the diameter outside the obstruction boundaries [5,7,25]. Compared to single-vessel analysis, accuracy of %DS assessment significantly improved with the two bifurcation software packages (Table I, *P*-values; single-vessel analysis by CAAS vs. bifurcation segment analysis by CAAS: $P < 0.001$, single-vessel analysis by CAAS vs. bifurcation segment analysis by QAngio XA with a default setting: $P < 0.001$). However, the accuracy of %DS was better in CAAS than QAngio XA with a default setting ($P = 0.041$). When the analysis was stratified according to the location of stenosis (Table I), the variance of %DS was prominent in SB. This is due to an obvious error of measurement when Y-shape algorithms is by default applied for Medina class (0,1,0). When the T-shape algorithm was forced for all analyses, the accuracy improved and becomes comparable with CAAS. It could be, therefore, recommended to systematically use T-shape algorithm when QAngio XA is used for bifurcation studies. Indeed, in the third Nordic bifurcation study [16,17], the T-shape model was chosen for all bifurcation analyses. This approach should give the best measurements of bifurcation lesions with a high accuracy and precision. Y shape could be considered when the specific Y-shape device (e.g., Axxess plus™ stent) [21] is being evaluated (Table III).

LIMITATION

The phantom design naturally has the inherent limitations of an artificial construction trying to mimic real life. The smooth and static walls of the phantoms neither resemble the jagged irregular appearance of the coronary vessel walls, especially after balloon dilation, nor they reflect movement with each cardiac cycle.

CONCLUSION

The conventional single-vessel QCA method is inaccurate in bifurcation lesions, underestimating RVD and %DS in the PMV with overestimation of these parameters in the DMV and SB. CAAS bifurcation software accurately measured MLD, RVD, and %DS when compared to the PDs. When the default bifurcation algorithms (T shape, Y shape) of the QAngio XA system was automatically selected, QAngio XA demonstrated a higher MLD, RVD, and %DS than CAAS and the PDs. However, if the T-shape algorithm is consistently used in the QAngio XA bifurcation method, the accuracy in measuring RVD and %DS improved and became comparable to the CAAS bifurcation method. Therefore, CAAS bifurcation software and QAngio XA bifurcation software (when the T shape is systematically used) are both suitable for quantitative assessment of bifurcation lesion.

ACKNOWLEDGMENTS

The authors wish to express their sincere appreciation to Dr. Jean-Paul Aben and Dr. Johan H.C. Reiber for the critical review of manuscript.

REFERENCES

1. Keane D, Gronenschild E, Slager C, Ozaki Y, Haase J, Serruys PW. In vivo validation of an experimental adaptive quantitative coronary angiography algorithm to circumvent overestimation of small luminal diameters. Cathet Cardiovasc Diagn 1995;36:17–24.
2. Janssen JP, Koning G, de Koning PJ, Tuinenburg JC, Reiber JH. A novel approach for the detection of pathlines in x-ray angiograms: The wavefront propagation algorithm. Int J Cardiovasc Imaging 2002;18:317–324.
3. Ramcharitar S, Onuma Y, Aben JP, Consten C, Weijers B, Morel MA, Serruys PW. A novel dedicated quantitative coronary analysis methodology for bifurcation lesions. EuroIntervention 2008;3:553–557.
4. Goktekin O, Kaplan S, Dimopoulos K, Barlis P, Tanigawa J, Vatankulu MA, Koning G, Tuinenburg JC, Mario CD. A new quantitative analysis system for the evaluation of coronary bifurcation lesions: Comparison with current conventional methods. Catheter Cardiovasc Interv 2007;69:172–180.
5. Lansky A, Tuinenburg J, Costa M, Maeng M, Koning G, Popma J, Cristea E, Gavit L, Costa R, Rares A, Van Es GA, Lefevre T, Reiber H, Louvard Y, Morice MC, European Bifurcation Angiographic S-C. Quantitative angiographic methods for bifurcation lesions: A consensus statement from the european bifurcation group. Catheter Cardiovasc Interv 2009;73:258–266.
6. Girasis C, Schuurbiers JC, Onuma Y, Aben JP, Weijers B, Boersma E, Wentzel JJ, Serruys PW. Two-dimensional quantitative coronary angiographic models for bifurcation segmental analysis: In vitro validation of CAAS against precision manufactured plexiglas phantoms. Catheter Cardiovasc Interv 2011;77:830–839.
7. Girasis C, Schuurbiers JC, Onuma Y, Aben JP, Weijers B, Morel MA, Wentzel JJ, Serruys PW. Advances in two-dimensional quantitative coronary angiographic assessment of bifurcation lesions: Improved small lumen diameter detection and automatic reference vessel diameter derivation. EuroIntervention 2012;7:1326–1335.
8. Tuinenburg JC, Koning G, Rares A, Janssen JP, Lansky AJ, Reiber JH. Dedicated bifurcation analysis: Basic principles. Int J Cardiovasc Imaging 2011;27:167–174.
9. Tuinenburg JC, Janssen JP, Kooistra R, Koning G, Corral MD, Lansky AJ, Reiber JH. Clinical validation of the new t- and y-shape models for the quantitative analysis of coronary bifurcations: An interobserver variability study. Catheter Cardiovasc Interv 2013;81:E225–E236.

10. Girasis C, Schuurbiers JC, Onuma Y, Serruys PW, Wentzel JJ. Novel bifurcation phantoms for validation of quantitative coronary angiography algorithms. Catheter Cardiovasc Interv 2011; 77:790–797.
11. Girasis C, Onuma Y, Schuurbiers JC, Morel MA, van Es GA, van Geuns RJ, Wentzel JJ, Serruys PW, 5th meeting of the European Bifurcation C. Validity and variability in visual assessment of stenosis severity in phantom bifurcation lesions: A survey in experts during the fifth meeting of the european bifurcation club. Catheter Cardiovasc Interv 2012;79:361–368.
12. Girasis C, Schuurbiers JC, Muramatsu T, Aben JP, Onuma Y, Soekhradj S, Morel MA, van Geuns RJ, Wentzel JJ, Serruys PW. Advanced three-dimensional quantitative coronary angiographic assessment of bifurcation lesions: Methodology and phantom validation. EuroIntervention 2013;8:1451–1460.
13. Colombo A, Bramucci E, Sacca S, Violini R, Lettieri C, Zanini R, Sheiban I, Paloscia L, Grube E, Schofer J, Bolognese L, Orlandi M, Niccoli G, Latib A, Airoldi F. Randomized study of the crush technique versus provisional side-branch stenting in true coronary bifurcations: The cactus (coronary bifurcations: Application of the crushing technique using sirolimus-eluting stents) study. Circulation 2009;119:71–78.
14. Korn HV, Yu J, Ohlow MA, Huegl B, Schulte W, Wagner A, Wassmer G, Gruene S, Petek O, Lauer B. Interventional therapy of bifurcation lesions: A timi flow-guided concept to treat side branches in bifurcation lesions–a prospective randomized clinical study (thueringer bifurcation study, thuebis study as pilot trial). Circ Cardiovasc Interv 2009;2:535–542.
15. Hildick-Smith D, de Belder AJ, Cooter N, Curzen NP, Clayton TC, Oldroyd KG, Bennett L, Holmberg S, Cotton JM, Glennon PE, Thomas MR, Maccarthy PA, Baumbach A, Mulvihill NT, Henderson RA, Redwood SR, Starkey IR, Stables RH. Randomized trial of simple versus complex drug-eluting stenting for bifurcation lesions: The british bifurcation coronary study: Old, new, and evolving strategies. Circulation 2010;121:1235–1243.
16. Niemela M, Kervinen K, Erglis A, Holm NR, Maeng M, Christiansen EH, Kumsars I, Jegere S, Dombrovskis A, Gunnes P, Stavnes S, Steigen TK, Trovik T, Eskola M, Vikman S, Romppanen H, Makikallio T, Hansen KN, Thayssen P, Aberge L, Jensen LO, Hervold A, Airaksinen J, Pietila M, Frobert O, Kellerth T, Ravkilde J, Aaroe J, Jensen JS, Helqvist S, Sjogren I, James S, Miettinen H, Lassen JF, Thuesen L, Nordic-Baltic PCISG. Randomized comparison of final kissing balloon dilatation versus no final kissing balloon dilatation in patients with coronary bifurcation lesions treated with main vessel stenting: The nordic-baltic bifurcation study III. Circulation 2011;123:79–86.
17. Holm NR, Hojdahl H, Lassen JF, Thuesen L, Maeng M. Quantitative coronary analysis in the nordic bifurcation studies. Int J Cardiovasc Imaging 2011;27:175–180.
18. Yamashita T, Nishida T, Adamian MG, Briguori C, Vaghetti M, Corvaja N, Albiero R, Finci L, Di Mario C, Tobis JM, Colombo A. Bifurcation lesions: Two stents versus one stent–immediate and follow-up results. J Am Coll Cardiol 2000;35:1145–1151.
19. Sheiban I, Albiero R, Marsico F, Dharmadhikari A, Tzifos V, Pagnotta P, Montorfano M, Leonardo F, Saba P, Di Mario C, Colombo A. Immediate and long-term results of "t" stenting for bifurcation coronary lesions. Am J Cardiol 2000;85:1141–1144, A1149.
20. Al Suwaidi J, Berger PB, Rihal CS, Garratt KN, Bell MR, Ting HH, Bresnahan JF, Grill DE, Holmes DR Jr. Immediate and long-term outcome of intracoronary stent implantation for true bifurcation lesions. J Am Coll Cardiol 2000;35:929–936.
21. Grube E, Buellesfeld L, Neumann FJ, Verheye S, Abizaid A, McClean D, Mueller R, Lansky A, Mehran R, Costa R, Gerckens U, Trauthen B, Fitzgerald PJ. Six-month clinical and angiographic results of a dedicated drug-eluting stent for the treatment of coronary bifurcation narrowings. Am J Cardiol 2007;99:1691–1697.
22. Onuma Y, Muller R, Ramcharitar S, van Geuns RJ, Louvard Y, Morel MA, Morice MC, Davis R, Kaplan AV, Lefevre T, Grube E, Serruys PW. Tryton I, first-in-man (fim) study: Six month clinical and angiographic outcome, analysis with new quantitative coronary angiography dedicated for bifurcation lesions. EuroIntervention 2008;3:546–552.
23. Onuma Y, Serruys PW, Kukreja N, Veldhof S, Doostzadeh J, Cao S, Stone GW, Spirit, II, Investigators III. Randomized comparison of everolimus- and paclitaxel-eluting stents: Pooled analysis of the 2-year clinical follow-up from the spirit II and III trials. Eur Heart J 2010;31:1071–1078.
24. Cutlip DE, Chauhan MS, Baim DS, Ho KK, Popma JJ, Carrozza JP, Cohen DJ, Kuntz RE. Clinical restenosis after coronary stenting: Perspectives from multicenter clinical trials. J Am Coll Cardiol 2002;40:2082–2089.
25. Keane D, Haase J, Slager CJ, Montauban van Swijndregt E, Lehmann KG, Ozaki Y, di Mario C, Kirkeeide R, Serruys PW. Comparative validation of quantitative coronary angiography systems. Results and implications from a multicenter study using a standardized approach. Circulation 1995;91:2174–2183.

3.3 Inter-Core Lab Variability in Analyzing QCA for Bifurcation Lesions

Comparison between two-dimensional and three-dimensional quantitative coronary angiography bifurcation analyses for the assessment of bifurcation lesions: A sub-analysis of the TRYTON pivotal IDE coronary bifurcation trial.

JACC Cardiovasc Interv. 2015 Feb;8(2):305-14.
[Original research paper, IF 7.44]

Grundeken MJ, **Ishibashi Y**, Généreux P, LaSalle L, Iqbal J, Wykrzykowska JJ, Morel MA, Tijssen JG, de Winter RJ, Girasis C, Garcia-Garcia HM, Onuma Y, Leon MB, Serruys PW.

Inter–Core Lab Variability in Analyzing Quantitative Coronary Angiography for Bifurcation Lesions

A Post-Hoc Analysis of a Randomized Trial

Maik J. Grundeken, MD,* Yuki Ishibashi, MD, PhD,† Philippe Généreux, MD,‡ Laura LaSalle, MPH,‡ Javaid Iqbal, MD,† Joanna J. Wykrzykowska, MD, PhD,* Marie-Angèle Morel, BSc,§ Jan G. Tijssen, PhD,*§ Robbert J. de Winter, MD, PhD,* Chrysafios Girasis, MD,§‖ Hector M. Garcia-Garcia, MD, PhD,†§ Yoshinobu Onuma, MD, PhD,†§ Martin B. Leon, MD,‡ Patrick W. Serruys, MD, PhD¶

ABSTRACT

OBJECTIVES This study sought to evaluate inter-core lab variability in quantitative coronary angiography (QCA) analysis of bifurcation lesions.

BACKGROUND QCA of bifurcation lesions is challenging. To date there are no data available on the inter-core lab variability of bifurcation QCA analysis.

METHODS The randomized Tryton IDE (Tryton Pivotal IDE Coronary Bifurcation Trial) compared the Tryton Side Branch Stent (Tryton Medical, Durham, North Carolina) with balloon angioplasty as side branch treatment. QCA was performed in an angiographic subcohort (n = 326) at 9-month follow-up. Inter-core lab variability of QCA analysis between the Cardiovascular Research Foundation and the Cardialysis core labs was evaluated before and after alignment of the used QCA methodology using angiographic data derived from this angiographic follow-up cohort.

RESULTS In the original analysis, before alignment of QCA methodology, the mean difference between the core labs (bias) was large for all QCA parameters with wide 95% limits of agreement (1.96 × SD of the bias), indicating marked variability. The bias of the key angiographic endpoint of the Tryton trial, in-segment percentage diameter stenosis (%DS) of the side branch, was 5.5% (95% limits of agreement: −26.7% to 37.8%). After reanalysis, the bias of the in-segment %DS of the side branch reduced to 1.8% (95% limits of agreement: -16.7% to 20.4%). Importantly, after alignment of the 2 core labs, there was no longer a difference between both treatment groups (%DS of the side branch: treatment group A vs. group B: 34.4 ± 19.4% vs. 32.4 ± 16.1%, p = 0.340).

CONCLUSIONS Originally, a marked inter-core lab variability of bifurcation QCA analysis was found. After alignment of methodology, inter-core lab variability decreased considerably and impacted angiographic trial results. This latter finding emphasizes the importance of using the same methodology among different core labs worldwide. (Tryton Pivotal Prospective, Single Blind, Randomized Controlled Study to Evaluate the Safety & Effectiveness of the Tryton Side Branch Stent Used With DES in Treatment of de Novo Bifurcation Lesions in the Main Branch & Side Branch in Native Coronaries [TRYTON]; NCT01258972) (J Am Coll Cardiol Intv 2015;8:305–14) © 2015 by the American College of Cardiology Foundation.

From the *Amsterdam Heart Center, Academic Medical Center, Amsterdam, the Netherlands; †Thoraxcenter, Erasmus Medical Center, Rotterdam, the Netherlands; ‡Cardiovascular Research Foundation, New York, New York; §Cardialysis B.V., Rotterdam, the Netherlands; ‖First Cardiology Department, Onassis Cardiac Surgery Center, Athens, Greece; and the ¶International Centre for Circulatory Health, National Heart and Lung Institute, Imperial College London, London, United Kingdom. Dr. Généreux has received speaking fees from Abbott Vascular; and consults for Cardiovascular Systems Inc. Dr. Wykrzykowska has received speaking and consulting fees from Abbott, Tryton Medical, and Stentys. Dr. Leon is member of the Scientific Advisory Board for Abbott Vascular, Boston Scientific, and Medtronic; and is the principal investigator of the Tryton Bifurcation Study. All other authors have reported that they have no relationships relevant to the contents of this paper to disclose.

Manuscript received September 25, 2014; revised manuscript received December 4, 2014, accepted December 17, 2014.

ABBREVIATIONS AND ACRONYMS

%DS = percentage diameter stenosis

CI = confidence interval

CRF = Cardiovascular Research Foundation

IDE = investigational device exemption

MLD = minimal lumen diameter

QCA = quantitative coronary angiography

RVD = reference vessel diameter

Ever since the late 1970s, visual estimation of the severity of a stenosis on coronary angiography has been regarded as unreliable due to a marked intra- and interobserver variability (1,2). Therefore, quantitative coronary angiography (QCA) was introduced in the mid-1980s to provide an objective and reproducible quantification of coronary lesions (3,4). QCA parameters have been widely used as primary and secondary endpoints in numerous randomized clinical trials evaluating the efficacy of new technologies in percutaneous coronary interventions and the effect of new pharmaceutical agents on coronary artery disease progression/regression (5-7).

Due to the fractal geometry of the coronary tree, there is a natural tapering of the bifurcation, with differences in reference vessel diameter (RVD) among the proximal main branch, distal main branch, and side branch (8,9). Due to this natural tapering, the interobserver variability of visual estimation of lesion severity increases even more in bifurcation lesions (10). Furthermore, conventional QCA algorithms have the limitation of being inaccurate in bifurcation lesions because they have been developed and validated in a single straight coronary segment (11). To improve the accuracy of QCA in bifurcation lesions, dedicated bifurcation algorithms were developed, which subsequently have been used in recent clinical trials on bifurcation treatment (12-16).

To eliminate the potential bias stemming from the investigators, QCA analysis in clinical trials is usually performed at independent core laboratories (core labs). These core labs aim to provide unbiased and reproducible results by using validated QCA software and by using standard operating procedures during QCA analysis. Although intraobserver and interobserver variability of bifurcation QCA algorithms have been investigated before (14,16,17), to date no data are available on the differences in bifurcation QCA measurements between core labs. This study aimed to examine inter-core lab variability by comparing the QCA results of 2 core labs using data from the 9-month angiographic follow-up cohort of the randomized trial on the Tryton Side Branch Stent (Tryton Medical, Durham, North Carolina).

METHODS

SETTING. Tryton IDE (Tryton Pivotal IDE Coronary Bifurcation Trial), an investigational device exemption (IDE) randomized trial, compared the Tryton Side Branch Stent with side branch balloon angioplasty, both in combination with a regular drug-eluting stent in the main branch, for the treatment of de novo true coronary bifurcation lesions. The primary endpoint (powered for noninferiority), at 9-month follow-up, was the difference in the occurrence of target vessel failure, defined as the composite of cardiac death, Q-wave or non-Q-wave target vessel myocardial infarction (>3× the upper limit of normal of creatine kinase isoenzyme), and target vessel revascularization. The key secondary endpoint (powered for superiority) was in-segment percentage diameter stenosis (%DS) of the side branch in a pre-specified subgroup of 374 subjects (with an expected loss to follow-up of 15%) undergoing planned repeat angiography at 9 months (the angiographic follow-up cohort).

Two core labs were assigned to perform different types of analyses in the angiographic follow-up cohort of the Tryton IDE trial. The Cardiovascular Research Foundation (CRF, New York, New York) was assigned to perform 2-dimensional QCA analysis of the complete angiographic follow-up cohort. Cardialysis B.V. (Rotterdam, the Netherlands) was assigned to perform 3-dimensional QCA and intravascular ultrasound analyses and for this purpose 9-month follow-up angiograms of 130 subjects included in the angiographic follow-up cohort were available at Cardialysis. Besides 3-dimensional QCA and intravascular ultrasound analyses, Cardialysis also performed 2-dimensional QCA analysis in this subgroup. The inter-core lab variability of the 9-month 2-dimensional QCA analysis between the 2 core labs was investigated in these 130 subjects. This initial analysis indicated diverging angiographic results between the 2 core labs (**Figure 1A**). Thereafter, both core labs disclosed and shared their QCA analysis plans to unravel potential explanations for these differences. Both core labs decided to perform a reanalysis of the total angiographic follow-up cohort using an identical QCA analysis plan, which they had agreed on (**Table 1**).

INITIAL QCA ANALYSIS PLAN OF CRF. At the start of the Tryton IDE trial, the dedicated bifurcation QCA algorithms were not yet validated against precision phantoms. Therefore, the initial QCA analysis plan of the trial, approved by the U.S. Food and Drug Administration and used for the main publication, included the use of a conventional single-vessel QCA algorithm (QAngio XA, version 7.2.34, Medis Medical Imaging Systems, Leiden, the Netherlands). For each bifurcation, 2 analyses were performed: one from the proximal main branch to the distal main branch, and the

other from the proximal main branch to the side branch. First, calibration was performed using the guiding catheter and then, the region of interest was defined by indicating its proximal (i.e., in the proximal main branch) and distal (i.e., in the side branch or distal main branch) boundaries (**Figure 2B**). Hereafter, the QCA software automatically detected the vessel contour based on the change in brightness of the pixels (**Figure 2C**) (4). Then, the analysts were allowed to manually edit the vessel contour whenever the contour did not appeared to be smooth or appropriately delineated (Online Figure 1). Because conventional single-vessel QCA software does not recognize the side branch origin, segmentation of the bifurcation lesion was performed manually, with the carinal point as the beginning of the side branch segment (**Figure 2E**). For the side branch, a single point 5 mm distal to the balloon/stent edge was taken as the reference vessel diameter (RVD) (**Figure 2F**). The %DS was calculated as follows: (RVD of the side branch - minimal lumen diameter [MLD] of the side branch) / RVD of the distal side branch (**Figure 2F**). For the main branch, the RVD was defined as the average of the reference diameter in the "normal" segments proximal and distal to the stent. The %DS in the main branch was calculated by using the MLD and the averaged RVD. QCA measurements were performed on a single "worst" projection (i.e., the projection in which the stenosis looks most severe).

INITIAL QCA ANALYSIS PLAN OF CARDIALYSIS. Cardialysis used a dedicated bifurcation software algorithm for their QCA analysis on bifurcation lesions (Coronary Angiography Analysis System [CAAS], version 5.9, Pie Medical Imaging, Maastricht, the Netherlands) (13,18). For each bifurcation, only 1 analysis needed to be performed. The bifurcated region of interest—including the proximal main branch, distal main branch, and side branch—was defined by indicating its proximal (i.e., in the proximal main branch) and distal (i.e., in both the side branch and the distal main branch) boundaries (**Figure 3A**). After the automatic vessel contour detection (**Figure 3B**), analysts were not allowed to manually edit the vessel contour, except in the cases where the vessel contour was erroneously detecting a side branch or other overlapping contours instead of the vessel contour itself (Online Figure 2). The point of bifurcation is automatically determined by the software and is defined as the mid-point of the largest circle that can be fitted in the bifurcation area, touching all 3 contours (**Figure 3C**) (19). The centerlines of each of the 3 segments meet at the point of bifurcation (**Figure 3C**). Segmentation of the bifurcation in 3 individual segments was performed automatically using the point of bifurcation and centerlines as previously described (19). The %DS was automatically calculated using the interpolated RVD at the MLD site of each segment (**Figures 3E to 3G**). All QCA measurements were performed on at least 2 projections (if available), and the average from all projections were reported.

FIGURE 1 Influence of Core Lab Alignment on the QCA Trial Results

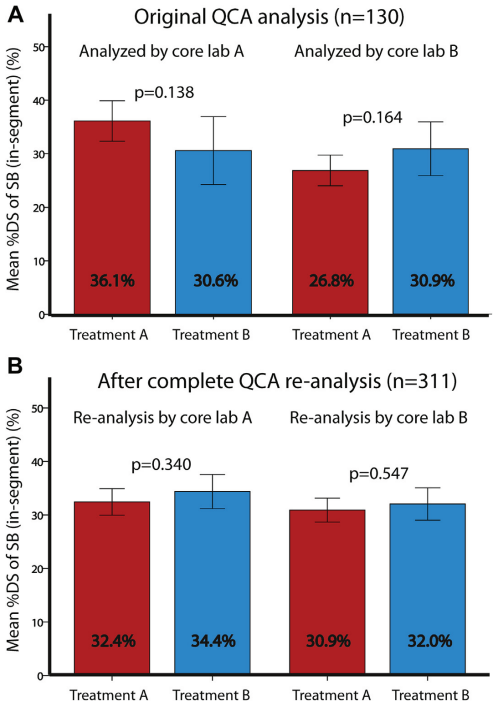

(A) The divergent results are shown of the initial quantitative coronary analysis (QCA), in a subgroup of 130 patients, with regard to in-segment diameter stenosis of the side branch at 9-month follow-up. **(B)** After reanalysis of the complete angiographic cohort (n = 311), both core labs show similar results.

ALIGNMENT OF QCA ANALYSIS PLANS BETWEEN BOTH CORE LABS FOR THE REANALYSIS. After establishing the differences in QCA plans, the 2 core labs agreed to perform a post-hoc reanalysis. It was decided to use

TABLE 1 Initial QCA Analysis Plans of Both Core Laboratories and After Alignment

	Initial QCA Analysis Plan CRF	Initial QCA Analysis Plan Cardialysis	Aligned QCA Analysis Plan for Reanalysis
QCA software used			
Software type	QAngio XA (Medis)	CAAS (Pie Medical)	CAAS
Version	Version 7.2.34	Version 5.9	Version 5.9 (Cardialysis) and 5.11 (CRF)
Algorithm used	Single-vessel algorithm, separately applied on the main and side branch	Dedicated bifurcation algorithm	Dedicated bifurcation algorithm
QCA analysis			
Vessel contour detection	Manual editing was allowed after automatic vessel contour detection	Automatic contour detection with restricted use of manual editing	Automatic contour detection with restricted use of manual editing
Segmentation	User-defined, manual segmentation	Automatic segmentation	Automatic segmentation
RVD of the MB	The average of the distal and proximal user-defined MB references	Interpolated reference automatically generated by the software	Interpolated reference automatically generated by the software
RVD of the SB	User-defined distal SB segment	Interpolated reference automatically generated by the software	Interpolated reference automatically generated by the software
Number of views used	Single, "worst" view was used	Average of ≥2 views to account for lumen eccentricity	Single, "worst" view was used

CAAS = Coronary Angiography Analysis System; CRF = Cardiovascular Research Foundation; MB = main branch; QCA = quantitative coronary angiography; RVD = reference vessel diameter; SB = side branch.

the dedicated CAAS bifurcation software for reanalysis, considering the superior accuracy and precision of this method compared with single-vessel algorithms (12). After delineating the region of interest and the automatic detection of the vessel contours, the analysts were not allowed to manually edit the vessel contour, except in cases were the vessel contour was erroneously not following the vessel contour, as previously described (Online Figure 2). Segmentation of the bifurcation was performed automatically by the software and the %DS was calculated using the interpolated RVD at the site of the MLD in each segment. All QCA measurements were performed on a single worst projection. Both core labs performed their QCA on exactly the same frame, which was selected by the CRF core lab.

STATISTICAL ANALYSES. The individual signed differences of both core labs were averaged; the mean of these signed differences (bias) was used as a measure of accuracy and the standard deviation as a measure of precision (20). The agreement between both core labs with regard to the measurement of %DS of the side branch (in-segment) was evaluated by nonparametric orthogonal regression analysis using the Passing-Bablok method (21). The differences in %DS of the side branch between core labs were also displayed using Bland-Altman plots: the mean of both core lab measurements were plotted on the horizontal axis against the individual signed differences of both core labs on the vertical axis. The 95% limits of agreement (mean difference [bias] ± 1.96 SD of the bias) were determined as the measure of variability. For the Passing-Bablok regression analysis, STATA (version 12, StataCorp LP, College Station, Texas) was used. All other statistical analyses were performed using the SPSS software package (version 21.0, IBM, Chicago, Illinois).

RESULTS

INTER-CORE LAB VARIABILITY. Inter-core lab variability of the initial QCA analysis of the 130 subjects is shown in **Table 2**. Core lab A systematically measured larger RVD, MLD, and %DS in both main branch and side branch compared with Core Lab B. Furthermore, the 95% limits of agreement were wide for all QCA parameters, indicating a marked variability between both core labs. The average difference in the in-segment %DS of the side branch (the key secondary endpoint of the Tryton IDE trial, powered for superiority) was 5.54%, with the 95% limits of agreement between -26.74% and 37.82% (**Figure 4**). Passing-Bablok orthogonal linear regression analysis showed systematic as well as proportional bias between both core labs with regard to the measurement of in-segment %DS of the side branch, with an intercept of 7.1% (95% confidence interval [CI]: 4.5% to 10.0%) and a slope of 0.62 (95% CI: 0.50 to 0.74) (**Figure 4**).

From the 374 patients included in the pre-specified angiographic cohort, 326 patients returned for repeat angiography (87%). From these 326 patients, 311 matched cases were used to assess the inter-core lab variability after QCA reanalysis. In 15 cases, angiography was not available for both core labs due to missing or corrupt CDs. After reanalysis of the total angiographic cohort using the same QCA analysis

FIGURE 2 Initial QCA Analysis Plan of CRF Using a Single-Vessel Algorithm

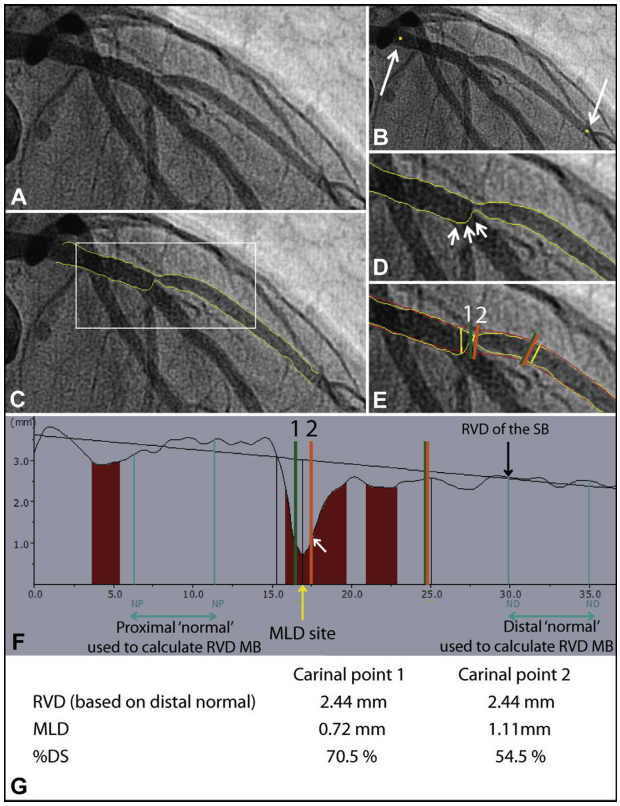

	Carinal point 1	Carinal point 2
RVD (based on distal normal)	2.44 mm	2.44 mm
MLD	0.72 mm	1.11mm
%DS	70.5 %	54.5 %

G

(A) Diagnostic angiogram of a patient with a left anterior descending-diagonal branch bifurcation lesion. QCA was performed using the conventional single-vessel algorithm of QAngio XA (Medis) software. The region of interest of the diagonal branch was defined by indicating the proximal and distal boundaries (**B; long white arrows**). Hereafter, the QCA software automatically detected the vessel contour based on the change in brightness of the pixels **(C). (D)** The software detected the contour in the so-called polygon of confluence. Note that the software detected the outermost vessel wall, opposite to the side branch ostium, as vessel contour **(short white arrows)**. Then, segmentation is performed manually. **(E)** Two examples of different segmentations with different side branch origins (**green line 1 vs. orange line 2**) are shown, illustrating the potential bias introduced by the manual segmentation. **(F)** The diameter function as displayed in the QCA report. Note that a difference in segmentation of the side branch origin (**green line 1 vs. orange line 2**), results in a difference of in-segment side branch minimal lumen diameters (0.72 mm **[yellow arrow]** vs. 1.11 mm **[white arrow]**), because the true minimal lumen diameter of the complete region of interest (0.72 mm) was not included in the side branch segment by the second segmentation **(orange line 2). (G)** The percentage diameter stenosis was calculated for the initial trial results by using the diameter of the distal normal segment as the reference vessel diameter. Note how differences in side branch segmentation resulted in differences in percentage diameter stenosis of the side branch. Note that this figure is included for illustrative purposes and it does not represent actual analyses performed in the trial. CRF = Cardiovascular Research Foundation; QCA = quantitative coronary angiography.

FIGURE 3 Initial QCA Analysis Plan of Cardialysis Using a Bifurcation Algorithm

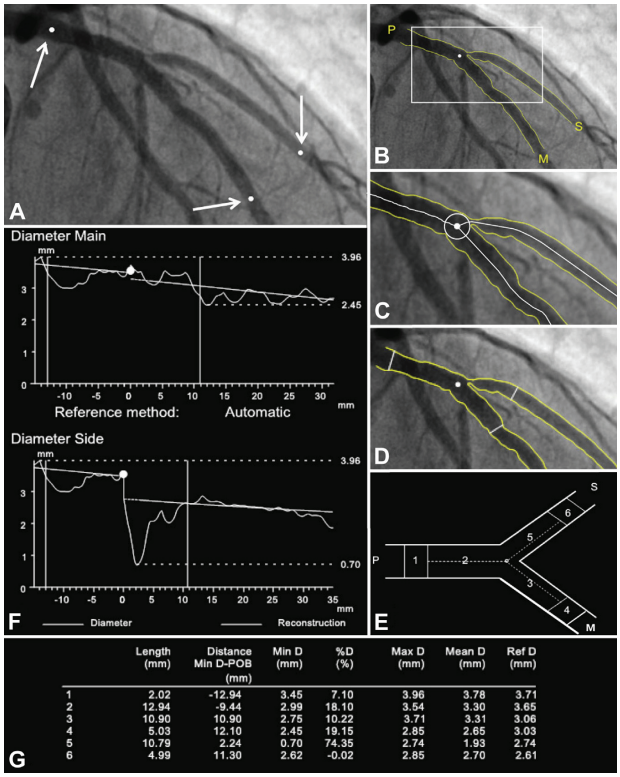

	Length (mm)	Distance Min D-POB (mm)	Min D (mm)	%D (%)	Max D (mm)	Mean D (mm)	Ref D (mm)
1	2.02	-12.94	3.45	7.10	3.96	3.78	3.71
2	12.94	-9.44	2.99	18.10	3.54	3.30	3.65
3	10.90	10.90	2.75	10.22	3.71	3.31	3.06
4	5.03	12.10	2.45	19.15	2.85	2.65	3.03
5	10.79	2.24	0.70	74.35	2.74	1.93	2.74
6	4.99	11.30	2.62	-0.02	2.85	2.70	2.61

QCA analysis of the same bifurcation lesion as in Figure 2, now performed using the dedicated bifurcation algorithm of the Coronary Angiography Analysis System (CAAS) software. The bifurcated region of interest was defined by indicating the boundaries in the proximal main branch, distal main branch, and side branch **(A; white arrows)**. After automatic detection of the vessel contour **(B),** analysts were not allowed to further edit the vessel contour manually. **(C)** The point of bifurcation (POB) and the 3 centerlines. Before the software calculates the QCA parameters, the analysts defined the proximal and distal ends of the main branch stent and the distal end of the Tryton stent/balloon in the side branch **(D; white lines). (E)** The 3 segments of the bifurcation (segments 2, 3, and 5) plus the proximal and distal 5-mm stent/balloon edges (segments 1, 4, and 6) are shown. **(F)** The QCA diameter function of the proximal main branch and distal daughter vessels (i.e., distal main branch and side branch) is shown. Note that each subsegment has its own interpolated reference diameter function, based on the complete bifurcated region of interest (**white vertical lines** corresponding with the **white lines** in **D**, indicating the stent/balloon edges). **(G)** The QCA parameters are shown as they are displayed in the QCA report. Note that the in-segment side branch stenosis calculation is based on the interpolated reference diameter at the site of the minimal lumen diameter. Note that this figure is included for illustrative purposes and does not represent actual analyses performed in the trial. QCA = quantitative coronary angiography.

plan with the same frame and QCA bifurcation software, less systematic bias was observed (Table 2). The side branch in-segment QCA measurements were almost identical between both core labs; only small average differences were observed with regard to the MLD (-0.0297 mm; 95% limits of agreement: -0.4683 to 0.4089 mm) and the RVD (0.0227 mm; 95% limits of agreement: -0.4193 to 0.4647 mm),

TABLE 2 Table Showing the Inter-Core Lab Variability Before and After Alignment of Core Lab Methodologies

	Initial Analysis (n = 130)			After Reanalysis of Both Core Labs (n = 311)		
	Mean Signed Differences (Bias)	Standard Deviation (Precision)	95% Limits of Agreement	Mean Signed Differences (Bias)	Standard Deviation (Precision)	95% Limits of Agreement
Main branch						
RVD, mm	0.2710	0.4216	−0.5553 to 1.0973	−0.0108	0.3464	−0.6681 to 0.6897
In-segment MLD, mm	0.1445	0.4420	−0.7218 to 1.0108	−0.0101	0.2652	−0.5299 to 0.5097
In-segment %DS, %	2.81	13.42	−23.47 to 29.11	−0.04	11.44	−22.46 to 22.38
In-stent MLD, mm	0.2030	0.4271	−0.6341 to 1.0401	−0.0084	0.3006	−0.5976 to 0.5808
In-stent %DS, %	0.48	12.10	−23.24 to 24.20	0.69	11.85	−22.54 to 23.92
Side branch						
RVD, mm	0.2240	0.3376	−0.4377 to 0.8857	0.0227	0.2255	−0.4193 to 0.4647
In-segment MLD, mm	0.0322	0.4574	−0.8643 to 0.9287	−0.0297	0.2238	−0.4683 to 0.4089
In-segment %DS, %	5.54	16.47	−26.74 to 37.82	1.84	9.45	−16.68 to 20.36

%DS = percentage diameter stenosis; MLD = minimal lumen diameter; RVD = reference vessel diameter.

resulting in an average difference in %DS of 1.8% (95% limits of agreement: -16.7% to 20.4%) (**Figure 4**). Finally, orthogonal linear regression analysis showed a marked improvement in reproducibility between core labs with regard to the measurement of in-segment %DS of the side branch. The intercept of the orthogonal regression line was close to 0%, with 0% being enclosed in the 95% CI (intercept: 0.8%, 95% CI: -0.8% to 2.5%), suggesting there was no systematic bias. The slope of the orthogonal regression line was closer to the identity line with the identity line almost being enclosed in the 95% CI, suggesting only a minimal proportional bias between both core labs after reanalysis (slope: 0.94, 95% CI: 0.88 to 0.99) (**Figure 4**).

Initial QCA analysis in the subgroup of 130 patients showed diverging results between both core labs with regard to the Tryton IDE trial key secondary endpoint of in-segment %DS of the side branch (**Figure 1A**). However, after complete reanalysis using contemporary bifurcation QCA software without the routine use of manual contour editing and manual segmentation, both core labs showed similar results with regard to in-segment %DS of the side branch (**Figure 1B**).

DISCUSSION

Our study, for the first time, has highlighted a marked inter-core lab variability in bifurcation QCA measurements due to the use of different QCA software and methodology. After using the same QCA bifurcation software and aligning the methodology of the QCA core labs, the inter-core lab variability improved considerably. Furthermore, after aligning the QCA methodology, we have demonstrated that the trial results were affected. These findings emphasize the importance of standardization of QCA methodology among the different core labs.

The steering committee did acknowledge the methodological differences between core labs that have been raised retrospectively after the database have been locked for the IDE submission to the U.S. Food and Drug Administration. During the designing phase of the trial, however, the validation of the CAAS bifurcation QCA algorithm against a precision bifurcation phantom model was not yet published (14), and therefore the bifurcation algorithm not yet integrated in the core lab responsible for the baseline and follow-up QCA analyses. It was decided to report the data according to the initial approved methodological plan and analysis in the main paper, while reporting the post-hoc QCA results using the bifurcation software in the Online Appendix (22).

USE OF SINGLE-VESSEL VERSUS DEDICATED BIFURCATION SOFTWARE. One of the potential explanations for the differences in the initial analysis was the use of a single-vessel QCA algorithm, which is less accurate than a dedicated bifurcation algorithm is and introduces a systematic bias for several reasons (8,12). Due to the fractal geometry of the epicardial coronary tree, there is a natural tapering of the coronaries with different vessel diameters proximal to and distal from each bifurcation (9). When using a single-vessel algorithm, the interpolated reference is determined by the diameters of the proximal and distal branches, which are by definition unequal, resulting in a systematic underestimation of the RVD and %DS in the proximal main branch, and an overestimation of the RVD and %DS in the distal main branch and side branch (8). In addition, if the reference diameter is selected from a normal segment distal to the balloon/stent in

FIGURE 4 Inter-Core Lab Variability Between CRF and Cardialysis Before and After Alignment of Methodology With Regard to the In-Segment Percentage Side Branch Stenosis

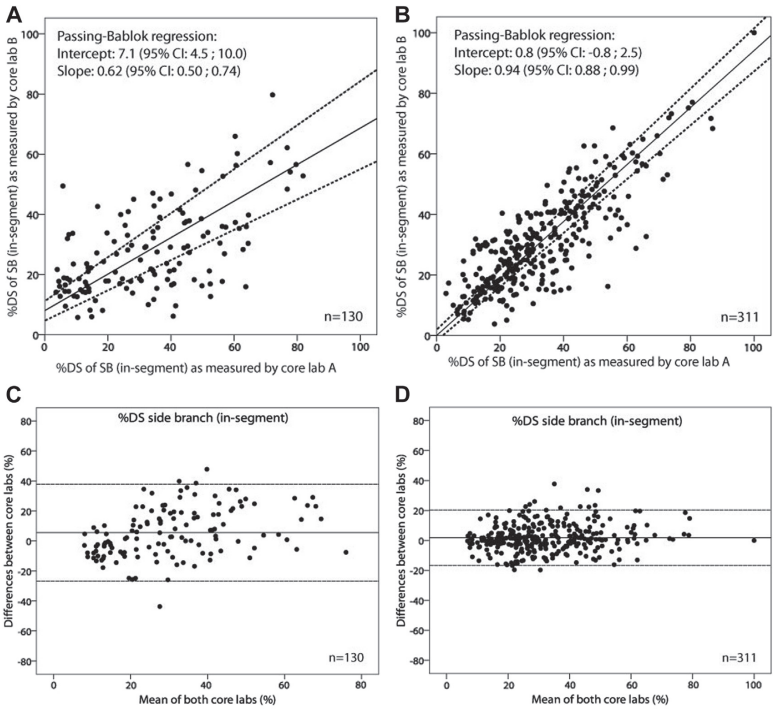

(A) shows a weak agreement between CRF and Cardialysis with regard to the initial measurements of the in-segment side branch stenosis at 9-month follow-up. **(B)** shows a considerable improved agreement between CRF and Cardialysis after reanalysis of the total cohort (**solid lines** = orthogonal regression lines, **dashed lines** = 95% confidence intervals of these regression lines). **(C and D)** show Bland-Altman plots of in-segment side branch stenosis, with the mean between core labs on the horizontal axis plotted against the signed differences on the vertical axis. The **solid lines** represent the mean difference, whereas the **dashed lines** indicate the 95% limits of agreement (1.96 × SD of the mean difference). Note that after reanalysis **(D)**, the mean difference between core labs was smaller, with less wide limits of agreement indicating improved accuracy and precision. CRF = Cardiovascular Research Foundation.

the side branch to calculate the %DS, this can introduce a subjective random error when compared with the interpolated reference diameter based on the vessel contour of the complete region of interest encompassing the side branch (Figure 2). Furthermore, in the so-called polygon of confluence, the single-vessel software is not able to define the vessel contour automatically and often requires manual editing, potentially introducing another factor of random error (Figure 2D, Online Figure 1). Finally, single-vessel algorithms do not recognize the origin of the distal branches, requiring manual segmentation, which may introduce another bias (Figures 2E and 2F).

MANUAL CONTOUR EDITING. Another potential explanation for the differences in the initial analysis was the difference in allowance for manual corrections. Lack of smoothness of the automatic contour delineation, observed when the angiogram is

of suboptimal quality (23), should be accepted as such. Manual editing will introduce subjectivity (Online Figure 1) and should be allowed only in those cases where the algorithm erroneously detects other structures than the vessel contour (side branches, for example). Analysts should use the "restriction function" to exclude an area for the automatic contour detection instead of completely redrawing it themselves (Online Figure 2). All corrections and adjustments made after completion of the QCA analysis should be captured by audit trails and final approval of the QCA should be electronically signed to fulfill the Code of Federal Regulation Title 21, part 11 (CFR 21, part 11) guideline of the U.S. Food and Drug Administration, which defines the criteria for reliable electronic data capturing.

REMAINING INTER-CORE LAB VARIABILITY COMPARED WITH THE ACCURACY AND PRECISION OF THE BIFURCATION SOFTWARE. Although the reproducibility improved remarkably after aligning the core lab methodology, some systematic bias remained. This remaining inter-core lab bias for the in-segment side branch QCA parameters was 0.0227 mm (RVD), -0.0297 mm (MLD), and 1.84% (%DS) (**Table 2**). We believe this is acceptable, considering that the intrinsic accuracy of the CAAS bifurcation software, calibrated on a precision phantom model, was comparable to this bias: −0.032 mm (side branch RVD), −0.017 mm (side branch MLD), and 0.88% (side branch %DS) (12).

Inter-core lab variability (standard deviation of the bias) after reanalysis was 0.2255 mm for the in-segment side branch RVD, 0.2238 mm for the in-segment side branch MLD, and 9.45% for the in-segment %DS. This variability is a little higher as would have been expected from the phantom validation, which showed precision of the bifurcation software of 0.075 mm (side branch RVD), 0.123 mm (side branch MLD), and 5.35% (side branch %DS) (12). This somewhat higher variability might be explained by differences in calibration. Whereas the calibration in the phantom validation study was performed using a grid in a static model, the calibration in the current study was performed using the guiding catheter in close proximity of the beating heart. Although calibration is preferably performed in the same frame as the QCA analysis, sometimes this is not possible and calibration in another frame is needed, which may introduce extra variability. Given the fact that most angiograms have a calibration factor of ~0.2000 mm/pixel, a precision with regard to measuring the MLD and RVD being around this number can be considered as acceptable.

IMPLICATIONS. Although core lab analysts are ideally blinded to the treatment groups to minimize bias, this is not always possible. This is a major limitation, which is not restricted to the current Tryton IDE trial, but also applies to other trials such as trials comparing metallic stents with bioresorbable scaffolds or different types of transcatheter aortic valves. This is important to realize because device and pharmaceutical companies cover the costs of the analysis, which makes core labs not completely independent. Therefore, it is vital to use a methodology in which the analysis is performed as automatically as possible to minimize human subjectivity, with manual corrections restricted to a minimum.

It seems to remain challenging to aim for standardization of QCA methodology in various core labs worldwide (11). Our study has highlighted the importance of using the same QCA methodology among different core labs, using software validated on the same high-resolution calibrated bifurcation phantom model (10,14,16,24), to ensure reproducibility and objectivity. Although standard operating procedures are often not shared because they are considered intellectual property of the core lab, we believe it is important to share at least the key factors of the QCA methodology to ensure reproducible and generalizable results. Considering cross-validation, using 2 distinct core labs, of a prespecified proportion of patients enrolled might even be a valid option to ensure identification of any potential issues precluding data accuracy and reproducibility.

STUDY LIMITATIONS. Because the agreed QCA reanalysis plan included the use of exactly the same angiographic view and frame, selected by 1 of the core labs, this study did not investigate the role of frame selection on the inter-core lab variability. Although it has been shown that differences in frame selection from the same angiographic view does not influence the accuracy and variability to a large extent (25), differences in selection of the angiographic view itself is a major determinant of variability in QCA (26).

CONCLUSIONS

We found a marked inter-core lab variability in QCA of bifurcation lesions when different QCA methodologies were used, including difference in software use (single-vessel vs. dedicated bifurcation software), differences in allowance for manual vessel contour correction, and differences in the method for segmentation (automatic vs. manual). However, when

the same methodology was used, inter-core lab variability decreased considerably. More importantly, QCA results of the trial were affected following alignment of the methodology. This latter finding emphasizes the importance of using the same QCA methodology among different core labs worldwide.

REPRINT REQUESTS AND CORRESPONDENCE: Dr. Patrick W. Serruys, International Centre for Circulatory Health, NHLI, Imperial College London, Royal Brompton Campus, London SW7 2AZ, United Kingdom. E-mail: patrick.w.j.c.serruys@gmail.com.

REFERENCES

1. Zir LM, Miller SW, Dinsmore RE, Gilbert JP, Harthorne JW. Interobserver variability in coronary angiography. Circulation 1976;53:627-32.

2. Galbraith JE, Murphy ML, de Soyza N. Coronary angiogram interpretation: interobserver variability. JAMA 1978;240:2053-6.

3. Serruys PW, Reiber JH, Wijns W, et al. Assessment of percutaneous transluminal coronary angioplasty by quantitative coronary angiography: diameter versus densitometric area measurements. Am J Cardiol 1984;54:482-8.

4. Reiber JH, Serruys PW, Kooijman CJ, et al. Assessment of short-, medium-, and long-term variations in arterial dimensions from computer-assisted quantitation of coronary cineangiograms. Circulation 1985;71:280-8.

5. Garg S, Serruys PW. Coronary stents: current status. J Am Coll Cardiol 2010;56:S1-42.

6. Lichtlen PR, Hugenholtz PG, Rafflenbeul W, Hecker H, Jost S, Deckers JW, the INTACT Group Investigators. Retardation of angiographic progression of coronary artery disease by nifedipine: results of the International Nifedipine Trial on Antiatherosclerotic Therapy (INTACT). Lancet 1990; 335:1109-13.

7. de Feyter PJ, Vos J, Deckers JW. Progression and regression of the atherosclerotic plaque. Eur Heart J 1995;16 Suppl I:26-30.

8. Lansky A, Tuinenburg J, Costa M, et al., for the European Bifurcation Angiographic Subcommittee. Quantitative angiographic methods for bifurcation lesions: a consensus statement from the European Bifurcation Group. Catheter Cardiovasc Interv 2009;73:258-66.

9. Finet G, Gilard M, Perrenot B, et al. Fractal geometry of arterial coronary bifurcations: a quantitative coronary angiography and intravascular ultrasound analysis. EuroIntervention 2008; 3:490-8.

10. Girasis C, Onuma Y, Schuurbiers JC, et al. Validity and variability in visual assessment of stenosis severity in phantom bifurcation lesions: a survey in experts during the fifth meeting of the European Bifurcation Club. Catheter Cardiovasc Interv 2012;79:361-8.

11. Keane D, Haase J, Slager CJ, et al. Comparative validation of quantitative coronary angiography systems: results and implications from a multicenter study using a standardized approach. Circulation 1995;91:2174-83.

12. Ishibashi Y, Grundeken MJ, Nakatani S, et al. In vitro validation and comparison of different software packages or algorithms for coronary bifurcation analysis using calibrated phantoms: implications for clinical practice and research of bifurcation stenting. Catheter Cardiovasc Interv 2014 Jul 24 [E-pub ahead of print].

13. Onuma Y, Müller R, Ramcharitar S, et al. Tryton I, First-In-Man (FIM) study: six month clinical and angiographic outcome, analysis with new quantitative coronary angiography dedicated for bifurcation lesions. EuroIntervention 2008;3: 546-52.

14. Girasis C, Schuurbiers JC, Onuma Y, et al. Two-dimensional quantitative coronary angiographic models for bifurcation segmental analysis: in vitro validation of CAAS against precision manufactured plexiglas phantoms. Catheter Cardiovasc Interv 2011;77:830-9.

15. Holm NR, Hojdahl H, Lassen JF, Thuesen L, Maeng M. Quantitative coronary analysis in the Nordic Bifurcation studies. Int J Cardiovasc Imaging 2011;27:175-80.

16. Girasis C, Schuurbiers JC, Onuma Y, et al. Advances in two-dimensional quantitative coronary angiographic assessment of bifurcation lesions: improved small lumen diameter detection and automatic reference vessel diameter derivation. EuroIntervention 2012;7:1326-35.

17. Tuinenburg JC, Janssen JP, Kooistra R, et al. Clinical validation of the new T- and Y-shape models for the quantitative analysis of coronary bifurcations: an interobserver variability study. Catheter Cardiovasc Interv 2013;81:E225-36.

18. Magro M, Wykrzykowska J, Serruys PW, et al. Six-month clinical follow-up of the Tryton side branch stent for the treatment of bifurcation lesions: a two center registry analysis. Catheter Cardiovasc Interv 2011;77:798-806.

19. Ramcharitar S, Onuma Y, Aben JP, et al. A novel dedicated quantitative coronary analysis methodology for bifurcation lesions. EuroIntervention 2008;3:553-7.

20. Reiber JH. Why and how should QCA systems be validated? In: Serruys PW, Foley DP, de Feyter PJ, editors. Quantitative Coronary Angiography in Clinical Practice. Dordrecht, the Netherlands: Kluwer Academic Publishers, 1994:1-7.

21. Passing H, Bablok L. A new biometrical procedure for testing the equality of measurements from two different analytical methods: application of linear regression procedures for method comparison studies in clinical chemistry, part I. J Clin Chem Clin Biochem 1983;21:709-20.

22. Généreux P, Kumsars I, Lesiak M, et al. A randomized trial of a dedicated bifurcation stent versus provisional stenting in the treatment of coronary bifurcation lesions. J Am Coll Cardiol 2015;65:533-43.

23. Reiber JH, van der Zwet PM, Koning G, et al. Accuracy and precision of quantitative digital coronary arteriography; observer-, as well as short- and medium-term variabilities. In: Serruys PW, Foley DP, de Feyter PJ, editors. Quantitative Coronary Angiography in Clinical Practice. Dordrecht, the Netherlands: Kluwer Academic Publishers, 1994:7-26.

24. Girasis C, Schuurbiers JC, Onuma Y, Serruys PW, Wentzel JJ. Novel bifurcation phantoms for validation of quantitative coronary angiography algorithms. Catheter Cardiovasc Interv 2011;77:790-7.

25. Reiber JH, van Eldik-Helleman P, Kooijman CJ, Tijssen JG, Serruys PW. How critical is frame selection in quantitative coronary angiographic studies? Eur Heart J 1989;10 Suppl F:54-9.

26. Jost S, Deckers J, Nikutta P, et al., for the International Nifedipine Trial on Antiatherosclerotic Therapy Investigators. Influence of the selection of angiographic projections on the results of coronary angiographic follow-up trials. Am Heart J 1995;130:433-9.

KEY WORDS bifurcation, bifurcation lesions, percutaneous coronary interventions, quantitative coronary angiography, Tryton Side Branch Stent

APPENDIX For supplemental figures, please see the online version of this paper.

3.4 Comparison Between Two-dimensional and Three-dimensional QCA

Comparison Between Two-dimensional and Three-dimensional Quantitative Coronary Angiography For the Assessment of Bifurcation Lesions:
A Sub-analysis of the TRYTON Pivotal IDE Coronary Bifurcation Trial.

Catheter Cardiovasc Interv. 2015 Sep;86(3).
[Original research paper, IF 2.40]

Muramatsu T, Grundeken MJ, **Ishibashi Y**, Nakatani S, Girasis C, Campos CM, Morel MA, Jonker H, de Winter RJ, Wykrzykowska JJ, García-García HM, Leon MB, Serruys PW, Onuma Y; TRYTON Pivotal IDE Coronary Bifurcation Trial Investigators.

Comparison Between Two- and Three-dimensional Quantitative Coronary Angiography Bifurcation Analyses for the Assessment of Bifurcation Lesions: A Subanalysis of the TRYTON Pivotal IDE Coronary Bifurcation Trial

Takashi Muramatsu,[1,2] MD, PhD, Maik J. Grundeken,[3] MD, Yuki Ishibashi,[1] MD, PhD, Shimpei Nakatani,[1] MD, Chrysafios Girasis,[1,4] MD, Carlos M. Campos,[1,5] MD, Marie-Angèle Morel,[6] BSC, Hans Jonker,[6] BSC, Robbert J. de Winter,[3] MD, PhD, Joanna J. Wykrzykowska,[3] MD, PhD, Hector M. García-García,[1,6] MD, PhD, Martin B. Leon,[7] MD, Patrick W. Serruys,[8*] MD, PhD, and Yoshinobu Onuma,[1] MD, PhD, On behalf of the TRYTON Pivotal IDE Coronary Bifurcation Trial Investigators

Background: Three-dimensional (3D) quantitative coronary angiography (QCA) provides more accurate measurements by minimizing inherent limitations of two-dimensional (2D) QCA. The aim of this study was to compare the measurements between 2D and 3D QCA analyses in bifurcation lesions. Methods and Results: A total of 114 cases with non-left main bifurcation lesions in the TRYTON pivotal IDE Coronary Bifurcation Trial (ClinicalTrials.gov: NCT01258972) were analyzed using a validated bifurcation QCA software (CAAS 5.10, Pie Medical Imaging, Maastricht, the Netherlands). All cases were analyzed in matched projections between pre- and post-procedure. The 2D analysis was performed using one of two angiographic images used for 3D reconstruction showing a larger distal bifurcation angle. In the treated segments (stent and balloon), there were no differences in minimal luminal diameter (MLD) between 2D and 3D, while diameter stenosis (DS) was significantly higher in 2D compared to 3D both pre-procedure and post-procedure (53.9% for 2D vs. 52.1% for 3D pre-procedure, $P < 0.01$; 23.2% for 2D vs. 20.9% for 3D post-procedure, $P = 0.01$). In the sub-segment level analysis, lengths of proximal main branch, distal main branch, and side branch were consistently shorter in 2D compared to 3D both pre-procedure and post-procedure. Using 3D QCA, the anatomic location of the smallest MLD or the highest DS was relocated to a different bifurcation sub-segment in a considerable proportion of the patients compared to when 2D-QCA was used (kappa values: 0.50 for MLD, 0.55 for DS). Conclusions: Our data showed differences in addressing anatomical severity and

[1]Thoraxcenter, Erasmus Medical Center, Rotterdam, The Netherlands
[2]Department of Cardiology, Fujita Health University Hospital, Toyoake, Japan
[3]Amsterdam Heart center, Academic Medical Center, Amsterdam, The Netherlands
[4]First Cardiology Department, Onassis Cardiac Surgery Center, Athens, Greece
[5]Department of Interventional Cardiology, Heart Institute (InCor), University of São Paulo Medical School, São Paulo, Brazil
[6]Cardialysis, B.V., Rotterdam, The Netherlands
[7]Cardiovascular Research Foundation/Columbia University Medical Center, New York Presbyterian Hospital, New York, New York
[8]International Centre for Circulatory Health, NHLI, Imperial College London, London, United Kingdom

Conflict of interest: The TRYTON IDE trial have been sponsored and funded by Tryton Medical, Inc. Drs. Grundeken, Wykrzykowska, and de Winter declare the funding from Tryton Medical for the TRYTON Pivotal IDE Coronary Bifurcation Trial received by their institution (Academic Medical Center, Amsterdam, The Netherlands). The rest of authors have reported that they have no relationships relevant to the contents of this article to disclose.

Additional Supporting Information may be found in the online version of this article.

*Correspondence to: Patrick W. Serruys, MD, PhD, International Centre for Circulatory Health, NHLI, Imperial College London, London, The United Kingdom. E-mail: patrick.w.j.c.serruys@gmail.com

Received 26 November 2014; Revision accepted 8 March 2015

DOI: 10.1002/ccd.25925
Published online 24 April 2015 in Wiley Online Library (wileyonlinelibrary.com)

location of coronary bifurcation lesions between in vivo 2D and 3D QCA analyses. More studies are needed to investigate potential clinical benefits in using 3D approach over 2D QCA for the assessment of bifurcation lesions.

Key words: coronary bifurcation; three-dimensional; quantitative coronary angiography

INTRODUCTION

Quantitative coronary angiography (QCA) has been introduced in the mid-eighties to overcome the shortcomings of visual assessment of stenosis severity, such as a marked inter- and intra-observer variability [1–4]. Conventional two-dimensional (2D) QCA has been accepted as an objective and reproducible method to quantify coronary lesion severity, and QCA parameters have been accepted as surrogate endpoints in numerous randomized clinical trials evaluating the efficacy of new technologies in percutaneous coronary interventions (PCI) and the effect of new pharmaceutical agents on coronary artery disease progression/regression [5–7].

Even in the era of drug-eluting stents (DES), bifurcation lesions have still been recognized as one of the most challenging lesion subsets [8,9]. As a consequence of the fractal geometry of the coronary tree, there is a natural step-down of diameters proximal and distal to the bifurcation [10,11]. The interpolation method of the single-vessel QCA algorithms to estimate the reference vessel diameter (RVD) is therefore inaccurate, structurally underestimating the RVD and percentage diameter stenosis (DS) in the proximal main branch (MB), and overestimating the RVD and DS of the distal MB and side branch (SB) [11,12] Dedicated bifurcation 2D QCA algorithms have therefore been developed to improve the accuracy of QCA in bifurcation lesions [12–14].

However, 2D bifurcation techniques also include several inherent limitations, such as vessel overlap and foreshortening that can lead to inaccurate angiographic assessment. Three-dimensional (3D) QCA techniques have been developed to overcome these limitations, improving the accuracy of QCA, as shown in a phantom bifurcation model [15]. To date, however, comparisons between 2D and 3D bifurcation QCA have not yet been performed in real life. The aim of this study was therefore to compare the angiographic measurements between 2D and 3D QCA analyses in human coronary bifurcation lesions using validated bifurcation QCA analysis software.

METHODS

Study Overview

The TRYTON Pivotal IDE (Investigational Device Exemption) Coronary Bifurcation Trial is a prospective, multicenter, single-blind, randomized controlled study to evaluate the safety and efficacy of the Tryton side branch stent (Tryton Medical, Durham, NC) in coronary bifurcation lesions [16]. Patients with single *de novo* lesion in a non-left main bifurcation were randomized in a 1:1 fashion to either the Tryton stent or SB balloon angioplasty (SBBA), both in conjunction with a DES in the MB.

The details of the Tryton side branch stent were described elsewhere [16–18]. The Tryton stent is a balloon-expandable cobalt chromium (CoCr) bare-metal stent with strut thickness of 84 μm. It is comprised of three zones (a distal side branch, a transition, and a proximal MB zone), and is implanted in the SB before an approved conventional DES was implanted in the MB. The study protocol was approved by the institutional review boards or medical ethics committees at each participating center. This study was registered at ClinicalTrials.gov (identifier: NCT01258972). Written informed consent was obtained for all enrolled patients. In the present analysis, angiographic data were pooled and analyzed regardless of randomization.

Quantitative Coronary Angiography Assessment

Off-line QCA analyses were performed using the Cardiovascular Angiography Analysis System software (CAAS 5.10, Pie Medical Imaging, Maastricht, The Netherlands) in an independent angiographic core laboratory (Cardialysis B.V., Rotterdam, The Netherlands). The treated segments were defined by three borders. The proximal MB border was defined by the proximal MB DES stent edge, the distal MB border was defined by the distal MB DES stent edge, and the SB border was defined by either the distal Tryton stent edge or the distal marker of the most distal balloon used in the case of SBBA (Fig. 1). The in-segment analyses included the treated segment plus 5 mm proximally to the proximal border of MB, and 5-mm distally to the distal borders of MB and SB.

Only matched pre- and post-procedural projections were used for QCA analyses. Calibration was performed automatically in both 2D and 3D analysis with the geometric data of acquisitions provided through the DICOM headers. Three-dimensional QCA analyses were performed first, using two angiographic images separated by a viewing angle of $\geq 30^{\circ}$. Subsequently,

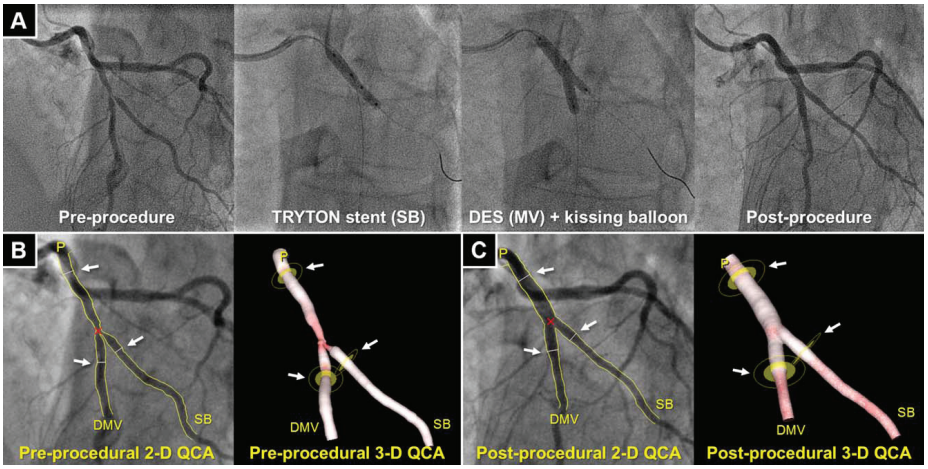

Fig. 1. Treatment procedure using the Tryton stent and the definition of the treated segment. A bifurcation lesion was observed in the mid segment of left anterior descending artery and a diagonal branch (left in panel A). After pre-dilatation, a Tryton stent was implanted toward the side branch (center left), then a drug-eluting stent was implanted through the Tryton stent in the main vessel (center right). The final angiogram showed good results (right). The treated segments were delineated using three white lines (see white arrows) at the proximal main branch (PMB), distal main branch (DMB), and side branch (SB) in the matched projections (white arrows, pre-procedure in panel B and post-procedure in panel C). Specifically, the proximal and distal borders of the main vessel were set at the proximal and distal edge of the DES implanted, respectively. In this case, the distal border of side branch was defined as the distal edge of the Tryton stent.

2D analyses were performed by using one of the angiographic images used in 3D QCA with the largest distal BA (Fig. 2).

Minimal lumen diameter (MLD), DS, and RVD were quantified pre- and post-procedurally. The MLD in the 3D QCA analysis was derived from the absolute minimal lumen area using the so-called "equivalent diameters" methodology, as previously published [19] (Supporting Information, Fig. S1). The RVD was calculated with automatic reference obstruction analysis [13], and the DS was automatically calculated from the MLD and the RVD. The QCA analyses were performed according to the six-segment model (BSM6) [14] plus the 3-mm ostial SB segment of the 11-segment model (BSM11) (Fig. 3) [14]. Bifurcation angle (BA) values were calculated according to the methodology described previously [13,19]. Binary stenosis was defined as the presence of stenosis with a DS of $\geq$50%.

Statistical Analysis

Continuous variables were expressed as mean $\pm$ SD and categorical variables as counts and percentages. Comparisons were performed by paired *t* test for continuous variables and chi-squared test for categorical variables. Agreements between 2D and 3D analyses in detecting the sub-segment with the smallest MLD or the highest DS were evaluated using kappa statistics. A *P* value $<$0.05 was considered statistically significant. Statistical analyses were performed using SPSS Statistics version 21 (IBM, Armonk, NY).

RESULTS

Study Population

A total of 114 patients (114 bifurcation lesions, matched between pre- and post-procedure) were used for the paired 2D and 3D analyses (Supporting Information, Fig. S2).

Subsegment Level Analysis

Subsegment analyses based on the BSM6 model are shown in Table I. Preprocedurally, 2D-MLD was smaller than 3D-MLD in the proximal MB, while the 2D-MLD was larger than 3D-MLD in the SB. Postprocedurally, 2D-MLD was smaller than 3D-MLD in

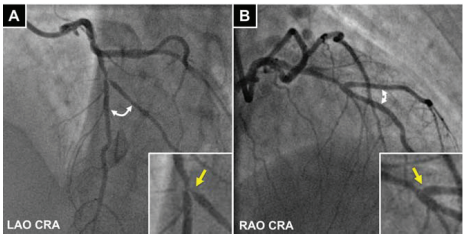

Fig. 2. Two-dimensional (2D) and three-dimensional (3D) QCA assessments. Severe stenosis was evident at the ostium of side branch (yellow arrows) in the LAO cranial view (panel A), while this part was overlapped and "hidden" by the overlapping main vessel in the RAO cranial view (panel B). An angiogram with the largest bifurcation angle between distal main branch and side branch was used for 2D quantitative coronary angiography assessment in the current analysis (e.g., the panel A in this case).

the distal MB. Specifically at the ostial SB, there were no differences in MLD between 2D and 3D QCA (both pre- and post-procedure). Pre-procedural RVD was consistently larger in 2D QCA than in 3D QCA in the proximal MB, distal MB, and SB. Post-procedural RVD was larger with 2D QCA only in the proximal MB, while in the other segments the RVD was similar between 2D QCA and 3D QCA. These differences in MLD and RVD resulted in differences in pre- and post-procedural DS in the proximal MB and ostial SB (Fig. 4). Segment lengths were consistently shorter with 2D QCA than with 3D QCA in all sub-segments, both pre- and post-procedure.

Treated Segment Level Analysis

There were no differences in either in-segment MLD or treated segment MLD between 2D and 3D QCA both pre- and post-procedure (Table II). Conversely, 2D QCA showed a trend toward a higher in-segment DS compared to 3D QCA, while in the treated segment DS appeared to be significantly higher in 2D QCA than in 3D QCA both pre-procedure ($53.9\% \pm 12.4\%$ vs. $52.1\% \pm 11.3\%$, $P < 0.01$) and post-procedure ($23.2\% \pm 10.9$ vs. $20.9\% \pm 11.9\%$, $P = 0.01$) (Fig. 5).

Bifurcation Angle Analysis

Bifurcation angle analyses are shown in Table III. Proximal bifurcation angles ($BA_{PMB\text{-}SB}$) were significantly larger in 2D QCA than in 3D QCA both pre-procedure and post-procedure, while there were no differences in pre- and post-procedural distal bifurcation angles ($BA_{DMB\text{-}SB}$) between 2D and 3D QCA. Post-procedurally $BA_{PMB\text{-}SB}$ became significantly larger and $BA_{DMB\text{-}SB}$ became significantly smaller in both 2D and 3D QCA.

Comparisons of Locations With the Smallest MLD or the Highest DS Between 2D and 3D QCA

Pre-procedural locations with the smallest MLD and the highest DS among sub-segments based on the BSM6 model are shown in Fig. 6. There were apparent inconsistencies in location (i.e., sub-segments) having in-segment smallest MLD and highest DS between 2D and 3D analyses. In the BSM6 model, 2D QCA indicated 49 cases and 3D QCA indicated

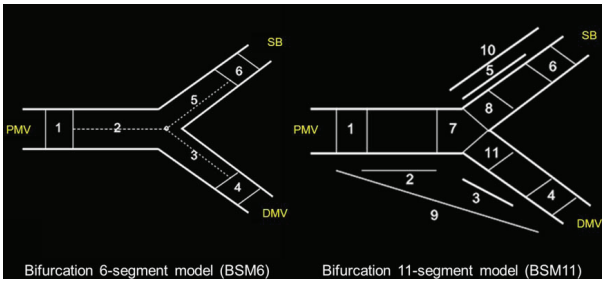

Fig. 3. Bifurcation segment models in the cardiovascular angiography analysis system (CAAS). A composite of segments 2, 3, and 5 in bifurcation six-segment model (BSM6) corresponds to the "treated segment," where the stents were implanted or balloons were dilated, including the proximal main branch (PMB), distal main branch (DMB) and side branch (SB) respectively. The segments 2, 3, and 5 are divided by the point of bifurcation (POB) defined as the point where all the centerlines meet and the midpoint of the largest circle/sphere that can reach all three contours in bifurcation [13]. Segments 1, 4, and 6 correspond to 5-mm segments beyond the treated segment (left panel). Segment 8 in BSM11 reflects 3-mm ostial segments of SB (right panel). In this study, "in-segment" corresponds to a composite of all segments in BSM6.

TABLE I. Subsegment Level Analysis (Paired Samples *N* = 114)

Variables	Paired samples ($N = 114$) 2-D QCA	3-D QCA	*P* value
Pre-procedure			
Proximal main branch (segment 2 in BSM6)			
MLD (mm)	1.75 ± 0.65	1.84 ± 0.61	<0.01
RVD (mm)	3.00 ± 0.57	2.71 ± 0.51	<0.01
DS (%)	41.4 ± 19.5	31.7 ± 19.4	<0.01
Length (mm)	8.34 ± 4.23	9.25 ± 4.72	<0.01
Binary stenosis rate, *n* (%)	40 (35.1)	25 (21.9)	0.03
Distal Main Branch (segment 3 in BSM6)			
MLD (mm)	1.32 ± 0.36	1.33 ± 0.37	0.68
RVD (mm)	2.24 ± 0.40	2.21 ± 0.40	0.08
DS (%)	40.2 ± 15.6	38.9 ± 15.3	0.28
Length (mm)	9.87 ± 5.27	11.63 ± 6.56	<0.01
Binary stenosis rate, *n* (%)	36 (31.6)	27 (23.7)	0.18
Side Branch (segment 5 in BSM6)			
MLD (mm)	1.29 ± 0.38	1.22 ± 0.41	0.02
RVD (mm)	2.08 ± 0.36	1.99 ± 0.33	<0.01
DS (%)	37.8 ± 15.8	38.9 ± 16.7	0.46
Length (mm)	6.23 ± 1.86	6.79 ± 2.23	<0.01
Binary stenosis rate *n* (%)	30 (26.3)	29 (25.4)	0.88
Ostial Side Branch (segment 8 in BSM11)			
MLD (mm)	1.42 ± 0.41	1.44 ± 0.45	0.63
RVD (mm)	2.08 ± 0.35	1.99 ± 0.33	<0.01
DS (%)	31.6 ± 16.3	28.1 ± 16.9	0.02
Length (mm)	2.95 ± 0.39	2.94 ± 0.41	0.57
Binary stenosis rate *n* (%)	18 (15.8)	9 (7.9)	0.07
Post-procedure			
Proximal main branch (segment 2 in BSM6)			
MLD (mm)	2.89 ± 0.39	2.89 ± 0.38	0.91
RVD (mm)	3.28 ± 0.44	3.11 ± 0.42	<0.01
DS (%)	11.52 ± 7.25	6.86 ± 6.64	<0.01
Length (mm)	8.01 ± 4.02	8.70 ± 4.35	<0.01
Binary stenosis rate, *n* (%)	0 (0.0)	0 (0.0)	1.00
Distal Main Branch (segment 3 in BSM6)			
MLD (mm)	2.38 ± 0.32	2.42 ± 0.34	0.04
RVD (mm)	2.66 ± 0.32	2.66 ± 0.31	0.84
DS (%)	10.35 ± 8.37	9.28 ± 6.11	0.14
Length (mm)	10.05 ± 5.04	11.40 ± 6.03	<0.01
Binary stenosis rate, *n* (%)	0 (0.0)	0 (0.0)	1.00
Side branch (segment 5 in BSM6)			
MLD (mm)	1.78 ± 0.39	1.75 ± 0.40	0.23
RVD (mm)	2.18 ± 0.31	2.15 ± 0.42	0.37
DS (%)	18.28 ± 14.13	18.61 ± 13.17	0.77
Length (mm)	6.41 ± 2.03	6.66 ± 2.23	0.09
Binary stenosis rate, *n* (%)	4 (3.5)	2 (1.8)	0.41
Ostial side branch (segment 8 in BSM11)			
MLD (mm)	1.81 ± 0.40	1.85 ± 0.39	0.08
RVD (mm)	2.19 ± 0.31	2.16 ± 0.42	0.3
DS (%)	17.58 ± 13.66	14.14 ± 11.62	<0.01
Length (mm)	2.97 ± 0.44	2.96 ± 0.43	0.61
Binary stenosis rate *n* (%)	4 (3.5)	1 (0.9)	0.18

MLD = minimal luminal diameter, RVD = reference vessel diameter, DS = diameter stenosis, BSM = bifurcation segment model.

63 cases having the smallest pre-procedural MLD within the SB (segment 5 in the BSM6 model). Similarly, 2D and 3D QCA indicated the SB as the location of the highest pre-procedural DS in 27 and 40 cases, respectively. For the agreement between 2D and 3D QCA in determining the location of the subsegment with the smallest pre-procedural MLD, the kappa value was 0.50. For the agreement to determine the location of the highest pre-procedural DS, the kappa value was 0.55.

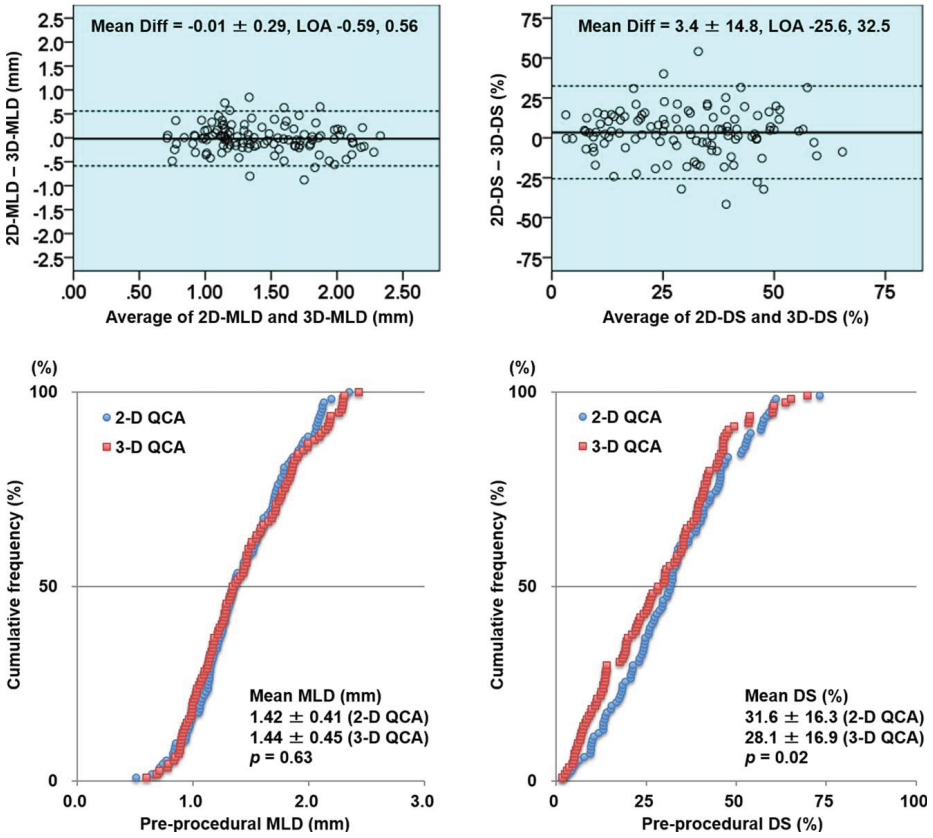

Fig. 4. Bland–Altman plots and cumulative frequency distribution (CFD) curves of pre-procedural MLD and DS in the ostial side branch. In the Bland–Altman plots (upper panels), solid lines indicate the mean difference between 2D and 3D analyses and dotted lines indicate the upper and lower limit of agreement (LOA). In the CFD curves (lower panels), blue circles indicate 2D QCA and red squares indicate 3D QCA. MLD = minimal luminal diameter, DS = diameter stenosis.

DISCUSSION

The main findings of this study can be summarized as follows: (1) DS were estimated to be higher when 2D QCA was used as compared when 3D QCA was used, specifically within the SB ostium; (2) in most sub-segments, this difference was based on larger RVD as measured with 2D QCA, while MLDs were similar between 2D and 3D, except for the proximal MB (pre-procedure) and distal MB (post-procedure), in which the difference in DS was explained by a smaller MLD measured by 2D QCA; (3) segment lengths appeared to be shorter in 2D than in 3D QCA; (4) bifurcation angles were influenced by 2D and 3D analyses; and (5) the agreement between 2D and 3D QCA to define the locations with the smallest MLD and the highest DS was poor.

There have been two studies that compared 2D and 3D QCA in bifurcation lesions [20,21]. However, these studies used different software with different analysis

TABLE II. Treated Segment Level Analysis

	Paired samples ($N = 114$)		
Variables	2D QCA	3D QCA	P value
In-segment (whole segment in BSM6)			
Smallest MLD (mm)			
Pre-procedure	1.07 ± 0.27	1.05 ± 0.29	0.43
Post-procedure	1.56 ± 0.34	1.60 ± 0.34	0.08
Largest DS (%)			
Pre-procedure	53.96 ± 12.25	52.09 ± 11.31	0.06
Post-procedure	32.39 ± 10.93	28.66 ± 10.40	0.08
Treated segment (segment 2, 3, 5 in BSM6)			
Smallest MLD (mm)			
Pre-procedure	1.07 ± 0.28	1.05 ± 0.30	0.47
Post-procedure	1.76 ± 0.37	1.74 ± 0.39	0.36
Largest DS (%)			
Pre-procedure	53.87 ± 12.40	52.09 ± 11.31	<0.01
Post-procedure	23.21 ± 10.88	20.89 ± 11.89	0.01

BSM = bifurcation segment model, MLD = minimal luminal diameter, DS = diameter stenosis.

algorithms for the 2D and 3D QCA analyses. We demonstrated that the CardiOp-B system (Paeion Medical, Rosh Ha'ayin, Israel), used for the 3D QCA analyses in both studies, was less accurate with respect to the measurements of luminal diameter and area when compared to the CAAS system [22]. We then applied the CAAS bifurcation analysis algorithms systematically to 2D and 3D QCA that has been validated in the plexiglas bifurcation phantom models with excellent inter- and intra-observer reproducibility [14,15,23]. In the present study, sub-segment level analysis based on the BSM6 model showed a trend toward higher DS in 2D QCA than in 3D QCA. The differences in DS between the two QCA approaches could partially be explained by a larger RVD found with 2D QCA. The RVD at the MLD site is an interpolated reference diameter based on the non-stenotic lumens of the analyzed region of interest. In some sub-segments, a larger RVD determined with 2D analysis might imply an overestimation of the non-stenotic regions, resulting in a larger interpolated RVD at the MLD site as compared to 3D analysis. Another possible explanation is that the luminal shape at the MLD site is often not circular (concentric plaque), but elliptical (eccentric plaque). 3D QCA derived MLD is calculated as an "equivalent diameter" based on the circular assumption of the cross-section (Supporting Information, Fig. S1). For the current study, 2D analysis was based on a single projection, which could result in a smaller MLD if the projection was perpendicular on the smallest diameter of the elliptical lumen. Furthermore, we found a low agreement between 2D and 3D QCA to define the location of the smallest in-segment MLD. As a result, there might also be a difference in DS because the MLD was located in a somewhat different site, even in the same sub-segment, because the two modalities uses different methodology to calculate the MLD (i.e., smallest area in 3D vs. smallest diameter in 2D) as mentioned above. Consequently, the interpolated RVD might be larger at that site leading to higher DS.

Accuracy in length derivation is one of advantages of 3D QCA by minimizing possible vessel foreshortening commonly seen in 2D QCA [15,19,24]. In the present study, the length of each sub-segment (proximal MB, distal MB, and SB) appeared to be significantly shorter in 2D than in 3D QCA. This finding is in line with previous studies that showed the superiority of 3D to 2D QCA in determining the segment length [22,24–27]. This advantage of 3D QCA may help interventional cardiologists in their decision making of appropriate device length when treating bifurcation lesions.

Recently more attention has been drawn to the BA assessment since the relative change between systolic and diastolic BA was related to clinical outcomes after distal left main PCI [28,29]. Theoretically, 3D QCA provides more accurate BA compared to 2D QCA by calculating the vectors of proximal MB, distal MB, and SB separately in a three-dimensional approach, minimizing the influence of vessel overlap [19]. In the present study, significant differences were observed only in $BA_{PMB\text{-}SB}$ and not in $BA_{DMB\text{-}SB}$.This might be explained by the fact that the projection with the largest $BA_{DMB\text{-}SB}$ was selected for 2D QCA analysis, which might be considered as the most optimal view for 2D BA assessment if 3D QCA is not available (Fig. 2).

The present study also highlights the fact that 2D and 3D QCA detected different locations of the smallest pre-procedural MLD or the highest pre-procedural DS in bifurcation lesions. Indeed the kappa values suggested insufficient agreement between the two analysis approaches (kappa: 0.50 for the smallest MLD sites and 0.55 for the highest DS sites). From the clinical perspective, it has been reported that the DS measured by dedicated 2D bifurcation QCA algorithm showed a better correlation with invasive fractional flow reserve (FFR) than that by a conventional single-vessel 2D QCA technique, and this advantage was more pronounced in SB [30]. It is also noteworthy that Yong et al. demonstrated that 3D QCA derived measurements showed better predictive ability in detecting functionally significant stenosis determined by invasive FFR as compared to 2D QCA derived measurements in simple lesions [27]. Therefore, the dedicated bifurcation 3D QCA algorithm may provide more accurate information not only on anatomical severity but also on

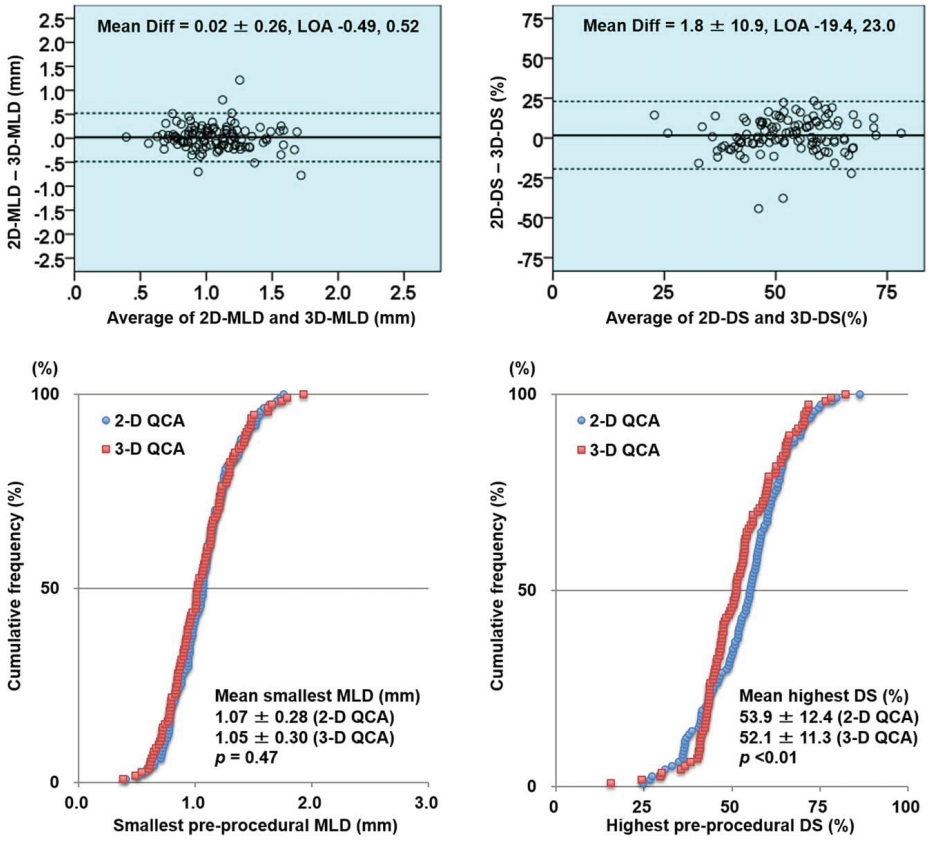

Fig. 5. Bland–Altman plots and cumulative frequency distribution (CFD) curves of the smallest pre-procedural MLD and the highest pre-procedural DS in the treated segment. In the Bland–Altman plots (upper panels), solid lines indicate the mean difference between 2D and 3D analyses and dotted lines indicate the upper and lower limit of agreement (LOA). In the CFD curves (lower panels), blue circles indicate 2D QCA and red squares indicate 3D QCA (lower panels). MLD = minimal luminal diameter, DS = diameter stenosis.

location of stenosis to be treated in the clinical setting, although we cannot use the current data to support this statement.

Study Limitations

First, we presented neither inter- nor intra-observer reproducibility of QCA analyses in the present study. Our group has already reported the excellent inter- and intra-observer reproducibility in both 2D and 3D QCA analyses in the previous literature [14,15,23]. The results may be different when using other software with different algorithms for bifurcation analysis. Second, we consistently applied one of the two angiographic images with the largest $BA_{DMB\text{-}SB}$ to the 2D analysis since such a view is usually considered as a more suitable 2D view specifically for the anatomical evaluation of ostial SB that is the most susceptible part of the bifurcation to vessel overlap (Fig. 3). Nevertheless, image selection may have an impact on the comparison between 2D and 3D QCA derived parameters.

TABLE III. Bifurcation Angle Analysis (Paired Sample $N = 114$)

Bifurcation angle, degree	Paired samples ($N = 114$) 2D QCA	3D QCA	P value
Pre-procedure			
Proximal MB-SB	141.3 ± 22.8	137.4 ± 17.5	0.04
Distal MB-SB	61.9 ± 21.9	59.0 ± 16.2	0.08
Post-procedure			
Proximal MB -SB	153.0 ± 18.2	144.3 ± 14.3	<0.01
Distal MB-SB	51.7 ± 18.9	51.4 ± 13.8	0.85

Bifurcation angle, degree	Paired samples ($n = 114$) Pre-procedure	Post-procedure	P value
2D QCA			
Proximal MB -SB	141.3 ± 22.8	153.0 ± 18.2	<0.01
Distal MB -SB	61.9 ± 21.9	51.7 ± 18.9	<0.01
3-D QCA			
Proximal MB -SB	137.4 ± 17.5	144.3 ± 14.4	<0.01
Distal MB -SB	59.0 ± 16.2	51.4 ± 13.8	<0.01

MB = main branch, SB = side branch.

CONCLUSIONS

There were differences in addressing anatomical severity and location of coronary bifurcation lesions between in vivo 2D and 3D QCA analyses. Whereas DS was in general higher with 2D QCA, lesion length was shorter with 2D QCA than with 3D QCA. No differences could be detected in distal bifurcation angles ($BA_{DMB\text{-}SB}$) in the present study, although a difference in the proximal bifurcation angles ($BA_{PMB\text{-}SB}$) was evident between the two algorithms. The MLD sites or the highest DS sites by 2D assessment relocated to different sub-segments in a considerable proportion of the patients when using 3D assessment. More studies are needed to investigate the potential clinical benefit in using 3D approach over 2D QCA for the assessment of bifurcation lesions.

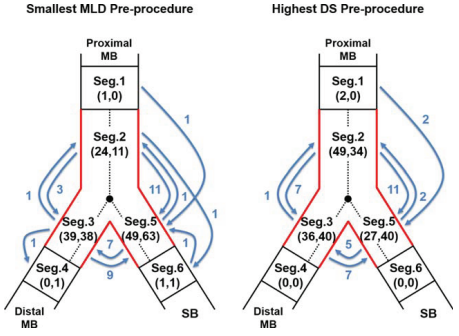

Fig. 6. Locations of subsegments with smallest MLD and highest DS pre-procedure. In-segment smallest MLD (left panel) and highest DS (right panel) were identified and their locations were classified according to the BSM6 model in 2D and 3D QCA analyses. Numbers in brackets (2D, 3D) indicate the number of cases in which smallest MLD or highest DS were located in each corresponding segment. Curved blue arrows indicate the number of cases and directions of change in location with smallest MLD or highest DS by 2D QCA when analyzed by 3D QCA. MLD = minimal luminal diameter, DS = diameter stenosis, MB = main branch, SB = side branch.

ACKNOWLEDGMENTS

The authors wish to express their sincere appreciation to Mr. Folkert Tijdens (Pie Medical Imaging, Maastricht, The Netherlands) for technical assistance.

REFERENCES

1. Serruys PW, Reiber JH, Wijns W, et al. Assessment of percutaneous transluminal coronary angioplasty by quantitative coronary angiography: Diameter versus densitometric area measurements. Am J Cardiol 1984;54:482–488.
2. Reiber JH, Serruys PW, Kooijman CJ, et al. Assessment of short-, medium-, and long-term variations in arterial dimensions from computer-assisted quantitation of coronary cineangiograms. Circulation 1985;71:280–288.
3. Zir LM, Miller SW, Dinsmore RE, Gilbert JP, Harthorne JW. Interobserver variability in coronary angiography. Circulation 1976;53:627–632.
4. Galbraith JE, Murphy ML, de SN. Coronary angiogram interpretation. Interobserver variability. JAMA 1978;240:2053–2056.
5. Garg S, Serruys PW. Coronary stents: Current status. J Am Coll Cardiol 2010;56:S1–S42.
6. Lichtlen PR, Hugenholtz PG, Rafflenbeul W, Hecker H, Jost S, Deckers JW. Retardation of angiographic progression of coronary artery disease by nifedipine. Results of the International Nifedipine Trial on Antiatherosclerotic Therapy (INTACT). INTACT Group Investigators. Lancet 1990;335:1109–1113.
7. de Feyter PJ, Vos J, Deckers JW. Progression and regression of the atherosclerotic plaque. Eur Heart J 1995;16 (Suppl I):26–30.
8. Rathore S, Terashima M, Katoh O, et al. Predictors of angiographic restenosis after drug eluting stents in the coronary arteries: Contemporary practice in real world patients. EuroIntervention 2009;5:349–354.
9. van Werkum JW, Heestermans AA, Zomer AC, et al. Predictors of coronary stent thrombosis: The Dutch Stent Thrombosis Registry. J Am Coll Cardiol 2009;53:1399–1409. [PMC][10.1016/j.jacc.2008.12.055] [19371823]
10. Finet G, Gilard M, Perrenot B, et al. Fractal geometry of arterial coronary bifurcations: A quantitative coronary angiography and intravascular ultrasound analysis. EuroIntervention 2008;3:490–498.
11. Lansky A, Tuinenburg J, Costa M, et al. Quantitative angiographic methods for bifurcation lesions: A consensus statement from the European Bifurcation Group. Catheter Cardiovasc Interv 2009;73:258–266.
12. Ishibashi Y, Grundeken MJ, Nakatani S, et al. In vitro validation and comparison of different software packages or algorithms for coronary bifurcation analysis using calibrated phantoms: Implications for clinical practice and research of bifurcation stenting. Catheter Cardiovasc Interv 2015;85:554–563.

13. Ramcharitar S, Onuma Y, Aben JP, et al. A novel dedicated quantitative coronary analysis methodology for bifurcation lesions. EuroIntervention 2008;3:553–557.
14. Girasis C, Schuurbiers JC, Onuma Y, et al. Two-dimensional quantitative coronary angiographic models for bifurcation segmental analysis: In vitro validation of CAAS against precision manufactured plexiglas phantoms. Catheter Cardiovasc Interv 2011;77:830–839.
15. Girasis C, Schuurbiers JC, Muramatsu T, et al. Advanced three-dimensional quantitative coronary angiographic assessment of bifurcation lesions: Methodology and phantom validation. EuroIntervention 2013;8:1451–1460.
16. Généreux P, Kumsars I, Lesiak M, et al. A randomized trial of a dedicated bifurcation stent versus provisional stenting in the treatment of coronary bifurcation lesions. J Am Coll Cardiol 2015;65:533–543.
17. Grundeken MJ, Asgedom S, Damman P, et al. Six-month and one-year clinical outcomes after placement of a dedicated coronary bifurcation stent: A patient-level pooled analysis of eight registry studies. EuroIntervention 2013;9:195–203.
18. Grundeken MJ, Stella PR, Wykrzykowska JJ. The Tryton side branch stent for the treatment of coronary bifurcation lesions. Expert Rev Med Dev 2013;10:707−716. [PMC][10.1586/17434440.2013.848165] [24164662]
19. Onuma Y, Girasis C, Aben JP, et al. A novel dedicated 3-dimensional quantitative coronary analysis methodology for bifurcation lesions. EuroIntervention 2011;7:629–635. [PMC][10.4244/EIJV7I5A100] [21930468]
20. Galassi AR, Tomasello SD, Capodanno D, et al. A novel 3D reconstruction system for the assessment of bifurcation lesions treated by the mini-crush technique. J Interv Cardiol 2010;23:46–53. [PMC][10.1111/j.1540-8183.2009.00512.x] [20002960]
21. Dvir D, Assali A, Lev EI, Ben-Dor I, Battler A, Kornowski R. Percutaneous interventions in unprotected left main lesions: Novel three-dimensional imaging and quantitative analysis before and after intervention. Cardiovasc Revasc Med 2010;11:236–240.
22. Ramcharitar S, Daeman J, Patterson M, et al. First direct in vivo comparison of two commercially available three-dimensional quantitative coronary angiography systems. Catheter Cardiovasc Interv 2008;71:44–50.
23. Girasis C, Schuurbiers JC, Onuma Y, et al. Advances in two-dimensional quantitative coronary angiographic assessment of bifurcation lesions: Improved small lumen diameter detection and automatic reference vessel diameter derivation. EuroIntervention 2012;7:1326–1335.
24. Meerkin D, Marom H, Cohen-Biton O, Einav S. Three-dimensional vessel analyses provide more accurate length estimations than the gold standard QCA. J Interv Cardiol 2010;23:152–159.
25. Tsuchida K, van der Giessen WJ, Patterson M, et al. In vivo validation of a novel three-dimensional quantitative coronary angiography system (CardiOp-B): Comparison with a conventional two-dimensional system (CAAS II) and with special reference to optical coherence tomography. EuroIntervention 2007;3:100–108.
26. Bruining N, Tanimoto S, Otsuka M, et al. Quantitative multimodality imaging analysis of a bioabsorbable poly-l-lactic acid stent design in the acute phase: A comparison between 2- and 3D-QCA, QCU and QMSCT-CA. EuroIntervention 2008;4:285–291.
27. Yong AS, Ng AC, Brieger D, Lowe HC, Ng MK, Kritharides L. Three-dimensional and two-dimensional quantitative coronary angiography, and their prediction of reduced fractional flow reserve. Eur Heart J 2011;32:345–353. [PMC][10.1093/eurheartj/ehq259] [20705695]
28. Girasis C, Serruys PW, Onuma Y, et al. 3-Dimensional bifurcation angle analysis in patients with left main disease: A substudy of the SYNTAX trial (SYNergy Between Percutaneous Coronary Intervention with TAXus and Cardiac Surgery). JACC Cardiovasc Interv 2010;3:41–48.
29. Girasis C, Farooq V, Diletti R, et al. Impact of 3-dimensional bifurcation angle on 5-year outcome of patients after percutaneous coronary intervention for left main coronary artery disease: A substudy of the SYNTAX trial (synergy between percutaneous coronary intervention with taxus and cardiac surgery). JACC Cardiovasc Interv 2013;6:1250–1260.
30. Sarno G, Garg S, Onuma Y, et al. Bifurcation lesions: Functional assessment by fractional flow reserve vs. anatomical assessment using conventional and dedicated bifurcation quantitative coronary angiogram. Catheter Cardiovasc Interv 2010;76:817–823.

Chapter 4

Long Term Assessment of Bioresorbable Scaffolds

4.1 Echogenicity as a surrogate for Bioresorbable Scaffolds degradation

Echogenicity as a surrogate for bioresorbable everolimus-eluting scaffold degradation: analysis at 1-, 3-, 6-, 12- 18, 24-, 30-, 36- and 42-month follow-up in a porcine model.

Int J Cardiovasc Imaging. 2015 Jan 28.
[Original research paper, IF 2.32]

Campos CM, **Ishibashi Y**, Eggermont J, Nakatani S, Cho YK, Dijkstra J, Reiber JH, Sheehy A, Lane J, Kamberi M, Rapoza R, Perkins L, Garcia-Garcia HM, Onuma Y, Serruys PW.

Echogenicity as a surrogate for bioresorbable everolimus-eluting scaffold degradation: analysis at 1-, 3-, 6-, 12- 18, 24-, 30-, 36- and 42-month follow-up in a porcine model

Carlos M. Campos · Yuki Ishibashi · Jeroen Eggermont · Shimpei Nakatani · Yun Kyeong Cho · Jouke Dijkstra · Johan H. C. Reiber · Alexander Sheehy · Jennifer Lane · Marika Kamberi · Richard Rapoza · Laura Perkins · Hector M. Garcia-Garcia · Yoshinobu Onuma · Patrick W. Serruys

Received: 27 November 2014 / Accepted: 10 January 2015 / Published online: 28 January 2015

Abstract The objective of the study is to validate intravascular quantitative echogenicity as a surrogate for molecular weight assessment of poly-l-lactide-acid (PLLA) bioresorbable scaffold (Absorb BVS, Abbott Vascular, Santa Clara, California). We analyzed at 9 time points (from 1- to 42-month follow-up) a population of 40 pigs that received 97 Absorb scaffolds. The treated regions were analyzed by echogenicity using adventitia as reference, and were categorized as more (hyperechogenic or upperechogenic) or less bright (hypoechogenic) than the reference. The volumes of echogenicity categories were correlated with the measurements of molecular weight (Mw) by gel permeation chromatography. Scaffold struts appeared as high echogenic structures. The quantification of grey level intensity in the scaffold-vessel compartment had strong correlation with the scaffold Mw: hyperechogenicity (correlation coefficient = 0.75; $P < 0.01$), upperechogenicity (correlation coefficient = 0.63; $P < 0.01$) and hyper + upperechogenicity (correlation coefficient = 0.78; $P < 0.01$). In the linear regression, the R^2 for high echogenicity and Mw was 0.57 for the combination of hyper and upper echogenicity. IVUS high intensity grey level quantification is correlated to Absorb BVS residual molecular weight and can be used as a surrogate for the monitoring of the degradation of semi-crystalline polymers scaffolds.

Keywords Absorb · Bioresorbable vascular scaffold · Degradation · Echogenicity · IVUS · Porcine

Abbreviations

IVUS	Intravascular ultrasound
BRS	Bioresorbable scaffolds
PLLA	Poly-l-lactide-acid
PDLLA	Poly-D, L-lactide
Mw	Molecular weight
Absorb	Poly-l-lactide-acid everolimus eluting
BVS	bioresorbable scaffold
CAD	Coronary artery disease

Impact on daily practice

Changes in bioresorbable vascular scaffolds (BRS), design and compositions may affect their degradation and loss of

Electronic supplementary material The online version of this article (doi:10.1007/s10554-015-0591-4) contains supplementary material, which is available to authorized users.

C. M. Campos · Y. Ishibashi · S. Nakatani · Y. K. Cho · H. M. Garcia-Garcia · Y. Onuma · P. W. Serruys (✉)
Department of Interventional Cardiology, Thoraxcenter, Erasmus University Medical Centre, s-Gravendijkwal 230, 3015 CE Rotterdam, The Netherlands
e-mail: p.w.j.c.serruys@erasmusmc.nl

C. M. Campos
Heart Institute (InCor), University of São Paulo Medical School, Sao Paulo, Brazil

J. Eggermont · J. Dijkstra · J. H. C. Reiber
Leiden University Medical Center, Leiden, The Netherlands

A. Sheehy · J. Lane · M. Kamberi · R. Rapoza · L. Perkins
Abbott Vascular, Santa Clara, CA, USA

H. M. Garcia-Garcia
Cardialysis, Rotterdam, The Netherlands

P. W. Serruys
International Centre for Circulatory Health, NHLI, Imperial College London, London, UK

biomechanical characteristics (with the risk of late recoil) and may be associated with a second wave of arterial wall inflammation. Therefore, studying the BRS degradation is crucial to fully understand this technology. The present work validates echogenicity as a surrogate for polylactide scaffold degradation.

Introduction

Bioresorbable vascular scaffolds (BRS) are a novel approach to the interventional treatment of coronary artery disease (CAD), providing short-term vascular scaffolding combined with drug-delivery capability. They may offer potential advantages compared to metallic drug-eluting stents (e.g. adaptive remodeling, restoration of vasomotion and late luminal enlargement). The so called 4th revolution in coronary artery disease revascularization steered extensive scientific research in BRS developments [1–3].

It has been shown that the designs and materials of BRS platforms—either metallic or polymeric—influence the resorption process [3–5]. Considering the variety of possible platforms, it is necessary to establish tools capable of monitoring the degradation process and its correlated mechanical characteristics.

Intravascular ultrasound-derived parameters have shown to be useful to assess the BRS resorption of metallic and polymeric scaffolds in humans [6–8]. One of the most studied intravascular ultrasound (IVUS) techniques to evaluate the resorption process is called differential echogenicity [8, 9]. This method consists in an automated and quantitative three-dimensional analysis of coronary tissue components scored for echogenicity using as reference the mean level of the adventitia brightness [9] where scaffold struts appear as bright hyperechogenic structures. In clinical studies, a continuous decrease of echogenicity over time has been shown in regions treated with BRS, being putatively correlated to BRS degradation [7, 8]. However, in serial human assessments, changes in the adventitia and plaque-media compartment of the treated regions during the follow-up period could possibly affect these interpretations [10–14].

The objectives of the current study were: (1) to describe a novel method of echogenicity for tissue analysis; (2) to evaluate its reproducibility; and (3) to assess its aptitude to assess the BRS degradation process through a direct correlation with the molecular weight (Mw) in a preclinical model using a drug-eluting poly-l-lactide-acid (PLLA) bioresorbable scaffold (Absorb BVS, Abbott Vascular, Santa Clara, California).

Methods

Study devices

The device used in the present preclinical study is the same used in Cohort B of the ABSORB clinical trial [15, 16]. Absorb is a balloon-expandable BRS that consists of a polymer backbone of Poly (L-lactide) (PLLA) coated with a thin layer of a 1:1 mixture of Poly-D, L-lactide (PDLLA) polymer with the antiproliferative drug everolimus to form an amorphous drug-eluting coating matrix containing 100 μg of everolimus/cm^2 of scaffold [17].

Experimental model

For validation purposes, we analyzed non-atherosclerotic Yorkshire-Landrace swine which had been implanted with Absorb BVS via femoral access according to published procedures [18]. Absorb sizes were matched to the vessel size at a target balloon-to-artery ratio of 1.0–1.1 (10 % overstretch). Each animal received a single Absorb (3.0 × 18 mm for 1-, 3-, and 6-month and 3.0x12 mm for 12- to 42-month) in 2 or 3 main coronary arteries. Forty pigs (98 arteries) underwent IVUS acquisition and were then euthanized at 1-month (n = 12 scaffolds), 3-(n = 12), 6-(n = 14), 12-(n = 12), 18-(n = 12), 24-(n = 12), 30-(n = 8), 36-(n = 8) or 42-months (n = 8). Each scaffold had quantification of polymer degradation by gel permeation chromatography (GPC). Experimental studies received protocol approval from the institutional animal care and use committee and were conducted in accordance with American Heart Association guidelines for pre-clinical research and the Guide for the Care and Use of Laboratory Animals (National Institutes of Health 2010).

Gel permeation chromatography (GPC)

A previously reported GPC method, with a slightly modified sample extraction/purification process, was employed to investigate the degradation of polymer over time by evaluating the number-average molecular weight (Mn) of polymer in the Absorb [19]. In the present method, the extraction and purification of the polymer was repeated up to five times until the polymer was fully extracted from the tissue (i.e., the polymer signal in the last extract below the quantitation limit of 0.3 mg/mL). The samples were analyzed prior at 1-, 3-, 6-, 12-, 18-, 24-, 30-, 36- and 42-months after implantation.

IVUS acquisition and analysis

All IVUS runs were acquired with 40 MHz mechanical systems, using Galaxy V2.02 (Boston Scientific, MA,

USA) at 1-, 3-, 6- and 12-month follow-ups and iLab at 18-, 24-, 30-, 36- and 42-month (Boston Scientific, MA, USA). We used motorized pullback of 0.5 mm/s with a frame rate of 30 frames/second. The regions of interest were restrict to the scaffolded areas, identified by the first and the last cross-sectional IVUS frame in which scaffold struts could be identified and/or where the proximal or distal metallic markers could be identified. Vessel, scaffold and lumen contours were delimited every 0.5 mm blind to molecular weight results. We analysed four compartments by IVUS: the luminal, scaffold, vessel and the neointimal volume (vessel volume-lumen volume). The scaffold was delineated semiautomatically at the luminal leading edge of the struts and the lumen was delineated at the inner detectable tissue (Fig. 1).

To evaluate inter-observer reproducibility, 2 readers (C.C. and Y.I.) independently analyzed 30 segments randomly selected from the total number of the investigated segments. To determine intra-observer reproducibility, one reader (C.C.) analyzed these segments twice, with the second reading occurring 3 months later. The inter- and intra-observer reproducibility were good according to the conventional norms [20] (hyperechogenicity inter-observer interclass correlation coefficient [ICC] = 0.80, intra-observer ICC = 0.95; hypoechogenicity: inter-observer ICC = 0.78, intra-observer ICC = 0.97; upperechogenicity: inter-observer ICC = 0.92, intra-observer ICC = 0.97) (Supplementary material).

Automatic quantitative echogenicity analysis

The principle of echogenicity has been previously described elsewhere [9, 21, 22]. Echogenicity aims to classify the vessel wall components located between the luminal boundary and the external elastic membrane (EEM) into categories based on their grey-level intensity in B-mode IVUS images rather than based on radiofrequency ultrasound signal analysis [23–26] (Fig. 1). Here we quantified 5 tissue types: hypoechogenic, hyperechogenic, calcified, upperechogenic and unknown.

Comparison with the adventitia allows for normalization with respect to transducer variability, gain settings and across populations [21]. However, in the analysis of atherosclerotic tissue, the adventitia can be partially obscured or darkened as a result of the guide-wire shadowing or the presence of dense tissue (e.g. calcium) which reduces the average grey-level values of the adventitia. Therefore, these parts need to be excluded from the reference adventitial area. To determine the reference adventitia area in each frame, the full adventitial area located just outside the EEM is first determined based on a minimum (0.01 mm) and maximum (0.21 mm) distance from the EEM contour (Fig. 1). To remove the low echogenic parts of the adventitia an adaptive threshold value for the entire adventitia area is determined based on Otsu's method [27]. Otsu's method is a classic automatic non-parametric threshold selection method which maximizes the between-class variance. Next, the adventitial area is divided into 2-degree wide sectors. If more than half of the pixels inside of a sector is below the adaptive threshold, the sector is excluded from the reference adventitia area. Finally, the histograms of the reference adventitial areas of the individual frames are combined into a global adventitia grey-level intensity histogram and the median value is computed as a threshold. Cross-section pixels with an intensity lower than the median value are classified as hypoechogenic, pixels with an intensity higher than the median value threshold are classified as hyperechogenic.

Calcified plaque is typically identified in B-mode IVUS images as a highly echogenic area creating an acoustic shadow [21]. To determine the high-intensity grey-level threshold for highly echogenic components we use the adaptive threshold selection method described in [28]. First Otsu's method is applied to the entire grey-level histogram of an image resulting in an optimal threshold value. In the next 2 iterations, Otsu's method is applied to the histogram of all intensities above the threshold found in the previous step. Next, we apply an in-house developed acoustic shadow detection algorithm. Highly echogenic areas with a grey-level intensity higher than the high-intensity threshold but without acoustic shadow behind them are classified as upperechogenic, while highly echogenic areas with acoustic shadow are classified as calcified and the shadow itself is classified as unknown. The entire method has been implemented and tested in QCU-CMS-Research v4.69 (research version of QIvus, developed by the Leiden University Medical Center) [29].

Data analysis

Continuous variables are presented as mean ± SD or medians (interquartile range). The ANOVA test was used to compare continuous variables. As we had different scaffold lengths we normalized all measurements by the mean length for all pigs as described previously [30]. This adjusts for differing segment lengths across animals, thereby providing equal weighting of each individual in the calculation of echogenicity volumes. The residual scaffold molecular weight by GPC was compared to the echogenicity findings and the correlation coefficient was used as a measure of the degree of relationship (Pearson's correlation coefficient). A linear regression was used to evaluate if hyper and/or upperechogenicity were able to predict the residual molecular weight. A

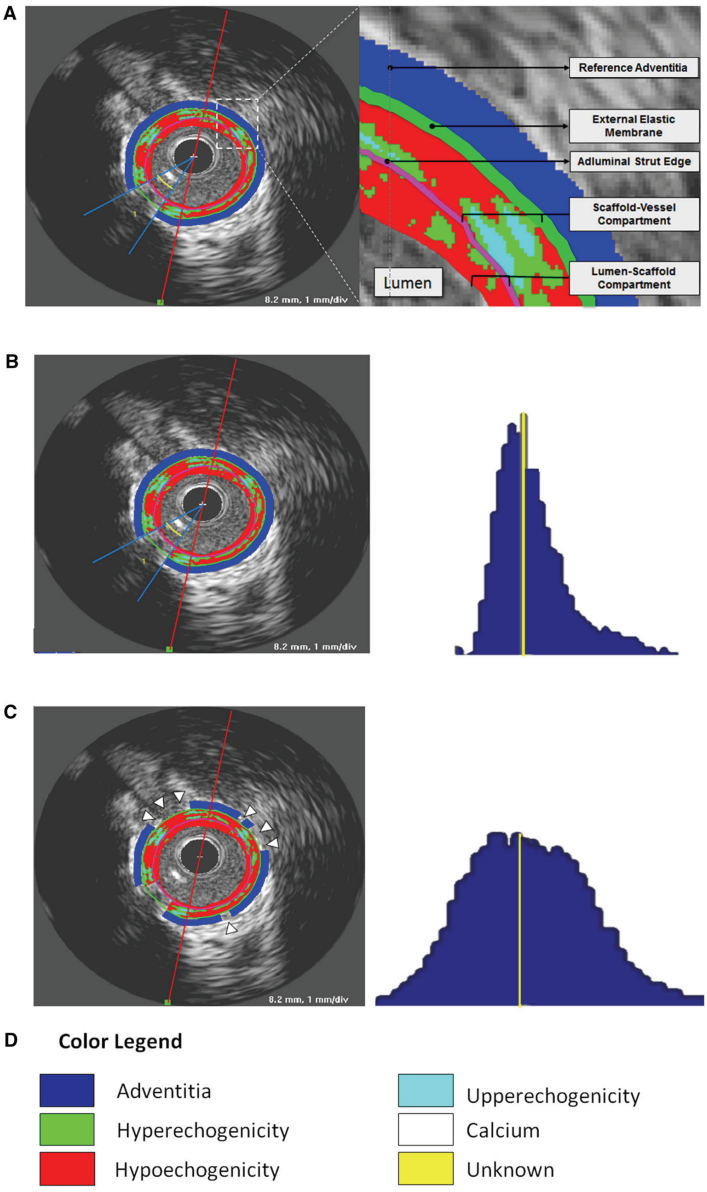

Fig. 1 Differential echogenicity methodology. **a** The first step was to determine the lumen-scaffold and scaffold-vessel compartments by defining the vessel, lumen and luminal scaffold contours in every 0.5 mm. After guidewire masking, the software identifies the adventitia as a ring between 0.01 and 0.21 mm outside vessel contours. **b** However, if the software uses as reference the whole layer around the vessel contour, it will include low intensity structures (e.g., pericardium, side branches, low attenuated tissues, etc.) resulting in a histogram with a non-normal distribution (*right panel*). **c** The present software detects automatically high signal adventitia as reference, excluding low intensity structures (*arrow heads*). The *right panel* shows that the combination of high signal adventitia in all frames obtains a bell shaped normally distributed histogram. The yellow line represents the referential adventitial median value. **d** The color legend of each echogenicity classification is provided. As we used a non-atherosclerotic porcine model there was no calcification and unknown tissue. Nevertheless, the present software is able to detect theses tissues

hierarchical cluster analysis using Ward's method (Squared Euclidean distance) was applied for hyper + upperechogenicity and hypoechogenicity volumes. The differences were regarded significant when $P < 0.05$ (two-tailed). SPSS version 21.0 (SPSS Inc., Chicago, Illinois) was used for all statistical analyses.

Results

The main grey scale IVUS volumetric findings are shown in Fig. 2 and the comparisons between each group are given in the supplementary material (Tables 2-5). The mean scaffold length was 16.5 mm. Compared with 1-month follow-up, the vessel, scaffold and lumen volumes had a trend to be larger after 18-month follow-up. These three aforementioned volumes were significantly larger at 36- and 42-month. Additionally, the neointima had the biggest volume at 1-month follow-up, being similar among groups thereafter (Fig. 3).

Differential echogenicity and molecular weight

Table 1 summarizes the main findings on differential echogenicity and mean Mw at each time point. The highest total hypoechogenicity volume was found at 1-month follow-up, the time point with also the highest neointimal hyperplasia as aforementioned. The lumen-scaffold compartment had an increase in hyper + upperechogenic volumes up to 12-month and subsequently a decrease until 42-month. Using the as reference the 1-month group, the hyper + upperechogenic decreased significantly in the scaffold vessel compartment after 12 months (supplementary material).

The GPC results indicated a continuous decrease in molecular weight over time. The rate of reduction was slower during the first 6-months of scaffold implantation followed by a more rapid decline thereafter, being fully resorbed 36-months after implantation (Fig. 2).

To validate the scaffold degradation by echogenicity we took into consideration the hyper- and upperechogenicity in

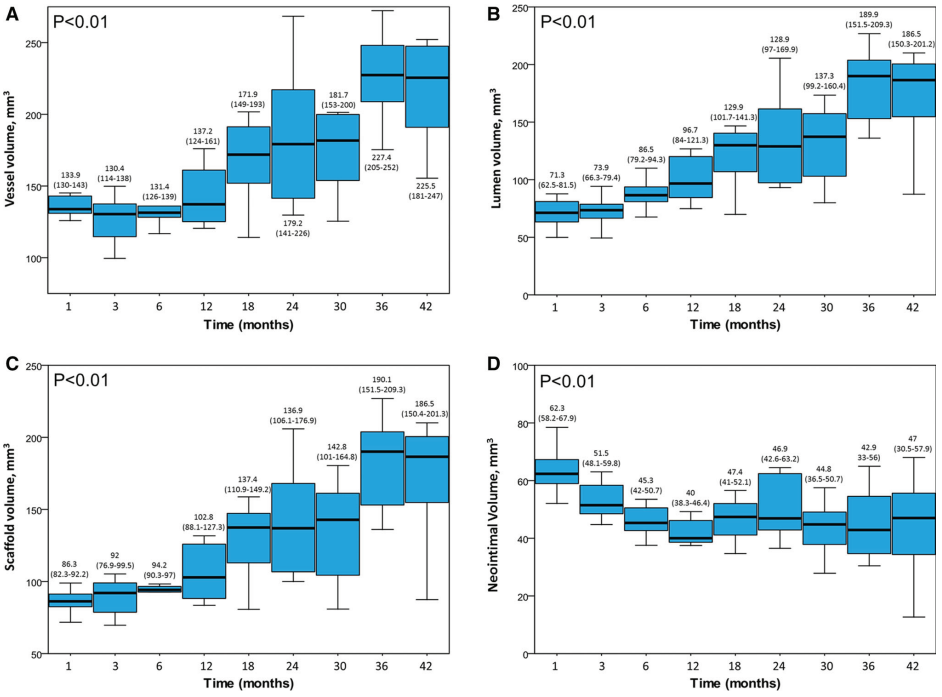

Fig. 2 Grey Scale intravascular ultrasound volumetric findings at different time points. **a** Vessel volume; **b** Lumen Volume; **c** Scaffold Volume and **d** Neointimal Volume. Values are median and interquartile range

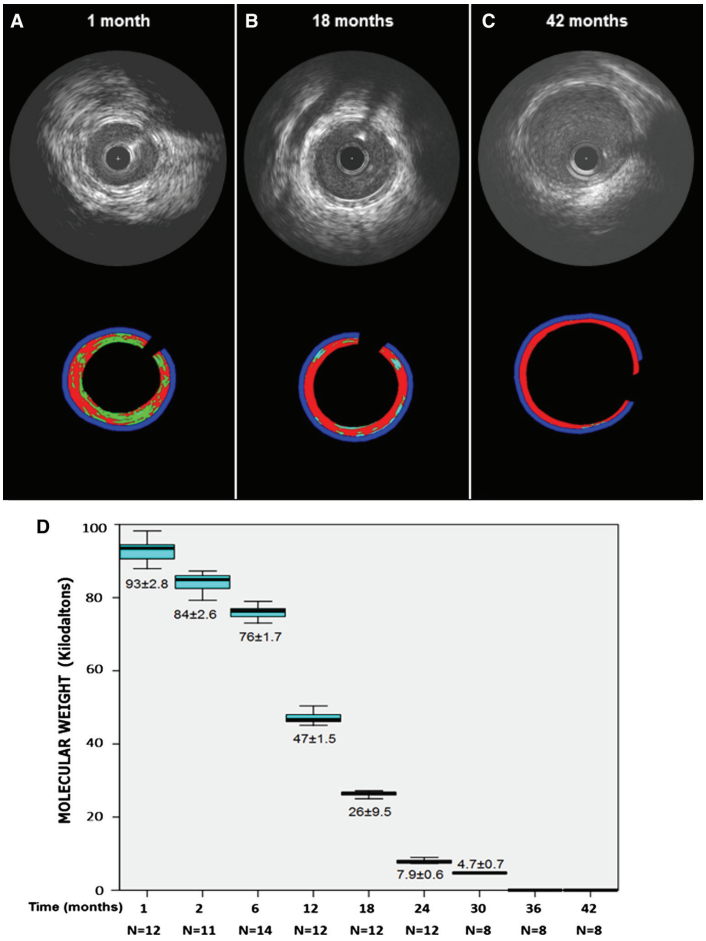

Fig. 3 IVUS echogenicity analysis at 1- (**a**), 18- (**b**) and 42-month (**c**). The high echogenic (including hyper = *light green* and upper = *light blue*) parameters decrease over time. **d** Gel permeation chromatography (GPC) for the assessment of degradation of Absorb showing the in vivo degradation of polymer of Absorb over time

the scaffold-vessel compartment (Fig. 1). As shown in Table 1, the earlier IVUS were more likely to present higher grey-level intensity (hyper + upperechogenicity). The scaffold-vessel hyperechogenicity (Pearson correlation coefficient = 0.75; $P < 0.01$), upperechogenicity (Pearson correlation coefficient = 0.63; $P < 0.01$) and hyper + upperechogenicity (Pearson correlation coefficient = 0.78; $P < 0.01$) had strong correlation with the scaffold molecular weight. As shown in Fig. 4, in linear regression, the best correlation found in linear regression model for molecular weight was scaffold-vessel hyper + upperechogenicity (R squared = 0.57; $P < 0.01$); i.e., all grey-level intensity higher than median adventitia in the scaffold-vessel compartment should be considered for monitoring the degradation process of this semi-crystalline polymers scaffold. Post-Hoc comparisons between each group are given in the supplementary material (Tables 6-8).

Additionally, a cluster analysis was run for scaffold-vessel hyper + upperechogenicity and hypoechogenicity. It produced five clusters, among which the variables were significantly different in the main (Fig. 5). The comparison among clusters of hyper + upperechogenicity showed a clear positive association scaffold-vessel hyper + upperechogenicity and molecular weight (Fig. 5).

Table 1 Differential echogenicity findings and polymer molecular weight by gel permeation chromatography

	1 Month (n = 12)	3 Months (n = 12)	6 Months (n = 14)	12 Months (n = 12)	18 Months (n = 12)	24 Months (n = 12)	30 Months (n = 8)	36 Months (n = 8)	42 Months (n = 8)	*P* value for overall comparison
Total hypoechogenicity Volume (mm^3)	49.3 ± 6.9	34.7 ± 6.8	31.4 ± 5.5	28.7 ± 4.5	33.3 ± 6.2	42.2 ± 8	28.4 ± 7	38.6 ± 12.2	37.6 ± 14.3	<0.01
% Total hypoechogenicity	79.4 ± 4.9	68.3 ± 7.8	70.3 ± 6.5	71.6 ± 6.7	80.5 ± 5.0	86.8 ± 5.4	78.1 ± 6.1	89.7 ± 4.3	92.0 ± 3.4	<0.01
Total hyperechogenicity volume (mm^3)	8.5 ± 2.7	8.7 ± 4	6.6 ± 1	6.5 ± 2.8	4.8 ± 1	3.9 ± 1.5	4.3 ± 1.3	2.8 ± 1.2	2.2 ± 1.1	<0.01
% Total Hyperechogenicity	13.6 ± 3.6	17.2 ± 7.0	15.5 ± 2.7	16.1 ± 6.1	11.8 ± 2.4	8.0 ± 2.6	12.0 ± 2.9	6.7 ± 2.5	5.3 ± 1.9	<0.01
Total upperechogenicity volume (mm^3)	6.3 ± 3.5	13.7 ± 5	12.9 ± 3.6	14.1 ± 7.1	9.5 ± 5.5	6.1 ± 3.6	11.3 ± 4.3	3.9 ± 2.1	2.9 ± 1.9	<0.01
% Total upperechogenicity	7.0 ± 3.9	14.5 ± 5.5	14.1 ± 5.3	12.3 ± 5.3	7.7 ± 4.0	5.2 ± 2.9	9.9 ± 3.4	3.7 ± 1.9	2.8 ± 1.6	<0.01
Total hyper and upperechogenicity volumes (mm^3)	14.9 ± 4.5	22.4 ± 5.2	19.6 ± 4.4	20.6 ± 6.8	14.4 ± 6.1	10 ± 4.9	15.6 ± 5.3	6.7 ± 3.16	5.1 ± 3	<0.01
% Total hyper and upperechogenicity	20.6 ± 4.9	31.7 ± 7.8	29.7 ± 6.5	28.4 ± 6.7	19.5 ± 5.1	13.2 ± 5.4	21.9 ± 6.1	10.3 ± 4.3	8.1 ± 3.4	<0.01
Lumen-scaffold hypoechogenicity Volume (mm^3)	13.6 ± 5.5	13.4 ± 4.3	7.7 ± 7.5	3.9 ± 1.9	6.7 ± 2.5	7.8 ± 4.1	2.9 ± 2	0 ± 0.1	0 ± 0.1	<0.01
% Lumen-scaffold hypoechogenicity	91.9 ± 4.3	88.8 ± 4.5	88.4 ± 4.1	80.5 ± 11.6	89.3 ± 3.7	92.3 ± 2.9	86.1 ± 4.5	22.0 ± 41.3	44.5 ± 48.3	<0.01
Lumen-scaffold hyperechogenicity volume (mm^3)	1.25 ± 0.9	1.5 ± 0.8	1.2 ± 1.8	0.8 ± 0.5	0.4 ± 0.2	0.3 ± 0.2	0.3 ± 0.2	0	0	<0.01
% Lumen-scaffold hyperechogenicity	8.1 ± 4.4	10.7 ± 4.7	11.0 ± 3.8	19.0 ± 11.6	6.5 ± 3.0	4.0 ± 2.0	9.9 ± 3.5	1.8 ± 5.0	3.7 ± 8.7	<0.01
Lumen-scaffold upperechogenicity volume (mm^3)	1.9 ± 1.3	6.6 ± 2.8	6.6 ± 2.8	9.3 ± 5.1	6.6 ± 3.9	3.8 ± 2.2	7.7 ± 3.22	2.4 ± 1.4	1.8 ± 1.3	<0.01
% Lumen-scaffold upperechogenicity	0.1 ± 0.1	0.5 ± 0.7	0.5 ± 0.7	0.4 ± 0.5	4.2 ± 0.9	3.1 ± 1.2	4.0 ± 1.7	1.2 ± 3.4	1.8 ± 51	<0.01
Lumen-scaffold hyper and upperechogenicity Volumes (mm^3)	3.2 ± 1.5	8.1 ± 3.1	7.9 ± 2.6	10.1 ± 5.4	7.1 ± 4	4.1 ± 2.4	8 ± 3.3	2.4 ± 1.4	1.8 ± 1.3	<0.01
% Lumen-scaffold hyper and upperechogenicity	8.1 ± 4.3	11.2 ± 4.5	11.6 ± 4.1	19.5 ± 11.6	10.7 ± 37	7.1 ± 2.9	13.9 ± 4.5	3.0 ± 8.4	5.5 ± 10.3	<0.01
Scaffold-vessel hypoechogenicity volume (mm^3)	35.7 ± 4	21.3 ± 5.1	23.8 ± 9.3	24.9 ± 4.6	26.6 ± 4.9	34.4 ± 7.9	25.5 ± 7.9	38.5 ± 12.2	37.7 ± 14.3	<0.01
% Scaffold-vessel hypoechogenicity	75.5 ± 6.0	59.6 ± 8.6	66.9 ± 8.3	70.1 ± 6.9	78.4 ± 6.2	85.3 ± 6.3	77.0 ± 6.3	89.7 ± 4.3	91.9 ± 3.4	<0.01
Scaffold-vessel hyperechogenicity volume (mm^3)	7.3 ± 2	7.2 ± 4.2	5.4 ± 2.3	5.7 ± 2.5	4.4 ± 0.9	3.5 ± 1.3	4 ± 1.4	2.8 ± 1.1	2.2 ± 1.2	<0.01
% Scaffold-vessel hyperechogenicity	15.4 ± 4.1	19.5 ± 7.3	16.3 ± 2.9	15.9 ± 5.7	13.1 ± 2.8	8.9 ± 3.0	12.3 ± 3.0	6.7 ± 2.5	5.3 ± 1.9	<0.01
Scaffold-vessel upperechogenicity volume (mm^3)	4.4 ± 2.6	7.1 ± 2.5	6.3 ± 1.8	4.8 ± 2.1	2.9 ± 1.7	2.3 ± 1.4	3.5 ± 1.5	1.5 ± 0.8	1.1 ± 0.8	<0.01
% Scaffold-vessel upperechogenicity	9.2 ± 5.3	20.8 ± 8.3	16.7 ± 6.7	14.4 ± 6.4	8.5 ± 4.9	5.8 ± 3.5	10.7 ± 3.7	3.7 ± 1.9	2.8 ± 1.6	<0.01

Table 1 continued

	1 Month (n = 12)	3 Months (n = 12)	6 Months (n = 14)	12 Months (n = 12)	18 Months (n = 12)	24 Months (n = 12)	30 Months (n = 8)	36 Months (n = 8)	42 Months (n = 8)	*P* value for overall comparison
Scaffold-vessel hyper and upperechogenicity volumes (mm^3)	11.7 ± 3.4	14.3 ± 3.8	11.7 ± 3.8	10.5 ± 2.4	7.3 ± 2.3	5.8 ± 2.7	7.5 ± 2.7	4.3 ± 1.9	3.2 ± 1.9	<0.01
% Scaffold-vessel hyper and Upperechogenicity	24.6 ± 6.0	40.4 ± 8.6	33.1 ± 8.3	29.9 ± 6.9	21.7 ± 6.2	14.7 ± 6.3	23.0 ± 6.3	10.4 ± 4.3	8.1 ± 3.4	<0.01
Molecular weight (kDa)	92.9 ± 2.8	84.2 ± 2.5	76 ± 1.7	47.1 ± 1.5	26.2 ± 0.9	7.9 ± 0.6	4.7 ± 73.9	0	0	<0.01

Discussion

In the present study, using IVUS grey scale derived parameters we attempted to assess the degradation process of the Absorb poly-L-lactide bioresorbable everolimus-eluting scaffold at multiple time points in a porcine model. The major findings of this study can be summarized as follows: (1) hyperechogenic and upperechogenic thresholds had strong and positive correlations with the scaffold molecular weight assessment; (2) the combination of hyper and upperechogenicity could be used as a surrogate for the chromatographic assessment of scaffold molecular weight and (3) echogenicity demonstrated good inter- and intra-observer reproducibility (Supplementary Material).

The present manuscript describes a new software designed to assess the differential echogenicity and, for the first time, ascertained the correlation between IVUS grey scale intensities and quantitative assessment of Mw by GPC. The first novelty is that it was not necessary to use ECG gating and therefore, it is not needed a dedicated IVUS console or post-processing correction. The robustness of this method and the aforementioned good reproducibility demonstrate, for the first time, good correlation of echogenicity with the degradation of the scaffold without being mandatory correction for motion artifacts [30].

Image resolution can be defined as the capability of making distinguishable the individual parts of an object. Therefore, the use of 40 MHz IVUS catheter in the present study has potential to be more precise to detect scaffold degradation than the previous methodology with the 20 MHz ultrasound [7, 31]. Ultrasound at a center frequency of 10 MHz has demonstrated to detect decline in the acoustic impedance of PLA when molecular weight varied from 60 to 24 kDa, but further decrease in molecular weight to 15 kDa did not result in discernible change [32]. In the present study, working with the higher resolution of the 40 MHz IVUS catheter, we were able to detect acoustic differences in 150 m thick samples degrading from $\sim$100 to <4 kDa.

The use of ultrasound to monitor the degradation process of polymers has been initially proposed with a wave pulse-echo method in an in vitro essay [31]. Wu succeeded to monitor by ultrasound the degradation process of three biodegradable polymers: poly(glycolic acid) (PGA), poly(L-lactic acid) (PLLA) and 50:50 poly(D, L-lactide-co-glycolide) (PDLLG) [33]. Another IVUS based approach to detect the resorption process in human is virtual histology [6]. The spectral analysis of the raw backscattered ultrasound misrepresents polymeric struts as dense calcium (DC) and necrotic core (NC). As these parameters are shown to decrease over time after implantation, they have been correlated putatively with resorption [6, 16, 34, 35].

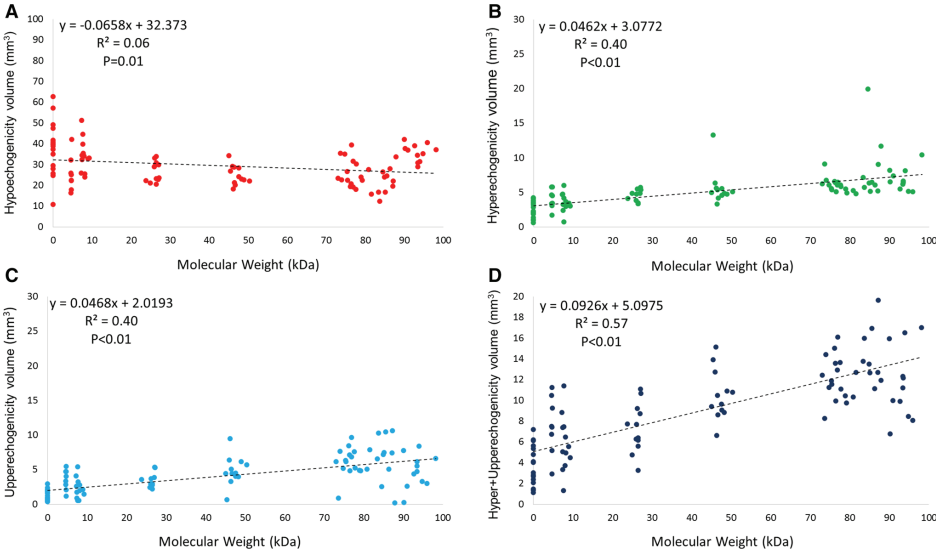

Fig. 4 Linear regressions between molecular weight and echogenicity derived parameters in the scaffold-vessel compartment

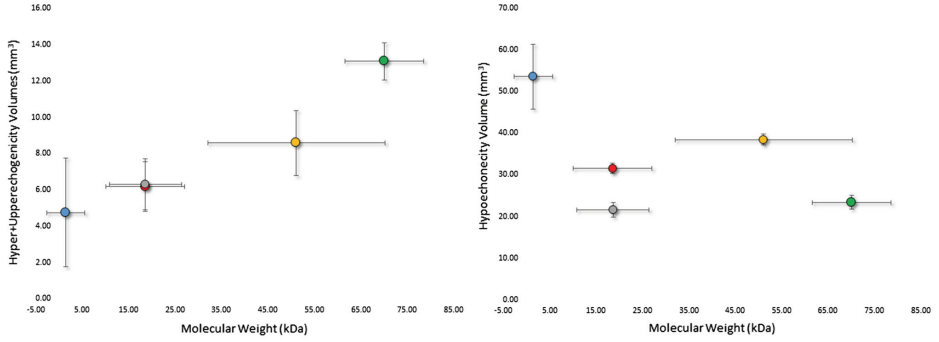

Cluster	1 (n=22)	2 (n=34)	3 (n=19)	4 (n=18)	5 (n=5)	P
Parameter						
Hyper+Upperechogenicity Volume, (mm³)	4.75±2.41	6.19±2.93	6.31±2.75	8.59±4.02	13.08±2.92	<0.01
Hypoechogenicity Volume, (mm³)	53.58±6.31	31.56±2.46	21.56±3.60	38.43±2.97	23.37±4.75	<0.01
Molecular Weight, (kDa)	1.48±3.30	18.54±17.09	18.63±17.09	51.13±43.10	70.08±24.42	<0.01

Fig. 5 A hierarchical cluster analysis labeled by animal was run for scaffold-vessel hyper + upperechogenicity and hypoechogenicity. Cluster 2 and 3 had similar hyper + upperechogenicity but statistically significant greater hypoechogenicity volumes in the cluster 2. Cluster 3 and 5 had similar hypoechogenicity but markedly higher hyper + upperechogenicity volumes in cluster 5. There was a clear positive association between scaffold-vessel hyper + upperechogenicity and molecular weight. The sample sizes are number of scaffolds included in each pig cluster. The values are mean ± standard deviation and the errors bars are 95 % confidence interval

Previously, echogenicity has been used to assess paired serial acoustic properties of coronary plaques in BRS-treated segments in the clinical setting [7, 8, 35]. It has been shown that these segments had an increase in hyperechogenic tissue after implantation which decreased over time [7, 8, 35]. The aforementioned methodology succeeds to document the progressive decrease of high intensity grey level tissues in both metallic and polymeric BRS [8, 35].

However, until now, the link between echogenicity and the degradation process has been hypothetically assumed. The pending question was whether temporal plaque changes could interfere with the multistage degradation of the polymer and confound the echogenicity analysis. It has been shown that coronary atherosclerosis is a dynamic phenomenon and numerous factors can influence the atherosclerotic changes as detected by IVUS-derived parameters. For instance, statin treatment may reduce the percentage lipid volume index over time [13] and may increase the calcified plaque component [11]. Additionally, there is a significant decrease in NC (16 %) and DC (30 %) content in coronary plaque located behind the struts of the everolimus-eluting bioresorbable vascular scaffold [36]. All the above-mentioned confounding factors might influence the acoustic properties in the lumen-vessel compartment and hinder the clinical relevance of echogenicity for BRS degradation assessment.

As we have used a porcine non-atherosclerotic model, we did not have the confounding presence of coronary artery disease, thus enabling the evaluation of Poly-L-Lactide's echogenic characteristics over time. Hyperechogenic, upperechogenenic and hyper + upperechogenic tissues had strong and positive correlations between echogenicity and the degradation process. Echogenicity is determined by the difference in acoustic impedance between two mediums, which is proportional to density and acoustic velocity. The acoustic velocity is proportional to the square root of the stiffness (bulk and shear moduli). Many factors impact the stiffness of PLA, including molecular weight, polydispersity, crystallinity, orientation of crystalline microstructure, and other environmental conditions [37]. As a result, one would expect to change the impedance of PLA as it degrades and molecular weight to have a generalized relationship to this decline.

Qualitatively, the correlation was however not perfectly linear. For instance, at 1-month the combination hyper + upper tended (without statistical significance; Table 6, supplementary material), in average, to be lower than at 3-months whereas the molecular weight had a continuous decrease in the same period. From the ultrasonic point of view, the significantly higher neointimal hyperplasia (Fig. 2) at 1-month might have affected the ultrasound penetration and therefore the echogenicity interpretation. Additionally, the scaffold-vessel hyper + upperechogenicity at 30-months was numerically comparable to that at 18-month. However, the degradation process may be influenced by individual biological factors and it has to be emphasized that these assessments were not serial. However, we showed a consistent individual positive correlation between the molecular weight and echogenicity (Figs. 4 and 5).

Limitations

Arteries used for molecular weight assessment could not be evaluated histologically. Therefore, changes in the observed echogenicity (both lumen-scaffold and scaffold-vessel) could not be related to the histologic changes over time [19, 38]. As this study has been performed in a non-atherosclerotic model, it should be acknowledged that the rate of degradation has not been confirmed in atherosclerotic coronary arteries. However, as the degradation of PLLA is a hydrolytically driven and not enzymatically driven process, it is expected that the rates would be largely equivalent.

We could not test the reproducibility of the echogenicity IVUS findings in the two different consoles. However as we worked at the same ultrasound frequency (40 MHz) and the tissue classifications were normalized by the individual adventitia grey scale intensity we could show a robust correlation between scaffold degradation and high echogenic parameters. It has been shown that the comparison with the adventitia allows for normalization with respect to transducer variability, gain settings and across populations [21].

The changes in vessel, lumen, scaffold and neointima volumes over time are in line with the serial IVUS findings in the pre-clinical model and clinical setting showing progressive increase in vessel, lumen area and scaffold area [16, 18, 39, 40]. However, in the porcine model the somatic growth can influence our findings [39]. As we do not have the IVUS at baseline we could not normalize these geometrical changes for the increase in the reference vessel size. Nevertheless, this information has been described in the literature and are beyond the main scope of the current manuscript.

Conclusion

IVUS high intensity grey level quantification is correlated to Absorb scaffold residual molecular weight assessment. Echogenicity is a reproducible technique which could be considered as a surrogate assessment of polylactide molecular weight decrease as assessed by chromatography and allows for monitoring of the degradation of semi-crystalline polymeric scaffolds.

Acknowledgments The authors acknowledge Dave Pinson and Katherine Fu (Abbott Vascular) for their technical contributions in GPC analysis. The authors also acknowledge Michael Frie and the staff of American Preclinical Services (Minneapolis, MN) for their care and attention in successful completion of the in life phase of this study. The present study was sponsored by Abbott Vascular, Santa Clara, California.

Conflict of interest Alexander Sheehy, Marika Kamberi, Richard Rapoza and Laura Perkins are full-time employee of Abbott Vascular, Santa Clara, California, and at the time of this work, Jennifer Lane also was a full-time employee of Abbott Vascular. The others authors have no conflict of interest and did not receive grants or financial support from industry or from any other source to prepare this manuscript.

References

1. Iqbal J, Onuma Y, Ormiston J, Abizaid A, Waksman R, Serruys P (2013) Bioresorbable scaffolds: rationale, current status, challenges, and future. Eur Heart J
2. Wykrzykowska JJ, Onuma Y, Serruys PW (2009) Vascular restoration therapy: the fourth revolution in interventional cardiology and the ultimate "rosy" prophecy. EuroIntervention 5 Suppl F:F7-F8
3. Garcia-Garcia HM, Serruys PW, Campos CM, Muramatsu T, Nakatani S, Zhang YJ, Onuma Y, Stone GW (2014) Assessing Bioresorbable Coronary Devices: Methods and Parameters. JACC Cardiovasc Imaging 7:1130–1148
4. Campos CM, Muramatsu T, Iqbal J, Zhang YJ, Onuma Y, Garcia-Garcia HM, Haude M, Lemos PA, Warnack B, Serruys PW (2013) Bioresorbable drug-eluting magnesium-alloy scaffold for treatment of coronary artery disease. Int J Mol Sci 14:24492–24500
5. Campos CM, Lemos PA (2014) Bioresorbable vascular scaffolds: novel devices, novel interpretations, and novel interventions strategies. Catheter Cardiovasc Interv 84:46–47
6. Garcia-Garcia HM, Gonzalo N, Pawar R, Kukreja N, Dudek D, Thuesen L, Ormiston JA, Regar E, Serruys PW (2009) Assessment of the absorption process following bioabsorbable everolimus-eluting stent implantation: temporal changes in strain values and tissue composition using intravascular ultrasound radiofrequency data analysis. A substudy of the ABSORB clinical trial. EuroIntervention 4:443–448
7. Bruining N, de Winter S, Roelandt JR, Regar E, Heller I, van Domburg RT, Hamers R, Onuma Y, Dudek D, Webster MW, Thuesen L, Ormiston JA, Cheong WF, Miquel-Hebert K, Veldhof S, Serruys PW (2010) Monitoring in vivo absorption of a drug-eluting bioabsorbable stent with intravascular ultrasound-derived parameters a feasibility study. JACC Cardiovasc Interv 3:449–456
8. Waksman R, Prati F, Bruining N, Haude M, Bose D, Kitabata H, Erne P, Verheye S, Degen H, Vermeersch P, Di Vito L, Koolen J, Erbel R (2013) Serial observation of drug-eluting absorbable metal scaffold: multi-imaging modality assessment. Circ Cardiovasc Interv 6:644–653
9. Bruining N, Verheye S, Knaapen M, Somers P, Roelandt JR, Regar E, Heller I, de Winter S, Ligthart J, Van Langenhove G, de Feijter PJ, Serruys PW, Hamers R (2007) Three-dimensional and quantitative analysis of atherosclerotic plaque composition by automated differential echogenicity. Catheter Cardiovasc Interv 70:968–978
10. Puri R, Libby P, Nissen SE, Wolski K, Ballantyne CM, Barter PJ, Chapman MJ, Erbel R, Raichlen JS, Uno K, Kataoka Y, Tuzcu EM, Nicholls SJ (2014) Long-term effects of maximally intensive statin therapy on changes in coronary atheroma composition: insights from SATURN. Eur Heart J Cardiovasc Imaging 15:380–388
11. Nozue T, Fukui K, Yamamoto S, Kunishima T, Umezawa S, Onishi Y, Tohyama S, Hibi K, Sozu T, Terashima M, Michishita I (2013) Time course of statin-induced changes in coronary atherosclerosis using intravascular ultrasound with virtual histology. Coron Artery Dis 24:481–486
12. Zhao Z, Witzenbichler B, Mintz GS, Jaster M, Choi SY, Wu X, He Y, Margolis MP, Dressler O, Cristea E, Parise H, Mehran R, Stone GW, Maehara A (2013) Dynamic nature of nonculprit coronary artery lesion morphology in STEMI: a serial IVUS analysis from the HORIZONS-AMI trial. JACC Cardiovasc Imaging 6:86–95
13. Hattori K, Ozaki Y, Ismail TF, Okumura M, Naruse H, Kan S, Ishikawa M, Kawai T, Ohta M, Kawai H, Hashimoto T, Takagi Y, Ishii J, Serruys PW, Narula J (2012) Impact of statin therapy on plaque characteristics as assessed by serial OCT, grayscale and integrated backscatter-IVUS. JACC Cardiovasc Imaging 5:169–177
14. Lee IS, Bourantas CV, Muramatsu T, Gogas BD, Heo JH, Diletti R, Farooq V, Zhang Y, Onuma Y, Serruys PW, Garcia-Garcia HM (2013) Assessment of plaque evolution in coronary bifurcations located beyond everolimus eluting scaffolds: serial intravascular ultrasound virtual histology study. Cardiovasc Ultrasound. 11:25
15. Serruys PW, Onuma Y, Dudek D, Smits PC, Koolen J, Chevalier B, de Bruyne B, Thuesen L, McClean D, van Geuns RJ, Windecker S, Whitbourn R, Meredith I, Dorange C, Veldhof S, Hebert KM, Sudhir K, Garcia-Garcia HM, Ormiston JA (2011) Evaluation of the second generation of a bioresorbable everolimus-eluting vascular scaffold for the treatment of de novo coronary artery stenosis: 12-month clinical and imaging outcomes. J Am Coll Cardiol 58:1578–1588
16. Serruys PW, Onuma Y, Garcia-Garcia HM, Muramatsu T, van Geuns RJ, de Bruyne B, Dudek D, Thuesen L, Smits PC, Chevalier B, McClean D, Koolen J, Windecker S, Whitbourn R, Meredith I, Dorange C, Veldhof S, Hebert KM, Rapoza R, Ormiston JA (2013) Dynamics of vessel wall changes following the implantation of the Absorb everolimus-eluting bioresorbable vascular scaffold: a multi-imaging modality study at 6, 12, 24 and 36 months. EuroIntervention
17. Serruys PW, Onuma Y, Ormiston JA, de Bruyne B, Regar E, Dudek D, Thuesen L, Smits PC, Chevalier B, McClean D, Koolen J, Windecker S, Whitbourn R, Meredith I, Dorange C, Veldhof S, Miquel-Hebert K, Rapoza R, Garcia-Garcia HM (2010) Evaluation of the second generation of a bioresorbable everolimus drug-eluting vascular scaffold for treatment of de novo coronary artery stenosis: six-month clinical and imaging outcomes. Circulation 122:2301–2312
18. Lane JP, Perkins LE, Sheehy AJ, Pacheco EJ, Frie MP, Lambert BJ, Rapoza RJ, Virmani R (2014) Lumen gain and restoration of pulsatility after implantation of a bioresorbable vascular scaffold in porcine coronary arteries. JACC Cardiovasc Interv
19. Onuma Y, Serruys PW, Perkins LE, Okamura T, Gonzalo N, Garcia-Garcia HM, Regar E, Kamberi M, Powers JC, Rapoza R, van Beusekom H, van der Giessen W, Virmani R (2010) Intracoronary optical coherence tomography and histology at 1 month and 2, 3, and 4 years after implantation of everolimus-eluting bioresorbable vascular scaffolds in a porcine coronary artery

model: an attempt to decipher the human optical coherence tomography images in the ABSORB trial. Circulation 122:2288–2300
20. Fleiss JL (ed) (1986) The design and analysis of clinical experiments. Wiley, New York
21. Rasheed Q, Dhawale PJ, Anderson J, Hodgson JM (1995) Intracoronary ultrasound-defined plaque composition: computer-aided plaque characterization and correlation with histologic samples obtained during directional coronary atherectomy. Am Heart J 129:631–637
22. Schartl M, Bocksch W, Koschyk DH, Voelker W, Karsch KR, Kreuzer J, Hausmann D, Beckmann S, Gross M (2001) Use of intravascular ultrasound to compare effects of different strategies of lipid-lowering therapy on plaque volume and composition in patients with coronary artery disease. Circulation 104:387–392
23. Sathyanarayana S, Carlier S, Li W, Thomas L (2009) Characterisation of atherosclerotic plaque by spectral similarity of radiofrequency intravascular ultrasound signals. EuroIntervention 5:133–139
24. Nair A, Kuban BD, Tuzcu EM, Schoenhagen P, Nissen SE, Vince DG (2002) Coronary plaque classification with intravascular ultrasound radiofrequency data analysis. Circulation 106:2200–2206
25. Nair A, Margolis MP, Kuban BD, Vince DG (2007) Automated coronary plaque characterisation with intravascular ultrasound backscatter: ex vivo validation. EuroIntervention 3:113–120
26. Okubo M, Kawasaki M, Ishihara Y, Takeyama U, Kubota T, Yamaki T, Ojio S, Nishigaki K, Takemura G, Saio M, Takami T, Minatoguchi S, Fujiwara H (2008) Development of integrated backscatter intravascular ultrasound for tissue characterization of coronary plaques. Ultrasound Med Biol 34:655–663
27. Otsu N (1979) A threshold selection method from gray-level histograms. IEEE Transactions on Systems, Man and Cybernetics 9:62–66
28. Santos Filho ESY, Tanaka A, Yoshizawa M (2008) Detection and quantification of calcifications in intravascular ultrasound images by automatic thresholding. Ultrasound Med Biol 34:160–165
29. Koning G, Dijkstra J, von Birgelen C, Tuinenburg JC, Brunette J, Tardif JC (2002) Advanced contour detection for three-dimensional intracoronary ultrasound: a validation–in vitro and in vivo. Int J Cardiovasc Imag 18:235–248
30. Mintz GS, Garcia-Garcia HM, Nicholls SJ, Weissman NJ, Bruining N, Crowe T, Tardif JC, Serruys PW (2011) Clinical expert consensus document on standards for acquisition, measurement and reporting of intravascular ultrasound regression/progression studies. EuroIntervention 6(1123–30):9
31. Wu HC, Shen FW, Hong X, Chang WV, Winet H (2003) Monitoring the degradation process of biopolymers by ultrasonic longitudinal wave pulse-echo technique. Biomaterials 24:3871–3876
32. Parker NG, Mather ML, Morgan SP, Povey MJ (2010) Longitudinal acoustic properties of poly(lactic acid) and poly(lactic-co-glycolic acid). Biomed Mater 5:055004
33. Chen S, Hong Y, Scherer SJ, Schartl M (2001) Lack of ultraviolet-light inducibility of the medakafish (Oryzias latipes) tumor suppressor gene p53. Gene 264:197–203
34. Sarno G, Onuma Y, Garcia Garcia HM, Garg S, Regar E, Thuesen L, Dudek D, Veldhof S, Dorange C, Ormiston JA, Serruys PW (2010) IVUS radiofrequency analysis in the evaluation of the polymeric struts of the bioabsorbable everolimus-eluting device during the bioabsorption process. Catheter Cardiovasc Interv 75:914–918
35. Brugaletta S, Gomez-Lara J, Serruys PW, Farooq V, van Geuns RJ, Thuesen L, Dudek D, Koolen J, Chevalier B, McClean D, Windecker S, Smits PC, de Bruyne B, Whitbourn R, Meredith I, van Domburg RT, Sihan K, de Winter S, Veldhof S, Miquel-Hebert K, Rapoza R, Garcia-Garcia HM, Ormiston JA, Bruining N (2011) Serial in vivo intravascular ultrasound-based echogenicity changes of everolimus-eluting bioresorbable vascular scaffold during the first 12 months after implantation insights from the ABSORB B trial. JACC Cardiovasc Interv 4:1281–1289
36. Brugaletta S, Gomez-Lara J, Garcia-Garcia HM, Heo JH, Farooq V, van Geuns RJ, Chevalier B, Windecker S, McClean D, Thuesen L, Whitbourn R, Meredith I, Dorange C, Veldhof S, Rapoza R, Ormiston JA, Serruys PW (2012) Analysis of 1 year virtual histology changes in coronary plaque located behind the struts of the everolimus eluting bioresorbable vascular scaffold. Int J Cardiovasc Imaging 28:1307–1314
37. Henton DE, Gruber P, Lunt J, Randall J (2005) Polylactic acid technology. CRC Press, Boca Raton
38. Vorpahl M, Finn AV, Nakano M, Virmani R (2009) The bioabsorption process: tissue and cellular mechanisms and outcomes. EuroIntervention 5(Suppl F):F28–F35
39. Strandberg E, Zeltinger J, Schulz DG, Kaluza GL (2012) Late positive remodeling and late lumen gain contribute to vascular restoration by a non-drug eluting bioresorbable scaffold: a four-year intravascular ultrasound study in normal porcine coronary arteries. Circ Cardiovasc Interv 5:39–46
40. Durand E, Sharkawi T, Leclerc G, Raveleau M, van der Leest M, Vert M, Lafont A (2013) Head-to-head comparison of a drug-free early programmed dismantling polylactic acid bioresorbable scaffold and a metallic stent in the porcine coronary artery: six-month angiography and optical coherence tomographic follow-up study. Circ Cardiovasc Interv

4.2 Light intensity after implantation of bioresorbable scaffolds

Temporal evolution of strut light intensity after implantation of bioresorbable polymeric intracoronary scaffolds in the ABSORB cohort B trial-an application of a new quantitative method based on optical coherence tomography.

Circ Journal. 2014;78(8):1873-81.
[Original research paper, IF 3.69]

Nakatani S, Onuma Y, **Ishibashi Y**, Eggermont J, Zhang YJ, Campos CM, Cho YK, Liu S, Dijkstra J, Reiber JH, Perkins L, Sheehy A, Veldhof S, Rapoza R, van Es GA, Garcia-Garcia HM, van Geuns RJ, Serruys PW; ABSORB Cohort B investigators.

Temporal Evolution of Strut Light Intensity After Implantation of Bioresorbable Polymeric Intracoronary Scaffolds in the ABSORB Cohort B Trial

– An Application of a New Quantitative Method Based on Optical Coherence Tomography –

Shimpei Nakatani, MD; Yoshinobu Onuma, MD, PhD; Yuki Ishibashi, MD, PhD; Jeroen Eggermont, PhD; Yao-Jun Zhang, MD, PhD; Carlos M. Campos, MD; Yun Kyeong Cho, MD, PhD; Shengnan Liu; Jouke Dijkstra, PhD; Johan H.C. Reiber, PhD; Laura Perkins, PhD; Alexander Sheehy, PhD; Susan Veldhof, BSc; Richard Rapoza, PhD; Gerrit-Anne van Es, PhD; Hector M. Garcia-Garcia, MD, PhD; Robert-Jan van Geuns, MD, PhD; Patrick W. Serruys, MD, PhD on behalf of the ABSORB Cohort B investigators

Background: Quantitative light intensity analysis of the strut core by optical coherence tomography (OCT) may enable assessment of changes in the light reflectivity of the bioresorbable polymeric scaffold from polymer to provisional matrix and connective tissues, with full disappearance and integration of the scaffold into the vessel wall. The aim of this report was to describe the methodology and to apply it to serial human OCT images post procedure and at 6, 12, 24 and 36 months in the ABSORB cohort B trial.

Methods and Results: In serial frequency-domain OCT pullbacks, corresponding struts at different time points were identified by 3-dimensional foldout view. The peak and median values of light intensity were measured in the strut core by dedicated software. A total of 303 corresponding struts were serially analyzed at 3 time points. In the sequential analysis, peak light intensity increased gradually in the first 24 months after implantation and reached a plateau (relative difference with respect to baseline [%Dif]: 61.4% at 12 months, 115.0% at 24 months, 110.7% at 36 months), while the median intensity kept increasing at 36 months (%Dif: 14.3% at 12 months, 75.0% at 24 months, 93.1% at 36 months).

Conclusions: Quantitative light intensity analysis by OCT was capable of detecting subtle changes in the bioresorbable strut appearance over time, and could be used to monitor the bioresorption and integration process of polylactide struts. (*Circ J* 2014; **78:** 1873–1881)

Key Words: Bioresorbable vascular scaffold; Bioresorption; Coronary artery disease; Light intensity analysis; Optical coherence tomography

Fully bioresorbable scaffolds (BRS) are a novel approach to interventional treatment of coronary artery disease, and this new era has been dubbed the fourth revolution in percutaneous coronary revascularization.[1,2] The biological advantages of a transient device include late lumen enlargement with wall thinning, restoration of vasomotion and return of pulsatility, which are important in effecting optimal repair of the vessel wall, potentially reducing adverse events such as late/very late neoatherosclerosis and stent/scaffold thrombosis.[2–4]

Received February 5, 2014; revised manuscript received April 11, 2014; accepted April 27, 2014; released online June 18, 2014 Time for primary review: 18 days

Thoraxcenter, Department of Cardiology, Erasmus MC (S.N., Y.O., Y.I., Y.-J.Z., C.M.C., Y.K.C., H.M.G.-G., R.-J.v.G., P.W.S.), Cardialysis (G.-A.v.E., H.M.G.-G., P.W.S.), Rotterdam; Leiden University Medical Center, Leiden (J.E., S.L., J.D., J.H.C.R.); Medis Medical Imaging Systems BV, Leiden (J.H.C.R.), The Netherlands; Abbott Vascular, Santa Clara, CA (L.P., A.S., S.V., R.R.), USA; and International Centre for Circulatory Health, NHLI, Imperial College London, London (P.W.S), UK

Appendix lists the investigators who contributed to OCT image acquisition in the ABSORB cohort B trial.

Mailing address: Yoshinobu Onuma, MD, Thoraxcenter, Ba-583 's Gravendijkwal 230 3015, CE Rotterdam, The Netherlands. E-mail: yoshinobuonuma@gmail.com

ISSN-1346-9843 doi:10.1253/circj.CJ-14-0143

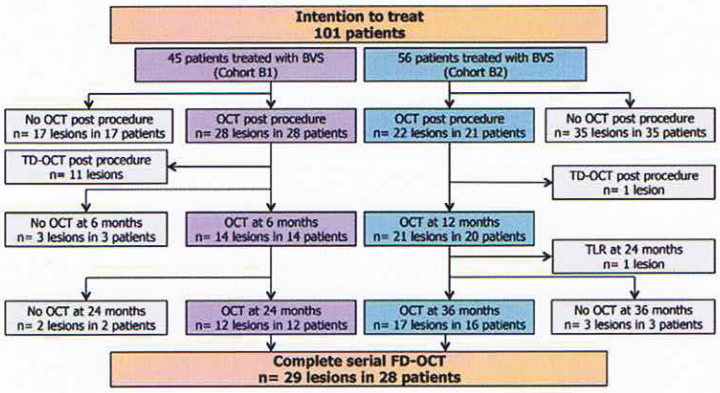

Figure 1. Flow chart of serial FD-OCT investigation in Cohort B of the ABSORB clinical trial. OCT, optical coherence tomography; FD-OCT, frequent-domain OCT; TD-OCT, time-domain OCT.

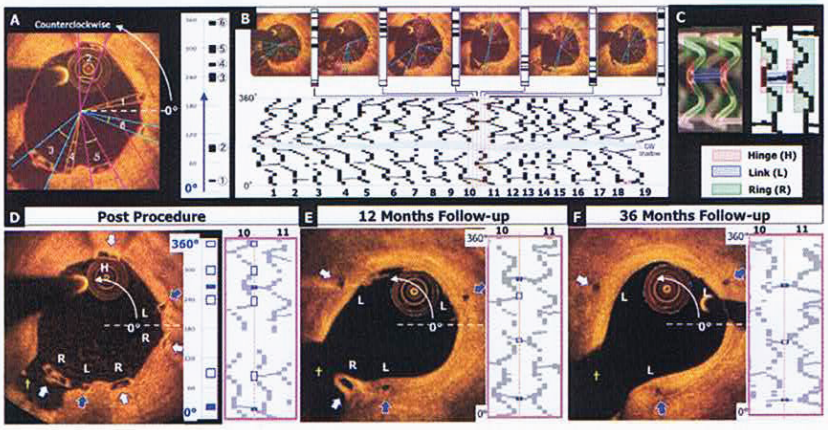

Figure 2. Strut core matching at serial time points confirmed by 3D foldout view. Lumen contour is drawn and the strut angle defined as the angle created by 2 lines originating from the center of gravity of the lumen to the edges of the visualized struts. By taking the position at 3 o'clock as the 0° reference angle, the angular orientation of each strut can be visualized in the 2D cross-section as indicated in the 3D foldout view. (**A**) By correlating the cross-sectional angular position with the longitudinal distance from the distal edge of the scaffold (defined as at least 1 strut detected in a cross-section) for each visualized strut, the 3D foldout view of a scaffold can be constructed.[18] (**B**) Foldout view of a 3×18 mm scaffold with 19 circular rings connected by 54 longitudinal links. The 3D foldout view confirms the location of matched or unmatched struts in a ring (R in white), link (L in white) or a hinge (H in white) in (**C**) and (**D**). The corresponding cross-sections were identified post procedure (**D**) and at 12 (**E**) and 36 months (**F**) by using a side branch (yellow cross) as an anatomical landmark. The corresponding struts were then selected by identifying those with a similar angular orientation in the corresponding cross-sections. However, some struts need confirmation on the 3D foldout view. For example, in (**D**), post procedure, in the cross-sections there are 2 visualized struts close in their angular orientations (350° and 20°), while at 12 (**E**) and 36 (**F**) months there is only one small strut visualized at 20°. The 3D foldout views at 12 and 36 months demonstrate that this small strut is located in a link connecting the 10th and 11th rings, and the 3D foldout view post procedure shows that the strut at 20° is also located in a link connection; thus, this strut is confirmed as correctly matched. Accordingly, the blue arrows show the corresponding struts and the white arrows show the non-corresponding struts.

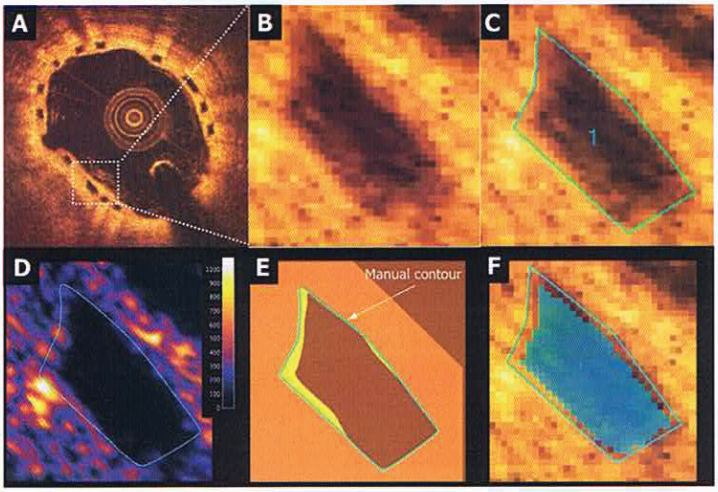

Figure 3. Strut core for light intensity assessment (region of interest, ROI). (**A**,**B**) OCT visualization of Absorb BVS strut consisting of a core area surrounded by reflective borders that are the interfaces between strut core and lumen or strut core and neointima/vessel wall. The struts "frame" can only be assessed unequivocally post procedure.[12] (**C**–**F**). Contours at follow-up of a strut core of interest visually delineated by manually drawn contours (**C**) and light intensity mapping around the strut core (**D**). The manually drawn borders of a strut core at follow-up often includes the reflective strut frame borders, so that part of the bright reflective frame can be misclassified as strut core region (**E**). Strut core region after automatic subtraction of 2 pixels inside the manual contours (**F**).

The current-generation BRS are constructed of either a polymer or a metallic alloy.[5] A variety of polymers with different chemical compositions and bioresorption times are in the preclinical and/or clinical stages of investigation. The most frequently used polymer is poly-L-lactide (PLLA).[2]

After implantation of a PLLA scaffold in vivo, the polymeric struts are progressively hydrolyzed and replaced by a provisional matrix; as it is released, the monomeric component, lactic acid, is metabolized via the Krebs cycle into carbon dioxide and water, with complete resorption occurring within approximately 24–36 months.[6] The duration of bioresorption is influenced by the initial molecular weight (MW) of the main component and the presence of oligomer, monomer and/or solvents.[6] After completion of bioresorption, the provisional matrix becomes cellularized with connective tissue; the struts eventually become fully integrated into the surrounding vessel wall and their OCT "footprint" becomes undetectable.[7]

In previous preclinical and clinical studies of the first-generation Absorb scaffold, 4 subgroups of strut appearance on OCT were visually categorized: "black box, dissolved bright box, dissolved black box or open box".[7] However, in those studies, the categorization showed only moderate reproducibility (k=0.58); therefore, more reproducible and/or quantitative methods were warranted. Quantitative light intensity analysis of the strut core is a method that could enable assessment of the light reflectivity of the resorbing polymer, its replacement by a provisional matrix and its vessel wall integration after cellularization by de novo connective tissue.[8–10] The aim of this report was to describe the methodology of light intensity analysis, to demonstrate the reproducibility of the assessment and to apply the method in serial OCT images collected post procedure and at 6, 12, 24 and 36 months follow-up in the ABSORB cohort B studies.[11]

Methods

Study Population

The OCT data used in the current analysis were obtained in the ABSORB Cohort B trial, a multicenter single-arm trial assessing the safety and performance of the Absorb™ everolimus-eluting bioresorbable vascular scaffold (BVS; Abbott Vascular, Santa Clara, CA, USA) in the treatment of 101 patients with a maximum of 2 de novo native coronary artery lesions.[12] The Absorb BVS consists of a semicrystalline PLLA backbone, coated with a thin amorphous layer of poly-D,L-lactide containing the antiproliferative agent everolimus. The details of inclusion and exclusion criteria have been described previously.[12] In this trial, 23 lesions in 23 patients were serially imaged by OCT post procedure and at 6 and 24 months (Cohort B1), and 19 lesions in 18 patients were serially investigated post procedure and at 12 and 36 months (Cohort B2).[11] Per study protocol, all patients were treated uniformly with a 3×18 mm BVS. To avoid variation in light intensity because of different types of the light imaging system used (ie, time-domain OCT [TD-OCT] vs. frequency-domain OCT [FD-OCT]), cases of investigation by TD-OCT were excluded from the analysis (n=12). In total, 87 pullbacks in 29 cases of truly serial FD-OCT were included in this study (**Figure 1**).

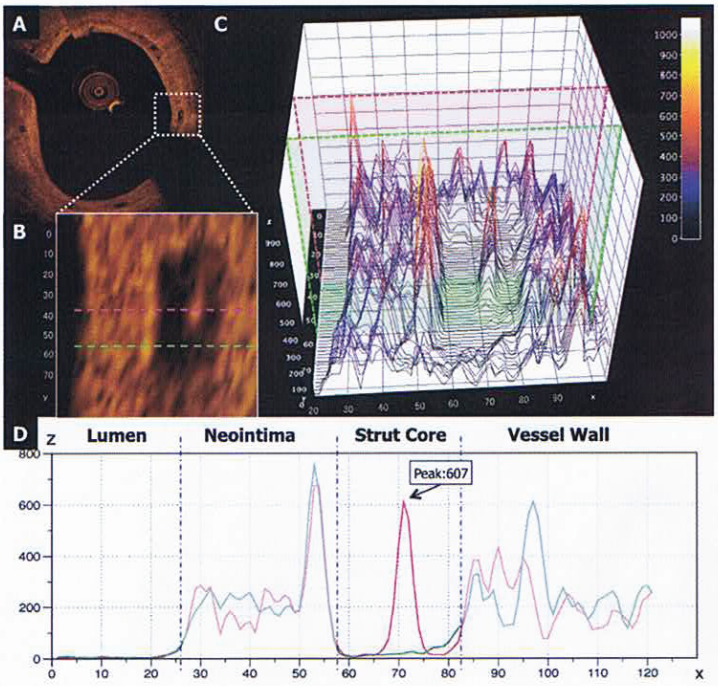

Figure 4. Two-dimensional and three-dimensional presentations of light intensity of the strut core. (**A**,**B**) Single strut located at 3 o'clock (0° reference angle) on this single cross-section of a scaffold implanted 36 months before. Inside the core region (**B**), there is a focus of high light intensity. The pink dotted line passes through this focus. The green dotted line crosses the strut core without passing the high-intensity spot. (**C**) 3D mapping of light intensity with 2 individual light profiles corresponding to the pink and green dotted (**B**) and continuous lines (**D**). The dotted blue lines in (**D**) indicate the region of interest (ROI). X and Y axis scales are in pixels, the Z axis has a dimensionless intensity value.

Method of Strut Matching

Preclinical studies suggest that the speed at which struts integrate into the arterial wall could vary within a single device depending on the location of the struts.[7] Therefore, in our analysis, strut-by-strut matching was performed to ascertain that the light intensity was repeatedly measured at the same site in the scaffold.[13–16] Using landmarks such as metallic markers or side branches, the corresponding cross-sections were identified at the different time points of follow-up. In corresponding OCT cross-sections, visualized struts' cores were matched by identifying struts with similar angular orientation in the 2D cross-section. This strut level matching was further confirmed by using a 3-D foldout view of the scaffold (**Figures 2C–E**).[13–16]

In every cross-section with at least 1 scaffold strut, the lumen contour was drawn, and the strut angle was defined as the angle created by 2 lines originating from the center of the gravity of the lumen to the edges of the struts, taking the position at 3 o'clock as the 0° angle of reference (**Figure 2A**).[13] By correlating the cross-sectional angular position of the struts with the longitudinal distance of each strut from the distal edge of the scaffold, a 3D foldout view of a scaffold can be constructed and thereby confirms the location of a matched or unmatched struts in a ring, link or a hinge (**Figure 2C**).[16]

Light Intensity Analysis

Light intensity analysis was performed using dedicated software (QCU-CMS v4.69 research version, Leiden, The Netherlands). Raw images in original polar format were used to ensure that interpolation, dynamic range compression or other image processing did not alter the signal and bias the analysis. The OCT image of an Absorb BVS strut consists of a "black core" area, surrounded by reflective borders created by the following interfaces because of differences in refraction index: at baseline, the lumen-polymer interface and the abluminal polymer-vessel wall interface and at follow-up, a neointima-strut core interface and an abluminal strut core-vessel wall interface. These interfaces are depicted in **Figure 3**.

The contours of the strut core of interest were delineated manually by visual inspection in a Cartesian image that were created from the raw polar images. The manually drawn bor-

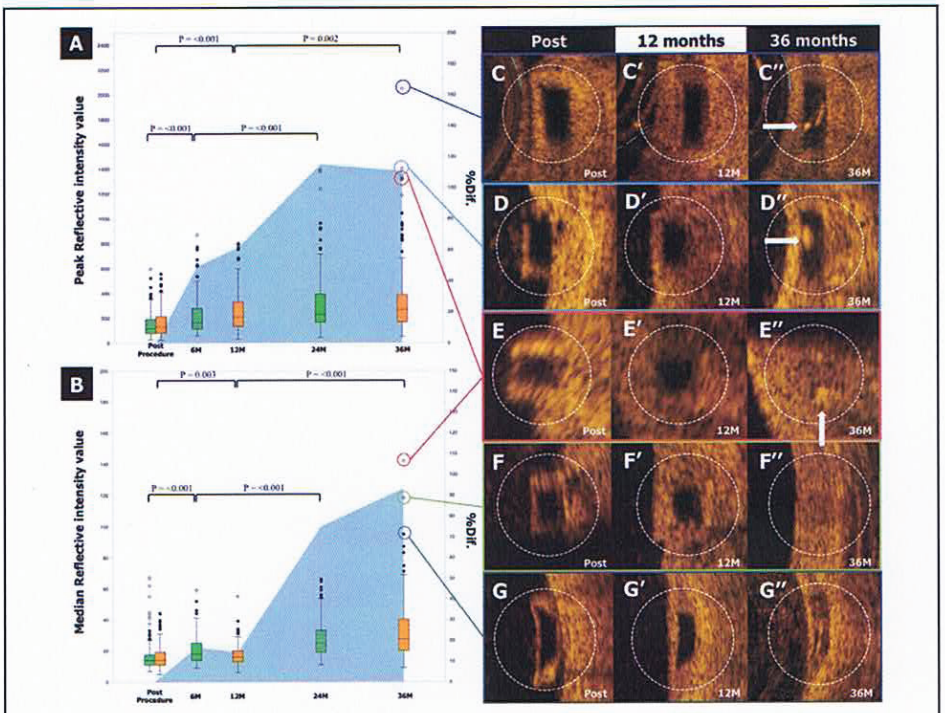

Figure 5. Change in peak and median intensity values over time with examples of serial highest peak or median intensity changes. (**A**,**B**) Whisker plots of peak and median intensity values (dimensionless) of corresponding strut cores in peak and median light intensities. Blue shadow curves depict the average of relative changes from baseline to follow-up (right vertical axis scale in percent, % difference). (**C''–E''**) Struts with the highest peak intensity values at 36 months. Corresponding struts post procedure (**C–E**) and 12 months (**C'–E'**) after implantation. (**C'',D''**) At 36 months, the corresponding struts on visual inspection still have a "black box" appearance but now include a high-intensity spot (arrows). (**E''–G''**) Struts with the highest median intensity values at 36 months. Corresponding struts post procedure (**E–G**) and 12 months (**E'–G'**) after implantation. These strut cores with high median values show increased light reflection of the entire core, which according to our previous categorized nomenclature could have been visually categorized as dissolved bright (**E''**), dissolved black (**F''**) or open (**G''**) box.[19]

ders of a strut core region often included complex reflective interfaces between the strut core and the surroundings, so that part of the bright reflective OCT frame of the strut (easily discernable at baseline) could become included in the strut core area at follow-up (**Figures 3C–E**) The interobserver manual delineation of the region of interest (ROI) could vary by 1 or 2 pixels (10–20 micron). To substantially reduce such a variability in ROI contours, 2 pixels inside of the manual contour were automatically subtracted (**Figure 3F**).

Although the strut borders at follow-up were no longer detectable because of changes in strut appearance, the contours at baseline were manually superimposed on the follow-up images (**Figure 5F''**). In addition, the malapposed struts and struts located at the ostium of the side branch post procedure were excluded in the current analysis. Furthermore, struts with post-procedure scattering center, which is a focal hyperintense signal in the strut core without apparent contact with either the axial or transversal strut edge and derived from polymer crazing caused by mechanical deformation of scaffold during crimping and deployment, were excluded in this analysis.[16,17]

The peak and median intensity values (dimensionless) of the strut core were then measured by the dedicated software (**Figure 4**). To evaluate interobserver reproducibility, 2 readers (S.N. and Y.I.) independently analyzed 400 struts randomly selected from the total number of investigated struts (n=909). To determine intraobserver reproducibility, 1 reader (S.N.) analyzed the struts twice, with the second reading occurring 3 months later. The inter- and intraobserver reproducibility were good according to the conventional norms[18] (peak intensity value: interobserver ICCa=0.92, intraobserver ICCc=0.89, median intensity value: interobserver ICCa=0.91, intraobserver ICCc=0.93; **Table S1**, **Figure S1**).

Table. Peak and Median Intensity Values at Several Time Points After Implantation of Bioresorbable Polymeric Intracoronary Scaffolds in the ABSORB Cohort B Trial

	Peak intensity value		Median intensity value	
	Cohort B1 (n=141)	Cohort B2 (n=162)	Cohort B1 (n=141)	Cohort B2 (n=162)
Post procedure, median [IQR]/ mean (SD)	117.0 [79.0 to 194.0]/ 149.5 (100.2)	131.0 [81.5 to 214.3]/ 157.4 (95.48)	14.0 [11.0 to 17.8]/ 17.1 (10.4)	14.0 [11.0 to 19.9]/ 15.8 (7.8)
M, median [IQR]/mean (SD)				
6	162.0 [112.5 to 279.5]/ 221.5 (162.2)	–	18.0 [14.0 to 25.0]/ 20.7 (9.4)	–
12	–	206.5 [133.5 to 330.3]/ 254.1 (178.4)	–	16.0 [13.0 to 20.0]/ 17.2 (7.4)
24	228.0 [162.0 to 393.5]/ 322.9 (247.0)	–	25.0 [19.0 to 33.0]/ 28.2 (12.3)	–
36	–	265.0 [163.5 to 386.0]/ 347.7 (302.8)	–	27.5 [20.0 to 40.3]/ 32.5 (19.4)
Dif., median [IQR]				
6M-Post	48.0 [–36.5 to 147.5]	–	3.0 [–1.0 to 9.5]	–
12M-Post	–	72.5 [–21.5 to 194.0]	–	1.8 [–2.0 to 6.0]
24M-6M	72.0 [38.5 to 108.5]	–	6.0 [0.8 to 15.0]	–
36M-12M	–	32.0 [–69.5 to 201.5]	–	11.0 [4.4 to 22.0]
P value				
Post-1st FUP	<0.001	<0.001	<0.001	0.003
1st–2nd FUP	<0.001	0.002	<0.001	<0.001
Post-2nd FUP	<0.001	<0.001	<0.001	<0.001

All P-values are calculated by Wilcoxon paired test. Continuous variables are presented as the mean±standard deviation (SD) or median with interquartile range (IQR). FUP, follow up; M, months.

Statistical Analysis

All statistical analyses were performed using the statistical software package SPSS version 21.0 (SPSS Inc, Chicago, IL, USA). Continuous variables are presented as the mean±standard deviation or median with interquartile ranges. Paired comparisons between post procedure and follow-up were done by Wilcoxon's signed rank test. Values of $P<0.05$ were considered statistically significant.

Results

In 87 serial pullbacks (19 lesions) performed either at 6 and 24 months (cohort B1) or at 12 and 36 months (cohort B2), 423 cross-sections were matched using anatomical landmarks. After strut level matching, a total of 303 corresponding struts (141 struts in cohort B1, 162 struts in cohort B2) were serially analyzed at 3 time points (909 strut images). Both peak and median intensity values over time are tabulated in Table, and the whisker plots of peak and median intensity values of the corresponding struts with the blue shadow curves representing the average relative change from baseline to follow-up are shown in Figure 5. The changes in absolute values for both parameters in the serial paired analysis are highly significant. In a relative difference analysis, the peak light intensity value increased gradually in the first 24 months after implantation (relative difference [%Dif.]: 49.4% at 6 months, 61.4% at 12 months, 115.0% at 24 months) and reached a plateau (%Dif.: 110.7% at 36 months), while the median intensity value increased significantly at 24 months (%Dif: 14.3% at 12 months, 75.0% at 24 months) and kept increasing at 36 months (93.1% at 36 months).

Mean plus 1 standard deviation of the measurement of the parameters was used as arbitrary threshold criteria for defining 4 groups: (1) struts with low peak and median light intensity values, (2) struts with high peak and low median intensity values, (3) struts with low peak and high median intensity values, and (4) struts with high peak and median intensity values.

The categorization into 4 groups helps in evaluating the changes of the strut appearance over time. At 36 months, 16.6% of the strut cores no longer has the appearance of those with low median and low peak intensities. This percentage is expected to rise dramatically at 5 years.

Struts with the highest peak or median intensity values at 3 years are exemplified in Figure 5. In 2 out of 3 struts with the highest peak intensity value, the strut core still appeared as a "black box" but contained isolated bright spots (arrows in Figures 5C",D"), Three struts with high median intensity values showed an increase in the light reflection of the entire strut (Figures 5E"–G").

Discussion

The main findings of this study using the new methodology of light intensity assessment are: (1) serial quantification of light intensity in matched strut cores is feasible and reproducible when using dedicated software and (2) the peak and median intensity values increase gradually in the serial light intensity analysis, a phenomenon presumably related to bioresorption and/or the integration process of the resorbable device.

Bioresorption Process Monitoring by Light Intensity

Preclinical studies have demonstrated that the MW of the first-generation Absorb BVS becomes undetectable by gel permeation chromatography 24 months after implantation, and the polylactide is replaced by a provisional matrix that gradually integrates into the arterial wall.[7] Using visual qualitative assessment only, OCT is unable to monitor MW loss or to detect replacement of the polymer by this provisional matrix. In the current study using a quantitative method, there was an overall

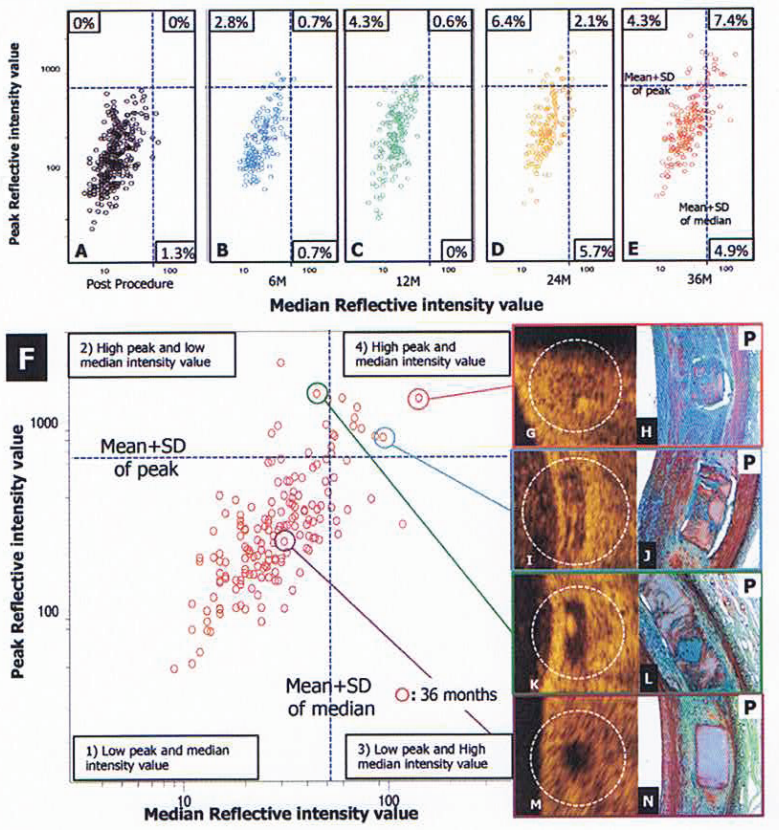

Figure 6. Quantitative light intensity assessment of strut integration on optical coherence tomography (OCT). (**A–E**) Scatter plots of the peak and median values post procedure and at 6, 12, 24 and 36 months. (**F**) Scatter diagram of the peak and median intensity values of each individual strut core at 36 months (dotted blue lines represent the light intensity values of the mean+1 SD for both parameters. According to these 2 threshold criteria, the strut cores are classified into 4 groups: (1) struts with low peak and low median light intensity values, (2) struts with high peak and low median intensity values, (3) struts with low peak and high median intensity values, and (4) struts with high peak and high median intensity values. The majority of struts are still categorized as having low peak/low median intensity value (M), which could correspond to struts without cellularization, but presumably occupied by provisional matrix (N). This panel also includes histological examples obtained from Absorb BVS implanted porcine coronary arteries at 36 moths after implantation and stained by Movat's pentachrome staining (red: smooth muscle cell/protein; blue-green: provisional matrix with staining characteristics comparable to that of proteoglycan; yellow: collagen). Strut cores with high median intensity value could (**G,I**) correspond to those that have been substantially cellularized with homogeneous connective tissue infiltration (**H**) such that the integration into the vessel wall is almost complete. (**I**) Strut core with high median and peak intensities suggesting that connective tissue infiltration is more modest (**J**). The strut cores with high peak/low median intensities (**K**) could correspond to struts that are focally cellularized with infiltration of connective tissue on histology (**L**).

increase in peak light intensity values from baseline to 24 months, followed by a plateau; these changes could reflect early connective tissue infiltration forming foci of cellularization in the provisional matrix; preliminary investigations (data not shown) in a porcine model suggest that specific interpretation (Figure 6L).

Integration Process on OCT

In previous preclinical studies, OCT assessment by visual inspection was sensitive enough to monitor the integration process after bioresorption ("strut footprint" becoming undetectable on OCT).[7] In the present study, by using peak and median intensity values (Figure 6), the struts could be categorized into

4 groups (see above).

In the current follow-up (36 months), the majority of struts (83.6%) still retained low peak and low median intensity values (Figure 6M), an observation that could correspond to strut cores without cellularization, but exclusively replaced by provisional matrix in the porcine model (Figure 6N). The strut cores with high peak intensity but low median intensity values (Figure 6K) could correspond to struts with focal cellularization according to histology in the porcine model (Figure 6L), whereas strut cores with high median intensity values (Figures 6G,I) could correspond to struts that have been fully cellularized in the porcine model (Figures 6H,J). Indeed, high median light intensity might reflect a more homogeneous replacement of struts with connective tissue whereby it is no longer possible to detect a demarcation between the de novo tissue replacing the pre-existing strut and the surrounding arterial wall, ultimately rendering the foci of the pre-existing struts undetectable by OCT (Figure 6H).

However, these hypothetical correlations between light intensity and histological changes need to be further cross-validated in the porcine model and investigated in patients with a follow-up of 5 years (March–November 2014). It is our expectation that most of these sites at 5 years will have high median intensity values and therefore will be no longer be detectable on OCT. In summary, categorization by peak/median light intensity value could be used to quantify the integration process of struts made of polylactide.

Clinical Implication of Light Intensity Analysis

The preclinical investigation of scaffolded porcine coronary artery models at 2, 3 and 4 years, combining OCT and histology, indicated that the last process in the integration of struts involves their complete replacement with connective tissue and maturation (shrinkage) of this tissue. This same process of cellularization and contracture also occurs clinically and may correspond to vessel wall thinning, the latter of which could contribute to lumen enlargement with/without adaptive remodeling. The current method of light intensity analysis could be applied clinically to assess the degree of strut/scaffold integration after implantation. Therefore, by using the classification of struts based on quantitative light intensity values, clinicians could assess the stage of scaffold integration that heralds late lumen enlargement.

From the regulatory perspective, it is mandatory to investigate the rate of biodegradation/bioresorption of each device, because the rate can vary according to the manufacturing process of PLLA (extrusion, molding, microfiber braiding etc), even in devices made of the same MW PLLA with an identical scaffold design.[19,20] Moreover, the rate at which a device becomes integrated into the tissue can also vary according to its anatomical placement, the nature of the tissue underlying the scaffold (normal or pathological) and the location of each strut against the wall (apposition, malapposition or side-branch ostium).[21] Considering the fact that the translucent polymeric scaffold initially does not interfere with imaging of the underlying plaque, the interaction between strut integration and underlying plaque could be also assessed with OCT.

Study Limitations

In the current study, OCT imaging was optional per protocol and cases of events were excluded, so only 28 of 101 patients (27.7%) with truly serial OCT were analyzed, which might under-represent the total cohort and relevant outcomes. Using the dedicated software algorithm, automatic exclusion of the outer circumferential pixels from the strut core could overlook changes around the border of a strut core. Theoretically, neointimal tissue on the endoluminal side of a strut core might influence the light intensity value of the strut cores; however, the median light intensity value of a strut core had no significant correlation with the thickness and median light intensity value of the neointimal tissue covering the endoluminal side of struts (Figures S2,S3).

Conclusions

The current analysis demonstrated that strut-by-strut serial light intensity analysis of the bioresorbable strut core is feasible and reproducible. The changes in peak intensity values at early time points may be related to focal cellularization, whereas the evolution of peak/median intensity values at later time points could reflect the integration process. Ongoing analysis of a porcine model up to 42 months will help in the interpretation of the 60-month (March–November 2014) OCT analysis of the sequential cohort of patients in the ABSORB cohort B1 and B2 trials.

Acknowledgments

The authors thank Renu Virmani for her preparation and interpretation of the preclinical histological samples from which the images were taken.

Disclosures

Conflict of Interest Statement: L. Perkins, A. Sheehy, S. Veldhof and R. Rapoza are full-time employees of Abbott Vascular, which sponsored the Cohort B trial.

References

1. Serruys PW, Garcia-Garcia HM, Onuma Y. From metallic cages to transient bioresorbable scaffolds: Change in paradigm of coronary revascularization in the upcoming decade? *Eur Heart J* 2012; **33:** 16–25b.
2. Onuma Y, Serruys PW. Bioresorbable scaffold: The advent of a new era in percutaneous coronary and peripheral revascularization? *Circulation* 2011; **123:** 779–797.
3. Raber L, Magro M, Stefanini GG, Kalesan B, van Domburg RT, Onuma Y, et al. Very late coronary stent thrombosis of a newer-generation everolimus-eluting stent compared with early-generation drug-eluting stents: A prospective cohort study. *Circulation* 2012; **125:** 1110–1121.
4. Nakazawa G, Otsuka F, Nakano M, Vorpahl M, Yazdani SK, Ladich E, et al. The pathology of neoatherosclerosis in human coronary implants bare-metal and drug-eluting stents. *J Am Coll Cardiol* 2011; **57:** 1314–1322.
5. Iqbal J, Onuma Y, Ormiston J, Abizaid A, Waksman R, Serruys P. Bioresorbable scaffolds: Rationale, current status, challenges, and future. *Eur Heart J* 2014; **35:** 765–776.
6. Vorpahl M, Finn AV, Nakano M, Virmani R. The bioabsorption process: Tissue and cellular mechanisms and outcomes. *EuroIntervention* 2009; **5**(Suppl F)**:** F28–F35.
7. Onuma Y, Serruys PW, Perkins LE, Okamura T, Gonzalo N, Garcia-Garcia HM, et al. Intracoronary optical coherence tomography and histology at 1 month and 2, 3, and 4 years after implantation of everolimus-eluting bioresorbable vascular scaffolds in a porcine coronary artery model: An attempt to decipher the human optical coherence tomography images in the ABSORB trial. *Circulation* 2010; **122:** 2288–2300.
8. Tearney GJ, Bouma BE. Shedding light on bioabsorbable stent struts seen by optical coherence tomography in the ABSORB trial. *Circulation* 2010; **122:** 2234–2235.
9. Sheehy A, Gutierrez-Chico JL, Diletti R, Oberhauser JP, Glauser T, Harrington J, et al. In vivo characterisation of bioresorbable vascular scaffold strut interfaces using optical coherence tomography with Gaussian line spread function analysis. *EuroIntervention* 2012; **7:** 1227–1235.
10. Templin C, Meyer M, Muller MF, Djonov V, Hlushchuk R, Dimova I, et al. Coronary optical frequency domain imaging (OFDI) for in vivo evaluation of stent healing: Comparison with light and electron microscopy. *Eur Heart J* 2010; **31:** 1792–1801.
11. Serruys PW, Onuma Y, Garcia-Garcia HM, Muramatsu T, van

Geuns RJ, de Bruyne B, et al. Dynamics of vessel wall changes following the implantation of the Absorb everolimus-eluting bioresorbable vascular scaffold: A multi-imaging modality study at 6, 12, 24 and 36 months. *EuroIntervention* 2014; **9:** 1271–1284.
12. Serruys PW, Onuma Y, Ormiston JA, de Bruyne B, Regar E, Dudek D, et al. Evaluation of the second generation of a bioresorbable everolimus drug-eluting vascular scaffold for treatment of de novo coronary artery stenosis: Six-month clinical and imaging outcomes. *Circulation* 2010; **122:** 2301–2312.
13. Okamura T, Garg S, Gutierrez-Chico JL, Shin ES, Onuma Y, Garcia-Garcia HM, et al. In vivo evaluation of stent strut distribution patterns in the bioabsorbable everolimus-eluting device: An OCT ad hoc analysis of the revision 1.0 and revision 1.1 stent design in the ABSORB clinical trial. *EuroIntervention* 2010; **5:** 932–938.
14. Gutierrez-Chico JL, van Geuns RJ, Regar E, van der Giessen WJ, Kelbaek H, Saunamaki K, et al. Tissue coverage of a hydrophilic polymer-coated zotarolimus-eluting stent vs. a fluoropolymer-coated everolimus-eluting stent at 13-month follow-up: An optical coherence tomography substudy from the RESOLUTE All Comers trial. *Eur Heart J* 2011; **32:** 2454–2463.
15. Gomez-Lara J, Radu M, Brugaletta S, Farooq V, Diletti R, Onuma Y, et al. Serial analysis of the malapposed and uncovered struts of the new generation of everolimus-eluting bioresorbable scaffold with optical coherence tomography. *JACC Cardiovasc Interv* 2011; **4:** 992–1001.
16. Gutierrez-Chico JL, Radu MD, Diletti R, Sheehy A, Kossuth MB, Oberhauser JP, et al. Spatial distribution and temporal evolution of scattering centers by optical coherence tomography in the poly(L-lactide) backbone of a bioresorbable vascular scaffold. *Circ J* 2012; **76:** 342–350.
17. Radu MD, Onuma Y, Rapoza RJ, Diletti R, Serruys PW. In vivo visualisation by three-dimensional optical coherence tomography of stress crazing of a bioresorbable vascular scaffold implanted for treatment of human coronary stenosis. *EuroIntervention* 2012; **7:** 1461–1463.
18. Fleiss J. The design and analysis of clinical experiments. New York: Wiley, 1986.
19. Serruys PW, Ormiston JA, Onuma Y, Regar E, Gonzalo N, Garcia-Garcia HM, et al. A bioabsorbable everolimus-eluting coronary stent system (ABSORB): 2-year outcomes and results from multiple imaging methods. *Lancet* 2009; **373:** 897–910.
20. Ormiston JA, Serruys PW, Onuma Y, van Geuns RJ, de Bruyne B, Dudek D, et al. First serial assessment at 6 months and 2 years of the second generation of ABSORB everolimus-eluting bioresorbable vascular scaffold: A multi-imaging modality study. *Circ Cardiovasc Interv* 2012; **5:** 620–632.
21. Gutierrez-Chico JL, Gijsen F, Regar E, Wentzel J, de Bruyne B, Thuesen L, et al. Differences in neointimal thickness between the adluminal and the abluminal sides of malapposed and side-branch struts in a polylactide bioresorbable scaffold: Evidence in vivo about the abluminal healing process. *JACC Cardiovasc Interv* 2012; **5:** 428–435.

Appendix

The list of investigators who contributed to OCT image acquisition in the ABSORB cohort B trial.

Robert-Jan van Geuns, MD, PhD (n=14), Evald Christiansen, MD (n=12), Dariusz Dudek, MD (n=8), Dougal McClean, MD (n=7), Jacques Koolen, MD, PhD (n=7), John A Ormiston, MB, ChB, PhD (n=7), Bernard Chevalier, MD (n=7), Stefan Windecker, MD (n=6), Pieter C. Smits, MD, PhD (n=6), Bernard de Bruyne, MD, PhD (n=5), Robert Whitbourn, MD (n=3).

Supplementary Files

Supplementary File 1

Inter- and intraobserver reproducibility of the light intensity value analysis of strut core

Influence of neointimal tissue on the endoluminal side of a strut core for the light intensity value of strut cores

Table S1. Inter- and intraobserver variability of peak and median intensity values

Figure S1. Inter- and intraobserver reproducibility analysis.

Figure S2. Neointimal thickness and the median light intensity value of the neointimal tissue covering the endoluminal side of struts.

Figure S3. Influence of neointimal tissue for the light intensity value of strut cores.

Please find supplementary file(s);
http://dx.doi.org/10.1253/circj.CJ-14-0143

4.3 Bioresorption and Vessel Wall Integration of bioresorbable scaffolds

Bioresorption and Vessel Wall Integration of A Fully Bioresorbable Polymeric Everolimus-Eluting Scaffold: Optical Coherence Tomography (OCT), Intravascular Ultrasound (IVUS) and Histological 3 Study in Porcine Model with Four Years Follow-up.

JACC Cardiovasc Interv. 2016 in press.
[Original research paper, IF 7.44]

Nakatani S, **Ishibashi Y**, Perkins L, Eggermont J, Sotomi Y, Grundeken MJ, Dijkstra J, Rapoza R, Virmani R, Serruys,PW, Onuma Y.

TRANSLATIONAL

Bioresorption and Vessel Wall Integration of a Fully Bioresorbable Polymeric Everolimus-Eluting Scaffold

Optical Coherence Tomography, Intravascular Ultrasound, and Histological Study in a Porcine Model With 4-Year Follow-Up

Shimpei Nakatani, MD,[a] Yuki Ishibashi, MD, PhD,[a] Yohei Sotomi, MD,[b] Laura Perkins, DVM, PhD,[c] Jeroen Eggermont, PhD,[d] Maik J. Grundeken, MD,[b] Jouke Dijkstra, PhD,[d] Richard Rapoza, PhD,[c] Renu Virmani, MD,[e] Patrick W. Serruys, MD, PhD,[f] Yoshinobu Onuma, MD, PhD[a]

ABSTRACT

OBJECTIVES The aim of the present study was to investigate the relationship between the integration process and luminal enlargement with the support of light intensity (LI) analysis on optical coherence tomography (OCT), echogenicity analysis on intravascular ultrasound, and histology up to 4 years in a porcine model.

BACKGROUND In pre-clinical and clinical studies, late luminal enlargement has been demonstrated at long-term follow-up after everolimus-eluting poly-L-lactic acid coronary scaffold implantation. However, the time relationship and the mechanistic association with the integration process are still unclear.

METHODS Seventy-three nonatherosclerotic swine that received 112 Absorb scaffolds were evaluated in vivo by OCT, intravascular ultrasound, and post-mortem histomorphometry at 3, 6, 12, 18, 24, 30, 36, 42, and 48 months.

RESULTS The normalized LI, which is the signal densitometry on OCT of a polymeric strut core normalized by the vicinal neointima, was able to differentiate the degree of connective tissue infiltration inside the strut cores. Luminal enlargement was a biphasic process at 6 to 18 months and at 30 to 42 months. The latter phase occurred with vessel wall thinning and coincided with the advance integration process demonstrated by the steep change in normalized LI (0.26 [interquartile range (IQR): 0.20 to 0.32] at 30 months versus 0.68 [IQR: 0.58 to 0.83] at 42 months, $p < 0.001$).

CONCLUSIONS In this pre-clinical model, late luminal enlargement relates to strut integration into the arterial wall. Quantitative LI analysis on OCT could be used as a surrogate method for monitoring the integration process of poly-L-lactic acid scaffolds, which could provide insight and understanding on the imaging-related characteristics of the bioresorption process of polylactide scaffolds in human. (J Am Coll Cardiol Intv 2016;9:838–51)

From the [a]ThoraxCenter, Erasmus Medical Center, Rotterdam, the Netherlands; [b]Academic Medical Center, University of Amsterdam, Amsterdam, the Netherlands; [c]Abbott Vascular, Santa Clara, California; [d]Leiden University Medical Center, Leiden, the Netherlands; [e]CVPath Institute, Gaithersburg, Maryland; and the [f]International Centre for Circulatory Health, National Heart and Lung Institute, Imperial College London, London, United Kingdom. This study was funded by Abbott Vascular. Drs. Perkins and Rapoza are full-time employees of Abbott Vascular. Drs. Serruys and Onuma are members of the advisory board of Abbott Vascular. Dr Virmani receives research support from Abbott Vascular, BioSensors International, Biotronik, Boston Scientific, Medtronic, MicroPort Medical, OrbusNeich Medical, SINO Medical Technology, and Terumo Corporation; has speaking engagements with Merck; receives honoraria from Abbott Vascular, Boston Scientific, Lutonix, Medtronic, and Terumo Corporation; and is a consultant for 480 Biomedical, Abbott Vascular, Medtronic, and W.L. Gore. All other authors have reported that they have no relationships relevant to the contents of this paper to disclose.

Manuscript received December 22, 2015; accepted January 15, 2016.

As an alternative approach to metal drug-eluting stents, fully bioresorbable polymeric drug-eluting scaffolds provide transient vessel support with drug-delivery capability. As the scaffold begins to resorb, the vessel is no longer caged, and therefore luminal area as well as vessel area could increase simultaneously without creating evagination (1-5). The everolimus-eluting scaffold (Absorb; Abbott Vascular, Santa Clara, California) consists of a semicrystalline poly-L-lactic acid (PLLA) backbone coated by a thin amorphous layer of poly-D,L-lactic acid containing the antiproliferative agent everolimus. After implantation, the polylactide strut progressively degrades by hydrolysis, and its molecular weight starts to decrease from its initial molecular

SEE PAGE 852

weight of around 100 kDa (molecular weight loss) (6). The PLLA molecules remain at the implanted site until the polymeric chains become small enough to diffuse from the site into the surrounding tissue (mass loss). As small oligomers or monomers gradually leave the site, there is progressive replacement by a provisional matrix initially composed of a milieu of extracellular matrix components. This initially acellular provisional matrix is gradually cellularized with connective tissues, and the struts and footprints eventually become fully integrated into the surrounding neointimal tissue of the vessel wall (6,7).

It is well-established that the scaffolding efficacy of the device is related to the timing of molecular weight reduction and the loss of mechanical integrity (8). However, at a late phase, it is still unclear whether the integration of strut footprints is associated with the late luminal enlargement. In the pre-clinical assessment of fully bioresorbable scaffolds, it is therefore important to assess the processes of molecular weight loss and integration in vivo. In humans, intravascular imaging has been used in vivo as a surrogate marker to understand the bioresorption and integration process, but the correlation between the surrogate assessment and the true bioresorption process needs to be established.

On intravascular ultrasound (IVUS), quantitative echogenicity has been demonstrated to correlate with the molecular weight of PLLA (9). On optical coherence tomography (OCT), the visual categorizations of strut appearance have previously been demonstrated to correlate with the integration process (10). However, this visual categorization was limited by its moderate reproducibility (k = 0.58). Recently, log-transformed optical coherence tomographic signal measurement (light intensity analysis) of strut cores was introduced as a feasible and reproducible method to assess the degree of strut integration after scaffold implantation (11). In humans, the median intensity value of strut cores increased significantly at 24 months and kept increasing up to 36 months, and most of pre-existing struts were indiscernible at 60 months on OCT (**Figure 1**). It was hypothesized

ABBREVIATIONS AND ACRONYMS

IQR = interquartile range

IVUS = intravascular ultrasound

OCT = optical coherence tomography

PLLA = poly-L-lactic-acid

TD = time-domain

print & web 4C/F PO

FIGURE 1 Strut Appearance on Optical Coherence Tomography of Revision 1.0 (Used in the ABSORB Cohort A Study) and Revision 1.1 (Used in the ABSORB Cohort B Study) of the Absorb Device

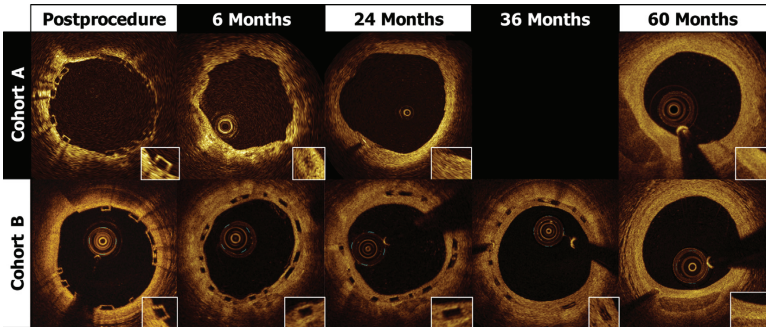

The time to complete degradation of the Absorb A device was approximately 2 years, whereas that for the Absorb B device was approximately 3 years, resulting in the different appearance of strut cores on optical coherence tomography over time in Absorb B devices compared with that of Absorb A devices in humans (5,26).

that light reflectivity is correlated with connective tissue infiltration of the strut cores. However, this hypothetical correlation between light intensity and histological changes has so far not been demonstrated with strut histology-matched light intensity.

The aim of this study was to demonstrate the relationship between light intensity and histological changes with regard to strut integration at 3, 6, 12, 18, 24, 30, 36, 42, and 48 months in a porcine coronary artery model. In addition, IVUS echogenicity analysis was also assessed to monitor early changes in molecular weight.

METHODS

The present study was conducted from 2009 to 2013. Eight nonatherosclerotic juvenile domestic crossbred farm swine and 65 Yucatan mini-swine underwent Absorb scaffold implantation with a targeted balloon-to-artery ratio of 1.0:1.1. Each animal received a single everolimus-eluting scaffold (Absorb; 3.0 × 18 mm for 1, 3, and 6 months and 3.0 × 12 mm for 12 to 48 months) in 1 or 2 main coronary arteries. The Absorb scaffold used in the present study is the same as the device used in cohort B of the ABSORB clinical trials. Seventy-three pigs with 112 Absorb scaffolds implanted were examined by OCT at baseline and anesthetized at the designated endpoints with the optical coherence tomographic and IVUS examinations at 3 months (n = 10 Absorb scaffolds in 8 farm swine), as well as 6 (n = 10 Absorb scaffolds in 8 Yucatan mini-swine), 12 (n = 11 in 7), 18 (n = 12 in 7), 24 (n = 12 in 7), 30 (n = 12 in 8), 36 (n = 12 in 8), 42 (n = 13 in 8), and 48 (n = 20 in 12) months (Figure 2).

Optical coherence tomographic acquisition was executed by the frequency-domain optical coherence tomographic imaging system (C7 Dragonfly or Dragonfly Duo, St. Jude Medical, St. Paul, Minnesota), with the exception of a few early investigations performed with the time-domain (TD) OCT imaging system in 2 animals. IVUS runs were acquired with 40-MHz mechanical systems, using Galaxy version 2.02 or iLab (Boston Scientific, Natick, Massachusetts). After performing intravascular imaging studies (OCT and IVUS), animals were humanely euthanized. Hearts were excised and pressure perfused with 0.9% saline solution, followed by pressure perfusion fixation with 10% neutral buffered formalin overnight in preparation for histology. Embedded arteries were divided into a minimum of 3 blocks representing the proximal, medial, and distal regions of the scaffold. Duplicate 4- to 6-mm sections from each of the

FIGURE 2 Study Flowchart of the Pigs Receiving Absorb Scaffolds Evaluated by Optical Coherence Tomography, Intravascular Ultrasound, and Histology

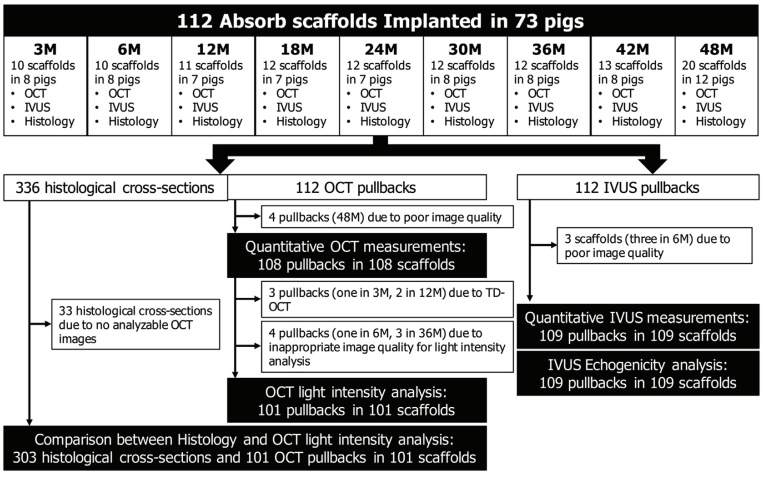

IVUS = intravascular ultrasound; M = month; OCT = optical coherence tomography.

3 blocks were collected, and each was stained with Movat's pentachrome and hematoxylin and eosin for evaluation by light microscopy.

Experimental studies received protocol approval from the Institutional Animal Care and Use Committee and were conducted in accordance with American Heart Association guidelines for pre-clinical research and the Guide for the Care and Use of Laboratory Animals (National Institutes of Health, 1996).

HISTOLOGICAL CATEGORIZATION OF STRUT AND STRUT FOOTPRINT. On histology, the integration grade of each strut was semiquantitatively classified into 6 groups according to the connective tissue composition within a strut core in Movat's pentachrome-stained sections: 0) acellular, no connective tissue composition; 1) hypointegration, 1% to 10% connective tissue composition; 2) low integration, 11% to 25% connective tissue composition; 3) moderate integration, 26% to 50% connective tissue composition; 4) moderate to high integration, 51% to 75% connective tissue composition; and 5) high integration, >75% connective tissue composition. **Figure 3** shows examples of strut appearance on the basis of histological classification of integration (10).

OPTICAL COHERENCE TOMOGRAPHIC QUANTITATIVE MEASUREMENTS. Cross sections with unacceptable image quality for measurements due to suboptimal flushing (4 scaffolds at 48 months) were excluded from the quantitative analysis and light intensity analysis. Quantitative measurements (scaffold area, incomplete scaffold apposition area, and neointimal area) were performed in the scaffolded segment and periscaffolded segments (within 5 mm proximal and distal to the stent edge) at 1-mm intervals according to previously published methods (12). As the porcine coronary artery grows, the luminal area in the periscaffolded segment (reference luminal area) is enlarged (2,13). To compare the time-dependent changes, the normalized scaffold and luminal area was calculated as the ratio of the scaffold and lumen to the reference luminal area (2).

OPTICAL COHERENCE TOMOGRAPHIC LIGHT INTENSITY ANALYSIS OF STRUT CORES. Because the light intensity values vary between TD and frequency-domain OCT, images obtained by TD OCT (1 scaffold at 3 months and 2 at 12 months) were excluded from the light intensity analysis. Pull-backs with high intraluminal signal intensity with shadows

FIGURE 3 Light Intensity Analysis on Optical Coherence Tomography and Categorization on Histology

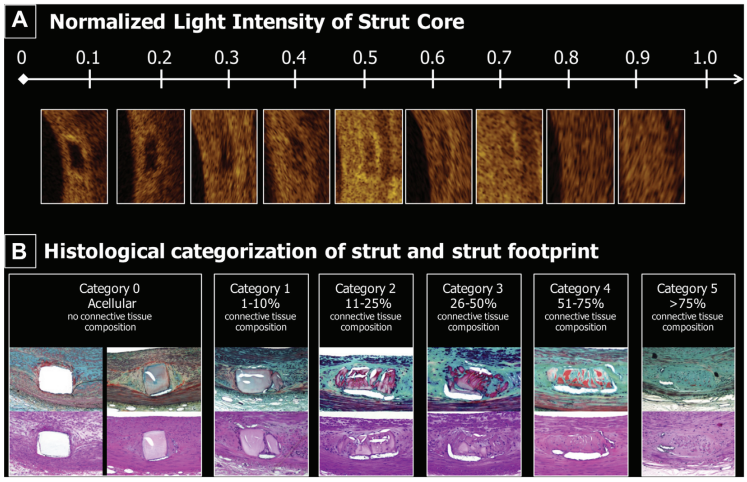

Representative strut appearance according to the normalized light intensity on optical coherence tomography **(A)** and histological categorization **(B)** of the strut core and footprint.

TABLE 1 Light Intensity Analysis in Matched Struts Over Time

Time Point (months)	Matched Struts	Accellular Struts	Integrated Struts					p Value
		0. Acellular: No connective Tissue Composition	1. Hypointegration: 1%–10% Connective Tissue Composition	2. Low Integration: 11%–25% Connective Tissue Composition	3. Moderate Integration: 26%–50% Connective Tissue Composition	4. Moderate to High Integration: 51%–75% Connective Tissue Composition	5. High Integration: >75% Connective Tissue Composition	
3	228	220 (96.5%)	8 (3.5%)	–	–	–	–	
6	255	231 (90.6%)	24 (9.4%)	–	–	–	–	
12	219	194 (88.6%)	20 (9.1%)	4 (1.8%)	1 (0.5%)	–	–	
18	310	256 (82.6%)	37 (11.9%)	16 (5.2%)	1 (0.3%)	–	–	
24	251	199 (79.3%)	38 (15.1%)	14 (5.5%)	–	–	–	
30	294	222 (75.5%)	46 (15.6%)	24 (8.2%)	2 (0.7%)	–	–	
36	214	29 (13.6%)	38 (17.8%)	85 (4.0%)	34 (15.9%)	13 (6.1%)	15 (7.0%)	
42	334	–	1 (3.0%)	14 (4.2%)	158 (47.3%)	92 (27.5%)	69 (20.7%)	
48	350	–	1 (2.9%)	29 (8.3%)	106 (30.3%)	124 (35.4%)	90 (25.7%)	
Normalized light intensity		0.16 [0.11–0.23]	0.25 [0.17–0.38]*	0.43 [0.32–0.61]†	0.65 [0.54–0.77]‡	0.72 [0.58–0.88]	0.80 [0.67–0.96]	<0.001

*p < 0.05 versus category 0, †p < 0.05 versus category 1, and ‡p < 0.05 versus category 2, performed by performed by post hoc multiple comparison.

due to suboptimal flushing were excluded from the light intensity analysis (1 scaffold at 6 months, 3 at 36 months, and 4 at 48 months).

Light intensity analysis of the strut cores was performed using dedicated software (QCU-CMS version 4.69 [research version]; Leiden, the Netherlands). Raw images with 16 bits in original polar format were used to ensure that interpolation, dynamic range compression, or other image processing did not alter the signal and bias the analysis. The contours of strut cores were delineated manually with "box-shape" by visual inspection in Cartesian images (Online Figure 1) (11). According to the strut contours, the median light intensity values were computed with the subtraction of 2 pixels inside of the manual strut core contour by the software automatically, as described previously (11).

To minimize bias in light intensity measurement caused by the variation in optical signal due to eccentric location of the optical coherence tomographic catheter or the uneven distribution of neointima on top of the strut, the light intensity values of strut cores were normalized by the median light intensity value of the interstrut neointima in the vicinity (bilaterally 22.5° wide originating from the strut center) of each strut (referred to as the normalized light intensity of strut cores) (Online Figure 1).

The light intensity analysis was performed in cross sections at intervals of 1 mm and additionally in the OCT-imaged struts matched with histology. **Figure 3** shows examples of strut appearance on the basis of normalized light intensity of strut cores on OCT.

MATCHING OF STRUTS ON HISTOLOGY AND OCT. To correlate strut cores and histology at a strut level, 1 observer (Y.O.) aware of the histological image selected the matched OCT-histology cross sections at each time point using landmarks such as side branches, metallic radiopaque markers, or the appearance of neointima and media (Online Appendix). In the selected cross sections of OCT and histology, individual struts were further matched by identifying struts with similar angular orientation and peculiar appearance of struts (strut-level matching) (Online Figure 2). To ensure accurate identification of the strut areas by OCT and histology, especially at later time points (36, 42, and 48 months), when struts are more integrated and thus more difficult to identify, strut contours drawn on optical coherence tomographic analysis were superimposed on histology to match the strut core regions and to calculate the percentage of infiltration by connective tissue normalized for the strut footprint area.

These matched strut images were sent to the independent optical coherence tomographic analyst (S.N.) and the pathologist (L.P.). The normalized light intensity of the OCT-imaged strut and the histological categorization of integration of this strut into the surrounding neointimal tissue was blinded to the observer who had performed the matching.

ECHOGENICITY ANALYSIS IN IVUS GRAYSCALE. IVUS quantitative analysis (vessel, scaffold, and luminal area) was performed in 0.5-mm intervals in the scaffolded segment and periscaffolded segments (defined by a length 5 mm proximal and distal to the stent edge). The normalized vessel area was calculated as the ratio of the vessel to the reference vessel area, and the normalized scaffold and luminal area was calculated as the ratio to the reference luminal area.

According to the contours of lumen and vessel, the dedicated software (QCU-CMS version 4.69 [research

FIGURE 4 Normalized Light Intensity and Histological Findings in Matched Strut Cores

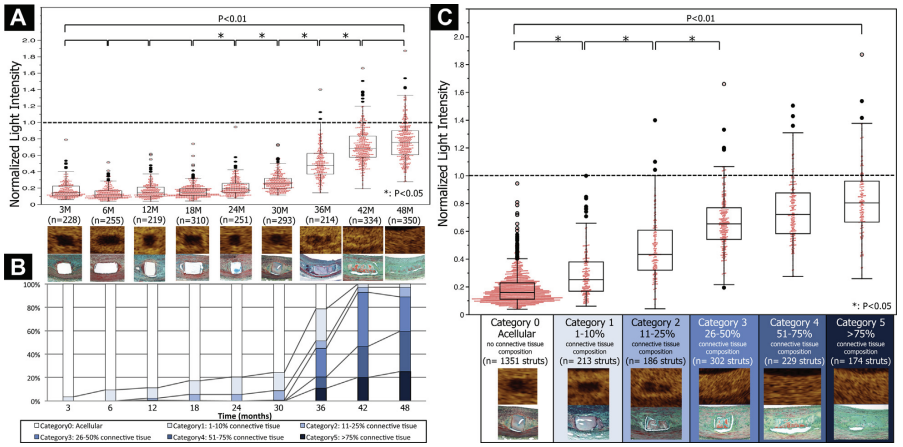

(A) Whisker plots combined with scatterplots of matched strut cores in normalized light intensity (dimensionless) over time. Normalized light intensity increased gradually between 18 and 30 months, then surged between 30 and 42 months and approached 1.0 at 48 months. **(B)** Changes in histological categories of struts over time. The rate of acellular struts decreased gradually during the first 30 months, then abruptly decreased from 75.5% at 30 months to 13.6% at 36 months. Spontaneously, the frequency of moderately to highly integrated struts (histological grade ≥3) increased from 0.7% to 94% between 30 and 42 months. After 42 months, there was no strut without integration. **(C)** Correlation between normalized light intensity on optical coherence tomography and histological categorization on whisker plots in combination with scatterplots. Normalized light intensity was significantly different between categories 0 and 1 ($p < 0.05$), between categories 1 and 2 ($p < 0.05$), and between categories 2 and 3 ($p < 0.05$). There were no significant differences in normalized light intensity among categories 3, 4, and 5. M = month.

version]) calculates the areas of 5 tissue types categorized by using the median brightness of the adventitia as a reference in the lumen-vessel compartments automatically: 1) hypoechogenic, 2) hyperechogenic, 3) calcified, 4) upper echogenic, and 5) unknown (9).

STATISTICAL ANALYSIS. All statistical analyses were performed using the SPSS version 23.0 (SPSS, Chicago, Illinois). Normality of distributions was tested with the Kolmogorov-Smirnov statistic. Continuous variables are presented as mean ± SD or median (interquartile range [IQR]), as indicated in the tables. Generalized estimating equations modeling was performed to take into an account the clustered nature of >1 scaffold analyzed from the same pig, which might result in unknown correlations among measurements within these scaffold clusters. Categorical variables are presented as absolute values and percentages. Relations between histological categories and normalized light intensity of strut cores were analyzed by Spearman's rank-order correlation. Bayesian analysis of normalized light intensity included estimation of area under the receiver-operating characteristic, curve with the optimal cut-off value for the detection of the onset of "strut integration" into the neointimal surrounding and the shift to "moderate to high filtration into the strut core," with associated sensitivity and specificity. A modification of the classification of Swets (13) was used to classify diagnostic efficiency of normalized light intensity according to the values of the area under the curve as low (<0.70), moderate (0.70 to 0.90), or high (>0.90).

RESULTS

In total, 336 histological cross sections and 112 optical coherence tomographic pull-backs were available (**Figure 2**). After excluding 4 optical coherence tomographic pull-backs because of impaired image quality, 108 pull-backs were analyzed for quantitative measurements. Of 108 pull-backs, 7 were excluded from the light intensity analysis for

TABLE 2 Optical Coherence Tomographic Quantitative Measurements

Quantitative Measurement	3 months (n = 10)	6 months (n = 10)	12 months (n = 11)	18 months (n = 12)	24 months (n = 12)	30 months (n = 12)	36 months (n = 12)
Mean scaffold area (mm^2)	7.05 ± 0.64	7.33 ± 0.51	7.82 ± 1.98	9.47 ± 2.39	9.90 ± 2.33	11.72 ± 2.97	10.49 ± 1.58
Minimum scaffold area (mm^2)	5.96 ± 1.24	6.42 ± 0.46	6.71 ± 1.61	8.33 ± 2.45	8.95 ± 2.21	10.81 ± 2.77	9.32 ± 1.45
Normalized scaffold area	0.95 ± 0.17	1.08 ± 0.23	1.08 ± 0.24	1.07 ± 0.24	1.10 ± 0.19	1.07 ± 0.07	1.35 ± 0.22
Mean luminal area (mm^2)	4.04 ± 0.62	4.37 ± 0.64	5.28 ± 1.12	6.49 ± 2.33	6.96 ± 2.25	8.45 ± 2.63	7.27 ± 1.48
Minimum luminal area (mm^2)	3.30 ± 0.96	3.33 ± 0.71	4.37 ± 0.85	5.56 ± 2.43	5.99 ± 1.95	7.47 ± 2.53	6.31 ± 1.54
Normalized luminal area	0.54 ± 0.13	0.65 ± 0.16	0.73 ± 0.13	0.72 ± 0.19	0.76 ± 0.16	0.77 ± 0.20	0.93 ± 0.17
Mean neointimal area (mm^2)	2.76 ± 0.60	2.69 ± 0.39	2.38 ± 0.98	2.71 ± 0.34	2.71 ± 0.31	3.00 ± 0.55	2.90 ± 0.54
Neointimal thickness on top of struts (μm)	218 ± 73	208 ± 15	151 ± 72	165 ± 47	162 ± 42	159 ± 38	179 ± 47
Area stenosis (%)	29.9 ± 8.8	27.8 ± 7.1	19.4 ± 6.5	20.7 ± 8.0	19.6 ± 6.7	17.9 ± 6.0	20.2 ± 5.4
Mean reference luminal area (mm^2)	7.69 ± 1.69	7.03 ± 1.49	7.29 ± 1.03	8.97 ± 1.92	9.11 ± 2.08	11.21 ± 2.39	7.97 ± 1.77
	n = 1,369 struts in 9 pigs	n = 1,646 struts in 9 pigs	n = 904 struts in 9 pigs	n = 1,364 struts in 12 pigs	n = 1,030 struts in 12 pigs	n = 1,134 struts in 12 pigs	n = 1,365 struts in 9 pigs
Normalized light intensity	0.17 (0.15–0.19)	0.15 (0.14–0.18)	0.14 (0.12–0.15)	0.19 (0.18–0.22)	0.25 (0.21–0.29)	0.3 (0.28–0.32)	0.55 (0.55–0.64)

Continued on the next page

technical reasons (3 because of TD OCT and 4 because of inappropriate image quality for light intensity analysis), resulting in 101 OCT pull-backs available for light intensity analysis. After excluding 33 histological cross sections because of lack of analyzable OCT pull-backs, 2,979 struts were identified in 303 histological cross sections. Using sectorial approximate locations and landmarks such as metallic radiopaque markers, side branches, and neointimal formation, a total of 2,455 struts were matched between OCT and histology.

LIGHT INTENSITY ANALYSIS OVER TIME. The light intensity analysis in 2,455 matched struts over time is summarized in Table 1 and Figure 4A. There was no significant difference in the normalized light intensity of strut cores until 18 months after scaffold implantation: 0.14 (IQR: 0.11 to 0.22) at 3 months, 0.12 (IQR: 0.08 to 0.17) at 6 months, 0.15 (IQR: 0.10 to 0.21) at 12 months, and 0.15 (IQR: 0.11 to 0.19) at 18 months. The normalized light intensity increased gradually between 18 and 30 months (0.19 [IQR: 0.14 to 0.26] at 24 months; $p = 0.001$ vs. 18 months; 0.26 [IQR: 0.20 to 0.32] at 30 months; $p < 0.001$ vs. 24 months). After 30 months, the normalized light intensity surged until 42 months: 0.48 (IQR: 0.37 to 0.62) at 36 months ($p < 0.001$ vs. 30 months) and 0.68 (IQR: 0.58 to 0.83) at 42 months ($p < 0.001$ vs. 36 months) and was close to 1.0 at 48 months (0.76 [IQR: 0.61 to 0.90]; $p = 1.00$ vs. 42 months), suggesting that the strut cores were completely integrated into the surrounding tissue.

HISTOLOGICAL FINDINGS. The categorization of histological integration of 2,455 matched struts over time is summarized in Table 1 and Figure 4B. From 3 to 12 months, the struts were completely separated from the lumen by a thin, fibromuscular neointima and had well-defined, squared appearances. Most of the struts were classified as acellular (96.5% at 3 months, 90.6% at 6 months, and 88.6% at 12 months). From 18 to 30 months, the strut footprints maintained their discrete borders but began to appear blue with Movat's pentachrome. The percentage of acellular struts decreased gradually (82.6% at 18 months, 79.3% at 24 months, and 75.5% at 30 months). Six months later (at 36 months), the percentage of acellular struts has abruptly decreased to 13.6%, and the strut footprints were generally colonized by connective tissue. These strut footprints further progressed up to the point at which the strut footprint was only poorly discernible. Twenty-nine percent of matched struts were classified as grade ≥3 (>25% of cellularization and connective tissue composition). After 42 months, there was no strut without integration, and the rate of highly integrated struts increased gradually up to 48 months. At 48 months, 61.1% of matched struts showed >50% of connective tissue composition.

COMPARISON BETWEEN OPTICAL COHERENCE TOMOGRAPHIC LIGHT INTENSITY ANALYSIS AND HISTOLOGICAL CLASSIFICATION. The correlation between the normalized light intensity on OCT and histological categorization of 2,455 matched struts is summarized in Table 1 and Figure 4C. There were significant differences among the histological categories with respect to normalized light intensity: 0.16 (IQR: 0.11 to 0.23) in category 0 (acellular), 0.25 (IQR: 0.17 to 0.38) in category 1 (1% to 10%), 0.43 (IQR: 0.32 to 0.61) in category 2 (11% to 25%), 0.65 (IQR: 0.54 to 0.77) in category 3 (26% to 50%), 0.72 (IQR: 0.58 to

TABLE 2 Continued

42 months (n = 13)	48 months (n = 16)	p Value								
		Overall	6 vs. 3 months	12 vs. 3 months	18 vs. 3 months	24 vs. 3 months	30 vs. 3 months	36 vs. 3 months	42 vs. 3 months	48 vs. 3 months
12.14 ± 2.00	12.64 ± 1.72	<0.001	0.182	0.238	0.002	<0.001	<0.001	<0.001	<0.001	<0.001
11.02 ± 2.31	11.60 ± 1.76	<0.001	0.138	0.209	0.004	<0.001	<0.001	<0.001	<0.001	<0.001
1.22 ± 0.18	1.20 ± 0.15	0.001	0.137	0.244	0.246	0.044	0.189	<0.001	0.001	<0.001
9.27 ± 2.02	9.69 ± 1.61	<0.001	0.116	<0.001	0.001	<0.001	<0.001	<0.001	<0.001	<0.001
8.41 ± 2.30	8.81 ± 1.80	<0.001	0.924	<0.001	0.005	<0.001	<0.001	<0.001	<0.001	<0.001
0.93 ± 0.16	0.92 ± 0.13	<0.001	0.098	0.002	0.022	<0.001	0.002	<0.001	<0.001	<0.001
2.57 ± 0.22	2.63 ± 0.24	0.241	0.714	0.352	0.802	0.766	0.345	0.562	0.284	0.48
138 ± 34	140 ± 19	<0.001	0.689	0.056	0.04	0.021	0.016	0.128	<0.001	<0.001
15.0 ± 5.0	14.6 ± 2.2	<0.001	0.476	0.002	0.007	0.001	<0.001	0.001	<0.001	<0.001
10.09 ± 2.01	10.68 ± 1.80	<0.001	0.346	0.485	0.128	0.051	<0.001	0.703	0.004	<0.001
n = 1,335 struts in 13 pigs	n = 1,894 struts in 16 pigs									
0.8 (0.77–0.87)	0.82 (0.79–0.83)	<0.001	0.296	0.426	0.565	0.001	<0.001	<0.001	<0.001	<0.001

0.88) in category 4 (51% to 75%), and 0.80 (IQR: 0.67 to 0.96) in category 5 (>75%) ($p < 0.01$). In paired comparison, normalized light intensity was significantly different between categories 0 and 3, whereas there were no significant differences between categories 3 and 5 (**Table 1**, **Figure 4C**). In Spearman rank-order correlation analysis, there was a significant positive correlation between histological category of integration and normalized light intensity of strut cores ($r = 0.791$; $p < 0.01$).

Receiver-operating characteristic curves demonstrated that the diagnostic efficiency of the normalized light intensity of strut cores for the detection of the onset of the "strut integration" into the surrounding neointima (histological category ≥1, area under the curve 0.924, cutoff value 0.326) and for the detection of the shift to "moderate to high filtration into the strut core" (histological category ≥3, area under the curve 0.965, cutoff value 0.413) were excellent (Online Figure 3).

QUANTITATIVE MEASUREMENTS ON OCT. The optical coherence tomographic quantitative measurements and light intensity analysis of strut cores performed in 1-mm interval cross sections are summarized in **Table 2** and Online Figure 4. At baseline, there were no significant difference in scaffold and flow area among all time-point groups (scaffold area, $p = 0.113$; flow area, $p = 0.124$). Compared with 3 months (0.54 ± 0.13), the normalized luminal area was significantly larger after 12 months ($p < 0.05$). The neointimal thickness on top of struts decreased significantly at 48 compared with 3 months (218 ± 73 μm at 3 months vs. 140 ± 19 μm at 48 months, $p < 0.001$).

The light intensity analysis of strut core in 1-mm intervals was in line with the matched struts, showing a surge between 30 and 42 months.

QUANTITATIVE MEASUREMENTS AND ECHOGENICITY CHANGES ON IVUS. The IVUS quantitative measurements and echogenicity analysis on the basis of 0.5-mm-interval cross sections are summarized in **Table 3**. The area of vessel wall (including media and neointima) did not change over time, whereas the thickness of vessel wall significantly decreased at 48 months (0.33 ± 0.06 mm) compared with 3 months (0.41 ± 0.05 mm) ($p < 0.001$).

The hyperechogenicity plus upper echogenicity area, a surrogate parameter for the molecular weight of PLLA (9), significantly decreased during the first 24 months (0.42 [IQR: 0.29 to 0.56] at 24 months vs. 1.10 [IQR: 1.07 to 1.48] at 3 months, $p < 0.001$).

DISCUSSION

The main findings of the present analysis are as follows (**Figures 5 and 6A**). First, following polymeric scaffold implantation, the normalized light intensity of strut cores did not change between 3 and 18 months; thereafter it gradually increased from 18 to 30 months, but the change in light intensity significantly surged between 30 and 42 months. Second, the histological evaluation showed that the frequency of acellular strut cores (absence of tissue infiltration) remained the same up to 12 months and then gradually decreased up to 30 months and began to dramatically change between 30 and 42 months, virtually disappearing at 48 months. Third, in matched struts for OCT and histology, the normalized

TABLE 3 Intravascular Ultrasound Quantitative Measurements

Quantitative Measurement	3 months (n = 10)	6 months (n = 7)	12 months (n = 11)	18 months (n = 12)	24 months (n = 12)	30 months (n = 12)
Mean vessel area, mm^2	8.30 ± 1.12	8.66 ± 1.34	8.86 ± 1.93	10.79 ± 2.46	11.86 ± 2.53	11.81 ± 3.31
Normalized vessel area by reference vessel area	0.94 ± 0.19	1.06 ± 0.18	0.99 ± 0.12	1.04 ± 0.12	1.05 ± 0.13	0.99 ± 0.17
Mean scaffold area, mm^2	5.81 ± 1.17	6.12 ± 1.20	6.39 ± 1.82	8.16 ± 2.30	8.74 ± 2.06	9.13 ± 3.00
Normalized scaffold area by reference luminal area	0.76 ± 0.15	0.92 ± 0.16	0.82 ± 0.14	0.93 ± 0.15	0.86 ± 0.13	0.84 ± 0.17
Mean luminal area, mm^2	4.59 ± 0.88	4.96 ± 1.02	5.01 ± 1.18	6.73 ± 2.23	7.11 ± 2.01	7.89 ± 2.79
Normalized luminal area by reference luminal area	0.60 ± 0.10	0.74 ± 0.13	0.65 ± 0.12	0.76 ± 0.16	0.70 ± 0.12	0.72 ± 0.16
Mean neointimal area + media	3.73 ± 0.73	3.70 ± 0.45	4.01 ± 1.20	4.03 ± .0.60	4.75 ± 0.67	3.95 ± 0.61
Vessel wall thickness (thickness between lumen and vessel)	0.41 ± 0.05	0.40 ± 0.03	0.35 ± 0.11	0.39 ± .0.08	0.44 ± 0.04	0.36 ± 0.02
Mean reference vessel area, mm^2	8.96 ± 1.54	8.30 ± 1.63	8.93 ± 1.53	10.46 ± .2.60	11.39 ± 2.65	12.06 ± 3.18
Mean reference luminal area, mm^2	6.08 ± 1.29	5.60 ± 1.27	6.56 ± 1.07	8.06 ± .2.24	8.74 ± 2.08	9.61 ± 2.68
Echogenicity analysis						
Mean upper, mm^2	0.4 (0.30–0.46)	0.3 (0.17–0.34)	0.22 (0.16–0.29)	0.26 (0.17–0.29)	0.26 (0.16–0.28)	0.25 (0.16–0.27)
Mean hyper, mm^2	0.73 (0.64–1.04)	0.78 (0.74–0.84)	0.46 (0.38–0.65)	0.65 (0.23–0.83)	0.24 (0.10–0.35)	0.24 (0.16–0.32)
Mean upper + hyper, mm^2	1.10 (1.07–1.48)	0.98 (0.90–1.16)	0.8 (0.68–0.87)	0.91 (0.47–1.10)	0.42 (0.35–0.60)	0.46 (0.43–0.54)

Continued on the next page

light intensity was able to differentiate the degree and intensity of connective tissue infiltration inside the strut cores. Using a cutoff value of 0.413, the normalized light intensity could detect the advanced process of integration of the strut cores (histological grade ≥3) with an accuracy of 0.922. Fourth, the optical coherence tomographic quantitative measurements demonstrated that the scaffold and luminal area normalized to the reference luminal area increased between 30 and 36 months. The neointimal thickness on top of the struts and the black core strut thickness (if visible) decreased concurrently between 36 and 42 months. Fifth, the IVUS quantitative measurements were in line with the results of optical coherence tomographic measurements but were not as discrete as those of OCT. The area of neointima plus media in absolute value did not show a significant change over time, whereas there was a thinning of the vessel wall (thickness between lumen and vessel) due to the late luminal enlargement. Finally, the upper echogenicity plus hyperechogenicity area steadily decreased during the first 24 months, reflecting the early loss of molecular weight.

LUMINAL ENLARGEMENT IN THE FIRST 2 YEARS: LOSS OF MECHANICAL INTEGRITY AND ADAPTIVE EXPANSION TO THE INHERENT ARTERIAL GROWTH OF THE MODEL. One of the most important findings of the present study is that there are 2 phases of vessel and luminal growth in 4 years after implantation of the Absorb bioresorbable scaffold. On IVUS and OCT, the first significant luminal and scaffold enlargement occurs between 6 to 18 months, whereas the second occurs between 30 and 42 months (**Figure 6A**). Of note, these luminal gains were not observed following permanent metallic stent implantation, because of the permanent mechanical caging (2,14).

The first growth of the scaffold and luminal area seems to be related to the loss of mechanical integrity and the natural growth of coronary artery. The Absorb device loses its mechanical strength 6 months after implantation (15,16). On OCT, at 3 months, luminal and scaffold area is normalized by the reference lumen smaller than the reference area (0.54), but after 6 months, and coinciding with the loss of mechanical integrity, the scaffold and lumen started to follow the enlargement of reference area (normalized lumen area at 12 to 30 months: 0.72 to 0.77). The current animal study was performed in the Yucatan pig model, which is known to have inherent coronary arterial growth over time (2,17).

SECOND-PHASE LUMINAL ENLARGEMENT: INTEGRATION OF STRUT CORE. The second phase of vessel remodeling, which occurred between 30 and 42 months, is presumably due to the integration process. During this period, the normalized luminal area further increased from 0.77 to 0.93. On histology, rapid integration of the struts in the surrounding neointima was observed. The frequency of moderately to highly integrated struts (histological grade ≥3) increased from 0.7% to 94%, which was clearly illustrated by the surge of light intensity inside the strut core void on OCT.

During the infiltration of connective tissue into the provisional matrix, the thickness of the neointima on top of struts decreased. It is still unclear whether maturation from a provisional matrix to collagen-rich connective tissue may further influence

TABLE 3 Continued

36 months (n = 12)	42 months (n = 13)	48 months (n = 20)	p Value							
			Overall	6 vs. 3 months	12 vs. 3 months	18 vs. 3 months	24 vs. 3 months	30 vs. 3 months	36 vs. 3 months	42 vs. 3 months	48 vs. 3 months
11.21 ± 1.65	13.37 ± 1.83	13.43 ± 1.64	<0.001	0.596	0.478	0.002	<0.001	0.004	<0.001	<0.001	<0.001
1.08 ± 0.10	1.07 ± 0.08	0.97 ± 0.06	0.005	0.203	0.521	0.135	0.124	0.552	0.042	0.048	0.734
8.50 ± 1.26	10.47 ± 1.44	10.14 ± 1.28	<0.001	0.57	0.396	0.001	<0.001	0.002	<0.001	<0.001	<0.001
0.94 ± 0.11	0.96 ± 0.07	0.86 ± 0.07	0.001	0.07	0.429	0.012	0.109	0.282	0.003	<0.001	0.041
7.04 ± 1.22	9.21 ± 1.26	9.45 ± 1.18	<0.001	0.428	0.391	0.002	<0.001	0.001	<0.001	<0.001	<0.001
0.78 ± 0.10	0.85 ± 0.07	0.81 ± 0.08	<0.001	0.033	0.341	0.007	0.06	0.055	<0.001	<0.001	<0.001
4.19 ± 0.61	4.13 ± 0.72	3.99 ± 0.16	0.005	0.925	0.48	0.274	0.001	0.469	0.085	0.2	0.365
0.39 ± 0.05	0.35 ± 0.05	0.33 ± 0.06	<0.001	0.824	0.056	0.666	0.176	0.019	0.385	0.006	<0.001
10.50 ± 1.97	12.57 ± 2.18	13.96 ± 1.79	<0.001	0.347	0.959	0.061	0.004	0.003	0.027	<0.001	<0.001
7.98 ± 1.62	9.79 ± 1.63	10.57 ± 1.45	<0.001	0.436	0.369	0.007	<0.001	<0.001	0.003	<0.001	<0.001
0.18 (0.12-0.20)	0.18 (0.11-0.20)	0.11 (0.07-0.14)	<0.001	0.056	0.001	<0.001	<0.001	<0.001	<0.001	<0.001	<0.001
0.25 (0.14-0.34)	0.19 (0.17-0.31)	0.10 (0.07-0.16)	<0.001	0.688	0.003	0.022	<0.001	<0.001	<0.001	<0.001	<0.001
0.42 (0.29-0.56)	0.38 (0.32-0.50)	0.22 (0.15-0.29)	<0.001	0.197	<0.001	0.001	<0.001	<0.001	<0.001	<0.001	<0.001

mechanotransduction by improving the transmission of mechanical signal (18). The stimulation of initial smooth muscle cells can induce matrix metalloproteinase release, which plays a key role in matrix deposition and reorganization by collagen type I deposition that leads to negative arterial remodeling and potential neointimal shrinkage (18–21).

CLINICAL IMPLICATIONS. The present analysis confirms that 1) OCT light intensity correlated with the integration process and that 2) IVUS echogenicity can detect early changes in molecular weight. By using IVUS echogenicity, molecular weight loss could be monitored, and the timing of loss of mechanical integrity could be predicted. Without any reference to gel permeate chromatography in vivo, it would be clinically useful to judge by echogenicity the degree of biodegradation related to the loss of mechanical strength and subsequent restoration of mechanotransduction.

Optical coherence tomographic light intensity is more sensitive for the integration process, which is associated with the thinning of the vessel wall as well as very late luminal enlargement. By using the classification of strut (using a proposed cutoff of 0.413 for infiltration greater than 25%), clinicians can assess the stage of integration that heralds late luminal enlargement.

When the quantitative light intensity analysis is applied to the human data obtained from ABSORB cohort B (**Figure 6B**), the light intensity surge had not yet been detected at 36 months (the average of normalized light intensity was 0.22 in 161 sequentially matched struts). This suggests that the integration process in humans is somewhat slower than that in animals and that either late luminal enlargement could commence later than 3 years or that the underlying plaque fails to allow positive remodeling because it is rich in type I collagen.

The influence of the underlying plaque on the integration process remains unclear. In previous clinical studies, the Absorb scaffold was associated with a decrease of the plaque area on IVUS in the long term when compared with post-implantation (22). It was questioned whether this is due to the disappearance of struts or the real reduction of atherosclerotic plaque. In the present animal study, the area of neointima plus media remained unchanged throughout the 4-year follow-up period, whereas vessel wall thickness was reduced as a result of the very late luminal expansion or conversion of type III collagen to type I with cross-linking of collagen (**Figure 6A**). This suggests that the integration of the struts does not significantly affect the area of neointima plus media but induces the expansion of the lumen and the vessel, which could be mediated by the mechanotransduction and the restoration of shear stress (1).

FROM VISUAL CATEGORIZATION TO QUANTITATIVE MEASUREMENT OF LIGHT INTENSITY. In the present analysis, we used quantitative assessment of light intensity, which is more reproducible than visual assessment. The method has been applied to optical coherence tomographic analysis of struts in humans. The intraclass correlation coefficient for interobserver variability was as high as 0.91 (11).

The present OCT analysis using the second iteration of the Absorb device showed that using a cutoff of 0.413, the measured light intensity can

FIGURE 5 Change of Strut Core on Histology, Optical Coherence Tomography, and Intravascular Ultrasound From 3 to 48 Months

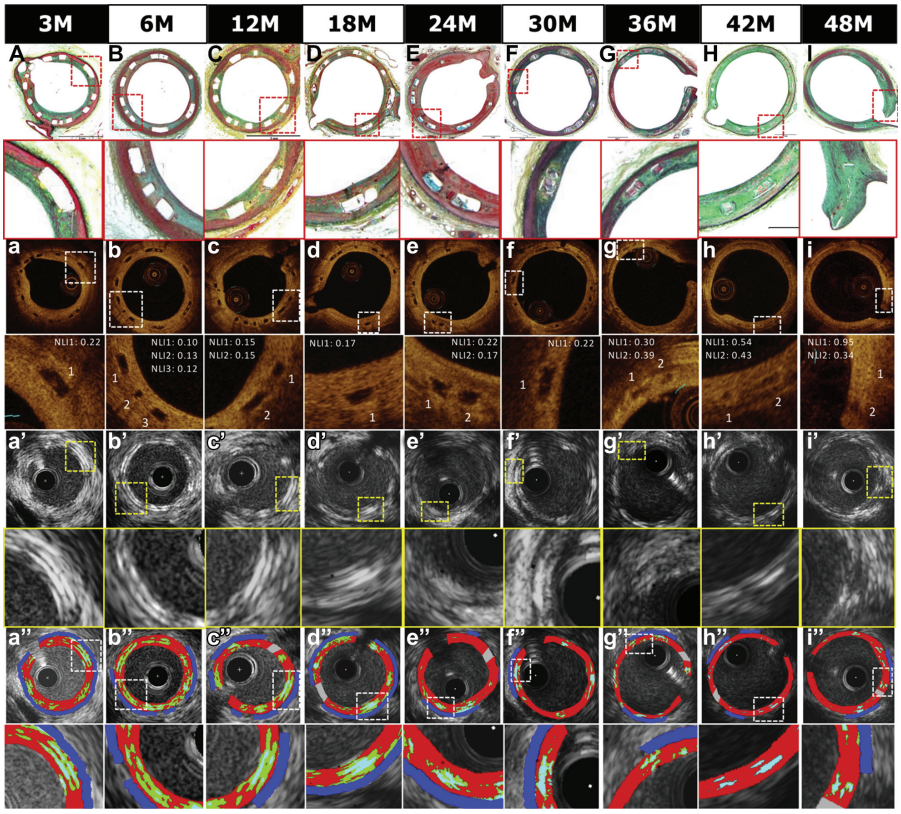

The figure summarizes the changes in strut cores from 3 to 48 months in the matched struts between histology **(A–I)**, optical coherence tomography (OCT) **(a–i)**, intravascular ultrasound (IVUS) grayscale **(a′–i′)**, and IVUS echogenicity **(a″–i″)**. During the first 18 months, the struts were completely sequestered from the lumen by a thin and fibromuscular neointima with well-defined and squared edge on histology. **(A–D)** Although the normalized light intensity (NLI) on OCT showed low values **(a–d)**, the echogenicity of struts on IVUS decreased gradually (light blue area plus green area in **a″–d″**). At 24 and 30 months, the strut footprints had discrete borders but started to be replaced by provisional matrix **(E)**, followed by infiltration by connective tissue on histology **(F–I)**. The NLI slightly increased **(e,f)**, whereas the echogenicity of struts reached to plateau **(e″,f″)**. On histology, the filtration inside of strut void rapidly advanced between 30 and 42 months **(G,H)**. Correspondingly, the normalized intensity on OCT surged **(g,h)**. At 48 months, the integration of strut cores was almost complete **(I)**, and the NLI reached a plateau **(i′)**. Light blue indicates upper echogenicity, and light green indicates hyperechogenicity.

differentiate moderately to highly integrated struts from low-integrated struts with an accuracy of 0.922. This integration progressively occurs between 30 and 42 months after implantation, which seems to be the critical timing for maximal vessel remodeling.

The other possible optical coherence tomographic methods to evaluate the bioresorption process include the refractive index or dispersion to differentiate the provisional matrix and polymer, or birefringence analysis using polarization-sensitive

FIGURE 6 Relationships Among Quantitative Light Intensity Analysis, Luminal Area, and Echogenicity in Animal and Human Models

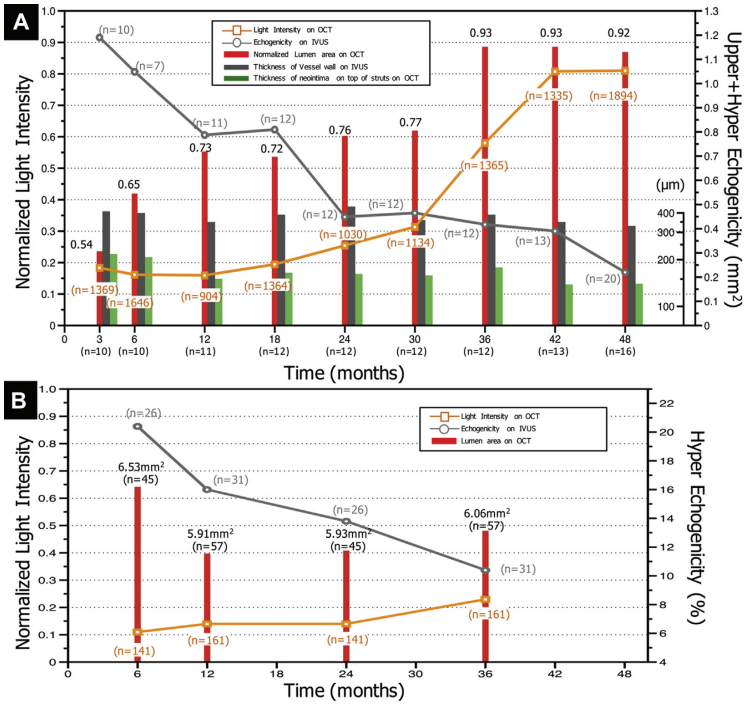

(A) The relationships among quantitative light intensity, normalized luminal area, and echogenicity with superimposed wall thickness and neointimal thickness on top of struts in swine. There are 2 periods of facilitated enlargement of normalized luminal area **(red bar)**. The first enlargement of lumen occurs during the first 30 months, which could be related to the loss of mechanical integrity and the natural growth of the coronary artery. During this period, the upper echogenicity plus hyperechogenicity area on intravascular ultrasound (IVUS) echogenicity decreased and reached a plateau **(gray line)**. The second luminal enlargement occurred between 30 and 42 months. During this period, the normalized light intensity on optical coherence tomography (OCT) surged **(orange line)**. In addition, the vessel wall thickness **(gray bar)** was reduced with the thinning of the neointima on top of struts **(green bar)**. **(B)** The relationships among quantitative light intensity, luminal area, and echogenicity in humans. In the ABSORB cohort B trial, at 36 months IVUS echogenicity had decreased **(gray line)**, whereas the normalized light intensity on OCT had not yet surged (the average of normalized light intensity was 0.22 at 36 months; orange line). Luminal area did not change significantly from 12 to 36 months.

OCT (23). In terms of quantitative measurement, OCT is presumably more close to the in vivo dimension than histomorphometric measurement, because of the absence of vessel shrinkage from histological preparation (24).

On histology, we used a semiquantitative scale to classify the degree of integration. Theoretically, the infiltration rate of connective tissues into the strut footprint could also be quantifiable on histology; however, because of tissue shrinkage due to formalin fixation and dehydration with tissue processing, it is unclear which segment of the vessel may be most affected. It is likely to be proteoglycans, which are water rich, and dehydration affects water-rich areas more than other regions. It was also possible that the strut footprint could deform during the histological

processing; after 4 years, the original area occupied by the polymeric strut is poorly discernible by light microscopy, which made quantitative measurement on histology difficult. The use of time-of-flight secondary iron mass spectroscopic analysis might facilitate future pre-clinical studies to quantify the degrees of degradation and integration (25).

STUDY LIMITATIONS. The present study was performed in a healthy porcine model without atherosclerosis, so the generalizability of the concepts to human is therefore limited. The methodology for normalization is not necessarily applicable to humans, because homogeneity of neointima is different between human and porcine models. The expected complex relationships among plaque burden, mechanotransduction, luminal enlargement and vascular remodeling, and natural coronary artery growth are not yet elucidated in the current models, although the initial molecular weight loss due to depolymerization is not different between human and pigs, because the process is purely chemical via hydrolysis.

From a regulatory perspective, it is mandatory to investigate the process of bioresorption of each fully bioresorbable scaffold, because the rate can vary according to the manufacturing process. The current assessment for monitoring bioresorption and integration process by echogenicity on IVUS and light intensity on OCT could be applied only to scaffolds made of PLLA, with similar molecular weights and similar manufacturing processes, but it could not be applied to other scaffolds made of different materials (e.g., magnesium), with different molecular weights (e.g., Igaki-Tamai) or different manufacturing processes (e.g., Mirage).

CONCLUSIONS

In this pre-clinical model, luminal enlargement is a biphasic process in which the latter phase likely relates, at least in part, to strut integration of the Absorb scaffold into the arterial wall. The quantitative light intensity analysis of strut cores on OCT could be used as a surrogate method for monitoring matrix infiltration and integration of collagen-rich connective tissue within the polymeric struts that coincide with the time of late luminal enlargement. These intravascular methods may provide insight and understanding of the imaging-related characteristics of the bioresorption process of various polylactide scaffolds in human.

REPRINT REQUESTS AND CORRESPONDENCE: Dr. Yoshinobu Onuma, Thoraxcenter, Ba-583, 's Gravendijkwal 230, 3015 CE Rotterdam, the Netherlands. E-mail: yoshinobuonuma@gmail.com.

PERSPECTIVES

WHAT IS KNOWN? Visual categorizations of strut appearance of bioresorbable scaffolds on OCT have previously been demonstrated to correlate with the integration process with limited reproducibility. Light intensity analysis of strut cores has been introduced as a feasible and reproducible method for a quantitative assessment of strut integration after scaffold implantation.

WHAT IS NEW? In a porcine pre-clinical model, IVUS echogenicity analysis and light intensity analysis on OCT were well correlated with the depolymerization process of the strut and the integration process after the complete bioresorption, respectively. The late luminal enlargement observed between 3 and 4 years seems to be related to strut integration.

WHAT IS NEXT? Further studies are needed to evaluate the generalizability of the concepts to human and to elucidate the expected complex relationships among plaque burden, mechanotransduction, luminal enlargement and vascular remodeling, and natural coronary artery growth.

REFERENCES

1. Serruys PW, Garcia-Garcia HM, Onuma Y. From metallic cages to transient bioresorbable scaffolds: change in paradigm of coronary revascularization in the upcoming decade? Eur Heart J 2012;33:16–25.

2. Lane JP, Perkins LE, Sheehy AJ, et al. Lumen gain and restoration of pulsatility after implantation of a bioresorbable vascular scaffold in porcine coronary arteries. J Am Coll Cardiol Intv 2014;7:688–95.

3. Onuma Y, Dudek D, Thuesen L, et al. Five-year clinical and functional multislice computed tomography angiographic results after coronary implantation of the fully resorbable polymeric everolimus-eluting scaffold in patients with de novo coronary artery disease: the ABSORB cohort A trial. J Am Coll Cardiol Intv 2013;6:999–1009.

4. Radu MD, Raber L, Kalesan B, et al. Coronary evaginations are associated with positive vessel remodelling and are nearly absent following implantation of newer-generation drug-eluting stents: an optical coherence tomography and intravascular ultrasound study. Eur Heart J 2014;35:795–807.

5. Serruys PW, Onuma Y, Garcia-Garcia HM, et al. Dynamics of vessel wall changes following the implantation of the absorb everolimus-eluting bioresorbable vascular scaffold: a multi-imaging modality study at 6, 12, 24 and 36 months. Eurointervention 2014;9:1271–84.

6. Otsuka F, Pacheco E, Perkins LE, et al. Long-term safety of an everolimus-eluting bioresorbable vascular scaffold and the cobalt-chromium XIENCE V stent in a porcine coronary artery model. Circ Cardiovasc Interv 2014;7:330–42.

7. Vorpahl M, Finn AV, Nakano M, Virmani R. The bioabsorption process: tissue and cellular mechanisms and outcomes. Eurointervention 2009;5 Suppl F:F28–35.

8. Middleton JC, Tipton AJ. Synthetic biodegradable polymers as orthopedic devices. Biomaterials 2000;21:2335–46.

9. Campos CM, Ishibashi Y, Eggermont J, et al. Echogenicity as a surrogate for bioresorbable everolimus-eluting scaffold degradation: analysis at 1-, 3-, 6-, 12–18, 24-, 30-, 36- and 42-month follow-up in a porcine model. Int J Cardiovasc Imaging 2015;31:471–82.

10. Onuma Y, Serruys PW, Perkins LE, et al. Intracoronary optical coherence tomography and histology at 1 month and 2, 3, and 4 years after implantation of everolimus-eluting bioresorbable vascular scaffolds in a porcine coronary artery model: an attempt to decipher the human optical coherence tomography images in the ABSORB trial. Circulation 2010;122:2288–300.

11. Nakatani S, Onuma Y, Ishibashi Y, et al. Temporal evolution of strut light intensity after implantation of bioresorbable polymeric intracoronary scaffolds in the ABSORB cohort B trial. Circ J 2014;78:1873–81.

12. Serruys PW, Onuma Y, Ormiston JA, et al. Evaluation of the second generation of a bioresorbable everolimus drug-eluting vascular scaffold for treatment of de novo coronary artery stenosis: six-month clinical and imaging outcomes. Circulation 2010;122:2301–12.

13. Swets JA. Measuring the accuracy of diagnostic systems. Science 1988;240:1285–93.

14. Strandberg E, Zeltinger J, Schulz DG, Kaluza GL. Late positive remodeling and late lumen gain contribute to vascular restoration by a non-drug eluting bioresorbable scaffold: a four-year intravascular ultrasound study in normal porcine coronary arteries. Circ Cardiovasc Interv 2012;5:39–46.

15. Oberhauser JP, Hossainy S, Rapoza RJ. Design principles and performance of bioresorbable polymeric vascular scaffolds. Eurointervention 2009;5 Suppl F:F15–22.

16. Onuma Y, Serruys PW. Bioresorbable scaffold: the advent of a new era in percutaneous coronary and peripheral revascularization? Circulation 2011; 123:779–97.

17. Lowe HC, Schwartz RS, Mac Neill BD, et al. The porcine coronary model of in-stent restenosis: current status in the era of drug-eluting stents. Catheter Cardiovasc Interv 2003;60:515–23.

18. Chien S. Mechanotransduction and endothelial cell homeostasis: the wisdom of the cell. Am J Physiol Heart Circ Physiol 2007;292:H1209–24.

19. Deguchi JO, Aikawa E, Libby P, et al. Matrix metalloproteinase-13/collagenase-3 deletion promotes collagen accumulation and organization in mouse atherosclerotic plaques. Circulation 2005; 112:2708–15.

20. Galis ZS, Khatri JJ. Matrix metalloproteinases in vascular remodeling and atherogenesis: the good, the bad, and the ugly. Circ Res 2002;90: 251–62.

21. Nagase H, Visse R, Murphy G. Structure and function of matrix metalloproteinases and TIMPs. Cardiovasc Res 2006;69:562–73.

22. Sarno G, Bruining N, Onuma Y, et al. Morphological and functional evaluation of the bioresorption of the bioresorbable everolimus-eluting vascular scaffold using IVUS, echogenicity and vasomotion testing at two year follow-up: a patient level insight into the ABSORB A clinical trial. Int J Cardiovasc Imaging 2012;28:51–8.

23. Tearney GJ, Bouma BE. Shedding light on bioabsorbable stent struts seen by optical coherence tomography in the ABSORB trial. Circulation 2010;122:2234–5.

24. Gogas BD, Radu M, Onuma Y, et al. Evaluation with in vivo optical coherence tomography and histology of the vascular effects of the everolimus-eluting bioresorbable vascular scaffold at two years following implantation in a healthy porcine coronary artery model: implications of pilot results for future pre-clinical studies. Int J Cardiovasc Imaging 2012;28:499–511.

25. Ninomiya S, Ichiki K, Yamada H, et al. Precise and fast secondary ion mass spectrometry depth profiling of polymer materials with large Ar cluster ion beams. Rapid Commun Mass Spectrom 2009; 23:1601–6.

26. Simsek C, Karanasos A, Magro M, et al. Long-term invasive follow-up of the everolimus-eluting bioresorbable vascular scaffold: five-year results of multiple invasive imaging modalities. Eurointervention 2016;11:996–1003.

KEY WORDS **biodegradable polymer, bioresorbable scaffold, coronary intervention, intravascular ultrasound, optical coherence tomography, pathology**

APPENDIX **For additional methods and supplemental figures, please see the online version of this article.**

4.4 Receding of aneurysm after implantation of bioresorbable scaffolds

Development and receding of a coronary artery aneurysm after implantation of a fully bioresorbable scaffold.

Circulation. 2015 Feb 24;131(8):764-7.
[Case report, IF 14.95]

Nakatani S, **Ishibashi Y**, Suwannasom P, J Grundeken M, Høj Christiansen E, Onuma Y, Serruys PW; ABSORB Cohort B Investigators.

Development and Receding of a Coronary Artery Aneurysm After Implantation of a Fully Bioresorbable Scaffold

Shimpei Nakatani, MD; Yuki Ishibashi, MD, PhD; Pannipa Suwannasom, MD; Maik J. Grundeken, MD; Evald Høj Christiansen, MD, PhD; Yoshinobu Onuma, MD, PhD; Patrick W. Serruys, MD, PhD; on behalf of the ABSORB Cohort B Investigators

A 83-year-old man included in the ABSORB cohort B trial underwent successful percutaneous coronary intervention of the middle left anterior descending artery with a 3.0×18-mm bioresorbable scaffold (Absorb, Abbott Vascular, CA) that was postdilated with a 3.0-mm noncompliant balloon at 24 atm (Figure 1A and 1B). The 2-dimensional and 3-dimensional (3D) optical coherence tomography (OCT) confirmed the absence of structural discontinuity after the procedure (Figure 2B and Figure 3A'). At 6 months, the planned angiography showed the absence of restenosis but an ectasia in the scaffolded segment (Figure 1C). Intravascular ultrasound revealed a focal vessel and lumen enlargement (17.93 mm^2 [Δ+20.5%] and 6.99 mm^2 [Δ+9.6%], respectively, in the matched cross-section analysis; Figure 2C), whereas 3D OCT suggested a deformation of the scaffold in the 2-mm segment of the ectasia (Figure 3B'). At 18 months, the planned multislice computed tomography showed lumen dilatation in the scaffolded segment (Figure 1D). At 2 years, on angiography, the ectatic lesion in the scaffold became aneurysmal (50% increase compared with the adjacent reference vessel; Figure 1E). Intravascular imaging revealed the increase in the vessel area and lumen area (20.90 mm^2 [Δ+40.5%] on intravascular ultrasound and 10.91 mm^2 [Δ+35.7%] on OCT, respectively, from baseline; Figure 1E and 1F), whereas 3D OCT showed a focal cleavage of the scaffold rings and a bulge of the vessel in the segment free from the scaffold struts (Figure 3C and C'). Five years after implantation, angiography revealed that the aneurysm was still present but had become smaller compared with the previous time points (Figure 1F). Intravascular ultrasound and OCT demonstrated the diminished vessel and lumen area (17.11 mm^2 [Δ−18.1%] and 8.78 mm^2 [Δ−19.5%], respectively, from 2 years; Figure 2G and 2H), making the scaffold indiscernible on OCT.

In general, aneurysm after drug-eluting device implantation is attributed to residual dissection and deep arterial wall injury and to inflammatory and allergic reactions to the drug, polymer, or device such as metal. In rare cases, a fully bioresorbable poly(L-lactide) acid prosthesis can cause inflammation.[1] Further insight can be obtained from the 3D reconstructions of the OCT signal (Figure 3A', 3B', and 3C'), in which the pattern of the struts can qualitatively outline the time history of the aneurysmal expansion. From implantation to 6 months, the wall distended and displaced the strut pattern without an apparent change in intracrown angulations, indicating a wall distention that occurred while the strut material was still continuous and minimally degraded. Further expansion from 6 to 24 months occurred in part after substantial polymer degradation had already occurred, as evidenced by the widening of intracrown angulations or complete separation of strut segments, indicating that strut migration follows wall migration entirely and continuity of struts has diminished to subpattern levels. Cross-sectional and longitudinal reconstructions of these segments appear to show that, although diameter is substantially distended, the arterial wall thickness over and under the struts is uniform in nature, an appearance inconsistent with severe inflammatory reactions to polymer.

Disclosures

Dr Serruys is a member of Advisory Board of Abbott Vascular.

References

1. Katsuragi YT, Gomi A, Sunaga A, Miyazaki K, Kamochi H, Arai F, Fukushima N, Sugawara Y. Intracerebral foreign body granuloma caused by a resorbable plate with passive intraosseous translocation after cranioplasty. *J Neurosurg Pediatr*. 2013;12:622–625. doi: 10.3171/2013.9.PEDS13187.

From the Thoraxcenter, Erasmus Medical Center, Rotterdam, The Netherlands (S.N., Y.I., P.S., Y.O.); Academic Medical Center, University of Amsterdam, Amsterdam, The Netherlands (M.G.); Aarhus University Hospital, Skejby, Aarhus, Denmark (E.H.C.); and International Centre for Circulatory Health, NHLI, Imperial College London, UK (P.W.S.).

Correspondence to Patrick W. Serruys, MD, PhD, International Centre for Circulatory Health, NHLI, Imperial College London, London, UK. E-mail patrick.w.j.c.serruys@gmail.com

(*Circulation*. 2015;131:764-767. DOI: 10.1161/CIRCULATIONAHA.114.014257.)

Circulation is available at http://circ.ahajournals.org DOI: 10.1161/CIRCULATIONAHA.114.014257

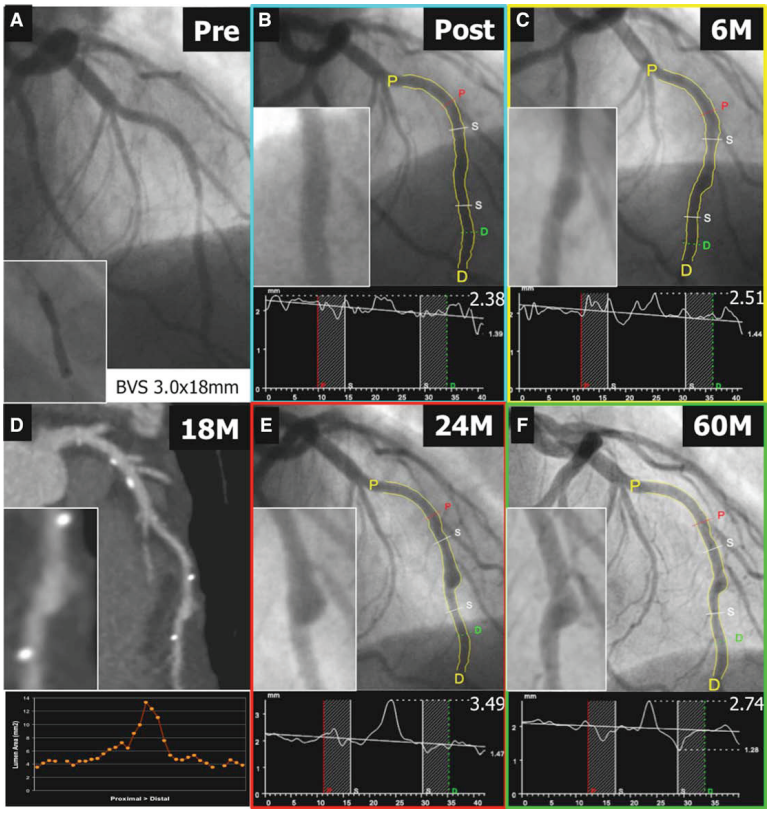

Figure 1. Coronary angiography of the left anterior descending artery before (**A**) and after (**B**) intervention at baseline. At 6 months, the planned angiography showed an ectasia in the scaffolded segment (**C**). The planned multislice computed tomography showed lumen dilatation in the scaffolded segment at 18 months (**D**). Repeat angiography demonstrated that the ectatic lesion in the scaffold became aneurysmal at 2 years (**E**) and diminished at 5 years (**F**).

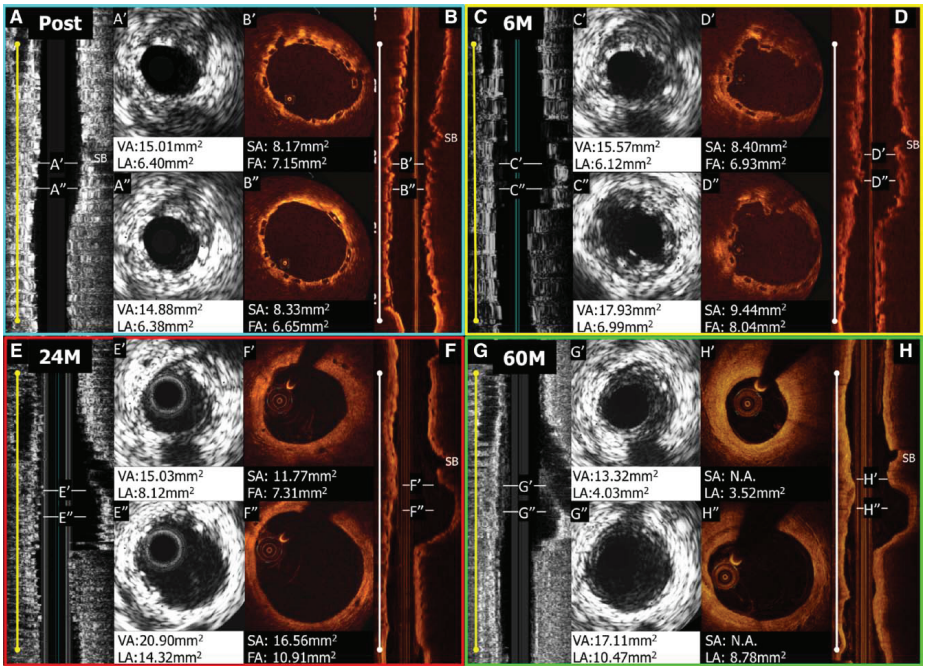

Figure 2. Intravascular ultrasound (IVUS) and optical coherence tomography (OCT) images from matched sites (aneurysm site and near proximal site) after the procedure (**A** and **B**), at 6 months (**C** and **D**), at 2 years (**E** and **F**), and at 5 years (**G** and **H**) after scaffold implantation. The white lines in the longitudinal view indicate the sites corresponding to the cross sections of **A'** to **H"**. Postprocedural OCT showed some malapposed struts but confirmed the absence of structural discontinuity. At 6 months, IVUS revealed a focal vessel and lumen enlargement (**C"**). IVUS and OCT revealed the increase in the vessel and the lumen area at 2 years (**E"** and **F"**) and the subsequent decrease in the aneurysm, with the scaffold becoming indiscernible on OCT at 5 years (**G"** and **H"**). FA indicates flow area; LA, lumen area; SA, scaffold area; and VA, vessel area.

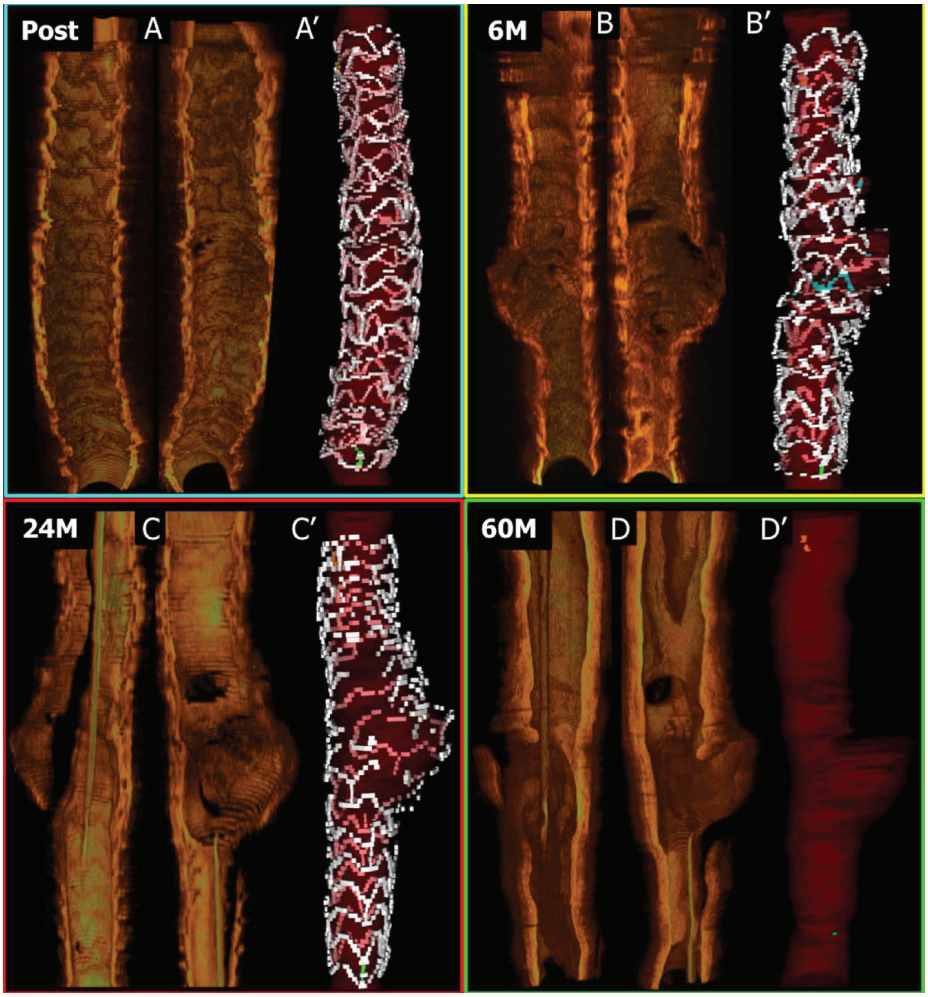

Figure 3. Three-dimensional (3D) reconstruction of cross-sectional images corresponding to the scaffold segment. **A'** through **D'** are reconstructed for emphasizing the scaffold structure. 3D optical coherence tomography (OCT) confirmed the absence of structural discontinuity after the procedure. At 6 months, 3D OCT suggested a deformation of the scaffold in the 2-mm segment corresponding to the ectasia (**B** and **B'**). At 2 years, 3D OCT showed a focal cleavage of the scaffold rings and a bulge of the vessel in the segment free from the scaffold struts (**C** and **C'**). At 5 years, the aneurysm started to reduce, with the scaffold becoming indiscernible on OCT (**D** and **D'**). In **A'** to **D'**, the yellow and green dots indicate the proximal and distal radiopaque makers. The blue struts indicate malapposed struts.

4.5 Multislice Computed Tomography Coronary Angiography assessment

A medium term follow-up by Multislice Computed Tomography Coronary Angiography assessing the persistent presence of Bioresorbable Vascular Scaffold metallic radiopaque markers at the site of implantation.

JACC Cardiovasc Interv. 2015 Jul;8(8):1130-2.
[Letter, IF 7.44]

Suwannasom P, Onuma Y, Campos CM, Nakatani S, **Ishibashi Y**, Grundeken MJ, Stanetic B, Nieman K, Jonker H, Garcia-Garcia HM, Serruys PW.On behalf of the investigators of ABSORB Cohort A, B and EXTENDs.

revascularization are needed. We also agree with Conti's opinion that, unless ischemia is present, collaterals do not appear angiographically; if the collateral provides excellent blood flow to ischemic myocardium, the collaterals will remain (2). Werner et al. (3) reported that even collaterals that appear well developed on angiography are not able to fully replace anterograde blood flow; therefore, restoring flow reserve does little to prevent myocardial ischemia. Our hypothesis was that well-developed collateral flow in patients with stable CTO lesions may partially protect the myocardium and the revascularization may allow complete maintenance of viable myocardium (4), and we identified long-term survival benefits of aggressive revascularization compared with medical therapy in our study. Unfortunately, because we did not routinely perform contralateral injections after successful revascularization of CTO in our practice, we could not identify the existence or disappearance of collaterals after CTO revascularization, as mentioned in Conti's letter. However, we agree with his hypothesis that the change of collateral flow after CTO revascularization in coronary angiography might correlate with whether ischemia of viable myocardium occurs or not. This hypothesis requires further detailed study.

As stated by Barbato and Wijns (1), our study might have reported a higher rate of successful percutaneous coronary intervention (PCI) or coronary bypass grafting (CABG) compared to previous studies of CTO revascularization. However, remarkable developments in the survival benefits posed by CTO revascularization are rapidly becoming a reality because CTO PCI techniques have improved and the experience of CABG has also increased. We anticipate that the survival benefits of aggressive reduction of remnant ischemia by revascularization or intensive medication in patients with CTO lesions will be verified by future large-scale randomized trials.

Woo Jin Jang, MD
Jeong Hoon Yang, MD, PhD
***Seung-Hyuk Choi, MD, PhD**
Young Bin Song, MD, PhD
Joo-Yong Hahn, MD, PhD
Jin-Ho Choi, MD, PhD
Wook Sung Kim, MD, PhD
Young Tak Lee, MD, PhD
Hyeon-Cheol Gwon, MD, PhD
*Division of Cardiology
Department of Medicine, Cardiac and Vascular Center
Samsung Medical Center
Sungkyunkwan University School of Medicine
#50, Irwon-dong, Gangnam-gu
Seoul 135-710
Republic of Korea
E-mail: sh1214.choi@samsung.com

http://dx.doi.org/10.1016/j.jcin.2015.05.012

Please note: The authors have reported that they have no relationships relevant to the contents of this paper to disclose. The first two authors contributed equally to this work.

REFERENCES

1. Barbato E, Wijns W. Are we ready for a new paradigm shift in percutaneous revascularization of chronically occluded vessels with well-developed collaterals?: from leaving 'em all to stenting 'em all. J Am Coll Cardiol Intv 2015;8:280–2.

2. Conti CR. Coronary artery collaterals. Clin Cardiol 2010;33:188–9.

3. Werner GS, Surber R, Kuethe F, et al. Collaterals and the recovery of left ventricular function after recanalization of a chronic total coronary occlusion. Am Heart J 2005;149:129–37.

4. Jang WJ, Yang JH, Choi SH, et al. Long-term survival benefit of revascularization compared with medical therapy in patients with coronary chronic total occlusion and well-developed collateral circulation. J Am Coll Cardiol Intv 2015;8:271–9.

Fate of Bioresorbable Vascular Scaffold Metallic Radio-Opaque Markers at the Site of Implantation After Bioresorption

The use of bioresorbable vascular scaffolds (BRS) is increasing in patients with coronary artery disease undergoing percutaneous coronary interventions. Because the devices are radiolucent on fluoroscopy, 2 adjacent cylindrical platinum markers are incorporated in the proximal and distal edges of the polymeric devices for precise scaffold deployment and post-dilation during the procedure. In addition, the metallic radio-opaque markers (MRMs) also provide anatomic landmarks for long-term follow-up when all the polymeric struts have been bioresorbed. There has been concern about the potential risk of MRM beads becoming dislodged from the device and embolized into the coronary bed after complete bioresorption of the polymeric struts. Beyond the biological hazard of MRMs embolization, the additional inconvenience is that the embolization may result in the incapacity to locate the coronary segment where the fully bioresorbed scaffold was implanted. Invasive assessment of BRS such as quantitative coronary angiography (QCA), intravascular ultrasound (IVUS), or optical coherence tomography (OCT) may be unable to detect the precise location of the MRMs either because of the

resolution of the imaging technique (QCA) or as a result of wire artifact (IVUS, OCT) or mimicry by heavy calcium (IVUS). Multislice computed tomography coronary angiography (MSCT) has provided reliable assessment of the angiographic results up to 3 to 5 years (1,2) after scaffold implantation with accurate detection of the position of MRMs and their blooming effect without being dependent on the rate of image acquisition and wire artifact. In order to dispel the question of embolization of MRMs, we evaluated the persistent presence and location at 18 months of the MRMs following implantation of these fully bioresorbable scaffolds.

We retrospectively pooled data from the ABSORB trials (ABSORB Cohort A, ABSORB Cohort B, and ABSORB EXTEND) in which 943 patients with de novo native coronary artery lesions were treated with the fully resorbable everolimus-eluting Absorb scaffold (Abbott Vascular, Santa Clara, California); the details and primary outcome of each trial have been published (2-4). Of these 943 patients, 165 patients with 168 lesions underwent MSCT at 18 months. A list of the MSCT scanners, the acquisition protocol, and the MSCT analysis are described in the Online Appendix.

To establish the persistent presence of the MRMs in MSCT, both qualitative and quantitative evidence were required. The qualitative evidence was the ability to identify both proximal and distal MRMs position. Because calcified nodules (CN) could mimic MRMs, 4 criteria were used to identify the position of the radio-opaque markers: 1) typical location and orientation of the MRMs; 2) marker-to-marker length; 3) topographical relationship of the radio-opaque markers with anatomic landmarks visualized on MSCT and conventional coronary angiography; and 4) blooming artifact and its peak attenuation. The description of criteria and examples of MSCT images by using these 4 criteria are provided in Online Figure 1. The quantitative evidence is the MSCT scaffold length compared with its nominal length.

The statistical analysis is detailed in the Online Appendix.

A total of 168 lesions (12 lesions in ABSORB Cohort A, 61 lesions in ABSORB Cohort B, and 95 lesions in the ABSORB EXTEND study) were analyzed, and the study profile is shown in Online Figure 2. A total of 348 MRMs were evaluated by both quantitative and qualitative analyses; all MRMs were detected at the implantation site; and there was no evidence of marker embolization to distal vascular beds. The median MSCT scaffold length was 18.0 mm (ranging from 12 mm to 36 mm; interquartile range [IQR]: 17 to 19 mm) as well as the median nominal scaffold length was 18.0 mm (ranging from 12 mm to 28 mm) (**Figure 1**).

FIGURE 1 MSCT Scaffold Length Compared With Nominal Scaffold Length

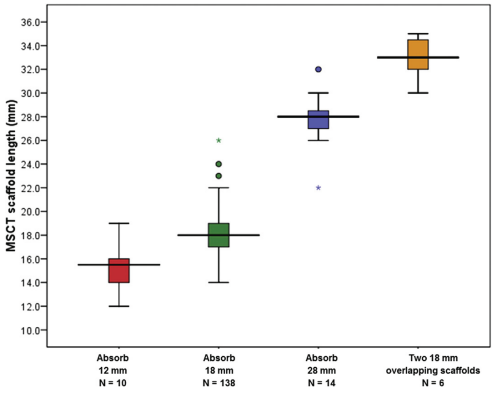

The median and the 1st and 3rd quartiles of each multislice computed tomography (MSCT) scaffold length corresponding to its nominal length are shown in **boxes**, and the minimum and maximum values as whiskers. The **asterisks and the dots above/below** indicate the outlier cases.

The median difference in length between MSCT scaffold length and nominal scaffold length was 0.0 mm (IQR: −1.0 to 1.0 mm). There was a moderate correlation between MSCT mean lumen area (Mean LA) and QCA Mean LA ($r = 0.54$, $p < 0.0001$). A good correlation was observed between MSCT Mean LA and IVUS Mean LA, and between MSCT Mean LA and OCT Mean LA ($r = 0.74$ and $r = 0.73$, respectively; $p < 0.0001$) (Online Figure 3). The Mean LA measured by MSCT was comparable to QCA, but statistically lower than IVUS and OCT (Online Table 1). The reproducibility of the 4 criteria to identify MRMs from CN was good, $r = 0.97$; $p < 0.0001$ (Online Figure 4).

The attenuation of MRMs was approximately 30% higher than dense CN attenuation, but there was nevertheless a modest overlap of the attenuation values; MRM attenuation was sometimes lower than 1,000 HU as a result of the partial volume effect. The median peak density of MRMs was 1,368 HU (IQR: 1,158 to 1,715 HU) in contrast to the median peak density of CN that was 946 HU (IQR: 844 to 1,133 HU).

The main findings of this study are the following: 1) according to the criteria, all MRMs were identified and located at the site of the initial implantation; 2) the MSCT Mean LA was comparable to the Mean LA measured by QCA but lower than OCT and IVUS; and 3) the reproducibility in detecting of MRMs by using 4 criteria was high.

However, the distinction between calcified spots and metallic markers with computed tomography is also not easy to determine compared with OCT. The possible advantages of OCT are the ability to: 1) distinguish the MRMs from underlying calcium more clearly than MSCT; 2) measure the embedment of the struts; and 3) evaluate the thickness of neointima because of a higher axial resolution of around 10 to 15 μm as compared with MSCT.

The limitation in this study is that the study result was able to confirm the persistent presence of MRMs only at medium-term follow-up, and the long-term results still require investigation.

In conclusion, MRM recognition by MSCT is critical for precise noninvasive assessment of the coronary location of all MRMs. On the basis of our study criteria, there was no evidence of MRMs dislodgement and embolization 18 months after scaffold implantation.

Pannipa Suwannasom, MD
Yoshinobu Onuma, MD, PhD
Carlos M. Campos, MD
Shimpei Nakatani, MD
Yuki Ishibashi, MD, PhD
Hiroki Tateishi, MD, PhD
Maik J. Grundeken, MD
Bojan Stanetic, MD
Koen Nieman, MD, PhD
Hans Jonker, BSc
Hector M. Garcia-Garcia, MD, PhD
***Patrick W. Serruys, MD, PhD**
on behalf of the investigators of ABSORB Cohort A, B and EXTEND trials

*International Center for Circulatory Health
NHLI, Imperial College London
London, United Kingdom
P.O. box 2125
Rotterdam 3000CC
the Netherlands
E-mail: patrick.w.j.c.serruys@gmail.com

http://dx.doi.org/10.1016/j.jcin.2015.04.010

Please note: The ABSORB trials were sponsored by Abbott Vascular. Dr. Nieman has received institutional research support from Siemens Medical Solutions, GE Healthcare, and Bayer HealthCare. Mr. Jonker is an employee of Cardialysis. Drs. Garcia-Garcia, Onuma, and Serruys are members of the Advisory Board of Abbott Vascular. All other authors have reported that they have no relationships relevant to the contents of this paper to disclose.

REFERENCES

1. Onuma Y, Dudek D, Thuesen L, et al. Five-year clinical and functional multislice computed tomography angiographic results after coronary implantation of the fully resorbable polymeric everolimus-eluting scaffold in patients with de novo coronary artery disease: the ABSORB cohort A trial. J Am Coll Cardiol Intv 2013;6:999-1009.

2. Serruys PW, Onuma Y, Garcia-Garcia HM, et al. Dynamics of vessel wall changes following the implantation of the absorb everolimus-eluting bioresorbable vascular scaffold: a multi-imaging modality study at 6, 12, 24 and 36 months. EuroIntervention 2014;9:1271-84.

3. Ormiston JA, Serruys PW, Regar E, et al. A bioabsorbable everolimus-eluting coronary stent system for patients with single de-novo coronary artery lesions (ABSORB): a prospective open-label trial. Lancet 2008;371:899-907.

4. Abizaid A, Ribamar Costa J Jr., Bartorelli AL, et al. The ABSORB EXTEND study: preliminary report of the twelve-month clinical outcomes in the first 512 patients enrolled. EuroIntervention 2014;10:1396-401.

APPENDIX For supplemental methods, statistical analysis, table, and figures, please see the online version of this article.

3-Year Follow-Up of the Balloon Elution and Late Loss Optimization Study (BELLO)

The optimal treatment of de novo small-vessel coronary artery disease remains unclear. The use of drug-eluting stents in this patient group are limited by high rates of restenosis (1) and the requirement of prolonged treatment with dual antiplatelet therapy. The use of drug-coated balloons (DCB) might be an alternative treatment option. There are currently limited data with regard to the long-term efficacy of this strategy (2), and currently no randomized data to support this approach. The BELLO (Balloon Elution and Late Loss Optimization) study (3) was an investigator-initiated, prospective, multicenter, single-blinded, active-treatment controlled clinical trial. In BELLO, 182 patients undergoing percutaneous revascularization of small coronary vessels (reference vessel diameter <2.8 mm by visual estimation) were randomly assigned in a 1:1 ratio to treatments with: 1) In.Pact Falcon paclitaxel DCB (Medtronic, Inc., Santa Rosa, California) dilation and provisional bare-metal stenting; or 2) paclitaxel-eluting stent (PES) (Taxus Liberté, Boston Scientific, Marlborough, Massachusetts) implantation as per standard clinical practice. We have shown that treatment of small-vessel disease with a paclitaxel DCB is associated with less angiographic late loss and similar rates of restenosis and revascularization as PES is at 1 year. Here we report the final pre-defined, protocol-mandated 3-year clinical follow-up results of this study population.

A total of 182 patients were enrolled at 15 Italian centers and randomized to treatment with DCB (n = 90) in 94 lesions or PES (n = 92) in 98 lesions. Patients were eligible if ≥18 years of age, with a diagnosis of stable or unstable angina or documented ischemia and a maximum of 2 angiographically significant de novo lesions <25 mm in length in native coronary arteries with a visually estimated reference

4.6 Edge vascular response following implantation of bioresorbable scaffolds

Scaffold and edge vascular response following implantation of everolimus-eluting bioresorbable vascular scaffold: a 3-year serial optical coherence tomography study.

JACC Cardiovasc Interv. 2014 Dec;7(12):1361-9
[Original research paper, IF 7.44]

Zhang YJ, Iqbal J, Nakatani S, Bourantas CV, Campos CM, **Ishibashi Y**, Cho YK, Veldhof S, Wang J, Onuma Y, Garcia-Garcia HM, Dudek D, van Geuns RJ, Serruys PW; ABSORB Cohort B Study Investigators.

Scaffold and Edge Vascular Response Following Implantation of Everolimus-Eluting Bioresorbable Vascular Scaffold

A 3-Year Serial Optical Coherence Tomography Study

Yao-Jun Zhang, MD, PhD,*† Javaid Iqbal, PhD,*‡ Shimpei Nakatani, MD,* Christos V. Bourantas, MD, PhD,* Carlos M. Campos, MD,* Yuki Ishibashi, MD, PhD,* Yun-Kyeong Cho, MD,* Susan Veldhof, RN,§ Jin Wang,§ Yoshinobu Onuma, MD, PhD,* Hector M. Garcia-Garcia, MD, PhD,* Dariusz Dudek, MD,‖ Robert-Jan van Geuns, MD, PhD,* Patrick W. Serruys, MD, PhD,*¶
on behalf of the ABSORB Cohort B Study Investigators

ABSTRACT

OBJECTIVES This study sought to investigate the in-scaffold vascular response (SVR) and edge vascular response (EVR) after implantation of an everolimus-eluting bioresorbable scaffold (BRS) using serial optical coherence tomography (OCT) imaging.

BACKGROUND Although studies using intravascular ultrasound have evaluated the EVR in metal stents and BRSs, there is a lack of OCT-based SVR and EVR assessment after BRS implantation.

METHODS In the ABSORB Cohort B (ABSORB Clinical Investigation, Cohort B) study, 23 patients (23 lesions) in Cohort B1 and 17 patients (18 lesions) in Cohort B2 underwent truly serial OCT examinations at 3 different time points (Cohort B1: post-procedure, 6 months, and 2 years; B2: post-procedure, 1 year, and 3 years) after implantation of an 18-mm scaffold. A frame-by-frame OCT analysis was performed at the 5-mm proximal, 5-mm distal edge, and 2-mm in-scaffold margins, whereas the middle 14-mm in-scaffold segment was analyzed at 1-mm intervals.

RESULTS The in-scaffold mean luminal area significantly decreased from baseline to 6 months or 1 year (7.22 ± 1.24 mm^2 vs. 6.05 ± 1.38 mm^2 and 7.64 ± 1.19 mm^2 vs. 5.72 ± 0.89 mm^2, respectively; both $p < 0.01$), but remained unchanged from then onward. In Cohort B1, a significant increase in mean luminal area of the distal edge was observed (5.42 ± 1.81 mm^2 vs. 5.58 ± 1.53 mm^2; $p < 0.01$), whereas the mean luminal area of the proximal edge remained unchanged at 6 months. In Cohort B2, the mean luminal areas of the proximal and distal edges were significantly smaller than post-procedure measurements at 3 years. The mean luminal area loss at both edges was significantly less than the mean luminal area loss of the in-scaffold segment at both 6-month and 2-year follow-up in Cohort B1 or at 1 year and 3 years in Cohort B2.

CONCLUSIONS This OCT-based serial EVR and SVR evaluation of the Absorb Bioresorbable Vascular Scaffold (Abbott Vascular, Santa Clara, California) showed less luminal loss at the edges than luminal loss within the scaffold. The luminal reduction of both edges is not a nosologic entity, but an EVR in continuity with the SVR, extending from the in-scaffold margin to both edges. (ABSORB Clinical Investigation, Cohort B [ABSORB B]; NCT00856856) (J Am Coll Cardiol Intv 2014;7:1361-9) © 2014 by the American College of Cardiology Foundation.

From the *Thoraxcenter, Erasmus Medical Center, Rotterdam, the Netherlands; †Nanjing First Hospital, Nanjing Medical University, Nanjing, China; ‡Department of Cardiovascular Science, University of Sheffield, Sheffield, United Kingdom; §Abbott Vascular, Diegem, Belgium; ‖Jagiellonian University, Krakow, Poland; and the ¶International Centre for Circulatory Health, NHLI, Imperial College London, London, United Kingdom. This study was sponsored by Abbott Vascular, Santa Clara, California. Dr. Geuns has received speaker honoraria from Abbott Vascular. S. Veldhof and J. Wang are full-time employees of Abbott Vascular. All other authors have reported that they have no relationships relevant to the contents of this paper to disclose.

Manuscript received February 3, 2014; revised manuscript received April 30, 2014, accepted June 19, 2014.

ABBREVIATIONS AND ACRONYMS

BMS = bare-metal stent(s)

BRS = bioresorbable scaffold(s)

BVS = bioresorbable vascular scaffold(s)

CI = confidence interval

DES = drug-eluting stent(s)

EVR = edge vascular response

IVUS = intravascular ultrasound

OCT = optical coherence tomography

SVR = in-scaffold vascular response

Restenosis in the segments adjacent to the proximal and distal edges of a permanent or transient coronary implant has been a concern for many years (1-5). In the metal drug-eluting stent (DES) era, studies demonstrated effective inhibition of neointimal hyperplasia reducing the risk of edge restenosis and the need for repeat intervention on the edges (6,7). Our group, using intravascular ultrasound (IVUS) imaging, previously investigated the edge vascular response (EVR) after implantation of fully bioresorbable scaffold (BRS) and reported a luminal area reduction at the proximal edge at 2-year follow-up (8).

SEE PAGE 1370

Optical coherence tomography (OCT) offers substantially superior resolution that allows a precise evaluation of luminal dimensions, edge dissections, and relevant vessel wall pathology (9-12). To date, no study has used serial OCT imaging to examine the EVR and its relationship with in-scaffold vascular response (SVR) at 3-year follow-up after BRS implantation. We hypothesized that the local changes in luminal dimensions at the edge of the Absorb Bioresorbable Vascular Scaffold (Absorb BVS) (Abbott Vascular, Santa Clara, California) are simply the extension of the changes in luminal dimension observed at the in-scaffold margins and not a separate pathological entity. This study aimed to evaluate the OCT-based SVR and EVR after Absorb BVS (Abbott Vascular) implantation in the ABSORB Cohort B (ABSORB Clinical Investigation, Cohort B) trial.

METHODS

STUDY DESIGN AND POPULATION. The ABSORB Cohort B trial was described in detail previously (12). Briefly, this was a nonrandomized, multicenter, single-arm trial that enrolled 101 patients (102 lesions) treated with the second-generation Absorb BVS (Abbott Vascular) (A complete list of the members of the ABSORB Cohort B Study appears in the Online Appendix). The participants were divided into 2 groups according to the pre-defined invasive follow-up: Cohort B1 at post-procedure, 6 months, and 2 years and Cohort B2 at post-procedure, 1 year, and 3 years. OCT was an optional examination conducted at selected centers with OCT capability and previous experience. The registry was approved by the ethics committee at each participating institution, and each patient gave written informed consent before inclusion.

STUDY DEVICE AND TREATMENT PROCEDURE. The Absorb BVS (Abbott Vascular) is a balloon-expandable scaffold consisting of a polymer backbone of poly-L-lactide coated with a thin layer of a 1:1

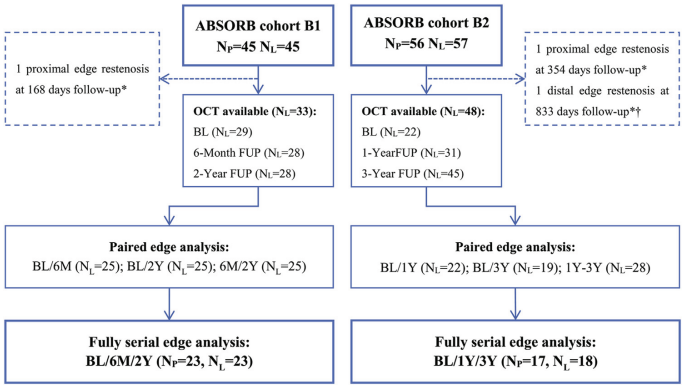

FIGURE 1 Flowchart of the Patients Included in the Current Analysis

*Edge restenoses in Cohort B that mandated repeat revascularization. †This case had in-segment restenosis at the distal margin of the scaffolded segment and distal edge. 1Y = 1 year; 2Y = 2 years; 3Y = 3 years; BL = baseline; FUP = follow-up; N_L = number of lesions; N_P = number of patients; OCT = optical coherent tomography.

mixture of amorphous poly-D,L-lactide polymer and the antiproliferative drug everolimus to form a drug-eluting coating matrix that contains 100 μg of everolimus per square centimeter of scaffold (13-15).

Target lesions were treated with routine interventional techniques, and pre-dilation was mandatory. The Absorb BVS (Abbott Vascular) inflation pressure did not exceed 16 atm, the burst pressure according to the product chart. Post-dilation with a balloon shorter than the implanted scaffold was at the discretion of the operator. OCT imaging was performed after optimal Absorb BVS (Abbott Vascular) implantation and at follow-up.

OCT ACQUISITIONS AND DATA ANALYSIS. OCT acquisitions were performed using 3 different commercially available systems: the M2 and M3 Time-Domain Systems and the C7XR Fourier-Domain System (LightLab Imaging, Westford, Massachusetts). OCT images were acquired at frame rates of 15.6, 20, and 100 frames/s with pullback speeds of 2, 3, and 20 mm/s in the M2 Time-Domain System (n = 11), M3 Time-Domain System (n = 11), and C7XR Fourier-Domain System (n = 101) (LightLab Imaging), respectively. All recordings were performed according to the recommended procedure for each OCT system (16). The OCT images acquired post-procedure and at follow-up were analyzed off-line, using proprietary LightLab Imaging software (St. Jude Medical Inc., St. Paul, Minnesota). Truly serial OCT data were defined as the patient undergoing OCT examinations at all 3 time points.

The SVR analysis included all 18-mm scaffold segments, analyzed at 1-mm intervals by an independent core laboratory (Cardialysis, Rotterdam, the Netherlands). The EVR analysis included the 5-mm proximal and distal edges, analyzed in a frame-by-frame fashion (128-μm interval for the M2, 150-μm interval for the M3, 200-μm interval for the C7). In addition, we performed a frame-by-frame analysis of changes in the lumen area at the 2-mm margins of the scaffold to explore the relationship between in-scaffold margins and the edges. The scaffold edge was defined as the first cross section exhibiting visible struts in a circumference <270° (10). If the 5-mm edge had a side branch with a vessel diameter ≥1.5 mm, the analysis included only frames between the scaffold's margin and the ostium of the side branch. If the vessel diameter of the side branch was <1.5 mm, only the frames at the ostium of the side branch were excluded. In addition, we excluded the cases that needed a bailout stent as well as the frames with insufficient assessment of the entire luminal circumference due to inadequate blood clearance or incomplete scanning perimeter. Edge dissection was defined as disruption of the endoluminal vessel surface at the proximal and distal edges (17).

TABLE 1 Baseline and Lesion Characteristics of Fully Serial OCT Available Patients

	Cohort B1 (n = 23)	Cohort B2 (n = 17)	Difference (95% CI)
Age, yrs	63.4 ± 9.8	61.6 ± 8.0	1.8 (−3.9 to 7.5)
Male	82.6	64.7	17.9 (−8.8 to 43.5)
Diabetes mellitus	4.3	5.9	−1.5% (−22.9 to 15.8)
Hypertension	52.2	70.6	−18.4 (−43.5 to 11.7)
Hypercholesterolemia	95.7	76.5	19.2 (−2.6 to 43.2)
Current smoker	21.7	29.4	−7.7% (−34.3 to 18.2)
Family history of CAD	52.2	66.7	−14.5% (−40.9 to 16.6)
Previous MI	43.5	12.5	31.0 (1.5-52.7)
History of PCI	26.1	11.8	14.3 (−12.0 to 36.4)
Unstable angina	17.4	5.9	11.5 (−12.0 to 31.8)
Target-lesion vessel, %			
LAD	26.1	11.1	15.0 (−10.6 to 36.9)
LCX	26.1	33.3	−7.3 (−33.9 to 19.3)
RCA	47.8	55.6	−7.7 (−35.0 to 21.4)
RVD before intervention	2.59 ± 0.40	2.57 ± 0.26	0.02 (−0.19 to 0.23)
Maximal balloon artery ratio	1.01 ± 0.15	1.05 ± 0.11	−0.04 (−0.12 to 0.05)
Maximal inflation pressure	18.4 ± 3.0	16.6 ± 5.3	1.8 (−1.1 to 4.7)

Values are mean ± SD or %.

CAD = coronary artery disease; CI = confidence interval; LAD = left anterior descending artery; LCX = left circumflex artery; MI = myocardial infarction; OCT = optical coherent tomography; PCI = percutaneous coronary intervention; RCA = right coronary artery; RVD = reference vessel diameter.

STATISTICAL ANALYSIS. Continuous variables are presented as mean ± SD or median (interquartile range). Binary variables are presented as count and percent. Absolute difference and 95% confidence interval (CI) of baseline characteristics was generated by normal approximation for continuous variables and Newcombe score method for binary variables. A paired *t* test or Wilcoxon signed rank test was used to compare SVR and EVR within groups at different time points. The normality of the data was determined with the D'Agostino Pearson test and verified by histogram plots. To evaluate the relationship of the lumen area

TABLE 2 In-Scaffold Vascular Response Analysis

	In-Scaffold Vascular Response (18 mm)			
Luminal Area Changes	Distal Subsegment (6 mm)	Middle Subsegment (6 mm)	Proximal Subsegment (6 mm)	p Value
Cohort B1				
6 months vs. baseline	−1.21 ± 0.79	−0.98 ± 0.68	−1.34 ± 0.79	0.27
2 yrs vs. 6 months	−0.44 ± 0.91	0.05 ± 1.46	0.12 ± 1.29	0.25
2 yrs vs. baseline	−1.65 ± 0.99	−0.94 ± 1.62	−1.22 ± 1.24	0.18
Cohort B2				
1 yr vs. baseline	−1.91 ± 1.24	−1.77 ± 1.10	−2.06 ± 0.87	0.73
3 yrs vs. 1 yr	−0.18 ± 0.93	0.26 ± 0.84	0.05 ± 0.72	0.29
3 yrs vs. baseline	−2.10 ± 1.59	−1.51 ± 1.23	−2.00 ± 1.03	0.36

Values are mean ± SD.

TABLE 3 Edge Vascular Response Analysis

Luminal Area	Cohort B1		Cohort B2	
Distal edge, 5 mm	6M	2Y	1Y	3Y
Baseline	5.42 ± 1.81		5.78 ± 2.04	
FUP (6M/2Y, 1Y/3Y)	5.58 ± 1.53	5.26 ± 1.40	5.63 ± 1.45	5.29 ± 1.77
Difference	0.19 ± 1.05	−0.16 ± 1.24	−0.14 ± 1.25	−0.49 ± 1.17
p value (BL vs. FUP)	<0.01	0.03	0.11	<0.01
Proximal edge, 5 mm	6M	2Y	1Y	3Y
Baseline	6.84 ± 2.86		7.27 ± 2.01	
FUP (6M/2Y, 1Y/3Y)	6.76 ± 2.63	6.75 ± 2.60	6.66 ± 1.74	6.51 ± 1.63
Difference	−0.07 ± 1.14	−0.08 ± 1.13	−0.61 ± 1.33	−0.76 ± 1.57
p value (BL vs. FUP)	0.31	0.25	<0.01	<0.01

Values are mean ± SD.
6M = 6 months; 1Y = 1 year; 2Y = 2 years; 3Y = 3 years; BL = baseline; FUP = follow-up.

within different segments of the scaffold (3 subsegments: proximal, middle, and distal), multilevel generalized estimating equation model fitting, with the mean lumen area as the response and the subsegments and the follow-up visits as categorical variables, were nested within each patient. Multiple comparisons were conducted without adjustment. Statistical significance was assumed at $p < 0.05$. All statistical analyses were performed with SAS version 9.1.3 (SAS Institute Inc., Cary, North Carolina).

RESULTS

STUDY POPULATION AND OCT ACQUISITION. A flowchart of the subjects included in the current

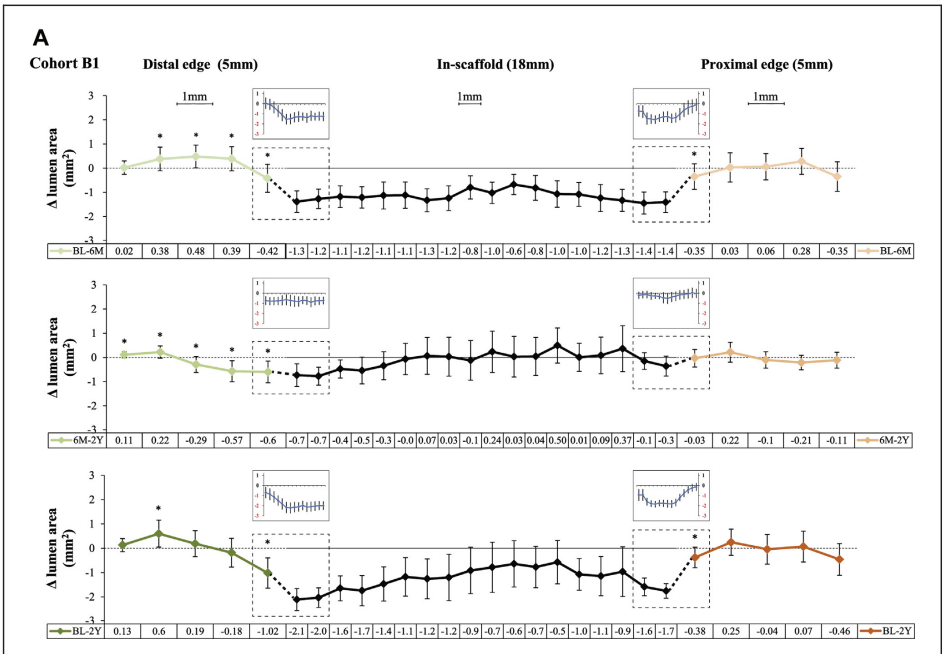

FIGURE 2 Scaffold and Its EVR

The images present the global mean luminal area changes including in-scaffold, 5-mm proximal and distal edges at follow-up. **(A)** Cohort B1. **(B)** Cohort B2. Mean luminal area of the 18-mm in-scaffold segment significantly decreased from baseline to 6-month or 1-year follow-up, but no change from 6 months to 2 years or 1 year to 3 years. The EVR analysis showed an increase in mean luminal area at the distal edge at 6 months and a reduction at both the proximal and distal edges at long-term follow-up. The transitional regions with a 200-μm interval analysis are presented in the embedded panels, indicating a continuous pattern of luminal reduction extending from the in-scaffold margins to the first 1 mm of proximal and distal edges. *Indicates a significant change in mean luminal area in each 1-mm interval at the proximal or distal edge ($p < 0.05$). EVR = edge vascular response; other abbreviations as in Figure 1.

analysis is shown in Figure 1. A total of 183 OCT pullbacks at baseline and follow-up were performed in 80 patients (81 lesions). Twenty-three patients (23 lesions) in Cohort B1 and 17 patients (18 lesions) in Cohort B2 had truly serial OCT examinations at 3 different time points. Three patients who had a target lesion revascularization did not undergo OCT examination before the reintervention.

Baseline characteristics of the patients with truly serial OCT pullbacks are shown in Table 1. There was a greater prevalence of patients with previous myocardial infarction (43.5% vs. 12.5%; difference: 31.0%; 95% CI: 1.5% to 52.7%) and lesions in the left anterior descending artery in Cohort B1 (26.1% vs. 11.1%; difference: 15.0%; 95% CI: −10.6% to 36.9%) than in Cohort B2.

SVR ANALYSIS. In Cohort B1, there was a significant reduction in mean in-scaffold luminal area at 6 months (7.22 ± 1.24 mm^2 vs. 6.05 ± 1.38 mm^2, $p < 0.01$). However, the mean luminal area remained unchanged from 6 months to 2 years (5.97 ± 1.61 mm^2, $p = 0.75$). Similarly, in Cohort B2, there was a significant reduction in mean in-scaffold luminal area from baseline to 1 year (7.64 ± 1.19 mm^2 vs. 5.72 ± 0.89 mm^2, $p < 0.01$), but no change from 1 year to 3 years (5.81 ± 1.29 mm^2, $p = 0.60$).

At 3-year follow-up, there was no significant difference in behavior of the 3 in-scaffold subsegments (proximal, middle, and distal) (Table 2). The mean luminal area of proximal and middle subsegments numerically increased from 6 months to 2 years or 1 year to 3 years (B1: 0.12 ± 1.29 mm^2, 0.05 ± 1.46 mm^2; B2: 0.05 ± 0.72 mm^2, 0.26 ± 0.84 mm^2; respectively), whereas the mean luminal area of the distal segment numerically decreased (B1: −0.44 ± 0.91 mm^2, −0.18 ± 0.93 mm^2).

EVR ANALYSIS. The changes in mean luminal area of the proximal and distal edges at different time points are shown in Table 3. In Cohort B1, a significant increase in mean luminal area at the distal edge (5-mm

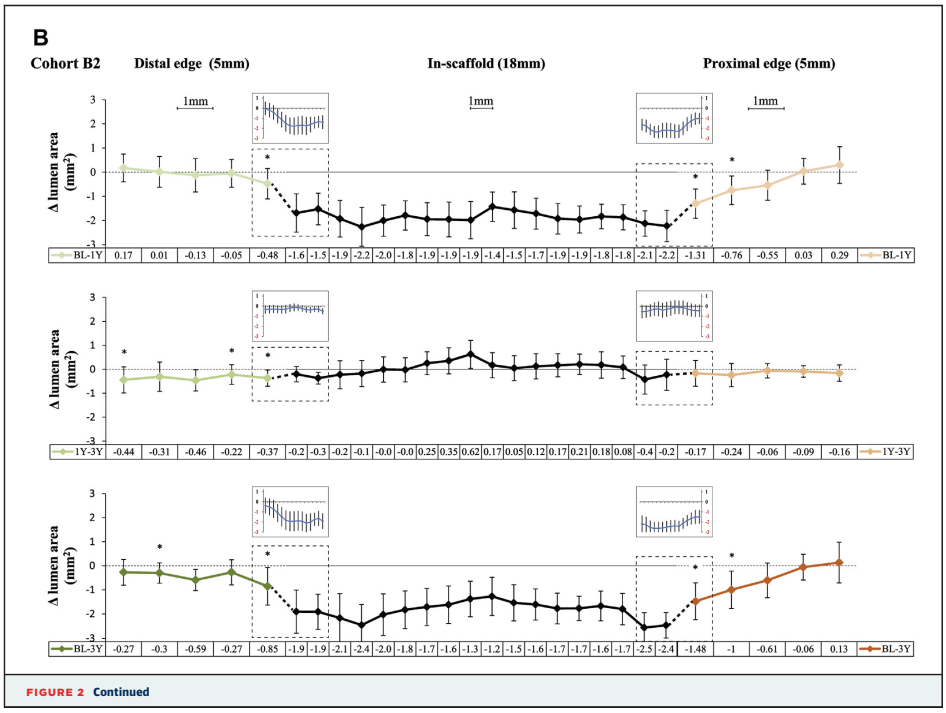

FIGURE 2 Continued

TABLE 4 Overall Vascular Response Analysis

Luminal Area Changes	Distal Edge, 5 mm	In-Scaffold, 18 mm	Proximal Edge, 5 mm	p Value (Distal vs. In-Scaffold)	p Value (Proximal vs. In-Scaffold)
Cohort B1					
6 months vs. baseline, mm^2	0.16 ± 1.05	−1.18 ± 1.06	−0.07 ± 1.14	<0.01	<0.01
2 years vs. baseline, mm^2	−0.16 ± 1.24	−1.23 ± 1.64	−0.08 ± 1.13	<0.01	<0.01
Cohort B2					
1 year vs. baseline, mm^2	−0.14 ± 1.25	−1.88 ± 1.29	−0.61 ± 1.33	<0.01	<0.01
3 years vs. baseline, mm^2	−0.49 ± 1.17	−1.85 ± 1.50	−0.76 ± 1.56	<0.01	<0.01

Values are mean ± SD.

segment) was observed at 6 months (5.42 ± 1.81 mm^2 vs. 5.58 ± 1.53 mm^2, $p < 0.01$) (Figure 2A), whereas at the proximal edge (5-mm segment), the mean luminal area remained unchanged (6.84 ± 2.86 mm^2 vs. 6.76 ± 2.63 mm^2, $p = 0.31$). In Cohort B2, the mean luminal area at the distal edge was unchanged at 1-year follow-up (5.78 ± 1.45 mm^2 vs. 5.63 ± 1.45 mm^2, $p = 0.11$) (Figure 2B). At 3-year follow-up, a significant reduction in the mean luminal area was observed at both edges (distal: 5.78 ± 2.04 mm^2 vs. 5.29 ± 1.77 mm^2; proximal: 7.27 ± 2.01 mm^2 vs. 6.51 ± 1.63 mm^2; both $p < 0.01$).

PATTERN OF CHANGES IN LUMINAL DIMENSIONS FROM IN-SCAFFOLD MARGINS TO EDGES. At all time points, reduction in the luminal area was observed in the first 1 mm of the edges, both proximally and distally, indicating a continuous pattern of luminal reduction extending from the scaffold margin to the proximal or distal edge (Figure 2). The overall reduction in mean luminal area at both edges was significantly less than the in-scaffold segments (all $p < 0.05$) (Table 4).

EDGE RESTENOSIS, EDGE DISSECTION, AND STENT THROMBOSIS. Of 101 patients in the entire ABSORB Cohort B trial, 2 patients (2.0%) had proximal edge restenosis and 1 patient (1%) had distal edge restenosis. Patients with the proximal edge restenosis had a repeat revascularization at day 168 and day 383, respectively. The patient with the distal edge restenosis had a repeat revascularization at day 833. These 3 patients were treated without previous OCT to examine edge restenosis. In 2 of these patients, a geographic miss (injured or diseased segment not covered by the device, balloon-artery ratio <0.9 or >1.3) was previously reported (15).

In total, 12 proximal (24%) and 21 distal (42%) edge dissection flaps were observed post-procedure. In the truly serial OCT analysis, 9 proximal (21%) and 16 distal (38%) edge dissection flaps were identified post-procedure, which decreased to 1 proximal (2%) and 2 distal (5%) at 6 months, only proximal 1 (2%) at 1-year follow-up, and none at 2- and 3-year follow-up (Figure 3). No scaffold thrombosis was reported in this trial.

DISCUSSION

This study, for the first time, reported OCT-derived EVR and SVR evaluation after Absorb BVS (Abbott Vascular) implantation at mid- and long-term follow-up. The primary findings are the following: 1) an increase in mean luminal area at the distal edge at 6 months; 2) a reduction in the mean luminal area at both edges at long-term (2- or 3-year) follow-up; 3) reduction in luminal area at the in-scaffold segment from baseline to 6 or 12 months, but no change from then onward. A uniform pattern of luminal reduction extending from the in-scaffold margins to the first 1-mm of the proximal and distal edges of the scaffold is also demonstrated, suggesting that the edge changes in luminal dimension is not a nosologic entity, but a progressive transition in luminal dimension from the in-scaffold margin to the edges.

EVOLUTION OF DEVICES AND EVR. The introduction of coronary metal stents has markedly reduced the risk of restenosis (14). The EVR in the era of bare metal stents (BMS) was mainly due to an increase in plaque and medial area and reduction in luminal area within the first 1 to 2 mm of the device (15,18). Radioactive stents, developed to reduce restenosis, were proved to be safe in initial studies (19,20), but led to a profound edge effect defined angiographically as a diameter stenosis of >50% at the proximal and distal stent edges (2,3). In the DES era, the EVR can also be influenced by the drug and polymer incorporated into the stent (21). A high degree of variability in EVR was identified among the different DES types (5). In the TAXUS II trial, paired-edge analyses with IVUS showed a significant increase in luminal area at the distal edge of paclitaxel-eluting stent compared with the BMS at 6 months, whereas a significant decrease in the luminal area was observed at the proximal edge (22). The beneficial effect of the paclitaxel-eluting stent was most notable in the area closest to its distal edge (23). Trials with the Endeavor stent (Medtronic, Minneapolis, Minnesota) demonstrated a reduction in the luminal area at both the proximal and distal edges, mainly due to negative remodeling, plaque growth, and rapid elution of zotarolimus (24,25). However, serial IVUS

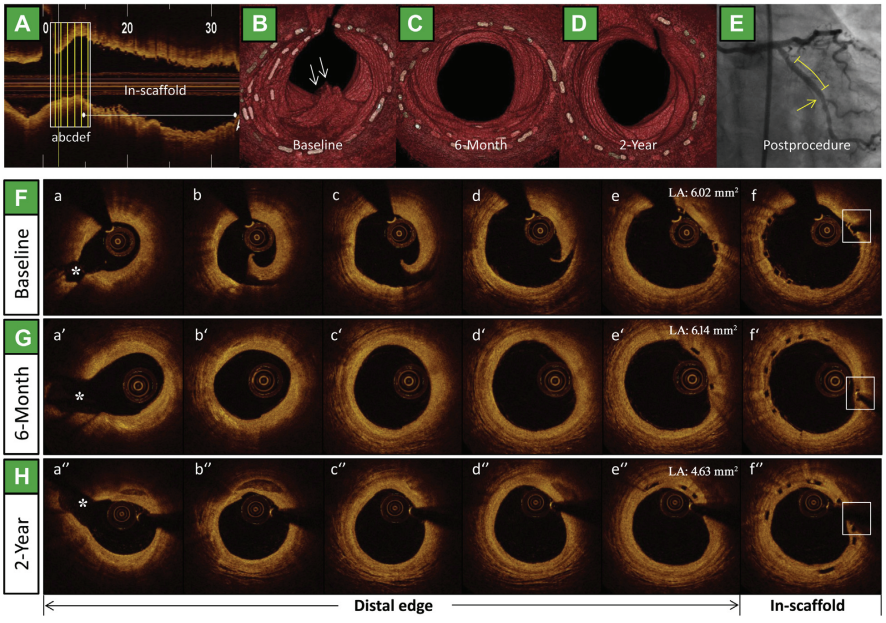

FIGURE 3 **Dissections at the Distal Edge**

(A) Longitudinal view of patients with distal dissection. **(B)** Three-dimensional reconstruction of optical coherence tomography pullbacks show that dissection is visible at distal edge **(double white arrow)**. **(C, D)** Three-dimensional reconstruction at 6-month and 2-year follow-up showed that dissection has healed. **(E)** No distal edge dissection **(arrow)** is visible from the post-procedure angiograms. The **curved line** indicates the scaffolded segment. **(F)** Dissection extends into at least the media from multiple cross-sectional views. **(G)** Increased luminal area without visible dissection at 6-month follow-up. **(H)** The luminal area decreased with detected calcific tissue at 2-year follow-up. LA = lumen area. *Indicates a side branch.

examination in sirolimus- and everolimus-eluting stents revealed an enlargement of the luminal area at the distal edge (26-28). Our results are in agreement with those of previous reports on metal everolimus-eluting stents (28), with a significant increase in the distal-edge luminal area and a nonsignificant decrease in the proximal edge at 6-month follow-up. The difference in behavior of the 2 edges can partially be explained by downstream diffusion of antiproliferative drug to the distal edge (21).

IN-DEPTH ANALYSIS OF EVR AND SVR. IVUS imaging has contributed to our understanding of EVR after BRS implantation. However, this approach has inherent limitations (e.g., poor resolution, cardiac motion artifacts) and makes it difficult to assess EVR precisely (29-31). The present study, performed with OCT, for the first time evaluated EVR in frame-by-frame (≤200 μm) fashion after Absorb BVS (Abbott Vascular) implantation and provided additional insights into the changes in luminal dimensions at the proximal and distal edges.

Our previous IVUS-based study demonstrated a nonsignificant reduction in luminal area at the distal edge at 6 months (32); however, accurate assessment with OCT has documented it to be a significant change. By the virtue of the high resolution of OCT, we also demonstrated that the pattern of in-scaffold luminal reduction extended progressively from the in-scaffold margins to the contiguous first 1 mm of the edges outside the scaffold, both proximally and distally, presumably related to neointimal

hyperplasia or neoatherosclerosis (33). In addition, the discrepancy with previous IVUS observations can also be attributed to the nonserial nature of the data in previous IVUS studies. Thus, we believe that OCT-based EVR evaluation with truly serial data can provide more reliable and precise information.

Finally, the SVR analysis presented here is consistent with the previous final 3-year report of the ABSORB Cohort B study (32). The analysis of changes in mean luminal area of different in-scaffold subsegments using a generalized estimating equation model did not show any significant difference in vascular response; however, there was a numerical increase in luminal area in the middle subsegment from 1 year to 3 years. Preclinical studies of the BRS have demonstrated that late luminal positive remodeling was observed at late follow-up (34). It will be interesting to re-evaluate this subsegment behavior at 5-year follow-up of the ABSORB Cohort B study.

CLINICAL IMPLICATIONS. The Absorb BVS (Abbott Vascular) does not produce a pathological edge effect that was seen with BMS or notoriously with radioactive stents. The stable luminal area after 6 to 12 months without late catch-up is a potential superiority of BRS over metal DES. In the ABSORB Cohort B trial, there were only 3 cases of edge restenosis, and 2 of them could be attributed to longitudinal geographic miss (13). Edge dissections, considered to be a trigger for early stent thrombosis, were often detected by post-procedure OCT in the present study; however, most of these dissections healed within 6 months, without any clinical adverse events.

STUDY LIMITATIONS. First, the number of patients in the current study is small; however, it is the largest and longest series available to date, and due to the truly serial OCT data, potential patient-to-patient variability was minimized. Second, OCT examination was not available for patients undergoing repeat revascularization, and, therefore, we decided to exclude these patients from this analysis. Finally, OCT cannot visualize external elastic lamina due to its low penetration, and, hence, changes in plaque media or vessel area cannot be assessed adequately.

CONCLUSIONS

In this study, truly serial OCT imaging was used to assess the EVR and SVR after Absorb BVS (Abbott Vascular) implantation up to 3-year follow-up. We found a significant increase in the luminal area at the distal edge at 6-month follow-up. However, at longer term (1, 2, and 3 years), the luminal area decreased at both edges, resulting in a repeat revascularization rate of 3%. In-scaffold luminal area significantly decreased from post-procedure to 6 months or 1 year, but remained unchanged from then onward. A continuous pattern of luminal loss extending from the in-scaffold margins to the first 1-mm of scaffold edges has suggested that the changes in luminal area at the edge of a BRS is not a nosologic entity in itself, but an extension of the in-scaffold response to the edges.

REPRINT REQUESTS AND CORRESPONDENCE: Dr. Patrick W. Serruys, International Centre for Circulatory Health, NHLI, Imperial College London, Royal Brompton Campus, London SW7 2AZ, United Kingdom. E-mail: p.w.j.c.serruys@gmail.com.

REFERENCES

1. Albiero R, Nishida T, Adamian M, et al. Edge restenosis after implantation of high activity (32)P radioactive beta-emitting stents. Circulation 2000;101:2454–7.

2. van Der Giessen WJ, Regar E, Harteveld MS, et al. "Edge Effect" of (32)p radioactive stents is caused by the combination of chronic stent injury and radioactive dose falloff. Circulation 2001;104:2236–41.

3. Serruys PW, Kay IP. I like the candy, I hate the wrapper: the (32)P radioactive stent. Circulation 2000;101:3–7.

4. Serruys PW, Ormiston JA, Sianos G, et al. Actinomycin-eluting stent for coronary revascularization: a randomized feasibility and safety study: the ACTION trial. J Am Coll Cardiol 2004;44:1363–7.

5. Gogas BD, Garcia-Garcia HM, Onuma Y, et al. Edge vascular response after percutaneous coronary intervention: an intracoronary ultrasound and optical coherence tomography appraisal: from radioactive platforms to first- and second-generation drug-eluting stents and bioresorbable scaffolds. J Am Coll Cardiol Intv 2013;6:211–21.

6. Serruys PW, Silber S, Garg S, et al. Comparison of zotarolimus-eluting and everolimus-eluting coronary stents. N Engl J Med 2010;363:136–46.

7. Windecker S, Serruys PW, Wandel S, et al. Biolimus-eluting stent with biodegradable polymer versus sirolimus-eluting stent with durable polymer for coronary revascularisation (LEADERS): a randomised non-inferiority trial. Lancet 2008;372:1163–73.

8. Gogas BD, Bourantas CV, Garcia-Garcia HM, et al. The edge vascular response following implantation of the Absorb everolimus-eluting bioresorbable vascular scaffold and the XIENCE V metallic everolimus-eluting stent. First serial follow-up assessment at six months and two years: insights from the first-in-man ABSORB Cohort B and SPIRIT II trials. EuroIntervention 2013;9:709–20.

9. Ormiston JA, Serruys PW, Onuma Y, et al. First serial assessment at 6 months and 2 years of the second generation of absorb everolimus-eluting bioresorbable vascular scaffold: a multi-imaging modality study. Circ Cardiovasc Interv 2012;5:620-32.

10. Gogas BD, Onuma Y, van Geuns RJ, Serruys PW. The edge vascular response following implantation of a fully bioresorbable device: 'a miss always counts'. Int J Cardiol 2012;158:455–7.

11. Gogas BD, Muramatsu T, Garcia-Garcia HM, et al. In vivo three dimensional optical coherence tomography. A novel imaging modality to visualize the edge vascular response. Int J Cardiol 2013;164:e35–7.

12. Serruys PW, Onuma Y, Dudek D, et al. Evaluation of the second generation of a bioresorbable everolimus-eluting vascular scaffold for the treatment of de novo coronary artery stenosis: 12-month clinical and imaging outcomes. J Am Coll Cardiol 2011;58:1578–88.

13. Nakatani S, Onuma Y, Ishibashi Y, et al. Early (before 6 months), late (6-12 months) and very late (after 12 months) angiographic scaffold restenosis in the ABSORB Cohort B trial. EuroIntervention 2014 Feb 27 [E-pub ahead of print].

14. Iqbal J, Gunn J, Serruys PW. Coronary stents: historical development, current status and future directions. Br Med Bull 2013;106:193–211.

15. Weissman NJ, Wilensky RL, Tanguay JF, et al. Extent and distribution of in-stent intimal hyperplasia and edge effect in a non-radiation stent population. Am J Cardiol 2001;88:248–52.

16. Tearney GJ, Regar E, Akasaka T, et al. Consensus standards for acquisition, measurement, and reporting of intravascular optical coherence tomography studies: a report from the International Working Group for Intravascular Optical Coherence Tomography Standardization and Validation. J Am Coll Cardiol 2012;59:1058–72.

17. Muramatsu T, Garcia-Garcia HM, Onuma Y, et al. Intimal flaps detected by optical frequency domain imaging in the proximal segments of native coronary arteries. Circ J 2013;77:2327–33.

18. Popma JJ, Leon MB, Moses JW, et al. Quantitative assessment of angiographic restenosis after sirolimus-eluting stent implantation in native coronary arteries. Circulation 2004;110:3773–80.

19. King SB 3rd, Williams DO, Chougule P, et al. Endovascular beta-radiation to reduce restenosis after coronary balloon angioplasty: results of the beta energy restenosis trial (BERT). Circulation 1998;97:2025–30.

20. Condado JA, Waksman R, Gurdiel O, et al. Long-term angiographic and clinical outcome after percutaneous transluminal coronary angioplasty and intracoronary radiation therapy in humans. Circulation 1997;96:727–32.

21. Wakabayashi K, Waksman R, Weissman NJ. Edge effect from drug-eluting stents as assessed with serial intravascular ultrasound: a systematic review. Circ Cardiovasc Interv 2012;5:305–11.

22. Serruys PW, Degertekin M, Tanabe K, et al. Vascular responses at proximal and distal edges of paclitaxel-eluting stents: serial intravascular ultrasound analysis from the TAXUS II trial. Circulation 2004;109:627–33.

23. Weissman NJ, Ellis SG, Grube E, et al. Effect of the polymer-based, paclitaxel-eluting TAXUS Express stent on vascular tissue responses: a volumetric intravascular ultrasound integrated analysis from the TAXUS IV, V, and VI trials. Eur Heart J 2007;28:1574–82.

24. Sakurai R, Hongo Y, Yamasaki M, et al. Detailed intravascular ultrasound analysis of Zotarolimus-eluting phosphorylcholine-coated cobalt-chromium alloy stent in de novo coronary lesions (results from the ENDEAVOR II trial). Am J Cardiol 2007;100:818–23.

25. Waseda K, Miyazawa A, Ako J, et al. Intravascular ultrasound results from the ENDEAVOR IV trial: randomized comparison between zotarolimus- and paclitaxel-eluting stents in patients with coronary artery disease. J Am Coll Cardiol Intv 2009;2:779–84.

26. Jimenez-Quevedo P, Sabate M, Angiolillo DJ, et al. Vascular effects of sirolimus-eluting versus bare-metal stents in diabetic patients: three-dimensional ultrasound results of the Diabetes and Sirolimus-Eluting Stent (DIABETES) Trial. J Am Coll Cardiol 2006;47:2172–9.

27. Jensen LO, Maeng M, Mintz GS, et al. Serial intravascular ultrasound analysis of peri-stent remodeling and proximal and distal edge effects after sirolimus-eluting or paclitaxel-eluting stent implantation in patients with diabetes mellitus. Am J Cardiol 2009;103:1083–8.

28. Shimohama T, Ako J, Yamasaki M, et al. SPIRIT III JAPAN versus SPIRIT III USA: a comparative intravascular ultrasound analysis of the everolimus-eluting stent. Am J Cardiol 2010;106:13–7.

29. Arbab-Zadeh A, DeMaria AN, Penny WF, Russo RJ, Kimura BJ, Bhargava V. Axial movement of the intravascular ultrasound probe during the cardiac cycle: implications for three-dimensional reconstruction and measurements of coronary dimensions. Am Heart J 1999;138:865–72.

30. von BC, de Vrey EA, Mintz GS, et al. ECG-gated three-dimensional intravascular ultrasound: feasibility and reproducibility of the automated analysis of coronary lumen and atherosclerotic plaque dimensions in humans. Circulation 1997;96:2944–52.

31. Bruining N, von BC, de Feyter PJ, et al. ECG-gated versus nongated three-dimensional intracoronary ultrasound analysis: implications for volumetric measurements. Cathet Cardiovasc Diagn 1998;43:254–60.

32. Gogas BD, Serruys PW, Diletti R, et al. Vascular response of the segments adjacent to the proximal and distal edges of the ABSORB everolimus-eluting bioresorbable vascular scaffold: 6-month and 1-year follow-up assessment: a virtual histology intravascular ultrasound study from the first-in-man ABSORB cohort B trial. J Am Coll Cardiol Intv 2012;5:656–65.

33. Serruys PW, Onuma Y, Garcia-Garcia HM, et al. Dynamics of vessel wall changes following the implantation of the Absorb everolimus-eluting bioresorbable vascular scaffold: a multi-imaging modality study at 6, 12, 24 and 36 months. EuroIntervention 2014;9:1271–84.

34. Strandberg E, Zeltinger J, Schulz DG, Kaluza GL. Late positive remodeling and late lumen gain contribute to vascular restoration by a non-drug eluting bioresorbable scaffold: a four-year intravascular ultrasound study in normal porcine coronary arteries. Circ Cardiovasc Interv 2012;5:39–46.

KEY WORDS Absorb BVS, bioresorbable scaffold, edge vascular response, in-scaffold vascular response, optical coherence tomography

APPENDIX For a complete list of the ABSORB Cohort B study investigators, please see the online version of this article.

Summary

SUMMARY AND CONCLUSIONS

Vessel Sizing, Acute Performance and Patient Outcome after Implantation of Bioresorbable Scaffolds

The use of bioresorbable scaffolds has several challenges that justify careful assessment of this technology. The performance of the second-generation Absorb bioresorbable everolimus-eluting scaffold was investigated in the ABSORB II as well as in the Cohort B1, Cohort B2, and ABSORB EXTEND studies, and demonstrated excellent clinical results. As the Absorb scaffold has a strict upper limit of expansion, assessment of pre-procedural Dmax of proximal and distal sites has been used for Absorb scaffold size selection in the ABSORB studies. The MACE and MI rates at 1 year were significantly higher in the scaffold oversize group (both proximal and distal Dmax values were smaller than the nominal size of the implanted scaffold) than in the scaffold nonoversize group (MACE: 6.6% vs. 3.3%, log-rank $p < 0.01$, all MI: 4.6% vs. 2.4%; log-rank $p= 0.04$), mainly driven by a higher rate of MI within 1 month after the procedure (3.5% vs. 1.9%; $p= 0.08$). Selection of an appropriate scaffold size according to the vessel Dmax showed a trend toward less frequent ID-TLR, whereas implantation of an oversized Absorb scaffold in a relatively small vessel may be associated with a higher risk of MACE at 1 year (chapter 1.1). The conformability of the stent has been described as the flexibility of a stent in its expanded state with adaptation to the natural shape of the vessel. A higher conformability of the stent is associated with less potential for vessel distortion and trauma. In the deployment of long coronary scaffolds/ stents (28mm in length), bioresorbable vascular scaffolds provides better conformability compared with metallic stents (chapter 1.2). Chapter 1.3 is the first randomized clinical trial (ABSORB II) to analyze the difference in frequencies of periprocedural myocardial infarction (PMI) and cardiac biomarker (CB) rise after implantation of Absorb scaffold or Everolimus eluting stent (EES). Incidence of any anatomic complications including side branch occlusion (SBO) assessed by angiography was similar between the 2 treatment arms (Absorb: 16.4% vs. EES: 19.9%, $p = 0.39$). There were no statistically significant differences in the incidence of CB rise and PMI between Absorb and EES. Treatment with overlapping devices was an independent determinant of per-protocol PMI (OR: 5.07, 95% CI: 1.78 to 14.41, $p = 0.002$). In addition, binary definition of PMI is not only dependent on the selection of CB but also on the thresholds of the CB rise which are arbitrarily chosen (chapter 1.3). In the ABSORB II randomized controlled trial, lower acute gain occurred more frequently in the Absorb arm

than in the Xience arm (3.46 mm2 vs. 4.27 mm2, p<0.001; risk ratio, 3.04; 95%CI, 1.94-4.76). The plaque morphology at the minimum lumen area (MLA) cross-section was not independently associated with acute gain. On angiography, device acute recoil was comparable but expansion of the device was different. The influence of post-dilatation on MLD was somewhat limited (chapter 1.4). The relationship between the IVUS geometrical morphologies and clinical events has never been investigated in the context of a randomized trial. The principal independent determinants of eccentric and asymmetric morphology of scaffold/stent post implantation were high pre-implantation EI [OR 0.03(0.00-0.31), p=0.003] and treatment with Absorb [OR 7.29(3.24-16.37), p<0.001]. Lesions with pre-implantation negative remodeling and high post-implantation AI were independently associated with 1-year DoCE (chapter 1.5). Despite rapid dissemination of an everolimus-eluting bioresorbable scaff old for treatment for coronary artery disease, no data from comparisons with its metallic stent counterpart are available. In ABSORB II trial, the everolimus-eluting bioresorbable scaff old showed similar 1-year composite secondary clinical outcomes to the everolimus-eluting metallic stent (chapter 1.6). In the BVS STEMI study, the Absorb scaffolds implantation in patients presenting with acute MI appeared feasible, with high rate of final TIMI-flow III and good scaffold apposition (chapter 1.7). Furthermore, the implantation of the everolimus eluting bioresorbable vascular scaffold in an expanded range of coronary lesion types and clinical presentations was observed to be safe and feasible with promising angiographic results and mid-term clinical outcomes (chapter 1.8).

Failure Mode of Bioresorbable Scaffolds

In the early Absorb studies, several technical failure and adverse events were documented. We thus summarised the cases who experienced subacute/late scaffold thrombosis or scaffold dislodgement. In the first 450 patients enrolled in the ABSORB EXTEND trial, all dislodgements occurred in the LCX, and in two cases dislodgement was observed after reinsertion of the same device. Two subacute scaffold thromboses and two late scaffold thromboses were observed. Two scaffold thromboses seemed to be related to either premature discontinuation of DAPT or resistance to clopidogrel (chapter 2.1). Potential mechanism causes of scaffold thrombosis could be: 1) suboptimal implantation resulting in underexpansion/acute incomplete strut apposition or acute disruption of struts; 2) platelet activation due to low shear stress created by the relatively thick strut; 3) delayed tissue

coverage in an overlapped segment; 4) discontinuation of DAPT or resistance to DAPT (chapter 2.2). We summarizes the rate of scaffold thrombosis in each individual report. Excluding the GHOST-EU registry, the rate of definite/probable scaffold thrombosis was 0.89% in all-comers, 0.68% in SAP, 1.71% in ACS and 0.67% in STEMI (chapter 2.2). In the ABSORB Cohort B trial, there were six cases of in-segment binary restenosis at the 3-year imaging and clinical follow-up,: two early ISR (<6 months), one late ISR (6-12 months) and three very late ISR (>12 months). Three of these ISR cases seemed to be induced by anatomical or procedural factors. In the other three cases, intravascular imaging (IVUS/OCT) demonstrated that the main mechanism of restenosis was significant intra-scaffold tissue growth, while the structural circularity and diameter of the scaffold were not affected (chapter 2.3).

Validation and application of bifurcation algorithm

The challenge in QCA of bifurcations is to assess an accurate reference diameter (RVD) to calculate the percent diameter stenosis (%DS). Conventional single-vessel QCA software is inaccurate in bifurcation lesions because it completely ignores the natural anatomy of the bifurcation, including the natural "step-down" in diameters after each bifurcation (chapter 3.1). Overestimation of the %DS of the distal main and side branch by single-vessel analysis may potentially have clinical implications. We are already aware that ostial side branch stenosis severity is overestimated with visual estimation. However, the side branch stenosis will also be overestimated when single-vessel QCA analysis is used pre-procedure, which may lead to the overtreatment of insignificant stenosis (chapter 3.1). Dedicated bifurcation software algorithms have been developed: currently, two different software packages are commercially available (CAAS and QAngio XA). The two software packages use slightly different approaches, but both have proven to be highly accurate when validated against precision-manufactured bifurcation phantoms (chapter 3.2). Single-vessel software use in bifurcation trials or first-in-man/registry studies on dedicated bifurcation stents with planned repeat angiography will lead to less accurate results of the side branch (chapter 3.2). A recent example was the Tryton IDE trial showing different QCA outcomes with dedicated bifurcation QCA from those with single-vessel QCA (chapter 3.3). The use of single-vessel software in such trials may therefore lead to an increased rate of ischaemia-driven target TLR of the side branch (chapter 3.3). Three-dimensional (3D) quantitative coronary angiography (QCA) provides more accurate measurements by

minimizing inherent limitations of two-dimensional (2D) QCA (chapter 3.4). There were differences in addressing anatomical severity and location of coronary bifurcation lesions between in vivo 2D and 3D QCA analyses. Whereas DS was in general higher with 2D QCA, lesion length was shorter with 2D QCA than with 3D QCA (chapter 3.4). The implantation of a bioresorbable scaffold is a new approach that provides transient vessel support with drug delivery capability, potentially without the limitations of permanent metallic implants.

Long Term Assessment of Bioresorbable Scaffolds

Using IVUS grey scale derived parameters, we attempted to assess the degradation process of the Absorb poly-L-lactide bioresorbable everolimuseluting scaffold at multiple time points in a porcine model. Hyperechogenic and upperechogenic thresholds had strong and positive correlations with the scaffold molecular weight assessment. The combination of hyper and upperechogenicity could be used as a surrogate for the chromatographic assessment of scaffold molecular weight (chapter 4.1). Quantitative light intensity analysis by OCT was capable of detecting subtle changes in the bioresorbable strut appearance over time, and could be used to monitor the bioresorption and integration process of polylactide struts (chapter 4.2). The quantitative OCT-light intensity analysis could be used as a surrogate method for monitoring the integration process of PLLA scaffolds throughout 5 years, which could help the clinicians to better interpret the human OCT images with regarding to the phases of integration process (chapter 4.3). Development and receding of a coronary artery aneurysm after implantation of a fully bioresorbable scaffold was documended in the Cohort B trial for 5 years (Chapter 4.4). Multislice computed tomography coronary angiography (MSCT) has provided reliable assessment of the angiographic results up to 3 to 5 years. The metallic radio-opaque markers (MRM) recognition by MSCT is critical for precise noninvasive assessment of the coronary location of all MRMs (chapter 4.5). We found a significant increase in the luminal area at the distal edge at 6-month follow-up. However, at longer term (1, 2, and 3 years), the luminal area decreased at both edges, resulting in a repeat revascularization rate of 3% (chapter 4.6).

CONCLUSIONS

In the randomised comparison, the Absorb everolimuseluting bioresorbable scaffolds showed similar one-year clinical outcomes to the everolimus-eluting Xience metallic stent,

and side branch occlusion and other angiographic complications are not different in the acute performance. Implantation of an oversized Absorb scaffold in a relatively small vessel appears to be associated with a higher 1-year MACE rate driven by more frequent early MI. In the early Absorb studies, several failure modes of bioresorbable scaffolds were documented. To avoid scaffold dislodgement, appropriate lesion preparation is mandatory. In case of unsuccessful initial delivery, a second insertion of the same scaffold should be avoided. Adherence to antiplatelet therapy is of paramount importance to avoid acute or subacute scaffold thrombosis. QCA bifurcation was validated and clinical applicable. IVUS, OCT and MSCT could be used to assess long term bioresorption and serial changes in lumen dimension.

Further investigation using intravascular imaging is needed to establish the relationship between acute potential mechanism and late adverse events.

May 2016,

Yuki Ishibashi

Samenvatting

Samenvatting en conclusies

Bepaling bloedvat diameter, acute prestaties en patiënten uitkomsten na implantatie van biologisch oplosbare stents (scaffolds).

Het gebruik van biologisch oplosbare stents heeft verschillende uitdagingen die een zorgvuldige evaluatie van deze technologie justificeert. De prestaties van de tweede generatie biologisch oplosbare everolimus-afgevende stents onderzocht in ABSORBII studie en ook in cohort B1/B2 en ABSORB-Extend studies laten goede klinische resultaten zien. Omdat de Absorb scaffold een strikte maximale bovengrens van expansie heeft, worden in de ABSORB studies de beoordeling van de pre-procedure Dmax (maximale-Diameter) van proximale en distale kanten van de scaffold gebruikt voor het selecteren van de juiste Absorb scaffold maat (diameter). De negatieve uitkomsten zoals dood, myocard infarct (MI), reinterventie (MACE) waren op 1 jaar aanzienlijk hoger in de patiënten groep met een te grote scaffold maat in relatie tot het bloedvat (zowel de proximale als distale Dmax waren kleiner dan de nominale maat van de geïmplanteerde scaffold) dan in de scaffold groep met een juiste scaffold maat zonder oversizing (MACE: 6,6% versus 3,3%, log-rank p <0,01, alle MI: 4,6% versus 2,4%; log-rank p= 0,04), voornamelijk gedreven door een hoger percentage van MI binnen 1 maand na de procedure (3,5% versus 1,9%; p= 0,08). Selectie van een geschikte grootte van de scaffold in relatie tot de Dmax van het bloedvat toonde een trend naar minder frequente reinterventies, terwijl het implanteren van een oversized Absorb scaffold in een relatief klein bloedvat kan worden geassocieerd met een hoger risico van MACE op 1 jaar (hoofdstuk 1.1). De verhoogde pasbaarheid (conformability) van de stent is omschreven als de flexibiliteit van een stent in de uitgerekte vorm met aanpassing aan de natuurlijke vorm van het bloedvat. Een betere conformabiliteit van de scaffold wordt geassocieerd met minder bloedvat vervorming en andere trauma. Bij de implantatie van lange coronaire scaffolds/ stents (28 mm lang) bieden biologisch oplosbare stents een betere/verhoogde pasbaarheid in vergelijking met metalen stents (hoofdstuk 1.2). In hoofdstuk 1.3 wordt de eerste gerandomiseerde klinische trial (ABSORB II) behandeld en wordt het verschil in frequentie van peri-procedure myocard infarct (PMI) en cardiale biomarker (CB) verhoging na implantatie van de biologisch oplosbare everolimus-afgevende stents (EWS) beschreven. Incidentie van anatomische complicaties waaronder zijtak occlusie (SBO) beoordeeld door angiografie was vergelijkbaar tussen de twee behandelings armen (de biologisch oplosbare

everolimus-afgevende stent (ABSORB): 16,4% *versus* de metalen everolimus-afgevende stent (XIENCE): 19,9%, p = 0,39). Er waren geen statistisch significante verschillen in de incidentie van CB verhoging en PMI tussen ABSORB en XIENCE. Behandeling met een overlappende stent/scaffold was een onafhankelijke factor van de per-protocol PMI (OR: 5,07, 95% CI: 1.78 tot 14.41, p = 0.002). Bovendien, is de binaire definitie van PMI niet alleen afhankelijk van de keuze van CB, maar ook van de keuze van de drempel (threshold) van de CB verhoging die willekeurig gekozen wordt (hoofdstuk 1.3). In de ABSORB II gerandomiseerde gecontroleerde trial, zien we in de scaffold arm vaker een lagere acute gain (winst in diameter) dan in de XIENCE arm (3,46 mm2 vs. 4.27 mm2, P<0,001; risico ratio, 3.04; 95%CI, 1.94-4.76). De morfologie van de plaque op het punt van de minimale lumen dwarsdoorsnede (MLA) was niet onafhankelijk geassocieerd met acute gain. Op angiografie, was de acute recoil (afname in diameter/terugveren) vergelijkbaar tussen de ABSORB en de XIENCE maar de expansie tussen de twee producten was verschillend. De invloed van post-dilatatie op de minimale lumen diameter (MLD) was enigszins beperkt (hoofdstuk 1.4). De relatie tussen de IVUS geometrische morfologie en klinische gebeurtenissen is nooit onderzocht in het kader van een gerandomiseerde trial. De belangrijkste onafhankelijke determinanten van excentrische en asymmetrische morfologie van scaffold/stent na implantatie zijn hoge pre-implantatie EI [OR 0.03 (0.00-0.31), p=0.003] en behandeling met Absorb [OR 7.29(3.24-16.37), p<0,001]. Vernauwingen met pre-implantatie negatieve remodeling en hoge post-implantatie AI zijn onafhankelijk geassocieerd met 1 jaar gebeurtenissen (Device oriented Cardiac Endpoints; dood, infarct, reinterventie) (hoofdstuk 1.5). Ondanks een snelle verspreiding van de biologisch oplosbare everolimus-afgevende stents voor behandeling van coronaire hartziekte, zijn er nog geen gegevens beschikbaar van vergelijkingen met zijn metalen counterpart. In de ABSORB II studie, laat de biologisch oplosbare everolimus-afgevende stent soortgelijke 1 jaar samengestelde secundaire klinische resultaten zien dan de everolimus-afgevende metalen stent (hoofdstuk 1.6). De BVS STEMI-studie laat zien dat de implantatie van de biologisch oplosbare everolimus-afgevende stents mogelijk is bij patiënten met een acuut myocard infarct met een goede TIMI flow III en een goede scaffold appositie in de bloedvatwand (hoofdstuk 1.7). Bovendien blijkt de implantatie van de biologisch oplosbare everolimus-afgevende stents in een uitgebreid scala van coronaire laesies types en klinische presentaties veilig en haalbaar met goede angiografische en tussentijdse klinische resultaten (hoofdstuk 1.8).

Failure Mode van biologisch oplosbare stents

In het begin van de ABSORB studies werden er diverse technische problemen en ongewenste klinische gebeurtenissen gedocumenteerd. Wij hebben gevallen van subacute/late scaffold trombose en van scaffold dislodgement gerapporteerd. In de eerste 450 patiënten gerekruteerd in de ABSORB EXTEND studie gebeurde alle dislodgements in de LCX, en in twee gevallen werd dislodgement waargenomen na het opnieuw inbrengen van *dezelfde* scaffold. Twee subacute scaffold thromboses en twee late scaffold thromboses werden waargenomen. Twee scaffolds thromboses lijken te zijn gelieerd aan een voortijdige beëindiging van DAPT of resistentie voor clopidogrel (hoofdstuk 2.1). Potentiële oorzaken van scaffold trombose kunnen zijn: 1) suboptimale implantatie met onder expansie/acute onvolledige strut aanhechting (appositie) of acute ontwrichting van struts; 2) bloedplaatjes activatie door lage shear stress veroorzaakt door de relatief dikke struts; 3) vertraagde weefsel dekking in een segment met overlappende struts; 4) onderbreking/ stoppen van DAPT of resistentie tegen DAPT (hoofdstuk 2.2). We hebben het percentage scaffold trombose samengevat in elk individueel verslag. Met uitzondering van de ghost-eu registrie, het percentage van de definitieve/waarschijnlijke scaffold trombose 0,89% in all-comer patiënten, 0,68% in stabiele patiënten, 1,71% in acute patiënten en 0,67% in ST-elevation myocardial infarction (hoofdstuk 2.2). In de ABSORB cohort-B trial, waren er zes gevallen van in-segment restenosis (ISR) tijdens de 3-jarige klinische follow-up met beeldvorming: twee vroege ISR (<6 maanden), één late ISR (6-12 maanden) en drie zeer late gevallen van ISR (>12 maanden). Drie van deze ISR gevallen blijken te worden geïnduceerd door anatomische of procedurele factoren. In de drie andere gevallen, heeft intravasculaire imaging (IVUS/OCT) aangetoond dat het belangrijkste mechanisme van restenosis significante intra-scaffold weefselgroei is, terwijl de structurele circulariteit en de diameter van de scaffolds niet werden beïnvloed (hoofdstuk 2.3).

Validatie en toepassing van bifurcatie algoritme

De uitdaging van QCA in bifurcaties is het beoordelen van een nauwkeurige referentie diameter (RVD) voor het berekenen van percentage diameter stenose [%DS]. Conventionele single-bloedvat QCA software is onnauwkeurig in bifurcatie laesies omdat deze software volledig voorbij gaat aan de natuurlijke anatomie van de bifurcatie, waaronder de natuurlijke "step-down" in diameters na iedere zijtak/ bifurcatie (hoofdstuk 3.1).

Overschatting van de %DS van de distale hoofdtak en zijtak door single-bloedvat analyse hebben mogelijkerwijs klinische implicaties. We weten al dat een ostiale zijtak vernauwing wordt overschat met visuele analyse. Echter, deze ostiale zijtak vernauwing wordt ook overschat wanneer single-bloedvat QCA analyse wordt gebruikt pre-procedure, wat kan leiden tot de overbehandeling van onbeduidende vernauwingen (hoofdstuk 3.1). Speciale bifurcatie software-algoritmen zijn ontwikkeld; momenteel zijn twee verschillende softwarepakketten commercieel verkrijgbaar (CAAS en QAngio XA). Deze twee softwarepakketten gebruiken enigszins verschillende methoden, maar beide hebben zijn uiterst nauwkeurig wanneer gevalideerd tegen precisie vervaardigde bifurcatie fantomen (hoofdstuk 3.2). Single-bloedvat analyse software gebruikt in bifurcatie en first-in-man/register studies met toegewijde bifurcatie stents met geplande follow-up angiografie zal leiden tot minder nauwkeurige resultaten (hoofdstuk 3.2). Een recent voorbeeld hiervan is de Tryton IDE studie die verschillende QCA resultaten laat zien wanneer speciale bifurcatie QCA wordt gebruikt vergeleken met singel-bloedvat QCA (hoofdstuk 3.3). Het gebruik van single-bloedvat QCA software in dergelijke processen kan dan ook leiden tot een foutieve mate van reinterventie van de zijtak (hoofdstuk 3.3). Driedimensionale (3D) kwantitatieve coronaire angiografie (QCA) verschaft nauwkeurigere metingen door het minimaliseren van inherente beperkingen van tweedimensionale (2D) QCA (hoofdstuk 3.4). Er zijn verschillen tussen in-vivo 2D en 3D QCA-analyses in aanpak van de anatomische vernauwing en van de locatie van coronaire bifurcaties. DS% was in het algemeen hoger met 2D-QCA, laesie lengte was korter met 2D-QCA dan met 3D-QCA (hoofdstuk 3.4). De implantatie van een biologisch oplosbare stent met medicijn afgevende capaciteit en met kortstondige support van het bloedvat is een nieuwe benadering, mogelijk zonder de beperkingen van permanente metalen implantaten.

Lange termijn beoordeling van biologisch oplosbare stents

Met IVUS afgeleide parameters, hebben we geprobeerd om in het varkensmodel op meerdere tijdstippen het afbraak proces te analyseren van de poly-L-lactide bioresorbable everolimus-eluting Absorb. Hyperechogenic en upperechogenic drempels hadden een sterke en positieve correlaties met de beoordeling van het molecuulgewicht van de scaffold. De combinatie van hyper en upperechogenicity konden worden gebruikt als surrogaat voor de chromatografische analyse van het molecuulgewicht van de scaffold (hoofdstuk 4.1). Kwantitatieve lichtintensiteit analyse door OCT kunnen subtiele veranderingen

detecteren in het uiterlijk van de bioresorbable strut in de loop van de tijd, en kan worden gebruikt voor bewaking van de bioresorption- en integratieproces van de polylactide struts (hoofdstuk 4.2). De kwantitatieve OCT-lichtintensiteit analyse gedurende 5 jaar kan worden gebruikt als surrogaat voor het integratieproces van PLLA scaffolds die de artsen kunnen helpen om de menselijke OCT beelden beter te kunnen interpreteren met betrekking tot het integratie proces (hoofdstuk 4.3). Ontwikkeling en afname van een coronaire bloedvat aneurysma voor 5 jaar na implantatie van een volledig bioresorbable scaffold is gedocumenteerd in Absorb cohort B trial (hoofdstuk 4.4). Multislice computertomografie coronaire angiografie (MSCT) heeft gezorgd voor een betrouwbare beoordeling van de angiografische resultaten van 3 tot 5 jaar. De herkenning van de metalen radio-opaque marker (MRM) van de scaffold door MSCT is essentieel voor nauwkeurige niet-invasieve evaluatie van alle MRMs in het bloedvat (hoofdstuk 4.5). We vonden een significante toename in de luminal area aan de distale rand bij 6 maanden follow-up. Echter, op langere termijn (1, 2 en 3 jaar) is de luminal area afgenomen aan beide kanten wat resulteerde in 3% re-interventies (hoofdstuk 4.6).

Conclusies

In de gerandomiseerde vergelijking, de biologisch oplosbare everolimus-afgevende stent (ABSORB) vertoonden soortgelijke eenjarige klinische resultaten dan de metalen everolimus-afgevende stent (XIENCE), en zijtak occlusie en andere angiografische complicaties verschillen niet in de acute prestaties. Implantatie van een oversized Absorb scaffold in een relatief klein bloedvat lijkt geassocieerd te worden met een hogere 1-jaar MACE percentage gedreven door vroege myocard infarcten. In het begin van de Absorb studies zijn diverse tekortkomingen van bioresorbable scaffolds gedocumenteerd. Om het vroegtijdig breken van scaffolds te voorkomen is een nauwkeurige laesie voorbereiding verplicht. In geval van een niet-succesvolle eerste poging, moet een tweede poging met eenzelfde scaffold worden vermeden. Naleving van antiplatelet therapie is van het allergrootste belang om acute of subacute scaffold trombose te voorkomen. Bifurcatie QCA werd gevalideerd en is klinische toepasbaar. IVUS, CTO en MSCT kunnen worden gebruikt voor het beoordelen van langdurige bioresorption en seriële veranderingen in lumen dimensie.

Nader onderzoek met behulp van intravasculaire beeldvorming is vereist om de relatie tussen acute potentiële mechanisme en late ongewenste gebeurtenissen te bevestigen.

Mei 2016, Yuki Ishibashi

Curriculum Vitae

CURRICULUM VITAE

Yuki Ishibashi, M.D., Ph.D.

Division of Cardiology, Department of Internal Medicine,

St. Marianna University School of Medicine

2-16-1 Sugao, Miyamae-ku, Kawasaki city, Kanagawa, 216-8511, Japan

E-mail: ishibashi15@yahoo.co.jp

DATE and PLACE OF BIRTH:

5th January, 1978 Iwate-prefecture, Japan

NATIONALITY:

Japanese

EDUCATION:

Doctor of Philosophy in Medicine
St. Marianna University Graduate School (Kawasaki-city, Kanagawa-prefecture, Japan)
October 6, 2010

Doctor of Medicine in Medicine
St. Marianna University School of Medicine (Kawasaki-city, Kanagawa-prefecture, Japan)
April 1997 to March 2003

WORK EXPERIENCES:

Chief Physician in the Division of Cardiology, Department of Internal Medicine, St. Marianna University School of Medicine, Kanagawa, Japan
April 2015 to present

Erasmus University Medical Center, Thoraxcenter, Rotterdam, The Netherlands (Research Fellow in Interventional Cardiology)
April 2013 to March 2015

Chief Physician in the Division of Cardiology, Department of Internal Medicine, St. Marianna University School of Medicine, Kanagawa, Japan
April 2012 to March 2013

Chief Physician in the Department of Cardiology,
St. Marianna University Yokohama-city Seibu Hospital, Kanagawa, Japan
April 2010 to March 2012

Physician in the Division of Cardiology, Department of Internal Medicine, St. Marianna University School of Medicine, Kanagawa, Japan
April 2006 to March 2010

Senior Resident in the Division of Cardiology, Yokohama Sakae Kyosai Hospital, Federation of National Public Service Personnel Mutual Associations, Kanagawa, Japan
April 2005 to March 2006

Junior Resident in the Division of Cardiology, Department of Internal Medicine, St. Marianna University School of Medicine, Kanagawa, Japan
April 2003 to March 2005

QUALIFICATIONS:

Ph.D.
St. Marianna University Graduate School (No.1312) 2010/10/6

Master
FESC (Fellowship of the ESC) 2016/11

Board Certified Member of the Japanese Association of Cardiovascular Intervention and Therapeutics (No. 00547) 2010/10/01

Board Certified Member of the Japanese Circulation Society (No. 17908) 2010/04/01

Registered Instructor of Japanese Cardiac Rehabilitation (No. 092077) 2009/09/01

Board Certified Member of the Japanese Society of Internal Medicine (No. 33515) 2007/10/01

M.D.
St. Marianna University School of Medicine (No. 437895) 2003/05/10

AWARDS and HONORS:

2010.01 Exemplary Works Best Abstract Award at Complex Cardiovascular Therapeutics 2010

PROFESSIONAL ASSOCIATION:

The Japanese Circulation Society
The Japanese Society of Internal Medicine
Japanese Association of Cardiovascular Intervention and Therapeutics
Japanese Association of Cardiac Rehabilitation

PUBLICATIONS: Scientific journal

1. Edge Vascular Response After Resorption of the Everolimus-Eluting Bioresorbable Vascular Scaffold - A 5-Year Serial Optical Coherence Tomography Study.

Tateishi H, Suwannasom P, Sotomi Y, Nakatani S, **Ishibashi Y**, Tenekecioglu E, Abdelgani M, Cavalcante R, Zeng Y, Grundeken MJ, Albuquerque FN, Veldhof S, Onuma Y, Serruys PW; investigators of the ABSORB Cohort B study.
Circ J. 2016 Mar 3.

2. Aortic annulus displacement assessed by contrast left ventriculography during invasive coronary angiography as a predictor of adverse events.

Kuwata S, Yoneyama K, Suzuki K, Izumo M, Mizukoshi K, Koyama K, **Ishibashi Y**, Mitarai T, Kamijima R, Kongoji K, Harada T, Akashi YJ.
J Cardiol. 2016 Feb 16.

3. Relation between bioresorbable scaffold sizing using QCA-Dmax and clinical outcomes at 1 year in 1232 patients from three study cohorts (ABSORB Cohort B, ABSORB EXTEND and ABSORB II).

Ishibashi Y, Nakatani S, Suwannasom P, Grundeken MJ, Garcia-Garcia HM, Bartorelli A, Whitbourn R, Chevalier B, Abizaid A, Ormiston JA, Rapoza R, Veldhof S, Onuma Y, Serruys PW
JACC cardiovasc. Interv. 2015 Nov;8(13):1715-26.

4. Incidence and Potential Mechanism(s) of Post-Procedural Rise of Cardiac Biomarker in Patients With Coronary Artery Narrowing After Implantation of an Everolimus-Eluting Bioresorbable Vascular Scaffold or Everolimus-Eluting Metallic Stent.

Ishibashi Y, Muramatsu T, Nakatani S, Sotomi Y, Suwannasom P, Grundeken MJ, Cho YK, Garcia-Garcia HM, van Boven AJ, Piek JJ, Sabaté M, Helqvist S, Baumbach A, McClean D, de Sousa Almeida M, Wasungu L, Miquel-Hebert K, Dudek D, Chevalier B, Onuma Y,
Serruys PW.
JACC Cardiovasc Interv. 2015 Jul;8(8):1053-63

5. First generation versus second generation drug-eluting stents for the treatment of bifurcations: 5-year follow-up of the LEADERS all-comers randomized trial.

Grundeken MJ, Wykrzykowska JJ, **Ishibashi Y**, Garg S, de Vries T, Garcia-Garcia HM, Onuma Y, de Winter RJ, Buszman P, Linke A, Ischinger T, Klauss V, Eberli F, Corti R, Wijns W, Morice MC, di Mario C, Meier B, Jüni P, Yazdani A, Copt S, Windecker S, Serruys PW.
Catheter Cardiovasc Interv. 2015 Dec 9.

6. Incidence and potential mechanism of resolved, persistent and newly acquired malapposition three days after implantation of self-expanding or balloon-expandable stents in a STEMI population: insights from optical coherence tomography in the APPOSITION II study.

Nakatani S, Onuma Y, **Ishibashi Y**, Karanasos A, Regar E, Garcia-Garcia HM, Tamburino C, Fajadet J, Vrolix M, Witzenbichler B, Eeckhout E, Spaulding C, Reczuch K, La Manna A, Spaargaren R, Capodanno D, Van Langenhove L, Verheye S, Serruys PW, van Geuns RJ.
EuroIntervention. 2015 Nov 10;11(7)

7. Comparative analysis method of permanent metallic stents (XIENCE) and bioresorbable poly-L-lactic (PLLA) scaffolds (Absorb) on optical coherence tomography at baseline and follow-up.

Nakatani S, Sotomi Y, **Ishibashi Y**, Grundeken MJ, Tateishi H, Tenekecioglu E, Zeng Y, Suwannasom P, Regar E, Radu MD, Räber L, Bezerra H, Costa MA, Fitzgerald P, Prati F, Costa RA, Dijkstra J, Kimura T, Kozuma K, Tanabe K, Akasaka T, Di Mario C, Serruys PW, Onuma Y.
EuroIntervention. 2015 Oct 9;11(6).

8. Comparison between two- and three-dimensional quantitative coronary angiography bifurcation analyses for the assessment of bifurcation lesions: A subanalysis of the TRYTON pivotal IDE coronary bifurcation trial.

Muramatsu T, Grundeken MJ, **Ishibashi Y**, Nakatani S, Girasis C, Campos CM, Morel MA, Jonker H, de Winter RJ, Wykrzykowska JJ, García-García HM, Leon MB, Serruys PW, Onuma Y; TRYTON Pivotal IDE Coronary

Bifurcation Trial Investigators.
Catheter Cardiovasc Interv. 2015 Sep 1;86(3):E140-9.

9. Dual antiplatelet therapy, drug-eluting stents and bioresorbable vascular scaffolds: Evolutionary perspectives.

Albuquerque FN, Bortnick A, Iqbal J, **Ishibashi Y**, Stone GW, Serruys PW.
Catheter Cardiovasc Interv. 2015 Aug 10.

10. Fate of Bioresorbable Vascular Scaffold Metallic Radio-Opaque Markers at the Site of Implantation After Bioresorption.

Suwannasom P, Onuma Y, Campos CM, Nakatani S, **Ishibashi Y**, Tateishi H, Grundeken MJ, Stanetic B, Nieman K, Jonker H, Garcia-Garcia HM, Serruys PW; investigators of ABSORB Cohort A, B and EXTEND trials.
JACC Cardiovasc Interv. 2015 Jul;8(8):1130-2.

11. Definite and probable bioresorbable scaffold thrombosis in stable and ACS patients.

Ishibashi Y, Nakatani S, Onuma Y.
EuroIntervention. 2015 Jul 22;11(3):e1-2.

12. Association between inflammatory biomarkers and thin-cap fibroatheroma detected by optical coherence tomography in patients with coronary heart disease.

Koyama K, Yoneyama K, Mitarai T, **Ishibashi Y**, Takahashi E, Kongoji K, Harada T, Akashi YJ.
Arch Med Sci. 2015 Jun 19;11(3):505-12.

13. A Rare Case of Spontaneous Dissection in a Left Internal Mammary Artery Bypass Graft in Acute Coronary Syndrome.

Koyama K, Yoneyama K, Tsukahara M, Kuwata S, Mitarai T, Kamijima R, **Ishibashi Y**, Tanabe Y, Kongoji K, Harada T, Akashi YJ.
JACC Cardiovasc Interv. 2015 Jun;8(7):996-7

14. The need for dedicated bifurcation quantitative coronary angiography (QCA) software algorithms to evaluate bifurcation lesions.

Grundeken MJ, **Ishibashi Y**, Ramcharitar S, Tuinenburg JC, Reiber JH, Tu S, Aben JP, Girasis C, Wykrzykowska JJ, Onuma Y, Serruys PW.
EuroIntervention. 2015 May;11 Suppl V:V44-9

15. Risk stratification in 3-vessel coronary artery disease: Applying the SYNTAX Score II in the Heart Team Discussion of the SYNTAX II trial.

Campos CM, Stanetic BM, Farooq V, Walsh S, **Ishibashi Y**, Onuma Y, Garcia-Garcia HM, Escaned J, Banning A, Serruys PW; SYNTAX II Study Group.
Catheter Cardiovasc Interv. 2015 May 6.

16. Validity of SYNTAX score II for risk stratification of percutaneous coronary interventions: A patient-level pooled analysis of 5,433 patients enrolled in contemporary coronary stent trials.

Campos CM, Garcia-Garcia HM, van Klaveren D, **Ishibashi Y**, Cho YK, Valgimigli M, Räber L, Jonker H, Onuma Y, Farooq V, Garg S, Windecker S, Morel MA, Steyerberg EW, Serruys PW.
Int J Cardiol. 2015 May 6;187:111-5

17. Echogenicity as a surrogate for bioresorbable everolimus-eluting scaffold degradation: analysis at 1-, 3-, 6-, 12- 18, 24-, 30-, 36- and 42-month follow-up in a porcine model.

Campos CM, **Ishibashi Y**, Eggermont J, Nakatani S, Cho YK, Dijkstra J, Reiber JH, Sheehy A, Lane J, Kamberi M, Rapoza R, Perkins L, Garcia-Garcia HM, Onuma Y, Serruys PW.
Int J Cardiovasc Imaging. 2015 Mar;31(3):471-82.

18. In vitro validation and comparison of different software packages or algorithms for coronary bifurcation analysis using calibrated phantoms: implications for clinical practice and research of bifurcation stenting.

Ishibashi Y, Grundeken MJ, Nakatani S, Iqbal J, Morel MA, Généreux P, Girasis C, Wentzel JJ, Garcia-Garcia HM, Onuma Y, Serruys PW.
Catheter Cardiovasc Interv. 2015 Mar;85(4):554-63.

19. Early (before 6 months), late (6-12 months) and very late (after 12

months) angiographic scaffold restenosis in the ABSORB Cohort B trial.
Nakatani S, Onuma Y, **Ishibashi Y**, Muramatsu T, Iqbal J, Zhang YJ, van Geuns RJ, Ormiston JA, Serruys PW.
EuroIntervention. 2015 Mar;10(11):1288-98.

20. Development and receding of a coronary artery aneurysm after implantation of a fully bioresorbable scaffold.
Nakatani S, **Ishibashi Y**, Suwannasom P, Grundeken MJ, Høj Christiansen E, Onuma Y, Serruys PW; ABSORB Cohort B Investigators.
Circulation. 2015 Feb 24;131(8):764-7.

21. Inter-core lab variability in analyzing quantitative coronary angiography for bifurcation lesions: a post-hoc analysis of a randomized trial.
Grundeken MJ, **Ishibashi Y**, Généreux P, LaSalle L, Iqbal J, Wykrzykowska JJ, Morel MA, Tijssen JG, de Winter RJ, Girasis C, Garcia-Garcia HM, Onuma Y, Leon MB, Serruys PW.
JACC Cardiovasc Interv. 2015 Feb;8(2):305-14.

22. A bioresorbable everolimus-eluting scaffold versus a metallic everolimus-eluting stent for ischaemic heart disease caused by de-novo native coronary artery lesions (ABSORB II): an interim 1-year analysis of clinical and procedural secondary outcomes from a randomised controlled trial.
Serruys PW, Chevalier B, Dudek D, Cequier A, Carrié D, Iniguez A, Dominici M, van der Schaaf RJ, Haude M, Wasungu L, Veldhof S, Peng L, Staehr P, Grundeken MJ, **Ishibashi Y**, Garcia-Garcia HM, Onuma Y.
Lancet. 2015 Jan 3;385(9962):43-54.

23. Short-term effects of Nano+™ polymer-free sirolimus-eluting stents on native coronary vessels:an optical coherence tomography imaging study
Suwannasom P, Benit E, Gach O, von Birgelen C, Hofma S, Bo X, Zhang Y-J, Nakatani S, **Ishibashi Y**, Onuma Y, García-García HM, Gao R, Serruys PW
AsiaIntervention 2015;1:57-70

24.Scaffold and edge vascular response following implantation of everolimus-eluting bioresorbable vascular scaffold: a 3-year serial optical coherence tomography study.
Zhang YJ, Iqbal J, Nakatani S, Bourantas CV, Campos CM, **Ishibashi Y**, Cho YK, Veldhof S, Wang J, Onuma Y, Garcia-Garcia HM, Dudek D, van Geuns RJ, Serruys PW; ABSORB Cohort B Study Investigators.
JACC Cardiovasc Interv. 2014 Dec;7(12):1361-9.

25.Periprocedural myocardial injury and right bundle branch block during coronary optical coherence tomography in an acute coronary syndrome patient with severe coronary ectasia.
Koyama K, Yoneyama K, Mitarai T, Kobayashi Y, Saito M, Oono T, Kuwata S, **Ishibashi Y**, Kongoji K, Akashi YJ, Harada T.
Int J Cardiol. 2014 Dec 20;177(3):1113-5.

26.Fast virtual functional assessment of intermediate coronary lesions using routine angiographic data and blood flow simulation in humans: comparison with pressure wire - fractional flow reserve.
Papafaklis MI, Muramatsu T, **Ishibashi Y**, Lakkas LS, Nakatani S, Bourantas CV, Ligthart J, Onuma Y, Echavarria-Pinto M, Tsirka G, Kotsia A, Nikas DN, Mogabgab O, van Geuns RJ, Naka KK, Fotiadis DI, Brilakis ES, Garcia-Garcia HM, Escaned J, Zijlstra F, Michalis LK, Serruys PW.
EuroIntervention. 2014 Sep;10(5):574-83.

27.Simultaneous occlusion of left anterior descending and left circumflex arteries by very late stent thrombosis: vascular response to drug-eluting stents assessed by intravascular ultrasound.
Yamawaki M, Onuma Y, Nakano M, Muramatsu T, Nakatani S,
Ishibashi Y, Ishimori H, Hirano K, Ito Y, Tsukahara R, Muramatsu T.
Heart Vessels. 2014 Jul 17.

28.Lessons learned from acute and late scaffold failures in the ABSORB EXTEND trial.
Ishibashi Y, Onuma Y, Muramatsu T, Nakatani S, Iqbal J, Garcia-Garcia HM, Bartorelli AL, Whitbourn R, Abizaid A, Serruys PW; ABSORB EXTEND Investigators.

EuroIntervention. 2014 Aug;10(4):449-57.

29. Temporal evolution of strut light intensity after implantation of bioresorbable polymeric intracoronary scaffolds in the ABSORB cohort B trial-an application of a new quantitative method based on optical coherence tomography.

Nakatani S, Onuma Y, **Ishibashi Y**, Eggermont J, Zhang YJ, Campos CM, Cho YK, Liu S, Dijkstra J, Reiber JH, Perkins L, Sheehy A, Veldhof S, Rapoza R, van Es GA, Garcia-Garcia HM, van Geuns RJ, Serruys PW; ABSORB Cohort B investigators.

Circ J. 2014;78(8):1873-81.

30. Implications of a bioresorbable vascular scaffold implantation on vessel wall strain of the treated and the adjacent segments.

Bourantas CV, Garcia-Garcia HM, Campos CA, Zhang YJ, Muramatsu T, Morel MA, Nakatani S,Gao X, Cho YK, **Ishibashi Y**, Gijsen FJ, Onuma Y, Serruys PW.

Int J Cardiovasc Imaging. 2014 Mar;30(3):477-84.

31. In-stent protrusion after implantation of a drug-eluting stent in a honeycomb-like coronary artery structure: complete resolution over 6 months and the role of optical coherence tomography imaging in the diagnosis and follow-up.

Koyama K, Yoneyama K, Mitarai T, Kuwata S, **Ishibashi Y**, Kongoji K, Akashi YJ.

JACC Cardiovasc Interv. 2014 May;7(5):e39-40.

32. Everolimus-eluting bioresorbable vascular scaffolds for treatment of patients presenting with ST-segment elevation myocardial infarction: BVS STEMI first study.

Diletti R, Karanasos A, Muramatsu T, Nakatani S, Van Mieghem NM, Onuma Y, Nauta ST, **Ishibashi Y**, Lenzen MJ, Ligthart J, Schultz C, Regar E, de Jaegere PP, Serruys PW, Zijlstra F, van Geuns RJ.

Eur Heart J. 2014 Mar;35(12):777-86.

33. A rare adult case of corrected transposition of the great vessels with

situs inversus with a single coronary artery and an atrial septal defect.
Kuwata S, Yoneyama K, Izumo M, **Ishibashi Y**, Hayashi A, Yamauchi M, Musha H, Akashi YJ.
Int J Cardiol. 2013 Oct 3;168(3):e91-3.

34.A case reports; Effective use of Tadalafil in a patient with pulmonary hypertension and silent thyroiditis induced by pregnancy.
Mitarai T, **Ishibashi Y**, Yamauchi M, Musha H, Miyake F
Theraputic Research 2012 (33) 7

35.Relevance of I-BMIPP delayed scintigraphic imaging for patients with angina pectoris - a pilot study.
Koyama K, Akashi YJ, Kida K, Suzuki K, **Ishibashi Y**, Musha H, Banach M.
Arch Med Sci. 2011 Jun;7(3):428-32.

36.Significance of 99mTc-sestamibi myocardial scintigraphy after percutaneous coronary intervention in patients with acute myocardial infarction.
Akashi YJ, Ashikaga K, Takano M, Izumo M, **Ishibashi Y**, Kida K, Yoneyama K, Suzuki K, Miyake F, Banach M.
Med Sci Monit. 2011 Feb 25;17(3):CR140-5.

37.Impact of contrast-induced nephropathy and cardiovascular events by serum cystatin C in renal insufficiency patients undergoing cardiac catheterization.
Ishibashi Y, Yamauchi M, Musha H, Mikami T, Kawasaki K, Miyake F.
Angiology. 2010 Nov;61(8):724-30.

38.Peak time of acute coronary syndrome in patients with sleep disordered breathing.
Ishibashi Y, Osada N, Sekiduka H, Izumo M, Shimozato T, Hayashi A, Kida K, Yoneyama K, Takahashi E, Suzuki K, Tamura M, Akashi YJ, Inoue K, Omiya K, Miyake F, Izawa K, Watanabe S.
J Cardiol. 2009 Apr;53(2):164-70.

39.Relationship between sleep-disordered breathing level and acute onset time of congestive heart failure.
Yoneyama K, Osada N, Shimozato T, **Ishibashi Y**, Hayashi A, Takahashi E, Kida K, Suzuki K, Tamura M, Inoue K, Akashi YJ, Omiya K, Miyake F, Izawa KP, Watanabe S.
Int Heart J. 2008 Jul;49(4):471-80.

40.A Comparative Study in the Same Patients Treated with the 4 French Acist Power Injection System and the 5 French Manual Catheterization Technique.
Ishibashi Y, Yamauchi M, Musha H, Mikami T, Kawasaki K, Miyake F
The St. Marianna Medical Journal 2008; 36: 427-433.

41.Small dense low-density lipoprotein cholesterol is a useful marker of metabolic syndrome in patients with coronary artery disease.
Nozue T, Michishita I, **Ishibashi Y**, Ito S, Iwaki T, Mizuguchi I, Miura M, Ito Y, Hirano T.
J Atheroscler Thromb. 2007 Aug;14(4):202-7.

42.Functional capacity, skeletal muscle strength, and skeletal muscle volume in patients with myocardial infarction.
Kida K, Osada N, Akashi YJ, Sekizuka H, Izumo M, **Ishibashi Y**, Shimozato T, Hayashi A, Yoneyama K, Takahashi E, Suzuki K, Tamura M, Inoue K, Omiya K, Miyake F.
Int Heart J. 2006 Sep;47(5):727-38

43.Bacterial meningitis and cerebral hemorrhagic infarction caused by infective endocarditis.
Ishibashi Y, Honma H, Yamada K, Takahashi Y, Samejima H
Neurological Medicine 2004 Feb. (60) 209-211

44.A case of diagnosis of Bartter Syndrome after pregnancy
Ishibashi Y, Shima Y, Hagimoto K, Sato T, Kimura K
Proceedings of the Congress on Electrolyte Metabolism 2004 (31) 23-27

PUBLICATIONS: TextBook

1. ABSORB, Bioresorbable Vascular Scaffold. A scientific Compendium IV from 2006 to 2014.
Ishibashi Y, Bill Gogas, Onuma Y, Serruys PW

PRESENTATIONS: International (first author only)

1. Ishibashi Y.
QCA-Dmax as guidance for appropriate size selection and deployment of the Absorb scaffold(s) in 1232 patients from three study cohorts (ABSORB Cohort B, ABSORB EXTEND and ABSORB II): Impact on the clinical outcomes at 1 year. ESC 2015, August, London.

2. Ishibashi Y.
Incidence and Potential Mechanism(s) of Post-Procedural Rise of Cardiac Biomarker in Patients With Coronary Artery Narrowing After Implantation of an Everolimus Eluting Bioresorbable Vascular Scaffold or Everolimus Eluting Metallic Stent
The 79nd annual meeting of the Japanese Circulation Society. April. 2015,Osaka.

3. Ishibashi Y.
Critical appraisal of quantitative coronary angiography: Insights from calibrated phantoms. EBC 2014, Oct. Bordeaux.

4. Ishibashi Y.
In vitro validation of two bifurcation algorithms of quantitative coronary angiography in calibrated phantoms: comparison with a CAAS ™ system and with a QAngio XA™. Euro PCR 2014, May. Paris

5. Ishibashi Y.
Acute angiographic and Six-Month Clinical Outcomes after Implantation of Everolimus-eluting Bioresorbable Scaffolds in Long Lesions (>32mm)

ACC 2014, March Washington

6. Ishibashi Y.
The value of fractional flow reserve in predicting myocardial protective effect in patients with previous myocardial infarction undergoing percutaneous coronary intervention. ESC 2011, August, Paris.

7. Ishibashi Y.
The value of cystatin C in predicting contrast-induced acute kidney injury in patients with chronic kidney disease undergoing percutaneous coronary intervention. ESC 2011, August, Paris.

8. Ishibashi Y.
Contrast-Induced Acute Kidney Injury in Patients with Chronic Kidney Disease undergoing Percutaneous Coronary Intervention.
The 75nd annual meeting of the Japanese Circulation Society. 2011, April.

9. Ishibashi Y.
Cystatin C provides Prognostic efficacy than Other Parameters for Stratifying Risk in Patients with Acute Coronary Syndrome.
The 75nd annual meeting of the Japanese Circulation Society. August. 2011,Yokohama.

10. Ishibashi Y.
Myocardial Injury after Percutaneous Coronary Intervention Using Fractional Flow Reserve in Patients with Coronary Artery Disease.
The 75nd annual meeting of the Japanese Circulation Society. August. 2011,Yokohama.

11. Ishibashi Y.
Impact of Contrast-Induced Nephropathy and Cardiovascular Events by Serum Cystatin C in Patients with Renal Insufficiency Undergoing Cardiac Catheterization. ESC 2010, August, Stockholm.

12. Ishibashi Y.
Cystatin C is Useful Marker for Contrast-Induced Nephropathy in the Erderly Patients with Coronary Artery Disease. ESC 2010, August,

Stockholm.

13. Ishibashi Y.
Cystatin C is Useful Marker for Contrast-induced Nephropathy in the Elderly Patients with Stable Angina.
The 74nd annual meeting of the Japanese Circulation Society. March. 2010, Kyoto.

14. Ishibashi Y.
Cystatin C Before Catheterization is Useful Marker for Contrast-induced Nephropathy. Complex Cardiovascular Therapeutics 2010, January, Kobe.

15. Ishibashi Y.
Cystatin C is Useful Marker for Contrast-Induced Nephropathy Undergoing Cardiac Catheterization. ESC 2009, August, Barcelona.

16. Ishibashi Y.
The significance of 123I-BMIPP delayed scintigraphic imagings in patients with vasospastic angina. International Conference of Nuclear Cardiology 2009, May, Barcelona.

17. Ishibashi Y.
The Relationship antihypertensive effect level and Clinical Blood Pressure Changes after Continuous Positive Airway Pressure Treatment in patients with Obstructive Sleep Apnea.
The 73nd annual meeting of the Japanese Circulation Society. March. 2009, Ossaka.

18. Ishibashi Y.
Cystatin C is Useful Marker for Contrast-induced Nephropathy in Patients with Renal Insufficiency Undergoing Cardiac Angiography.
The 73nd annual meeting of the Japanese Circulation Society. March. 2009, Osaka.

AREA of RESEARCH INTEREST:

Interventional Cardiology
Clinical Cardiology
Exercise Physiology
Contrast induced nephropathy

Appendix

Appendix:

Appendix 1: Compendium

ABSORB Bioresorbable Vascular Scaffold: Scientific compendium 2006-2014

Ishibashi Y, Gogas B, Onuma Y, Serruys PW

Appendix 2: QCA and FFR

Fast virtual functional assessment of intermediate coronary lesions using routine angiographic data and blood flow simulation in humans: comparison with pressure wire - fractional flow reserve.

Papafaklis MI, Muramatsu T, **Ishibashi Y**, Lakkas LS, Nakatani S, Bourantas CV, Ligthart J, Onuma Y, Echavarria-Pinto M, Tsirka G, Kotsia A, Nikas DN, Mogabgab O, van Geuns RJ, Naka KK, Fotiadis DI, Brilakis ES, Garcia-Garcia HM, Escaned J, Zijlstra F, Michalis LK, Serruys PW.

EuroIntervention. 2014 Sep;10(5):574-83 **[Original research paper, IF 3.76]**

Appendix 3: Comparison methods of metallic stents and Absorb scaffolds

Comparative analysis method of permanent metallic stents (XIENCE) and bioresorbable poly-L-lactic (PLLA) scaffolds (Absorb) on optical coherence tomography at baseline and follow-up.

Nakatani S, Sotomi Y, **Ishibashi Y**, Grundeken MJ, Tateishi H, Tenekecioglu E, Zeng Y, Suwannasom P, Regar E, Radu MD, Räber L, Bezerra H, Costa MA, Fitzgerald P, Prati F, Costa RA, Dijkstra J, Kimura T, Kozuma K, Tanabe K, Akasaka T, Di Mario C, Serruys PW, Onuma Y.

EuroIntervention. 2015 Oct 9;11(6). **[Original research paper, IF 3.76]**

Appendix 4: Incidence and relevance of angina

The incidence and relevance of site-reported versus patient reported angina: insights from the ABSORB II randomized trial comparing Absorb everolimus eluting bioresorbable scaffold with XIENCE everolimus eluting metallic stent.

Grundeken MJ, White RM, Hernandez JB, Dudek D, Cequier A, Haude M, van Boven AJ, Piek JJ, Helqvist S, Sabate M, **Ishibashi Y**, Staehr P, Veldhof S, Cheong WF, de Winter RJ, Garcia-Garcia HM, Wykrzykowska JJ, Onuma Y, Serruys PW, Chevalier B.

European Heart Journal – Quality of Care and Clinical Outcomes. 2015 Sep.

Appendix 5: DAPT review

Dual antiplatelet therapy, drug-eluting stents and bioresorbable vascular scaffolds: Evolutionary perspectives.
Albuquerque FN, Bortnick A, Iqbal J, **Ishibashi Y,** Stone GW, Serruys PW.
Catheter Cardiovasc Interv. 2015 Aug 10. **[Review paper, IF 2.40]**

Appendix 6: OCT assessment in STEMI
Incidence and potential mechanism of resolved, persistent and newly acquired malapposition three days after implantation of self-expanding or balloon-expandable stents in a STEMI population: insights from optical coherence tomography in the APPOSITION II study.
Nakatani S, Onuma Y, **Ishibashi Y**, Karanasos A, Regar E, Garcia-Garcia HM, Tamburino C, Fajadet J, Vrolix M, Witzenbichler B, Eeckhout E, Spaulding C, Reczuch K, La Manna A, Spaargaren R, Capodanno D, Van Langenhove L, Verheye S, Serruys PW, van Geuns RJ.
EuroIntervention. 2015 Nov 10;11(7). **[Original research paper, IF 3.76]**

Appendix 7: OCT assessment in Angina
Short-term effects of Nano+™ polymer-free sirolimus-eluting stents on native coronary vessels: an optical coherence tomography imaging study.
Suwannasom P, Benit E, Gach O, von Birgelen C, Hofma S, Bo X, Zhang Y-J, Nakatani S, **Ishibashi Y**, Onuma Y, García-García HM, Gao R, Serruys PW
AsiaIntervention 2015;1:57-70 **[Original research paper, IF: none]**

Appendix 8: Syntax II trial
Risk stratification in 3-vessel coronary artery disease: Applying the SYNTAX Score II in the Heart Team Discussion of the SYNTAX II trial.
Campos CM, Stanetic BM, Farooq V, Walsh S, **Ishibashi Y**, Onuma Y, Garcia-Garcia HM, Escaned J, Banning A, Serruys PW; SYNTAX II Study Group.
Catheter Cardiovasc Interv. 2015 Nov 15;86(6):E229-38. **[Original research paper, IF 2.40]**

Appendix 9: Syntax II trial
Validity of SYNTAX score II for risk stratification of percutaneous coronary interventions: A patient-level pooled analysis of 5,433 patients enrolled in contemporary coronary stent trials.
Campos CM, Garcia-Garcia HM, van Klaveren D, **Ishibashi Y**, Cho YK, Valgimigli M,

Räber L, Jonker H, Onuma Y, Farooq V, Garg S, Windecker S, Morel MA, Steyerberg EW, Serruys PW.
Int J Cardiol. 2015 May 6;187:111-5. **[Original research paper, IF 2.32]**

Appendix 10: BVS in ACS
Are BVS suitable for ACS patients? Support from a large single center real live registry.
Felix CM, Onuma Y, Fam JM, Diletti R, **Ishibashi Y**, MD, Karanasos A, Everaert BRC, van Mieghem NM, Daemen J, de Jaegere1, PPT, Zijlstra P, Regar ES, van Geuns RJM
Submitted **[Original research paper, IF xx]**

Appendix 11: Vessel wall strain using Absorb scaffolds
Implications of a bioresorbable vascular scaffold implantation on vessel wall strain of the treated and the adjacent segments.
Bourantas CV, Garcia-Garcia HM, Campos CA, Zhang YJ, Muramatsu T, Morel MA, Nakatani S, Gao X, Cho YK, **Ishibashi Y**, Gijsen FJ, Onuma Y, Serruys PW.
Int J Cardiovasc Imaging. 2014 Mar;30(3):477-84. [Original research paper, IF 2.32]

Acknowledgement

ACKNOWLEDGEMENTS

First, I would like to thank you for your support during my staying in Rotterdam, which lasted about two year. I would like to take this opportunity to offer my sincere gratitude to the people of Erasmus MC and CARDIALYSIS for their warm support.

In March 2012, I visited Rotterdam for the first time to receive an interview with Prof. Serruys. In spite of my poor English, he welcomed me very warmly and made discussions about future projects in Rotterdam. After the interview, I belonged to the Erasmus MC Thoraxcenter and the team of Prof. Serruys as a research fellow since April-2013 until March-2015. I was always in CARDIALYSIS as well as my colleagues even in the weekend and shared frustration and happiness. I shall remember the rest of my life that I was able to meet with you all.

Dearest my promotor Professor Serruys, I deeply appreciate for everything you gave me in Rotterdam. You taught me the fun of science and the condition of having strong feelings. I'll do my best to show you my growth someday.

Dear my good mentor Yoshi-sensei, I appreciate all your support during my stay in Rotterdam. This thesis would not be possible without your numerous help and factory of ideas. I am also grateful that you were so kind to take care of my family (Emi and Kyosuke).

Dear Hanny, definitely you are the "Mother" of fellows. I am grateful that you were so kind to take care of my family as well as my support.

Dear Marie-angele Morel and Hector, many thanks for everything you kindly supported to me and a nice friendship with Japanese fellows. Dank u wel.

Dear Paul, Sylvie and Wendel, many thanks for your great friendship with me. I never forget to talk with you. It was good experience to be part of the editorial board with the EuroIntervention.

Dear research fellows in Rotterdam: Taka-sensei (Japan), Christos (Greece), Yaojun (China), Javaid (UK), Roberto (Italy), Yun Kyeong (South Korea), Shimpei-sensei (Japan), Maik (The Netherlands), Carlos (Brazil), Hiroki-sensei (Japan), Pannipa (Thailand), Erhan (Turkey), Bojan (Bosnia and Herzegovina), Yaping (China), Yohei-sensei (Japan), it was my great pleasure to work with you even for a short time in Rotterdam. Hope everyone to become a great senior interventional cardiologist and let's collaborate in the future studies.

Dear everyone in CARDIALYSIS, I must thank many staffs working in the CARDIALYSIS:

Gerrit-Anne van Es, Monique Schuijer, Bianca Backx, Anne Marie Bruinsma, Jeannette Ana Guimaraes, Ton de Vries, Michael Swart, Joost de Vries, Coby Bouwman, Ravindra Pawar, Jamal Khachabi, Marije Hoogen, Glenda Bochove, and Hans Jonker for their kind friendship and technical assistance. Osama-san, many thanks for your support and friendship.

Herewith I would also like to introduce of My Prof. Yoshihiro J. Akashi (St. Marianna University School of Medicine, Kawasaki, Japan). I must thank you for giving me a chance to move to Rotterdam from Kawasaki. My next goal is to further improve three important components of St. Marianna University School of Medicine (i.e. clinical work, academic research, and education).

Finally, my special thanks to my parents (Kanji and Yuko), wife (Emi) and son (Kyosuke). Now I am very happy thanks to my parents. Despite all difficulties in Rotterdam for my wife and son, you supported me mentally. Thank you very much.

I am grateful to all the people for every encounter.

April 2016,

With my best regards,

Yuki Ishibashi